Oral Session Program

Room 802 A: Soil and Water - Nutrient runoff -			
A1-1	Oct.27 11:00-11:15	Assessing impacts of Nutrient Runoff from corn field with Climate change Using APEX model An Yongbin・Hong Eun Mi・Choi Soon Kun・Ahn Jin-Hyuk・Bak HyeongJin	1
A1-2	Oct.27 11:15-11:30	Analysis of Nutrient Loss in Cropland Using the APEX Model: Effects of Environmental Characteristics and Climate Change Ahn Jin-Hyuk・Bak Hyeongjin・Jung Se yoon・Ahn Yongbin・Jun Sang-Min・Choi Soonkun・Hong Eunmi	3
A1-3	Oct.27 11:30-11:45	Evaluation of Nutrient Runoff Reduction Effects of Fertilizer Application BMPs in Paddy Fields Using the APEX-Paddy Model Bak Hyeongjin・Ahn Jin-Hyuk・An Yongbin・Jung Se yoon・Jun Sang-Min・Choi Soonkun・Hong Eunmi	5
A1-4	Oct.27 11:45-12:00	An Integrated Watershed-Reservoir Modeling Approach for Assessing Hydrodynamics, Sedimentation, and Nutrient Transport in Deji Reservoir, Taiwan Perodes Rozal Jemima・Yu Cheng-Wei・Monredondo Alayaay Mark Lloyd	7
A1-5	Oct.27 12:00-12:15	Refinement of a Total Nitrogen Dynamics Model by Introducing High Temporal Resolution in the Imbanuma Cyclic Irrigation Area Iwasaki Shunya・Iida Toshiaki	9
A1-6	Oct.27 12:15-12:30	Dynamics of water and nutrient flow in a cyclic irrigation scheme for paddy fields in Imbanuma Irrigation Area, Chiba Prefecture, Japan Adiyaksa Ilham Putra・Okura Fumi・Kato Tasuku	10
Room 810 A: Soil and Water - Long term prediction, Drought -			
A2-1	Oct.27 11:00-11:15	Quantifying Soil Moisture Drydown Patterns Using Satellite Observations for Drought Early Warning Sasamoto Daichi・Tsujimoto Kumiko・Ohta Tetsu	12
A2-2	Oct.27 11:15-11:30	Characterization of Flash Droughts on the Korean Peninsula Using Satellite-Derived Soil Moisture Lee Hee-Jin・Nam Won-Ho	14
A2-3	Oct.27 11:30-11:45	Meteorological Drought Thresholds in Cambodia Using the Standardized Precipitation Index Ol Kimsor・Junichiro Takeuchi・Chung Sarit・Masayuki Fujihara	16
A2-4	Oct.27 11:45-12:00	Application and Evaluation of Long-Term Ensemble Precipitation Forecasts for Reservoir Inflow Prediction Tai Yuan-Li・Cheng Ke-Sheng・Lin Yun-Ching・Lee Ching-Teng・Pan Chi	18
A2-5	Oct.27 12:00-12:15	Impact of Climate Change-Induced Rainfall Pattern Shifts on Marine Resources in Kafuri Bay Tabata Toshinori・Tanaka So・Harada Masayoshi・Ozaki Akinori	20
A2-6	Oct.27 12:15-12:30	Irrigation as an Adaptation Strategy for Tea Cultivation under Climate Change Matsushita Yoshihiro・Takeuchi Junichiro・Hama Takehide・Fujihara Masayuki	22
Room 811 A: Soil and Water - Reclaimed water, Microorganisms -			
A3-1	Oct.27 11:00-11:15	Analysis of Biochar Effects on Sorghum Soil under Irrigation with Reclaimed Water from the Kinmen Distillery Liao Yi-Tai・Chiang Li-Chi・Liao Ci-Jyun・Chen Feng-Wen・Tan Yun-Wei	24
A3-2	Oct.27 11:15-11:30	Advancing sustainable rice farming through biochar integration with treated wastewater irrigation to combat greenhouse gas emissions Buates Jittrera・Phung Duc Luc・Watanabe Toru	26
A3-3	Oct.27 11:30-11:45	Microbial Responses to Metal Oxide Nanoparticles in Composted Sewage Sludge: Implications for Greenhouse Gas Emissions in Paddy Soils Phung Duc Luc・Nguyen Thi-Thanh Binh・Vu The Anh・Nishiyama Masateru・Watanabe Toru	28
A3-4	Oct.27 11:45-12:00	Enhancing Reclaimed Water Usage in Paddy Farming Huang Ben Hung-Pin・Huang Yin-Chen	30
A3-5	Oct.27 12:00-12:15	Phytoplankton Community Structure Changes and Occurrence Patterns Associated with Cyanobacterial Blooms in the Upstream Region of Lake Soyang Lee Seungyun・Kim Seonggyeoum・Yeom Hojeong・Choi Hyejeong・Hong Eunmi	32

A3-6	Oct.27 12:15-12:30	Changes in Phytoplankton Communities in Lake Uiam in Response to Climatic and Hydro-environmental Factors Kim Seonggyeoum・Lee Seungyun・Choi Hyejeong・Baek Kyongoh・Hong Eunmi	34
Room 804 A: Soil and Water - Soil -			
A4-1	Oct.27 11:00-11:15	Evaluating the Effect of Near-Surface Soil Moisture Profiles on Microwave Brightness Temperatures Using C-band Radiometry Tsujimoto Kumiko・Ohta Tetsu・Kaihotsu Ichirow	36
A4-2	Oct.27 11:15-11:30	Effect of Biomass-Derived Hydrogels as Soil Amendment on Heavy Metal Immobilization in Paddy and Upland Soils He Kung-Hui	38
A4-3	Oct.27 11:30-11:45	Cellulose nanofibers boost soil water availability and plant growth under deficit irrigation Mori Yasushi・Ngo Thuy An	40
A4-4	Oct.27 11:45-12:00	Evaluating Evapotranspiration and Irrigation Efficiency in Subtropical Rice Fields under AWD Management WU Dong-Hong・Wu Pei-Jhen・Tsai Hsuan-Ju・Lee Shin-Ruei	42
A4-5	Oct.27 12:00-12:15	Impacts of Soil Structure on Gas Diffusivity in Regenerative Agriculture Fields Yukari Yanagi・Sakai Masaru・Kiyoshi Nagasu	44
A4-6	Oct.27 12:15-12:30	Evaluation of the amount of water erosion by mineral composition Nishimura Taku・Yamasaki Takuhei・Gonoi Rin	46
Room 802 A: Soil and Water - Hydrological model -			
A5-1	Oct.27 13:30-13:45	A Systematic Review of Lumped and Conceptual Rainfall-Runoff Models: Performance, Hybridization, Uncertainty and Data Integration Rahmon Abiodun Salau・Qudus Adeyi・Adisa Hammed Akinsoji・Kyung Sook Choi	48
A5-2	Oct.27 13:45-14:00	On the Optimal Configuration of a Distributed Hydrological Model subject to Different Grid Sizes and Lateral Boundary Conditions Chen Chia-Jeng・Liu Jian-Jun	50
A5-3	Oct.27 14:00-14:15	Evaluation of Fecal Coliform Export from Agricultural Watersheds under Climate Change Scenarios Using the SWAT Model Jung Se yoon・Hong Eunmi・Ahn Jin Hyuk・Bak Hyeong Jin・Lee Seonah	52
A5-4	Oct.27 14:15-14:30	Evaluation of Climate Change and Agricultural Management Impacts on Hydrology and Water Quality Using SWAT+ Kim Min-Jin・Nam Won-Ho・Hong Eun-Mi・Jun Sang-Min・Choi Soon-Kun・Kim Seongjoon	54
A5-5	Oct.27 14:30-14:45	Assessing Crop Water Stress and Irrigation Benefits Using the SWAT Model: A Case Study of the Wu River Basin Cheng An-Rou・Chiang Li-Chi・Lin Guan-Zhou	56
A5-6	Oct.27 14:45-15:00	Coupled SWAT and CE-QUAL-W2 Modeling of Nutrient Transport from Watershed to Reservoir: A Case Study of the Feitsui Reservoir, Taiwan Wu Yu-Ting・Chiang Li-chi	57
A5-7	Oct.27 15:00-15:15	Groundwater Modeling and Adaptation Strategies under Climate Change in the Lanyan River Basin: Applications of SWAT+ and LSTM Hao-Hung Chiang・Li-Chi Chiang	60
Room 810 A: Soil and Water - Water use -			
A6-1	Oct.27 13:30-13:45	Assessment of the Agricultural Water Cycle and Resource Utilization Using the EPA-SWMM Model Shin Ji-Hyeon・Nam Won-Ho	62
A6-2	Oct.27 13:45-14:00	Evaluating the Impact of Input Data Structure on ANN-Based Runoff Modeling Maga Kim・Jin-yong Choi	64
A6-3	Oct.27 14:00-14:15	Growth responses of two green manure crops to treatments with non-sulfur photosynthesis bacteria and wastewater sludge Chun-Hank Ko・Bo-Xiang Lee・Ping-Yuan Yang・Chihhao Fan・Tang-Long Shen	66
A6-4	Oct.27 14:15-14:30	Optimizing Water Application Strategies for Climate-Resilient Amaranthus Production in Paddy Field: Insights from On-Farm Experiments in Northern Ghana Salifu Eliasu・Yamada Masakazu・Alhassan Mohammed Issah	68

A6-5	Oct.27 14:30-14:45	A Strategic Framework for Agricultural Water Allocation Using Modern Portfolio Theory HU Ming-Che・WANG Li-Kuan・WEN Tzai-Hung	70
A6-6	Oct.27 14:45-15:00	Optimizing Agricultural Water Distribution with Network Flow Model Chang-Ying Lee・Ming-Che Hu・Ching-Pin Tung	71
A6-7	Oct.27 15:00-15:15	Rapid Expansion of Irrigation through Participatory Irrigation Management in Madhya Pradesh, India: Key Features of Transformation Yokoyama Kenichi・Ishii Atsushi	73
Room 811 A: Soil and Water - Water quality -			
A7-1	Oct.27 13:30-13:45	Application of Time-Lapse Ion-Exchange Resin Capsules for Assessing Spatial Characteristics of Irrigation Water Pollution: A Case Study in the Dali Area, Taichung City, Central Taiwan Tan Yun Wei・Chen Feng Wen・Wang Man Zhing・Hsieh Ming Yang・Li Ting Yi	75
A7-2	Oct.27 13:45-14:00	Twenty Years of NPS Pollution Research in Korea: Insights from the Han River Basin Lee Seonah・Hong Eunmi	77
A7-3	Oct.27 14:00-14:15	Modeling the spatiotemporal dynamics of dissolved oxygen minima in a temperate reservoir using CE-QUAL-W2 Yeom Hojeong・Kim Yoonhee・Kim Bomchul・Hong Eunmi	79
A7-4	Oct.27 14:15-14:30	Raising Rice Productivity Through Oxygen-Enriched Irrigation Water Arif Chusnul・Purnomo Azzahra Putri Kayla・Wibowo Andrehan・Sutoyo Sutoyo・Purwanto Aris Yohannes・Taufik Muh	81
A7-5	Oct.27 14:30-14:45	Portable Minapadi Model and Its Performance for Urban Farming Julianto Tri Baskoro・Setiawan Indra Budi・Saptomo Krido Satyanto・Liyantono Liyantono	82
A7-6	Oct.27 14:45-15:00	Estimation of spring season fish assessment index (FAI) using PyCaret-based AutoML algorithm in South Korea Kim Yong Won・Lee Yonggwan・Chung Jeehun・Jun Wonjun・Kim Seongjoon	84
Room 804 A: Soil and Water - Groundwater -			
A8-1	Oct.27 13:30-13:45	Integrating Modified Sheet-Pipe Technology in Rice Field Subsurface Water Management Saptomo Krido Satyanto・Putra Heriansyah・Junaedi Ahmad・Iqbal Muhammad Raihan・Alghifari Faiq Muhammad・Hamzah Hadyanti Ayda	86
A8-2	Oct.27 13:45-14:00	The Impact of Alternate Wetting and Drying (AWD) on Methane Emissions and Groundwater Recharge in Organic Paddy Fields Hsu Shao-Yiu・Liao Ying-Chi・ Tsai Yi-Zhih・Yang Zhi-Wei	88
A8-3	Oct.27 14:00-14:15	Assessment of Salinity and Soil Loss in Reclaimed Land Under Climate Change Using the APEX Model Lee Ye-Jun・Nam Won-Ho・Kwak Jin-Hyeob・Lee Kwang-Seung	91
A8-4	Oct.27 14:15-14:30	Time-dependent groundwater flows with similarity properties Togo Shuntaro・Unami Koichi・Fujihara Masayuki	93
A8-5	Oct.27 14:30-14:45	Spatio-temporal variability assessment of groundwater level in the drought-prone region in India. Dhivar Nanasaheb Yuvraj・Jha Kumar Madan・Fujihara Masayuki	95
A8-6	Oct.27 14:45-15:00	Water reuse and groundwater augmentation－Focus on New Valley, Egypt－ Abdelhafez A Ahmed・Yoshida Shuichiro	97
Room 701 B: Agricultural Facilities - Concrete structure -			
B1-1	Oct.27 11:00-11:15	Multi-Domain Joint Learning for Crack Detection in-service Agricultural Infrastructure under Varying Illumination Conditions using UAV Imagery Tanaka Hiromu・Shibano Kazuma・Suzuki Tetsuya	98
B1-2	Oct.27 11:15-11:30	Quantitative Internal Damage Assessment of Irrigation and Drainage Concrete Structures by X-ray CT image-based DCNN IKEDA KOKI・Shibano Kazuma・Mukai Moeka・Suzuki Tetsuya	100
B1-3	Oct.27 11:30-11:45	Influence of Input Frequency on Ultrasonic Velocity in Concrete Cores with Large Aggregate Moeka Mukai・Kazuma Shibano・Tetsuya Suzuki	102
B1-4	Oct.27 11:45-12:00	A Study on Simplified Monitoring Methods for Water Leakage Evaluation in Aging Irrigation Reservoirs LI YIXUAN・Matsui Moe・Nakamura Naoki・Sato Mari	104

B1-5	Oct.27 12:00-12:15	Strain behavior and mechanical properties of admixture-added mortars during air and water curing Hirotsugu Suzuki・Kiyohito Yamamoto	106
Room 701 B: Agricultural Facilities - Facilities -			
B2-1	Oct.27 13:30-13:45	Three-dimensional evaluation of in-service corroded steel sheet piles using laser scanning Hagiwara Taiki・Takahashi Yuto・Shibano Kazuma・Tanaka Hiromu・Ikeda Koki・Chiyoda Atsushi・Suematsu Kakutaro・Fujitani Yuta・Suzuki Tetsuya	108
B2-2	Oct.27 13:45-14:00	Non-Contact Detection of Water Pressure Transient Damping in Leakage Pipeline using DIC and TTBTs Techniques Takahashi Yuto・Hagiwara Taiki・Tsubota Toma・Suzuki Tetsuya	110
B2-3	Oct.27 14:00-14:15	Comparison of Future Drought Vulnerability Based on Water Resource Systems in North and South Korea Shin Hyeon-Wook・Nam Won-Ho	112
B2-4	Oct.27 14:15-14:30	Quantitative Assessment of Agricultural Reservoir Response to Extreme Events with Consideration of Storage Capacity Variations Yang Mi-Hye・Nam Won-Ho	114
B2-5	Oct.27 14:30-14:45	Predicting water distribution amount using deep learning in the Aichi Irrigation Project Taisei Hamaguchi・Keigo Noda・Masashi Kiguchi・Taichi Sano・Taikan Oki	116
B2-6	Oct.27 14:45-15:00	Evaluation of Open-Source Digital Elevation Models for Watershed Hydrology Simulation MISHRA KUMAR SURENDRA・PRASHANT PRASHANT・LOHANI KUMAR ANIL	118
Room 702 C: Rural Planning and Ecosystem Services - Ecosystem services -			
C1-1	Oct.27 11:00-11:15	Estimating rice NDVI-peaks with use of variety-specific time-series curves Onishi Kyohei・Nagano Takanori・Yoshikawa Natsuki・Motonaga Yoshitaka	119
C1-2	Oct.27 11:15-11:30	Impact of Climate Change-induced Warming on Adult Morphology in *Sympetrum frequens* Shogo Sato・Hiroshi Jinguji	121
C1-3	Oct.27 11:30-11:45	Comparative Analysis of Fish Habitat Suitability Characteristics in Han River Basin, South Korea Lee Hyeokjin・Song Inhong	123
C1-4	Oct.27 11:45-12:00	Modeling the Ecosystem Conservation Function of Agricultural Ponds in Urbanizing Regions Jo Hamaguchi・Masayasu Maki・Koshi Yoshida・Tasuku Kato・Keigo Noda	124
C1-5	Oct.27 12:00-12:15	Estimation of Habitat Suitability Index Based on Water Quality Using Parametric Distributions in Korea Jang Seongju・Lee Hyeokjin・Song Inhong	126
C1-6	Oct.27 12:15-12:30	SPATIOTEMPORAL ANALYSIS OF HYDROLOGICAL CONNECTIVITY IN A FLOODPLAIN WETLAND USING GEOSTATISTICAL METHODS: A CASE STUDY OF BAKHIRA WILDLIFE SANCTUARY, INDIA Pandey Ashish・Rawat Manish・Yadav Basant・Gupta Kumar Praveen	128
Room 702 C: Rural Planning and Ecosystem Services - Rural Planning -			
C2-1	Oct.27 13:30-13:45	Life cycle impact assessment of radioactive isotope release on the rice paddy fields environment Fong Chin・Fan Chihhao・Hsieh Cheng-I・Lin Wen-sheng	131
C2-2	Oct.27 13:45-14:00	Spatio-temporal characterization of compound heat and drought extremes in South Korea Qudus Adeyi・ Deepak Chaulagain・Kyung Sook Choi	133
C2-3	Oct.27 14:00-14:15	Water Scarcity Risk for Paddy Field Development Project in Pre-Modern Japan: Case Study of the Kinu-Kokai River Basin. EKPELIKPEZE Russell Adonis・ASADA Yohei・ISHII Atsushi	135
C2-4	Oct.27 14:15-14:30	Optimizing Irrigation Water Allocation in Sonosari Irrigation Area, Malang Regency Using Deterministic Dynamic Programming to Enhance Utilization Efficiency and Agricultural Profitability Lufira Dara Rahmah・Limantara Montarcih Lily・Hamdany Ivan Muhammad	137

C2-5	Oct.27 14:30-14:45	A Preliminary Study on the Relationship between Tourism and Agriculture & Fishery NISHINO Takanori・WAKABAYASHI Takashi	138
C2-6	Oct.27 14:45-15:00	Factors Shaping Successful Participatory Irrigation Management in Vietnam: The Roles of Multi-Functional Cooperatives and the Public Sector TRAN HONG MINH・ISHII ATSUSHI・DOAN DOAN TUAN・SHIN MOONO・TRAN VIET DUNG・ASADA YOHEI・NGUYEN DUY TIEN	140
C2-7	Oct.27 15:00-15:15	Functions and structures of Water User Associations (WUAs) in Egypt: A Focus on New Valley Governorate El Gwely Samir・Iwasaki Erina・Sugiura Mikiko	142
Room 703 D: Latest Smart Technologies - Smart facilities -			
D1-1	Oct.27 11:00-11:15	Development of a Drought Monitoring Method Using Multiple Vegetation Indices Derived from PlanetScope Imagery Choi Hyeok-Jae・Nam Won-Ho・Jeon Min-Gi・Moon Min-Kyu・Hong Eun-Mi・Park Jeong-Hwan	143
D1-2	Oct.27 11:15-11:30	Comparative Assessment of CHIRPS v2.0 and v3.0 for Satellite-Based Agricultural Drought Monitoring in South Korea Mun Young-Sik・Nam Won-Ho	145
D1-3	Oct.27 11:30-11:45	Parcel-Level Crop Classification from Structured SITS Features and Clustering Based Analysis Jaejun Gou・Seongju Jang・Jinseok Park・Hyeokjin Lee・Inhong Song	147
D1-4	Oct.27 11:45-12:00	Applying GeoAI to Paddy Area Estimation: A Case Study in Taibao, Taiwan Lee Zih-Ying・Liu Ting-Li・Shih Hsueh-Yen・Wijaya Candera	149
D1-5	Oct.27 12:00-12:15	Optimal IIS Deployment in Fragmented Paddy Fields via Geo-Clustering and Neighborhood Search Tian Runze・Noda Keigo・Takaki Kyoji	151
D1-6	Oct.27 12:15-12:30	Evaluating Smart Gate Control Effects on Water Allocation in Terminal Canals of Thai Paddy Irrigation Schemes Nakada Toru・Hitomi Tadayoshi・Nakaya Tetsuo・Diloksopon Attapan・Ngootip Sarayut・Yamauchi Katsuhiko	153
Room 703 D: Latest Smart Technologies - Infrastructure improvement -			
D2-1	Oct.27 13:30-13:45	Uncovering Stakeholders in Agricultural Irrigation Governance: A Corpus-Based Text Mining Approach YU JOU JOU・Yu Wei Cheng	155
D2-2	Oct.27 13:45-14:00	Implementation plan development and monitoring status for agricultural water resources in Korea under the Comprehensive Basin Water Management Plan yoon kwangsik	157
D2-3	Oct.27 14:00-14:15	Development of a Cascade Watershed Water Balance Model Integrating Agricultural Facilities Yoon Dong-Hyun・Nam Won-Ho	159
D2-4	Oct.27 14:15-14:30	Assessing the awareness of information and communications technology in construction among enterprises engaged in agricultural and rural development Yasushi Noguchi・Teruhito Miyamoto・Atsushi Ishii	161
D2-5	Oct.27 14:30-14:45	PHENOLOGY-BASED MAPPING OF DEEP-WATER FLOATING RICE IN MYANMAR USING GOOGLE EARTH ENGINE Rudiyanto Rudiyanto・Ginting Irawan Frisa・Fatchurrachman Fatchurrachman・Mohd Shah Ramisah・Che Soh Norhidayah	163
D2-6	Oct.27 14:45-15:00	Agricultural Street-View Survey System with Cabbage Field Object Detection Shih Hsueh-Yen・Liu Ting-Li・Ho Shin-Fu・Lee Zih-Ying・Wijaya Candera	164
D2-7	Oct.27 15:00-15:15	Experiments on Internet Environment Improvement in Mountainous Farmland Using Starlink and Mesh-net Wi-Fi Technology Masaru Mizoguchi・Yasuhiro Itakura	166

Poster Session Program

Room 803 A: Soil and Water		
P001	Crop Cultivation Activity Impacts Evaluation using Water-Energy-Food-Carbon-Water Quality Nexus Yoon PuReun・Kim Maga・Choi Jin-Yong・Hur Seung-Oh・Son Jeong-Woo	168
P002	Improved Water Efficiency of Paddy Farming through Alternate Wetting and Drying Irrigation in Central Taiwan Tsai Hsuan-Ju・Wu Pei-Jhen・Wu Dong-Hong・Lee Shin-Ruei	169
P003	Establishing Corn Crop Coefficients for Precision Irrigation in Sustainable Paddy Rotation Systems Lee Shin-Ruei	171
P004	Evaluation of Return Flow and Reuse Efficiency Using Water Cycle Simulation in Irrigation Canal Networks Lee Hyeon-Ji・Nam Won-ho・shin Ji-Hyeon	173
P005	Estimation of Discharge Amount After Using Water Curtain Water in Greenhouse Complexes During Winter Season Kim Sang Min	175
P006	Effect of Irrigation-Induced Distribution of Temperature and Nitrogen Concentration of Paddy Water on Rice Chalky Grain Yuta AMAKAWA・Kazuhiro NISHIDA・Tadashi TSUKAGUCHI・Keita KOBUCHI・Kazuya SHIRAISHI・Shuichiro YOSHIDA	176
P007	Methane gas emissions from meso-scale paddy soil columns affected by artificial macropore installation. Tanaka Nagatsuki・Mori Yasushi	178
P008	Development of a Climate-Resilient Paddy-Upland Crop Rotation Model: A Case Study of Baby Corn and Heat-Tolerant Rice in Subtropical Taiwan Sun Ping Wei・Li Charng Pei・Huang Li Han	180
P009	Effects of Lactobacillales Amendment and Soil Water Content on Carbon Dioxide and Methane Emissions in Paddy Soil Liyuan Chen・Kimihito Nakamura・Natsuki Nobe・Takanori Nagano	182
P010	The Effect of Soil Aggregation Forms to Water Content and Plant Biomass in Soil Columns Kento Tajiri・Yasushi Mori	184
P011	Molecular Characterization of Soil Organic Matter Using NMR and GC/MS in Relation to Total Carbon Content Horiuchi Moeri・Hayakawa Satoshi・Mori Yasushi	186
P012	Measurement of Guava Evapotranspiration in Southern Taiwan Gao Bi-Shuang・Hsieh Hung-Yeh・Syu Chien-Hui	188
P013	Determination of heat unit-based crop coefficient for rice in Taiwan Hou Ya-Ling・Wu Dong-Hong・Wu Pei-Jhen	190
P014	Optimizing Banana Cultivation with CROPWAT 8.0 and Drip Irrigation to Mitigate Water Competition in Paddy-Dominated Watersheds and Promote Climate-Resilient Agriculture Wang Wei-Chen・Chen Yu-Yi・Chen Hsueh-I・Syu Chien-Hui・Tsai Yao-Hsien・Lin Yung-Chou	192
P015	Detection of Initial Irrigation in Paddy Fields Using Remote Sensing Data for Monitoring Water Allocation in Traditional Irrigation System in Bali Wily Goldramijaya・Atiqotun Fitriyah・Fumi Okura・Tasuku Kato・Ni Nyoman Sulastri・I Wayan Tika・Sumiyati・Ida Ayu Gede Bintang Madrini・Mentari Kinasih	194
P016	Improving SWAT performance in a snow-dominated basin via a two-season precipitation lapse rate: Case study of the Tedori River, Japan TABACARU GHEORGHE ALEXANDRU・Fujihara Yoichi	196
P017	High-resolution satellite monitoring of alpine snow patches for watershed water resource variability analysis Nonaka Ryoma・Fujihara Yoichi・Ogawa Hiroshi・Chono Shunsuke・Ichion Eiji	198
P018	The Impact of Irrigation on Carbon Storage in Tea Plantations: Insights from the Static Chamber Method Huang Yan-Ning・Liao Kuo-Wei	200
P019	XGBoost-Based Assessment of Groundwater Levels Influenced by Irrigation and Meteorological Factors Chen Hui Chih・Ling You Ting・Zhuang Wei Ya・Wang Wei Sheng	202
P020	Analysis of salinity dynamics in the estuary of the Red River, Northern Vietnam Inoue Keishi・Kimura Masaomi・Yoshikawa Natsuki・Matsuno Yutaka	203

P021	Effects of automated weed control robots on methane emissions from paddy fields in mountain areas of Northeast Japan Kato Chihiro・Nakamura Tetsuya・Ookawa Taiichiro	205
P022	A Critical Review of Flood Risk Assessment Methodologies: Applicability and Framework for Agricultural Landscape Under Climate Change Adisa Hammed Akinsoji・Kyung Sook Choi	207
P023	Field Analysis of Infiltration Properties Before and After Restoration of Terraced Paddy Fields in Northern Taiwan Huang Qun-Zhan・Hsu Shao-Yiu	209
P024	Impact on agricultural irrigation under the influence of climate change and adaptation strategies for stabilizing agricultural irrigation water supply Huang Ya-Zhen・Fan Chihhao	211
P025	Linking Reservoir Water Level with Lumped Models for Estimating Inflow to Agricultural Reservoirs Kang Seokhun・Song Junghun	213
P026	Effect of irrigation with high nitrogen concentration water on the horizontal distribution and temporal changes in nitrogen concentration in a paddy field Kobuchi Keita・Nishida Kazuhiro・Yoshida Shuichiro	215
P027	Effects of Rice Straw Management on Greenhouse Gas Emissions and Soil Nitrogen Dynamics in Rice Paddy Soil Wang Shan-Li・Kao Chuan-Fu	217
P028	Quantifying Absorbed Water via Matric Potential to Improve Dielectric Models Hashimura Makoto	218
P029	Estimation of short-term rainfall magnitude and intensity using forecast data based on artificial intelligence Kwak Jihye・Kim Jihye・Kim Sinae・Park Seongjae・An Jaeyoung・Park Seonjae・Park Suhwan・Kang Moon Seong	220
P030	Probabilistic estimation of future rainfall erosivity under climate change using sub-hourly disaggregation of daily rainfall in South Korea Kim Sinae・Park Suhwan・Kwak Jihye・An Jaeyoung・Park Seongjae・Park Seonjae・Kang Moon-Seong	221
P031	High-resolution measurements of methane flux from paddy field Natsuki Nobe・Kimihito Nakamura・Liyuan Chen・Takanori Nagano	222
Room 812 B: Agricultural Facilities		
P040	Comparison of Drought Response Capacities Based on Water Resources Under Extreme Drought Conditions in South and North Korea Seo Jun-Yeong・Nam Won-Ho	224
P041	Flood Damage Assessment in an Agricultural Irrigation Area with Motorized Gate Application Kim Da Ye・Lee Gang Hoon・Lee Seung Wook	226
P042	Investigation into effects of aging degradation of rice husk envelope of subsurface drainage for paddy fields on water conductivity at entrance of drainpipe KAGEI Yuji・YOSHIDA Shuichiro・NISHIDA Kazuhiro	228
P043	Smart Agricultural Irrigation Enhances Management Efficiency Tsai, Ming-Dou	230
P044	A Study on Establishing Appropriate Hydrological Design Frequency Criteria for Agricultural Reservoirs So Euigeon・Yoo Seung-Hwan	232
P045	Post-earthquake Deformation Detection in Drainage Wells by UAV-LiDAR for Prevention of Secondary Disasters in Paddy Field Shibano Kazuma・Tanaka Hiromu・Inaba Kazunari・Suzuki Tetsuya	233
P046	Vulnerability Assessment of Agricultural Water Resources and Irrigation Reservoirs Using Multi-Model Ensembles Based on SSP Scenarios Kim Hayoung・Na Ra・Joo Donghyuk・Yoo Seung-Hwan・So Euigeon	235
P047	Estimation of Crack Width for Agricultural Infrastructure by Multimodal Approach with Point Cloud and Image Data Integration Tagami Keika・Tanaka Hiromu・Shibano Kazuma・Suzuki Tetsuya	236
P048	Estimation of irrigation water quality and the effects of abrasion and leaching on water quality kanehira Shusuke	238

P049	Development of Reservoir Operation Rules Using Machine Learning-Based Water Level Forecasting Yang Mi-Hye・Nam Won-Ho	240
P050	Performance evaluation of agricultural pipeline system based on TTBTs with artificial leakage Chiyoda Atsushi・Hagiwara Taiki・Takahashi Yuto・Tsubota Toma・Suematsu Kakutaro・Suzuki Tetsuya	242
P051	Non-Contact Detection of Irregular Vibrations in Pump Rotors using Infrared-Stress Method Suzuki Tetsuya・Oshima Keiichiro・Takahashi Yuto・Hagiwara Taiki	244
P052	Post-Earthquake Damage Assessment of Landslide Prevention Facilities by UAV-LiDAR Otaka Norihiro・Tanaka Hiromu・Shibano Kazuma・Fujimoto Yuji・Suzuki Tetsuya	245
Room 812 C: Rural Planning and Ecosystem Services		
P060	Estimation of Parameters in a Water Front Advance Model for Large-Scale Paddy Fields Koshiyamma Naoko・Otsu Takeshi	247
P061	Effects of Land Use on Soil Microbial Community Composition and Predicted Nitrogen Metabolism in Paddy and Dry Fields Shiau Yo-Jin・Chen Ting-Kai・Jhang Syu-Ruei・Chen Yi-Ying・Chou Charles C.-K.・Lee Chia-Wei・Chen Wei-Nai・Chang Chih-Chung・Chiang Chih-Feng	249
P062	Farmers' Perceptions of Farmland and Preferences for Land Management in Irrigated Areas: A Case Study of the Rwamagana District Irrigation Scheme, Republic of Rwanda KINOSHITA Kodai・MATSUNO Yutaka・NDAYISHIMIYE Alfred	251
P063	Enhancing Sustainable Agricultural Water Management through Participatory Local Governance: A Case Study from Korea Kim Da Ye・Maeng Seung Jin・Lee Eun Ryeong・Lee Bong Kuk	253
P064	Climate Change and Adaptation in Coastal Agriculture: Impacts on Nutrient Cycling and Water Resources Chen Chi Wen・Chen Yu Yen・Wang Wei Sheng	255
P065	Hierarchical and Non-hierarchical Cluster Analysis of Standard Watersheds Considering Hydrology, Water Quality, and Aquatic Ecosystem in South Korea Wonjun Jeon・Yonggwan Lee・Jeehun Chung・Yongwon Kim・Seongjoon Kim	257
P066	Ecological Impact of Treated Effluent Irrigation in Rice Paddies: A Case Study on Aquatic Organisms Liu Chen-Wuing・Lee Jin-Jing・Chen Feng-Wen・Cho Yu-Chien・Chen Guan-Jia・Kuo Mei-Hwa	259
P067	Development of a practical numerical model for predicting paddy field dam effect based on the actual field condition Abe Takaaki・Koshiyama Naoko・Hotta Nobuyuki	261
P068	Quantitative PCR method to detect the invasive bitterling fish in agricultural channels using environmental DNA Moriuchi Kaito・Otsuki Kanoko・Hamada Mayuko・Taniguchi Rintaro・Sumida Takanari・Katsuhara Koki・Nakata Kazuyoshi	263
P069	Development of a Multi-Faceted Evaluation Framework for Agricultural Reservoir Clusters toward Sustainable Management Masaomi Kimura・Satoshi Watanabe・Keigo Noda・Yutaka Matsuno	265
P070	Effects of restoration methods on freshwater mussel distribution in the agricultural irrigation channels of Okayama City, western Japan Taniguchi Rintaro・Sato Moyu・Moriuchi Kaito・Katsuhara Koki・Takeyama Tomohiro・Nakata Kazuyoshi	267
Room 812 D: Latest Smart Technologies		
P080	Improving Water Distribution and Reducing Labor in Hillside Irrigation Canals Using ICT Irrigation Devices Takeshita Shinichi・Pingkanon Maetawee	269
P081	Sentinel-2 Time-Series Analysis for Detection and Monitoring of Alternanthera philoxeroides Shinohara Kengo	271
P082	Groundwater Level Forecasting Based on Time Series Clustering and Transformer Chueh, Chia-Jung	273
P083	Water Stress Detection in Persimmon Cultivation Using A Pre-Trained Machine Leading Model Naoki Onishi・Atsushi Okayama・Yutaka Matsuno・Kuniomi Kimura	275
P084	Deep Learning-Based Estimation of Water Stress in Persimmon Trees for Data-Driven Irrigation Management Okayama Atsushi・Onishi Naoki・Kimura Masaomi・Sanada Rena・Matsuno Yutaka	277

P085	Fundamental Evaluation of Convolutional Neural Networks for Automatic Identification of Spider Mite Damage in Edible Roses (Rosa spp.) Rena Sanada・Honami Nakasuji・Atsushi Okayama・Munetaka Hosokawa・Masaomi Kimura・Yutaka Matsuno	279
P086	Effect of nighttime irrigation using automatic irrigation systems on preventing cold water damage of rice Nishida Kazuhiro・SHIRAISHI Kazuya・TSUKAGUCHI Tadashi・YOSHIDA Shuichiro・HIRAI Kazuyoshi・SUNAHASE Yuji	281
P087	Integrating Groundwater Forecasting and Climate Risk Mapping to Enhance Adaptive Water Management: A Case Study of Tainan, Taiwan Tsai Wen-Ping・Wang I-Hsuan・Tsang Pei-Ju	283
P088	Development of a Crop Yield Estimation Technique Based on Integrated Analysis of Hydrological and Growth Indicators in Paddy Fields Using SAR Imagery Chung Jeehun・Lee Yonggwan・Kim Yongwon・Jun Wonjun・Kim Seongjoon	284
P089	Integrated Application of Ultrafiltration and Fine Bubble Diffusion in a Hybrid Recirculating Aquaculture-Paddy Farming System Teuku Assiddiqi Devan・Setiawan Indra Budi	285
P090	Paddy Irrigation Tools developed on Farmers Viewpoint OZAWA Yoshihiro	286
P091	A Differentiable Two-Layer Energy Balance Model Coupled with a Residual Temporal Convolutional Network for Sparse-Observation Paddy Water Depth Inversion Xie Wenpeng・Kimura Masaomi・Li Hongmei・Tian Runze	288
P092	Analysis of Critical Input Features in LSTM-Based Inundation Forecasting Optimized by Multi-Objective Genetic Algorithms Jhong Bing-Chen・Chang Hsiang-Kuan・Chu Jung-Lien	289

Assessing impacts of Nutrient Runoff from corn field with Climate Change Using APEX model

Yong Bin An [1], Eunmi Hong [1*], Soon-Kun Choi[2], Jin-Hyuk Ahn[1], Hydeongjin Bak[3], Hojeong Yeom[3]

[1] Department of Environmental science, Kangwon National University, Chuncheon, (Gangwon State) 24341, Republic of Korea

[2] National Institute of Agricultural Sciences, Wanju, (Jeonbuk State) 55365, Republic of Korea

[3] Interdisciplinary Program in Earth Environmental System Science & Engineering, Kangwon National University, Chuncheon, (Gangwon State) 24341, Republic of Korea

* Corresponding author. Email: eunmi.hong@kangwon.ac.kr

Abstract (10 pt, Times New Roman, Bold)

Excessive nutrient runoff from agricultural land is a primary cause of water quality degradation and eutrophication. As rainfall patterns change due to climate change, the risk of nutrient loss and soil erosion from farmlands increases.

This study aimed to assess the impact of climate change on nutrient loss from an agricultural field by utilizing the APEX (Agricultural Policy/Environmental eXtender) model. A field plot was established at the Kangwon National University farm, and hydrological and water quality monitoring system was installed. The collected samples were analyzed for total nitrogen (TN) and total phosphorus (TP) according to standard methods. The APEX (Agricultural Policy/Environmental eXtender) model, which is suitable for evaluating environmental changes at the field scale, was selected to evaluate nutrient runoff under climate change scenarios.

The collected monitoring data will be used to calibrate and validate the APEX model. The validated model will then be used to apply climate change scenarios, and the results will be analyzed to evaluate the effects of climate change on nutrient loss from farmland.

Keywords: Agricultural field, APEX, Climate change, Nutrient loss

1. Introduction

Soil erosion and nutrient runoff from agricultural activities are one of the primary causes of water pollution (Tapa et al., 2025). Worldwide, the excessive application of fertilizers to increase crop yields has led to an over-accumulation of nutrients in the soil. Soil and nutrients discharged from farmlands act as a non-point source of pollution, contributing to significant pollution loads in aquatic ecosystems (Yang et al., 2025). Therefore, managing nitrogen and phosphorus runoff is necessary to reduce non-point source pollution.

As a result of abnormal temperatures and changes in rainfall patterns due to climate change, nutrient runoff from farmlands is expected to increase (Lee et al., 2024). Changes in regional hydrological patterns can lead to altered transport characteristics of nutrient discharge. (Chang et al., 2023). In particular, the increasing frequency and intensity of extreme rainfall is a major future issue influencing the runoff of soil and nutrients. The need to evaluate the impact of climate change on nutrient runoff has become critical.

To address these issues, it is first necessary to understand the mechanisms of surface runoff and nutrient loss in response to rainfall. Research to evaluate runoff loads and better understand the underlying mechanisms has been conducted through field monitoring under various conditions. However, such studies are limited by constraints like time and cost. To overcome the limitations of assessing non-point source pollution through direct observation, various watershed hydrological models have been introduced. Among these, the Agricultural Policy/Environmental eXtender (APEX) model is widely used in agricultural management due to its suitability for farm and small watershed scale studies.

The APEX model is useful for simulating the effects of various farming activities and conservation practices, and it has also been widely applied to evaluate future climate impacts based on historical data. Recently, as the risk of nutrient runoff from farmlands due to climate change has increased, numerous studies have used the APEX model to investigate nutrient runoff under future climate conditions. However, since the APEX model was developed for U.S. landscapes and agricultural practices, there are limitations in applying it directly to Korean farmlands. In Korea, the APEX-Paddy model has been developed to reflect the characteristics of rice paddy cultivation and has been used to evaluate runoff loads and climate change impacts (Kamruzzaman et a., 2020). Nevertheless, research using the APEX model to assess non-point source pollution from upland fields under future climate change remains insufficient.

This study aims to evaluate nutrient runoff under future climate change in a conventional corn–cabbage double-cropping system using the APEX model. A field plot was established to provide input data for the APEX model, as well as calibration and validation datasets. Based on this, we aim to verify the applicability of the APEX model for future climate impact assessment in Korea.

2. Materials and Methods

2.1. Study Area

This study was conducted by establishing a field plot at the Kangwon National University farm in Chuncheon, Gangwon Province, South Korea. The experimental plot, measuring 5 m in width and 14.5 m in length, had a slope of approximately 2.8%. The soil was identified as Jigog series, which is close to sandy loam and belongs to Hydrologic Soil Group D.

2.2. Monitoring & Analysis

To use as input data for the model, runoff was measured for each rainfall event in 2025 and water quality was analyzed. Corn was grown in the spring and summer, and fall cabbage was grown in the autumn. The corn

variety used was Zea mays L. cv. Dubaemat Chal, and the fall cabbage variety was Brassica rapa subsp. pekinensis (Lour.) Hanelt cv. Buram3ho. A 1/100 runoff sampler (Korean Patent Application 10-2013-0050011) was installed at the outlet of the field plot to measure runoff volume and collect runoff samples. Water quality samples were stirred after the rainfall event and collected into sample bottles before being transported to the lab for the analysis of Total Nitrogen and Total Phosphorus, according to the Water Pollution Standard Method. Weather data were obtained from the Chuncheon ASOS weather station near the plot.

2.3. APEX model

To evaluate nutrient runoff from the field, the APEX (version 1501) model with the APEXeditor (J. M. O Leyton, 2019) spreadsheet interface was used. The APEX model input data includes soil, weather, land use, slope, and crop management.

For weather data, daily average maximum and minimum temperatures, daily precipitation, average relative humidity, daily average wind speed, and solar radiation were collected from the Chuncheon ASOS weather station.

For soil data, Korean soil data provided by Heuktoram were accessed and used in the APEX soil database.

For the nutrient runoff evaluation, the model was calibrated for key parameters related to runoff, nitrogen, and phosphorus export. This study identified commonly used parameters through a literature review (Yang et al., 2025). These parameters were manually calibrated within their given ranges using R^2 (coefficient of determination), NSE (Nash-Sutcliff model efficiency), and PBIAS (percentage bias).

2.4. Future climate change scenarios

In this study, we aimed to evaluate future nutrient runoff from the field based on future climate scenarios. We obtained climate data for Korea based on a Global Climate Model (GCM) and SSP (Shared Socioeconomic Pathways) scenarios from the National Institute of Agricultural Sciences, Rural Development Administration. Based on this data, we plan to reflect future climate scenarios in the model.

3. Results and Discussion

The results of this study are preliminary and the APEX model is currently undergoing calibration and validation. We calibrated the APEX model parameters based on runoff, TN, and TP data from corn and fall cabbage rainfall events in 2025. A total of nine parameters—four related to runoff, two to TP, and three to nitrogen—were selected through a literature review. Since runoff calibration must precede the calibration of nitrogen and phosphorus loads, we are currently performing runoff parameter calibration.

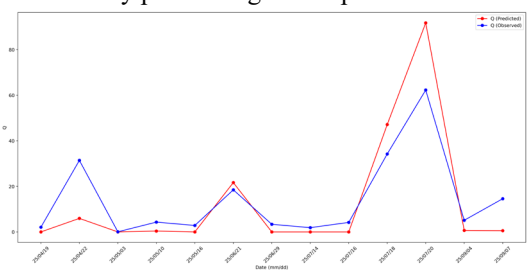

Figure 1. Comparison of observed and simulated data results during the study period

The runoff calibration results were an R^2 of 0.84, an NSE of 0.51, and a PBIAS of 9.01%, which were evaluated as Good, Satisfactory, and Good levels, respectively. Based on these results, we will proceed with the calibration of total nitrogen and total phosphorus parameters. Once the calibration for runoff, total phosphorus, and total nitrogen is complete, we plan to set up future climate scenarios and use the APEX model to simulate total nitrogen and total phosphorus loads.

Table 1. An example of table.

Index	R2	NSE	PBIAS (%)
Discharge	0.84	0.51	9.01

4. Conclusions

Based on this study's results, the APEX model was found to satisfactorily simulate runoff, with R^2, NSE, and PBIAS all evaluated as above a satisfactory level. We will use these results to complete the TN and TP parameter calibration. Following this, we plan to perform simulations based on climate change scenarios to evaluate future changes in nutrient runoff.

Acknowledgements

This study was conducted by National Academy of Agricultural Sciences under the project titled 'Development of impact, vulnerability assessment and adaptation technology for agricultural nutrient runoff, water quality under changes in climate and cropping system' (00396736) funded by the Rural Development Administration.

References

Chang, D., Li, S., & Lai, Z.,2023. Effects of extreme precipitation intensity and duration on the runoff and nutrient yields. Journal of Hydrology, 626, 130281.

Kamruzzaman, M., Hwang, S., Choi, S. K., Cho, J., Song, I., Jeong, H., ... & Yoo, S. H.,2020. Prediction of the effects of management practices on discharge and mineral nitrogen yield from paddy fields under future climate using APEX-paddy model. Agricultural Water Management, 241, 106345.

Lee, J.-M., Yeob, S.-J., Jun, S.-M., Lee, B., Yang, Y., and Choi, S.-K.,2024. Evaluation of non-point pollution loads in corn-autumn Kimchi cabbage cultivation areas by fertilizer application levels using the APEX model. Journal of the Korean Society of Agricultural Engineers, 66(5),15-27.

Thapa, A., Aryal, N., Reba, M. L., Teague, T. G., Payne, G. K., & Pieri, A.,2025. Modeling of conservation practices' effects on nutrients and sediment load reduction from commercial cotton fields using APEX. Journal of Agriculture and Food Research, 21, 101889.

Yang, Y., Choi, S. K., Lee, B. M., Jun, S. M., Lee, J. M., & Yeob, S. J.,2025. Evaluation of Phosphorus Runoff Reduction in Sloped Upland with Furrow Vegetative Cover Using the APEX Model. Journal of The Korean Society of Agricultural Engineers, 67(2), 69-81.

Analysis of Nutrient Loss in Cropland Using the APEX Model : Effects of Environmental Characteristics and Climate Change

Jin-Hyuk Ahn[1], Hyeongjin Bak[2], Yongbin An[1], Se yoon Jung[2], Sang-Min Jun[3], Soon-Kun Choi[3], Eunmi Hong[4*]

[1] Department of Environmental Science, Kangwon National University, Chuncheon, Gangwon State 24341, Republic of Korea

[2] Interdisciplinary Program in Earth Environmental System Science & Engineering, Kangwon National University, Chuncheon, Gangwon State 24341, Republic of Korea

[3] National Institute of Agricultural Sciences, Wanju, (Jeonbuk State) 55365, Republic of Korea

[4]Associate Professor, Interdisciplinary Program in Earth Environmental System Science & Engineering, Kangwon National University, Chuncheon, Gangwon State 24341, Republic of Korea

* Corresponding author. Email: Eunmi.Hong@kangwon.ac.kr

Abstract

Cropland is a major non-point source of nutrient loss, particularly during rainfall events. To manage this effectively, there is a growing need for scientific evidence that enables the proactive identification of fields vulnerable to nutrient loss. However, studies conducted in Korea have been carried out under varying climatic conditions, limiting the ability to clearly distinguish environmental vulnerability factors at the field scale. In this study, the Agricultural Policy/Environmental eXtender (APEX) model was developed based on monitoring data from Korea to evaluate the influence of environmental characteristics on nutrient loss under uniform climatic conditions. Model input data included daily climate records from the Korea Meteorological Administration and runoff, total phosphorus (TP) load data collected from previous studies. Soil data was obtained from the 'Detailed soil maps' provided by the National Institute of Agricultural Sciences, and operation schedules were referenced from the Rural Development Administration's 'Nongsaro' database. As most prior studies in Korea were conducted over short periods (less than one year), all available data were used for model calibration, and model validation could not be performed. The calibrated model was then applied with consistent climate inputs to analyze nutrient loss characteristics according to field-specific environmental conditions, thereby providing a scientific basis for assessing field-scale nutrient loss vulnerability. Additionally, the calibrated model was run with climate change scenarios (SSP) to simulate future nutrient loss trends under climate change. This was intended to proactively identify fields that may become more vulnerable due to climate change in the future.

Keywords: APEX model, Field-scale evaluation, Nutrient loss, SSPs(Shared Socioeconomic Pathways).

1. Introduction

Cropland is a major non-point source of nutrient loss, particularly during rainfall events. To ensure effective management, it is essential to establish scientific evidence that enables the proactive identification of fields vulnerable to nutrient loss. In this study, the Agricultural Policy/Environmental eXtender (APEX) model was developed based on monitoring data collected in Korea, and the influence of field-specific environmental characteristics on nutrient loss was evaluated under uniform climatic conditions. In addition, future climate scenarios were applied to assess the vulnerability of nutrient loss from each cropland under future climatic conditions.

2. Materials and Methods

2.1. Data source

The model input data included daily climate records from the Korea Meteorological Administration and runoff and nutrient load data collected from previous studies. Soil data were obtained from the 'Detailed Soil Map' provided by the National Institute of Agricultural Sciences, and operation schedules were referenced from the Rural Development Administration's 'Nongsaro' database.

Table 1. field-specific environmental characteristics.

Site No.	Crop	Slope (%)	Slope Length (m)	Ref.
1	Radish	20.0	250	NIER (2010)
2	Kimchi cabbage	28.0	120	
3	Soybean	3.2	79	Kim (2010)
4	Soybean	27.5	30	
5	Kimchi cabbage	9.0	49.3	Won (2014)
6	Sweet potato	8.5	35	NIER (2010)
7	Perilla	3.0	30	NIER (2012)
8	Perilla	8.0	30	

2.2. Calibration of APEX model

The APEX model was calibrated against runoff and nutrient loss, and only the most sensitive parameters identified through sensitivity analysis using APEX-CUTE were selected for calibration, while the remaining parameters were retained at their default values. Model performance was evaluated following the criteria proposed by Moriasi et al. (2015).

2.3. Climate Scenario

In this study, nutrient losses from croplands were analyzed for the current period (2011–2020) and the future period (2021–2100). For the current period, to control for climatic variability and evaluate nutrient loss

characteristics under different environmental factors, the average of nationwide meteorological observations from 2011 to 2020, provided by the Korea Meteorological Administration, was applied to all APEX models. For the future period, meteorological data were derived from the SSP climate change scenarios provided by the National Institute of Agricultural Sciences, using ensemble values from 18 GCMs. In this case as well, nationwide mean values were applied to minimize the influence of climatic variability. In addition, the future climate was divided into the Short-term (2021–2040), Mid-term (2041–2070), and Long-term (2071–2100) for analysis.

3. Results and Discussion

3.1. Calibration of APEX model

Model calibration showed satisfactory performance for runoff (R^2, NSE, PBIAS) across all sites, whereas TP load exhibited unsatisfactory PBIAS at some sites, likely due to the use of standard fertilizer application rates.

Table 2. Performance indicator values of APEX model.

Site No.	Runoff Depth(mm)			TP Load(kg/ha)		
	R^2	NSE	PBIAS	R^2	NSE	PBIAS
1	0.68	0.50	-1.35	0.62	0.56	-0.65
2	0.76	0.71	-3.44	0.80	0.79	-1.73
3	0.83	0.68	0.13	0.74	0.56	48.95
4	0.95	0.95	-0.17	0.78	0.62	19.12
5	0.88	0.51	6.38	0.78	0.62	19.12
6	0.67	0.66	0.25	0.46	0.39	19.97
7	0.99	0.99	-1.52	0.73	0.72	3.99
8	0.99	0.99	-1.51	0.68	0.65	-2.00

3.2. Field-specific phosphorus load

Based on APEX model estimates under uniform climate conditions, the average total phosphorus load (kg/ha/event) was highest in Kimchi cabbage at a 28% slope, followed by Perilla at 3% and 8% slopes, Kimchi cabbage at a 9% slope, Radish at a 20% slope, Soybean at a 27.5% slope, Sweet potato at an 8.5% slope, and Soybean at a 3.2% slope.

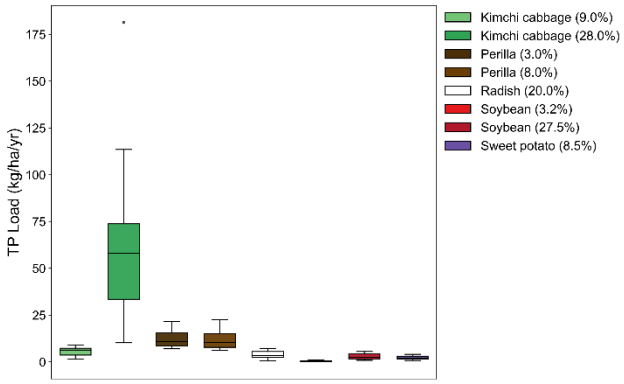

Figure 1. Total phosphorus load (kg/ha/event) for each field estimated by the APEX model during 2011–2020 in Korea.

3.3. Total phosphorus load under the SSP5-8.5 scenarios

All croplands exhibited the lowest phosphorus loads in the short-term period, with an overall increasing trend toward the long-term. Unlike the current period (2011–2020), the highest total phosphorus loads were observed in Perilla fields with 3.0% and 8.0% slopes, followed by Radish (20.0%), Kimchi cabbage (28.0%), Sweet potato (8.5%), Soybean (27.5%), Kimchi cabbage (9.0%), and Soybean (3.2%).

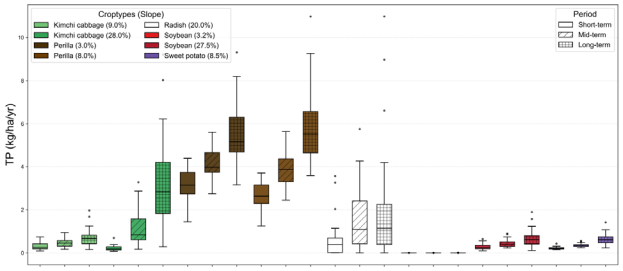

Figure 2. Total phosphorus load (kg/ha/yr) for each cropland estimated by the APEX model under the SSP5-8.5 scenario during the Short-term (2021–2040), Mid-term (2041–2070), and Long-term (2071–2100) periods.

4. Conclusions

In this study, the APEX model was developed based on Edge-of-Field monitoring data collected in Korea to identify environmental conditions highly susceptible to nutrient loss and to analyze nutrient loss sensitivity under future climate scenarios. In future research, the established model will be applied with Best Management Practices (BMPs) to evaluate field-scale vulnerability to nutrient loss.

Acknowledgements

"Development of Adaptation Technologies and Vulnerability Assessment of Agricultural Runoff and Irrigation Water Quality under Changing Climate and Cropping Systems" (Project No. 00396736), funded by the National Institute of Agricultural Sciences, Rural Development Administration, Republic of Korea.

References

Kim, K.-C. (2010). Comparison of Non-point Source Pollution Discharge Characteristics between Sandy Flat and Sloping Fields in Gangwon Province (Master's thesis). Kangwon National University. Gangwon-do.

Moriasi, D. N., Gitau, M. W., Pai, N., & Daggupati, P. (2015). HYDROLOGIC AND WATER QUALITY MODELS: PERFORMANCE MEASURES AND EVALUATION CRITERIA. Transactions of the ASABE, 58(6),1763-1785. https://doi.org/10.13031/trans.58.10715

Natlonal institute of environmental research. (2010). Long-term monitoring of nonpoint source pollution from major land uses (4), TRKO201800026365. Incheon, Korea: Natlonal institute of environmental research.

Natlonal institute of environmental research. (2012). A Long-Term Monitoring for the Non-Point Sources Discharge, T000038375. Incheon, Korea: Natlonal institute of environmental research.

Won, Chul Hee, Shin, Min Hwan, Lee, Su In, Kum, Dong Hyuk, Lim, Kyoung Jae, & Choi, Joong Dae. (2014). Effects of Surface Cover and Soil Amendments on the NPS load Reduction from Alpine Fields. Journal of The Korean Society of Agricultural Engineers, 56(3), 47–53.

Evaluation of Nutrient Runoff Reduction Effects of Fertilizer Application BMPs in Paddy Fields Using the APEX-Paddy Model

Hyeongjin Bak[1], Jin-Hyuk Ahn[2], Yongbin An[2], Se yoon Jung[1], Sang-Min Jun[3], Soon-Kun Choi[3], Eunmi Hong[4*]

[1]Interdisciplinary Program in Earth Environmental System Science & Engineering, Kangwon National University, Chuncheon, Gangwon-do 24341, Republic of Korea

[2]Department of Environmental science, Kangwon National University, Chuncheon, (Gangwon State) 24341, Republic of Korea

[3]National Institute of Agricultural Sciences, Wanju, (Jeonbuk State) 55365, Republic of Korea

[4]Associate Professor, Interdisciplinary Program in Earth Environmental System Science & Engineering, Kangwon National University, Chuncheon, Gangwon-do 24341, Republic of Korea

* Corresponding author. Email: Eunmi.hong@kangwon.ac.kr

Abstract

Nutrient runoff from paddy fields is a contributor to the eutrophication of aquatic ecosystems. To mitigate this issue, various Best Management Practices (BMPs) have been developed and implemented. However, a major limitation of conventional BMPs, such as reducing fertilizer application rates, is their low on-site applicability due to farmers' concerns over potential crop yield reduction. Consequently, there has been increasing interest in new BMPs that focus on improving fertilizer use efficiency and minimizing nutrient loss. To compare the effectiveness of these emerging BMPs with existing ones, long-term monitoring of experimental plots under controlled conditions is necessary, but this process is both costly and time-consuming. To overcome the limitations of field-based research, this study utilized the APEX-Paddy model to compare and evaluate the effects of several BMPs. This research established the APEX-Paddy model based on field monitoring data from a paddy field. The study then simulated various BMP scenarios, including reduced fertilizer application, increased drainage outlet height, the application of controlled-release fertilizers via side-deep placement, and deep placement fertilization. The nutrient runoff reduction effects of each scenario were then compared and evaluated.

Keywords: APEX-Paddy model, BMPs, Nutrient runoff, Paddy fields

1. Introduction

Nutrient runoff from paddy fields has long been identified as a major cause of eutrophication and water quality degradation in aquatic ecosystems. To mitigate this issue, various Best Management Practices (BMPs) have been developed and implemented. Historically, BMPs focused on non-point source pollution reduction in paddy fields have primarily involved fertilizer reduction and water management through methods like increasing the drainage outlet height. However, simply reducing fertilizer application tends to have low on-site applicability due to farmers' concerns over potential crop yield reduction (Yu et al., 2022).

To address this limitation, research and field application of BMPs that improve fertilization methods to suppress nutrient loss while maintaining the same total fertilizer application rate have been expanding. Examples include deep placement fertilization and the use of controlled-release fertilizers. However, agricultural non-point source pollution is highly dependent on regional heterogeneities such as weather conditions, soil type, and farming practices. This often leads to different studies reporting varying reduction efficiencies for the same BMP, which makes it difficult to generalize and quantitatively compare their effects.

Therefore, while long-term monitoring of experimental plots under identical conditions is required to accurately determine the reduction effects of each BMP, this approach is extremely costly and time-consuming. To compensate for these constraints, there has been a growing trend of using agricultural models like APEX and SWAT to simulate BMP scenarios and evaluate their effectiveness. This study, therefore, applies the APEX-Paddy model, which can reflect the unique flooded environment of paddy fields and simulate various BMPs, to quantitatively compare and evaluate the nutrient runoff reduction effects of multiple applicable BMPs.

2. Materials and Methods

2.1. Model Input Data

The study site was an experimental paddy field in the Iksan region of Jeollabuk-do, where the model was constructed based on field data collected during the 2013 farming season from May to September. The input data used for model construction are as follows. Daily meteorological data from the Jeonju ASOS station of the Korea Meteorological Administration were used as climate input. Soil data were built upon the Heuktoram detailed soil maps from the National Institute of Agricultural Sciences. Farming and water management data, including the farming schedule and water level data, were obtained from prior field studies. Additionally, detailed information on the farming schedule not included in the field data was supplemented by referencing information from the Rural Development Administration's 'Nongsaro' and a separate study by Choi (2019).

2.2. Model Calibration and Validation

To ensure the accuracy of the model, calibration was performed using monthly cumulative runoff (Q) and total nitrogen (TN) runoff load data. For the sensitivity analysis of relevant parameters, the Enhanced Morris method was implemented in Python (Campolongo, F et al., 2005). Parameters identified as highly sensitive were manually calibrated. The model's goodness-of-fit was evaluated using the Coefficient of Determination (R2), Nash–Sutcliffe Efficiency (NSE), and PBIAS metrics. The model's performance was assessed based on the criteria proposed by Moriasi et al. (2015).

2.3. BMP Scenario

To assess the effectiveness of BMPs in reducing non-point source pollution in paddy fields, five scenarios were established.

First, the conventional practice (CP) scenario, which served as a control group, was based on field data from the monitoring site. In this scenario, nitrogen fertilizer was applied at a rate of 121.1 kgN/ha, and the drainage outlet height was maintained at 7 cm after mid-season drainage.

In the drainage outlet raising (DOR) scenario, the drainage outlet height was raised to 12 cm after mid-season drainage to enhance the water storage capacity of the paddy field.

In the reduced fertilization (RF) scenario, nitrogen application was reduced by approximately 25% to the recommended rate of 90 kgN/ha.

For the controlled-release fertilizer and side-deep placement (CRF+SDP) scenario, fertilizer was applied at a soil depth of 4 cm simultaneously with transplanting. To represent the sustained release effect of the controlled-release fertilizer, which lasts for 90 days, the application was approximated by a split application at 10-day intervals.

Finally, in the deep-placement (DP) scenario, the entire amount of fertilizer was applied at a soil depth of 27 cm as a basal application before the paddy field was flooded.

3. Results and Discussion

3.1. APXE-Paddy Model Calibration Results

As a result of the APEX-Paddy model calibration, both Q and TN exhibited Satisfactory or better performance across all evaluation indices (Table 1.).

Table 1. Calibration Statistics for Q and TN.

Variable	R2	NSE	PBAIS
Q	0.990	0.956	-14.76
	Very good	Very good	Satisfactory
TN	0.957	0.849	17.65
	Very good	Very good	Satisfactory

3.2. BMP and TN Runoff

An evaluation of the effectiveness of BMPs in reducing TN runoff load during the farming season showed that the DP scenario was the most effective, reducing the TN load by 68% compared to the CP scenario. The CRF+SDP scenario achieved a 28% reduction, while the RF scenario resulted in an 18% reduction. In contrast, the DOR scenario showed a negligible effect, with only a 2.5% reduction in TN load (Figure 1.).

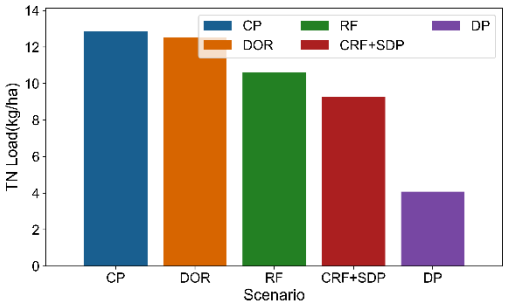

Figure 1. Growing-Season Cumulative TN load by scenario.

Analysis of the monthly TN runoff load (Figure 2.) revealed that both RF and DOR scenarios exhibited a peak TN runoff load during the early farming season (May to June), similar to the CP scenario. Conversely, the DP and CRF+SDP scenarios demonstrated significantly lower TN runoff loads during this initial period. These results suggest that improving fertilization methods can effectively mitigate the initial peak runoff load, leading to a successful reduction of TN runoff throughout the entire farming season.

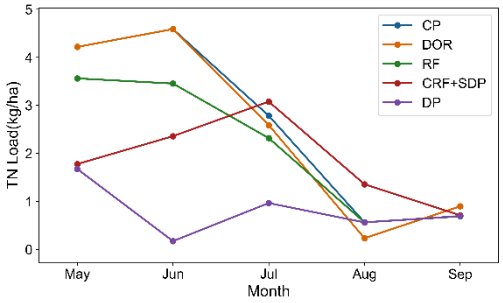

Figure 2. Growing-Season Monthly TN load by BMP scenario.

4. Conclusions

This study utilized the APEX-Paddy model to compare the effectiveness of various BMPs in paddy fields. The analysis revealed that improving fertilization methods, as represented by the DP and CRF+SDP scenarios, was significantly more effective at reducing TN runoff during the farming season than simply adjusting fertilizer application rates. Notably, these method-based BMPs successfully mitigated the peak TN runoff load that typically occurs in the early farming season, leading to a successful reduction in overall nutrient runoff.

Acknowledgements

“ Development of Adaptation Technologies and Vulnerability Assessment of Agricultural Runoff and Irrigation Water Quality under Changing Climate and Cropping Systems” (Project No. 00396736), funded by the National Institute of Agricultural Sciences, Rural Development Administration, Republic of Korea.

References

Campolongo,F.,Cariboni,J.,Saltelli,A.,Schoutens,W.,2005. Enhancing the Morris method. In: Hanson,K.M.,Hemez,F.M.(Eds.), Sensitivity Analysis of Model Output. Los Alamos National Laboratory, pp.369–379.

Choi,S.-K.,2019. APEX-Paddy model development and climate change impact assessment for paddy rice. Ph.D. dissertation, Seoul National University, Seoul, Korea. https://www.riss.kr/link?id=T15113325

Kim,K.,Kang,M.S.,Song,I.,Song,J.-H.,Park,J.,Jun,S.M.,Jang,J.R.,Kim,J.S.,2016. Effects of controlled drainage and slow-release fertilizer on nutrient pollutant loads from paddy fields. J. Korean Soc. Agric. Eng.,58(1),1–10. doi:10.5389/KSAE.2016.58.1.001

Moriasi,D.N.,Gitau,M.W.,Pai,N.,Daggupati,P.,2015. Hydrologic and water quality models: performance measures and evaluation criteria. Trans. ASABE,58(6),1763–1785. doi:10.13031/trans.58.10715.

Yu,C.-H.,Choi,J.-Y.,Kim,W.-K.,Kim,J.-M.,Jeong,J.-W.,2022. Current status and improvement directions of nonpoint source pollution management for agricultural water. Korea Rural Economic Institute.

An Integrated Watershed-Reservoir Modeling Approach for Assessing Hydrodynamics and Sedimentation Patterns in Deji Reservoir, Taiwan

Jemima R. Perodes[1,2] and Cheng-Wei Yu[2*]

[1] Department of Bioenvironmental Systems Engineering, National Taiwan University, Taipei City 106, Taiwan

[2] Central Mindanao University, Maramag, Bukidnon 8714, Philippines

* Corresponding author. Email: cwjyu@ntu.edu.tw

Abstract

Sediment loading from upland watersheds into downstream reservoirs poses a significant challenge for water resources management, as it can reduce storage capacity and deteriorate water quality. In the case of the Deji Reservoir in central Taiwan, this issue is of particular concern. To assess the influence of upland inputs on reservoir water quality, an integrated modeling framework was employed to simulate watershed hydrology, sediment transport processes, and reservoir hydrodynamics. The SWAT model was used to simulate streamflow and sediment load across the watershed while CE-QUAL-W2 was used for reservoir hydrodynamic and water quality modeling.

Results show spatial and temporal variability of sediment transport. In-reservoir deposition was concentrated near the river-reservoir transition zone, particularly during low-flow conditions.

Keywords: SWAT, CE-QUAL-W2, model coupling

1. Introduction

Reservoirs are critical infrastructure for various uses such as water supply, food control, and hydropower. However, sedimentation and hydrodynamic changes can affect their capacity and functionality.

Sediment is supplied primarily by watershed erosion, which is intensified by land use change, deforestation, and extreme rainfall (Walling, 2006). Increased sediment yield reduces storage and modifies hydrodynamic conditions, with implications for operational efficiency and downstream ecology (Kondolf et al., 2014).

Watershed models such as SWAT simulate runoff and sediment yield at the basin scale (Arnold et al., 1998). These models, however, do not resolve in-reservoir processes such as deposition, resuspension, and density-driven transport (Wu et al., 2020). Reservoir models including CE-QUAL-W2 are designed to represent hydrodynamics, stratification, and sediment dynamics, but they require accurate inflow inputs (Cole & Wells, 2008).

Because of these limitations, coupling watershed and reservoir models provides a more complete representation of sediment delivery and fate. Such an approach improves predictions of how land use and climate variability affect reservoir sedimentation (Borah & Bera, 2004).

This study applies a model coupling approach to assess the hydrodynamics and sedimentation in Deji Reservoir, Taichung, Taiwan. The findings of this work will contribute to improving reservoir operations and sediment management strategies.

2. Materials and Methods

2.1 Study area

Deji Reservoir is located in the upper reaches of Dajia River in Heping District, Taichung City, Taiwan. The 600-square-kilometer catchment area is mainly made up of mountainous and forested terrain. The location has a subtropical climate characterized by high humidity and rainfall of around 2500 mm average per year. Meteorological stations and stream gages are distributed within the watershed. Built between 1969 and 1974, the reservoir is impounded by a thin concrete arch dam that stands 180 meters tall, making it the highest dam in Taiwan. Although mainly used for hydroelectric power generation, it also serves for irrigation, flood control, and water supply purposes.

2.2 Watershed modeling using SWAT

The upstream watershed was modeled using the physically based modeling tool SWAT. Watershed delineation was carried out using a 20-m resolution digital elevation model to define watershed boundaries, sub-basins, river reaches, and flow paths. Daily meteorological inputs from 2012 to 2021 (i.e., precipitation, relative humidity, wind speed, solar radiation, and minimum and maximum temperatures) were incorporated into the model. Model performance was evaluated using the coefficient of determination (R^2), Nash–Sutcliffe efficiency (NSE), and percent bias (PBIAS).

2.3 Watershed-reservoir integration

Uni-directional external coupling was performed to integrate the two systems. Streamflow rate, water temperature, and sediment load from SWAT were inputted into CE-QUAL-W2.

2.4 Reservoir modeling using CE-QUAL-W2

CE-QUAL-W2, a laterally averaged hydrodynamic and water quality model, was employed to simulate reservoir processes. A high-resolution bathymetric dataset (1 m) was used to discretize the reservoir into longitudinal segments of 200 m and vertical layers of 1 m. Hydrodynamic simulations with variable time steps were forced using time-series inputs of inflow and outflow, along with meteorological variables including air temperature, wind speed, solar radiation, dew point temperature, and cloud cover.

3. Results and Discussion

3.1 Performance of the models

The watershed model performance during both calibration and validation was generally satisfactory based on the NSE, R^2, and PBIAS criteria, consistent with standards recommended for SWAT modeling studies (Moriasi et al., 2007; Arnold et al., 2012).

For streamflow, NSE values ranged from 0.72 to 0.75 during calibration and 0.68 to 0.78 during validation. R^2 ranged from 0.72 to 0.73 during calibration and slightly

decreased to 0.60 to 0.68 during validation. PBIAS values during calibration were low (3.6% to 3.9%), which indicates a slight tendency toward overestimation.

Table 1. Performance of the watershed model

Variable	Station	NSE	R^2	PBIAS
Streamflow (cms)	Calibration			
	SB-10	0.72	0.72	3.9
	SB-12	0.68	0.78	-14.9
	Validation			
	SB-10	0.73	0.75	3.6
	SB-12	0.60	0.61	3.6
Sediment load (tons/d)	Calibration			
	SB-10	0.59	0.60	-8.8
	SB-12	0.54	0.62	-21.6
	Validation			
	SB-10	0.59	0.64	9.3
	SB-12	0.53	0.53	5.5

3.2 Watershed processes

The rainfall patterns across the simulation period were highly variable, with distinct high-intensity events corresponding to peaks in streamflow. The model captured the timing and magnitude of most streamflow events with reasonable accuracy (Table 1), with NSE values of 0.72–0.75 during calibration and 0.68–0.78 during validation. Sediment load simulations showed weaker but acceptable performance, with NSE values of 0.53–0.59 and R^2 values of 0.53–0.64, consistent with the known difficulty of modeling sediment yield. Overall, the watershed model satisfactorily reproduced the hydrologic and sediment responses needed as input to the reservoir model.

Figure 1 shows the simulated streamflow and suspended sediment concentration at the watershed outlet. The hydrograph shows seasonal variability, while the sediment series reflects event-driven peaks and lower background levels during baseflow conditions.

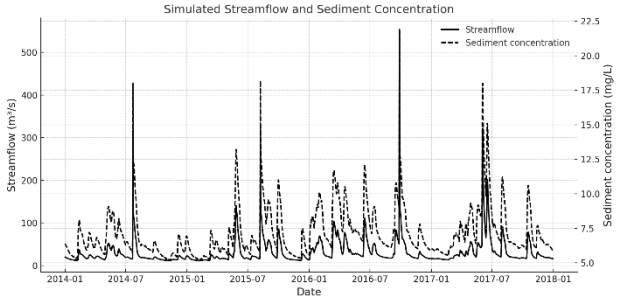

Figure 1. Simulated streamflow and sediment concentration

3.3 In-reservoir dynamics

Water balance was maintained by adjusting bathymetric parameters until simulated water surface elevations matched observations, with good agreement between observed and simulated fluctuations. The maximum reservoir level was capped at 1408 m a.s.l., with excess inflows released as spill. The model reproduced seasonal stratification patterns, with a summer thermocline forming between 22 and 28 m depth and temperatures ranging from ~25 °C at the surface to ~15 °C at the bottom, while winter months were nearly isothermal (15–18 °C). Simulated suspended sediment concentrations tracked observed values which reproduced peaks during high inflow events, although underestimated, and lower concentrations during baseflow periods. These results indicate that the model can represent the essential hydrodynamic and sediment dynamics of the reservoir.

3.4 Future directions

As an extension of this study, the scope will be expanded to include nutrient transport within the watershed and nutrient dynamics in the reservoir. Furthermore, the potential impacts of climate change, land use change, and management practices on the watershed–reservoir system will be evaluated.

4. Conclusions

This study demonstrated the use of an integrated SWAT–CE-QUAL-W2 framework to evaluate watershed processes and in-reservoir dynamics in Deji Reservoir. The watershed model reproduced streamflow with satisfactory accuracy and provided spatially and temporally variable sediment inputs. The reservoir model captured water balance, thermal stratification, and suspended sediment concentration dynamics. Together, the coupled models provide a reasonable representation of the delivery and fate of sediment in the watershed–reservoir system which can be a tool to support sediment management and operational planning for multipurpose reservoirs.

Acknowledgements

The authors would like to acknowledge the financial support and assistance provided by the Deji Reservoir Watershed Management Committee.

References

Arnold, J. G., Srinivasan, R., Muttiah, R. S., & Williams, J. R. (1998). Large area hydrologic modeling and assessment, part I: Model development. *Journal of the American Water Resources Association, 34*(1), 73–89.

Arnold, J. G., Moriasi, D. N., Gassman, P. W., Abbaspour, K. C., White, M. J., Srinivasan, R., ... & van Griensven, A. (2012). SWAT: Model use, calibration, and validation. *Transactions of the ASABE*, 55(4), 1491–1508.

Borah, D. K., & Bera, M. (2004). Watershed-scale hydrologic and nonpoint-source pollution models: Review of applications. *Transactions of the ASAE, 47*(3), 789–803. https://doi.org/10.13031/2013.16110

Cole, T. M., & Wells, S. A. (2008). *CE-QUAL-W2—A two-dimensional, laterally averaged, hydrodynamic and water-quality model, Version 3.6 (Instruction Report EL-08-1).* U.S. Army Engineer Research and Development Center.

Kondolf, G. M., Gao, Y., Annandale, G. W., Morris, G. L., Jiang, E., Zhang, J., *et al.* (2014). Sustainable sediment management in reservoirs and regulated rivers: Experiences from five continents. *Earth's Future, 2*(5), 256–280.

Moriasi, D. N., Arnold, J. G., Van Liew, M. W., Bingner, R. L., Harmel, R. D., & Veith, T. L. (2007). Model evaluation guidelines for systematic quantification of accuracy in watershed simulations. *Transactions of the ASABE*, 50(3), 885–900.

Walling, D. E. (2006). Human impact on land–ocean sediment transfer by the world's rivers. *Geomorphology, 79*(3–4), 192–216.

Wu, X., Bi, N., Syvitski, J. P. M., Saito, Y., Xu, J., Nittrouer, J. A., Bianchi, T. S., Yang, Z., & Wang, H. (2020). Can reservoir regulation along the Yellow River be a sustainable way to save a sinking delta? *Earth's Future, 8*(12), e2020EF001587.

Refinement of a Total Nitrogen Dynamics Model by Introducing High Temporal Resolution in the Imbanuma Cyclic Irrigation Area

Iwasaki Shunya・Iida Toshiaki

Abstract

At Imbanuma lake in eastern Japan, the cyclic irrigation system adopted since 2010 has been expected to reduce the effluent nutrient load from the surrounding agricultural land to the lake. It has been pointed out that the effectiveness of nutrient runoff suppression could be improved by more efficient operation of pumping stations in the cyclic irrigation system. In order to explore the optimal pump operation, Tamagawa et al. (2022) developed a hydrological water quality model based on a tank model. However, as the model calculation was performed daily, it was unable to incorporate realistic operations such as irrigation operations by farmers or frequent pump operations. In the present study, based on Tamagawa et al. (2022), a hydrological water quality model which simulates the nitrogen movement in the watershed with the calculation interval of one hour was developed. The nitrogen process modules in the model handling denitrification, crop nitrogen uptake, and soil nitrogen accumulation were reorganized in accordance with the hourly calculation interval.

The development of this model contributes to establishing a simulation foundation for implementing adaptive and effective pump operation strategies aimed at reducing nutrient runoff in the target region. This presentation describes the structural modifications made to the nitrogen model and discusses how these changes influence simulation behavior. The refined framework is expected to support more responsive and precise analysis of the cyclic irrigation system in paddy field regions.

Dynamics of water and nutrient flow in a cyclic irrigation scheme for paddy fields in Imbanuma irrigation area, Chiba Prefecture, Japan

Ilham Putra Adiyaksa [1], Fumi Okura [2], Tasuku Kato [1*]

[1] United Graduate School of Agricultural Science, Tokyo University of Agriculture and Technology, 3-5-8 Saiwaicho, Fuchu, Tokyo 183-8509, Japan

[2] Japan International Research Center for Agricultural Sciences, 1-1 Ohwashi, Tsukuba, Ibaraki 305-8686, Japan

* Corresponding author. Email: taskkato@go.tuat.ac.jp

Abstract

Cyclic irrigation systems are implemented in paddy cultivation to enhance water use efficiency and minimize nutrient pollution. This study examines water and nutrient dynamics in the Imbanuma irrigation area, Chiba Prefecture, Japan, over a two-year period (2022–2023), with a focus on two paddy field blocks. Total nitrogen (T-N) and total phosphorus (T-P) were monitored biweekly and monthly to assess nutrient flows under a dual-subsystem framework.

In 2022, low rainfall (410 mm during the planting period) led to the highest proportional water intake from Imbanuma Lake and minimal discharge. In contrast, 2023 saw higher rainfall (554 mm during the planting period) and increased discharge volumes, resulting in a negative water balance. Nutrient input from the lake increased due to elevated T-N concentrations, but higher discharge in 2023 led to lower T-N and T-P retention in the system compared to 2022. Nutrient losses from the first subsystem of paddy fields, up to 7.8% for T-N and 2.0% for T-P, suggesting strong nutrient retention within the paddy fields.

These results highlight the critical role of flow dynamics in nutrient accumulation, providing insights for managing water quality in recycled irrigation systems.

Keywords: cyclic irrigation, irrigation water quality, water and mass balance

1. Introduction

Cyclic irrigation systems are implemented in paddy field regions to enhance water use efficiency and reduce water consumption by recycling drainage water. In Japan, this method has been adopted in some different regions (Feng et al., 2004; Hama et al., 2011; Takeda & Fukushima, 2006) to support sustainable rice cultivation and mitigate non-point source pollution, which contributes to eutrophication in downstream water bodies, in particular Imbanuma Lake, as one of the most polluted lakes in Japan (Tsutsui, 2020). However, concerns remain regarding the accumulation of nutrients, such as nitrogen (N) and phosphorus (P), within the system, particularly due to the repeated reuse of water. Regular monitoring of nutrients and evaluating the impact of hydrological processes on nutrient accumulation is essential.

This study investigates the dynamics of water and nutrient flows in a cyclic irrigation system for paddy fields located in the Imbanuma irrigation area, Chiba Prefecture, Japan. Through monthly and biweekly monitoring, we aim to quantify the hydrological processes in transporting water and nutrients across the system and assess their implications for water quality sustainability.

2. Materials and Methods

The study was conducted in 2022-2023 in the Imbanuma irrigation area, Chiba Prefecture, covering the Shiroyama and Jinbee paddy field blocks. Total nitrogen (T-N) and total phosphorus (T-P) concentrations were measured biweekly during the planting period (April–August) and monthly during the non-planting period.

2.1. Water Balance Analysis

Water balance analysis was conducted following the procedure described by Okura et al. (2025). The water balance for the entire system was calculated using Equation 1.

$$\Delta WB = W - O + \mathrm{R} - ET_c - IR_{ncb_all} \quad (1)$$

where ΔWB is the change of water storage, W is the water supplied from Imbanuma Lake, O is the amount of discharge water back to Imbanuma Lake, R is rainfall, ET_c is crop evapotranspiration, and IR_{ncb_all} is irrigation water supplied to non-cyclic blocks. The unit of each parameter is in $m^3\ h^{-1}$.

2.2. Mass Balance Analysis

The masses of T-N and T-P were calculated by multiplying the nutrient concentrations by the corresponding water volumes and then dividing by the total area of 523.9 ha. The mass balance for the entire system was calculated using Equation 2.

$$\Delta MB = M_W - M_O + M_R - M_{IR_ncb_all} \quad (2)$$

where ΔMB is the remaining nutrient of T-N and T-P, M_W is the nutrient mass from Imbanuma Lake, M_O is the nutrient mass discharged back to Imbanuma Lake, M_R is nutrient mass supplied from rainfall, $M_{IR_ncb_all}$ is nutrient mass loss to the non-cyclic blocks. The unit of each parameter is in $kg\ ha^{-1}$.

3. Results and Discussion

Rainfall in 2022 was notably low compared to previous years, with a total of only 410 mm during the planting period, while it increased slightly to 554 mm in 2023. ETc was recorded at 600 mm in 2022 and 688 mm in 2023, respectively.

3.1. Water Balance Analysis

Due to the low rainfall in 2022 during the planting period, the proportion of water intake from Imbanuma Lake was the highest. However, in terms of total volume, more water was drawn from the lake in 2023. In 2022, the low rainfall resulted in the lowest discharge volume returning to Imbanuma Lake. In contrast, in 2023, the combination of increased water intake from the lake and moderate rainfall led to a higher discharge back to the lake (Table 1). As a result, the water balance in 2023 was negative, indicating that total outflows exceeded inflows.

Table 1. Water Balance in 2022 and 2023.

Unit: 1000 m^3		**2022**	**2023**
Inflow	*W*	7,955	9,178
	R	2,148	2,901
	Subtotal	10,103	12,079
Outflow	*O*	835	3,237
	ET	3,145	3,603
	IR_ncb	5,312	5,407
	Subtotal	9,291	12,247
ΔWB	Inflow-Outflow	812	-168

3.2. Mass Balance Analysis

There was an increase in T-N concentration in the waters of Shiroyama, Jinbee, and Imbanuma Lake, which contributed to a higher nutrient input from Imbanuma Lake in 2023 (Table 2). However, in the same year, a significant discharge back to Imbanuma Lake also led to increased nutrient outflow. As a result, the T-N mass balance in 2023 was lower than in 2022.

A similar trend was observed for the T-P mass balance. Although T-P concentrations in Imbanuma Lake did not change significantly between 2022 and 2023, the higher outflow in 2023 resulted in a lower remaining T-P mass within the system (Table 3).

Table 2. Mass Balance of T-N in 2022 and 2023.

Unit: kg. ha^{-1}	**2022**	**2023**
M_W	15.72	23.85
M_R	2.03	2.74
M_O	1.59	8.24
$M_{IR_ncb_all}$	11.34	15.83
ΔMB	4.81	2.52

Table 3. Mass Balance of T-P in 2022 and 2023.

Unit: kg. ha^{-1}	**2022**	**2023**
M_W	1.09	1.36
M_R	0.37	0.50
M_O	0.15	0.59
$M_{IR_ncb_all}$	0.79	0.93
ΔMB	0.52	0.33

Based on the monthly analysis, most nutrients appear to be utilized or retained within the paddy fields, as also reported in previous studies (Gu & Yang, 2022; Neitsch et al., 2011). Consequently, nutrient losses from the paddy fields are relatively small, with values of up to 7.8% for T-N and 2.0% for T-P.

4. Conclusions

This study highlights the importance of understanding water and nutrient flow dynamics in cyclic irrigation systems for paddy fields. The dual-year analysis in the Imbanuma irrigation area revealed that rainfall variability and intake volume from Imbanuma Lake significantly influenced both water balance and nutrient transport. In 2022, low rainfall led to a greater reliance on lake water and minimal discharge, resulting in relatively higher nutrient retention. In contrast, 2023 experienced greater nutrient input due to increased concentrations in lake water, but also higher outflow, resulting in lower net nutrient accumulation within the system.

Despite variability in hydrological conditions, nutrient losses from the paddy fields remained consistently low, indicating that most nutrients were retained or utilized within the system. This confirms the buffering capacity of flooded rice fields and supports the sustainability of cyclic irrigation when managed appropriately.

The findings suggest that monitoring nutrients and applying mass balance approaches can support informed decisions regarding irrigation management. Future research should explore EC flux losses via percolation to provide a more comprehensive assessment of environmental impacts. This study contributes to the development of climate-smart, water-efficient agricultural systems in regions practicing water reuse.

References

Feng, Y. W., Yoshinaga, I., Shiratani, E., Hitomi, T., & Hasebe, H. (2004). Characteristics and behavior of nutrients in a paddy field area equipped with a recycling irrigation system. *Agricultural Water Management*, *68*(1), 47–60. https://doi.org/10.1016/j.agwat.2004.02.012

Gu, J., & Yang, J. (2022). Nitrogen (N) transformation in paddy rice field: Its effect on N uptake and relation to improved N management. *Crop and Environment*, *1*(1), 7–14. https://doi.org/10.1016/j.crope.2022.03.003

Hama, T., Nakamura, K., Kawashima, S., Kaneki, R., & Mitsuno, T. (2011). Effects of cyclic irrigation on water and nitrogen mass balances in a paddy field. *Ecological Engineering*, *37*(10), 1563–1566. https://doi.org/10.1016/j.ecoleng.2011.03.032

Neitsch, S. L., Arnold, J. G., Kiniry, J. R., & Williams, J. R. (2011). *Soil and Water Assessment Tool Theoretical Documentation Version 2009*. Texas Water Resources Institute.

Okura, F., Kamei, A., & Kato, T. (2025). Water balance analysis of hydrological processes in cyclic irrigation: A case study of the Imbanuma irrigation area in Chiba, Japan. *Journal of Hydrology: Regional Studies*, *57*, 102111. https://doi.org/10.1016/j.ejrh.2024.102111

Takeda, I., & Fukushima, A. (2006). Long-term changes in pollutant load outflows and purification function in a paddy field watershed using a circular irrigation system. *Water Research*, *40*(3), 569–578. https://doi.org/10.1016/j.watres.2005.08.034

Tsutsui, S. (2020). *Water Environment Administrations of Lakes in Japan*. Ministry of Environment, Japan. https://www.ilec.or.jp/wp-content/uploads/2efb9012c80131b2d19aad6f1e20c947.pdf

Quantifying Soil Moisture Drydown Patterns Using Satellite Observations for Droughts Early Warning

Daichi Sasamoto [1*], Kumiko Tsujimoto [1], Tetsu Ohta[2]

[1] Graduate School of Environmental, Life, Science and Technology, Okayama University, Okayama, 700-8530, Japan

[2] U-PRIMO, Okayama, 700-0016, Japan

* Corresponding author. Email: ps6l2a3r@s.okayama-u.ac.jp

Abstract

Drought early warning is critical for mitigating agricultural and ecological impacts, but timely detection remains challenging. Satellite-based soil moisture observations offer a unique opportunity to monitor land surface hydrological processes with high spatial and temporal coverage, particularly in regions where direct field measurement data are limited. In this study, we followed the method of (Sehgal et al, 2021) and attempted a similar approach to estimate drydown patterns and soil moisture retention properties at each grid from satellite data. We can use the properties for developing an early drought detection system. One difference from the original study is that the original study used SMAP soil moisture data provided by NASA, but we tried to use AMSR-2 data from JAXA and SMOS data from ESA. SMAP, AMSR-2 and SMOS are satellite missions developed by different agencies to provide global soil moisture data. We initially attempted to use AMSR-2 data. However, it showed dry bias and limited accuracy, so we switched to using SMOS data which is more accurate data. In the future, we aim to further improve the reliability of this study through the integrated use of SMAP, AMSR and SMOS. In the previous year, we also worked on a drought detection method based on the self-calibrating Palmer Drought Severity Index (Wells et al, 2004) using meteorological data. Our final goal is to develop a more accurate global drought detection system through the integrated evaluation of these methods.

Keywords: flash drought, remote sensing data, AMSR, SMOS

1. Introduction

Drought is a meteorological disaster caused by reduced precipitation and rising temperatures, leading to agricultural losses and wildfires. In recent years, the damage caused by rapidly intensifying droughts, known as “flash droughts,” triggered by precipitation deficits and anomalously high temperatures, has become increasingly severe. [1] In this study, we utilized both satellite-based soil moisture observations and in-situ soil moisture data to estimate “Soil Water Retention Parameters” (SWRPeff), following the methodology of previous research (Sehgal et al. 2021a). Using these parameters, we calculated the “Flash Drought Severity Index” (FDSI) (Sehgal et al. 2021b), an index for detecting the occurrence of flash droughts, and carried out its evaluation and analysis.

2. Materials and Methods

2.1. Data set

We used soil moisture data observed by the Advanced Microwave Scanning Radiometer (AMSR) and the Soil Moisture and Ocean Salinity (SMOS) satellite. AMSR, developed by the Japan Aerospace Exploration Agency (JAXA), is a microwave radiometer-based mission for monitoring the water cycle. [2] SMOS, developed by the European Space Agency (ESA), is designed to observe soil moisture and ocean salinity using microwave instruments.[3]

For direct soil moisture measurements, we used data from the International Soil Moisture Network (ISMN), which provides a globally coordinated database of in-situ soil moisture observations.[4]

The data used in this study cover the period from January 1, 2015, to December 31, 2021. The analysis targeted multiple global sites, including the United States and Australia, where flash drought events have been reported.

2.2. Methodology

As shown in Figure 1, the soil moisture drydown process was divided into four phases according to the amount of soil moisture: (1) Gravity drainage, (2) Wet, (3) Transitional, and (4) Dry. The boundary between phases 1 and 2 defines field capacity(θ_{GW}), between phases 2 and 3 defines the critical point(θ_{WT}), and between phases 3 and 4 defines the wilting point(θ_{TD}). This definition is based on the previous study (Laio et al. 2001). This framework represents the soil moisture drydown curve.

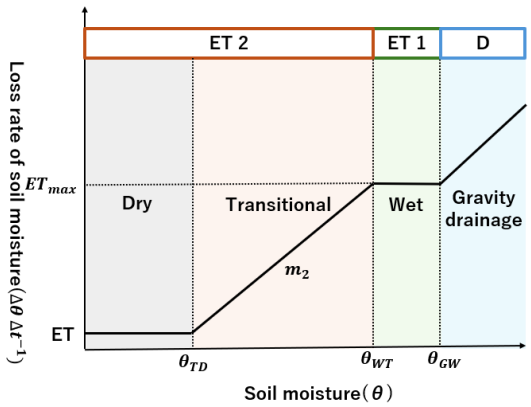

Figure 1. Soil moisture loss function

The soil moisture loss, expressed by Equation (1), was derived from the soil moisture data.

$$\Delta\theta/\Delta t = -(\theta_t - \theta_{t-1}) \qquad (1)$$

A nonlinear least squares method was then applied to construct the drydown curve and estimate θ_{GW}, θ_{WT} and θ_{TD}.

Subsequently, we calculated FDSI, which is composed of two indicators: Soil Moisture Stress (SMS) and the Relative Rate of Drydown (RRD). At time t, $FDSI_t$ is determined from SMS_t and RRD_t, which are calculated using data from the preceding 30 days (from t-30 to t). FDSI takes values between 0 and 1, where larger values indicate more severe drought conditions. FDSI values ≥ 0.71 indicate the occurrence of flash drought.

3. Results and Discussion

As a case study, we present results for Montana, USA, where severe flash drought damage was reported around May 2017 (Otkin et al. 2024).

3.1. SWRPeff

Table 1 shows the estimated values of SWRPeff. These values were compared against those derived from the Harmonized World Soil Database (HWSD) [5]. Although the estimates obtained from AMSR, SMOS, and ISMN showed similar trends, the values derived from soil moisture data were generally smaller than those from HWSD. In particular, the values of θ_{TD} were notably underestimated.

Table 1. Estimated SWRPeff

	θ_{GW} $(m^3\ m^{-3})$	θ_{WT} $(m^3\ m^{-3})$	θ_{TD} $(m^3\ m^{-3})$
AMSR	0.243	0.190	0.030
SMOS	0.219	0.149	0.018
ISMN	0.302	0.194	0.080
HWSD	0.349	-	0.202

3.2. FDSI

Figure 2 presents the time series of FDSI in Montana, USA, from 2015 to 2019, where severe flash drought impacts were reported around May 2017 (Otkin, 2024). The FDSI calculated using AMSR data consistently showed high values, while those calculated from SMOS and ISMN data showed similar trends. In 2017, both SMOS and ISMN results indicated a sharp increase in FDSI values beginning in late May, exceeding 0.71 during August and September, effectively capturing the reported flash drought event. However, false detections (values ≥ 0.71 during non-drought periods) were also observed, indicating the need for further improvements in detection accuracy.

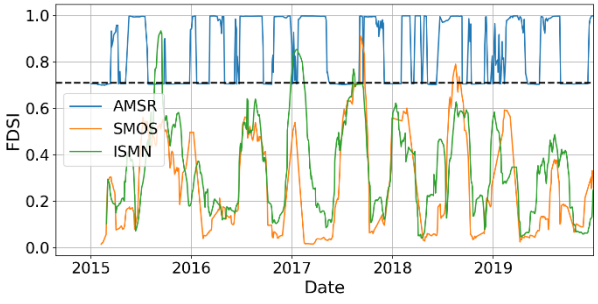

Figure 2. Time series of the FDSI

3.3. Discussion

This study successfully estimated SWRPeff and calculated FDSI using satellite-based soil moisture data. Previous attempts that combined HWSD-based estimates of SWRPeff with satellite soil moisture data failed to capture FDSI appropriately, as the HWSD values did not reflect the satellite-specific characteristics. By estimating SWRPeff directly from each dataset, we were able to calculate FDSI effectively for SMOS and ISMN data. However, the AMSR-based results were less reliable, likely due to strong dry bias, as indicated by abnormally high SMS values. This suggests that bias correction must be prioritized when using data with known systematic errors.

4. Conclusions

In this study, we estimated SWRPeff and calculated FDSI using soil moisture data. Although the accuracy of results varied depending on the dataset used, this approach enabled the detection of flash droughts without relying on other meteorological data. These findings highlight the extended utility of soil moisture data in global drought monitoring.

Acknowledgements

The authors gratefully acknowledge the financial support provided by the Kinoshita Memorial Foundation for Academic Research Activities, the Japan Aerospace Exploration Agency (JAXA) under the Earth Observation Research Program (25RT000181), and the “Initiative for Realizing Diversity in the Research Environment” from the Ministry of Education, Culture, Sports, Science and Technology (MEXT), Japan.

References

F.Laio, A. P., L.Ridolfi, I.Rodriguez-Iturbe. (2001). Plants in water-controlled ecosystems: active role in hydrologic processes and response to water stress II. Probabilistic soil moisture dynamics. Advances in Water Resource, 24, 707-723.

Otkin, J. A., Zhong, Y., Ford, T. W., Anderson, M. C., Hain, C., Hoell, A., Svoboda, M., & Wang, H. (2024). Multivariate Evaluation of Flash Drought Across the United States. Water Resources Research, 60(11). https://doi.org/10.1029/2024wr037333

Sehgal, V., Gaur, N., & Mohanty, B. P. (2021a). Global Surface Soil Moisture Drydown Patterns. Water Resources Research, 57(1). https://doi.org/10.1029/2020wr027588

Sehgal, V., Gaur, N., & Mohanty, B. P. (2021b). Global Flash Drought Monitoring Using Surface Soil Moisture. Water Resources Research, 57(9). https://doi.org/10.1029/2021wr029901

[1] National Integrated Drought Information System (NIDIS), 2025. What is drought, Flash Drought. https://www.drought.gov/what-is-drought/flash-drought Accessed September 2, 2025.

[2] Japan Aerospace Exploration Agency (JAXA), 2025. AMSR Learning Site. https://www.eorc.jaxa.jp/AMSR/learning/index_ja.html Accessed September 3, 2025.

[3] European Space Agency (ESA), 2025. SMOS Mission Overview. https://earth.esa.int/eogateway/missions/smos Accessed September 3, 2025.

[4] International Soil Moisture Network (ISMN), 2025. About ISMN. https://ismn.earth/en/ Accessed September 8, 2025.

[5] Food and Agriculture Organization of the United Nations (FAO), 2025. Harmonized World Soil Database v1.2. https://www.fao.org/soils-portal/data-hub/soil-maps-and-databases/harmonized-world-soil-database-v12/en/ Accessed September 8, 2025.

Characterization of Flash Droughts on the Korean Peninsula Using Satellite-Derived Soil Moisture

Hee-Jin Lee [1], Won-Ho Nam [2*]

[1] Ph.D Student, Department Integrated System Engineering, Hankyong National University, Anseong, Republic of Korea

[2] Professor, School of Social Safety and Systems Engineering, National Agricultural Water Research Center, Hankyong National University, Anseong, Republic of Korea

* Corresponding author. Email: wonho.nam@hknu.ac.kr

Abstract

Flash droughts are rapid-onset events that can severely Flash droughts are rapid-onset events that can severely impact agriculture and water resources, particularly under increasing climate variability. This study assessed flash drought characteristics across the Korean Peninsula using the Flash Drought Intensity Index (FDII), focusing on frequency, duration, and intensity. Results highlighted PA, GW_N, and GW_S as recurrent high-risk regions, with cropland and forest areas showing pronounced sensitivity to rapid soil moisture depletion. In contrast, urban areas exhibited disproportionately high values that are likely overestimated due to surface heterogeneity. A comparison with the evapotranspiration-based Evaporative Stress Percentile (ESP) revealed strong temporal correspondence, with both indices frequently detecting flash drought events simultaneously. Contrary to the expectation that evapotranspiration-based indicators enable earlier detection, FDII identified events at comparable timings, demonstrating its diagnostic capability. AMSR2-based FDII provided higher precision, while SMAP-based FDII showed higher recall and broader coverage, albeit with signs of over-detection. These findings underscore the practical value of soil moisture–based indices in capturing flash drought dynamics and suggest that integrating FDII with evapotranspiration-based indicators can enhance monitoring accuracy, strengthen early warning systems, and support drought risk management across vulnerable regions of the Korean Peninsula.

Keywords: Flash drought, The Korean Peninsula, Flash Drought Intensity Index (FDII), Soil moisture

1. Introduction

Flash droughts are defined as rapid-onset events triggered by abrupt shifts in weather and environmental variables associated with climate anomalies. Soil moisture is widely recognized as one of the most reliable variables for flash drought detection and early warning systems. This study conducts a comprehensive assessment of flash drought characteristics and detection performance across the Korean Peninsula, focusing on their frequency, duration, and intensity based on satellite-derived soil moisture data. In addition, it evaluates spatial variations by quantifying flash drought intensity across land cover types and examines the feasibility of soil moisture–based monitoring through comparison with an evapotranspiration-based drought index.

2. Materials and Methods

This was conducted in four steps: (1) collecting land cover and satellite imagery data for the Korean Peninsula; (2) calculating flash drought index using satellite-derived soil moisture; (3) analyzing flash drought characteristics across regions and land cover types; and (4) computing an evapotranspiration-based index for comparison.

2.1. Data collection

Satellite-based soil moisture datasets were derived from the Advanced Microwave Scanning Radiometer-2 (AMSR2) and the Soil Moisture Active Passive (SMAP) missions. For comparison and analysis of flash droughts, a 4-week composite Evaporative Stress Index (ESI) provided by SERVIR was utilized.

2.2. Flash Drought Intensity Index (FDII)

The FDII is a metric that quantifies flash drought intensity using two key components: the rate of intensification (FD_INT) and the average drought severity (DRO_SEV). It evaluates flash droughts by jointly considering the magnitude of the rapid decline in soil moisture and the duration required for recovery above a predefined threshold. This approach has since been adapted for multivariate drought monitoring frameworks that incorporate multiple drought indicators. (Otkin et al., 2024).

2.3. Evaporative Stress Percentile (ESP)

The ESP was calculated across the Korean Peninsula using historical ESI-4wk records. Based on the percentile classification defined by the U.S. Drought Monitor (USDM), flash drought occurrences were identified according to the ESP criteria proposed by Li et al. (2024).

3. Results and Discussion

3.1. Flash drought frequency and duration maps

FD_INT captures the rapid decline in soil moisture, indicating flash drought onset, while DRO_SEV quantifies duration based on periods below the 20th-percentile threshold. Using these metrics, flash drought frequency (FDF) and duration (FDD) were derived from AMSR2 and SMAP (Fig. 1).

AMSR2-based FDF was higher in PA, HH, GW_N, GW_S, and GS, whereas SMAP-based FDF showed elevated values across North Korea and in GG and GW_S. Both consistently highlighted PA, GW_N, and GW_S as high-frequency regions.

FDD, expressed in weeks, revealed longer drought durations in GW_S for both datasets, with AMSR2 showing higher values in GW_S, GS, and CC, and SMAP in HG and HH. Anomalous values occurred in coastal boundaries, reflecting uncertainties in soil moisture retrievals near water bodies due to salinity and seawater intrusion.

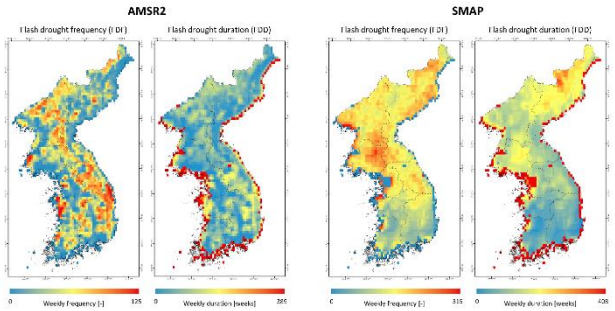

Figure 1. Flash drought frequency and duration from 2017 to 2024.

3.2. Characteristics by land cover type

flash drought frequency (FDF) and intensity per unit area were calculated for each land cover type (Fig. 2). SMAP-based FDII indicated relatively high intensities, with AMSR2 and SMAP showing consistent spatial patterns. Urban areas, though limited in extent, showed disproportionately high FDF and intensity—especially in HG, PA, GW_N, and GW_S—but these values may be overestimated due to impervious surfaces and small area representation. Excluding urban regions, cropland in HG and GW_S exhibited high FDF, while PA and GW_N showed higher intensity relative to frequency. In HH, forests had the highest FDF and intensity, with AMSR2 and SMAP showing notably different magnitudes.

Overall, HG, HH, PA, GW_S, and GW_N consistently displayed high flash drought intensity per unit area across all land cover types.

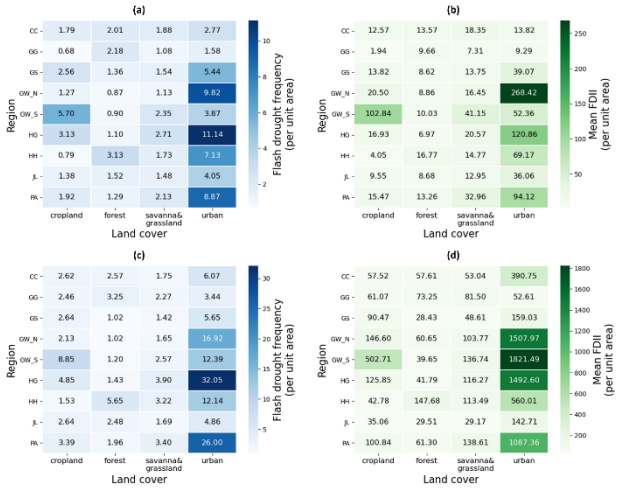

Figure 2. Flash drought frequency and intensity per unit area by land cover type

3.3. Comparison of flash drought detection

Time-lag analysis (Fig. 3) was performed to assess the detection capability of FDII relative to ESP. Most regions showed lag values clustered near zero, indicating strong temporal correspondence, with zero-lag events occurring most frequently. Contrary to the expectation that ESI detects flash droughts earlier, FDII detected events at timings comparable to evapotranspiration-based indices. Precision, recall, and F1-scores were calculated at lag = 0, showing that AMSR2-based FDII achieved higher precision (conservative but reliable), while SMAP-based FDII had higher recall and broader coverage, likely due to over-detection. Although F1-scores ranged from 0.35 to 0.65, the consistency across indices supports their complementary use in capturing flash drought dynamics.

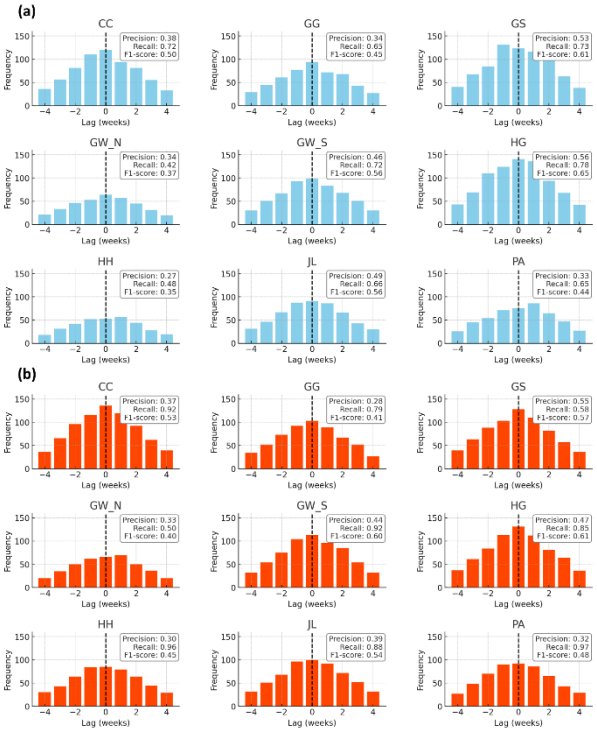

Figure 3. Time-lag analysis of flash drought events between FDII and ESP

4. Conclusions

This study quantified flash drought characteristics across the Korean Peninsula using satellite-derived soil moisture and compared results with an evapotranspiration-based index. FDII effectively captured the frequency, duration, and intensity of flash droughts, consistently identifying high-risk regions such as PA, GW_N, and GW_S. Land cover analysis revealed strong sensitivity in cropland and forest areas, while urban results were likely overestimated due to surface heterogeneity. Time-lag analysis demonstrated that FDII detected events at timings comparable to ESP, with complementary strengths between AMSR2- and SMAP-based datasets. These findings highlight the value of soil moisture–based indices for operational drought monitoring and their potential integration into multi-indicator frameworks for improved early warning.

Acknowledgements

This work was supported by Korea Environment Industry & Technology Institute (KEITI) through Water Management Program for Drought Project, funded by Korea Ministry of Environment (MOE) (RS-2023-00230286).

References

Li, P., Jia, L., Lu, J, Jiang, M., and Zheng, C., 2024. A new evapotranspiration-based drought index for flash drought identification and monitoring. Remote Sens., 16(5), 780.

Otkin, J. A., Zhong, Y., Ford, T.W., Anderson, M.C., Hain, C., Hoell, A., Svoboda, M., and Wang, H., 2024. Multivariate evaluation of flash drought across the United States. Water Resour. Res., 60(11), e2024WR037333.

Meteorological Drought Thresholds in Cambodia Using the Standardized Precipitation Index

Ol Kimsor [1*], Junichiro Takeuchi [1], Chung Sarit [1], Masayuki Fujihara [1]

[1] Graduate School of Agriculture, Kyoto University, Kyoto, Japan

* Corresponding author. Email: kimsor.ol168@gmail.com

Abstract

This study investigates meteorological drought thresholds in Cambodia using the Standardized Precipitation Index (SPI), with the goal of strengthening drought monitoring and supporting agricultural resilience. Although Cambodia is highly vulnerable to drought, particularly in rainfed farming systems, most previous studies have placed greater emphasis on floods. In this research, 22 years of rainfall data (2001–2022) from 21 stations, derived from NASA's IMERG satellite product, were used to calculate SPI at 1-month and 3-month timescales. The 1-month SPI was applied to identify short-term drought thresholds, while the 3-month SPI was used to validate historical drought events. The results indicate that mild to moderate droughts occur frequently, whereas extreme events are relatively rare. Monthly drought thresholds were also developed for stations including Banteay Meanchey and others, capturing seasonal rainfall patterns and basin-specific vulnerabilities. Alongside rainfall analysis, rice yield trends were examined, highlighting a strong link with fertilizer use. Despite the occurrence of droughts, rice yields have continued to rise, suggesting that improved agricultural practices and inputs may help buffer against drought impacts. Overall, this study provides a scientific basis for defining drought conditions and informing water resource management. By establishing location-specific thresholds, it offers practical guidance for stakeholders to support sustainable agriculture.

Keywords: rainfall, agriculture, paddy yield, fertilizer

1. Introduction

Drought is one of the major environmental issues in Cambodia, causing considerable economic damage, especially in agriculture. Since a large share of the population depends on farming, long dry periods can strongly affect people's livelihoods. Rice production, which needs a high amount of water, is particularly at risk because many farmers rely only on rainfall for irrigation. In some areas, traditional farming methods also make crops more vulnerable to failure during droughts. With this strong dependence on rainfall, it is important to study precipitation patterns to improve drought monitoring and preparedness. This research focuses on defining rainfall thresholds that reflect drought severity in order to strengthen mitigation measures.

2. Materials and Methods

2.1. Study area

Cambodia, located in southern Mainland Southeast Asia, borders Thailand, Laos, Vietnam, and the Gulf of Thailand. It lies between 10°-15°N latitude and 102°-108°E longitude, covering a total area of 181,035 km² (Figure 1). The country has a tropical monsoon climate with two seasons: a dry season (November-April) and a wet season (May-October). Annual rainfall ranges from 1,200 mm to 2,000 mm, with coastal areas receiving up to 3,000 mm (Phy et al., 2022). The average temperature is 28°C, peaking at 38°C in April and dropping to 17°C in January (Thoeun, 2015). Cambodia also has five main river basin groups, namely Tonle Sap, Three S, Upper Mekong, Lower Mekong, and Coastal Catchments (Salvadore et al., 2017).

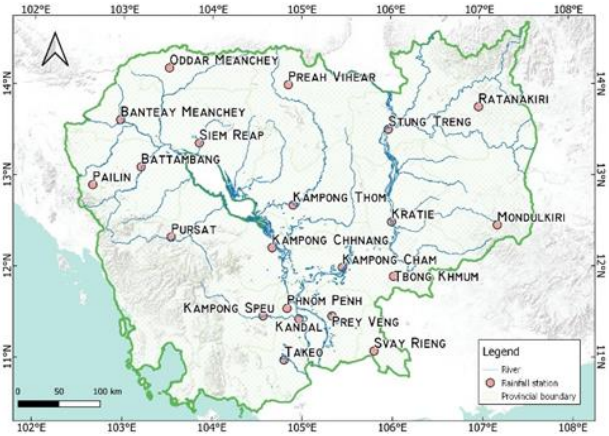

Figure 1. Study area.

2.2. Data acquisition

For this study, rainfall data for all 21 stations were sourced from the IMERG (Integrated Multi-satellitE Retrievals for Global Precipitation Measurement) Version 7 satellite product, which is publicly accessible through NASA's data archive. The dataset spans 22 years, covering the period from January 1st, 2001, to December 31st, 2022. In addition, data on rice yield and fertilizer application rates were obtained from the Food and Agriculture Organization (FAO) of the United Nations.

2.3. Standardized Precipitation Index (SPI)

The SPI, first introduced by McKee et al. (1993), is one of the most commonly applied precipitation-based indices for assessing wet and dry conditions across different timescales. In this study, SPI was computed using the SPI Generator software developed by the National Drought Mitigation Center. This tool was used to produce monthly SPI values at both 1-month and 3-month timescales for all 21 stations within the study area.

$$SPI = \frac{X - \mu}{\sigma} \qquad (1)$$

where X is the precipitation for the given period, μ is the mean precipitation of the period, and σ is the standard deviation of the precipitation for the period.

The SPI results were interpreted by focusing on negative values (rainfall deficits). Each negative value was assessed based on its magnitude and classified into mild, moderate, severe, or extreme drought according to the threshold ranges. This allowed us to identify the intensity of drought conditions over time at each station.

3. Results and Discussion

3.1. Assessment of drought severity

Figure 2 shows the monthly SPI at a 3-month timescale from 2001 to 2022 for Prey Veng, one of Cambodia's main rice-producing provinces. The SPI values range between 2 and -2, with positive values displayed in blue and negative values in red. The negative values indicate below-average rainfall, which is especially noticeable in the early years of the record, with Prey Veng showing a strong dry pattern. This points to recurring drought conditions influencing the climate in this important agricultural area and underlines the vulnerability of rainfed farming. In Prey Veng, the most notable drought began in mid-2001, gradually lessened, but continued with fluctuations until about 2005. Additional dry periods were observed around 2010, 2016, and 2020, each marked by considerable severity.

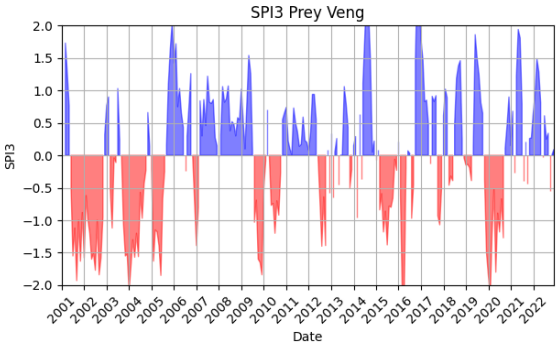

Figure 2. SPI 3-month timescale.

3.2. Meteorological drought thresholds

Figure 3 shows the monthly drought thresholds for Banteay Meanchey in the Tonle Sap River Basin. The orange shading illustrates different drought severity levels, where light orange represents mild drought, and darker shades indicate moderate, severe, and extreme conditions as rainfall decreases. The rainy season generally begins in May, reaches its peak in September, and declines by November. For this station, at least 125 mm of rainfall is needed during the peak month to avoid being classified as an extreme meteorological drought.

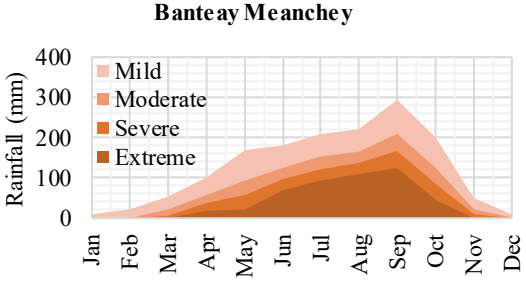

Figure 3. Monthly drought thresholds.

3.3. Rice yield and its relation to rainfall and fertilizer

Figure 4 illustrates the relationship between rice yield and fertilizer use from 2002 to 2022. Fertilizer use was low until 2006, while rice yield still rose from about 1.8 to 2.6 tons/ha. From 2007 onward, fertilizer application increased gradually, reaching around 30 kg/ha by 2021, which corresponded with a steady rise in rice yield. The correlation between fertilizer use and yield is strong, with a coefficient of 0.84, indicating that fertilizer played a key role in boosting productivity. Despite drought years, rice yields did not experience major declines, suggesting that improved inputs helped buffer the impacts of rainfall shortages.

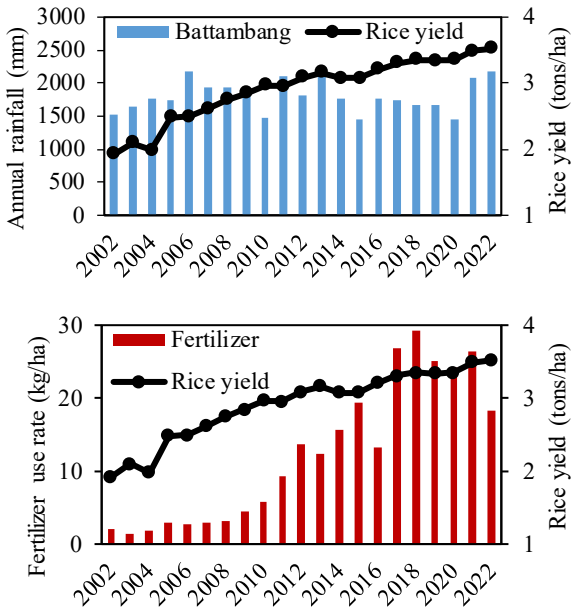

Figure 4. Rice yield compared to rainfall and fertilizer.

4. Conclusions

In summary, this study emphasizes the value of defining meteorological drought thresholds that reflect Cambodia's agricultural conditions. Using the SPI provides a practical approach for monitoring drought severity and regional patterns. The results offer useful insights for farmers and stakeholders, supporting preparedness and more sustainable farming practices. Nevertheless, the findings indicated that SPI had only a limited relationship with agricultural production, suggesting that yields are less dependent on rainfall variability and more strongly influenced by other factors, one of which is fertilizer application.

References

McKee, T. B., Doesken, N. J., Kleist, J. 1993. The relationship of drought frequency and duration to time scales. Proceedings of the 8th Conference on Applied Climatology, 17(22), 179-183.

Phy, S. R., Sok, T., Try, S., Chan, R., Uk, S., Hen, C., Oeurng, C. 2022. Flood Hazard and Management in Cambodia: A Review of Activities, Knowledge Gaps, and Research Direction. In Climate (Vol. 10, Issue 11), 162. https://doi.org/10.3390/cli10110162

Salvadore, E., Michailovsky, C., Coerver, B., Bastiaanssen, W., IHE-Delft, W. A. E. 2017. Water Accounting in selected Asian river basins: Pilot study in Cambodia. https://www.wateraccounting.org/files/projects/adb/phase1/Cambodia%20Water%20Accounting%20Final%20Report%20(2017).pdf (last accessed on July 22, 2025).

Thoeun, H. C. 2015. Observed and projected changes in temperature and rainfall in Cambodia. Weather and Climate Extremes, 7, 61-71. https://doi.org/10.1016/J.WACE.2015.02.001

Application and Evaluation of Long-Term Ensemble Precipitation Forecasts for Reservoir Inflow Prediction

Yuan-Li Tai[1*], Ke-Sheng Cheng[2], Yun-Ching Lin[1], Ching-Teng Lee[1], Chi Pan[1]

[1] Central Weather Administration, Taipei, Taiwan, R.O.C.

[2] Center for Weather and Climate Disaster Research, National Taiwan University, Taipei, Taiwan, R.O.C.

* Corresponding author. Email: leonmax306@gmail.com

Abstract

In water resource management and decision-making, it is essential to evaluate the anticipated hydrological conditions of an entire cropping season prior to its commencement in order to implement appropriate water allocation strategies. Consequently, long-term precipitation forecasts play a critical role in water resource planning. In this study, we applied long-term ensemble precipitation forecasts to predict reservoir inflows and evaluated the forecast performance, aiming to effectively capture long-term hydrological trends.

We utilized ensemble monthly precipitation hindcast data from Central Weather Administration Regional Spectral Model to generate probabilistic precipitation forecasts for the Shihmen Reservoir catchment. Assuming a monotonic correspondence between catchment rainfall and reservoir inflow, the probabilistic precipitation forecasts are transformed into forecast probability distributions of reservoir inflow using a quantile mapping approach. The theorem of probability integral transform, along with the Kolmogorov-Smirnov (K-S) test, is employed to assess whether the observed inflow data follow the forecast probability distribution. Results from the K-S test indicate that the cumulative probability values of observed inflow conform to a uniform distribution when mapped to the forecast distribution, suggesting that the forecast probability distributions of inflow are reliable. This method not only provides a quantitative evaluation of forecast performance but also reveals characteristics such as potential overestimation or underestimation of the mean and variance through the analysis of cumulative probability plots.

Keywords: Kolmogorov-Smirnov goodness-of-fit test, cumulative probability plot, Probabilistic forecast, Performance evaluation.

1. Introduction

In Taiwan, the nationwide average annual rainfall is approximately 2,500 mm. Nevertheless, only 20% of the annual rainfall occurs during the dry season (November to April). Water resource management and water shortage risk assessment in the dry season are of critical importance in Taiwan. Hsieh et al. (2016) conducted a water shortage risk assessment for the Jianan Irrigation District in southern Taiwan based on historical streamflow data. Tsai et al. (2023) presented an innovative risk-based irrigation decision making approach for the Shihmen Reservoir Irrigation District in northern Taiwan by using the reservoir inflow data. In practical application, considering precipitation forecasts in addition to historical flow data enables a more effective assessment of water shortage risk. In this study, we apply the ensemble precipitation forecasts to construct the forecast probability distribution of reservoir inflow. Several methods are implemented to evaluate the performance of the reservoir inflow prediction. The evaluation results for the Shihmen Reservoir in Taiwan are presented and discussed accordingly.

2. Materials and Methods

Central Weather Administration Regional Spectral Model (CWARSM) is a dynamic model developed by CWA. The concept of CWARSM was first proposed in 2003, which adopts the National Centers for Environmental Prediction (NCEP) RSM's perturbation concept for lateral boundary treatment, making it suitable for consistent long-term and seasonal predictions (Juang et al. 2003). The model was first evaluated at 30-km resolution and a 2-month lead time in forecast mode. As computing efficiency has improved, CWARSM has now developed forecasts with a 12-km resolution and 9-month lead time. In our research, hindcast data from 1991 to 2020, with 30 ensemble members, are used.

The ensemble forecast is often used to obtain some indication of the uncertainty in the prediction, but it is not obvious how the ensemble members can be used to indicate forecast uncertainty (Troccoli et al. 2008). In seasonal climate forecasts, tercile-category probabilistic forecasts are commonly conducted. A simple way to show forecast uncertainty is to estimate the category probabilities by the proportions of ensemble members having outcomes within each category. Let the tercile categories be expressed as C_1, C_2, and C_3, with t_1 and t_2 being the first and second terciles. The terciles are monthly specific and are calculated from forecast values of all years. The probabilities of C_1, C_2, and C_3 are calculated by

$$\mathrm{P}(\mathrm{C}_1) = \frac{\sum_{i=1}^{30} 1_{\{x_i<t_1\}}}{30}$$

$$\mathrm{P}(\mathrm{C}_2) = \frac{\sum_{i=1}^{30} 1_{\{t_1<x_i<t_2\}}}{30}$$

$$\mathrm{P}(\mathrm{C}_3) = \frac{\sum_{i=1}^{30} 1_{\{x_i>t_2\}}}{30}$$

where $1_{\{x_i<t_1\}}$ is the indicator function and x_i is the monthly rainfall of the i-th ensemble member.

Assuming a monotonic correspondence between the monthly catchment rainfall and reservoir inflow, tercile-forecast probabilities of the reservoir inflow and rainfall are identical. Let the probability distribution of reservoir inflow belong to a location-scale family. Given two quantiles q_1 and q_2, the location parameter (α) and scale parameter (β) can be calculated as follows (Cook, 2010):

$$\alpha = \frac{q_1 F_Z^{-1}(p_2) - q_2 F_Z^{-1}(p_1)}{F_Z^{-1}(p_2) - F_Z^{-1}(p_1)}$$

$$\beta = \frac{q_2 - q_1}{F_Z^{-1}(p_2) - F_Z^{-1}(p_1)}$$

where Z is the same distribution family with location 0 and scale 1 and F_Z is its cumulative distribution function (CDF).

After the forecast probability distribution of reservoir

inflow was estimated, some methods were employed to evaluate the adequacy of the distribution model. The Kolmogorov-Smirnov goodness-of-fit test (Mood et al. 1974), or Kolmogorov-Smirnov (K-S) test, is a nonparametric test used to test whether the samples come from a given reference probability distribution. The K-S statistics D_n is the maximum of the distance between empirical CDF and the given reference CDF, that is

$$\mathrm{D_n} = \sup_{-\infty<x<\infty} |F_n(x) - F(x)|$$

The critical region of the K-S test statistics D_n depends on sample size n. If it rejects the null hypothesis, it suggests that the sample data do not come from the given probability distribution.

3. Results and Discussion

In Taiwan, various types of storms contribute to heavy rainfall during different seasons. Therefore, the forecast probabilities were partitioned into three groups, the Mei-Yu season (May-June), summer season (July-October), and winter-to-spring season (December-April) (Cheng et al. 2024).

We evaluated the performance of reservoir inflow probabilistic forecast with a 1-month lead time at Shihmen Reservoir in northern Taiwan. The results of the K-S test are presented in Table 1. All the tests in different seasons do not reject the null hypothesis. It indicates that the forecast distribution can well characterize the observed reservoir inflow data.

Table 1. K-S test for forecast performance evaluation.

Season	KS statistics, D_n	Sample size, n	p value
Mei-Yu	0.1409	60	0.1819
Summer	0.0985	120	0.1943
Winter-to-spring	0.0574	180	0.5978

The cumulative probability plot of the empirical CDF ($\mathrm{F_n}(u)$) can reveal characteristics such as underconfident, overconfident, mean-underestimated, and mean-overestimated (Cheng et al. 2024). These plots in three different seasons are shown as Figure 1 to Figure 3. In Mei-Yu season, the forecast distribution is slightly overconfident and mean-overestimated. In summer season, the forecast distribution is slightly overconfident and mean-underestimated. In winter-to-spring season, the forecast distribution is well-calibrated.

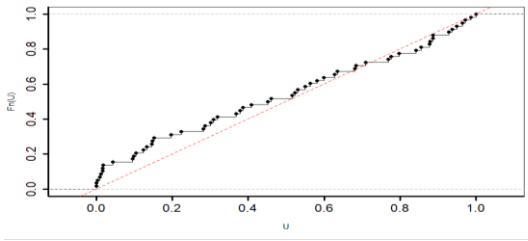

Figure 1. The CDF plot (Mei-Yu season).

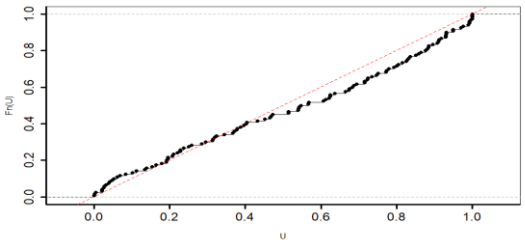

Figure 2. The CDF plot (summer season).

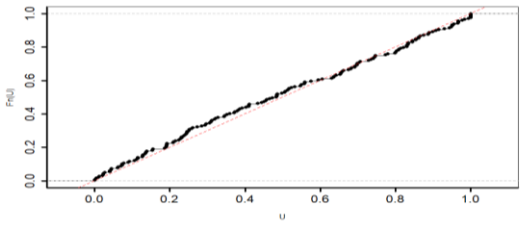

Figure 3. The CDF plot (winter-to-spring season).

4. Conclusions

This study applies the long-term ensemble precipitation forecasts from CWARSM to construct the forecast probability distribution of reservoir inflow using a quantile mapping approach. Several methods are implemented to evaluate the performance of the forecast distribution, including the Kolmogorov-Smirnov (K-S) test and the shape of the cumulative probability plot. The K-S test indicates that the forecast probability distributions of reservoir inflow are reliable across all seasons. The characteristics of the forecast probability distribution are identified from the cumulative probability plot, with the distribution showing the best performance in winter-to-spring season.

References

Cheng, KS., Yu, G., Tai, YL. et al., 2024. Hypothesis testing for performance evaluation of probabilistic seasonal rainfall forecasts. Geosci. Lett. 11, 27.

Cook, J. D., 2010. Determining distribution parameters from quantiles. UT MD Anderson Cancer Center Department of Biostatistics, Working Paper Series. https://www.johndcook.com/quantiles_parameters.pdf Accessed August 2, 2025.

Hsieh, HI., Su, MD., Wu, YC. et al., 2016. Water shortage risk assessment using spatiotemporal flow simulation. Geosci. Lett. 3, 2.

Juang, H.H., Shiao, C., Cheng, M., 2003. The Taiwan Central Weather Bureau Regional Spectral Model for Seasonal Prediction: Multiparallel Implementation and Preliminary Results. Monthly Weather Review, 131(8), 1832-1847.

Mood AM, Graybill FA, Boes DC., 1974. Introduction to the theory of statistics. McGraw-Hill, New York.

Troccoli, A., Harrison, M., Anderson, D. L., Mason, S. J. (Eds.)., 2008. Seasonal climate: forecasting and managing risk (Vol. 82). Springer Science & Business Media.

Tsai, SF., Wu, DH., Yu, GH., Cheng, KS., 2023. Risk-based irrigation decision-making for the Shihmen Reservoir Irrigation District of Taiwan. Paddy Water Environ 21, 497–508.

Impact of Climate Change-Induced Rainfall Pattern Shifts on Marine Resources in Kafuri Bay

Toshinori Tabata [1*], So Tanaka[2], Masayoshi Harada[1], Akinori Ozaki[3]

[1] Faculty of Agriculture, Kyushu University, Fukuoka City, Fukuoka, 819-0395, Japan

[2] Graduate School of Bioresource and Bioenvironmental Sciences, Kyushu University, Fukuoka City, Fukuoka 819-0395, Japan

[3] Institute of Tropical Agriculture Kyushu University, Fukuoka City, Fukuoka 819-0395, Japan

* Corresponding author. Email: ttabata@bpes.kyushu-u.ac.jp

Abstract

Kafuri Bay in Itoshima City, a productive shallow coastal area supporting aquaculture, has recently experienced declining fishery catches. To clarify the underlying causes, this study analyzed long-term water quality data (April 2010–December 2023) using Principal Component Analysis (PCA). Nine parameters (temperature, salinity, COD, DO, NH_4-N, NO_3-N, NO_2-N, PO_4-P, and chlorophyll-a) were examined at surface and bottom layers. PCA identified distinct environmental indicators. At the surface, S-PCS1 represented phytoplankton photosynthetic activity, S-PCS2 nutrient concentrations, and S-PCS3 winter DO. At the bottom, B-PCS1 indicated groundwater-derived winter nutrient input, B-PCS2 organic matter quantity, and B-PCS3 winter phytoplankton proliferation. Comparison of time-series patterns showed that peaks in S-PCS1 and S-PCS2 frequently coincided with heavy rainfall events, suggesting terrestrial runoff as a major nutrient source. Fishery production data showed clear linkages: aquaculture yields strongly correlated with surface nutrient concentration (S-PCS2), while boat fisheries were associated with bottom phytoplankton proliferation (B-PCS3). However, reduced catches in 2020 despite high B-PCS3 scores highlighted the importance of organic matter supply (B-PCS2) for sustaining productivity. These findings indicate that recent climate change-induced rainfall patterns (e.g., linear rainbands) destabilize nutrient inflow, reducing biological productivity and contributing to declining fishery resources. Future management strategies must therefore account for altered rainfall regimes to sustain coastal fisheries.

Keywords: Principal Component Analysis (PCA), Water Quality, Nutrients, Phytoplankton, Biological Productivity

1. Introduction

Kafuri Bay, located in the western part of Itoshima City, Fukuoka Prefecture, is a productive shallow coastal area featuring extensive tidal flats. It supports a thriving aquaculture industry, including the cultivation of prawns, small shrimp, bivalves, and oysters. However, local fishery operators have recently observed a decline in their catches, prompting an urgent need to identify the specific factors contributing to the reduction of marine resources. This decrease is likely a complex issue, potentially involving environmental changes and global climate change. Shallow coastal areas like Kafuri Bay are particularly susceptible to environmental fluctuations, which can significantly impact marine resources, thus requiring detailed investigations.

To address this critical problem, this study focused on investigating long-term changes in the water environment within Kafuri Bay. The primary objective was to identify specific environmental factors contributing to the observed decline in fishery resources. To achieve this, Principal Component Analysis (PCA), a multivariate analysis technique, was applied to accumulated water quality data from Kafuri Bay to examine the relationship between temporal changes in the bay's water environment and fluctuations in fishery catches.

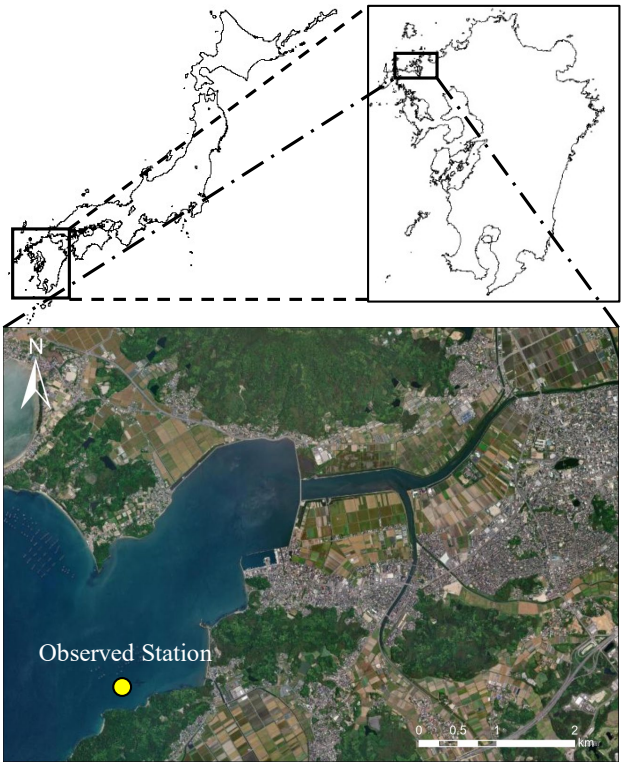

Fig. 1 Location of Kafuri bay and Water quality Station

2. Materials and Methods

This study utilized monthly water quality data collected from April 2010 to December 2023 in Kafuri Bay as shown in **Fig.1**. Data were obtained for both surface and bottom layers, encompassing nine parameters: Water Temperature (WT), Salinity (Sal), Chemical Oxygen Demand (COD), Dissolved Oxygen (DO), Ammonium Nitrogen (NH_4-N), Nitrate Nitrogen (NO_3-N), Nitrite Nitrogen (NO_2-N), Phosphate Phosphorus (PO_4-P), and Chlorophyll-a (Chl.a).

Principal Component Analysis was employed for multivariate statistical analysis to simplify data structures and identify key environmental factors. The PCA methodology involved standardizing each variable to a mean of 0 and a standard deviation of 1. A covariance matrix was then calculated, from which eigenvalues and

eigenvectors were derived. Principal components with an eigenvalue of 1 or greater were selected to explain maximum data variance. Finally, principal component scores were calculated by projecting the original data onto this component space. This PCA was applied to the monthly data of the nine water quality parameters for both surface and bottom layers across the study period.

3. Results and Discussion

Principal Component Analysis was performed on nine water quality parameters in Kafuri Bay from 2010 to 2023, identifying key environmental factors for both surface and bottom layers. For the surface layer (S-PCSs), S-PCS1 represented phytoplankton photosynthetic activation, prominent in summer, with high loadings for Water Temperature, COD, and Chlorophyll a. S-PCS2 indicated nutrient concentration, strongly linked to nitrogen and phosphorus. S-PCS3 showed seasonal Dissolved Oxygen (DO), with high scores reflecting winter DO and low scores suggesting potential summer hypoxia. In the bottom layer (B-PCSs), B-PCS1 represented winter groundwater-derived nutrient loads, influenced by warmer, low-DO groundwater. B-PCS2 indicated organic matter quantity, reflecting summer biological productivity from active surface photosynthesis. B-PCS3 denoted winter phytoplankton proliferation, driven by NH_4-N uptake.

Time-series comparison of principal component scores demonstrated a strong influence of terrestrial rainfall on the marine environment. Peaks in S-PCS1 (phytoplankton activation) and S-PCS2 (nutrient concentration) frequently coincided with heavy rainfall events. For example, in July 2018, daily rainfall exceeding 100 mm occurred just prior to the survey, suggesting that nutrient inflow from land, triggered by heavy rainfall, drove phytoplankton activation. This confirms rainfall as a major nutrient source for the bay.

Figure 2 shows the time-series of annual fish catch, aquaculture production in Kafuri Bay, and PC scores in surface and bottom layers. Comparing these environmental trends with annual fishery production data from the Chikuzen Sea Area revealed crucial relationships. Aquaculture production, which peaked at 1,185 tons in 2016, strongly correlated with the peak in S-PCS2 (nutrient concentration). The overall fluctuating trends in aquaculture also mirrored surface nutrient levels, underscoring the influence of marine nutrient concentration on yields. For boat fisheries, production peaked at 19,891 tons in 2015, coinciding with the peak of B-PCS3 (phytoplankton proliferation). This suggests that an increase in phytoplankton, a fundamental food source, contributed to improved fishery production. However, a discrepancy was noted in 2020: despite a peak in B-PCS3, boat fishery production was low. This was attributed to low B-PCS2 (organic matter quantity, an indicator of biological productivity) in the same year, highlighting that the supply of organic matter to the bottom layer is also critical for sustaining productivity.

The underlying cause of these dynamic changes in the marine water environment is strongly linked to recent climate change-induced shifts in rainfall patterns. Daily and monthly rainfall data at the Maebaru station revealed an increased frequency of short-duration, concentrated rainfall events (e.g., linear rainbands, guerrilla downpours)

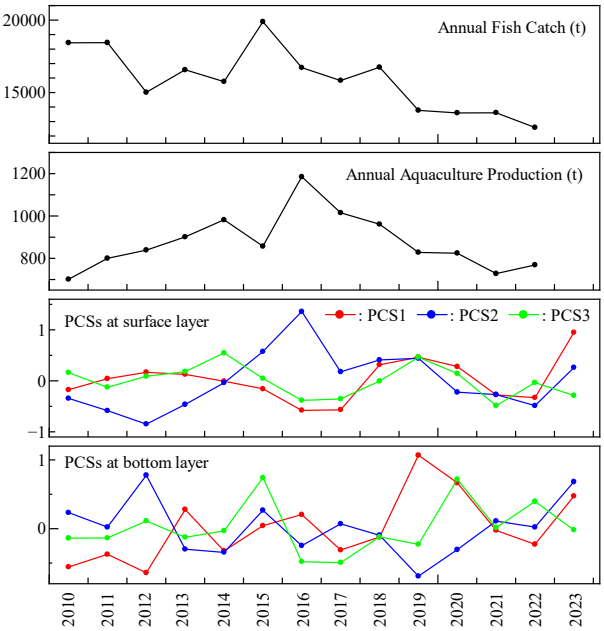

Fig.2 Annual fishery production and principal component scores (surface: S-PC1–3; bottom: B-PC1–3) in Kafuri Bay (2010–2023).

since 2017, alongside significant monthly variations in precipitation from 2019–2021. Coincidentally, fishery catches have decreased since 2019. This suggests that altered rainfall patterns create an unstable nutrient supply from terrestrial areas—characterized by sudden, large inflows during intense rains and insufficient input during dry periods—ultimately leading to a decline in marine biological productivity and impacting fishery catches in Kafuri Bay.

4. Conclusions

This study examined long-term water quality changes in Kafuri Bay and their relationship to fisheries using Principal Component Analysis (PCA). Surface productivity was mainly driven by phytoplankton activity and nutrient availability, while bottom-layer dynamics reflected groundwater-derived nutrients, organic matter supply, and phytoplankton proliferation. Comparison of time-series patterns indicated that heavy rainfall events triggered nutrient inflows that enhanced phytoplankton activity, but irregular rainfall also led to unstable nutrient supply. Fishery production trends reflected these dynamics—aquaculture yields correlated with surface nutrient concentrations, while boat fisheries depended on bottom phytoplankton and organic matter levels. Recent increases in short-duration, intense rainfall (e.g., linear rainbands, guerrilla downpours) have disrupted this balance, contributing to reduced biological productivity and declining catches. These results indicate that climate change-induced alterations in rainfall patterns are a key driver of fisheries decline in Kafuri Bay. Future nutrient management and fisheries strategies must therefore account for changing precipitation regimes to sustain productivity in shallow coastal ecosystems.

Acknowledgements

This research was partially supported by Itoshima City under the “Itoshima City University Collaboration Research Program for Problem-Solving”

Irrigation as an Adaptation Strategy for Tea Cultivation under Climate Change

Yoshihiro Matsushita [1*], Junichiro Takeuchi [1], Takehide Hama [1], Masayuki Fujihara [1]

[1] Graduate School of Agriculture, Kyoto University, Kyoto, 606-8502, Japan

* Corresponding author. Email: matsushita.keita.47e@st.kyoto-u.ac.jp

Abstract

Tea cultivation is particularly vulnerable to the impacts of climate change, as its growth, yield, and quality are closely linked to environmental factors such as temperature and precipitation. Adaptation strategies include molecular approaches, but their high costs and reliance on advanced infrastructure limit their widespread adoption. Therefore, this study aims to see if irrigation, which is more accessible, is effective against climate change and look for more effective ways of irrigation. This study uses the CUPPA-Tea model, which simulates the growth of tea, with the water balance model. In the simulation, ensemble weather prediction data for the past and the future with the rise of 4℃ provided by d4PDF are used, and some irrigation methods are considered. Simulation results show the average yield will decrease in the future due to more heat stress with the rise of temperature if the irrigation method, which is a planned one, is the same. Whereas trigger irrigation, which is done according to water stress, increases the yield little, cooling irrigation, which is done according to heat stress, achieved greater increase in the yield than the trigger one, though the yield is still less than the current one. However, this seems to be due to decreased water stress, not heat stress. In conclusion, irrigation could be effective as an adaptation strategy against climate change, but not enough to offset the full impact of climate change at all.

Keywords: CUPPA-Tea, d4PDF, cooling effect

1. Introduction

Tea (*Camellia sinensis*) is one of the world's most widely consumed beverages and a vital socioeconomic resource for millions worldwide. However, tea cultivation is particularly vulnerable to the impacts of climate change, as its growth, yield, and quality are closely linked to environmental factors such as temperature, precipitation (Han et al., 2017; Omer et al., 2025; Wang et al., 2021).

Adaptation strategies to mitigate the impacts of climate change on tea cultivation include a wide range of molecular approaches. However, the high costs of genomic technologies and their reliance on advanced infrastructure limit their widespread adoption in developing regions and for smallholder farmers (Omer et al., 2025).

In contrast, irrigation is more accessible for smallholder farmers than those advanced technologies are. Indeed, irrigation is one of the most employed measures to combat climate change, and shows statistically significant results in Assam, India (Baruah et al., 2021). Therefore, this study aims to see if irrigation is also effective against climate change in the future and look for more effective ways of irrigation.

2. Materials and Methods

2.1. Tea growth simulation model

This study uses the CUPPA-Tea model (Matthews and Stephens, 1998a, 1998b). It considers three phases of shoot development: S0 (rest), S1 (quiescent), S2 (bud-burst). Each shoot repeats these three phases according to the phenochron value, which is calculated as follows.

$$\frac{dA}{dt} = R_{max} \cdot f(T_{mi}) \cdot P(\varphi_i) \cdot g(\Phi) \quad (1)$$

where A is phenochron, t is time (day), R_{max} is 1.0 phenochron/day, $f(T_{mi})$, $P(\varphi_i)$ and $g(\Phi)$ are dimensionless zero-to-unity functions describing the effect of the mean temperature (T_{mi}, ℃), photoperiod (φ_i, h), and water stress (Φ, dimensionless) for day i on shoot development, respectively. When a shoot reaches a certain phenochron, it proceeds to the next phase.

2.2. Water balance model

For the water balance model, this study uses Fujiwara model (Fujiwara, 2008). It is a vertical one-dimensional numerical calculation model, whose governing equation is mixed-form Richards equation as follows.

$$\frac{d\theta}{dt} = -\frac{\partial}{\partial x}\left(-K(\psi)\frac{\partial h}{\partial x}\right) - t_r(x) \quad (2)$$

where θ is the water content, ψ is the soil water pressure head, t is the time, K is the unsaturated hydraulic conductivity, which is assumed to be isotropic, h (= ψ + x) is the hydraulic head, t_r is the root water extraction rate and x is the vertical coordinate (positive upward).

2.3. Climate data

For climate data, this study uses d4PDF (Mizuta et al., 2017) . It is an ensemble climate prediction database, and provides 100 members of past experiment (HPB) and 90 members of 4℃-rise experiment (HFB). This study uses past experiment data from 2008 to 2011 and 4℃-rise experiment data from 2051 to 2054 in Assam, India.

2.4. Irrigation methods

This study considers three kinds of irrigation. The first is planned irrigation, which takes place once a month from November to March, which is a dry season. The second is trigger irrigation, which takes place when the water stress value is below a certain one. The third is cooling irrigation, which takes place when the value of $f(T_{mi})$ in (1) is below a certain one, in addition to trigger irrigation. Calculation of cooling effect by irrigation is done using specific enthalpy as follows (Ghafarian et al., 2022).

$$H = c_{pa}T + y\left(c_{pw}T + L_w\right) \quad (3)$$

where H is the specific enthalpy (kJ kg^{-1}), c_{pa} is the specific heat of dry air at constant pressure (kJ kg^{-1} K^{-1}), T is the air temperature (℃), y is the absolute humidity (kg kg^{-1}), c_{pw} is the specific heat of water vapor at constant pressure (kJ kg^{-1} K^{-1}), L_w is the latent heat of vaporization of water (kJ kg^{-1}). Considering the conservation law as follows, the air

temperature after evapotranspiration (T_c) is calculated.

$$H(T, y) = H(T_c, y + ET) \quad (4)$$

where ET is evapotranspiration.

3. Results and Discussion

Table 1 shows the average total yield of each simulation. HPB-planned stands for past experiment with planned irrigation, HFB-planned stands for 4℃-rise experiment with planned irrigation, HFB-trigger stands for 4℃-rise experiment with trigger irrigation, and HFB-cooling stands for 4℃-rise experiment with trigger and cooling irrigation, respectively.

Table 1. Average total yield of each simulation (ton ha^{-1}).

Pattern	Average	Standard deviation
HPB-planned	5.87	0.12
HFB-planned	5.53	0.11
HFB-trigger	5.55	0.11
HFB-cooling	5.63	0.11

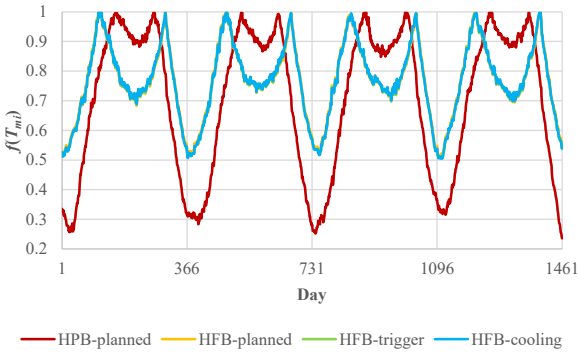

Figure 1. Daily $f(T_{mi})$ of each simulation.

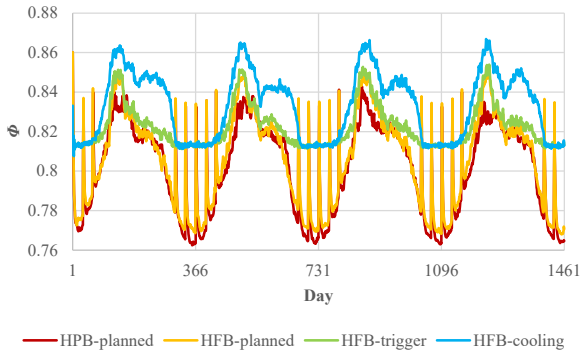

Figure 2. Daily Φ of each simulation.

The yield of HFB-planned is less than that of HPB-planned, and the difference is statistically significant ($p < 0.05$). This is thought to be because the values of $f(T_{mi})$ in HFB are lower in summer, which is the development season, than those of HPB with the rise of temperature (Figure 1), and that leads to slower growth and less yield.

The differences among different irrigation methods in HFB are much less than that of HPB-planned and HFB-planned, though they are statistically significant according to the multiple comparison procedure. The little difference between planned irrigation and trigger irrigation is thought to be because the values of the water stress function of both is almost the same in summer, the development season (Figure 2). On the other hand, the difference between HFB-trigger and HFB-cooling is rather larger. However, this seems to be because of the reduction of the water stress in summer (Figure 2), for $f(T_{mi})$ of three HFBs are almost indistinguishable (Figure 1). Nevertheless, the yield of HFB-cooling is still far less than that of HPB-planned.

4. Conclusions

In conclusion, irrigation could be effective as an adaptation strategy against climate change, but not enough to offset the full impact of climate change at all.

Acknowledgements

This study was financially supported by the JSPS KAKENHI (grant numbers 22KK0091).

References

Baruah, P., Handique, G. 2021. Perception of climate change and adaptation strategies in tea plantations of Assam, India. Environmental Monitoring and Assessment, 193, 165

Fujiwara, V. S. 2008. Decision-Support Model for Optimal FertilizerApplication and Irrigation Using Short- and Medium-Term Weather Forecasts. Master's thesis, Kyoto University

Ghafarian, F., Wieland, R., Nendel, C. 2022. Estimating the Evaporative Cooling Effect of Irrigation within and above Soybean Canopy. Water, 14, 319.

Han, W. Y., Huang, J. G., Li, X. et al. 2017. Altitudinal effects on the quality of green tea in east China: a climate change perspective. European Food Research and Technology, 243, 323–330

Matthews, R. B., Stephens, W. 1998a. CUPPA-Tea: a simulation model describing seasonal yield variation and potential production of tea. 1. Shoot development and extension. Experimental Agriculture, 34, 345-367

Matthews, R. B., Stephens, W. 1998b. CUPPA-Tea: a simulation model describing seasonal yield variation and potential production of tea. 2. Biomass production and water use. Experimental Agriculture, 34, 369-389

Mizuta, R., Murata, A., Ishii, M. et al. 2017. Over 5,000 Years of Ensemble Future Climate Simulations by 60-km Global and 20-km Regional Atmospheric Models. Bulletin of the American Meteorological Society, 98, 1383-1398

Omer, A. A. A., Zhang, C. H., Liu, J. et al. 2025. Comprehensive review of mapping climate change impacts on tea cultivation: bibliometric and content analysis of trends, influences, adaptation strategies, and future directions. Frontiers in Plant Science., 15, 1542793

Wang, P., Tang, J., Yuping, M. et al. 2021. Mapping threats of spring frost damage to tea plants using satellite-based minimum temperature estimation in China. Remote Sensing, 13, 2713

Analysis of Biochar Effects on Sorghum Soil under Irrigation with Reclaimed Water from the Kinmen Distillery

Yi-Tai Liao [1*], Li-Chi Chiang[1], Ci-Jyun Liao[1], Feng-Wen Chen[2], Yun-Wei Tan [2]

[1] Department of Bioenvironmental Systems Engineering, National Taiwan University, Taipei 10617, Taiwan

[2] Resource Division, Agricultural Engineering Research Center, 32061 Taoyuan City, Taiwan

* Corresponding author. Email: r11622026@ntu.edu.tw

Abstract

Agricultural irrigation accounts for about 70% of global water consumption. In recent years, climate change has reduced the availability of agricultural water resources, while floods and droughts have occurred with increasing frequency, making water shortages in arid regions more severe. Developing alternative water sources has therefore become a critical issue. This study carried out a field experiment in Kinmen County, an area facing severe water scarcity, using effluent from the Kinmen Kaoliang Liquor Distillery (KKL) for sorghum irrigation. The effluent is rich in nutrients but has high electrical conductivity, which may lead to soil salinization. To reduce this risk, it was diluted with Houlong Creek water to create five irrigation ratios: 0%, 20%, 40%, 60%, and 80% KKL. Each ratio was applied to two 8 × 4 m plots, divided into a control group and a biochar treatment group, where 2 kg of biochar was added. Results showed that biochar effectively reduced soil salinity, sodium accumulation, and plant sodium uptake, while preventing soil degradation and sodium toxicity.

Keyword: Wastewater、Irrigation、Sorghum、Biochar and soil salinization

1. Introduction

In recent years, climate change has intensified hydrological disasters, while population growth and rising environmental awareness have made water resource management a critical issue. Agricultural irrigation is the largest global water consumer (Tzanakakis et al., 2020), leading many countries to adopt treated wastewater as an alternative source, particularly in water-scarce regions (Ortega-Pozo et al., 2022). However, the high nutrient content of wastewater raises concerns of soil salinization, necessitating proper treatment before use. Climate change also threatens soil health and food security. Biochar, a widely used soil amendment, improves soil quality, enhances crop yields, and effectively mitigates salinity and sodicity (Andrade Foronda, 2022), making it a valuable tool for sustainable agriculture.

2. Materials and Methods

2.1. Experiment Design

This study was conducted at the Kinmen Country Agricultural Research and Extension Station (Fig. 1) from August 28, 2024, to February 11, 2025. Irrigation water consisted of effluent from the Kinmen Kaoliang Liquor Distillery mixed with Houlong Creek water at five ratios: 0%, 20%, 40%, 60%, and 80%, each stored in 2-ton tanks. For each ratio, plots were divided into a control group and a biochar treatment group, with the latter receiving an additional 2 kg of biochar. The crop grown was sorghum, cultivar Taichung No. 5 (Sorghum bicolor L. Moench).

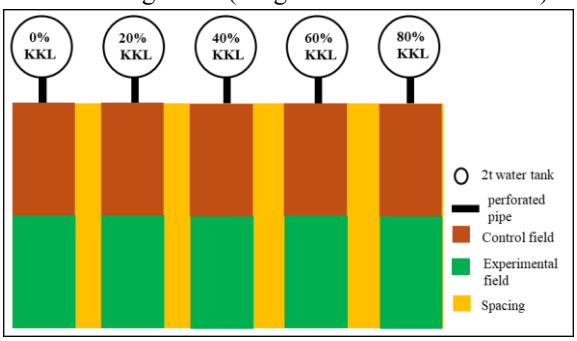

Figure 1. Field Design

2.2. Experiment Analysis

2.2.1 Water Analysis

Two 500 mL water samples were collected and preserved separately, one without acidification and the other acidified by adding appropriate amount of nitric acid for elemental analysis. The basic properties of the water samples, including pH and electrical conductivity, were measured using a handheld meter, while the elemental composition of the irrigation water was analyzed with in ICP-OES. The experiment involved three irrigation events conducted on 2024/12/09, 2024/12/24, 2025/01/15.

2.2.2 Soil and Plant Analysis

A total of seven soil sampling events were conducted, with four points selected in the field for composite sampling. The samples were air-dried at 30 °C for 72 hours. For plant analysis, three sorghum plants were collected at harvest, oven-dried at 65 °C for 48 hours, and then separated into roots, stems, leaves, and panicles. Each part was ground into powder using a grinder and stored in sealed bag. For elemental analysis, 0.5 g of sample was digested with 8 mL of aqua regia (6 mL HCl + 2 mL HNO_3) using a microwave digestion system. The digestate was diluted to 50 mL, and elemental concentrations were determined using ICP-OES.

3. Results and Discussion

3.1. Irrigation water result

The results of the irrigation water quality analysis are shown in Table 1. The pH, electrical conductivity, and sodium content of the irrigation water increased with the proportion of Kinmen Kaoliang Liquor (KKL) effluent. The analysis also revealed that the irrigation water contained a high concentration of sodium.

Tabel 1. Results of irrigation water quality analysis

	0%	20%	40%	60%	80%
pH	7.3	7.68	7.99	8.1	8.19
EC (μS/cm)	803	1256	1942	2644	2836
Na(mg/L)	74.4	168.27	299.57	407.9	440.69

3.2 Soil electrical conductivity Change

As shown in Table 2, soil electrical conductivity (EC) values in all treatments were below 200 µS/cm before planting and increased after three irrigations. In the control plots, EC rose with the salinity of the irrigation water, whereas the increase was smaller in the biochar-treated plots. These results indicate that biochar effectively reduces soil salt accumulation (El-sayed et al., 2021), thereby helping to prevent salinity hazards.

3.3 Soil sodium accumulation

In addition to salinity, soil sodium accumulation was also assessed. Before planting, sodium concentrations were below 100 ppm, showing an overall trend of increasing after first irrigation, peaking after the second, and declining after the third. At nearly all sampling times, sodium levels in the control plots were higher than in the biochar-treated plots. This indicates that biochar can adsorb sodium (Yu et al., 2023) and reduce harmful ion buildup (Huang et al., 2023), thereby mitigating sodium toxicity and the risk of soil salinity and sodicity.

Table 2. Soil electrical conductivity results (unit: μS/cm)

Treatment	2024/08/28	2025/02/11	Difference
0%	69.33	160.63	91.3
0%+BC	200.93	282.57	81.64
20%	54.23	210.67	156.44
20%+BC	102.53	155.13	52.6
40%	61.13	337.8	276.67
40%+BC	113.83	211.23	97.4
60%	64.23	250.97	186.74
60%+BC	169.23	232.1	62.87
80%	71	323.33	252.33
80%+BC	205.67	456.97	251.3

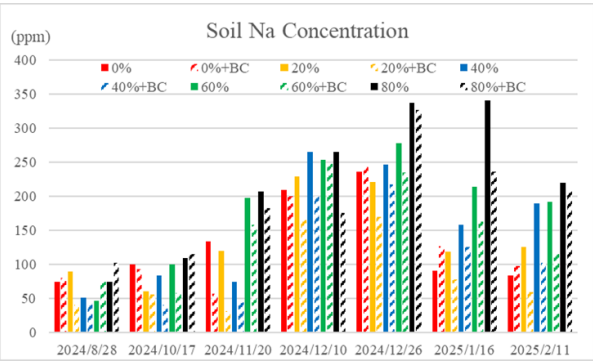

Figure 2. Accumulation of sodium concentration in soil

3.4 Plant sodium accumulation

At harvest, sodium accumulation in sorghum (Fig. 3) was highest in the roots, followed by panicles and stems, with the lowest in leaves. Concentrations in all plant parts increased with sodium levels in the irrigation water. Across treatments, the control group consistently showed higher sodium accumulation than the biochar group, indicating that biochar reduces sodium uptake in plants (Jin et al., 2018) and supports plant growth.

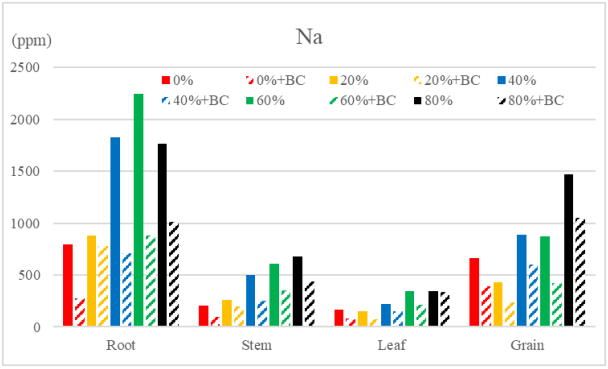

Figure 3. Accumulation of sodium concentration in plant tissues

4. Conclusions

This study examined soil salinity and sodicity induced by effluent irrigation and evaluated the mitigating role of biochar. Results showed that soil and plant elemental accumulation were positively correlated with effluent nutrient content. Biochar application effectively reduced soil salinity and sodium buildup in both soil and plants, thereby lowering the risks of sodicity and sodium toxicity. These findings suggest that biochar is a practical measure to prevent the negative impacts of effluent irrigation.

References

Andrade Foronda, D. (2022). *Reclamation of a Saline-Sodic Soil with Organic Amendments and Leaching*. Paper presented at the The 2nd International Laayoune Forum on Biosaline Agriculture.

El-sayed, M. E. A., Hazman, M., Abd El-Rady, A. G., Almas, L., McFarland, M., Shams El Din, A., & Burian, S. (2021). Biochar Reduces the Adverse Effect of Saline Water on Soil Properties and Wheat Production Profitability. *Agriculture, 11*(11).

Huang, K., Li, M., Li, R., Rasul, F., Shahzad, S., Wu, C., . . . Aamer, M. (2023). Soil acidification and salinity: the importance of biochar application to agricultural soils. *Front Plant Sci, 14*, 1206820.

Jin, F., Ran, C., Anwari, Q., Geng, Y., Guo, L., Li, J., . . . Shao, X. (2018). Effects of biochar on sodium ion accumulation, yield and quality of rice in saline-sodic soil of the west of Songnen plain, northeast China. *Plant, Soil and Environment, 64*(12), 612-618.

Ortega-Pozo, J. L., Alcalá, F. J., Poyatos, J. M., & Martín-Pascual, J. (2022). Wastewater Reuse for Irrigation Agriculture in Morocco: Influence of Regulation on Feasible Implementation. *Land, 11*(12).

Tzanakakis, V. A., Paranychianakis, N. V., & Angelakis, A. N. (2020). Water Supply and Water Scarcity. *Water, 12*(9).

Yu, J., Chang, J. S., Guo, H., Han, S., & Lee, D. J. (2023). Sodium ions removal by sulfuric acid-modified biochars. *Environ Res*, 235, 116592.

Advancing Sustainable Rice Farming through Biochar Integration with Treated Wastewater Irrigation to Combat Greenhouse Gas Emissions

Jittrera Buates [1*], Luc Duc Phung [1], Toru Watanabe [2]

[1] Japan Society for the Promotion of Science (JSPS); Faculty of Agriculture, Yamagata University, Yamagata, 997-8555, Japan

[2] Faculty of Agriculture, Yamagata University, Yamagata, 997-8555, Japan

* Corresponding author. Email: jittrera.b@gmail.com

Abstract

Agricultural greenhouse gas (GHG) emissions are a major driver of climate change, with rice cultivation being a significant contributor. Biochar (BC) application and alternate wetting and drying (AWD) have shown promise in reducing GHG emissions while improving crop productivity. However, limited research has investigated their integration with treated wastewater (TWW) irrigation. To address this gap, a microcosm experiment was conducted to evaluate three TWW-based rice production systems: (1) continuous surface irrigation (CSI), (2) CSI with BC (CSI+BC), and (3) AWD. These treatments were compared with conventional rice farming (control). Compared to the control, both CSI and CSI+BC considerably reduced cumulative CH_4 emissions by over 90%, while AWD increased CH_4 emissions by ~9%. Among the TWW systems, CSI produced the highest N_2O emissions, whereas CSI+BC and AWD achieved reductions of up to 68% relative to CSI. Nevertheless, all TWW systems emitted more N_2O than the control. AWD emerged as the system with the greatest global warming potential (GWP), in contrast to CSI+BC, which recorded the lowest, cutting it by 28-72% compared to the others. These findings suggest that BC, particularly when integrated with TWW, represents an effective climate-smart agricultural approach for reducing GHG emissions and supporting more resilient rice production systems.

Keywords: methane emissions, nitrous oxide emissions, organic amendment, water management, rice productivity

1. Introduction

Agriculture accounts for over three-quarters of Japan's CH_4 emissions and half of its N_2O emissions, with rice cultivation a major source driven by traditional flooded paddies (Fuhrmann-Aoyagi et al., 2024). This practice involves intensive chemical fertilizer (CF) and water use, resulting in substantial GHG emissions. To advance sustainable rice farming, it is essential to integrate strategies that reduce GHG emissions, conserve resources, and sustain crop productivity.

The simultaneous recycling of nutrients and water through TWW irrigation in rice cultivation presents a sustainable approach. Previous studies employing continuous sub-irrigation with TWW demonstrated significant CH_4 emission reductions and increased rice yield compared to conventional methods (Phung et al., 2021, 2020). Nonetheless, these studies identified a critical limitation, as TWW fertigation was associated with elevated N_2O emissions. BC application, as a soil organic amendment, is recognized as an effective strategy offering dual benefits by mitigating GHG emissions and enhancing crop productivity. Yang et al. (2019) and Gao et al. (2023) reported that BC altered denitrification gene abundance and microbial activity, thereby mitigating N_2O emissions by 20-22% compared to non-amended conditions. As an intermittent irrigation practice, AWD offers an alternative means of lowering N_2O emissions by up to 70% relative to continuous flooding (Loaiza et al., 2024).

Despite clear evidence supporting the advantages of both BC and AWD in mitigation potential, these approaches have yet to be implemented with TWW. This study aims to fill this gap by assessing the combined impact of TWW irrigation with either BC or AWD in rice production, comparing their performance to reduce GHG emissions against conventional practices.

2. Materials and Methods

2.1. Experimental design

A controlled microcosm experiment was conducted using acrylic chambers (32 × 40 × 60 cm) filled with 55 kg of air-dried sandy loam soil. A completely randomized design comprised three TWW-based irrigation regimes: (1) CSI, (2) CSI with BC amendment at 20 t ha^{-1} (CSI+BC), and (3) AWD. In CSI, TWW was continuously supplied from one side of the chamber, with excess water discharged via outlets positioned 5 cm above the soil surface. In AWD, chambers were reflooded to a 5 cm depth when the water table dropped to 15 cm below the soil surface. In these three treatments, TWW served as the sole source of irrigation water and nutrients. Additionally, the control received continuous flooding with tap water at a 5 cm depth. CF was applied twice: basal compound fertilizer (14-14-14; 80 kg N ha^{-1}) and urea topdressing (46% N; 40 kg N ha^{-1}). Each chamber contained four hills of uniform 30-day-old rice seedlings (*Oryza sativa* L., cv. Bekoaoba), transplanted at a spacing of 16 cm × 30 cm.

2.2. GHG emission measurement

CH_4 and N_2O fluxes were measured weekly using the static closed chamber method (Phung et al., 2020), with gas samples collected at 10-minute intervals and analyzed by gas chromatography. Gas fluxes were calculated using linear regression as described by Minamikawa et al. (2015). Cumulative emissions were estimated by linear interpolation and numerical integration between sampling dates. CH_4 and N_2O emissions were converted to CO_2 equivalents using 100-year GWP of 27 and 273, respectively (IPCC, 2021).

2.3. Statistical analysis

One-way analysis of variance (ANOVA) was performed using IBM SPSS Statistics (version 29.0.2.0; IBM Corp., Armonk, NY, USA). Differences between means were assessed using Tukey's honest significant difference (HSD) test with significance set at $p < 0.05$.

3. Results and Discussion

Significant reductions in cumulative CH_4 emissions of

92% or more were observed under CSI and CSI+BC ($p < 0.05$), while emissions from AWD were comparable to the control (Fig. 1a). Within the TWW systems, CSI+BC and AWD exhibited notable N_2O mitigation, achieving cumulative emission reductions of up to 68% relative to CSI; however, their emissions remained markedly elevated compared with the control ($p < 0.05$; Fig. 1b).

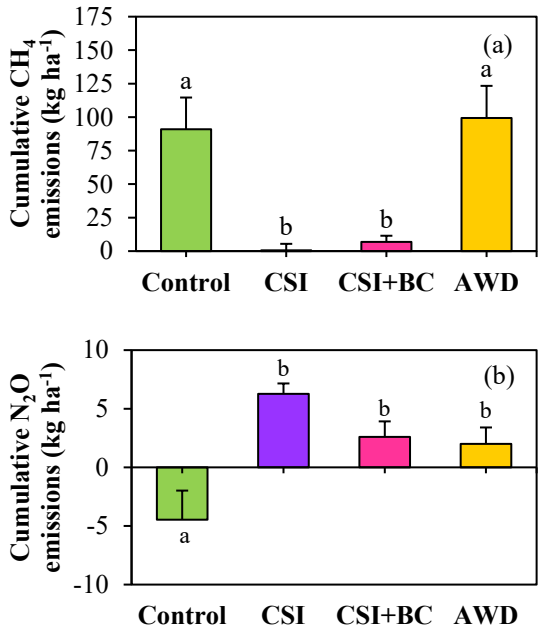

Figure 1. Cumulative emissions of CH_4 (a) and N_2O (b) under different treatments. Different letters denote statistically significant differences at $p < 0.05$.

CH_4 emissions were effectively mitigated under TWW irrigation schemes, particularly CSI and CSI+BC, due to enhanced oxygen transport from substantial amounts of dissolved oxygen in TWW into the soil, promoting CH_4 oxidation. BC addition with CSI further reduced N_2O emissions compared to CSI alone, probably by increasing soil pH following BC application and facilitating electron transfer to denitrifiers (Zhao et al., 2024). Conversely, AWD failed to reduce GHG emissions among the TWW regimes, particularly for CH_4. This was attributed to a greater release of stored CH_4 during re-wetting, accelerated by the availability of organic carbon in TWW, which serves as a substrate for methanogens.

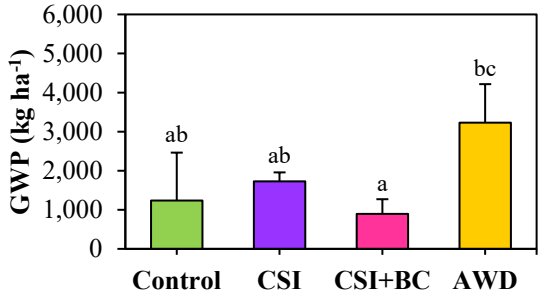

Figure 2. GWP under different treatments. Different letters denote statistically significant differences at $p < 0.05$.

Integrating CSI with BC proved the most successful strategy of diminishing GWP, attaining decreases of 28% and up to 72% relative to the control and other TWW fertigation practices (Fig. 2), respectively, thereby underscoring its strong potential to restrain GHG emissions and promote climate-conscious rice farming.

4. Conclusions

Applying BC in rice production systems irrigated with TWW efficiently cut down GWP and outperformed AWD. Although this CSI+BC treatment significantly suppressed CH_4 emissions, the higher N_2O emissions compared to conventional cultivation indicate that further optimization is needed to balance GHG trade-offs and ensure sustainable rice production over the long term.

References

Fuhrmann-Aoyagi, M.B., Miura, K., Watanabe, K., 2024. Sustainability in Japan's Agriculture: An Analysis of Current Approaches. Sustainability. https://doi.org/10.3390/su16020596

Gao, S., Peng, Q., Liu, X., Xu, C., 2023. The Effect of Biochar and Straw Return on N_2O Emissions and Crop Yield: A Three-Year Field Experiment. Agriculture. https://doi.org/10.3390/agriculture13112091

IPCC, 2021. Climate Change 2021: The Physical Science Basis. Contribution of Working Group I to the Sixth Assessment Report of the Intergovernmental Panel on Climate Change. Contrib. Work. Gr. I to sixth Assess. Rep. Intergov. panel Clim. Chang. 2, 2391.

Loaiza, S., Verchot, L., Valencia, D., Guzmán, P., Amezquita, N., Garcés, G., Puentes, O., Trujillo, C., Chirinda, N., Pittelkow, C.M., 2024. Evaluating Greenhouse Gas Mitigation through Alternate Wetting and Drying Irrigation in Colombian Rice Production. Agric. Ecosyst. Environ. 360, 108787. https://doi.org/10.1016/j.agee.2023.108787

Minamikawa, K., Tokida, T., Sudo, S., Padre, A., Yagi, K., 2015. Guidelines for Measuring CH_4 and N_2O Emissions from Rice Paddies by a Manually Operated Closed Chamber Method. Natl. Inst. Agro-Environmental Sci. Tsukuba, Japan 76.

Phung, L.D., Miyazawa, M., Pham, D.V., Nishiyama, M., Masuda, S., Takakai, F., Watanabe, T., 2021. Methane Mitigation is Associated with Reduced Abundance of Methanogenic and Methanotrophic Communities in Paddy Soils Continuously Sub-irrigated with Treated Wastewater. Sci. Rep. 11, 7426. https://doi.org/10.1038/s41598-021-86925-5

Phung, L.D., Pham, D.V., Sasaki, Y., Masuda, S., Takakai, F., Kaku, N., Watanabe, T., 2020. Continuous Sub-irrigation with Treated Municipal Wastewater for Protein-rich Rice Production with Reduced Emissions of CH_4 and N_2O. Sci. Rep. 10, 5485. https://doi.org/10.1038/s41598-020-62247-w

Yang, shihong, Xiao, Y., Sun, X., Ding, J., Jiang, Z., Xu, J., 2019. Biochar Improved Rice Yield and Mitigated CH_4 and N_2O Emissions from Paddy Field under Controlled Irrigation in the Taihu Lake Region of China. Atmos. Environ. 200, 69–77. https://doi.org/10.1016/j.atmosenv.2018.12.003

Zhao, Y., Jiang, H., Gao, J., Wan, X., Yan, B., Liu, Y., Cheng, G., Chen, L., Zhang, W., 2024. Effects of Biochar Application Methods on Greenhouse Gas Emission and Nitrogen Use Efficiency in Paddy Fields. Sci. Total Environ. 915, 169809. https://doi.org/10.1016/j.scitotenv.2023.169809

Microbial Responses to Metal Oxide Nanoparticles in Composted Sewage Sludge: Implications for Greenhouse Gas Emissions in Paddy Soils

Luc Duc Phung [1,2*], Binh Thi-Thanh Nguyen [3], Anh The Vu [3], Masateru Nishiyama [2], Toru Watanabe [2]

[1] Japan Society for the Promotion of Science (JSPS), Japan

[2] Faculty of Agriculture, Yamagata University, Tsuruoka, Yamagata 997-8555, Japan

[3] Graduate School of Agricultural Sciences, Yamagata University, Tsuruoka, Yamagata 997-8555, Japan

* Corresponding author. Email: lucphung@tds1.tr.yamagata-u.ac.jp

Abstract

The reuse of composted sewage sludge (CSS) offers a sustainable alternative to chemical fertilizers, but the presence of metal oxide nanoparticles (NPs) such as CuO and ZnO may pose risks to soil microbial function. This two-year pot experiment assessed how NP-contamianted CSS affected microbial communities in flooded rice systems. Results showed that CSS application increased total bacterial abundance and enriched copiotrophic phyla, but NP addition reduced bacterial counts by up to 56%, with subtle shifts toward stress-tolerant taxa. Methanogens and nitrifiers were more sensitive to NPs than methanotrophs and denitrifiers, with *Methanobacterium* and *Nitrosophaera* beng dominant in respective groups. NP treatments suppressed methanogen and nitrifier abundance by 2-5 folds but had limited effects on community structure. These microbial shifts could reduce CH_4 emissions while altering nitrification-denitrification balance, raising concerns about potential impaired N cycling in circular fertilizer systems. The study emphasizes the need to monitor microbial responses when applying biosolids containing engineered nanomaterials.

Keywords: Soil microbiome, metal oxide nanoparticles, methane emissions, nitrous oxide, rice paddies, biosolids.

1. Introduction

Composted sewage sludge (CSS) is a sustainable alternative to chemical fertilizers, enhancing soil fertility and closing nutrient loops. However, CSS may accumulate engineered nanoparticles (NPs), such as CuO and ZnO, originated from municipal wastewater, posing risks to soil microbial communities.

Soil microbes play key roles in greenhouse gas (GHG) regulation: methanogens and methanotrophs influence CH_4 fluxes, while nitrifiers and denitrifiers drive N_2O emissions. Disruption of these functional groups by NPs may undermine climate-smart cultivation strategies.

This study investigated the effects of CuO and ZnO NPs in CSS on microbial abundance, diversity, and the functional groups related to CH_4 and N_2O cycling over two years of flooded rice cultivation.

2. Materials and Methods

2.1. Experimental design

A two-year pot experiment (2023–2024) evaluated four treatments: CSS alone, CSS spiked with CuO NPs (1700 mg Cu kg^{-1}; CSS+CuOn), CSS with ZnO NPs (3500 mg Zn kg^{-1}; CSS+ZnOn), and CSS with a mixture of both NPs (CSS+Mix). NP concentrations complied with Council Directive 86/278/EEC (1986) for biosolid reuse. CSS were applied at 160 kg N ha^{-1}.

Rice was grown from May to September each year using standard agronomic practices. Treatments (n=3) were arranged in a completely randomized design in an open-sided greenhouse. Soil samples were collected at pre-transplantation (May 2023) and post-harvest (September 2023 and 2024), then stored at −80 °C.

2.2. Molecular analysis

Soil DNA was extracted from 0.25 g of frozen soil using the DNeasy PowerSoil Kit (QIAGEN, Hilden, Germany), quantified with a Qubit 4 fluorometer (Thermo Fisher Scientific, Waltham, Massachusetts, USA), and stored at −80 °C.

The 16S rRNA gene was amplified using 515f/806r primers and clustered into operational taxonomic unit (OTUs) at ≥97% similarity via Quantitative Insights into Microbial Ecology (QIIME) software package (Phung et al., 2021). Total bacterial abundance was quantified by qPCR (CFX96, Bio-Rad Laboratories, Inc. Hercules, CA, USA), and the relative abundances of methanogens, methanotrophs, nitrifiers, and denitrifiers were calculated from their respective marker genes relative to 16S rRNA gene copies (Phung et al., 2021).

3. Results and Discussion

3.1. Total bacterial abundance and diversity

The initial soil had a 16S rRNA gene copy number of 1.1×10^6 copies g^{-1} soil, which significantly increased to 2.5×10^6 copies g^{-1} soil after CSS application in 2023. However, CuO and ZnO NP contamination reduced bacterial abundance by 44–56%, and this suppression persisted in 2024 (Figure 1), indicating sustained stress on the soil microbiome.

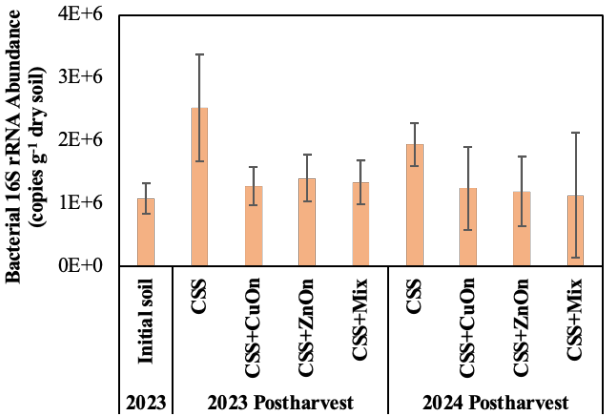

Figure 1. Abundance of bacterial 16S rRNA genes in paddy soils as affected by NP contamination in CSS.

At the phylum level, *Actinobacteriota* (~45–50%) dominated the initial soil. CSS application enriched copiotrophic *Proteobacteria* and *Bacteroidota* while reducing *Actinonacteriota* and *Acidobacteria* (Figure 2). NP treatments did not drastically alter phylum-level

structure, though CSS+CuOn and CSS+Mix showed slightly elevated proportions of stress-tolerant phyla (e.g., *Verrucomicrobiota*, *Chloroflexi*). Diversity indices (Shannon, Simpson, Pielou's Eveness) remained stable, suggesting that NPs reduced total bacterial abundance without major structural disruption.

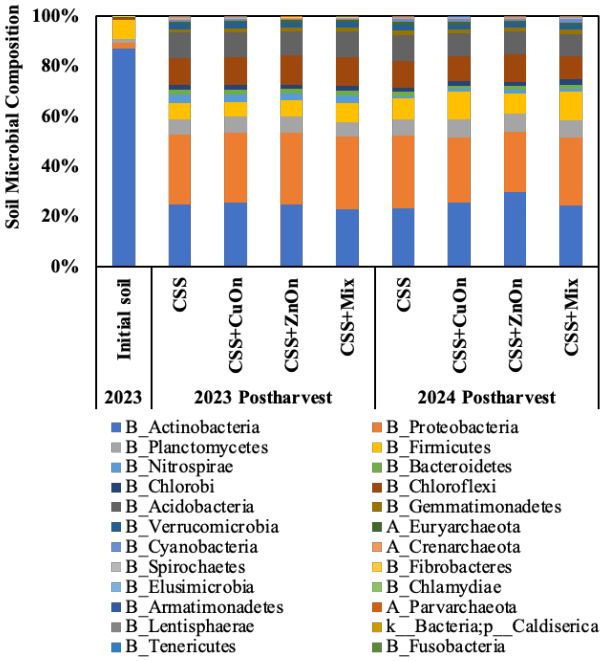

Figure 2. Microbial composition in paddy soils as affected by NP contamination in CSS.

3.2. Methanogenic and methanotrophic communities

Application of CSS markedly increased methanogen abundance from 2.0×10^3 to 2.2×10^4 copies g^{-1} soil in 2023, while NP treatments halved this effect, with CSS+Mix showing the lowest abundance (1.0×10^4 and 8.7×10^3 copies g^{-1} soil in 2023 and 2024, respectively; Table 1). Methanotrophs also increased under CSS (from 1.3×10^2 to 4.0×10^4 copies g^{-1} soil), but NP contamination reduced the population by ~50% (e.g., $1.9–2.2\times10^4$ copies g^{-1} soil), though partial recovery was occurred in 2024, especially under CSS+CuOn (3.0×10^4 copies g^{-1} soil).

Table 1. Abundance of methanogenic and methanotrophic groups as affected by NPs in CSS.

Treatment		Total count (copies g^{-1} soil)	
		Methanogen	Methanotroph
Pre-transplantation		2.0.E+03	1.3.E+02
2023	CSS	2.2.E+04	4.0.E+04
	CSS+CuOn	1.0.E+04	1.9.E+04
	CSS+ZnOn	1.1.E+04	2.2.E+04
	CSS+Mix	1.0.E+04	1.9.E+04
2024	CSS	2.5.E+04	3.5.E+04
	CSS+CuOn	1.5.E+04	3.0.E+04
	CSS+ZnOn	1.1.E+04	1.7.E+04
	CSS+Mix	8.7.E+03	2.8.E+04

Methanogens were dominated by *Methanobacterium*, while initial soils had higher shares of *Methanoregula*. Methanotrophs were consistently dominated by *Methylomonas*, with little variation across treatments. Overall, methanogens were more sensitive to NPs, potentially reducing CH_4 production under the application of contaminated CSS.

3.3. Nitrifier and denitrifier communities

Nitrifier abundance rose from 8.5×10^2 to 1.1×10^5 copies g^{-1} soil under CSS in 2023 but was sharply reduced under NP treatments, down to 7.0×10^3 copies g^{-1} soil under CSS+Mix (Table 2). In 2024, values remained low ($5.3\times10^3–1.3\times10^4$ copies g^{-1} soil. Denitrifiers increased from 2.1×10^4 to 4.9×10^4 copies g^{-1} soil under CSS, and slightly declined under NP treatments ($2.7–3.6\times10^4$ copies g^{-1} soil) across two years. These results suggest nitrifiers are more NP-sensitive than denitrifiers, with implications for nitrification-denitrification balance and potential N_2O regulation.

Table 2. Abundance of nitrifier and denitrifier groups.

Treatment		Total count (copies g^{-1} soil)	
		Nitrifier	Denitrifier
Pre-transplantation		8.5.E+02	2.1.E+04
2023	CSS	1.1.E+05	4.9.E+04
	CSS+CuOn	5.1.E+04	2.7.E+04
	CSS+ZnOn	1.2.E+04	3.3.E+04
	CSS+Mix	7.0.E+03	3.6.E+04
2024	CSS	1.3.E+04	3.5.E+04
	CSS+CuOn	5.3.E+03	3.6.E+04
	CSS+ZnOn	8.1.E+03	2.9.E+04
	CSS+Mix	6.4.E+03	2.8.E+04

AOA (*Nitrososphaera*) dominated nitrifier communities across all treatments, with only minor AOB presence. Denitrifier communities were primarily composed of *Pseudomonas* and *Bradyrhizobium*, with *Pseudomonas* becoming more prevalent under NP contaminated treatments.

4. Conclusions

Metal oxide nanoparticle contamination in composted sewage sludge reduced total bacterial abundance, notably suppressing methanogens and nitrifiers, while methanotrophs and denitrifiers were less affected. These selective shifts may lower CH_4 emissions but risk disrupting N cycling, underscoring the need for caution when reusing nanoparticle-contaminated biosolids in climate-smart agriculture.

Acknowledgements

We gratefully acknowledge the support of the Japan Society for the Promotion of Science for this research.

References

Council Directive 86/278/EEC (1986). Official Journal L 181, 12 June, pp. 6-12.

Phung, L.D., Miyazawa, M., Pham, D.V. et al. (2021). Methane mitigation is associated with reduced abundance of methanogenic and methanotrophic communities in paddy soils continuously sub-irrigated with treated wastewater. Sci Rep, 11, 7426. https://doi.org/10.1038/s41598-021-86925-5

Enhancing Reclaimed Water Usage in Paddy Farming

Hung-Pin Huang [1*], Yin-Chen Huang [2]

[1]Center for Weather and Climate Disaster Research, National Taiwan University, Taipei, 10617, Taiwan (R.O.C.)

[2] Institute for Materials Research (IMR), Tohoku University, Sendai, 9808577, Japan

* Corresponding author. Email: benhuang@ntu.edu.tw

Abstract

Effect of climate change results in frequently occurrence of extremely rainfall and drought events leading to operation pressure on traditional water supply. Paddy fields use large amounts of water and have high water quality requirements. Suitable treatment and satisfying the suggested quality standards of reclaimed water might decrease the pressure of water supply during drought season in Taiwan.

Keywords: Reclaimed water, Paddy field, Quality standard of reclaimed water

1. Introduction

The utilization of water is increasing in Taiwan. The amount of water was 100 billion m^3 in 2007, and 123 billion m^3 in 2024. In which, the highest usage of agricultural water was in 2007. The amount of agricultural water in 2007 was 33.71 billion m^3. The amount of agricultural water in 2024 was 20.80 billion m^3. Even though the percentage of agricultural water to total utilized water drew from 33.66% to 16.88%. The agriculture remains the largest utilizing object of water except hydraulic water.

2. Materials and Methods

The reclaimed water is used for high-leveled water of technology industry in Singapore. Australia, in accordance with the allowable limit for coliform group, separates usage of reclaimed water for both of contacted edible crops and noncontacted ones. In Japan, the reclaimed water is primarily used for toilet flushing and landscaping watering. There are restrictive and non-restrictive groups for urban reclaimed water, as well as contacted and noncontacted for agricultural usage in USA. In China, according to different ranks of sewage treatment, the irrigation crops are separated into three groups: priority recommended, recommended, and not recommended irrigation crops. In Israel, very high-quality reclaimed water for any crop without restrictions, and high-quality one with restrictions.

3. Results and Discussion

The characteristic of wastewater is exploited and then the treatment of wastewater, the considerations of utilizing reclaimed water and quality standard are discussed.

3.1. Characteristic of wastewater

Wastewater physicochemical characteristic includes turbidity, or TSS, TDS, pH, EC, SAR, organic loading such as BOD or COD, and nutrients such as total nitrogen and phosphorus. Excessive salts, organic matter or heavy metals in water will harm the growth of crops, change physicochemical and microbiological characteristics, and may even indirectly affect human health due to the relationship in the food chain.

Effluent without feasible treatment discharges from sewage treatment plant might affect soil properties, crop productivity and lead to serious risks to human health. (Cristina et al., 2015)

3.2. Treatments

Turbidity and coliform groups could be treated with coagulation, sedimentation, filtration, and disinfection. However, high proportion of total dissolved solids and chloride ions could be treated with nanofiltration and reverse osmosis, which are relatively expensive.

3.3. Ammonia nitrogen

Under the controlled conditions of concentrations of metals, toxic substances and organic pollutants, Zhang et al., (2004) used urban drainage water and clean water as irrigation sources to wheat field. The results showed that the yield of wheat irrigated with drainage water increased by 6.5-8.7%. The characteristics of rice affected by nitrogen include excessive growth of rice, excessively wide leaves, excessively long rice stalks, weak stalk joints that are prone to lodging, easy root rot, thick rice husks, reduced rice grain weight, delayed ear formation and reduced rice quality. (Chen, 1996; Hsu, 2005)

Up to now, the concentration of ammonia nitrogen in sewage effluent from Taiwan's water resource recovery center is too high to arrive the quality standard of irrigation water. The project to denitrification by membrane reactor for water reclamation needs to be started as soon as possible.

3.4. Soil salinization

The sodium groups in reclaimed water would be reserved in soil after evaporation or transpiration. Accumulation of sodium might affect the growth condition of crops. Even though drainage scheme in soil reclamation could discharge sodium groups from soil and lead to groundwater pollution. In general, effluent irrigation improves soil quality but risks salinization. (Huang, 2007; Brichi, 2025)

3.5. Organic matter

The high concentrations of organic wastewater could lead to increased ineffective tillering, extended growth period, excessive growth, affecting the development of maturity, resulting in a decrease in grain weight and an increase in the empty shell rate. (Chen, 1996)

3.6. Other sewage source

The diluted slaughterhouse and distillery wastewater which contain much organic matter could be used for farmland irrigation to increase crop yields. Even though some pollutants in wastewater could provide nutrients for crop growth and increase yields, it might also leave toxic residues in various parts of crops, directly affecting the quantity and quality of crops and indirectly harming humans or the soil properties. (Shilpi et al., 2018)

3.7. Stream water

Cho (2024) showed that irrigation water dividing from Shezi Creek caused higher risk of heavy metal, chloride ions and sulfate pollutions in paddy farmland than effluent of Yangmei water resource recovery center. Moreover, suitable arrangement of high proportion of ammonia nitrogen in reclaimed water might decrease usage of nitrogen fertilizers.

3.8. Other pollutants

Lin et al. (2024) got 66 and 30 pollutants from reclaimed water and stream water respectively in Taoyuan County. Medicament was the primary pollutants found in both irrigation waters. Forty-three pollutants were detected only in reclaimed water, including antidepressant sulpiride and sedative carbamazepine. Seven other pollutants, such as caffeine, were found only in stream water due to wastewater contamination.

Besides nitrate nitrogen and heavy metal substance, coliform group and virus need to be deleted from reclaimed water. Combing with UF and UV technology, reclaimed water without virus could be used successfully for agricultural irrigation in Japan.

3.9. Irrigation types

There is no sprinkler irrigation in the paddy fields so that it is not easy for reclaimed water contacting rice. Moreover, rice is not edible directly and need heat-treated or cooked so that it is not necessary to use very high-quality reclaimed water in paddy fields. The reclaimed water with high concentration of ammonia nitrogen might decrease the fertilizer usage by feasible dilution technology. However, farmers need to pay attention to biological, physical, and chemical pollutions.

3.10. Quality standard

With satisfying the quality criteria of pH, residual chlorine, and coliform, reclaimed water could be applied to raw food crops in Australian. In some states of USA, the reclaimed water quality must satisfy the higher criteria of BOD, TSS, turbidity and Fecal Escherichia coli for orchard, processed edible crops, or thick peel crops. The reclaimed water which satisfying lower criteria would be used for irrigation of pasture or ornamental plants.

The quality standard of reclaimed water in Taiwan includes pH, turbidity, TOC (total organic carbon), ammonia nitrogen, residual chlorine, and coliform. And, the reclaimed water is restricted to only use for flushing toilets, landscaping, watering, cleaning, and sprinkling to suppress dust.

Combing with the material of Chen et al. in 2008, The quality standard of reclaimed water applying to paddy fields is suggested:

- Biological items: parasite eggs, E. coli, F. coli, and Coliform.
- Physicochemical items: turbidity, pH, TSS, TDS, SAR, BOD, COD, TOC, ammonia nitrogen, residual chlorine, and persistent organic compounds.

4. Conclusions

In order to promote the utilization of reclaimed water, the following works need to be implemented:

- Accelerating study and develop the denitrification technology to lower down the ammonia nitrogen proportion in reclaimed water.
- Developing a power saving technology on deleting heavy metal substance, virus, and coliform group.
- Constructing public transporting pipe system, tax deduction, high guaranteed purchase price, low-cost water-scarce area to encourage farmers to use reclaimed water. Type your research findings here in the Conclusions section.

References

Brichi, L., Valani, G.P., Lyra, P.G., Gomes, T.M., and Rossi, F., 2025, Slaughterhouse Effluents and Soil Quality: A Review, Green Technologies and Sustainability, 3(4).

Chang, Y.T., Chen, F.W., Cho, Y.C., Tan, Y.W., Lin, H.T., Liu, C.W., Lee, J.J., Huang, H.H., and Zhao, B.H., 2022, Evaluation of the Efficiency of Emission Reduction and Adjustment of the Application of Effluent to Agricultural Irrigation, 2022 Conference of Taiwan Agricultural Engineers Society, 745-754.

Chen, F.W., Chen, S., and Lin H.T., 2008, A Study on Water Quality Standards of Different Targets Demand of Water with Application Reclaim Water, 2008 Conference of Taiwan Agricultural Engineers Society, 90-101.

Chen, H.K., Wang, K.L., and Huang, Y.T., 2007, Current Status of Urban Sewage Treatment Plants in Taiwan and Potential Utilization of Discharged Water, Water Conservation Quarterly, 47:9-21.

Chen, W.C., 1996, Impacts of Organic Wastewater on Crop Yields, Soil and Groundwater Quality, Master thesis, Department of Agricultural Engineering, National Taiwan University.

Chiang, L.C., Liao, C.J., Huang, C.H., and Chen, F.W., 2024, The Effect of Distillery Wastewater on Macroelements in The Sorghum Plant, J. of Taiwan Agricultural Engineering, 70(1):11-23.

Chinese Hydraulic Engineering Society, 2022, Technical code for irrigation with reclaimed water.

Cho, Y.C., 2024, The Feasibility Study of Effluent from Public Sewage Treatment Plants on Irrigated Paddy Field, Master Thesis, Dept. of Civil Engineering, National Taipei University of Technology.

Chou, L., and Ouyang, C.H., 2018, Facing New Challenges and Strategies in Promoting Recycled Water Utilization in Taiwan, CTCI Foundation.

Cristina, B.C, Ana Rita, L., Ivone, V.M., Elisabete, F. S., Célia, M. M. and Olga, C. N., 2015, Wastewater Reuse in Irrigation: A microbiological Perspective on Implications in Soil Fertility and Human and Environmental Health, Environment International, 75:117-135.

Hsu, P.C., 2005, The Effluent Reuse for Agricultural Irrigation from Municipal Wastewater Treatment Plants - A Case Study of the Pa-Li Wastewater Treatment Plant, Master Thesis, Institute of Environmental Engineering and Management, National Taipei University of Technology.

Huang, G.H., 2007, The Safety Use of Treated Waste Water for Irrigation in Agriculture, Renew of China Agricultural Science and Technology, 9(1):26-35.

Huang, T.F., 2008, Israel Water-saving Irrigation Study Report, Tea and Beverage Research Station, MOA.

Li, Y.F., Li, J.H., Zhao, W.X., and Wang, Z., 2015, Review on Irrigation Technology Applying Sewage Effluent—Advances and Prospects, Transactions of the Chinese Society for Agricultural Machinery, 46(6):102-110.

Lin, K.J., Chen, W.L., Liu, C.W., Chen, F.W., Cho, Y.C., Lee, J.J., and Wang, S.L., 2024, Applying High-resolution Mass Spectrometry to Investigating, The Small-molecule Changes in Rice due to Reclaimed Water Irrigation, 2024 Conference of Chinese Environmental Analytical Society.

Qin, G.S., Liu, J., Chen, C., Li, X.Y., Wang, Y.D., Wu, L.M., and Fang, K., 2024, Classified Treatment Technology and Refined Allocation of Reclaimed Water, Agricultural Engineering 14(1):127-132.

Shilpi, S., Seshadri, B., Sarkar, B., Bolan, N., Lamb, D. and Naidu, R., 2018, Comparative Values of Various Wastewater Streams as a Soil Nutrient Source, Chemosphere 192:272-281.

Zhang, C.P., Liu, H.L., Wu, W.Y., Qi, Z.M., Shi, Y.W., 2004, Research on the Utilization of Recycled (Sewage) Water for Irrigation, Beijing Water Resources, 4.

Phytoplankton Community Structure Changes and Occurrence Patterns Associated with Cyanobacterial Blooms in the Upstream Region of Lake Soyang

Seungyun Lee[1] Seonggyeoum Kim[2], Hojeong Yeom[2], Hyejeong Choi[3], Eunmi Hong[4*]

[1]Master's course, Department of Environmental Science, Kangwon National University

[2]Major in Environmental Science, Interdisciplinary Program in Earth Environmental System Science & Engineering, Kangwon National University

[3]Environmental Research Institute, Kangwon National University, Chuncheon, Gangwon state, 24341, Republic of Korea

[4]Associate Professor, Department of Environmental Science, College of Agriculture and Life Sciences, Kangwon National University

* Corresponding author. Email: eunmi.hong@kangwon.ac.kr

Abstract

This study aimed to investigate the temporal variation in phytoplankton community structure and its key environmental drivers in the upstream region of Lake Soyang. Sampling was conducted monthly at eight sites from June to October 2024 and March to May 2025, with biweekly sampling during cyanobacterial bloom periods (June–September). Phytoplankton were identified and counted under a microscope, and environmental variables, including temperature, nutrients, suspended solids, and chlorophyll-a, were measured. Biomass analysis indicated that diatoms (Navicula), cryptophytes (Cryptomonas), and chlorophytes (Scenedesmus) were generally dominant, while cyanobacteria (Dolichospermum, Microcystis) episodically prevailed at Gunchukgyo under high water temperature and nutrient levels. Community structure analysis showed that three upstream sites (Livingston Bridge, Naerincheon, Salgumi Bridge) shared similar assemblages, whereas Gunchukgyo exhibited distinct conditions with elevated water temperature and phosphorus, favoring cyanobacterial dominance. hese results suggest that rising water temperature and nutrient enrichment promote cyanobacterial dominance, directly affecting phytoplankton dynamics. While nutrient inputs have long persisted in the watershed, recent changes in community structure appear primarily driven by warming water temperatures.

Keywords: Cyanobacteria dominance, Nutrient enrichment, Water temperature

1. Introduction

Lake Soyang is a critical drinking water source for the Seoul metropolitan area, yet recurrent cyanobacterial blooms have recently occurred in its upstream region. Such blooms are closely associated with water quality deterioration and ecological imbalance, driven by rising water temperatures due to climate change, nutrient accumulation, and concentrated pollution sources in the watershed. In particular, the large-scale blooms observed in 2023 and 2024 highlighted the urgent need to understand how climatic and watershed changes influence phytoplankton community dynamics.

Therefore, this study aimed to examine the temporal and spatial variations in phytoplankton community structure in the upstream region of Lake Soyang and to identify the key environmental drivers of these changes. The results are expected to improve understanding of bloom formation mechanisms and provide baseline information for water quality management and ecosystem conservation.

2. Materials and Methods

2.1. Study area

Phytoplankton and environmental data were collected from five upstream sites of Lake Soyang: Livingston Bridge (LS), Naerincheon (NR), Salgumi Bridge (SG), Gunchuk Bridge (GC), and Golmal Bridge (GM). The monitoring period covered June to October 2024 and March to May 2025, with one to two surveys conducted per month. During this period, climatic data including precipitation and air temperature were obtained from the Korea Meteorological Administration (Inje-211 station) spanning 2015–2024, providing both long-term averages and 2024-specific records.

2.2. Analysis of Environmental Variables

Water quality parameters were analyzed following standardized procedures. Total nitrogen (TN) and total phosphorus (TP) were determined using UV–Visible spectrophotometry, while biochemical oxygen demand (BOD) and suspended solids (SS) were measured in accordance with the Water Pollution Standard Methods of the Ministry of Environment (2022). Chlorophyll-a (Chl-a) concentration was quantified using the UNESCO protocol.

2.3. Phytoplankton Enumeration and Taxonomic Identification

Phytoplankton samples were preserved with Lugol's iodine solution (1% v/v) and examined under an optical microscope (Olympus, Japan). Enumeration was conducted using the direct counting method, and taxa were identified to the genus level. Phytoplankton were identified to the genus level using established taxonomic references (Cox, 1996; Abé, 1980; Komárek & Zapomělová, 2007, 2008; Komárek, 2013; Li et al., 2000).

3. Results and Discussion

3.1. Phytoplankton Biomass and Relative Abundance

Phytoplankton biomass was predominantly composed of *Navicula* (Bacillariophyceae), *Cryptomonas* (Cryptophyceae), and *Scenedesmus* (Chlorophyceae), which consistently maintained high relative abundance

across most upstream sites.

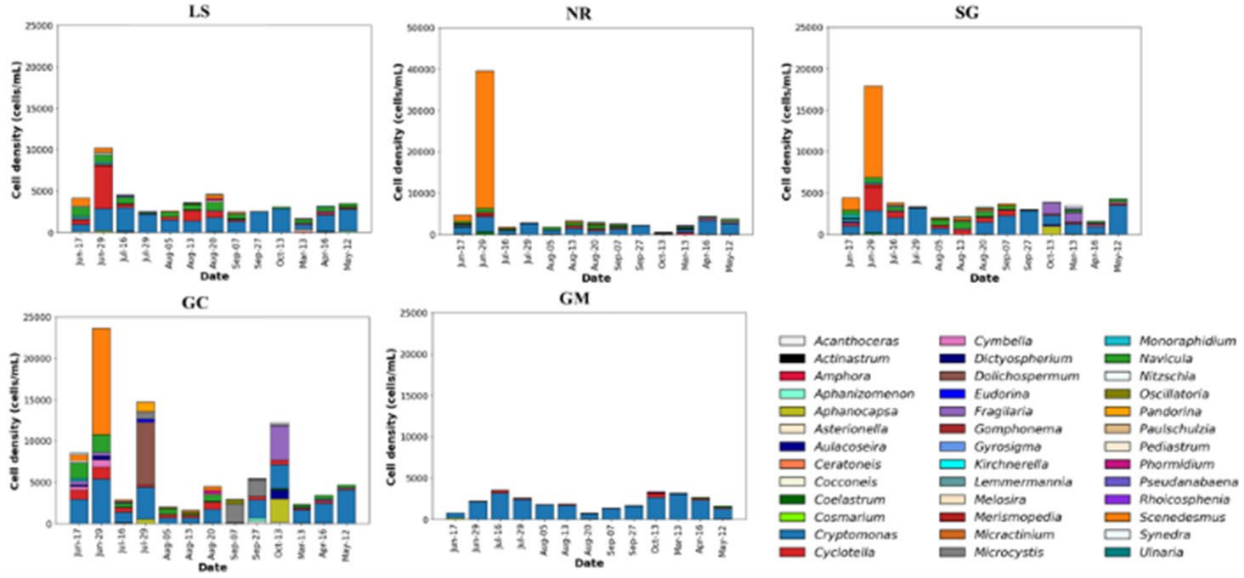

Figure 1. An example of a chart from Excel pasted here using Enhanced Metafile.

In contrast, cyanobacteria displayed episodic dominance at Gunchukgyo. On July 29, 2024, *Dolichospermum* reached 7,610 cells/mL, accounting for approximately 50% of the total assemblage, while on September 7, *Microcystis* attained 2,240 cells/mL, representing nearly 75% of the total community. These shifts indicate a pronounced replacement of diatoms, cryptophytes, and chlorophytes by cyanobacteria under conditions of elevated water temperature and nutrient availability.

3.2. Community Structure and Environmental Associations

Community structure analysis revealed clear spatial differentiation among the upstream sites. Livingston Bridge, Naerincheon, and Salgumi Bridge shared similar phytoplankton assemblages, characterized by the co-dominance of diatoms, cryptophytes, and chlorophytes under relatively stable environmental conditions. In contrast, Gunchukgyo displayed distinct community characteristics, marked by higher water temperature and elevated total phosphorus concentrations. Under these conditions, cyanobacteria such as Dolichospermum and Microcystis exhibited pronounced dominance, replacing other algal groups.

Multivariate analysis confirmed these site-specific patterns, with Gunchukgyo separating from the other upstream sites due to its unique environmental profile. This indicates that localized nutrient enrichment and warming exert strong influence on phytoplankton community composition.

Overall, the results demonstrate that while nutrient loading has been persistent in the watershed, the recent acceleration of warming is a critical driver shifting community structure toward cyanobacterial dominance, thereby altering upstream phytoplankton dynamics.

4. Conclusions

This study demonstrated that phytoplankton community structure in the upstream region of Lake Soyang is strongly influenced by environmental conditions, particularly water temperature and nutrient levels. The increasing dominance of cyanobacteria underscores the need for continuous monitoring and management strategies to mitigate bloom risks in this important freshwater ecosystem.

Acknowledgements

This research was supported by the project “Ecological Survey and Research on the Aquatic Environment of the Upstream Region of Lake Soyang” funded by Korea Water Resources Corporation (K-water), and by the Basic Science Research Program through the National Research Foundation of Korea (NRF), funded by the Ministry of Education (No. 2022R1C1C1010804). We gratefully acknowledge this support.

References

Journal articles:

Komárek, J., Zapomělová, E., 2007. Planktic morphospecies of the cyanobacterial genus *Anabaena* = subg. *Dolichospermum* – 1. part: coiled types. *Fottea*, 7(1), 1–31. DOI: 0.5507/fot.2007.001

Komárek, J., Zapomělová, E., 2008. Planktic morphospecies of the cyanobacterial genus *Anabaena* = subg. *Dolichospermum* – 2. part: straight types. *Fottea*, 8(1), 1–14. DOI: 10.5507/fot.2008.001

Li, R., Watanabe, M.M., Kawachi, M., 2000. Taxonomic studies of water-bloom-forming *Microcystis* (Cyanophyceae) in China with descriptions of new species. *Journal of Phycology*, 36, 981–991

Books;

Abé, T.H., 1980. Studies on the classification of dinoflagellates. Tokai University Press, Tokyo, 300 p.

Cox, E.J., 1996. *Identification of freshwater diatoms from live material.* Chapman & Hall, London, 158 p.

Changes in Phytoplankton Communities in Lake Uiam in Response to Climatic and Hydro-environmental Factors

Seonggyeoum Kim[1], Seungyun Lee[2], Hyejeong Choi[3], Kyongoh Baek[4], Eunmi Hong[5]*

[1] Interdisciplinary Program in Earth Environmental System Science & Engineering, Kangwon National University, Chuncheon, Gangwon state, 24341, Republic of Korea

[2] Department of Environmental science, Kangwon National University, Chuncheon, Gangwon state 24341, Republic of Korea

[3] Environmental Research Institute, Kangwon National University, Chuncheon, Gangwon state, 24341, Republic of Korea

[4] Department of Civil Engineering, Hankyong National University, Anseong, Gyeonggi-do, 17579, Republic of Korea

[5] Associate Professor, Department of Environmental science, Kangwon National University, Chuncheon, Gangwon state, 24341, Republic of Korea

* Corresponding author. Email: Eunmi.hong@kangwon.ac.kr

Abstract

Phytoplankton are key primary producers in freshwater ecosystems and serve as effective bioindicators for evaluating ecological status. They are increasingly recognized as sensitive tools for detecting early signals of environmental change, including climate warming and eutrophication. This study examined shifts in phytoplankton communities in Lake Uiam by comparing data collected a decade apart and analyzing the influence of climatic and hydro-environmental drivers. In 2024, monthly monitoring was conducted from June to November at three sites in the lake. Water quality variables included water temperature, dissolved oxygen, pH, chlorophyll-a, total nitrogen, total phosphorus, phosphate, nitrate, and total organic carbon. Phytoplankton samples were preserved in Lugol's solution, identified to the genus level, and enumerated by direct counting. Historical data from 2014–2015 at the same sites provided a baseline for comparison. Results showed that average phytoplankton abundance increased from ~4,800 cells mL^{-1} in 2014–2015 to 8,400 cells mL^{-1} in 2024. Community composition also shifted markedly: *Fragilaria*, *Cyclotella*, and *Rhodomonas* dominated in 2014–2015, whereas *Cryptomonas* and *Phormidium* were dominant in 2024. These findings suggest a transition from diatom-dominated assemblages under cooler, nutrient-rich conditions to cyanobacteria–cryptophyte communities under warmer, nutrient-enriched environments, highlighting the combined impacts of climate warming, altered inflows, and local anthropogenic pressures.

Keywords: climate change, eutrophication, community structure shift, cyanobacteria, Lake Uiam

1. Introduction

Phytoplankton represent less than 1% of global biomass but play a central role as primary producers in freshwater ecosystems by mediating energy flow and nutrient cycling(Field et al., 1998). They are highly sensitive to water quality factors such as temperature, pH, dissolved oxygen, and nutrients, and respond directly to external changes such as climate variability.

Recent climate change has increased water temperatures, altered precipitation patterns, flow variability, water residence time, and nutrient levels, significantly affecting freshwater ecosystem structure and function. These shifts influence phytoplankton diversity, community structure, and seasonal patterns. In particular, cyanobacteria under warm, nutrient-rich conditions can form harmful algal blooms, releasing toxins, degrading water quality, and posing risks to water management and public health. Thus, understanding phytoplankton dynamics is not only an ecological issue but also crucial for water quality management.

Lake Uiam, part of the North Han River system, is hydrologically connected to upstream dams and downstream reservoirs, making it a strategically important waterbody. However, studies on long-term community shifts and their links with environmental drivers remain limited. This study compares monitoring data from 2014–2015 and 2024 to examine how climatic and hydro-environmental changes have influenced phytoplankton community structures, providing baseline knowledge for ecosystem assessment and management strategies.

2. Materials and Methods

Lake Uiam, formed by the Uiam Dam on the North Han River, receives inflows from Lakes Soyang and Chuncheon and has a watershed of 7,709 km^2 with residence times of 6–11 days. Monitoring was conducted monthly from June to November 2024 at three sites: near the dam (UM1), mid-lake left bank (UM2), and mid-lake right bank (UM3), influenced by urban inflows.

Surface samples (0 m) were collected for in situ water temperature, pH, and dissolved oxygen, with laboratory analyses of chlorophyll-a, total nitrogen, total phosphorus, nitrate, phosphate, and total organic carbon. Phytoplankton were preserved in Lugol's solution, identified to genus level, and counted as cells mL^{-1}.

Taxa were classified using the CSR framework (C, S, R, and mixed strategies)(Reynolds et al., 2002; Reynolds, 2006). Statistical analyses included Spearman correlation to assess community changes and environmental drivers.

3. Results and Discussion

3.1. Climatic characteristics

Meteorological records from 2000 to 2024 indicated a significant warming trend in the Lake Uiam watershed, providing important background for interpreting ecological changes. The annual mean temperature ranged from 10.7 °C to 13.3 °C, with a clear increasing trend observed over the past 25 years, and summer mean reached 25.8 °C in 2024 ($p < 0.001$). While precipitation showed no clear long-term trend, more than half occurred in July–August, reflecting the monsoon climate. Against this background, our comparative analysis of 2014, 2015,

and 2024 revealed that summer warming may be one of the major factors influencing water quality and phytoplankton dynamics in Lake Uiam.

3.2. Phytoplankton community shifts

Phytoplankton abundance revealed distinct interannual contrasts, with average densities ranging from 1,560–8,320 cells/mL in 2014, 2,145–6,467 cells/mL in 2015, and 3,736–14,752 cells/mL in 2024. The highest peak occurred in September 2024 at UM3, reaching 26,116 cells/mL, nearly double the previous maxima. Alongside these quantitative changes, community composition also shifted markedly. While diatoms (Bacillariophyta) dominated in 2014–2015, cryptophytes (Cryptophyta, 36.8%) and cyanobacteria (Cyanophyta, 25.0%) dominated in 2024, indicating a fundamental transition from diatom-based assemblages to cryptophyte–cyanobacteria dominance under warmer and nutrient-enriched conditions. In 2014 and 2015, *Cyclotella* and *Fragilaria* together accounted for more than half of the total cell density, maintaining stable diatom dominance with only short-lived cyanobacterial peaks in summer. In contrast, 2024 was characterized by repeated dominance of *Microcystis*, *Phormidium*, *Dolichospermum*, and *Aphanizomenon*, with cyanobacteria persisting until late autumn. *Cryptomonas* also emerged as a key taxon, further elevating the contribution of cryptophytes. Overall, the 2024 community exhibited simplification, prolonged cyanobacterial dominance, and reduced functional balance compared to the earlier years.

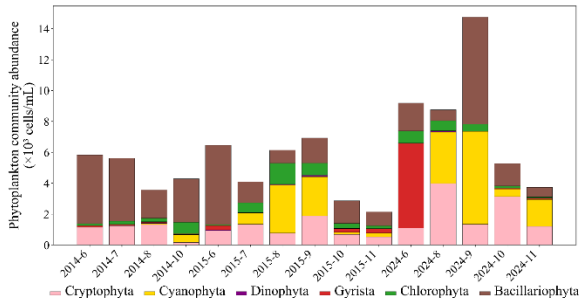

Figure 1. Temporal variations in phytoplankton Community abundance and composition at the phylum level.

3.3. Functional Group dynamics (CSR strategies)

Analysis of phytoplankton functional groups based on the CSR strategy revealed temporal shifts linked to climatic and hydro-environmental changes. In 2014, C (≈44%), S (≈30%), and R (≈27%) strategists were balanced, maintaining diversity. In 2015, R-strategists such as *Cyclotella* and *Aulacoseira* rose to nearly 50%, simplifying the community. In 2024, C (≈46%) and S (≈28%) strategists dominated, driven by *Synedra*, *Phormidium*, and especially *Microcystis*, whose late-summer blooms reduced C contributions. Spearman analysis showed S groups correlated positively with high temperature and negatively with dissolved oxygen, while nitrate favored CS groups. Overall, communities shifted along the CSR spectrum, with warming and eutrophication driving a transition from balanced or disturbance-driven assemblages to C–S dominance, underscoring phytoplankton adaptation under climate change.

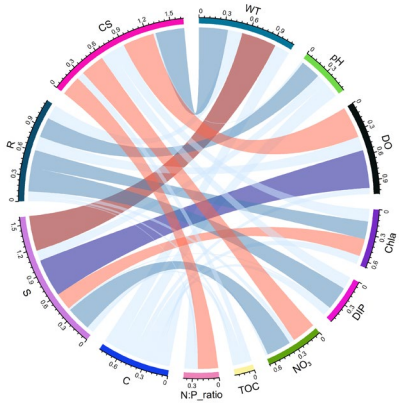

Figure 2. Chord diagram showing Spearman correlations between environmental variables and CSR functional groups of phytoplankton.

4. Conclusions

This study shows that climate change has significantly altered the water environment and phytoplankton community of Lake Uiam. Comparison of 2014–2015 and 2024 data revealed rising water temperatures, shifts in nutrient conditions, and restructuring of community dynamics. Cyanobacteria and cryptophytes increasingly replaced diatom assemblages, reflecting combined effects of warming, hydrological variability, and nutrient loading, heightening risks of harmful algal blooms. Functional group analysis showed a shift along the CSR spectrum, with stress-tolerant and competitive taxa prevailing under high-temperature, nutrient-rich conditions. These findings confirm phytoplankton are sensitive bioindicators of climate-driven ecosystem change. Importantly, they highlight that management strategies must go beyond nutrient reduction to include climate factors such as warming and altered hydrology. Considering both drivers is essential to anticipate ecological risks, protect drinking-water sources, and sustain freshwater ecosystem resilience. This research provides a critical basis for adaptive lake management under accelerating climate change.

Acknowledgements

This study was conducted with the support of the project titled “Investigation and Prediction of Hydraulics, Water Temperature, and Algal Behavior in Uiam Lake Based on the Discharge and Water Temperature Characteristics of Upstream Dams (Chuncheon Dam and Soyanggang Dam)” funded by the Wonju Regional Environmental Office of the Ministry of Environment, Republic of Korea.

References

Field, C. B., Behrenfeld, M. J., Randerson, J. T., & Falkowski, P. (1998). Primary production of the biosphere: integrating terrestrial and oceanic components. *science*, *281*(5374), 237-240.

Kruk C, Mazzeo N, Lacerot G, Reynolds CS. 2002. Classification schemes for phytoplankton: a local validation of a functional approach to the analysis of species temporal replacement. J Plankton Res 24: 901–912.

Reynolds CS. 2006. Ecology of phytoplankton. Cambridge, England: Cambridge University Press (UK), pp. 1–535.

Evaluating the Effect of Near-Surface Soil Moisture Profiles on Microwave Brightness Temperatures Using C-band Radiometry

Kumiko Tsujimoto [1*], Tetsu Ohta [2] , and Ichirow Kaihotsu [3]

[1] Graduate School of Environmental, Life, Natural Science and Technology, Okayama University, Okayama 700-8530, Japan

[2] Assistance Unit for Research and Engineering Development (U-PRIMO), Okayama 700-0016, Japan

[3] Graduate School of Integrated Arts and Sciences, Hiroshima University, Hiroshima 730-8521, Japan

* Corresponding author. Email: tsujimoto@okayama-u.ac.jp

Abstract

Satellite-based microwave remote sensing is widely used to estimate global soil moisture. However, because microwave penetration depth depends on frequency and soil moisture conditions, a persistent challenge in validation studies is identifying the soil depth represented by satellite-observed signals. This uncertainty complicates ground validation and limits algorithm development.

To address this issue, we conducted controlled experiments using C-band observations from the AMSR2 sensor aboard JAXA's GCOM-W satellite. A 1.8 m × 1.8 m plot was filled with weathered granite soil to a depth of 50 cm, with lateral flow restricted by impermeable plates. Soil moisture was measured at 1 cm intervals from the surface to 10 cm depth, and brightness temperatures were recorded with a portable C-band radiometer at both vertical and horizontal polarizations. Numerical simulations employed a process-based radiative transfer model linking soil moisture, dielectric properties, emissivity, and brightness temperature.

Comparisons between simulated and observed brightness temperatures enabled quantitative evaluation of vertical soil moisture distributions. Results show that even subtle near-surface variations significantly influence brightness temperature, underscoring the need to account for vertical heterogeneity in soil moisture retrieval algorithms.

Keywords: soil moisture, remote sensing, observation depth

1. Introduction

Large-scale, continuous monitoring of soil moisture is increasingly recognized as a key measure for addressing climate change. In response, satellite-based microwave remote sensing missions such as NASA's SMAP, ESA's SMOS, and JAXA's GCOM-W have been developed. Because microwaves are minimally affected by clouds and atmospheric water vapor, they provide all-weather observations and are highly effective for global monitoring.

Soil water content modifies the soil's complex permittivity, which determines emissivity; emissivity together with physical temperature defines the brightness temperature. Thus, by observing brightness temperature, soil moisture can be retrieved through radiative transfer models (RTMs). Comparisons between RTM simulations and in-situ measurements allow refinement of the models and improved retrieval accuracy. This study focuses on clarifying which depths of soil moisture and temperature most strongly influence the observed signal.

Microwave propagation in soil is governed by absorption and scattering, both dependent on the vertical distribution of moisture, temperature, and electrical conductivity. Consequently, the depth represented by observed brightness temperature—referred to as the effective penetration depth—varies with frequency and soil conditions, typically ranging from a few to about 10 cm. The objective of this study is to clarify the effects of vertical soil profiles of temperature, moisture, and electrical conductivity on effective penetration depth through combined field and laboratory experiments.

2. Materials and Methods

2.1. Field and laboratory experiments

The field experiment was conducted at Okayama University (Okayama City, Japan). A 1.8 m × 1.8 m plot was excavated to a depth of 50 cm. A permeable weed-control sheet was placed at the bottom, and plywood cutoff boards were installed along the sides to minimize lateral water movement, thereby creating a controlled experimental environment. Weathered granite soil (Masado) was then placed into the plot and lightly compacted to achieve a uniform bulk density.

Within this plot, ten soil moisture and temperature sensors (TDR type, ACC-TDR-315N, Acclima Inc.) were installed at depths from 1 to 10 cm below the surface at 1 cm intervals. These sensors recorded volumetric water content, soil temperature, and electrical conductivity every 10 minutes. Data were collected using a data logger (CR800, Campbell Scientific Inc.) connected to a personal computer. Simultaneously, surface brightness temperatures were observed with a microwave radiometer at 6.925, 7.3, 18, and 36 GHz for both vertical (V) and horizontal (H) polarizations. A photograph of the experimental plot is shown in Figure 1. Based on these data, the effects of vertical soil moisture and temperature profiles on microwave penetration depth were evaluated.

2.2. Numerical simulations

For numerical simulations, dielectric models describing the relationship between soil moisture and complex permittivity were combined with a surface roughness model to compute brightness temperatures

Photo 1. Field experiment setup.

under given soil conditions. Four dielectric models were employed: those proposed by Dobson, Mironov, and Wang & Schmugge, as well as a newly developed model by the authors. The Advanced Integral Equation Model (AIEM) was used for surface roughness. Field observations of soil moisture and temperature at 1 cm intervals from 1 to 10 cm depth served as input data, and brightness temperatures corresponding to each depth were calculated. The simulated results were then compared with observed brightness temperatures obtained from the radiometer.

3. Results and Discussion

Figure 1 shows selected cases of the observed vertical profiles of soil moisture and temperature, and Figure 2 compares calculated microwave brightness temperatures with measured brightness temperatures. In this example, the vertical profile indicates warmer and drier conditions near the soil surface. The calculated H-polarized brightness temperatures at depths of 1 and 2 cm were higher than the observed values, whereas the calculation for 4 cm depth agreed well with observations.

4. Conclusions

This study examined the influence of near-surface soil moisture profiles on microwave brightness temperatures using C-band radiometry combined with field observations and numerical simulations. The results clearly demonstrate that even small variations in vertical soil moisture distribution can produce significant differences in observed brightness temperatures.

These findings highlight the importance of explicitly considering near-surface heterogeneity in soil moisture retrieval algorithms. Conventional approaches that assume homogeneous profiles or use a single representative depth may underestimate the sensitivity of microwave signals to shallow soil layers. Incorporating vertical information into radiative transfer models will therefore improve the physical consistency of retrievals and enhance the accuracy of satellite-based soil moisture products.

Future research should extend this framework by including multi-frequency and multi-polarization analyses, as well as broader field validation across different soil types and climatic conditions. Such efforts will contribute to the development of more robust soil moisture retrieval algorithms and advance the application of satellite microwave observations in hydrology, climate studies, and agricultural management.

Acknowledgements

Meteorological data were obtained from instruments at Okayama University installed under the “Good Practice for Contemporary Educational Needs” program (MEXT, 2007). The authors thank Mr. Kimiaki Satomoto, and Drs. Kazuyoshi Nakata and Koki Katsuhara (Okayama University) for their support with the field experiments. The authors also acknowledge the support received through the provision of observational instruments, namely a data logger from Dr. Jun Asanuma (University of Tsukuba) and a microwave radiometer from Drs. Misako Kachi and Kentaro Aida (JAXA). This study was supported by JAXA (ER3AMF113, ER4AMF103-25RT000181), JSPS KAKENHI (25H00760, 23K26209, 19K04619), the Electric Technology Research Foundation of Chugoku, and the MEXT “Initiative for Realizing Diversity in the Research Environment.”

References

Fujii, H., Koike, T., Imaoka, K., 2009. Improvement of the AMSR-E algorithm for soil moisture estimation by introducing a fractional vegetation coverage dataset derived from MODIS data. J. Remote Sens. Soc. Japan, 29(1), 282–292. https://doi.org/10.11440/rssj.29.282

Njoku, E.G., Kong, J.A., 1977. Theory for passive microwave remote sensing of near-surface soil moisture. J. Geophys. Res., 82(20), 3108–3118. https://doi.org/10.1029/JC082i020p03108

Tsujimoto, K., Ohta, T., Fujii, H., Komatsu, M., 2022. Dielectric behavior of wet soils in the 1-36 GHz microwave range: Modeling and validation. J. Soil Phys., 151(0), 3-24. https://doi.org/10.34467/jssoilphysics.151.0_3

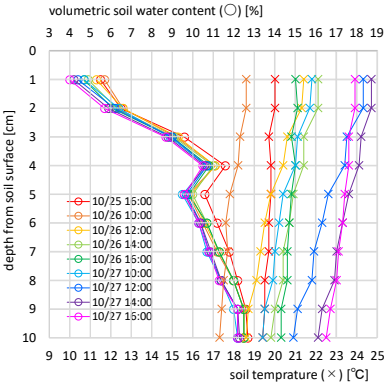

Figure 1. Selected cases of measured vertical profiles of soil moisture (○) and temperature (×), applied to the refinement of the microwave radiative transfer model.

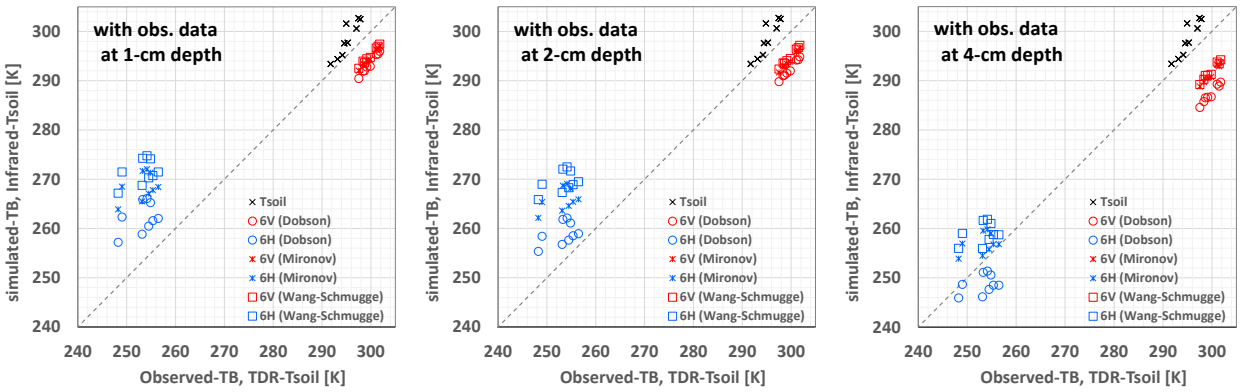

Figure 2. Comparison between observed and calculated brightness temperatures corresponding to measured soil temperature and moisture at different depths (from left: 1 cm, 2 cm, and 4 cm).

Effect of Biomass-Derived Hydrogels as Soil Amendment on Heavy Metal Immobilization in Paddy and Upland Soils

Kung-Hui He [1*], Shu-Yuan Pan [1]

[1] Department of Bioenvironmental Systems Engineering, National Taiwan University, Taipei, Taiwan ROC.

* Corresponding author. Email: jock122002@gmail.com

Abstract

This study developed a magnetic biomass-based hydrogel composed of nano zero-valent iron, chitosan, sodium alginate, and biochar (nZVI/CS/ALG/BC) for the immobilization and removal of heavy metals from contaminated soils. The hydrogel was magnetically modified to enable easy recovery from the soil environment, enhancing its field applicability. Adsorption experiments demonstrated that the material followed pseudo-first-order kinetics, and its isothermal adsorption behavior aligned well with the Langmuir model, indicating monolayer adsorption on a homogeneous surface. The kinetic model showed strong fits, with R^2 values ranging from 0.906 to 0.997. The pseudo-first-order rate constants (k_1) were 0.0035–0.0093 min^{-1} for Cu, 0.0047–0.0080 min^{-1} for Pb, and 0.0023–0.0069 min^{-1} for Cr, suggesting a high affinity for metal ions. As a soil amendment, the hydrogel also improves soil nutrient and moisture retention, reduces agricultural non-point source pollution, and enhances crop and soil health, aligning with sustainable remediation goals. Pot experiments in both paddy and upland soils were conducted to simulate heavy metal immobilization and migration. Concentrations in soil, leachate, plant tissues, and the hydrogel were monitored to assess immobilization performance. Additional tests using contaminated irrigation water were performed to evaluate metal transport among different environmental compartments. Overall, results confirm the hydrogel's potential as a multifunctional material for in-situ remediation and pollution control in agricultural soils.

Keywords: Recycling materials, heavy metals, green sustainable resilient remediation

1. Introduction

Heavy-metal pollution caused by industrial and agricultural activities has become a major threat to soil health and food security. Developing multifunctional, recyclable, and eco-friendly materials is thus essential for sustainable and resilient remediation.

This study developed a magnetic biomass-based hydrogel composite (nZVI/CS/ALG/BC), composed of nano zero-valent iron (nZVI), chitosan (CS), sodium alginate (ALG), and biochar (BC), designed to immobilize and remove heavy metals (Cu^{2+}, Pb^{2+}, Cr^{3+}) in contaminated soils. The material combines several mechanisms: nZVI provides strong reduction and precipitation effects, biochar and the polymer matrix enhance adsorption capacity, and its magnetic property enables rapid recovery and reuse. Beyond conventional one-time agents, this composite also improves soil water and nutrient retention, reduces agricultural non-point source pollution, and promotes overall soil health.

The design follows the concept of Green Resilient Remediation (GRR), emphasizing low energy consumption, renewability, and recyclability. By reducing chemical dependency and secondary pollution risks, the material lowers carbon emissions and supports circular economy principles. Simulated pot and field tests, coupled with mass-balance analysis, reveal heavy-metal transport pathways across the soil–water–plant system, demonstrating its stability and resilience for long-term farmland management.

In conclusion, the nZVI/CS/ALG/BC hydrogel composite shows high adsorption efficiency and strong alignment with sustainable remediation goals. Its scalability, recyclability, and low-carbon footprint highlight its potential as a practical solution for heavy-metal-contaminated farmland.

2. Materials and Methods

2.1. Biomass-Derived Hydrogels

CS/ALG/BC hydrogel beads were prepared by dissolving sodium alginate (1 g) and biochar (1 g) in 100 mL deionized water with 12 h stirring, forming a uniform black solution. Separately, chitosan (1 g) and $CaCl_2$ (0.5 g) were dissolved in 250 mL of 5% acetic acid until clear. The ALG/BC mixture was dropped into the CS/Ca^{2+} solution, where ionic crosslinking between Ca^{2+} and ALG generated spherical hydrogel beads. The beads were collected, washed with deionized water and ethanol, and dried at 60 °C for 24 h. The resulting CS/ALG/BC hydrogels showed high water retention and uniform biochar distribution, providing strong adsorption potential for heavy metals and indicating their applicability in soil remediation. (Facchi et al., 2018; Yu et al., 2024).

To load nZVI, dried CS/ALG/BC beads (1 g) were immersed with PEG-2000 (1 g, dispersant) in 100 mL of 0.1 M $FeSO_4$ solution (ethanol/water = 3:7) for 1 h to allow Fe^{2+} uptake. Under a nitrogen atmosphere, 70 mL of 0.3 M $NaBH_4$ was added dropwise, reducing Fe^{2+} to nano zero-valent iron (nZVI) that deposited within the pores and surfaces of the beads. The composite was washed repeatedly with deionized water and ethanol and dried at 60 °C for 24 h to obtain nZVI/CS/ALG/BC. This material combined the adsorption capacity of hydrogel–biochar with the reductive reactivity and magnetic properties of nZVI, enabling efficient heavy-metal removal and facilitating post-use recovery. (Tarekegn et al., 2021).

2.2. Adsorption test

Batch adsorption experiments were conducted using Cu^{2+}, Pb^{2+}, Cd^{2+}, and Cr^{3+} solutions at concentrations of 100, 200, and 400 mg/L. One gram of nZVI/CS/ALG/BC was added to 100 mL of each solution and stirred under controlled conditions. At intervals (0–240 min), 1 mL aliquots were withdrawn, diluted to 10 mL, filtered, and analyzed by ICP-OES to determine residual metal

concentrations. Adsorption efficiency and kinetic parameters were calculated from concentration changes. Fe release was simultaneously monitored to assess nZVI leaching, providing insights into the composite's structural stability and environmental safety during application.

2.3. Pot Simulation Experiment

Pot experiments were designed to simulate paddy and upland field conditions for evaluating heavy-metal immobilization and transport. In the paddy trial, rice was cultivated for 120 days at ~30 °C. In the upland trial, peanut (cash crop) and pak choi (sensitive crop) were selected. Background heavy-metal levels in soil, irrigation water, and hydrogel were measured before planting. After harvest, heavy-metal concentrations were determined in soil, leachate/runoff, plant tissues, and residual hydrogels to construct mass-balance flow diagrams. Soil nutrients (C, N, P) were also analyzed to evaluate the material's influence on fertility and nutrient cycling, providing a comprehensive assessment of its long-term remediation potential.

3. Results and Discussion

3.1. Biomass-Derived Hydrogels

Although chitosan (CS) and sodium alginate (ALG) can form hydrogels through intermolecular interactions, their network structure is relatively loose, making it difficult to maintain stable spherical beads. To address this issue, this study employed ionic crosslinking between ALG and calcium ions, successfully producing hydrogel beads with improved shape stability. However, the ALG–Ca^{2+} beads still became brittle after drying. To enhance stability, $CaCl_2$ was directly added into the CS solution, enabling rapid bead formation and the development of a dense outer "protective layer." This shell effectively prevented cracking during drying and endowed the beads with reversible swelling ability: dried beads could rehydrate and expand close to their original size. Moreover, nano zero-valent iron (nZVI), when immobilized on the hydrogel surface, naturally developed a thin oxide shell that protected the Fe(0) core from rapid oxidation, prolonging its reactivity. This oxide layer also provided negatively charged sites for electrostatic adsorption of heavy metals, giving the beads their typical reddish-brown appearance after drying, as shown in the core–shell schematic in Figure 1.

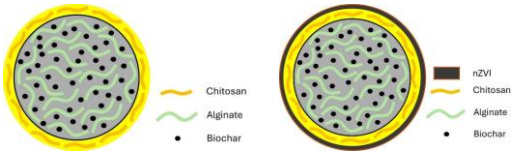

Figure 1. Schematic diagram of the structure of CS/ALG/BC and nZVI/CS/ALG/BC

3.2. Adsorption test

This study evaluated the adsorption behavior of CS/ALG/BC and nZVI/CS/ALG/BC composites toward heavy metal solutions. For CS/ALG/BC, the adsorption of Cu, Pb, and Cr increased with time under initial concentrations of 100, 200, and 400 mg/L. The process was rapid at the beginning, then gradually slowed until reaching equilibrium, with higher initial concentrations enhancing total uptake. A similar trend was observed for nZVI/CS/ALG/BC, which also exhibited fast adsorption followed by saturation, with higher concentrations further improving adsorption capacity. Kinetic analysis showed that both materials fit the pseudo-first-order model, with R^2 values ranging from 0.918–0.996 for CS/ALG/BC and 0.906–0.997 for nZVI/CS/ALG/BC. Isotherm fitting indicated that the Langmuir model provided maximum adsorption capacities (Qmax) of 1.062, 0.278, and 0.743 mmol/g for Cu, Pb, and Cr, respectively, with nZVI/CS/ALG/BC. Meanwhile, the Freundlich model suggested stronger Cu affinity for unmodified CS/ALG/BC, whereas nZVI modification significantly enhanced Pb adsorption.

4. Conclusions

This study successfully prepared structurally stable and magnetic nZVI/CS/ALG/BC hydrogel beads. The addition of $CaCl_2$ to the chitosan solution enhanced bead integrity after drying, improved reversible swelling in water, and promoted the formation of a dense outer layer, increasing durability. Nano zero-valent iron (nZVI) was then loaded onto the bead surfaces and pores, producing a composite with both adsorption and magnetic properties, facilitating subsequent recovery and reuse. Adsorption tests showed that CS/ALG/BC and nZVI/CS/ALG/BC rapidly removed Cu, Pb, and Cr, reaching saturation over time, with higher initial concentrations further improving uptake. Kinetic analysis indicated pseudo-first-order behavior (R^2 = 0.906–0.997), while Langmuir isotherm fitting was optimal (R^2 = 0.997–0.999), yielding maximum adsorption capacities (Qmax) of 1.062, 0.278, and 0.743 mmol/g for Cu, Pb, and Cr, respectively. Freundlich modeling suggested that unmodified CS/ALG/BC favored Cu adsorption, whereas nZVI modification enhanced Pb removal. Future pot experiments will simulate heavy-metal dynamics in soils under resilient remediation and assess the practical restoration potential of the hydrogel material.

References

Facchi, Débora P., André L. Cazetta, Edmilson A. Canesin, Vitor C. Almeida, Elton G. Bonafé, Matt J. Kipper, and Alessandro F. Martins.'New magnetic chitosan/alginate/Fe3O4@SiO2 hydrogel composites applied for removal of Pb(II) ions from aqueous systems', Chemical Engineering Journal, 337: 595-608. (2018)

Tarekegn, M. M., A. M. Hiruy, and A. H. Dekebo.'Nano zero valent iron (nZVI) particles for the removal of heavy metals (Cd2+, Cu2+ and Pb2+) from aqueous solutions', RSC Adv, 11: 18539-51. (2021)

Yu, Kejin, Lina Yang, Siyu Zhang, Hong Song, Shengnan Wang, and He Liu. 'A novel chitosan-based hydrogel microspheres for efficient heavy metal-ion adsorption', Materials Today Communications, 41. (2024)

Cellulose nanofibers boost soil water availability and plant growth under deficit irrigation

Yasushi Mori [1*], An Thuy Ngo [1,2]

[1] Graduate School of Environmental and Life Science, Okayama University, Okayama, 700-8530, Japan

[2] An Giang University – Vietnam National University Ho Chi Minh City, 97000, Vietnam

* Corresponding author. Email: yasushim@cc.okayama-u.ac.jp

Abstract

Water scarcity is a critical constraint on global food security, exacerbated by climate change and rising water demand. Innovative soil amendments are needed to improve water retention, increase irrigation efficiency, and support crop growth under limited water supply. Cellulose nanofibers (CNF), characterized by their nanoscale structure and remarkable hydrophilicity, show promise as sustainable superabsorbent materials. However, their capacity to improve plant-available water (PAW), seed germination, crop growth, and irrigation water use efficiency (IWUE) remains poorly quantified. This study evaluated CNF applications (0–1%) in sandy (MS) and silty loam (PS) soils under three irrigation regimes (100%, 50%, and 25% PAW). Results demonstrated that CNF substantially increased soil PAW (up to 110% in sandy soil and 88% in silty loam at 1% CNF). Germination assays with spinach seeds revealed no phytotoxic effects and significant improvements under water stress, with germination index enhancements up to 214% at I25. Greenhouse experiments showed that CNF enabled plants to maintain growth comparable to full irrigation even with 50% less water. IWUE improved markedly, with maximum gains of 56% under full irrigation, 169% under moderate stress, and 120% under severe stress. Collectively, these findings highlight CNF as a promising amendment for water-limited agriculture, providing a pathway toward climate-resilient and sustainable farming systems.

Keywords: Cellulose nanofibers, available water, plant growth, deficit irrigation, water stress

1. Introduction

Agricultural productivity relies heavily on reliable soil water availability, which underpins nutrient uptake and physiological functioning of plants. Yet, climate change and human activity have intensified drought frequency even in traditionally humid regions, threatening food security. Addressing water scarcity requires strategies that conserve soil moisture and improve crop resilience.

Superabsorbent polymers (SAPs) have been studied for their ability to store and gradually release water. Among them, cellulose nanofibers (CNF) stand out for being biodegradable, renewable, and highly hydrophilic. Their nanoscale fibrillar structure enables high water absorption, but an essential question remains: does the water held within CNF matrices remain accessible to plant roots, or is it trapped at pressures beyond plant uptake capacity? Measuring PAW—the difference between field capacity (FC) and permanent wilting point (PWP)—is therefore critical to evaluate CNF's agricultural utility.

Equally important are the biological effects of CNF. Seed germination is sensitive to water stress and soil amendments, and plant growth under deficit irrigation reflects both soil water retention and physiological tolerance. Moreover, IWUE, which relates biomass to irrigation water used, is a key metric for sustainable farming in water-limited environments. While CNF has been studied for its soil moisture effects, its integrated role in PAW, germination, growth, and IWUE remains underexplored.

This study addressed these gaps by testing CNF-amended soils under multiple irrigation regimes and soil types. Specifically, we examined: (i) changes in PAW; (ii) seed germination percentage and index; (iii) plant growth responses; and (iv) IWUE. By doing so, we aimed to clarify whether CNF could serve as a practical amendment for sustainable crop production in drought-prone regions.

2. Materials and Methods

CNF powders derived from plant pulp were applied at 0%, 0.1%, 0.5%, and 1% by weight to sandy (MS) and silty loam (PS) soils collected in Southeast Asia.

PAW determination was performed using pressure plate and dew point techniques to measure FC (–10 kPa) and PWP (–1500 kPa).

Germination tests used spinach (Spinacea oleracea), a drought-sensitive crop. Ten sterilized seeds per treatment were incubated at three irrigation levels: full irrigation (I100), moderate deficit (I50), and severe deficit (I25). Germination percentage (GP) and germination index (GI) were recorded over 15 days.

Plant growth experiments were conducted in a greenhouse with potted spinach. Irrigation was maintained at I100, I50, or I25 by weighing pots daily. Shoot height and fresh weight were measured after 55 days.

IWUE was calculated as the ratio of aboveground biomass to total irrigation water applied.

Soil microstructure was examined with scanning electron microscopy (SEM). Statistical analyses (ANOVA, regression) assessed treatment effects.

3. Results and Discussion

3.1. PAW enhancement by CNF

Figure 1. shows the plant available water of MS and PS. CNF substantially increased soil PAW by elevating FC more than PWP. At 1% CNF, PAW rose by 110% in sandy soil and 88% in silty loam compared to unamended controls. SEM revealed that CNF filled macro- and mesopores, creating finer pore networks that retained capillary water. Correlation analysis confirmed that CNF dosage strongly influenced PAW and FC, while soil properties contributed more to PWP. These findings establish CNF as an effective water reservoir, releasing moisture in the range accessible to plant roots.

3.2. Effects on seed germination

Under full irrigation, CNF did not significantly increase germination percentage but accelerated

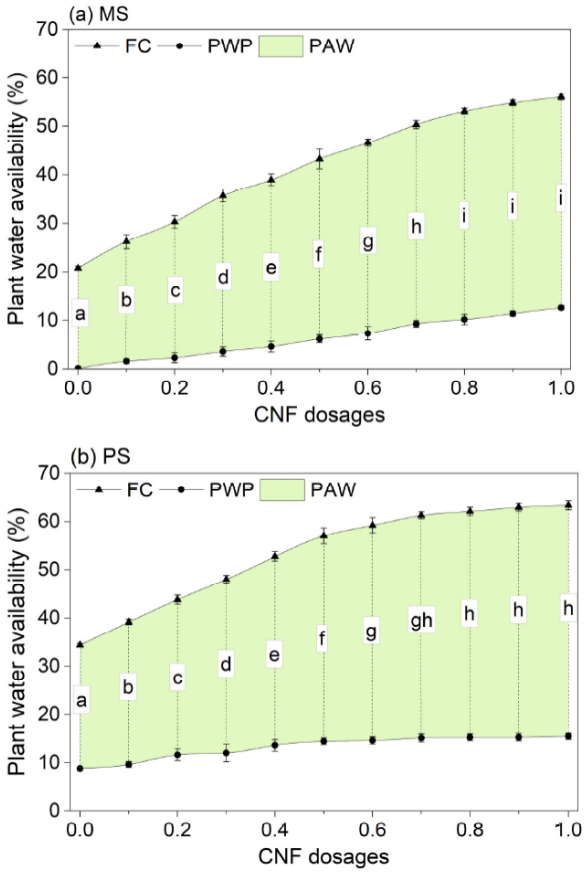

Figure 1. Plant available water of MS (a) and PS (b) improved by CNF. Letters indicate significant differences among treatments (ANOVA, $p < 0.05$). MS, masa soil; PS, paddy soil.

germination speed, confirming its non-phytotoxic nature. Under deficit irrigation, CNF dramatically improved GP and GI. At I50, 1% CNF boosted GP by up to 64% and GI by 163%; at I25, enhancements reached 125% and 214%, respectively. Regression analysis showed that CNF reduced the sensitivity of germination outcomes to irrigation levels, indicating that CNF stabilized moisture availability during early plant development.

3.3. Effects on plant growth

Plant growth declined sharply under deficit irrigation without CNF, with biomass losses of up to 83% at I25. CNF amendments mitigated these effects: at I50, plants with 1% CNF maintained height and weight nearly equal to those under full irrigation, despite receiving 50% less water. Even under severe stress (I25), CNF-treated plants sustained significantly higher growth than controls. These results indicate that CNF helps plants maintain physiological processes under drought by extending soil moisture availability.

3.4. Irrigation water use efficiency (IWUE)

CNF consistently improved IWUE. At 1% CNF, IWUE rose by 56% under I100, 169% under I50, and 120% under I25. These gains show that CNF enables higher biomass production per unit of irrigation water, particularly under deficit regimes. Such improvements are highly relevant in regions facing recurrent droughts, where maximizing crop output with minimal water input is essential.

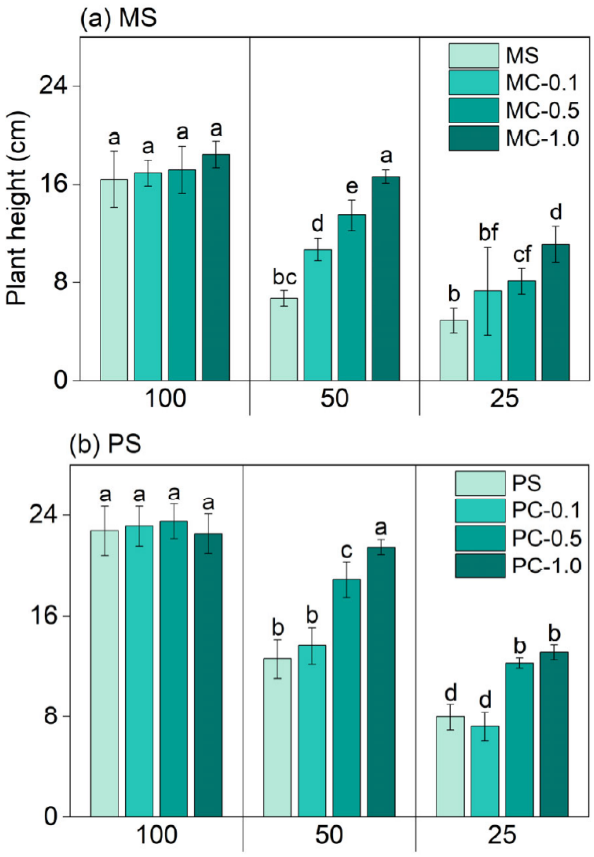

Figure 2. Plant height of MS and PS under various irrigation levels. MS amended with 0.1%, 0.5%, and 1% CNF are referred to as MC-0.1, MC-0.5, and MC-1.0. PS with similar dosages are referred to as PC-0.1, PC-0.5, and PC-1.0, respectively. MS, masa soil; PS, paddy soil.

4. Conclusions

This study provides strong evidence that cellulose nanofibers enhance soil and crop resilience to water stress. CNF significantly increased PAW in both sandy and silty loam soils, improved seed germination under drought, enabled plant growth comparable to full irrigation with 50% less water, and substantially enhanced IWUE. These findings confirm that CNF acts as a multifunctional amendment, simultaneously addressing soil water conservation and crop productivity.

Future research should assess CNF's long-term stability in field conditions, interactions with soil nutrients, and economic feasibility at scale. Nevertheless, this study highlights CNF as a sustainable material with practical potential to support agriculture in water-limited and climate-stressed environments.

Acknowledgements

The authors are grateful to Dr. Jun Kano at Graduate School of Environmental, Life, Natural Science and Technology, Okayama University for his advice on SEM measurement. This study was partially supported by the Japan Society for the Promotion of Science NEXT Program (GS021, 2011–2014), KAKENHI (B) (26292127, 2014–2016), KAKENHI (A) (17H01496, 2017–2020), KAKENHI (A) (21H04747, 2021–2024), and KAKENHI (S) (24H00057, 2024-2028).

Evaluating Evapotranspiration and Irrigation Efficiency in Subtropical Rice Fields under AWD Management

Dong-Hong Wu[1*] Pei-Jhen Wu[2], Hsuan-Ju Tsai[3], Shin-Ruei Lee[2]

[1] Department of Agronomy, National Chung Hsing University, Taichung City, 40227, Taiwan

[2] Crop Science Division, Taiwan Agricultural Research Institute, Ministry of Agriculture, Taichung City, 413008, Taiwan

[3] Agricultural Technology Translation Center, Taiwan Agricultural Research Institute, Ministry of Agriculture, Taichung City, 413008, Taiwan

* Corresponding author. Email: dhwu@nchu.edu.tw

Abstract

Rice cultivation in Taiwan is characterized by a mechanized farming system and a biannual cropping pattern, leading to concentrated water usage. Additionally, increasing competition for water resources due to extreme climate events has frequently resulted in fallow policies. Understanding water demand at different growth stages is crucial for optimizing water resource allocation and ensuring stable rice production. This study was conducted in central Taiwan from 2023 to 2024, with two cropping seasons per year under an alternate wetting and drying (AWD) irrigation system. Prior to the experiment, soil analyses were performed, and microclimate weather stations, water level sensors, and water vapor flux instruments were installed to collect data on water use and actual evapotranspiration (ETc). Reference evapotranspiration (ETo) was estimated using meteorological data to calculate crop coefficients (Kc) and analyze water demand at different growth stages. Results indicated that ETc and ETo increased gradually during the first cropping season with rising temperatures, whereas they decreased in the second season. The crop coefficient showed minor variations across growth stages and cropping seasons, averaging between 0.76 and 0.85. In terms of water balance, rainfall contributed 25% of the total water input in the first season, with irrigation accounting for 75%, while in the second season, rainfall exceeded 50%, with irrigation contributing approximately 41–48%. Regardless of the cropping season, ETc ranged from 352 to 445 mm, accounting for 21–32% of total water input, with the remaining water percolating into the soil, recharging groundwater, or flowing into downstream fields.

1. Introduction

Rice is the most extensively cultivated crop in Taiwan. Although mechanized farming and intensive biannual cropping have increased productivity, they have also resulted in highly concentrated water usage. With the rising frequency of extreme climate events, competition for water resources has intensified, leading to frequent fallow periods. Effective water resource management, particularly understanding the water demand at different rice growth stages, is essential for optimizing water allocation and enhancing production efficiency.

2. Materials and Methods

2.1. Experimental season:

Years: 2023, 2024, **Cropping Seasons**: First season (1st): Mar-Jun ; Second season (2nd): Jul-Oct Location: Central Taiwan (Wufeng District, Taichung City), Variety: Tainung No. 71.

2.2. Water Management:

The Alternate Wetting and Drying (AWD) irrigation model was applied. After irrigating with 5 cm of water, irrigation was resumed the next day when the water level naturally dropped to 0 cm above the soil surface. This process was repeated in cycles. During the drying period, the field was drained for several days, while during the heading stage, the soil surface was kept moist.

2.3. Data Collection and Analysis:

Soil analysis was conducted before the experiment, and microclimate weather stations, flow meters, water level gauges, and water vapor flux equipment were installed to collect water usage and actual evapotranspiration (ETc) data. Meteorological data were combined to estimate reference evapotranspiration (ETo) and calculate crop coefficients (Kc) to analyze water demand at each growth stage and evaluate the water balance.

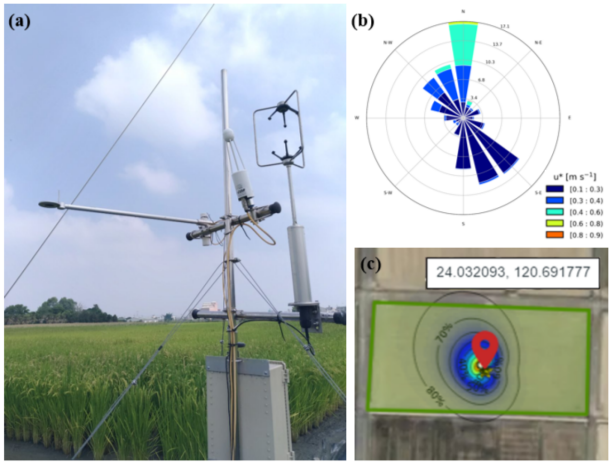

Figure 1. Collection of actual evapotranspiration (ETc) from the experimental field using a water vapor flux instrument (a), observation of wind direction and wind speed (b), and the data collection area (c).

3. Results and Discussion

Rice growth was divided into four stages: Initial, Development, Mid, and Late Season. An analysis of two consecutive years showed distinct patterns in evapotranspiration (ETc) and reference evapotranspiration (ETo). In the first cropping season, ETc and ETo gradually

increased with rising temperatures **(Fig 2a, b)**, with average daily ETc values of 3.44, 4.01, 3.94, and 4.65 mm/day. In the second season, ETc showed a decreasing trend **(Fig 2d, e)**, with averages of 3.95, 4.25, 3.75, and 2.73 mm/day. The crop coefficient (Kc) remained stable across growth stages and seasons, averaging 0.76–0.85**(Fig 2c, f).**

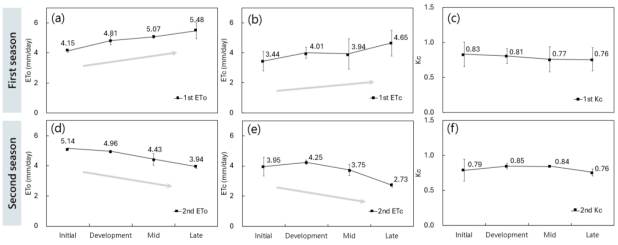

Figure 2. Changes in average reference evapotranspiration (ETo), actual evapotranspiration (ETc), and crop coefficients (Kc) across growth stages.

In terms of water balance (Fig 3), the first cropping season coincided with Taiwan's dry season, during which rainfall accounted for only 25% of the total water input, while irrigation contributed approximately 75% to meet evapotranspiration demands and seepage. This irrigation volume was significantly higher than that of the second season. In contrast, the second cropping season occurred during Taiwan's rainy season, with rainfall contributing over 50% of the total water input, while irrigation accounted for about 41–48%. For both the first and second cropping seasons, evapotranspiration ranged from 352 to 445 mm, representing 21–32% of total water use. The remaining water was utilized for soil infiltration, groundwater recharge, or overflow to downstream areas.

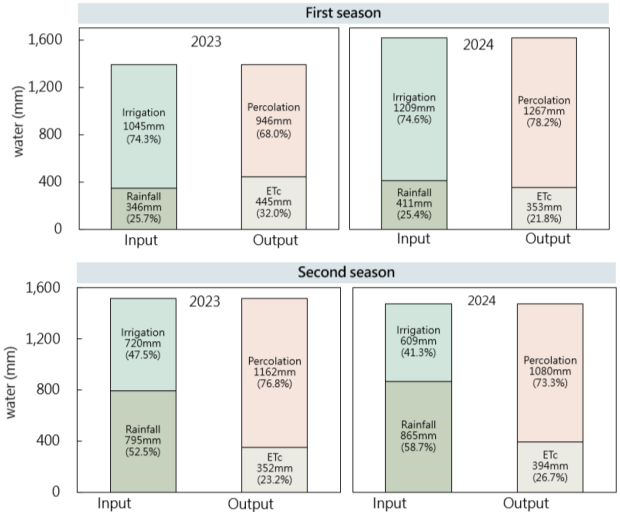

Figure 3. Water Balance for the First and Second Cropping Seasons, 2023-2024.

4. Conclusions

Crop evapotranspiration can be estimated using crop coefficients and meteorological factors. Combined with reservoir storage levels and rainfall forecasts, this serves as a reference indicator for water resource allocation and the implementation of agricultural management strategies.

Impacts of Soil Structure on Gas Diffusivity in Regenerative Agriculture Fields

Yukari Yanagi [1*], Sakai Masaru [1] and Kiyoshi Nagasuga [1]

[1] Graduate School of Bioresources, Mie University, 1577 Kurimamachiya, Tsu, 514-8507, Japan

* Corresponding author. Email: *525m222@m.mie-u.ac.jp*

Abstract

Regenerative agriculture incorporates practices such as cover cropping, reduced tillage, and minimal agrochemical use. Soils under these systems are hypothesized to develop natural structural features—macropores, cracks, and biopores—via root penetration and soil faunal activity. To assess their functional role, we examined soil physical properties, focusing on gas diffusivity. Two sample types were prepared: (1) intact soil cores (100 cm³) from regenerative fields and (2) repacked soils adjusted to the same bulk density but disrupted by sieving (⩽ 2 mm). The gas diffusion coefficient was measured as an indicator of aeration and pore network tortuosity. Soil water retention curves were also analyzed to evaluate water-holding capacity and pore size distribution, with emphasis on macropore volume. Intact soils showed greater macropore volume (>1500 μm) and, especially at wetter matric potentials, higher diffusivity and lower tortuosity than repacked soils. These results highlight the importance of preserving natural soil structure for improved aeration and water retention under regenerative management.

Keywords: Regenerative Agriculture, Soil Gas Diffusivity, Soil Structure

1. Introduction

Maintaining soil health is widely recognized as essential for sustainable agriculture and climate change mitigation. Conventional practices such as intensive tillage and monoculture often degrade soil structure and organic matter, reducing productivity and resilience. In contrast, regenerative agriculture emphasizes practices like reduced tillage, cover crops, and crop diversification, which are known to improve soil physical properties, including hydraulic conductivity, bulk density, and soil structure, as well as increase organic matter and aggregate stability, leading to enhanced water retention (Blanco‐Canqui & Ruis, 2020; Panagea et al., 2021).

Despite these advances, little is known about how regenerative management affects soil gas transport properties, particularly the gas diffusion coefficient (D_p), a key indicator of aeration and microbial activity. This study evaluates D_p and its structural determinants under regenerative practices by comparing intact soil cores with repacked soils in which the natural structure was destroyed, thereby clarifying the role of macropores, cracks, and biopores in soil aeration.

2. Materials and Methods

2-1. Soil Samples

This study targeted three plots from two farms practicing regenerative agriculture. The first is a regenerative plot at the Mie University Farm, where cover crops were first grown in 2024. Soil was sampled on July 3, 2024.

The second and third plots were located in Menno Village Naganuma, Hokkaido: MV2, a converted paddy field planted with clover and orchard grass in its second year, and MV5, a fallow field in its fifth year that underwent shallow tillage to a depth of approximately 5 cm one week prior to sampling. Undisturbed soil cores (100 cm³, 5 cm diameter × 5.1 cm height) were collected at depths of 2.5 cm and 12.5 cm, with three replicates per depth. Disturbed samples were prepared by sieving the same soil (< 2 mm) and repacking it into the same 100 cm³ cylinders at the average bulk density of the corresponding undisturbed samples.

2-2. Experimental Methods

The soil water retention curves of each sample were determined using the hanging water column method, pressure plate method, and dew point potentiometer method. From the obtained curves, the relationship between air-filled porosity and matric potential, as well as the pore size distribution (PSD), were calculated. Air-filled porosity (ε) was determined as $\varepsilon = \theta s - \theta$, with θs denoting saturated volumetric water content and θ the actual volumetric water content. Gas diffusion coefficients (D_p) were measured at selected matric potentials during the water retention curve determination (h = −100, −300, −1000, and h < −1000 cm). **Figure 1** shows the apparatus used for the D_p measurements. After flushing the sealed diffusion chamber with nitrogen gas (initial O_2 concentration C_0), the top plate was opened to initiate diffusion (time t = 0), allowing ambient oxygen (concentration C_i) to diffuse through the soil sample. The increase in O_2 concentration (C) within the chamber was recorded at 15-second intervals using a galvanic O_2 sensor connected to a CR800 data logger. Each measurement lasted approximately 30 minutes.

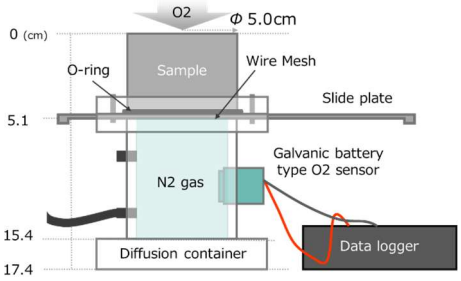

Figure 1 One-chamber apparatus used for measuring the soil gas diffusion coefficient (D_p, cm² s⁻¹).

The gas diffusion coefficient in soil D_p (cm² s⁻¹) was calculated using Currie's non–steady-state diffusion equation **(1)** (Currie, 1960).:

$$\frac{C(L_s,t)-C_i}{C_0-C_i}=\frac{2\varepsilon}{L_a}\cdot\frac{exp\left(-D_p\alpha_1^2\,t/\varepsilon\right)}{L_s\{\alpha_1^2+(\varepsilon/L_a)^2\}+\varepsilon/L_a} \qquad (1)$$

where L_s is the sample height (cm), ε is the air-filled porosity ($cm^3\ cm^{-3}$), L_a is the diffusion chamber height (cm), and α_1 (cm^{-1}) is the first positive root of $\varepsilon / L_s = \alpha\ tan(\alpha L_s)$.

The ratio of the measured diffusion coefficient to that in free air D_0 ($cm^2\ s^{-1}$) was calculated as the relative gas diffusion coefficient D_p / D_0. Furthermore, the tortuosity τ (dimensionless, –) was calculated from D_p / D_0 using the following equation **(2)** (Currie (1960), Ball (1981), Epstein (1989), and Moldrup et al. (2001)):

$$\tau = \frac{L_e}{L_s} = \sqrt{\varepsilon / (D_p / D_0)} \qquad (2)$$

here, tortuosity τ is defined as the ratio of the average capillary tube length, L_e, to the length of the porous media (soil sample), L_s along the major flow (diffusion) axis, in a tortuous (sinuous) capillary tube of uniform diameter. The equation assumes diffusion in a porous medium with pores consisting of tortuous and nonconstricted tubes with uniform and similar diameter.

3. Results and Discussion

Figure 2a (dotted line) shows the relationship between air-filled porosity and the relative gas diffusion coefficient (D_p/D_0) at 2.5 cm depth in the Mie field. In disturbed samples, D_p/D_0 showed a curved increase with porosity, whereas in intact samples it increased linearly, independent of bulk density (ρ_d). At low porosity (wet range), intact soils exhibited higher D_p/D_0 than disturbed ones. **Figure 3 ("Mie Field")** shows the increase in air-filled porosity and pore size distribution from water retention curves. In the wetter matric potential range ($h >$ −100 cm H_2O), intact samples had consistently higher air-filled porosity than disturbed ones. Disturbed soils contained more mesopores (~50 μm) but fewer macropores (>1500 μm).

Tortuosity (τ) patterns in **Figure 2a (solid line)** further highlight these differences. In intact samples, τ remained stable (1.7–2.2) across all ε. Disturbed samples showed very high τ (~15) at low ε, decreasing toward intact values with increasing ε. This indicates that disturbed soils had poorly connected pore networks, causing tortuous pathways, whereas intact soils maintained well-connected, relatively straight pores formed by roots and biopores—features of regenerative soils.

References

Blanco-Canqui, H., & Ruis, S. J. (2020). Cover crop impacts on soil physical properties: A review. Soil Science Society of America Journal, 84(5), 1527 – 1576. https://doi.org/10.1002/saj2.20129

Gulaiya, S., Kumar, M., Kumar, R., Kumar, R., Singh, N., Yadav, K., Singh, S., Kumar, D., & Rajpoot, A. S. (2024). Regenerative Agriculture: Integrating Soil Health, Carbon Management and Socio-ecological Outcomes. International Journal of Environment and Climate Change, 14(9),92–105. https://doi.org/10.9734/ijecc/2024/v14i94395

Currie, J. A. (1960). Gaseous Diffusion in Porous Media Part I—A Non-Steady State Method. British Journal of Applied Physics, 11, 314-317. https://doi.org/10.1088/0508-3443/11/8/302

Moldrup, P., T. Olesen, T. Komatsu, P. Schjønning, and D.E. Rolston. 2001. Tortuosity, diffusivity, and permeability in the soil liquid and gaseous phase. Soil Sci. Soc. Am. J. 65:613–623.

Epstein, N. (1989). On tortuosity and the tortuosity factor in flow and diffusion through porous media. Chem. Eng. Sci. 44:777–779.

Ball, B.C. (1981). Modeling of soil pores as tubes using gas permeabilities, gas diffusivities, and water release. J. Soil Sci. 32:465–481.

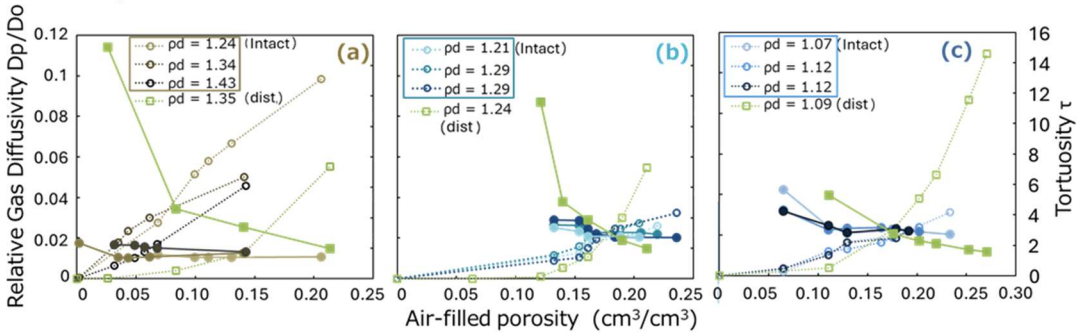

Figure 2 Relative gas diffusion coefficient (Dp/D0, dotted line) and tortuosity (τ, solid line) of disturbed and intact soil cores at 2.5 cm depth in (a) Mie field, (b) MV2, and (c) MV5.

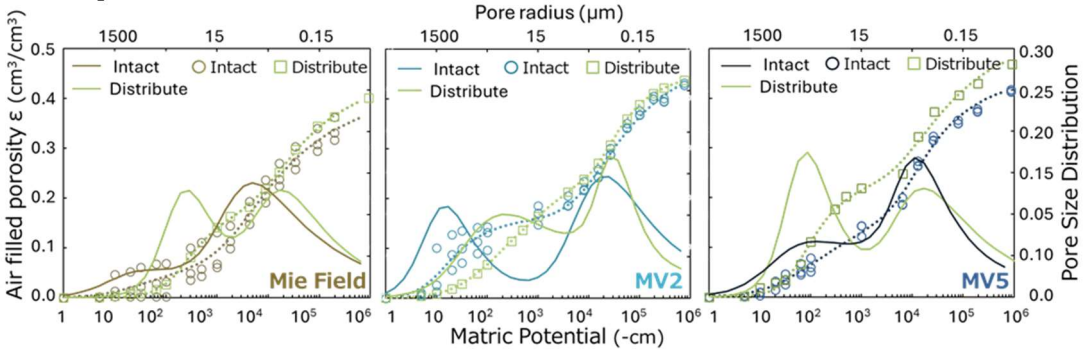

Figure 3 Air-filled porosity ratio and pore size distribution derived from the soil water retention curve for disturbed and intact samples at 2.5 cm depth.

Evaluation of the amount of water erosion by mineral composition

Taku Nishimura [1*], Rin Gonoi[2], Takuhei Yamasaki[1]

[1] Department of Biological and Environmental Engineering, The University of Tokyo, Bunkyo (Tokyo) 113-8657, Japan

[2] Rural Development Bureau, MAFF, Chiyoda (Tokyo) 100-8950, Japan

* Corresponding author. Email: atakun@g.ecc.u-tokyo.ac.jp

Abstract

It is difficult to identify the composition and source of sediments washed away by water erosion. In this study, considering the difference in Plagioclase content between Andisol and crushed basalt, the full pattern summation of X-ray diffraction spectra was used to determine the basalt content of eroded sediments. Andisol, with or without crushed basalt, was filled into a soil box with an 8% slope. Rainfall was applied at an intensity of 60 mm/h for 1 hour using a rainfall simulator, and surface runoff and eroded sediments were collected periodically. X-ray diffraction spectra were obtained using an X-ray diffractometer. The mineral content of the sediments was evaluated using the powdR software with Al_2O_3 as an internal standard. During rainfall events, soils containing 10% and 20% basalt resulted in sediment losses of 44 kg/ha and 59 kg/ha, respectively, for a runoff depth of 1 mm. This corresponds to the basalt loss of 1.8 and 10.2 kg/ha for a runoff depth of 1 mm. These results suggest that by focusing on mineral composition, it may be possible to estimate the source and settling location of sediments.

Keywords: Erosion, X-ray diffraction, full pattern summation, basalt.

1. Introduction

Since it is hard to identify sediments washed away by water erosion. attempts have been made to quantitatively discuss the composition and source of eroded sediments using various tracers such as radioactive elements, rare earth elements, and magnetic properties of minerals (Guzman et al., 2013). There are risks associated with the equipment required for quantification and soil contamination after the evaluation. Kurokawa et al. (2024) reported a quantitative evaluation of mineral compositions of agricultural soils using the full pattern summation of X-ray diffraction spectra. This would enable specific minerals as the safe tracer of soil erosion.

In this study, considering the difference in Plagioclase content between Andisol and crushed basalt, the full pattern summation of X-ray diffraction spectra was applied to determine basalt contents of soil and eroded sediments.

2. Materials and Methods

2.1 Materials

Andisol from Tsukuba, Ibaraki, Japan was mixed with 0, 10, and 20% crushed basalt (Sobue clay Inc.) with a grain size smaller than 0.1 mm. Mineral composition of the Andisol and basalt is shown in Table 1.

2.2 Rainfall experiment

The Andisol was packed into a soil box of 20 cm×50 cm×10 cm with an 8% slope. Simulated rainfall was applied at an intensity of 60 mm/h for 1 hour by using a rainfall simulator. The rainfall simulator sprays pressurized water from a VeeJet 11370 nozzle to produce raindrops. During the rainfall, surface runoff and eroded sediments were collected periodically (Photo 1).

2.3 Analysis of soil loss and mineral composition

After the halt of the rainfall, surface soil was sampled for X-ray diffraction. After oven drying, the mass of the eroded sediments was weighed. Then Al_2O_3 was added as an internal standard, and the mixed sample was finely milled. X-ray diffraction spectra were obtained using Miniflex600 (Rigaku). The mineral content of the sample was analyzed using the powdR software following the methodology outlined by Kurokawa et al. (2024)

Photo 1 Rainfall experiment

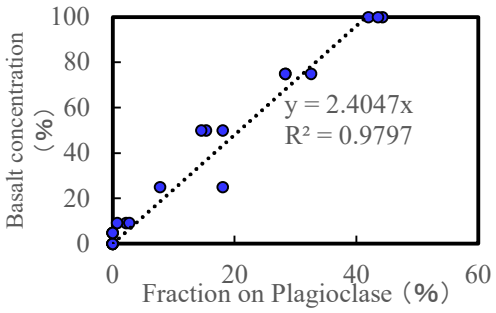

Figure 1 Plagioclase-Basalt relationship

Table 1 Mineral composition of the materials

	Micas	Quartz	Plagioclase	Smectite	Kaolin	Cristobalite	Amorphous	Others
Andisol	22.41	6.15	0.00	3.36	6.90	0.54	58.13	2.50
Basalt	30.35	2.21	43.31	11.12	0.00	4.00	0.00	9.01

3. Results and Discussion

3.1. Estimation of basalt concentration of soil samples

Several minerals showed a strong relationship with the basalt concentration of the soil sample. Plagioclase is relatively easily weathered, and the Andisol did not contain Plagioclase (Table 1). Figure 1 shows the relationship between Plagioclase and basalt concentration in a basalt-Andisol mixture, which yielded the highest regression coefficient. In the following, Figure 1 will be used to estimate the amount of basalt in soil.

3.2. Effects of basalt addition on runoff and basalt loss.

The physical properties of soil often change when materials such as basalt are added in, but in this rainfall experiment, the presence or absence of basalt did not make a significant difference in surface runoff (Figure 2).

Figure 3 shows the sediments discharge as a function of runoff rate. Though runoff rates were similar for with and without basalt addition, sediment discharge increased in the basalt 20% amendment. In addition, Andisol with higher basalt addition showed higher basalt concentration in the runoff (not shown). These could be the size of basalt particles. In this study, basalt was crushed to be equal to or less than 0.1 mm in diameter. This size of particle is, in general, susceptible to being uptaken by surface runoff.

3.3. Evaluation of basalt discharge.

Figure 4 shows the amount of basalt lost for each 1mm of surface runoff. During rainfall events, soils containing 10% and 20% basalt resulted in sediment losses of 44 and 59 kg ha^{-1}, respectively, for a runoff depth of 1 mm. This corresponds to basalt discharge of 1.8 and 10.2 kg ha^{-1} for each 1 mm of runoff.

Basalt was evenly mixed with Andisol; however, after the 60 mm rainfall, the surface soil at the upstream site had less basalt than the downstream site. This suggested that some of the eroded basalt at the upstream could settle down downstream of the soil box (Figure 5).

4. Conclusions

This study demonstrates that basalt concentration in eroded sediments can be fractionated using full-pattern summation of X-ray diffraction spectra with an internal standard. Although basalt discharge is affected by the initial basalt content of the soil, areal or band-shaped basalt application at the upstream of a field would make localized areas of erosion and deposition of basalt within the field. This would help to understand the erosion-sedimentation process of the field.

Acknowledgements

This study was supported by KAKENHI 24K01867.

References

Guzman, G., Quinton, J. N., Nearing, M. A., Mabit, L., Gomez, J. A. 2013 Sediment tracers in water erosion studies: current approaches and challenges. J Soils Sediments, 13, 816–833, doi.10.1007/s11368-013-0659-5

Kurokawa, K., Azuma, K., Nakao, A., Suzuki, A., Wakabayashi, S., Fujimura, S., Yanai, J. 2024 Examination of the reliability of X-ray powder diffraction analysis to determine mineral composition of soils. Soil Sci. Soc. of Am. J., 88(6), 1942-1958, doi.10.1007/s11368-013-0659-5, doi.org/10.1002/saj2.20757

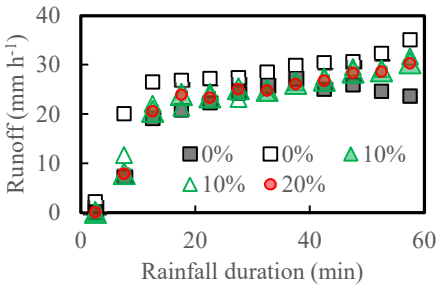

Figure 2 Basalt contents in eroded sediments during rainfall. The number in the figure is basalt addition.

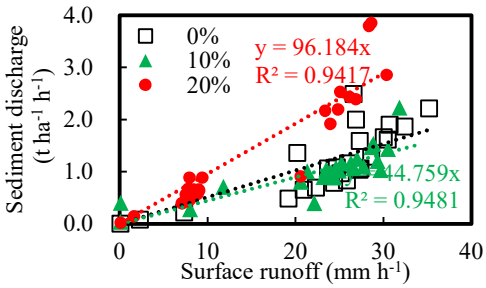

Figure 3 Sediment discharge during rainfall. The number in the figure is basalt addition.

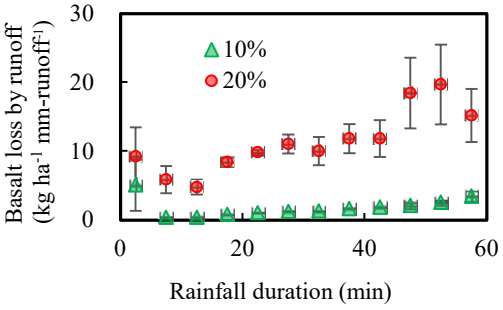

Figure 4 Amount of basalt lost per 1mm of surface runoff. The number in the figure is basalt addition.

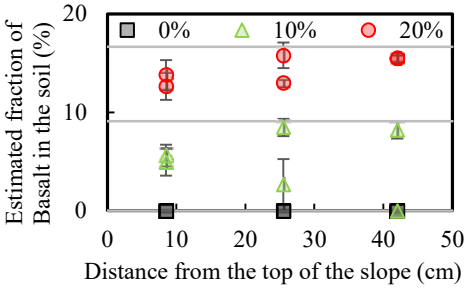

Figure 5 Basalt concentrations of surface soil after the rainfall experiment. The number in the figure is the basalt addition.

A Systematic Review of Lumped and Conceptual Rainfall-Runoff Models: Performance, Hybridization, Uncertainty and Data Integration

Rahmon Abiodun Salau[1]*, Qudus Adeyi[1], Adisa Hammed Akinsoji[1], Kyung Sook Choi[1,2,*]

[1] Department of Agricultural Civil Engineering, Kyungpook National University, Daegu 41566, Korea

2 Institute of Agricultural Science & Technology, Kyungpook National University, Daegu 41566, Korea

* Corresponding authors. ks.choi@knu.ac.kr

Abstract

This systematic review examines recent advances in lumped and conceptual rainfall–runoff models, focusing on their performance, calibration, validation, uncertainty treatment, and the emergence of hybrid approaches. Using the PRISMA protocol, forty-six studies published between 2019 and April 2025 were analyzed. Lumped models remain dominant, particularly HBV, GR4J, and AWBM, with Iran leading their application. The reviewed studies span 21 countries and 12 climate groups, most commonly semi-arid and temperate oceanic basins. Hybrid models represent 27% of studies, indicating a rising trend toward combining physical and data-driven approaches. Calibration practices vary, with manual, heuristic, and Bayesian methods coexisting, while validation remains weak—72% of studies use simple split-sample tests, and fewer than 10% employ cross-basin or spatio-temporal validation. Uncertainty assessment focuses largely on parameters, neglecting structural and input-related sources. Performance evaluation relies heavily on NSE, RMSE, and KGE, offering limited diagnostic insights into low-flow or bias-related errors. Overall, the field shows progress in hybridization and calibration sophistication but continues to lag in validation rigor and comprehensive uncertainty analysis. Future work should pursue integrated frameworks that balance interpretability, predictive accuracy, and robust uncertainty quantification to improve hydrological modelling under changing climate and land-use conditions.

Keywords: Rainfall-runoff modelling, lumped conceptual models, hybrid approaches, model calibration, uncertainty quantification, climate change adaptation

1. Introduction

The escalation of anthropogenic activities, coupled with rapid population growth, poses unprecedented challenges for managing water resources, particularly in agricultural regions that are highly vulnerable to climate change (Granata and Di Nunno, 2025). In numerous regions, particularly those characterized by arid and semi-arid climates, water scarcity has emerged as a critical concern due to both limited natural availability and increased demand, predominantly for irrigation purposes (Morante-Carballo et al., 2022). The accelerating pace of climate change further aggravates these challenges by altering hydrological patterns, reducing renewable water resources, and intensifying the occurrence of floods and droughts (Dixit et al., 2022). Consequently, accurate estimation and comprehensive understanding of water resources and their complex interactions are essential, particularly regarding runoff estimation and forecasting (Akbulut et al., 2023).

Rainfall-runoff (RR) models are broadly classified into three categories: physics-based models, physical-conceptual or "gray-box" models, and machine learning (ML) or "black-box" models (Jahanshahi et al.). Despite the development of a broad range of RR models, lumped conceptual models still underpin the field because they strike a balance between simplicity, interpretative value, and flexibility in the face of scarce hydrological data (Kant et al., 2025). Hybrid strategies that integrate physics-based or conceptual models with machine learning approaches have emerged as a promising way forward, offering improved predictive performance while retaining elements of physical interpretability (Kapoor et al., 2023). To provide a transparent and comprehensive synthesis of this evolving research landscape, this review systematically examines the performance, calibration practices, hybridization approaches, and data-integration strategies associated with lumped conceptual RR models following the PRISMA framework (Moher et al., 2010).

2. Materials and Methods

2.1. Literature Search Strategy

This study reviews lumped-conceptual models used for simulating runoff, discharge, reservoir inflow, or streamflow, with a particular focus on agricultural watersheds. A systematic approach was followed using the PRISMA framework, focusing on studies that applied lumped-conceptual rainfall-runoff models as base models. The Scopus database was selected as the primary source for literature retrieval. A structured Boolean search strategy combined terms such as "rainfall-runoff modelling," "conceptual models," "streamflow prediction," "calibration," and performance metrics like "Nash-Sutcliffe" and "Kling-Gupta."

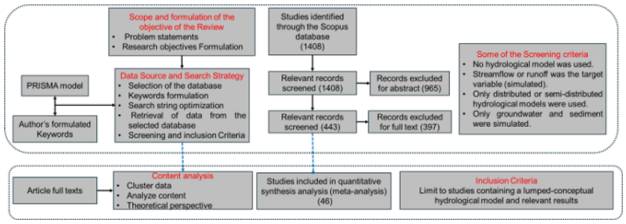

Fig. 1. Flowchart of the PRISMA technique

2.2. Selection Criteria

The search yielded 1,408 peer-reviewed articles published between 2019 and April 2025 in English. After screening through abstracts and excluding papers with distributed or semi-distributed models only, or those not focused on streamflow/runoff as the target variable, forty-six studies were selected based on relevance and data availability for comprehensive analysis.

3. Results and Discussion

3.1. Geographic and Climate Distribution

Twenty-three countries from six continents contributed to the reviewed literature, with Iran and South Korea as the largest contributors. The Köppen-Geiger climate classification revealed twelve distinct climate types, with hot semi-arid climate (BSh) demonstrating clear dominance at 47% occurrence, followed by temperate oceanic climate (Cfb) at 27%. Medium-sized watersheds (250-2500 km²) accounted for 72.5% of study areas, reflecting a focus on basins that balance hydrological complexity with management feasibility.

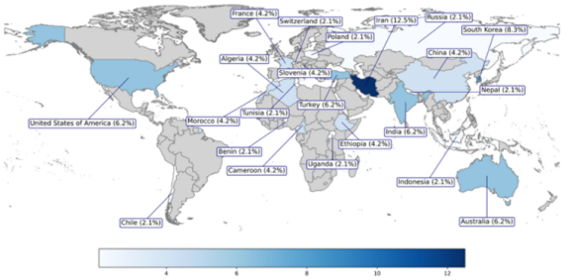

Fig.2.: Spatial Distribution of Reviewed Articles

3.2. Model Performance and Evaluation

GR4J, HBV, TANK, AWBM, IHACRES, and SIMHYD emerged as the most frequently applied lumped conceptual models. Hybrid models accounted for 27% of studies, demonstrating their growing prominence. Performance evaluation relied predominantly on NSE, RMSE, and KGE metrics. Conceptual models showed highest effectiveness in humid subtropical monsoon (Cwa, NSE = 0.85) and Mediterranean (Csa, NSE = 0.90) climates, while hybrid models consistently outperformed other types across all scales, achieving mean NSE of 0.84 in medium basins.

3.3. Calibration and Optimization

Manual calibration methods (24 occurrences) remain prevalent in lumped-conceptual models, though heuristic methods (12 occurrences) are increasingly adopted. Automated methods (14 occurrences) dominate data-driven models, while Bayesian approaches (9 occurrences) excel at uncertainty quantification. Optimization strategies include gradient-based (13), heuristic/metaheuristic (15), and hybrid methods (5), reflecting the field's shift toward systematic parameter estimation.

3.4. Validation and Uncertainty Assessment

Standard split-sample testing remains the most common validation approach (72% of studies), with only 10% adopting cross-basin or spatio-temporal protocols. Uncertainty assessment is dominated by parameter analysis (7 occurrences), while structural (5), input-related (4), and climate scenario uncertainties (3) remain underexplored. This reveals significant methodological gaps in validation robustness and comprehensive uncertainty treatment

4. Conclusions

This review underscores the persistent importance of lumped conceptual rainfall-runoff models while highlighting critical methodological transitions. The growth of hybrid approaches combining conceptual frameworks with machine learning represents a promising advancement, offering enhanced predictive performance with retained physical interpretability. However, validation practices remain disproportionately reliant on traditional split-sample testing, and uncertainty analysis concentrates on parameter ranges while neglecting structural, input, and scenario-related dimensions. Future progress requires embracing methodological pluralism through expanded ensemble and Bayesian methods, strengthened spatio-temporal validation protocols, and broader uncertainty treatment. Greater exploitation of emerging data streams from remote sensing, combined with strategic hybridization approaches, can enhance adaptability across hydroclimatic regions and deliver more reliable decision-making tools under climate and land-use change.

Acknowledgements

This work was supported by the National Research Foundation of Korea(NRF) grant funded by the Korea government(MSIT)(RS-2025-00562379).

References

Akbulut, U., Cifci, M.A., Aslan, Z., 2023. Hybrid Modeling for Stream Flow Estimation: Integrating Machine Learning and Federated Learning. Applied Sciences (Switzerland) 13. https://doi.org/10.3390/app131810203

Dixit, A., Madhav, S., Mishra, R., Srivastav, A.L., Garg, P., 2022. Impact of climate change on water resources, challenges and mitigation strategies to achieve sustainable development goals. Arabian Journal of Geosciences 15. https://doi.org/10.1007/s12517-022-10590-9

Granata, F., Di Nunno, F., 2025. Pathways for Hydrological Resilience: Strategies for Adaptation in a Changing Climate. Earth Systems and Environment. https://doi.org/10.1007/s41748-024-00567-x

Jahanshahi, A., Asadi, H., Gupta, H., 2025. A data fusion approach to enhancing runoff simulation in a semi-arid river basin. Environmental Modelling and Software 190. https://doi.org/10.1016/j.envsoft.2025.106468

Kant, C., Meena, R.S., Singh, S.K., 2025. A Critical Appraisal on Various Hydrological and Hydrodynamic Models. Water Conservation Science and Engineering. https://doi.org/10.1007/s41101-024-00328-x

Kapoor, A., Pathiraja, S., Marshall, L., Chandra, R., 2023. DeepGR4J: A deep learning hybridization approach for conceptual rainfall-runoff modelling. Environmental Modelling and Software 169. https://doi.org/10.1016/j.envsoft.2023.105831

Morante-Carballo, F., Montalván-Burbano, N., Quiñonez-Barzola, X., Jaya-Montalvo, M., Carrión-Mero, P., 2022. What Do We Know about Water Scarcity in Semi-Arid Zones? A Global Analysis and Research Trends. Water (Switzerland). https://doi.org/10.3390/w14172685

Moher, D., Liberati, A., Tetzlaff, J., Altman, D.G., 2010. Preferred reporting items for systematic reviews and meta-analyses: The PRISMA statement. International Journal of Surgery 8, 336–341. https://doi.org/10.1016/j.ijsu.2010.02.007

On the Optimal Configuration of a Distributed Hydrological Model subject to Different Grid Sizes and Lateral Boundary Conditions

Chia-Jeng Chen [1*], Jian-Jun Liu [1]

[1] Department of Civil Engineering, National Chung Hsing University, Taichung 402, Taiwan

* Email: cjchen@nchu.edu.tw

Abstract

Determining the most adequate grid size and lateral boundary conditions (e.g., land use and soil texture) is critical to distributed hydrological modeling, as they can exert significant influence over various hydrological processes, such as surface runoff generation, infiltration, and groundwater recharge. To enhance model performance in predicting river streamflow, this study assesses multiple configurations of a distributed hydrological model referred to as the Weather Research and Forecasting Hydrological modeling system (WRF-Hydro) in the Gaoping River Basin, southwestern Taiwan. This assessment encompasses three routing grid sizes (i.e., 100, 200, and 400 m), two land use scenarios (i.e., model default and survey data), two soil texture scenarios, and four rainfall amount categories, yielding a total of 48 distinct WRF-Hydro configurations. Observed rainfall data obtained from the Quantitative Precipitation Estimation and Segregation Using Multiple Sensors (QPESUMS) is used to drive WRF-Hydro for the assessment. As indicated by selected performance metrics evaluated between modeled and observed streamflow, we find that the effect of grid sizes is considerably more substantial than that of lateral boundary conditions. Specifically, the finer (100-m) and coarser (400-m) grid resolutions result in overestimated and underestimated streamflow, respectively, and the bias is proportional to the rainfall amount. The effect of lateral boundary conditions on streamflow reveals a prominent spatial discrepancy: The downstream and upstream regions demonstrate increased variability in streamflow simulations, attributable to alterations in land use and soil texture, respectively.

Keywords: WRF, WRF-Hydro, Coupled modeling

1. Introduction

Owing to the advancement of computational resource and availability of geospatial data, the resolution of various datasets serving as hydroclimatic model lateral boundary conditions (e.g., land use, soil texture, and elevation) has become increasingly refined and can significantly influence simulation accuracy (Bormann et al., 2009). In this context, distributed hydrological models have been evolving towards high to ultra-high resolutions (e.g., < 1 km) to better represent topographic variations, hydrological processes, and river network structures (Hoch et al., 2023). However, the benefits of increasing resolution are contingent upon topographic conditions (Aerts et al., 2022). Although improving soil moisture simulation and energy partitioning, higher resolution (i.e., smaller grid sizes) increases computational costs and may further induce modeling errors if the model structure and parameterization schemes are not adapted to the resolution (Shrestha et al., 2015). The coordination between high-resolution input data and model resolution, as well as the extent to which resolution settings affect simulation performance, remains insufficiently analyzed. This study thus aims to address this gap by applying the Weather Research and Forecasting Hydrological modeling system (WRF-Hydro) forced with high-resolution precipitation data to examine how different flow routing grid sizes and lateral boundary conditions affect streamflow simulation in the Gaoping River Basin (GRB), southwestern Taiwan.

2. Materials and Methods

2.1. Materials

2.1.1. QPESUMS

Precipitation data used in this study is the Quantitative Precipitation Estimation and Segregation Using Multiple Sensors (QPESUMS) system, developed by the Central Weather Administration (CWA) of Taiwan. This product is at a spatial resolution of 1 km and a temporal resolution of 10 minutes (Chang et al., 2021). The operational radar products employ a multi-radar variable synthesis technique that combines precipitation rate relationships derived from radar parameters such as reflectivity (Z), specific attenuation (A), and specific differential phase (K_{DP}). This approach accounts for the respective advantages and limitations of different radar variables under various precipitation conditions to enhance the accuracy of precipitation estimation.

2.1.2. Land use

The land use data employed in this study was obtained from the 2015 land use dataset published by the National Land Surveying and Mapping Center (NLSC) of Taiwan. This dataset was developed based on high-resolution aerial imagery, cadastral maps, and the Taiwan Geospatial One-Stop (TGOS) electronic map, complemented by partial field surveys. The NLSC classifies land use types across Taiwan into ten categories.

2.1.3. Soil texture

The soil texture data used in this study was developed by the Taiwan Agricultural Research Institute, Ministry of Agriculture. This dataset comprises 12 soil categories with a spatial resolution of 90 m. To enable its application in the WRF model, the soil texture was resampled to a resolution of 30 arc-seconds.

2.2. Methods

2.2.1.WRF-Hydro

In this study, WRF-Hydro was operated in stand-alone mode, driven by externally provided forcing files and static terrain data. The core land surface model (LSM) was Noah, which simulates the energy and water balance between the land surface and soil layers. Three routing grid resolutions, namely 100 m, 200 m, and 400 m, were configured in correspondence to the aggregation factors of

20, 10, and 5, respectively. According to the WRF-Hydro user manual, the routing model time step should be properly adjusted based on the spatial resolution to ensure numerical stability during simulations. The model configuration is summarized in Table 1.

Table 1. WRF-Hydro model configuration

Configuration option	Value/Option specified
Forcing time step	3600 (s)
Noah time step	3600 (s)
Output time step	3600 (s)
Sub-grid size	100, 200, 400 (m)
Routing model time step	6, 12, 24 (s)
Aggregation factor	20, 10, 5
Subsurface routing	On
Overland flow routing	On
Channel flow routing	On
Baseflow bucket model	On

2.2.2.Selected event

Based on the 24-hour accumulated precipitation from the nearest QPESUMS grid points to seven streamflow gauges in the GRB, daily accumulated rainfall events from 2016 to 2021 were classified into four categories: (1) 80–200 mm, (2) 200–350 mm, (3) 350–500 mm, and (4) >500 mm. Rainfall events corresponding to the four categories are listed in Table 2. Fig. 1 shows the spatial patterns of precipitation for the four selected events, highlighting the variations in rainfall intensity and location over the GRB.

Table 2. Selected rainfall events corresponding to four rainfall categories.

Date	Rainfall Category	Type
2016/06/13	80–200 mm/24 hr	Southwesterly flow
2017/07/31	200–350 mm/24 hr	Typhoon Haitang
2018/08/23	350–500mm/24 hr	Tropical depression
2021/08/07	>500 mm/24 hr	Typhoon Lupit

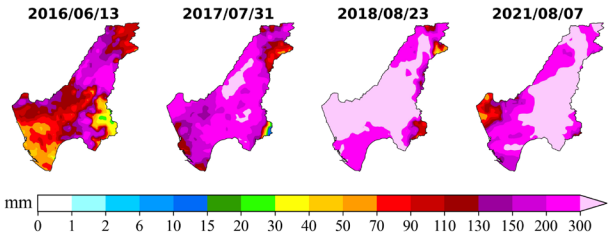

Fig. 1 Rainfall patterns of the four selected events in the Gaoping River Basin.

3. Results and Discussion

Figs. 2 and 3 present the streamflow hydrographs at the Dajean and Nanxiong stations in the GRB. Red, green, and blue lines represent routing grid sizes of 100 m, 200 m, and 400 m, respectively, with each color further divided into different input-data combinations (model default, land use updated, soil texture updated, or both updated). Results show that changes in the input-data combinations only exhibit a moderate effect on streamflow, whereas differences in the model grid sizes can result in substantial variations in streamflow. The higher impact of the model grid sizes on streamflow simulation is likely owing to the explicit scheme of WRF-Hydro in modeling overland and channel flows; the varying resolutions directly alter the aggregation of water volume and numerical integration, thereby affecting the total discharge.

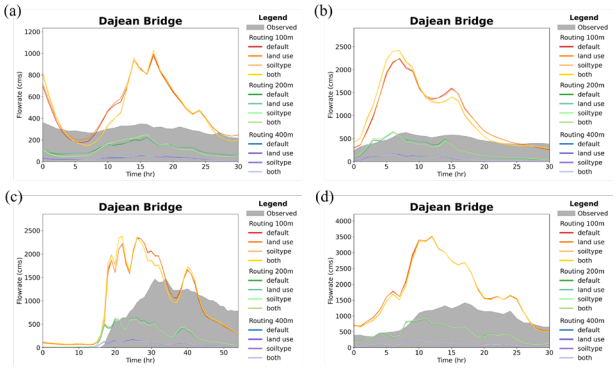

Fig. 2 Simulated streamflow at the Dajean station for the four rainfall events: (a) 2016/06/13, (b) 2017/07/31, (c) 2018/08/23, (d) 2021/08/07.

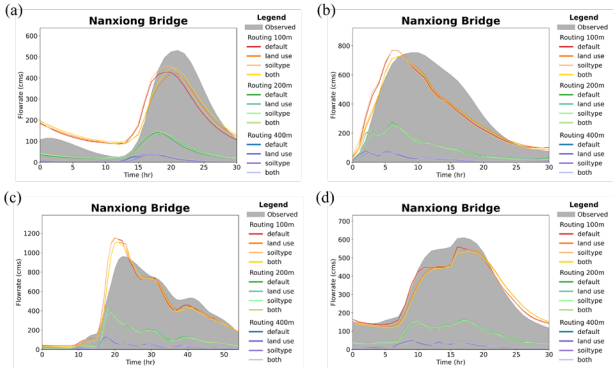

Fig. 3 As in Fig. 2, but at the Nanxiong station.

4. Conclusions

The simulation results indicate that grid sizes have a greater impact than the accuracy of the lateral boundary conditions on model performance. The underlying reasons for this finding require further verification and more case studies. Future work will involve more quantitative evaluations using model performance metrics.

References

Aerts, J.P., Hut, R.W., van de Giesen, N.C., Drost, N., van Verseveld, W.J., Weerts, A.H., Hazenberg, P., 2022. Large-sample assessment of varying spatial resolution on the streamflow estimates of the wflow_sbm hydrological model. Hydrol. Earth Syst. Sci., 26(16), 4407–4430.

Bormann, H., Breuer, L., Gräff, T., Huisman, J.A., Croke, B., 2009. Assessing the impact of land use change on hydrology by ensemble modelling (LUCHEM) IV: Model sensitivity to data aggregation and spatial (re-) distribution. Adv. Water Resour., 32(2), 171–192.

Chang, P.L., Zhang, J., Tang, Y.S., Tang, L., Lin, P.F., Langston, C., Howard, K., 2021. An operational multi-radar multi-sensor QPE system in Taiwan. Bull. Am. Meteorol. Soc., 102, E555–E577.

Hoch, J.M., Sutanudjaja, E.H., Wanders, N., Van Beek, R.L., Bierkens, M.F., 2023. Hyper-resolution PCR-GLOBWB: opportunities and challenges from refining model spatial resolution to 1 km over the European continent. Hydrol. Earth Syst. Sci., 27(6), 1383–1401.

Shrestha, P., Sulis, M., Simmer, C., Kollet, S., 2015. Impacts of grid resolution on surface energy fluxes simulated with an integrated surface-groundwater flow model. Hydrol. Earth Syst. Sci., 19(10), 4317–4326.

Evaluation of Fecal Coliform Export from Agricultural Watersheds under Climate Change Scenarios Using the SWAT Model

Se yoon Jung[1], Jin-Hyuk Ahn[2], Hyungjin Bak[1], Seonah Lee[1], Eunmi Hong[3*]

[1] Interdisciplinary Program in Earth Environmental System Science & Engineering, Kangwon National University, Chuncheon, (Gangwon state) 24341, Republic of Korea

[2] Department of Environmental science, Kangwon National University, Chuncheon, (Gangwon State) 24341, Republic of Korea

[3] Associate Professor, Department of Environmental science, Kangwon National University, Chuncheon, (Gangwon State) 24341, Republic of Korea

* Corresponding author. Email: Eunmi.hong@kangwon.ac.kr

Abstract

Fecal indicator bacteria are indirect indicators of the potential presence of pathogenic microorganisms that cause waterborne diseases, and their introduction into aquatic systems poses significant threats to public health and water quality. In agricultural areas, fecal coliforms (FC) can be released through various pathways, including livestock manure application, direct fecal deposition, and residual soil contamination, with their fate and transport strongly influenced by hydrometeorological conditions such as precipitation and temperature. With the increasing frequency and intensity of extreme weather events due to climate change, predicting and managing FC loading to surface waters has become more important. In this study, the Soil and Water Assessment Tool was used to simulate FC export from an agricultural watershed, assessing the impacts of temperature and precipitation changes under climate change scenarios. The study area is the Buk-myeon watershed in Gapyeong, and model inputs included daily climate data from the Korea Meteorological Administration and observed streamflow and FC concentrations from monitoring stations during 2012–2023. Agricultural schedules were referenced from the Rural Development Administration's "Nongsaro" database. The simulation period was set to 2012–2024, with the first three years used for warm-up, 2016–2020 for calibration, and 2021–2024 for validation. Future climate scenarios were incorporated to analyze FC export characteristics under projected changes. This study is expected to provide a scientific basis for preventing future microbial contamination in rivers by evaluating the sensitivity and response of FC export to climate-driven changes in precipitation and temperature.

Keywords: Agricultural area, Climate change, Fecal coliform, Soil and water assessment tool

1. Introduction

Waterborne diseases from pathogenic microorganisms are a significant public health threat, often linked to the use of contaminated river water for agricultural irrigation. As direct pathogen detection is difficult, Fecal Coliforms (FC) are widely used as an indicator of fecal contamination. Understanding the transport of FC in aquatic systems is therefore essential for protecting public health.

A primary source of this contamination is the land application of livestock manure, especially when it is incompletely composted. In South Korea, a substantial amount of inadequately treated manure, which contains high concentrations of pathogens, is applied to farmland. During rainfall, these pathogens are washed from fields into rivers, making compost maturity a critical factor in controlling water pollution.

Recently, climate change has increased the frequency of extreme weather events such as floods and droughts. Intense rainfall accelerates the runoff of pathogenic microorganisms from soil, while pollutants accumulated during dry periods can be flushed into rivers at high concentrations during the first rainfall. Furthermore, changes in temperature complicate the survival and die-off mechanisms of bacteria, making pollution prediction more difficult.

Therefore, to quantitatively predict FC runoff under climate change, this study constructed future climate projection data by integrating 18 SSP scenarios using a multi-model ensemble technique. This data was then applied to the Soil and Water Assessment Tool (SWAT) model to simulate and evaluate the characteristics of future FC runoff.

2. Materials and Methods

This study focused on the Jucheon River watershed in Hoengseong-gun, Gangwon state, which has been designated as a non-point source pollution management area.

Data from 2012 to 2024 were collected for the study: monthly streamflow and fecal coliform data from the Water Environment Information System, and daily weather data (minimum/maximum temperature, precipitation, average wind speed, and solar radiation) from the Korea Meteorological Administration. SWAT model input data, including the Digital Elevation Map, Land Use, and Soil Map, were sourced from the Korea Water Resources Corporation, Environmental Geographic Information Service, and Korean Soil Information System, respectively.

The study used 18 climate change scenario models presented in Hur et al. (2024), which were integrated into a single model through a multi-ensemble analysis. This research compared SSP2-4.5 and SSP5-8.5 to evaluate the scenario that assumes an intermediate level of climate change mitigation and socioeconomic development versus the scenario that assumes rapid socioeconomic development and high use of fossil fuels. The model was calibrated from 2016 to 2020 and validated from 2021 to 2024. After validation, the model's performance was evaluated using two objective functions, R^2 and KGE.

3. Results and Discussion

For Streamflow, the calibration results were an R^2 of

0.976 and a KGE of 0.945, while the validation results were an R^2 of 0.825 and a KGE of 0.821. For FC, the calibration results were an R^2 of 0.321 and a KGE of 0.440, and the validation results were an R^2 of 0.426 and a KGE of 0.539.

An analysis of future streamflow based on SSP scenarios shows a long-term increase from 2025 to 2100 for both SSP2-4.5 and SSP5-8.5. Notably, the increasing trend in the SSP5-8.5 scenario(slope=0.011) is more pronounced than in the SSP2-4.5 scenario(slope=0.006), suggesting that the magnitude of the streamflow increase may grow as the intensity of climate change deepens.

Furthermore, the maximum high flow occurred between 2025-2050 in the SSP2-4.5 scenario, whereas in the SSP5-8.5 scenario, it occurred between 2071-2100. This suggests that if we follow the SSP2-4.5 pathway, we should prepare for the near future, while for SSP5-8.5, preparation for the distant future is recommended.

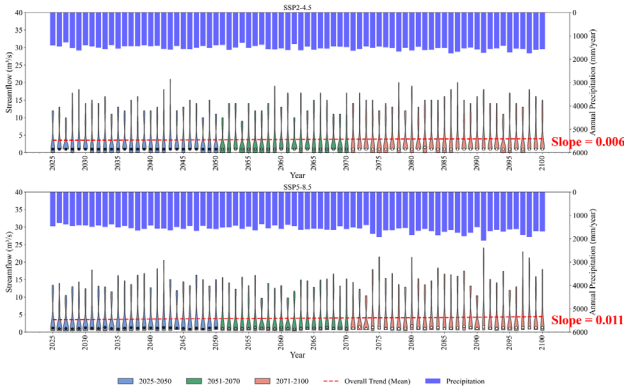

Figure 1. Violin Plot of Streamflow Time Series under SSP2-4.5 and SSP5-8.5 Scenarios

The analysis of FC concentrations under future climate change scenarios predicts a long-term increase in average concentrations for both the SSP2-4.5 and SSP5-8.5 scenarios, leading to a deterioration in future water quality. Notably, this downward trend is significantly steeper in the high-emission SSP5-8.5 scenario (slope=0.196) compared to the medium-emission SSP2-4.5 scenario (slope=0.088). This suggests that as climate change intensifies, microbiological water pollution could accelerate.

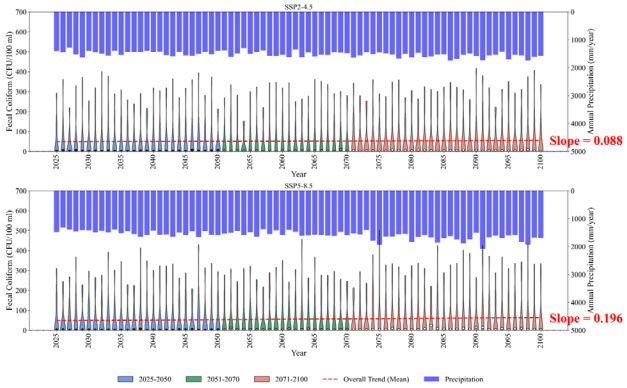

Figure 2. Time Series Violin Graph of FC for SSP2-4.5 and SSP5-8.5 Scenarios

A clear long-term increasing trend in the rate of exceeding water quality standards was evident across all scenarios. Under the 100 CFU/100 ml, Canadian federal water quality standard, the SSP5-8.5 scenario showed an increase from 11.20% in 2025-2050 to 12.78% in 2071-2100 , and under the 200 CFU/100 ml standard, it exhibited a significant increase from 20.19% to 21.94%. In contrast, the SSP2-4.5 scenario had a relatively smaller increase. Particularly in the 2071-2100, its exceedance rate for the 200 CFU/100 ml standard was 2.5 percentage lower than that of the SSP5-8.5 scenario (21.94%), demonstrating that the high-emissions greenhouse gas scenario exacerbates future water quality degradation.

Table 1. Rate of months exceeding water quality standards by scenario (Water for swimming : 100 CFU/100 ml, Water for recreation : 200 CFU/100 ml)

Standard	Scenarios	2025-2050	2051-2070	2071-2100
		%		
100 CFU/100 ml	SSP2-4.5	11.22	11.25	12.50
	SSP5-8.5	11.20	11.67	12.78
200 CFU/100 ml	SSP2-4.5	19.23	20.00	19.44
	SSP5-8.5	20.19	21.67	21.94

4. Conclusions

This study evaluated the export of FC from an agricultural watershed under climate change scenarios using the SWAT model. In both climate change scenarios (SSP2-4.5 and SSP5-8.5), streamflow showed a long-term increasing trend, with a more pronounced increase observed in the high-carbon emission scenario, SSP5-8.5. FC concentrations also increased over the long term in all scenarios, with a significantly steeper trend in the SSP5-8.5 scenario compared to the SSP2-4.5 scenario. This suggests that as climate change intensifies, fecal contamination in rivers could accelerate.

An analysis of the rate of exceeding water quality standards revealed a long-term increasing trend across all scenarios. Notably, for the SSP5-8.5 scenario, the exceedance rate for the 200 CFU/100 ml standard during the period 2071-2100 was 21.94%, which was 2.5 percentage points higher than in the SSP2-4.5 scenario. This demonstrates that the high-emission greenhouse gas scenario further exacerbates future water quality degradation.

Therefore, this study conducted a quantitative analysis of fecal contamination in rivers resulting from climate change in an agricultural region through modeling. The findings are expected to be utilized as foundational data for establishing countermeasures and management plans for the prevention of future water pollution.

Acknowledgements

This research was supported by Basic Science Research Program through the National Research Foundation of Korea (NRF) funded by the Ministry of Education (No. 2022R1C1C1010804)

References

Hur, J. N., Cho, J. P., Jo, S. R., Shim, K. M., Kim, Y. S., Kang, M. G., Oh, C. S., Seo, S. B. & Kim, E. S. (2024). SSP climate change scenarios with 1km resolution over Korean peninsula for agricultural uses. Korean Journal of Agricultural and Forest Meteorology, 26(1), 1-30.

Evaluation of Climate Change and Agricultural Management Impacts on Hydrology and Water Quality Using SWAT+

Min-Jin Kim [1], Won-Ho Nam [2*]

[1] Graduate Student, School of Social Safety and Systems Engineering, Hankyong National University, Anseong, Republic of Korea

[2] Professor, School of Social Safety and Systems Engineering, National Agricultural Water Research Center, Hankyong National University, Anseong, Republic of Korea

* Corresponding author. Email: wonho.nam@hknu.ac.kr

Abstract

Climate change is intensifying hydrological variability and exacerbating water quality issues in agricultural watersheds. In South Korea, increasing temperatures and the heightened frequency of extreme rainfall events are expected to accelerate non-point source pollution, particularly in rural areas dominated by agricultural activities. In this study, the Soil and Water Assessment Tool Plus (SWAT+) was applied to the upper Anseongcheon watershed, with the Geoncheon-ri streamflow station designated as the outlet. The watershed was delineated into 15 sub-basins and 1,917 hydrologic response units (HRUs), incorporating reservoirs and stream channels. Model calibration and validation were conducted using daily streamflow data from 2018 to 2024. Sensitivity analysis identified four dominant parameters, and model performance was evaluated as satisfactory (R^2 = 0.71, NSE = 0.64, PBIAS = –3.05%). The results demonstrate that SWAT+ provides reliable hydrological simulations for agricultural watersheds. Future work will extend the analysis to water quality, with emphasis on nutrient transport processes, and will integrate agricultural Best Management Practices (BMPs) to assess their effectiveness under climate change scenarios. This study establishes a robust modeling framework to support adaptive watershed management strategies under changing climatic and environmental conditions.

Keywords: hydrological variability, agricultural watershed, hydrological modeling, SSP scenarios, BMPs, watershed management

1. Introduction

Climate change has intensified hydrological variability and accelerated water quality deterioration in agricultural watersheds (Woo et al., 2025). In South Korea, rising temperatures combined with increasing rainfall intensity are projected to exacerbate non-point source pollution, particularly in rural regions where agricultural land use predominates (Sadiqi et al., 2024). These challenges highlight the urgent need for integrated approaches to assess watershed-scale responses under changing environmental conditions.

Advancements in hydrological modeling provide essential tools for quantitatively analyzing the interactions among climate drivers, land use, and management practices. The Soil and Water Assessment Tool Plus (SWAT+) has been widely recognized as a robust model for simulating streamflow, nutrient transport, and the impacts of agricultural management strategies (Bieger et al., 2017). By incorporating Shared Socioeconomic Pathways (SSPs) from the Coupled Model Intercomparison Project Phase 6 (CMIP6) alongside agricultural Best Management Practices (BMPs), it is possible to evaluate both potential climate-induced impacts and the effectiveness of mitigation measures in agricultural watersheds.

Accordingly, this study applies the SWAT+ model to the upper Anseongcheon watershed in Anseong, Gyeonggi Province, South Korea, to assess hydrological and nutrient dynamics under combined climate and management scenarios.

2. Materials and Methods

2.1. Study area

The study area is the upper Anseongcheon watershed, with the Geoncheon-ri streamflow station designated as the watershed outlet. The total area is 359.8 km², including Gosam, Geumgwang, and Madun reservoirs. Neighboring meteorological stations are located in Suwon, Icheon, and Cheonan. Based on the digital elevation model (DEM), the mean elevation and slope of the watershed are 112.9 m and 14.9%, respectively. Land use is dominated by forest (51.4%) and agriculture (38.6%). The dominant soil textures are sandy loam (43%) and loam (29%).

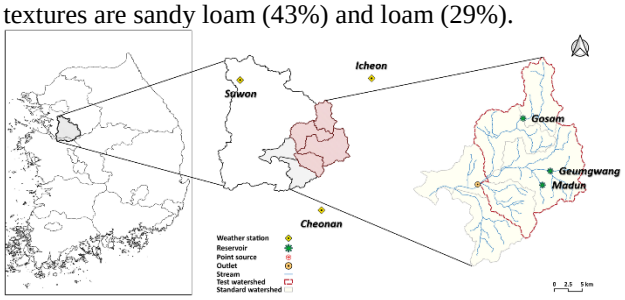

Figure 1. Locations of study area

2.2. SWAT+ model setup and calibration

The SWAT+ model was constructed using QSWAT+, a QGIS-based interface, to define subbasins and hydrologic response units (HRUs) and to incorporate reservoirs and stream networks. Input datasets included DEM (30 m resolution), land use data (2020, 7-class classification), a 1:25,000 detailed soil map, stream network data, meteorological records (1995–2024), daily streamflow data (2015–2024), and reservoir specifications.

Model calibration and validation were performed using observed daily streamflow data from the Geoncheon-ri station. The performance of the model was evaluated using the Nash-Sutcliffe Efficiency (NSE), coefficient of determination (R^2), and Percent Bias (PBIAS). Calibration was conducted for the period 2018–2021, and validation was performed for 2022–2024. The evaluation followed the recommended criteria of Moriasi et al. (2015), which define satisfactory performance as $R^2 > 0.60$, NSE > 0.50,

and PBIAS within ±15%.

2.3. Climate and Management scenarios

Climate change scenarios were based on the SSPs presented in the Intergovernmental Panel on Climate Change (IPCC) Sixth Assessment Report (AR6). Two scenarios, SSP1-2.6 and SSP5-8.5, were applied. To reduce projection uncertainty, a multi-model ensemble (MME) of 18 global climate models (GCMs) from CMIP6 was utilized. Future periods were divided into the near future (2040–2069) and the far future (2070–2099).

In addition, BMP scenarios were designed with reference to the Direct Payment for Public Interest program promoted by the Ministry of Agriculture, Food and Rural Affairs of Korea. These BMPs were combined with the climate scenarios to evaluate their effects on streamflow and nutrient transport.

3. Results and Discussion

3.1. Model setup results

The SWAT+ model was constructed for the upper Anseongcheon watershed, with a simulation period from 2015 to 2024. The years 2015–2017 were used as a pre-run to stabilize model initialization, while 2018–2024 served as the calibration and validation period. The watershed was delineated into 15 subbasins and 1,917 hydrologic response units (HRUs). This spatial discretization provided sufficient resolution to capture the heterogeneity of watershed hydrology.

3.2. Model calibration results

Sensitivity analysis identified four key parameters that strongly influenced streamflow: the baseflow recession constant (alpha), curve number (cn2), soil evaporation compensation factor (esco), and groundwater re-evaporation coefficient (revap_co). Automatic calibration yielded optimized values of alpha = 1.0, cn2 = 71.73, esco = 0.1, and revap_co = 0.02. These parameter adjustments improved the representation of infiltration, evapotranspiration, and groundwater–surface water interactions in the model.

Table 1. Streamflow calibration parameters

Parameters	Range	Calibration values
alpha	0 – 1	1
cn2	35 – 95	71.73
esco	0 – 1	0.1
revap_co	0.02 – 0.2	0.02

3.3. Model validation performance and applicability

Model validation was performed using daily streamflow data from the Geoncheon-ri station. The evaluation produced RMSE = 11.96 mm/day, R^2 = 0.71, NSE = 0.64, and PBIAS = –3.05%, which fall within the satisfactory performance thresholds suggested by Moriasi et al. (2015). Figure 2 compares observed and simulated streamflow, demonstrating that the SWAT+ model successfully reproduced both the magnitude and temporal variability of streamflow. These results confirm that SWAT+ is reliable for hydrological analysis in the Anseongcheon watershed and establish a solid foundation for subsequent climate change and management scenario applications.

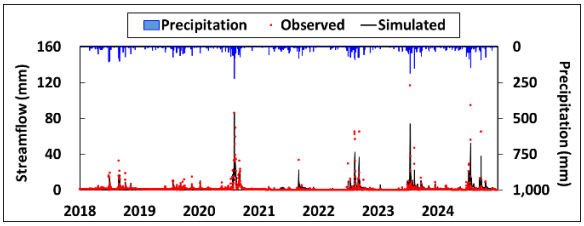

Figure 2. Hydrologic calibration and validation results (2018-2024)

4. Conclusions

This study developed and applied the SWAT+ model to the upper Anseongcheon watershed, with calibration and validation conducted using daily streamflow data from the Geoncheon-ri station. Sensitivity analysis and automatic calibration identified four key hydrological parameters, and the resulting performance statistics (R^2 = 0.71, NSE = 0.64, PBIAS = –3.05%) indicated that the model adequately reproduced streamflow dynamics. These results confirm the reliability of SWAT+ for hydrological applications in agricultural watersheds. Future research will extend the analysis to water quality by simulating nutrient transport processes, and will further incorporate agricultural BMPs to evaluate their combined effects with climate change scenarios. The findings of this study provide a robust modeling framework that can be used to support adaptive watershed management strategies, offering insights into both scientific understanding and practical policy development under future climate conditions.

Acknowledgements

This research was supported by the Rural Development Administration (RDA) through Cooperative Research Program for Agriculture Science & Technology Development, funded by Ministry of Agriculture, Food and Rural Affairs (MAFRA) [RS-2024-00396736].

References

Bieger, K., Arnold, J.G., Rathjens, H., White, M.J., Bosch, D.D., Allen, P.M., Volk, M., and Srinivasan, R., 2017. Introduction to SWAT+, a completely restructured version of the Soil and Water Assessment Tool. J. Am. Water Resour. Assoc., 53(1), 115–130.

Moriasi, D., Gitau, M., Pai, N., and Daggupati, P., 2015. Hydrologic and water quality models: Performance measures and evaluation criteria. Trans. ASABE, 58, 1763–1785.

Sadiqi, S.S.J., Nam, W.H., Lim, K.J., and Hong, E., 2024. Investigating nonpoint source and pollutant reduction effects under future climate scenarios: A SWAT-based study in a highland agricultural watershed in Korea. Water, 16(1), 179.

Woo, S., Kim, W., Chang, S.W., and Chung, I.M., 2025. Seasonal hydrologic responses to climate change based on a CMIP6 multi-model ensemble: A case study of An-Seong watershed in South Korea. J. Hydrol. Reg. Stud., 60, 102491.

Assessing Crop Water Stress and Irrigation Benefits Using the SWAT Model: A Case Study of the Wu River Basin

Cheng An-Rou・Chiang Li-Chi・Lin Guan-Zhou

Abstract

In response to the challenges posed by climate change, including altered rainfall patterns and increased crop water demands, this study aims to evaluate crop water stress and dry-season irrigation requirements in Taiwan. It further investigates the impact of water deficits on crop growth and yield, and quantifies the benefits of various irrigation strategies. The Wu River Basin, located in central Taiwan, was selected as the study area. The Soil and Water Assessment Tool (SWAT), which integrates hydrological processes with crop growth simulation, was used to simulate agricultural hydrology and crop yield changes over the period from 2014 to 2023. To explore water stress across different crop growth stages, three irrigation scenarios were designed, each triggered when soil available water is depleted by 25%, 50%, and 75%, respectively. Simulation results indicate that during the dry season, rainfed crops experience significant water stress during critical stages such as flowering and grain filling, leading to substantial yield reductions. However, the implementation of appropriate irrigation strategies effectively alleviates water stress and enhances crop productivity, underscoring the importance of irrigation management under climate change conditions. This study establishes an analytical framework integrating hydrological and crop modeling to quantify the effects of irrigation strategies on crop growth and yield. The findings offer valuable insights for developing adaptive dry-season irrigation plans and regional water resource management, aiming to balance agricultural production with the sustainable development of watershed ecosystems.

Coupled SWAT and CE-QUAL-W2 Modeling of Nutrient Transport from Watershed to Reservoir: A Case Study of the Feitsui Reservoir, Taiwan

Yu-Ting Wu [1], Li-Chi Chiang[1*]

[1] Department of Bioenvironmental Systems Engineering, National Taiwan University, Taipei 10617, Taiwan

* Corresponding Author Email: lchiang@ntu.edu.tw

Abstract

Climate change has intensified the frequency of extreme rainfall events, amplifying uncertainties in water resource management and elevating the risk of nonpoint source pollution entering reservoirs, thereby posing challenges to water quality security. Feitsui Reservoir, as the primary public water supply for the Taipei metropolitan area, plays a critical role in regional water safety. This study integrates the SWAT hydrological model with the CE-QUAL-W2 water quality model to establish a coupled watershed–reservoir simulation framework. Climate indices were applied to identify extreme rainfall events and to evaluate the impacts of nonpoint source pollution on reservoir water quality under such conditions. Simulation results indicate that fertilization in tea plantations is the dominant source of nitrogen and phosphorus export, with pollutant loads markedly increasing during extreme rainfall, leading to short-term deterioration in total phosphorus concentrations and algal dynamics within the reservoir. The findings highlight that rational fertilization practices and nonpoint source pollution mitigation strategies are essential for maintaining reservoir water quality, thereby providing a scientific basis for watershed management and drinking water security.

Keywords: nonpoint source pollution; extreme events; water quality modeling; reservoir eutrophication

1. Introduction

Rising temperatures and intensifying extreme climate events are inducing complex impacts on water quality and aquatic ecosystems through alterations in precipitation and biogeochemical cycles(Varadharajan et al., 2022). However, climate-informed predictive approaches for water quality under extreme events remain highly complex, and research as well as practical applications in Asia are still relatively limited(Mishra, Alnahit, & Campbell, 2021). Previous studies have also reported that extreme rainfall can exert contrasting effects on water quality: it may dilute pollutant concentrations, yet it can also transport greater amounts of contaminants into water bodies, thereby accelerating reservoir water quality deterioration(Murphy, McCleskey, Martin, Writer, & Ebel, 2018). In this context, the present study integrates the SWAT hydrological model and the CE-QUAL-W2 water quality model to simulate nutrient inputs from the watershed and their effects on reservoir thermal structure and water quality responses, aiming to assess the combined impacts of extreme climate events and agricultural activities on reservoir water quality.

2. Materials and Methods

2.1. Study Area

The Feitsui Reservoir, located in northern Taiwan, serves as the primary public water supply source for the Taipei metropolitan area. The (Figure 1) covers approximately 303 km² and is characterized by a subtropical monsoon climate with an annual average precipitation exceeding 3,000 mm, mainly concentrated during the plum rain and typho watershed on seasons. Land use in the watershed is dominated by forest, while tea plantations represent the major agricultural activity. Fertilization in these areas contributes substantial nitrogen (N) and phosphorus (P) loads, posing potential nonpoint source pollution risks that may exacerbate water quality deterioration under extreme rainfall events.

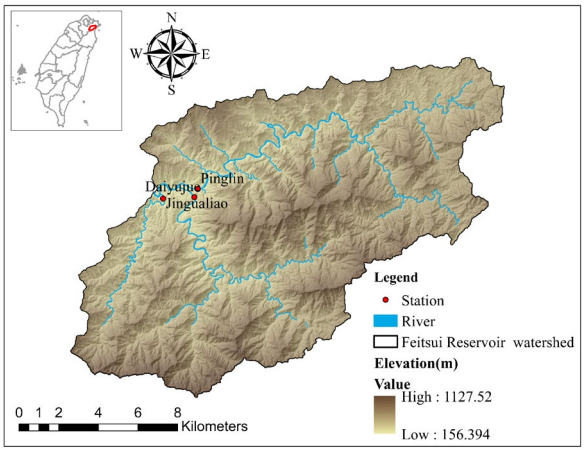

Figure 1 Feitsui Reservoir watershed

2.2. SWAT Model

SWAT(Soil and Water Assessment Tool) is a model developed by the United States Department of Agriculture (USDA). SWAT is a semi-distributed hydrological model primarily applied in non-point source pollution studies, water resource simulation and assessment, crop growth evaluation, and watershed management(G. Arnold et al., 2012)..The SWAT model was employed to simulate hydrological processes and N and P export in the upstream watershed. Required input data included a digital elevation model (DEM), soil distribution data, land use data, and daily meteorological data. Fertilizer application rates were defined according to crop fertilization guidelines. The simulation period spanned from 2010 to 2022. Model calibration and validation were conducted to ensure the reliability of both hydrological and water quality simulations.

2.3. CE-QUAL-W2 Model

CE-QUAL-W2, developed by the U.S. Army Corps of Engineers, has been applied to simulate in-reservoir water quality dynamics(Thomas M. Cole & Wells, 2006). Required input data included reservoir geometry (segment and layer), inflow data, and initial condition settings.

Inflow concentrations of N and P were derived from SWAT outputs, while initial conditions were based on monitoring data provided by the Feitsui Reservoir Administration. The simulation period was set from 2016 to 2022, to reproduce nutrient and algal dynamics within the reservoir.

2.4. Scenario design

In addition to the baseline scenario, an alternative management scenario was established by removing fertilizer applications in the calibrated model to compare nutrient outputs with and without fertilization. This scenario was designed to assess the contribution of agricultural fertilization to reservoir nutrient loading and to provide a reference for evaluating future management strategies.

3. Results and Discussion

3.1. SWAT Model Results

3.1.1 SWAT calibration and validation

Calibration and validation results demonstrated good performance in reproducing nutrient dynamics for the Pinglin and Daiyujue sub-watersheds, capturing both hydrological and pollutant transport characteristics. (Table 1&Table 2).

Table 1 Nitrate-N calibration & validation results

Station	Period	R^2	NSE	PBIAS(%)
PingLin	2013-2015	0.68	0.38	21.7
	2016-2017	0.76	0.38	23.8
Daiyujue	2013-2017	0.80	0.41	35.7
	2017-2018	0.60	0.43	28.2

Table 2 Phosphorus calibration & validation results

Station	Period	R^2	NSE	PBIAS(%)
PingLin	2013-2015	0.53	0.42	-12.6
	2016-2017	0.53	0.47	6.9
Daiyujue	2013-2017	0.46	0.37	-0.4
	2017-2018	0.47	0.34	-20.2

3.1.2 Comparison of Scenarios

Although agricultural land comprises only 5% of the total watershed area, fertilization substantially increased nitrate-N export. For instance, in the Pinglin sub-watershed (Figure 1), the mean monthly nitrate-N export under the no-fertilization scenario was 16,360, reflecting considerable background N contributions. With fertilization, the mean monthly export increased to 20,195, representing an increment of 3,836, or approximately 23%. These findings indicate that despite the limited proportion of agricultural land, fertilization practices can significantly elevate N loading.

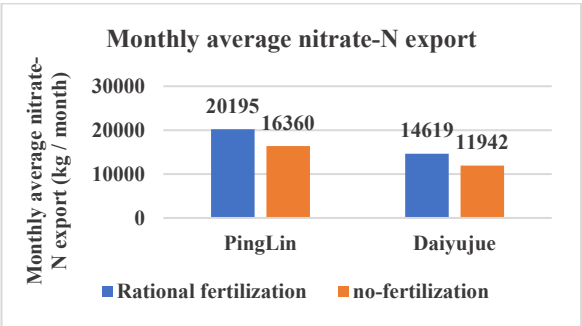

Figure 2 Monthly average nitrate-N export under fertilization and no-fertilization scenarios in the Pinglin sub-watershed.

3.2 CE-QUAL-W2 Model Results

3.2.1 Water Balance

The water balance simulation results of this study indicate an overall good performance. The model achieved a mean absolute error (MAE) of 1.48 and a root mean square error (RMSE) of 2.26, suggesting that the deviations between simulated and observed values remain within a reasonable range. The relative error (RE) was as low as 0.0093, reflecting high accuracy in total water volume estimation. The coefficient of determination (R^2) reached 0.90, demonstrating that the model effectively captured the variability of observed values.

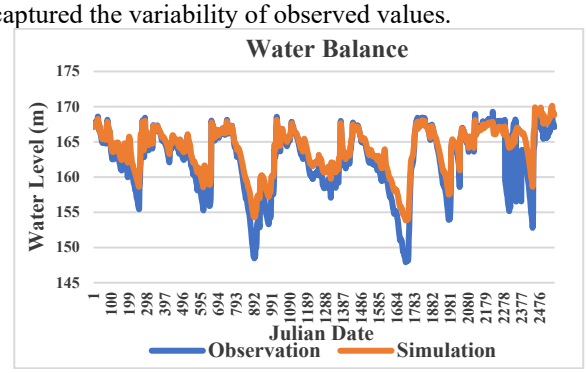

Figure 3 Water balance

3.2.2 Thermal stratification and water quality

Model results showed that thermal stratification developed in May and persisted until August. Surface water temperature rapidly increased to 28–30 °C, while bottom waters remained below 20 °C. The thermocline was located at depths of 8–15 m, and stratification led to the accumulation of nutrients and pollutants in the hypolimnion, heightening the risks of hypoxia and water quality deterioration. During the stratification period, nitrate nitrogen exhibited a clear vertical gradient. Concentrations were relatively low in the surface layer, increased with depth toward the metalimnion, and remained elevated in the hypolimnion. This pattern indicates that stratification restricted vertical mixing, leading to nitrate accumulation in deeper waters.

4. Conclusions

Agricultural fertilization is a critical driver of N export in the Feitsui Reservoir watershed, although background N contributions remain substantial and should not be overlooked in management planning. Reservoir thermal stratification and mixing processes exert direct control over water quality dynamics, particularly during high-risk summer periods.

References

G. Arnold, J., N. Moriasi, D., et al. (2012). SWAT: Model Use, Calibration, and Validation. *Transactions of the ASABE, 55*(4), 1491-1508. doi:https://doi.org/10.13031/2013.42256

Mishra, A., Alnahit, A., et al. (2021). Impact of land uses, drought, flood, wildfire, and cascading events on water quality and microbial communities: A

review and analysis. *Journal of Hydrology, 596*, 125707. doi:https://doi.org/10.1016/j.jhydrol.2020.125707

Murphy, S. F., McCleskey, R. B., et al. (2018). Fire, Flood, and Drought: Extreme Climate Events Alter Flow Paths and Stream Chemistry. *Journal of Geophysical Research: Biogeosciences, 123*(8), 2513-2526. doi:https://doi.org/10.1029/2017JG004349

Thomas M. Cole, & Wells, S. A. (2006). CE-QUAL-W2: A two-dimensional, laterally averaged, Hydrodynamic and Water Quality Model, Version 3.5. *Instruction Report EL-06-1, US Army Engineering and Research Development Center, Vicksburg, MS.*

Varadharajan, C., Appling, A., et al. (2022). Can machine learning accelerate process understanding and decision-relevant predictions of river water quality? *Hydrological Processes, 36*. doi:10.1002/hyp.14565

Groundwater Modeling and Adaptation Strategies under Climate Change in the Lanyan River Basin: Applications of SWAT+ and LSTM

Hao-Hung Chiang [1*], Li-Chi Chiang[1]

[1] Department of Bioenvironmental Systems Engineering, National Taiwan University, Taipei 10617, Taiwan

* Corresponding author. Email: r13622036@ntu.edu.tw

Abstract

Amid intensifying climate extremes and growing water scarcity, this study develops a two-stage "Physics × Machine Learning" framework for the Lanyang River Basin. In Stage 1 (ML-1), both the magnitude and frequency of AR6 GCM inputs are corrected, and the bias-adjusted data drive SWAT+ for initial groundwater simulations. In Stage 2 (ML-2), groundwater dynamics—including water levels, recharge, and baseflow—are further modeled to support adaptation strategies. Data are structured as follows: 1990–2014 for a day-of-year (DOY) baseline, 2015–2024 for training and validation, and post-2025 for scenario simulations.

Temperature correction applies residual learning, with LSTM predicting Obs–GCM residuals of Tmax and Tmin, followed by DOY-based quantile mapping. Precipitation correction employs a MoE-LSTM with wet/dry gating and multi-quantile loss to learn daily quantiles and rainfall probability, with tail-weighted learning enhancing extremes. Outputs are post-processed with ECDF-based DOY-QM, isotonic regression, and drizzle filtering. Validation (2015–2024) shows strong improvements: Tmax (r = 0.796, RMSE = 3.52 °C), Tmin (r = 0.832, RMSE = 2.68 °C), calibrated wet-day probabilities near 1:1, and reduced high-quantile biases.

By jointly correcting magnitude and probability while retaining long-term signals, ML-1 provides reliable climate inputs for SWAT+. ML-2 then captures nonlinear groundwater responses, enabling evaluation of adaptation strategies for irrigation and domestic water use.

Keyword: Groundwater、LSTM、SWAT+

1. Introduction

To address groundwater management under intensifying climate extremes, this study develops a two-stage "Physics × Machine Learning" framework for the Lanyan River Basin in Taiwan (Figure 1). In the first stage (ML-1),daily AR6 GCM inputs are corrected while retaining long-term climate signals. The corrected data are used to drive SWAT+, and subsequently, in the second stage (ML-2), groundwater dynamics are analyzed to support adaptation planning.

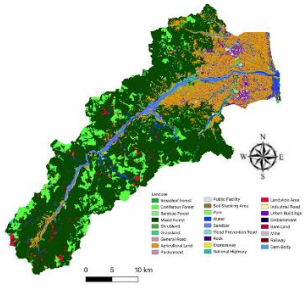

Figure 1 Land use distribution of Lanyan river basin

2. Materials and Methods

The research workflow first establishes a DOY (day-of-year) baseline using 1990–2014 data to preserve long-term climate trends. Data from 2015–2024 are used for training and validation of ML-1, while data after 2025 are applied in scenario simulations. For temperature correction, a residual learning approach is employed: an LSTM model predicts the residuals between observations and GCM simulations of Tmax and Tmin (Themeßl, 2011), which are then added back to GCM data,

followed by fine-scale adjustment through DOY-QM (Wang,2024).For precipitation correction, a Mixture-of-Experts LSTM (Li et al., 2022) with wet/dry-day gating is introduced, combined with a multi-quantile loss function to simultaneously generate daily q50, q80, q90, and q95 quantiles and wet-day probability p. Tail-weighted learning (Frame et al., 2021) is incorporated to improve the representation of extreme events. Outputs are then post-processed with ECDF-based DOY-QM and isotonic regression to align distributions and probability reliability, along with a drizzle-filtering mechanism. The same distributional adjustment is also applied to relative humidity data (Wang & Gao, 2023).

3. Results and Discussion

3.1 Precipitation

The ML-1 precipitation distribution model (quantiles + wet-day probability) closely aligns with the 1:1 reference line in the 2015–2024 evaluation (Figure 2), indicating that forecasted rainfall probabilities match observed wet-day frequencies and are thus calibrated. The 30-day moving average of P50 (Figure 3) successfully reproduces the seasonal cycles and interannual variability of observations, with peak timing and magnitude largely consistent. Quantile deviation analysis shows that the raw GCM systematically underestimates higher quantiles (heavy and extreme rainfall) by up to tens of millimeters. After ML-1 correction, deviations from the median to upper quantiles are significantly reduced toward zero, with clear improvement in the tails, indicating enhanced performance in both rainfall magnitude and occurrence.

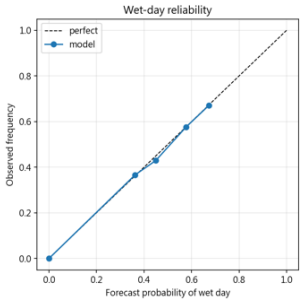

Figure 2 wet day reliability

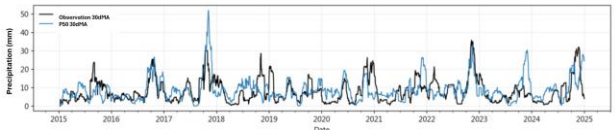

Figure 3 30-day moving average of P50

3.2 Maximum and Minimum Temperature

After residual learning correction, Tmax achieved r = 0.796, RMSE = 3.52 °C, MAE = 2.75 °C, Bias = −0.49 °C (Figures 4–5); Tmin achieved r = 0.832, RMSE = 2.68 °C, MAE = 2.00 °C, Bias = −0.12 °C (Figures 6–7). Time-series comparisons reveal that the corrected GCM consistently follows observed daily fluctuations, seasonal cycles, and interannual variations, with extreme highs and lows more closely aligned with observations. Current results demonstrate that ML-1 effectively corrects both distributions and probabilities while preserving long-term trends, making it suitable for threshold-risk and extreme-event assessments. Residual errors remain primarily in rare temperature extremes, which will be further addressed through tail-directed data augmentation and seasonal parameterization. ML-1 outputs will serve as inputs to SWAT+, while ML-2 will learn the residual, nonlinear spatiotemporal patterns of groundwater levels, recharge, and baseflow. Combined with SHAP-based interpretability analysis, these results will inform groundwater adaptation options and sustainability assessments to support irrigation and domestic water supply decision-making in the Lanyan River Basin.

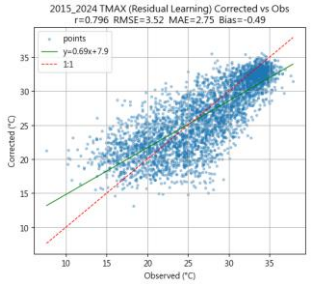

Figure 4 Correlation of corrected GCM Tmax with observations

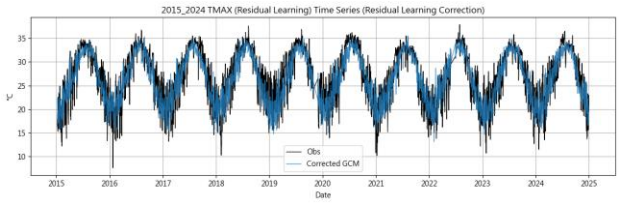

Figure 5 Time series of corrected GCM Tmax vs. observations

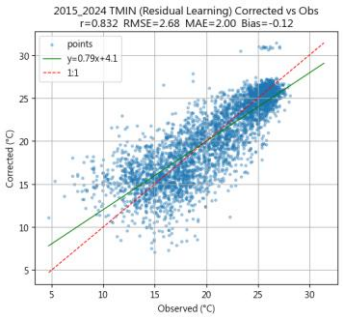

Figure 6 Correlation of corrected GCM Tmin with observations

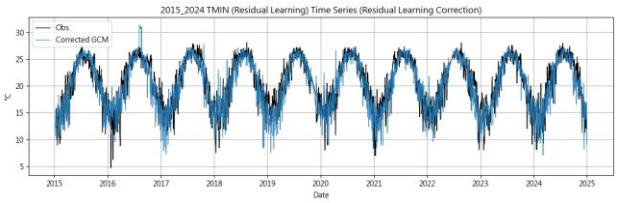

Figure 7 Correlation of corrected GCM Tmin with observations

References

1. Themeßl, M. J., Gobiet, A., & Leuprecht, A. (2011). Statistical bias correction of global simulated daily precipitation and temperature for the application of hydrological models. Journal of Hydrology, 395(3–4), 199–215.

2. Wang, F. (2024). Multivariate bias correction and downscaling of climate models. [Preprint]

3. Li, Y., Xu, J., & Anastasiu, D. C. (2022). An extremeadaptive time series prediction model based on probability-enhanced LSTM neural networks. arXiv preprint arXiv:2211.15891.

4. Frame, J., Kratzert, F., Klotz, D., Gauch, M., Lin & Nearing, G. S. (2021). Deep learning rainfall-runoff predictions of extreme events. Hydrology and Earth System Sciences Discussions, 2021, 1–27.

5. Wang, J., & Gao, Y. (2023). Generalized mixture model for extreme events forecasting in time series data. arXiv preprint arXiv:2310.07435.

Assessment of the Agricultural Water Cycle and Resource Utilization Using the EPA-SWMM Model

Ji-Hyeon Shin [1], Won-Ho Nam [2*]

[1] Ph.D Student, Department Integrated System Engineering, Hankyong National University, Anseong, Republic of Korea

[2] Professor, School of Social Safety and Systems Engineering, National Agricultural Water Research Center, Hankyong National University, Anseong, Republic of Korea

* Corresponding author. Email: wonho.nam@hknu.ac.kr

Abstract

As climate change intensifies, extreme weather events such as droughts and floods are becoming more frequent, increasing the occurrence of compound water-related disasters. In South Korea, agricultural water use accounts for about 41% of total water consumption, yet management remains largely empirical, leading to water losses, uneven distribution, and inefficiencies. Paddy fields, managed with bunds, make hydrological processes highly sensitive to climate variability and management practices. This study applied the Environmental Protection Agency's Storm Water Management Model (EPA-SWMM) to simulate agricultural water dynamics and evaluate two water management scenarios at the scale of individual water sources. Key components of the irrigation water cycle—supplied water, drainage and return flow, infiltration, evapotranspiration, and effective water use—were analyzed. The findings provide a scientific basis for developing efficient, climate-resilient agricultural water management strategies through a comprehensive understanding of water circulation processes.

Keywords: Irrigation, agricultural watershed, water circulation, hydrology-hydraulic modeling, SWMM

1. Introduction

Climate change has intensified extreme weather events, such as droughts and floods, increasing the occurrence of compound water-related disasters (Wilhite et al., 2000). In South Korea, agricultural water accounts for about 41% of total national use (MOE, 2020), yet its management still relies on empirical practices rather than quantitative monitoring, causing water losses and inefficiencies. Paddy fields dominate Korean agricultural watersheds and are managed using bunds to maintain ponded conditions, making the hydrological cycle highly sensitive to climate variability, cropping systems, and irrigation strategies. Assessing agricultural water circulation—including supply, usage, return flow, infiltration, and evapotranspiration—is essential to improve water-use efficiency. The Storm Water Management Model (EPA-SWMM) has recently been applied to simulate irrigation canal networks and evaluate dynamic gate control strategies, offering a more responsive framework than conventional approaches. This study applies an SWMM-based modeling framework to analyze irrigation water flow and assess two management scenarios, providing insights for efficient and climate-resilient agricultural water management.

2. Materials and Methods

2.1. Study area

The study area focuses on the Yongdang Reservoir, selected from agricultural reservoirs in the Han River basin with a storage capacity exceeding 5.0×10^6 m³. The reservoir has an effective storage capacity of 6.831×10^6 m³ and has been in operation since its completion in 1949. It was designed for a 10-year drought frequency and has a watershed area of 2,873 ha, an irrigated area of 922 ha, and a watershed ratio of 3.1. The irrigation network consists of 166 paddy fields, 2 main canals, and 21 sub canals, supported by 13 pumping stations and one weir for supplementary water supply. Among the total irrigated area, the primary water source covers 590 ha (64%), while supplementary sources cover 332 ha (36%).

2.2. Irrigation canal network modeling

The EPA-SWMM model was applied to simulate irrigation water supply by considering the geometry of agricultural facilities, including open channels, pipelines, and intake weirs (Rossman, 2010). By reversing the conventional stormwater network, the model simulated water distribution from a single source through main and lateral canals to individual paddy fields. The simulation period was from May 1 to September 10, 2024, with two water management scenarios: Scenario A, without gate control, and Scenario B, optimized by adjusting gate openings. In Scenario B, gate operations were modified based on Scenario A results to reduce water deficits and improve irrigation efficiency.

2.3. Agricultural water analysis factors

2.3.1.Agricultural water use and demand

Irrigation terms follow the Rationalization Plan for Agricultural and Rural Water Use (KRC, 2023). The total volume of water supplied to each paddy field was defined as irrigation water use (IWU). The irrigation water demand (IWD) was then calculated as the sum of IWU, canal losses (CL), and supplementary water required for distribution management (SW_{dm}). CL were estimated using the assigned values for each irrigation zone, as specified in the Rationalization Plan for Agricultural and Rural Water Use (MAFRA, 2014). SW_{dm} was assumed to be 7.5% of IWU. The calculation formulas for and are presented in Equations (1) and (2).

$$IWU = IWS_{pf} \quad (1)$$

$$IWD = IWU + CL + SW_{dm} \quad (2)$$

2.3.2. Irrigation return flow

In this study, the quick return flow and quick return flow rate (RF_Q) were analyzed at the scale of individual water sources, estimated using drainage volumes from the main (D_{mc}) and sub (D_{sc}) canals. The calculation formula for RF_Q is presented in Equation (3).

$$RF_Q = (D_{mc} + D_{sc}) \times 100(\%) \quad (3)$$

3. Results and Discussion

3.1. Agricultural water distribution simulation

To identify water-deficient areas and assess irrigation supply conditions, the ponding depth rate was analyzed, as shown in Figure 1. The results indicate that under Scenario A, most areas had a ponding depth rate below 60%, showing insufficient water supply and uneven distribution. In contrast, Scenario B achieved a higher ponding depth rate exceeding 80% in most regions, indicating a well-balanced water supply without significant water shortages.

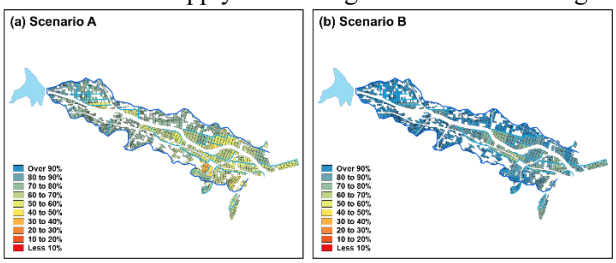

Figure 1. Analysis results of average ponding depth rates.

3.2. Agricultural water analysis

3.2.1.Agricultural water use and demand

In Scenario A, the irrigation water use and demand were estimated at 924 mm and 1,172 mm, respectively, whereas in Scenario B, they increased to 1,180 mm and 1,497 mm, respectively. These differences arise because the estimates were based on the irrigation water directly supplied to individual paddy fields. The higher values in Scenario B reflect more efficient water management with sufficient supply across the study area, while the lower values in Scenario A are attributed to the presence of water-deficient zones and uneven water distribution.

3.2.2. Irrigation return flow

Table 1 shows the analysis of irrigation return flow under the two scenarios. In Scenario A, the return flow accounted for 55% of the supplied water, whereas in Scenario B, it decreased to 47%. The lower return flow ratio in Scenario B indicates that optimized gate control reduced excessive drainage and enhanced overall irrigation efficiency compared to Scenario A.

Table 1. Analysis results of irrigation return flow.

Category	Supply (1,000 m³)	Irrigation return flow	
		(1,000 m³)	(%)
Scenario A	15,911	8,711	55
Scenario B	15,911	7,455	47

3.3. Agricultural water cycle analysis

Figure 2 shows the analysis of the irrigation water cycle under the two scenarios. In Scenario A, higher drainage and irrigation return flows were observed, while both irrigation water use and demand were relatively low, indicating inefficient water utilization. In contrast, Scenario B demonstrated optimized water management, with increased irrigation water use and demand, accompanied by reduced drainage and irrigation return flows. The differences in water cycle characteristics between the scenarios are attributed to gate-opening control and the spatiotemporal distribution of water supply. In Scenario A, the absence of gate control led to low ponding depth rates and inefficient water circulation, with increased return flows in over-supplied areas. In contrast, Scenario B utilized ponding depth analysis to identify water-deficient regions and adjusted gate openings to enable demand-oriented water distribution. As a result, ponding depth rates were maintained at higher levels, and irrigation return flows were minimized, indicating more efficient water use.

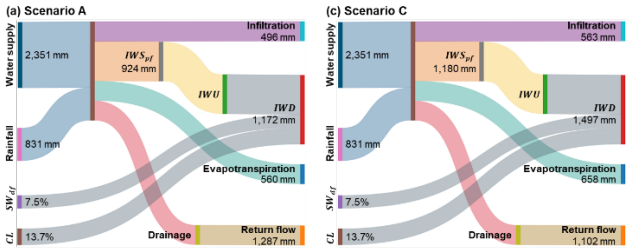

Figure 2. Results of the water circulation analysis in the irrigated area.

4. Conclusions

The concept of water circulation in irrigation reservoirs and districts has become increasingly important due to the rising frequency of droughts and floods under climate change. It plays a key role in enhancing agricultural productivity, sustainable water management, and environmental protection. This study emphasizes the need to estimate irrigation water use through supply network modeling and analyze circulation characteristics, including supply, drainage, return flow, use, and demand, at both water source and district scales. The findings provide a basis for improving water policies, ensuring timely supply, and supporting the sustainable use of rural resources. In the future, securing long-term monitoring of supply, drainage, and ponding depth will enable more accurate irrigation estimates and a better understanding of circulation dynamics.

Acknowledgements

This work was supported by Korea Institute of Planning and Evaluation for Technology in Food, Agriculture, and Forestry (IPET) through Intelligent Agricultural Infra Management for Climate Change Development Program, funded by Ministry of Agriculture, Food and Rural Affairs (MAFRA) (RS-2025-02219764).

References

Korea Rural Community Corporation (KRC), 2023. Rationalization Plan for Rural Water Use in Korea, 2023–2030. Korea Rural Community Corporation, Naju, Republic of Korea (in Korean).

Ministry of Agriculture, Food and Rural Affairs (MAFRA), 2014. Rural Water Use Rationalization Plan 2015–2024. Sejong, Republic of Korea (in Korean).

Ministry of Environment (MOE), 2020. Water for the Future 2020: Water and Climate Change. Daejeon, Republic of Korea (in Korean).

Rossman, L. A., 2010. Storm Water Management Model User's Manual Version 5.0. EPA/600/R-05/040, National Risk Management Research Laboratory, U.S. Environmental Protection Agency, Cincinnati, Ohio.

Wilhite, D. A., Hayes, M. J., Knutson, C., and Smith, K. H., 2000. Planning for drought: Moving from crisis to risk management. *Journal of the American Water Resources Association*, 36(4), 697–710.

Evaluating the Impact of Input Data Structure on ANN-Based Runoff Modeling

Maga Kim [1], Jin-yong Choi [2*]

[1] Department of Rural System Engineering, College of Agriculture and Life Sciences, Seoul National University, Seoul 08826, Republic of Korea

[2] Professor, Department of Rural System Engineering, College of Agriculture and Life Sciences, Seoul National University, Seoul 08826, Republic of Korea

* Corresponding author. Email: iamchoi@snu.ac.kr

Abstract

Runoff is a crucial factor in agricultural water resource planning and management because it has significant implications for various hydrological applications. The rainfall-runoff process represents the interaction between a watershed and rainfall. This process is highly non-linear and uncertain due to the complex relationships among topography, soil properties, vegetation, land use, and weather conditions, making modelization and calibration of parameters challenging and time-consuming.

The Artificial Neural Network (ANN) is a machine learning model that learns patterns from data and is considered suitable for analyzing non-linear natural phenomena. One advantage of the ANN model is that it does not require an explicit mathematical representation of physical processes. However, its performance strongly depends on the model structure and the input data used. For instance, depending on the model's purpose and desired output, the selection of critical input data varies. Moreover, selecting and designing an appropriate model structure based on the relationship between input and output data has a significant impact on model performance. In the hydrological field, numerous studies have estimated runoff using ANN with rainfall and antecedent runoff data. However, as runoff estimation periods become longer, the uncertainty in the rainfall-runoff process increases, and the influence of previous rainfall becomes more variable over time. However, few studies have incorporated this consideration when designing model inputs.

Therefore, in this study, we compare an ANN model that uses input data equally, a widely used approach, with a model that uses input data with different time structures.

Keywords: runoff, rainfall-runoff analysis, TANK model, artificial neural network.

1. Introduction

Runoff is a crucial factor in hydrological analysis for water resource management. Long-term runoff, as a continuous hydrological event, is especially important for determining reservoir capacity, allocating irrigation water, and establishing water resource plans. Since runoff originates from the watershed, which consists of complex factors such as topography, vegetation, land use, soil, and weather condition, rainfall-runoff processes are highly non-linear.

While existing linear models often disregarded such non-linearity, recent advances in computation have enabled improved interpretation (Oh et al., 2008). Artificial neural networks (ANNs), which imitate the human calculation process, are well suited for modeling non-linear natural phenomena and have been widely applied to rainfall-runoff analysis, rainfall distribution, drought, and groundwater flow.

Among conceptual models, the TANK model assumes several reservoirs and outlets to optimize parameters for runoff analysis. A modified three-stage TANK model has been used for small agricultural watersheds in Korea (Kim & Park, 1988; Kim & Kim, 2012; Ahn et al., 2015), but it is less accurate for large watersheds due to uniform parameters. Therefore, this study combines the TANK model and ANN: runoff estimated by the TANK model was used as training data for ANN and compared with ANN trained directly with rainfall and prior runoff.

2. Materials and Methods

In this study, the TANK model and ANN were combined to estimate the rainfall–runoff process. In the TANK–ANN model, antecedent runoff was replaced by the output of the TANK model, which allows runoff to be estimated without measured data from the preceding period. Furthermore, the results of the ANN model using antecedent runoff were compared with those of the TANK–ANN model.

2.1. Artificial neural network (ANN)

The ANN model, which simplifies the neuron and synapse of the human brain, is the computational model, made up of simple operators combinations. The ANN model can solve the problem only with given data, even if there's no algorithm or direct solving method (Yeo et al., 2010). Also, ANN models are valuable for modeling complex non-linear and multi-dimension In-Out relation.

The processing nodes, which are arranged on each layer, are the fundamental components of the ANN model. The outputs of the nodes from a layer deliver to nodes of the next layer through connection strength (Ryu et al., 2002). Multi-layer perceptron (MLP), which is the typical structure of ANN models, is consist of more than three layers mostly (Seo et al., 2017). The layer where information are entered called the input layer and the layer on which processed information appears called the output layer and all of the layer between the input layer and output layer called the hidden layer. The hidden layers can be many depending on the structure of the ANN model (Atkinson and Tatnall, 1997). MLP with hidden nodes, which is consist of three layers, performs the same operation as following equation.

$$\mathrm{o}(\mathbf{x}) = f\left(w_0 + \sum_{j=1}^{J} w_j \cdot f\left(w_{0j} + \sum_{i=1}^{n} w_{ij} x_i\right)\right)$$
$$= f\left(w_0 + \sum_{j=1}^{J} w_j \cdot f\left(w_{0j} + \mathbf{w}_j^T \mathbf{x}\right)\right)$$

where $x=\{x_i, i=1,2,\cdots,n\}$: input vector, f: activation function, o(x): output vector, w_0: bias for output nodes, w_j: connection strength, $w_{ij}=\{w_{ij}, i=1,2,\cdots,n\}$: connection strength vector of j^{th} hidden node, w_{0j}: bias for j^{th} hidden node (Günther and Fritsch, 2010).

2.2. TANK model

TANK model, which is developed by Sugawara, is a conceptual rainfall-runoff model (Sugawara, 1972). TANK model has a respectively simple algorithm for interpretation of complex rainfall-runoff phenomena and needs input data and parameters which is a lesser number (Koo et al., 2006). TANK model is consist of three or four conceptual tanks, and each tank has two or three discharge outlet. TANK model assumes the watershed as three or four stages of tanks, and carry out the runoff interpretation of watershed by optimizing parameters. TANK model simulates rainfall, evapotranspiration and surface runoff in the upper tank, and simulates interflow and infiltration conceptually by water transfer between each tank. TANK model has advantages that can be applied to watershed lacking in observational data because necessary input data and parameters for runoff interpretation are few, but it cannot ensure runoff interpretation for a watershed where parameters are not estimated (Kim and Kim, 2012).

In Korea Kim and Park (1988) suggested a modified 3-TANK model, which has three tanks and four discharge outlet, for upper stream watershed of the agricultural reservoir of Korea. In this study, the modified 3-TANK model is used for the estimation of runoff. The parameters of the TANK model are calculated according to the regression equations suggested by Kim and Park (1988).

3. Results and Discussion

In the study, cases 1, 2, and 3 were distinguished by input runoff data. Case 1 used only weather data, case 2 used observed antecedent runoff data, and case 3 estimated runoff with the TANK–ANN model, which used the TANK model's output instead of observed runoff data.

Cases 2 and 3, which utilized runoff data as input, showed better performance than case 1. In particular, during the validation phase, cases 2 and 3 achieved R2 values above 0.9, whereas case 1 recorded values below 0.9.

Table 1. Model result (statistical parameters)

Case	Runoff	R2	NSE	NSEln	PBIAS
1	-	0.833	0.832	0.359	8.392
2	Q	0.868	0.860	0.586	0.406
3	TANK	0.853	0.844	0.570	14.398

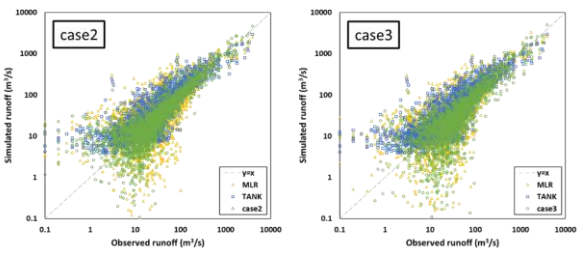

Figure 1. Scatter plot of MLR, TANK, and ANN

Cases 2 and 3 showed better performance than the TANK model and the MLR (Multiple Linear Regression) model, and their scatter plots exhibited a denser distribution.

4. Conclusions

The TANK–ANN model outperformed the TANK model and demonstrated comparable performance to the ANN model using observed runoff data. However, the use of observed data is limited for long-term runoff estimation, as such data are unavailable prior to the start of measurements. The findings of this study indicate that simulated runoff from the TANK model can effectively substitute for observed data in the TANK–ANN framework.

References

Ahn, J. S., Song, J. H., Kang, M. S., Song, I. H., Jun, S. M., Park, J. H. 2015. Regression equations for estimating the TANK model parameters. Journal of the Korean Socienty of Agricultural Engineers 57(4), 121-133.

Atkinson, P. M. & Tatnall, A. R. L. 1997. Introduction neural networks in remote sensing. International Journal of Remote Sensing 18(4), 699-709.

Günther, F. & Fritsch, S. 2010. Neuralnet: training of neural networks. The R Journal. 2(1), 30-38.

Kim, C. G. & Kim, N. W. 2012. Comparison of natural flow estimates for the Han river basin using TANK. Journal of Korean Water Resources Association 45(3), 301-316.

Kim, H. Y. & Park, S. W. 1988. Simulating daily inflow and release rates for irrigation reservoirs(I): modeling inflow rates by a linear reservoir model. Journal of the Korean Socienty of Agricultural Engineers 30(1), 50-62.

Koo, B. Y., Jung, I. W., Bae, D. H. 2006. A study on baseflow parameters estimation of TANK model. In Proceedings of the Korean Water Resources Association Conefrence, 1970-1974

Oh, C. R., Jin, Y. H., Kim, D. R., Park, S. C. 2008. Study on development of artificial neural network foecasting model using runoff, water quality data. Journal of Korean Water Resources Association 41(10), 1035-1044.

Ryu, J. H., Lee, S., Won, J. S., 2002. Weight determination of landslide factors using artificial neural networks. Economic and Environmental Geology 35(1), 67-74.

Seo, Y. M., Choi, E. H., Yeo, W. K. 2017. Reservoir water level forecasting using machine learning models. Journal of the Korean Society of Agricultural Engineers 59(3), 97-110.

Sugawara, E. O., 1972. Method of rainfall-runoff analysis, Kyouritsu Shuppan Co., Ltd., Tokyo, Japan.

Yeo, W. K., Seo, Y. M., Lee, S. Y., Ji, H. K. 2010. Study on water stage prediction using hybrid model of artificial neural network and genetic algorithm. Journal of Korean Water Resources Association 43(8), 721-731.

Growth responses of two green manure crops to treatments with non-sulfur photosynthesis bacteria and wastewater sludge

Chun-Hank Ko[1*] , Bo-Xiang Lee[1] , Ping-Yuan Yang[1] , Chihhao Fan[2] , Tang-Long Shen[3]

[1] School of Forestry and Resource Conservation, National Taiwan University, Taipei, Taiwna

[2] Department of Bioenvironmental Systems Engineering, National Taiwan University, Taipei, Taiwan

[3] Department of Plant Pathology and Microbiology, National Taiwan University, Taipei, Taiwan

* Corresponding author. Email: chunhank@ntu.edu.tw

Abstract

To promote sustainable agriculture and resource recycling, this study evaluated the effects of combining wastewater sludge with non-sulfur photosynthetic bacteria (PNSB) as a soil amendment on two green manure crops—*Sesbania cannabina* (Retz.) Poir and *Glycine max* (L.). Application of 20 t/ha sludge increased soil total carbon, total nitrogen, and available phosphorus by 14.2%, 67.3%, and 57%, respectively. The combination of 10 t/ha sludge with bacteria further enhanced phosphorus availability. Potassium and magnesium levels increased by 30% and 42%, and soil pH improved from acidic to near-neutral, indicating better nutrient retention. Sludge application led to dose-dependent increases in both soil heavy metal concentrations, with nickel and chromium levels sometimes exceeding pollution standards, and heavy metal accumulation in plant tissues. for example, soybean nickel uptake increased by 126.0% and Sesbania chromium uptake by 51.4% under specific treatments. Bioconcentration factor (BCF) confirmed that both crops accumulated nickel and chromium, with Sesbania showing high accumulation for both. Regarding carbon sequestration, soybean showed a 78% increase in CO_2 sequestration after 90 days with the 20 t/ha sludge and PNSB treatment, while sesbania increased by 46%. A positive correlation between CO_2 sequestration and heavy metal adsorption was observed, with soybean nickel uptake rising by 285%. Additionally, PNSB promoted earlier flowering in soybean, while excessive sludge might suppress root nodule formation in Sesbania.

Keywords: Wastewater sludge, Non-sulfur photosynthesis bacteria (*Rhodopseudomonas plustris*), soil fertility, Bioconcentration factor (BCF), Carbon sequestration

1. Introduction

Sludge generated from wastewater treatment plants contains abundant plant nutrients (such as nitrogen, phosphorus, and potassium) and organic matter, which can help improve soil structure, increase water retention capacity, and enhance microbial activity. However, untreated sludge often contains pathogens, heavy metals, and odorous organic compounds (such as hydrogen sulfide and VOCs), which may pose risks to crops and the environment, reducing its acceptance for field application.

To address these issues, common treatment techniques include thermal treatment, anaerobic digestion, composting, and lime stabilization. These stabilization methods can effectively reduce pathogens, minimize odors, and enhance nutrient stability. Among them, anaerobic digestion not only improves sludge stability and reduces volume, but also promotes carbon sequestration, reduces CO_2 and N_2O emissions, and in certain cases even results in net negative soil emissions. Composting, on the other hand, can convert sludge into odorless, highly stable organic matter with significant soil-improving effects (Li et al., 2024).Numerous studies have confirmed the multiple benefits of sludge application to crops and soils. For example, previous research found that appropriate application can promote hypocotyl growth and increase the yields of crops such as rapeseed, maize, and sunflower (Kominko et al., 2022).

Despite the high potential of sludge for soil application, heavy metal residues and accumulation remain the most critical potential risks. For example, zinc, cadmium, and mercury may be transformed into less bioavailable residual or oxidized forms during treatment, but under certain environmental conditions, they can still be released, absorbed by plants, and enter the food chain (Leila et al., 2017).

2. Materials and Methods

This study used short growth cycle green manure crops *Sesbania cannabina* (Sesbania) and *Glycine max* (Soybean) to investigate the effectiveness of anaerobic sludge and photosynthetic bacteria as soil amendments, with the aim of facilitating future applications in afforestation soils. The experiment compared five treatments: no amendment, sludge 10 t/ha, sludge 20 t/ha, sludge 10 t/ha + *Rhodopseudomonas palustris* (PNSB), and sludge 20 t/ha + *R. palustris*, to assess the effects of different sludge and photosynthetic bacteria application rates.

Carbon sequestration of the two green manure crops was measured under different treatments and sampling days. The physicochemical properties of the soil after 90 days of application were also compared, including total carbon, total nitrogen, available phosphorus, exchangeable potassium, and pH, to assess the differences in soil properties under different sludge application treatments.

This study also conducted analyses of the major heavy metals, examining their concentrations in the soil, Soybean, and Sesbania at different sampling times. In particular, the differences in zinc, nickel, copper, and chromium contents among soil, Soybean, and Sesbania were compared.

3. Results and Discussion

3.1. Using wastewater sludge and R. palustris as soil amendments to enhance soil carbon sequestration

This study employed short growth cycle green manure crops Sesbania and Soybean to rapidly screen and evaluate the effectiveness of anaerobic sludge and photosynthetic bacteria as soil amendments, with the aim of facilitating their future application in afforestation soils. The results of soil physicochemical properties after 90 days of application are shown in Table 1. The results indicate that both sludge application and sludge combined with PNSB treatment increased soil total carbon and nitrogen contents,

with total carbon increasing from 2.24% to a maximum of 2.53% and total nitrogen from 0.24% to 0.29%. This suggests that co-application with R. palustris can effectively enhance carbon fixation and nitrogen storage, promote nitrogen cycling and nutrient utilization by crops, and increase carbon storage and growth potential. Available phosphorus concentrations also increased significantly, especially under combined photosynthetic bacteria and sludge application, which may be related to microbial metabolism promoting phosphorus release. Exchangeable potassium levels generally increased with application rate, while pH rose from 5.48 in the control to above 6.5 in the photosynthetic bacteria treatment, improving the acidic soil environment.

Table 1. The soil properties analysis after 90 days under different conditions.

	Unit	Blank	Sludge 10 t/ha	Sludge 20 t/ha	Sludge 10 t/ha+ PNSB	Sludge 20 t/ha+ PNSB
TC	(%)	2.24	2.33	2.46	2.41	2.53
	(kg/ha)	36475	38025	40065	41866	43955
TN	(%)	0.24	0.25	0.26	0.27	0.29
	(kg/ha)	3884	4063	4259	4665	4961
AP	(mg/kg)	1037	1406	1628	1937	1563
EK	(mg/kg)	117.5	119.0	136.6	149.8	152.5
pH		5.48	6.48	5.42	6.53	6.55

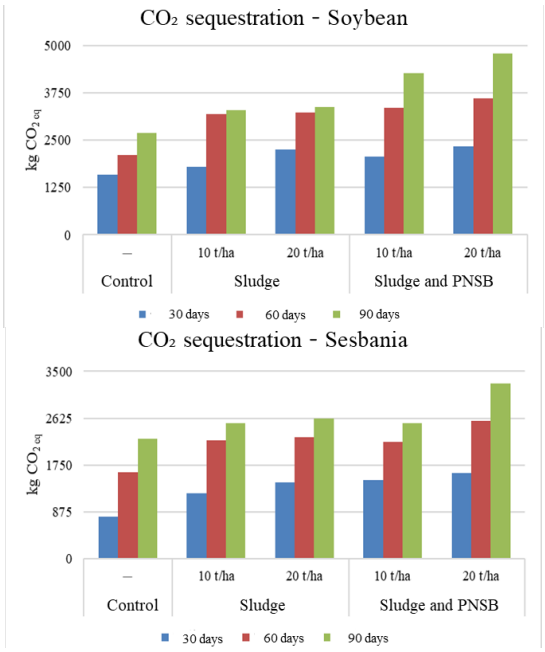

Fig. 1. Carbon sequestration of Soybean and Sesbania under different conditions after 30, 60 and 90 days.

Further comparison of CO_2 sequestration between the two crops (Figure 1) showed that, regardless of species, both sludge application and its combination with *R. palustris* effectively increased carbon sequestration. After 90 days, *Glycine max* reached the highest sequestration level at 4,795.54 kg CO_2-eq, while *Sesbania cannabina* sequestered approximately 3,276.32 kg CO_2-eq, indicating that *Glycine max* has a greater carbon fixation capacity. In addition, CO_2 sequestration for both crops increased steadily over time, reflecting the cumulative nature of carbon sink benefits. Notably, under *R. palustris* treatment, the increase between 30 and 90 days was significantly greater than that of sludge-only treatments, suggesting the potential role of *R. palustris* in enhancing plant photosynthesis and root development.

3.2. Heavy Metal Effects of Using Wastewater Sludge and PNSB as Soil Amendments

Since wastewater sludge often contains high levels of heavy metal contaminants, special caution is required when using it as a soil amendment. Therefore, this study conducted heavy metal analyses on soil, Soybean, and Sesbania at different sampling times. Heavy metal concentrations in the soil varied under different application treatments and showed a dose-dependent effect. The most notable change was observed for nickel, which increased from 131 mg/kg to 309 mg/kg as the sludge application rate increased. Given that nickel content in pure sludge was only 91 mg/kg, this increase is presumed to be related to the interactive release of nickel through association with oxides or organic matter.

Regarding the effect of photosynthetic bacteria, no significant differences were observed between treatments without additional R. palustris application. This may indicate that the short-term inhibitory effect of photosynthetic bacteria on certain heavy metals is unstable, highlighting the need for long-term monitoring to determine whether other strains possess stable heavy metal suppression capabilities.

Further analysis of heavy metal accumulation in crop tissues showed that under different sludge and photosynthetic bacteria treatments, the concentrations of Zn, Ni, Cu, and Cr in Soybean and Sesbania exhibited varying degrees of dose-dependent effects. For both species, the same types of heavy metals were predominantly accumulated, with nickel and chromium showing the highest levels. Within 90 days, Soybean accumulated Ni up to 126.0% (under the 20 t/ha sludge treatment), while Sesbania accumulated Cr up to 51.4% under the combined treatment of photosynthetic bacteria and 20 t/ha sludge.

4. Conclusions

Overall, the co-application of sludge and *R. palustris* not only improved soil physicochemical properties but also enhanced crop carbon sequestration efficiency, further promoting soil carbon sink potential and contributing to the reduction of agricultural system carbon footprints and sustainable management.

Acknowledgements

The authors acknowledge all the participants of the NSTC project.

References

Li, L., Li, H., Tong, L., & Lv, Y. (2024). Sustainable Agriculture Practices: Utilizing Composted Sludge Fertilizer for Improved Crop Yield and Soil Health. Agronomy, 14(4).

Kominko, H., Gorazda, K., & Wzorek, Z. (2022). Effect of sewage sludge-based fertilizers on biomass growth and heavy metal accumulation in plants. J Environ Manage, 305, 114417.

Leila, S., Mhamed, M., Hermann, H., et al. (2017). Fertilization value of municipal sewage sludge for Eucalyptus camaldulensis plants. Biotechnol Rep (Amst), 13, 8-12.

Optimizing Water Application Strategies for Climate-Resilient Amaranthus Production in Paddy Field: Insights from On-Farm Experiments in Northern Ghana

E. Salifu [1*], M. Yamada [2], I. M. Alhassan[1]

[1] School of Engineering, University for Development Studies, Tamale, Northern Region, Ghana

[2] Japan International Research Center for Agricultural Sciences, Tsukuba, Ibaraki Prefecture, Japan

* Corresponding author. Email: esalifu@uds.edu.gh

Abstract

In northern Ghana, water scarcity and climate variability pose a significant threat to smallholder agriculture and rural livelihoods, thereby necessitating the need for innovative and sustainable water management. The experiment assessed the effect of different irrigation frequencies (daily to weekly) and quantities (2 - 8 mm) on yield parameters of *Amaranthus cruentus*, as a secondary crop to rice, under two different fertilizer regimes. Key findings revealed that the average yield of Granulated Chemical Fertilizer (4.67 t ha^{-1}) and Burkina Phosphate Fertilizer (4.65 t ha^{-1}) treatments showed no significant difference. In terms of the water treatments, there was significant effect on yield. The T2 (twice daily of 4 mm irrigation) achieving the highest crop water productivity (CWP) of 1.26 kg m^{-3}, outperforming the control (once daily of 8 mm irrigation) which had CWP of 0.813 kg m^{-3} by 55% whilst maintaining moderate yield of 4.53 t ha^{-1} versus the control's 5.85 t ha^{-1}. The findings further revealed that for the best reduced water-use frequency with optimal CWP, the T4 (2 mm/day applied daily) could be considered under drip irrigation with organic mulching to further reduce evaporation. This could maintain yield within acceptable limits (80 % of control) while cutting water use by 75%. This study highlights that, farmers can reduce water use and application frequency significantly while maintaining yield, through aligning water application with crop water requirement. This underscores the viability of smart irrigation in enhancing climate resilience for smallholder farmers. These practices conserve scarce water resources through sustainable water utilization.

Keywords: *Amaranthus cruentus, Deficit irrigation, Crop water productivity, Climate resilience*

1. Introduction

Climate-induced water scarcity severely threatens smallholder farmers who rely on rainfed agriculture and dry-season vegetable production for livelihoods in northern Ghana (Acheampong, E.N. et al., 2014). Promoting the nutritious indigenous vegetable *Amaranthus cruentus* (*A. cruentus*) is a promising strategy due to its short growth cycle, high nutritional value, and adaptability to marginal conditions (Achigan-Dako et al., 2014), particularly as a secondary crop after rice cultivation. However, the crop cultivation is hindered by a knowledge gap — specifically, the lack of localized data on its crop water requirements and its response to efficient irrigation strategies under semi-arid conditions (FAO, 2017). The aim of the research is to evaluate different irrigation regimes to determine their effects on *A. cruentus* yield and crop water productivity.

2. Materials and Methods

2.1. Experimental Design and Treatments

The study was conducted during the 2023/2024 off-season at the Golinga irrigation scheme in the Northern Region of Ghana. In the scheme, *A. cruentus* was cultivated as a secondary crop following rice. The experiment used a 2×6 (comprising six water and two kinds of fertilizer) factorial Split-Plot Design with three replications, totaling 12 treatments and 36 plots. The water application treatments are presented in Table 1, based that 8mm day^{-1} is generally sufficient (Grubben and Denton, 2004), and farmers typically irrigate in the morning and afternoon. Two types of fertilizer are applied: Granulated Chemical Fertilizer (GCF, N20-P10-K10+3S, 300kg ha^{-1}) and Burkina Phosphate Fertilizer (BPF, calcinated rock phosphate, P^2O^5 18.5%, K^2O 14.9%). BPF is supplemented with Urea, Potassium fertilizer, and Sulfur fertilizer to achieve a composition similar to GCF. BPF was used because it has potential as a more cost-effective than GCF (Fukuda et al., 2021). The seedlings were grown in the nursery bed before being transplanted on 31 March 2024 to the trial field. Three harvests were conducted during a 90-day period following transplanting.

2.2. Data Collection and Analysis

Data was analyzed using a two-way ANOVA for a split-plot design in R Studio to determine the main and interaction effects of water and fertilizer treatments. Significant means were separated using Tukey's HSD test at a 5% significance level. Crop Water Productivity (CWP) was calculated as the fresh yield (t ha^{-1}) divided by the total irrigation water applied (m^3 ha^{-1}).

Table 1: Water application per treatment

Treat.	Freq.	Irrigation (mm time^{-1})	Total App. (mm d^{-1})
C	AM & PM, 7 d wk^{-1}	4	8
T1	PM, 7 d wk^{-1}	8	8
T2	AM & PM, 7 d wk^{-1}	2	4
T3	PM, 1 d 2 d^{-1}	8	4
T4	PM, 7 d wk^{-1}	2	2
T5	PM, 1 d wk^{-1}	8	1.14

3. Results and Discussion

Based on the data provided, a key finding is that water application is the primary factor influencing the yield, while fertilizer has no significant different effect (Table 2). In Table 3, the most notable insight is the equal yield between T2 and T4 (4.5 t ha^{-1}), despite T4 using half the water (1,800 m^3 ha^{-1} vs. 3,600 m^3 ha^{-1}). This highlights T4 as a superior, water-efficient strategy. The analysis of Crop Water Productivity (CWP) further supports this conclusion. T4 achieved the highest practical CWP of 2.52 kg m^{-3}, a remarkable 211 % increase over the control's 0.81 kg m^{-3}. While Treatment T5 had an even higher CWP, its disproportionately low yield of 3.87 t ha^{-1} makes it agronomically non-viable.

Table 2: Treatment effect on yield

Main Effect	p-value	Significance
Water Treatments	0.001	Significant
Fertilizer Treatments	0.221	Not Significant
Water × Fertilizer Interactions	0.085	Not Significant

Table 3: Crop water productivity of treatments

Treat.	Yield* (t ha^{-1})	Total Water Volume (m^3 ha^{-1})	CWP (kg m^{-3})
C	5.85	7,200	0.813
T1	4.96	7,200	0.689
T2	4.53	3,600	1.258
T3	4.18	1,800	2.322
T4	4.54	1,800	2.522
T5	3.87	146.6	26.40

*Yield means the average value of GCF and BPF treatment. The average yield of GCF is 4.67 t ha^{-1}, and BPF is 4.65 t ha^{-1}.

4. Conclusions and Recommendation

This study investigated optimal irrigation strategies for *A. cruentus* cultivated following rice in Northern Ghana. The findings indicate that irrigation volume and frequency significantly influenced both yield and CWP, whereas fertilizer type exhibited no statistically significant effect. Given the experimental site's history as a paddy rice cultivation area, future research should incorporate assessments of groundwater dynamics, particularly their impact on soil moisture retention and nutrient availability by applied fertilizer. The experiment was conducted during the dry season, a period characterized by increased competition for water resources due to domestic and livestock demands. Under these conditions, T4 achieved the highest CWP, suggesting its potential as a water-efficient option. Its yield was comparatively lower than that of the control and T1, which may limit its appeal to production-oriented farmers. However, it could be considered under drip irrigation with organic mulching to further reduce evaporation and increase the yield. This underscores the need for coordinated water resource management that accounts for both agricultural and non-agricultural water demands. As traditional vegetables such as *A. cruentus* are predominantly cultivated by women, it is imperative that water-use planning ensure equitable representation and address gender-specific needs. Furthermore, the successful adoption of water-saving techniques like T4 necessitates the establishment of demonstration plots and targeted extension activities to facilitate farmer understanding and acceptance.

References

Acheampong, E.N., Ozor, N. & Owusu, E.S. Vulnerability assessment of Northern Ghana to climate variability. Climatic Change 126, 31–44 (2014). https://doi.org/10.1007/s10584-014-1195-z

Achigan-Dako, E.G., Sogbohossou, O.E.D. & Maundu, P. Current knowledge on Amaranthus spp.: research avenues for improved nutritional value and yield in leafy amaranths in sub-Saharan Africa. Euphytica 197, 303–317 (2014). https://doi.org/10.1007/s10681-014-1081-9

FAO. Water for Sustainable Food and Agriculture. 2017. p16, ISBN 978-92-5-109977-3

Fukuda, M., Soma, DM., Iwasaki, S., Nakamura, S., et al. (2021). Site-specific responses of lowland rice to acidulated and calcined phosphate rock fertilizers in the Center-West region of Burkina Faso. PLOS ONE 16(4): e0250240. https://doi.org/10.1371/journal.pone.0250240.

Grubben, G.J.H., Denton, O.A. (2004). Plant Resources of Tropical Africa 2. Vegetables. PROTA Foundation, Wageningen, Netherlands / Backhuys Publishers, Leiden, Netherlands / CTA, Wageningen, Netherlands, 67-72.

A Strategic Framework for Agricultural Water Allocation Using Modern Portfolio Theory

HU Ming-Che・WANG Li-Kuan・WEN Tzai-Hung

Abstract

Taiwan's rainfall exhibits pronounced temporal and spatial unevenness, characterized by distinct wet and dry seasons. This imbalance, intensified by climate change, has led to persistent regional water shortages, particularly during the dry season. Managing agricultural water resources under these conditions poses growing challenges, given increasing climate variability, limited reservoir capacity, and rising water demand.

This study proposes an innovative agricultural water resource management model grounded in Modern Portfolio Theory (MPT). By applying MPT's mean-variance framework, the model treats diverse agricultural water sources as a portfolio, enabling the optimization of water allocation while minimizing supply risk. This approach strategically balances reliability and risk, enhancing the system's resilience to seasonal and regional fluctuations. The research develops a comprehensive MPT-based water allocation model to evaluate current management strategies and optimize distribution in water-scarce regions during the dry season. The resulting policy recommendations aim to support sustainable agricultural water use in Taiwan. By integrating risk analysis into water resource planning, this study offers a scientific and actionable framework for improving agricultural water management under climate uncertainty, promoting more efficient and equitable water distribution.

Optimizing Agricultural Water Distribution with Network Flow Model

Chang-Ying Lee [1], Ming-Che Hu [1*], Ching-Pin Tung[1]

[1] Department of Bioenvironmental System Engineering, National Taiwan University, Taipei, Taiwan

* Corresponding author: mchu@ntu.edu.tw

Abstract

This research aimed to provide a novel optimization network flow model in water resource distribution, particularly in agricultural water. Due to the severe extreme hydrological events that occurred in recent years, the water resource distribution in Taiwan has been seriously impacted. Furthermore, reducing agricultural water is a compromised policy in competition with domestic and industrial water demand. However, Long-term water supply reduction or fallowing will irreversibly impair the agriculture sector. This model could facilitate evaluating the policy for agricultural water distribution. The model is based on network flow programming and has three novel features: firstly, the hydrological data is adopted in terms of a time series function instead of constants during a specific time window; secondly, the function of water storage is considered in the model; thirdly, the hydrological data are transformed from the time domain to the frequency domain. This novel model exhibits practical significance for facilitating water agricultural water resources management and providing decision-support information for determining cropping policy.

Keywords: agricultural water, network flow, frequency domain.

1. Introduction

Agricultural water in Taiwan is meeting the challenges from the environment and the industries. The environmental challenges include climate change and extreme weather events. During 2000-2001, the southern region of Taiwan encountered severe drought events. In 2000, 19,000 ha of paddy fields were fallowed. In 2001, the fallowed paddy fields even reached 47,000 ha. The damages reimbursed by the Agriculture Department reached billions of NTD. The industrial challenges are mainly the high-tech industrial competition for water resources. When the water resources are scarce, the agricultural water is often saved for domestic and industrial demand for water.

Network flow and other programming methods has been used in water resources distribution. Sun et. al (1995) provided a general network programming algorithm solving the problem where the total supply and demand were balanced. The general model can separate the variables into network variables and non-network variables, which could be solved by network programming and other programming methods, respectively.

Labadie (2004) reviewed several advanced mathematical models in reservoir operation, some of which included probabilistic and fuzzy logic characteristics. He also predicted that neural networks could be broadly applied in the future.

Chou et. al (2014) provided an objective function in the network flow programming model to simulate reservoir operation and water resources allocation. He also defined cost coefficients of flow cost systematically and scientifically. Simulated examples in this study involved the operation of multiple inter-basin reservoirs.

In the original network flow model, constant flow is typically assumed, and the storage function is not considered. However, in water resources distribution, time-varying flow and storage functions are common and critical. Previous studies have neither treated the issues of time-varying flow in their models nor addressed the storage capacity at nodes to improve upon the limitations of the original network flow model. In this research, we provide our suggestions and methodology to tackle these issues.

2. Materials and Methods

Network flow model

As shown in Figure 1, this is the conceptual model of network flow. Nodes {A, B, C} are a collection of nodes in the network flow. Each node has inflow I(t), outflow O(t), demand D(t) and storage S(t). These nodes have interflow F(t). With the conceptual scheme, we can represent realistic reservoirs and the pipeline connecting them as a water supply network system.

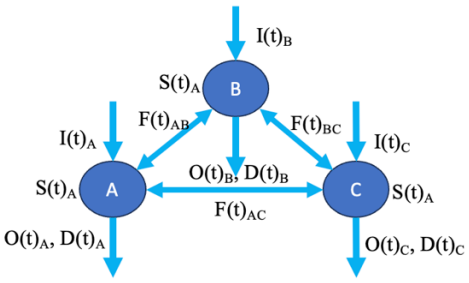

Figure 1. A conceptual scheme of network flow.

Fourier Series

When we consider a hydrological time series $f(t)$, we can transform it into a linear combination of periodical basis functions, we call it Fourier series of function $f(t)$.

$$f(t) = a_0 + \sum_{n=1}^{\infty}(a_n(\cos(nt) + b_n\sin(nt)) \quad (1)$$

$$a_0 = \frac{1}{2\pi}\int_{-\pi}^{\pi} f(t)dt \quad (2)$$

$$a_n = \frac{1}{\pi}\int_{-\pi}^{\pi} f(t)\cos(nt)dt \quad (3)$$

$$b_n = \frac{1}{\pi}\int_{-\pi}^{\pi} f(t)\sin(nt)dt \quad (4)$$

where a_0 is the mean value of f(t) during a period; a_n is the coefficient of the n-th cosine basis function;b_n is the coefficient of the n-th sine basis function.

Optimization

We need a criterion to find an "optimized" water distribution strategy. With this sense, in each node, we want the outflow to satisfy the demand as much as possible under the limitation of constraints. Since the hydrological time series is transformed into the frequency domain, we would like to optimize the decision variables in the frequency domain rather than in the time domain. Thus, we set up our optimization model as follows:

$$\text{Min } Z = (a_0^{out} - a_0^{DE})^2 + \sum_{n=1}^{N}(a_n^{OUT} - a_n^{DE})^2 + (b_n^{OUT} - b_n^{DE})^2 \quad (5)$$

$$\frac{dS(t)}{dt} = I(t) - O(t) \quad (6)$$

$$0 \le S(t) \le S_C \quad (7)$$

$$O(t) \ge 0 \quad (8)$$

Where $\{a_0^{out}, \{a_n^{OUT}\}_{n=1}^{N}, \{b_n^{OUT}\}_{n=1}^{N}\}$ are collection of coefficients of Fourier series of outflow O(t), and $\{a_0^{DE}, \{a_n^{DE}\}_{n=1}^{N}, \{b_n^{DE}\}_{n=1}^{N}\}$ are collection of coefficients of Fourier series of demand D(t). The objective function Z in Equation (5) is minimized such that the differences of corresponding coefficients between outflow and demand are as small as possible. Equation (6) is a mass balance condition to constrain the relation between outflow, inflow and storage of the node. Equation (7) is a limitation of storage S(t) under node storage capacity S_C and positive. Equation (8) is a positive constraint for outflow O(t).

3. Results and Discussion

3.1. Background of the research region

We built a virtual inter-basin water supply network of the southern region in Taiwan, as shown in Figure 2. The Tsengwen-Wushantou(TW) Reservoir is a two-reservoir system in charge of agricultural, domestic and industrial water supply. Nanhua(NH) Reservoir is in charge of the domestic and industrial water supply. Gaoping River Weir (GP) is in charge of the industrial and domestic water supply. TW and NH are connected by a two-way pipeline, whereas NH and GP are connected by a one-way pipeline from NH to GP.

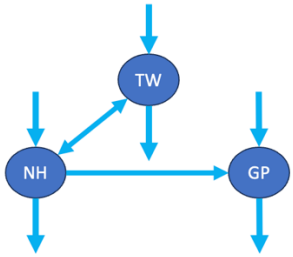

Figure 2. Reservoir network system of the southern region in Taiwan.

3.2. Result

From the Table 1, we can observe the water shortage amount between no connection operation and network connection operation. The total shortage amount is reduced by 7.9%. Though the shortage in NH has increased, the shortage in TW is reduced more.

We can also see the pattern of outflow and demand in TW as shown in the Figure. 3. The patterns of variation of outflow (blue line) and demand (orange line) in the time domain are quite similar. This feature is the result of minimizing the coefficients between outflow and demand in the frequency domain.

Table 1. Water shortage amount comparison.

Operation	TW ($10^4 m^3$)	NH ($10^4 m^3$)	GP ($10^4 m^3$)	Total ($10^4 m^3$)
No connection	26,141	19	682	26,841
Network connection	23,171	858	682	24,710
Improving rate(%)	11.4	-4415.8	0	7.9

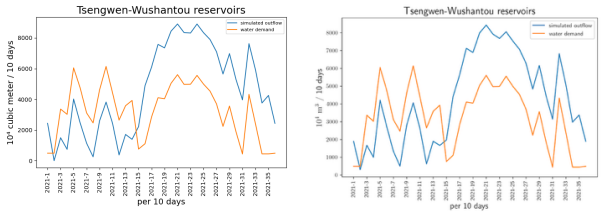

Figure 3. Tsengwen-Wushantou Reservoir outflow and demand time series, where the left is no connection

4. Conclusions

From the simulation result, the model could simulate the network connection of reservoirs crossing the basins. The water shortage can be reduced through the pipeline to balance the unevenness of inflow into the reservoirs. Thus, we can use this model to evaluate the network efficiency for the water supply network and assess the strategy of water distribution.

In summary, we can conclude that the novel model exhibits the following advantageous features:

1. parameters and variables in the model are denoted in terms of a function.
2. optimization in frequency domain
3. considering storage function in node
4. similarity of variation in the time domain between outflow and demand

References

Sun, Y. H., WG. Yeh, W., Hsu, N. S., & F. Louie, P. W. (1995). "Generalized network algorithm for water-supply-system optimization". *Journal of Water Resources Planning and Management*, *121*(5), 392-398.

Labadie, J. W. (2004). Optimal operation of multireservoir systems： State-of-the-art review. *Journal of water resources planning and management*, *130*(2), 93-111.

Chou, F. F., & Wu, C. W. (2014). "Determination of cost coefficients of a priority-based water allocation linear programming model–a network flow approach". *Hydrology and Earth System Sciences*, *18*(5), 1857-1872.

Rapid Expansion of Irrigation through Participatory Irrigation Management (PIM) in Madhya Pradesh (MP), India

Kenichi Yokoyama [1*], Atsushi Ishii [2]

[1] Graduate School of Science and Technology, Land and Water Resources Management, University of Tsukuba, Japan

[2] Institute of Life and Environmental Sciences, University of Tsukuba, Japan

* Corresponding author. Email: s2530252@u.tsukuba.ac.jp

Abstract

In 2010, Indian state of Madhya Pradesh reinforced participatory irrigation management (PIM) with rigorous pursuit of equitable water distribution, and has achieved near 3-fold increase in dry season irrigated area (IA). The study assessed impacts in individual schemes and their relations with water resource availability, scheme size, and other factors by collecting and analyzing scheme-wise annual operations data and design parameters. It was found that (i) IA has been significantly increased in individual schemes; (ii) increased IA is driven by improved irrigation efficiency (IE); (iii) annual IA is affected by available reservoir storage, (iv) changes are more significant for smaller schemes having had lower IA a priori, while larger schemes is achieving higher IA exceeding their design targets, possibly due to robustness to apply equitable distribution, stronger capacity of PIM institutions, and other factors such as infrastructure quality.

Keywords: Participatory irrigation management (PIM); Irrigation efficiency; Equitable water distribution; Sustainability; Water user associations

1. Introduction

PIM is pursued in many developing countries to enhance water use efficiency and sustainability, by forming water user associations (WUAs) and engage them in operation and maintenance (O&M) of irrigation facilities. However, its progress and impacts are less than expected, due to reasons including difficulties in building sufficient capacities (IWMI and FAO, 2008; ADB, 2017; Sato et al., 2007). However, MP state in India has shown a stunning case, where PIM was reinforced in 2010 and led to almost three-fold increase in dry season irrigation (from October to March) from 0.63 million hectare (ha) in 2009 to 1.79 million ha in 2021 in their large-scale schemes. In MP, equitable water distribution is rigorously pursued with specific measures including (i) seasonal irrigation planning is jointly done by Irrigation Department (ID) and WUAs, with qual allocation of about 500 mm; (ii) water is supplied by rotating canals for watering, during which tail-first water offtake is practiced; and (iii) close monitoring and control is done by ID and WUAs.

There are existing studies that have assessed the state-level macro impacts of PIM in MP. While initial impact in 2000s was marginal (Ghosh et al., 2019), significant macro impact of 2011 measures was noted (Julaniya et al., 2016; Shah et al., 2016). This study assessed their impacts at the individual scheme level and their relations with water resource availability, scheme size, and other factors.

2. Materials and Methods

Based on the available data in the public domain in India, a data set was established covering scheme wise irrigation performance and factors that may affect the performance. It comprises (i) annual records of 77 large-scale schemes in MP covering dry season IA and start- and end-of-season reservoir storage levels in 2009–23; (ii) scheme wise hydrological parameters: reservoir storage capacity and catchment area; and (iii) monthly rainfall (in eastern and western MP). The 77 schemes comprise 16 major (having design IA of more than 10,000 ha) and 61 medium (1,000–10,000 ha) schemes.

The study assessed the individual scheme wise changes in IA and irrigation efficiency (IE, derived from reservoir storage level and IA) before and after PIM reinforcement, and their relations with scheme size, start-of-season reservoir storage, and other unattributable factors, of which data are yet to be collected.

3. Results and Discussion

3.1 Change in irrigated are (IA) before and after PIM.

Figure 1 shows the annual IA and rainfall for all 16 major schemes and 20 medium schemes (largest 10 each in 5,000–10,000 ha and 1,000–5,000 ha categories).

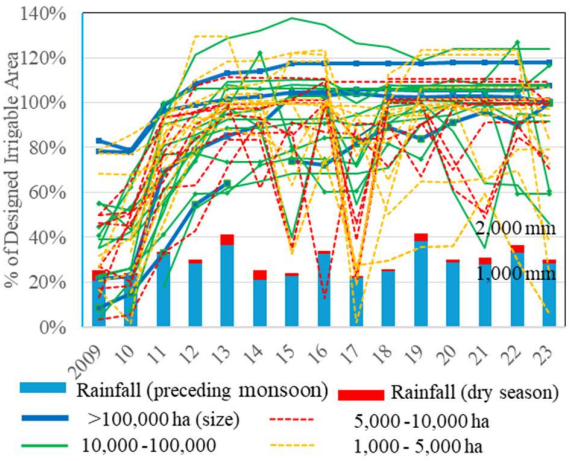

Figure 1. Annual Changes in Irrigated Area (2009-23)

IA increased substantially after PIM reinforcement and is sustained. The rate of IA compared with design IA in 77 schemes increased from 34% in 2009–11 to 88% in 2017–23 on average. Figure 1 shows that major schemes take longer years to reach full or maximum IA, some 3–5 plus years, compared with 2–3 years for medium schemes, possibly due to the need for spreading improved water distribution practices in larger areas. There is also high annual fluctuation for smaller schemes, while the largest four schemes (accounting for 58% of total design IA of 77 schemes) demonstrate highly stable IA.

3.2. Change in irrigation efficiency (IE) and start-of-season reservoir storage

Figure 2 presents the average IE of individual schemes during and after PIM reinforcement. IE is measured as hectare (ha) of land irrigated in the scheme by one million

cubic meter (MCM) of stored water. IE has improved by 94% on average. Most efficient 80% of schemes have IE of above 143 ha/MCM in 2017-23, improved from 84 ha/MCM in 2009-11. On the other hand, initial reservoir storage of dry seasons has reduced by 22% between 2009-11 and 2021-23 despite similar rainfall levels.

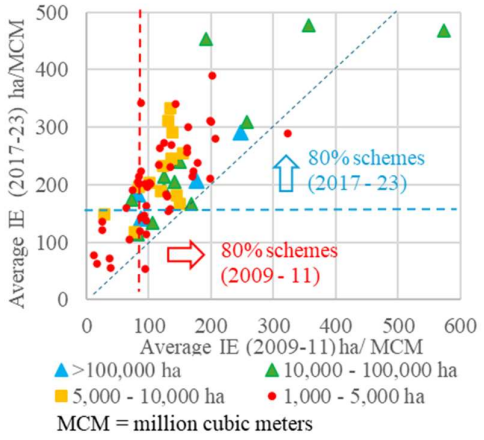

Figure 2. Average IE before and after PIM Reinforcement

Thus, in MP, IA increase is driven by improvement in IE, or better water distribution, despite declining water resources available. The latter may be due to change in water use pattern during the preceding monsoon, possibly the impact of paddy cultivation that has increased from 9.7% of net sown area in 2009 to 21.3% in 2023 in MP. Unless abated or managed well, this may eventually affect the sustainability of large dry season irrigation.

3.3. Impact of start-of-season reservoir storage on IA.

Figures 3 show the relations of reservoir storage with IA in selected drought and normal years for the same number of schemes as Figure 1. Dry season IA is critically influenced by the reservoir storage levels. The largest schemes (in blue) have stable storage, hence stable IA (as shown in Figure 1).

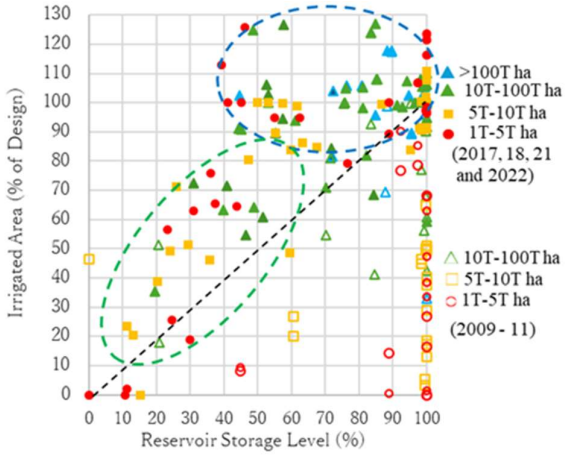

Figure 3. Relationship between reservoir storage and IA

As to the changes before and after PIM reinforcement, IA was generally low before, even at high reservoir storage. This is more evident in smaller schemes, which have shown much higher magnitude of changes after PIM reinforcement. On the other hand, larger schemes have higher IA after PIM exceeding design IA, hence showing higher performance. This may indicate the stronger PIM institutions in larger schemes, along with other factors such as quality of infrastructure and O&M.

Another notable feature is that irrigation schemes cope with lower reservoir storage down to 50–60% level by maintaining high IA while enhancing IE (blue dotted area), after which IA is adjusted downward (green dotted area). This indicates that, when available reservoir water is less than full, they maintain equitable water distribution in a fixed IA and increase IE (or reduce water applied). In this relation, equitable water distribution has been regarded as a principle of successful PIM by Sato et al. 2007c. Thus, the level of robustness of equitable distribution in the schemes could be another factor that may be contributing to higher IA and their sustainability.

4. Conclusion

In MP state in India, dry season irrigation increased substantially in individual major and medium schemes. This was driven by increased IE despite declining water availability of reservoirs. Their IA is critically dependent on reservoir storage available at its beginning. Larger schemes show higher IA stability due to stable storage availability. The change in IA after PIM reinforcement was higher in magnitude in medium schemes but this was due to their lower IA before 2011. The measures have brought major schemes achieving higher IA exceeding design level, possibly thanks to stronger PIM institutions and other reasons such as quality of infrastructure and O&M. They also cope with drought years by maintaining high IA as much as possible and sharing available storage and reducing water applied. The robustness of this equitable distribution practice may be another factor contributing to higher irrigation performance.

The above conclusion is drawn based on available data in the public domains. Further research and field surveys are planned to substantiate the data and analysis, collect further data on wider range of attributable factors, and analyze the mechanisms leading to the specific levels of irrigation performance in more details.

References

Asian Development Bank (ADB) 2017. Irrigation Subsector Guidance Note.

Ghosh G., Kolady D.E., Usha D., S. Gorain, S.K. Srivastava, B. Mondal, Aug. 2019. Spatio-temporal variations in effects of participatory irrigation management (PIM) reform in India: A panel data analysis, Agriculture Water Management, Volume 222, pp.48-61.

International Water Management Institute (IWMI) and Food and Agriculture Organization (FAO) 2008. Irrigation Management Transfer: Worldwide efforts and results.

Julaniya R.S., Singh M., Choubey M.G., and Biswaset S., 2016. A Management Approach to Increase Irrigated Area and Production in Madhya Pradesh, India, ICID 2nd World Irrigation Forum, Thailand

Satoh M., Kono K., Tassanee O., Ishii A., 2007. Principles and realization methodology of participatory water management, Journal of the Japanese Society of Irrigation, Drainages and Reclamation 75(7).

Shah T., Mishra G., Kela P., Chinnasamy P., 2016. Har Khet Ko Pani? (Water to Every Farm?) Emulate Madhya Pradesh's Irrigation Reform, IWMI-TATA Water Policy Program

Application of Time-Lapse Ion-Exchange Resin Capsules for Assessing Spatial Characteristics of Irrigation Water Pollution: A Case Study in the Dali Area, Taichung City, Central Taiwan

Yunwei Tan[1*], Fengwen Chen[1], Manzin Wang[2], Minyahng Xie[2], Tingyi Li[2]

[1] Agricultural Engineering Research Center, Taiwan

[2] Irrigation Agency Taichung Management, Taiwan

* Email: tan0710@aerc.org.tw

Abstract

Taiwan has long faced critical challenges in water quality management, particularly in regions characterized by the coexistence of agricultural and industrial activities. The Dali area of Taichung City represents a typical case where irrigation water is subject to persistent risks of heavy metal contamination due to discharges from both upstream and surrounding industrial sources. To systematically characterize the spatial distribution of potential contamination hotspots, this study employed Time-lapse Ion-Exchange Resin Capsules (TIERC) in the Dali area beginning in 2023 to conduct a series of heavy metal pollution assessments. Three field surveys were carried out across 19 monitoring sites within the study area. The degree of contamination was quantified using the Nemerow Pollution Index (NPI), while spatial interpolation was performed through the Inverse Distance Weighting (IDW) method to generate spatial pollution distribution maps. The NPI values obtained from the three monitoring campaigns ranged from 0.2~1.38, 0~1, and 0~1.48, respectively. The results indicate that the study area generally exhibited conditions ranging from no pollution to slightly pollution. Moreover, a strong spatial correspondence was observed between identified pollution hotspots and the distribution of local industrial clusters.

This study highlights the efficacy and applicability of TIERC as a low-cost, labor-efficient tool for the long-term monitoring of heavy metal accumulation in irrigation water. Furthermore, the temporal and spatial identification of irrigation water pollution characteristics provides a scientific basis for future agricultural irrigation management and pollution mitigation strategies.

Keywords: Irrigation Water quality, Point Source Pollution, Resin Capsules

1. Introduction

Agricultural areas are widely distributed across central Taiwan. However, irrigation districts in this region encompass rural, industrial, and metropolitan zones, where farmlands, factories, and residential areas are closely adjacent to one another. This land-use configuration has led to the discharge of heavy metal-containing industrial wastewater into irrigation channels, thereby deteriorating water quality and potentially causing soil contamination and food safety issues in agricultural lands. Nevertheless, factory wastewater discharges are often difficult to trace due to their sporadic, short-duration, high-concentration, and spatially dispersed nature (Lin, 2016), which makes it challenging for conventional grab sampling to capture such events. In this study, the use of TIERCs (Time Lapsed Exchange Resin Capsules) was adopted to record the temporal accumulation of pollutants in irrigation water. This technique offers the advantages of low cost, high efficiency, and reduced labor requirements, and is expected to facilitate the identification and narrowing down of potential pollution sources from industrial facilities (AERC, 2024).

2. Study area and Methods

2.1. Study area

This study was conducted in Dali, central Taiwan, where agricultural areas are irrigated through canal systems supplied by adjacent rivers. Given that farmlands in the downstream irrigation area have previously been affected by heavy metal contamination, this study employed TIERCs (Time-Integrated Exchange Resin Capsules) to further investigate potential pollution sources. A total of 19 monitoring sites were deployed during 2023, as shown in Figure 1.

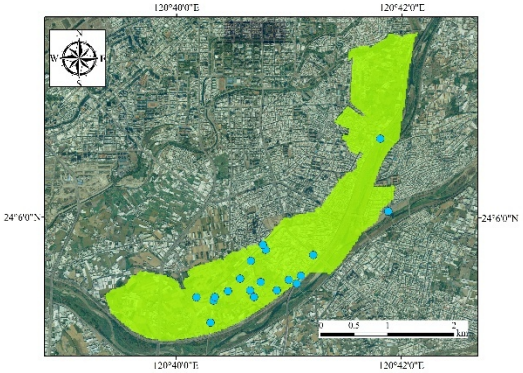

Figure 1. The study area.

2.2. Ion-Exchange The resin capsules

The TIERCs technique, developed by Zhang (2018), is typically deployed for 3~7 days to ensure adequate adsorption and avoid biofilm formation. After retrieval, capsules are rinsed to remove surface debris, and adsorbed heavy metals are measured using X-ray fluorescence (XRF) (Shih et al., 2019; Environmental Protection Administration, 2018). Metal-to-Sr concentration ratios are then calculated (Eq. 1), and NPI is used (Eq. 2) to identify sites with significant pollutant inputs.

$$X = \frac{C_x}{C_{Sr}} \quad (1)$$

$$X \geq \overline{X} + 2\sigma \quad (2)$$

In the formula: X is the ratio of a heavy metal concentration to Sr concentration; C_x is the concentration

of a heavy metal detected by XRF; C_{Sr} is the concentration of Sr detected by XRF; $\bar{X}$ is the average of the ratio of a heavy metal concentration to Sr concentration; σ is the standard deviation.

Figure 2. The TIERC.

In this study, the NPI was applied to assess overall environmental quality. The NPI integrates multiple heavy metal indicators by considering not only their average values but also highlighting the impact of the maximum single-factor index, thereby reflecting the potential hazard of the most dominant contaminant and enhancing the representativeness of the overall assessment results. The calculation formulas are presented in Equations (3)~(5).

$$P_n = \sqrt{\frac{P_i^2 + P_{i-\max}^2}{2}} \quad (3)$$

$$P_i = \frac{1}{n}\sum_{i=1}^{n}\left(\frac{C_i}{C_{si}}\right)^2 \quad (4)$$

$$P_{i-\max} = \frac{C_{\max}}{C_s} = \max\left(\frac{C_1}{C_{s1}}, \frac{C_2}{C_{s2}}, \ldots, \frac{C_n}{C_{s2}}\right) \quad (3)$$

In the formulas, Pn represents the comprehensive NPI; Pi is the pollution index of the i-th contaminant; Pi-max is the maximum single-factor pollution index; C_i is the measured concentration of the i-th contaminant; C_{si} is the standard limit value of the i-th contaminant; n is the number of evaluated contaminants; and C_s is the standard limit value of the contaminant with the highest pollution level.

Table1. The NPI classification.

Pn	Classification
$P_n \leqq 0.7$	No pollution
$0.7 \leqq P_n < 1.0$	Slight pollution
$1.0 \leqq P_n < 2.0$	moderate pollution
$2.0 \leqq P_n < 3.0$	Severe pollution
$P_n \geqq 3.0$	Extremely severe pollution

3. Results and Discussion

This study investigated irrigation water quality in Dali, central Taiwan, through three surveys in May, July, and September 2023 using TIERCs. The NPI and IDW interpolation were used to assess and map pollution levels. Results showed a consistent south-to-north gradient, with higher NPI values in mid- and downstream sections, especially around the Dali Industrial Park and Dali Creek, and lower values in upstream residential-agricultural areas. NPI values (0.2–1.48) indicated alert-level contamination. These findings suggest industrial effluents and surface runoff as major pollution sources. Enhanced monitoring, source tracking, and water treatment measures near industrial zones are recommended to reduce pollutant transport to downstream farmlands.

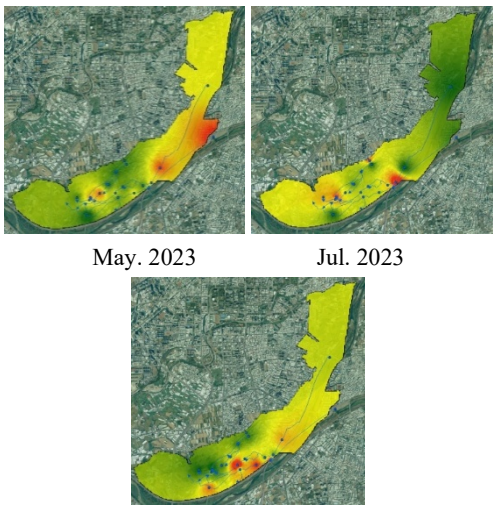

May. 2023 Jul. 2023

Sep.2023

Figure 3. The spatial estimation NPI of TIERCs.

4. Conclusions

The results indicate that irrigation system pollution in Dali is primarily concentrated around the Dali Industrial Park and along irrigation canals, suggesting that industrial activities play a dominant role in water contamination. In contrast, the northern areas, mainly agricultural and residential, exhibited lower pollution levels, indicating a strong spatial association between pollution sources and the clustering of factories. Moreover, the application of TIERCs demonstrates its potential for tracing water pollution sources.

References

[1] AERC, Agricultural engineering research center, ” The Investigation and Assessment of Irrigation Water Quality Monitoring and Potential Pollution Characteristics in Taichung Management Office Area in 2024, AERC-24-RR-08.

[2] AERC, Agricultural engineering research center, ”The investigation of water pollution in irrigation suspended period in Taichung management office area in 2021”, Taichung management office, irrigation agency, coincil of agriculture, excutive yuan, 2021, AERC-21-RR-11.

[3] AERC, Agricultural engineering research center, ”The water quality monitoring of high contaminated canals, advanced investigation of Nantun irrigation area and improvement planning of water quality in Datuliao canal, Taichung irrigation area in 2020”, Taichung management office, irrigation agency, coincil of agriculture, excutive yuan, 2020, AERC-20-RR-14.

[4] Agriharvest, “Wastewater discharge has nowhere to hide! this magical "capsule" can get the source through time and space”,2017.

[5] Environmental protection agency executive yuan, “National control and investigation plan for farmland with high heavy metal pollution potential (phase 5)”, EPA-105-GA02-03-A262.

[6] P.K. Shih, L.C. Chiang, S.C. Lin, T.K.Chang, W.C. Hsu, 2019," Application of Time-Lapse Ion Exchange Resin Sachets (TIERS) for Detecting Illegal Effluent Discharge in Mixed Industrial and Agricultural Areas, Taiwan", Sustainability 2019, 11, 3129; doi:10.3390/su11113129.

[7] S.C Lin,” Measuring Device with Ion-Exchange Resin and Measuring Method thereof”, national Pingtung university of science technology No.25.

[8] T.K. Chang,” Design and development of ion exchange resin time-lapse capsules for heavy metal monitoring”, ، soil and groundwater pollution remediation fund environmental protection agency executive yuan subsidy research and model field test project plan, 2018.

[9] Y.W. Tan, F.W. Chen, “Application of Ion Exchange Resin Capsules in Water Pollution Source Investigating in Taichung Area, Central Taiwan”, 2023, Published in Engineering Journal volume & issue, Vol. 38, no. 1,p. 67 Proceedings ISSN 2673-4591.

Twenty Years of NPS Pollution Research in Korea: Insights from the Han River Basin

Seonah Lee[1*], Eunmi Hong[2*]

[1] Integrated Ph.D. Program, Interdisciplinary Program in Earth Environmental System Science & Engineering, Kangwon National University, Chuncheon, Gangwon-do 24341, Republic of Korea

[2] Associate Professor, Interdisciplinary Program in Earth Environmental System Science & Engineering, Kangwon National University, Chuncheon, Gangwon-do 24341, Republic of Korea

* Corresponding author. Email: eunmi.hong@kangwon.ac.kr

Abstract

This study aims to explore the evolving research landscape of NPS pollution in the Han River Basin by organizing accumulated studies and examining their development across spatial, technological, and policy dimensions. For this purpose, final reports from the Han River Basin Environmental Baseline Survey (2003–2025) and 550 journal articles indexed in the Korean Citation Index (2001–2024) were collected and reviewed. Manual thematic coding was combined with bibliometric analysis to classify research topics, water quality parameters, applied technologies, and BMPs. Expert review was used to ensure consistency in classification.

Preliminary observations suggest that while earlier studies focused mainly on monitoring suspended solids (SS) and total phosphorus (TP), more recent work has gradually expanded to modeling, BMP evaluation, total organic carbon (TOC), and linkages with climate change and carbon neutrality. Policy milestones such as the introduction of the Total Load Management System (2004) and national NPS management master plans (2016, 2021) appear to coincide with shifts in research activity. Highland agriculture and urban impervious areas are often mentioned as potential hotspots, and straw mulching, vegetative buffer zones, and gabion walls have been examined as BMPs, though application criteria vary. Research on livestock manure management, urban NPS, and governance effectiveness remains relatively limited.

As an ongoing study, these findings are tentative and will be refined through further quantitative and systematic analysis. Ultimately, this research seeks to provide a structured basis for understanding long-term trends in NPS studies and to contribute to future strategies for sustainable watershed management and integrated environmental policy.

Keywords: non-point source pollution, Han River Basin, bibliometric analysis, environmental policy, BMPs, climate change, Watershed Management

1. Introduction

The Han River Basin is the largest watershed in Korea and serves as a crucial drinking water source for the metropolitan area (Im et al., 2020). However, non-point source (NPS) pollution has persisted as a key water quality concern due to factors such as highland agriculture, urban impervious expansion, and climate change (Ministry of Environment, 2020). Although the Environmental Baseline Survey has continuously addressed NPS issues since 2003, most studies have been fragmented in time and scope, making it difficult to interpret cumulative trends. This study seeks to address this gap by preliminarily analyzing the accumulated research to identify evolving themes and policy linkages.

2. Materials and Methods

This study applies to a systematic literature review and bibliometric analysis to examine the research trends and policy linkages of non-point source (NPS) pollution in the Han River Basin. The methodology was designed to ensure transparency and reproducibility.

2.1. Data collection

Two major data sources were used :

Environmental Baseline Survey reports (2003-2025) : Final reports from the Han River Basin Environmental Baseline Survey were collected, focusing on those explicitly addressing NPS issues. Where final reports lacked detail, supplementary information from annual reports was consulted.

Academic articles (2001–2024): A total of 550 peer-reviewed journal articles were retrieved from the Korean Citation Index (KCI) after applying screening criteria. Articles on atmospheric NPS were excluded, and only those directly related to water quality were retained

2.2. Selection criteria

Reports and papers were included if they clearly addressed NPS pollution in their objectives, methods, or conclusions. Duplicates, preliminary summaries, or studies without accessible full texts were excluded.

2.3. Classification and coding

Each document was manually reviewed to extract information on study objectives, target areas, water quality parameters, and applied BMPs. A Keyword-based coding framework was developed, and classification consistency was ensured through expert review by two additional water environment specialists.

2.4. Analytical approach

The analysis combined qualitative and quantitative components.

Temporal analysis: research was grouped into three policy phases (2004–2011, 2012–2020, 2021–2025) corresponding to the implementation of major NPS policies.

Spatial analysis: studies were categorized according to upper, middle, and lower basin characteristics.

Thematic analysis: research themes were mapped to categories such as monitoring, modeling, BMPs, and policy evaluation.

Bibliometric analysis: keyword frequency and co-

occurrence were analyzed to trace evolving research trends and policy linkages.

3. Results and Discussion

This section presents preliminary observations from the ongoing analysis and should be interpreted as indicative rather than conclusive.

3.1. Research themes

Early studies emphasized monitoring of suspended solids (SS) and total phosphorus (TP). More recent research shows a gradual expansion toward modeling, evaluation of BMPs, total organic carbon (TOC), and linkages with climate change and carbon neutrality.

3.2. Policy influence

Research activity appears to increase during periods following key policy milestones, including the introduction of the Total Load Management System in 2004 and the establishment of national NPS management plans in 2016 and 2021.

3.3. Spatial focus

Highland agricultural areas and urban catchments are frequently identified as potential hotspots for NPS pollution. However, studies addressing livestock manure management remain relatively scarce.

3.4. BMPs application

Straw mulching, vegetative buffer zones, and gabion walls are among the most frequently studied BMPs. Application criteria vary across studies, reflecting differences in crop type, soil condition, slope, and rainfall.

3.5. Limitations

While patterns are emerging, the analysis is ongoing. Final results will provide more robust insights through expanded quantitative evaluation and cross-validation.

4. Conclusions

This preliminary review indicates that NPS research in the Han River Basin has gradually shifted from monitoring-based studies to more diverse and interdisciplinary approaches, often aligning with major policy developments. Although the findings remain tentative, the analysis underscores the necessity of standardized long-term monitoring and data sharing, the establishment of region-specific BMP application guidelines, the expansion of research on participatory governance, and the stronger integration of NPS studies with climate change and carbon neutrality agendas. The ongoing work is expected to provide a structured basis for bridging research and policy, thereby contributing to the development of more effective and sustainable watershed management strategies.

Acknowledgements

This research was supported by the “Operation of Research Network and Establishment of the Master Plan for the Environmental Baseline Survey in the Han River Basin” (Project No. 202500330001), funded by the Han River Basin Environmental Office, Ministry of Environment, Republic of Korea, and by the “Development of Adaptation Technologies and Vulnerability Assessment of Agricultural Runoff and Irrigation Water Quality under Changing Climate and Cropping Systems” (Project No. 00396736), funded by the National Institute of Agricultural Sciences, Rural Development Administration, Republic of Korea.

References

Ministry of Environment, 2020. The 3rd Comprehensive Countermeasures for Stormwater Runoff and Nonpoint Source Pollution Management (2021–2025). Ministry of Environment, Sejong.

Im, J.K., Hwang, M.Y., Lee, E.H., Noh, H.R., and Yu, S.J., 2020. Pharmaceutical compounds in tributaries of the Han River watershed, South Korea. Environmental Research, 188, 109758. https://doi.org/10.1016/j.envres.2020.109758

Modeling the spatiotemporal dynamics of dissolved oxygen minima in a temperate reservoir using CE-QUAL-W2

Hojeong Yeom [1], Yoonhee Kim [2], Bomchul Kim [3], Eunmi Hong [3*]

[1] Interdisciplinary Program in Earth Environmental System Science & Engineering, Kangwon National University, Chuncheon, (Gangwon State) 24341, Republic of Korea

[2] Institute of Environmental Research, Kangwon National University, Chuncheon, (Gangwon State) 24341, Republic of Korea

[3] Department of Environmental Science, Kangwon National University, Chunchon, (Gangwon State) 24341, Republic of Korea

* Corresponding author. Email: eunmi.hong@kangwon.ac.kr

Abstract

Recent shifts in climate and intensified watershed development have altered the thermal and biogeochemical dynamics of reservoirs, challenging water-quality management. Dissolved oxygen (DO) minima are a key indicator of hypoxia threatening aquatic ecosystems. This study examines the spatiotemporal dynamics of DO minima in Lake Soyang, a temperate monomictic reservoir in South Korea, using the CE-QUAL-W2 hydrodynamic–water quality model. Simulations covered 2015–2024, with five years for calibration and five for validation, and used 1-km longitudinal segments and vertical layering. Results show that summer stratification maintained high DO in the epilimnion but promoted hypolimnetic depletion. Decreased inflow and extreme rainfall events reduced vertical mixing and oxygen supply to bottom waters, aggravating hypoxic conditions. By focusing on DO minima, this research identifies critical periods and locations of oxygen stress, providing insights for adaptive reservoir management under climate variability. The findings also create a basis for future model extensions that incorporate nutrient cycling and algal bloom risk, contributing to sustainable water-quality strategies in monsoonal, stratified lakes.

Keywords: CE-QUAL-W2, Climate variability, Dissolved oxygen (DO) minima, Lake Soyang

1. Introduction

Changing climate patterns and accelerated watershed development have profoundly influenced the thermophysical and biogeochemical dynamics of reservoirs, thereby adding complexity to water quality management. Rising air temperatures and increasing irregularities in rainfall patterns alter thermal stratification and mixing regimes. This causes variability in key water quality indicators such as dissolved oxygen (DO), nutrients, and algal distributions.

Among these indicators, DO serves as a fundamental determinant of aquatic ecosystem health, directly regulating the survival and habitat suitability of aquatic organisms. In particular, DO minima represent a critical threshold for diagnosing hypoxic or anoxic conditions, which can severely threaten benthic fish and invertebrate communities (Mallya, 2007). Consequently, understanding the spatiotemporal variability of DO minima in reservoirs is essential for ecosystem conservation and for developing effective water quality management strategies.

The dynamics of DO, however, are not governed solely by internal oxygen consumption processes but are shaped by the interplay of thermal stratification, inflow quantity and quality, meteorological variability, and reservoir operation practices. As a result, systematic assessment of oxygen depletion requires the application of hydrodynamic and water quality models capable of capturing high-resolution physical and biogeochemical processes (Pene et al., 2010).

The present study aims to investigate the spatiotemporal dynamics of DO minima in a temperate monomictic reservoir in South Korea using CE-QUAL-W2, a laterally averaged two-dimensional hydrodynamic and water quality model.

2. Materials and Methods

2.1. Study area

Soyang Lake is a deep, faulted reservoir located in northeastern Korea. Established in 1973, this reservoir is one of the deepest reservoirs in the region, with a maximum depth of over 90 metres. This reservoir exhibits strong summer stratification caused by the East Asian monsoon, resulting in prolonged periods of oxygen depletion in bottom waters. These characteristics make Soyang Lake an ideal location to study the spatiotemporal dynamics of dissolved oxygen minima due to changes in climatic and hydrological conditions.

2.2. Simulation period and dataset

The simulation was conducted over a 10-year period (2015 to 2024) and was divided into two stages: calibration (2015 to 2019) and validation (2020 to 2024). Meteorological forcing data, including temperature, wind speed, humidity, solar radiation, and precipitation, were provided by the Korea Meteorological Administration. Hydrological input data, such as inflow flow and inlet temperature, were derived from upstream stations. Reservoir operational data, including water level fluctuations and discharge records, were incorporated as boundary conditions.

2.3. Model configuration

The model was discretized into longitudinal sections approximately 1 km long, and vertical stratification was established to capture stratification and bottom water oxygen depletion. By applying more precise resolution to the upper water column and around the thermal zone, the expressiveness of the vertical mixing process has been improved. Simulated state variables included water temperature, dissolved oxygen, and oxygen dynamics-related components. Initial conditions were specified using observational monitoring data at the start of the simulation.

3. Results and Discussion

3.1. Calibration and validation of the CE-QUAL-W2

The Calibration was performed using observed water temperature and DO profiles from routine monitoring conducted by the Ministry of Environment. Model parameters related to vertical mixing, sediment oxygen demand, and reaeration coefficients were iteratively adjusted to minimize discrepancies between observed and simulated values. Model performance was evaluated using statistical indicators such as the root mean square error (RMSE), and coefficient of determination (R^2). Validation over the subsequent five-year period ensured the robustness and transferability of the calibrated parameter set.

3.2. Seasonal stratification and oxygen distribution

Preliminary simulations indicate that Lake Soyang develops strong summer stratification, separating oxygen-rich epilimnetic waters from oxygen-depleted hypolimnetic layers. While the epilimnion maintained sufficient DO, the hypolimnion tended to show minima driven by restricted mixing and oxygen demand.

3.3. Influence of hydrological variability

Initial results suggest that reduced inflow periods exacerbate oxygen depletion, whereas extreme rainfall events temporarily disrupt stratification. However, these events may also increase organic loading, accelerating oxygen consumption in deeper layers.

4. Conclusions

This study presents preliminary results on the spatiotemporal dynamics of DO minima in Lake Soyang using CE-QUAL-W2. Early simulations suggest that seasonal stratification, inflow variability, and extreme weather events play a key role in shaping oxygen dynamics. As the research is ongoing, further calibration and extended analyses will refine these findings and expand the discussion to include nutrient cycling and algal bloom risks.

Acknowledgements

This study was conducted with the support of “the National Long Term Ecological Research” (NIE-Unique Research-2025-01) from the National Institute of Ecology, “Basic Research” (No. 2022R1C1C1010804) from the National Research Foundation, and “Development of Adaptation Technologies and Vulnerability Assessment of Agricultural Runoff and Irrigation Water Quality under Changing Climate and Cropping Systems” (Project No. 00396736) from the National Institute of Agricultural Sciences, Republic of Korea.

References

Mallya, Y. J., 2007. The effects of dissolved oxygen on fish growth in aquaculture. The United Nations University Fisheries Training Programme, Final Project.

Pena, M. A., Katsev, S., Oguz, T., & Gilbert, D., 2010. Modeling dissolved oxygen dynamics and hypoxia. Biogeosciences, 7(3), 933-957. https://doi.org/10.5194/bg-7-933-2010

This extended abstract template was updated on September 15, 2025

Raising Rice Productivity Through Oxygen-Enriched Irrigation Water

Arif Chusnul・Purnomo Azzahra Putri Kayla・Wibowo Andrehan・Sutoyo Sutoyo

・Purwanto Aris Yohannes・Taufik Muh

Abstract

Improving rice productivity under sustainable water management is crucial in modern paddy farming. This study explores the application of oxygen-enriched irrigation water using fine bubbles technology (FBT) as a means to enhance rice yield and water quality. The experiment was conducted at Kinjiro Farm, Bogor, Indonesia, from February 25 to June 10, 2025. Four treatments were compared: two with FBT-FB-1 and FB-2-maintaining water levels at 7.04 cm and 7.17 cm above the soil surface, respectively, and two without FBT-the WET regime (-0.04 cm) and the conventional regime (CR) with 2.10 cm of standing water as control. Results showed that oxygen-enriched irrigation significantly boosted productivity, with FB-2 producing the highest yield at 8.00 tons/ha, followed by FB-1 at 6.20 tons/ha. In contrast, the WET and CR treatments yielded 2.42 and 5.76 tons/ha, respectively. Additionally, dissolved oxygen (DO) increased by 18.32% and 21.93% in FB-1 and FB-2, respectively. These findings suggest that integrating fine bubbles technology into irrigation practices can effectively raise rice productivity by improving oxygen availability and water conditions in paddy fields.

Portable Minapadi Model and Its Performance for Urban Farming

Baskoro Tri Julianto [1,2*], Budi Indra Setiawan [3], Satyanto Krido Saptomo [3], Liyantono [4,5], Euis Kania Kurniawati [2]

[1]Doctoral Program in Agricultural Engineering Science, Faculty of Agricultural Engineering and Technology, IPB University, IPB Dramaga Campus, Babakan, Bogor, West Java 16680, Indonesia.
[2]Department of Civil Engineering, Faculty of Science and Technology, University of Muhammadiyah Sukabumi, R. Syamsudin, S.H. Street No 50, Cikole, Sukabumi, West Java 43113, Indonesia.
[3]Department of Civil and Environmental Engineering, Faculty of Agricultural Engineering and Technology, IPB University, Lingkar Akademik Street, IPB Dramaga Campus, Babakan, Bogor, West Java 16680, Indonesia.
[4]Department of Mechanical and Biosystem Engineering, Faculty of Agricultural Engineering and Technology, IPB University, Lingkar Akademik Street, IPB Dramaga Campus, Babakan, Bogor, West Java 16680, Indonesia.
[5]Center for Environmental Research, PPLH Building Floors 2-4, IPB University, IPB Dramaga Campus, Babakan, Bogor, West Java 16680, Indonesia.

* Corresponding author. Email: 220701baskoro@ummi.ac.id

Abstract

The conversion of agricultural land to non-agricultural uses threatens urban food supply, despite the availability of unused open spaces with potential for food production. Cultivation techniques suitable for such areas and accessible to people with little or no farming experience are needed. This study developed and tested a portable Minapadi (rice–fish) culture model for urban farming and evaluated its performance. The experiment was conducted for one season (99 days), observing water balance, rice and fish production, and revenue. The system used automatic irrigation without electricity, consuming 738 mm of water with 54% efficiency. The Land and water productivity reached 3.62 tons/ha and 0.96 kg/m³, respectively. The Fish survival rate was 85% with a total production of 3.34 kg and feed efficiency of 2.74. The model generated IDR7,054.94/m³ from rice and IDR36,989.82/m³ from fish, totaling IDR44,044.76/m³. Findings demonstrate the potential of this portable Minapadi system to enhance urban agriculture.

Keywords: FONi, minapadi, revenue, rice and fish, urban farming

1. Introduction

Land conversion is currently a major problem in food security. The reduction of agricultural land means a reduction in food production. Therefore, every individual in their household or community is expected to be able to produce their own food. Urban agriculture is one solution to this problem. Nonpowered Automatic Fertigation, better known as FONi, is an innovative urban agricultural device that is claimed to be quite economical because it does not use electricity at all in its operation. This technology has also been used frequently in various studies. For example, Syafriyandi et al., (2023) used FONi technology for the cultivation of three vegetable crops, namely water lettuce, choy sum, and spinach, with land productivity of 9.60 kg/m^2; 12.30 kg/m^2, and 25.10 kg/m^2, respectively, and water productivity of 29.00 kg/m^3; 12.30 kg/m^3; and 52.40 kg/m^3, respectively. In addition, FONi has also been disseminated, particularly in the city of Tasikmalaya, West Java, Indonesia, which has shown quite satisfactory results (Muharomah et al., 2024). Another agricultural concept that has been applied is integrated rice and fish cultivation or better known as Minapadi. Minapadi is a way of raising fish in between rice plants as an interlude between two rice growing seasons or raising fish as a substitute for secondary crops in rice fields (Syuraihanah et al., 2024). The minapadi concept has been proven to provide benefits. Nurhayati et al., (2016)revealed that in Ciparay, West Java, the concept of minapadi can provide good economic and social results for the community in optimizing land use. By combining the concepts of FONi and Minapadi, it is hoped that food needs can be met at least at the lowest level. This study aims to test this hypothesis.

2. Materials and Methods

This research was conducted in Carang Pulang, West Java, Indonesia, from May to September 2025 with a total observation period of 99 days. A series of buckets and boxes measuring 2.0 m × 1.0 m × 0.4 m were used, arranged as interconnected vessels. Polybags were placed inside the boxes, and each polybag was planted with pre-germinated IPB 9G rice seedlings. Additionally, 15 red tilapia fish were released into each box. Two special boxs served as control parameters: one containing only rice plants and another containing only 30 red tilapia fish. At the end of the harvest season, an analysis of the yield was carried out, including the measurement of rice and fish weights, as well as water and land productivity. An illustration of the box arrangement is shown in the following figure.

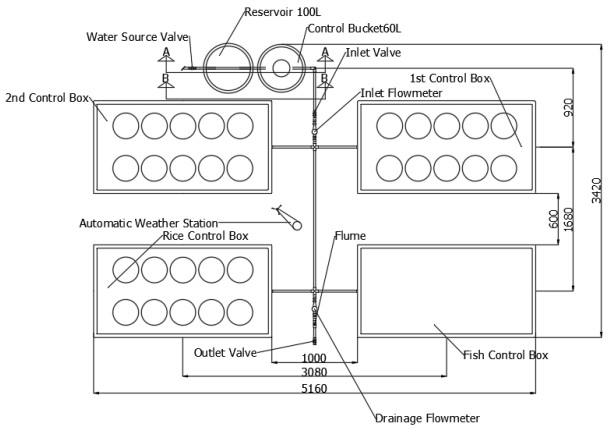

Fig 1. Plan of FONi system for minapadi model.

3. Results and Discussion

Climate data recorded by the AWS showed that the total accumulation of water entering and leaving the system was balanced, with rainfall amounting to 456.00 mm, irrigation water 281.92 mm, actual evapotranspiration 421.93 mm, and drainage 315.99 mm.

In agronomic aspects, the average rice plant height at harvest was 113 cm, with an average grain weight of 0.03 grams per grain. The total rice harvest was 2,460 grams, distributed as 825.00 grams in control box 1, 886.00 grams in control box 2, and 749.00 grams in the rice-only control box. Land productivity reached 3.62 tons/ha, while water productivity was 0.96 kg/m³ economically and 1.78 kg/m³ physically, with water use efficiency reaching 54.00%. As supporting evidence, a comparison of water productivity results from several previous studies was also carried out, as follows (Subari et al., 2012; Fuadi et al., 2016; Nabipour et al., 2024; Mondal et al., 2024).

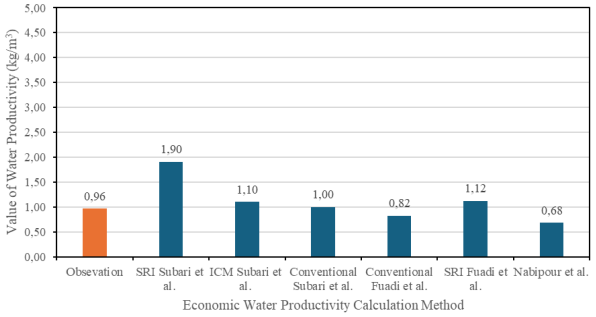

Fig 2. Economic water productivity.

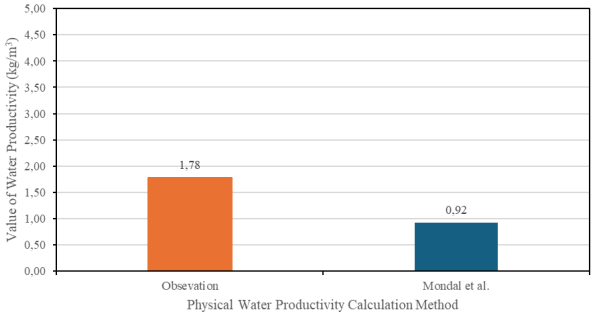

Fig 3. Physical water productivity.

In aquaculture aspects, the fish survival rate reached 85%, with a total harvest weight of 3,337 grams. However, this result was less satisfactory due to a relatively high feed conversion ratio of 2.74.

Economically, the total income generated from this Minapadi model performance test was IDR 44,044.76. This amount is quite substantial and reasonable, considering it combines the estimated sales of rice and fish without accounting for costs of materials, assembly, and maintenance.

4. Conclusions

From the research conducted, it can be concluded that the combination of the FONi system and the Minapadi concept is quite potential to be developed and applied on a limited scale within the community.

Acknowledgements

This abstract is a summary of a paper with the same title published in “Jurnal Keteknikan Pertanian Vol.13 No.2 pp 195-210, 2025” funded by the Ministry of Higher Education, Research and Innovation, Republic of Indonesia as part of Pendidikan Magister menuju Doktor untuk Sarjana Unggil (PMDSU) program.

References

Fuadi, N.A., Purwanto, M.Y.J., Tarigan, S.D., 2016. Kajian Kebutuhan Air dan Produktivitas Air Padi Sawah dengan Sistem Pemberian Air Secara SRI dan Konvensional Menggunakan Irigasi Pipa. JI 11, 23–32. https://doi.org/10.31028/ji.v11.i1.23-32

Mondal, U., Patra, S.K., Poddar, R., Sarkar, A., Das, N.C., Al-Shuraym, L.A., Sayed, S., Gaber, A., Hossain, A., 2024. The microsprinkler irrigation system influences the growth, yield, and water productivity and nutrient uptake of aerobic rice under humid subtropical climatic conditions. Paddy Water Environ. https://doi.org/10.1007/s10333-024-00988-4

Muharomah, R., Setiawan, B.I., Suwardi, S., 2024. Diseminasi Fertigasi Otomatis Nirdaya untuk Budidaya Sayuran di Kota Tasikmalaya. Agrokreatif. J. Ilm. Pengabdi. Kpd. Masy. 10, 156–165. https://doi.org/10.29244/agrokreatif.10.2.156-165

Nabipour, R., Yazdani, M.R., Mirzaei, F., Ebrahimian, H., Alipour Mobaraki, F., 2024. Water productivity and yield characteristics of transplanted rice in puddled soil under drip tape irrigation. Agricultural Water Management 295, 1–11. https://doi.org/10.1016/j.agwat.2024.108753

Nurhayati, A., Lili, W., Herawati, T., Riyantini, I., 2016. Derivatif Analysis of Economic and Social Aspect of Added Value Minapadi (Paddy-fish Integrative Farming) a Case Study in the Village of Sagaracipta Ciparay Sub District, Bandung West Java Province, Indonesia. Aquatic Procedia 7, 12–18. https://doi.org/10.1016/j.aqpro.2016.07.002

Subari, S., Joubert, M.D., Sofiyuddin, H.A., Triyono, J., 2012. Pengaruh Perlakuan Pemberian Air Irigasi pada Budidaya SRI, PTT dan Konvensional terhadap Produktivitas Air. JI 7, 28–42. https://doi.org/10.31028/ji.v7.i1.28-42

Syafriyandi, D., Setiawan, B.I., Arif, C., Suwardi, S., 2023. Performance of Automatic Unpowerer Subsurface Irrigation on Water-Lettuce, Choy-Sum, and Spinach Cultivations. JTEP 11, 268–278. https://doi.org/10.19028/jtep.011.3.268-278

Syuraihanah, K., Mulandari, K., Sukardi, P., Mardiyana, M., 2024. Determinasi Resiko Keamanan Pangan Berdasarkan Kandungan Escherichia coli Pada Ikan Budi Daya Mina Padi Banyumas. myh 3, 43. https://doi.org/10.20884/1.maiyah.2024.3.1.11711

Estimation of Spring Season Fish Assessment Index (FAI) using PyCaret-based AutoML Algorithm in South Korea

Yongwon Kim[1], Yonggwan Lee[2], Jeehun Chung[1], Wonjun Jeon[3], Seongjoon Kim[4*]

[1] Department of Civil, Environmental and Plant Engineering, Graduate School, Konkuk University, Seoul, Gwangjin-gu Neungdong-ro 05029, Republic of Korea

[2] Asia Infrastructure Research Center, Konkuk University, Seoul, Gwangjin-gu Neungdong-ro 05029, Republic of Korea

[3] Division of Civil and Environmental Engineering, Graduate School, Konkuk University, Seoul, Gwangjin-gu Neungdong-ro 05029, Republic of Korea

[4] Division of Civil and Environmental Engineering, College of Engineering, College of Engineering, Konkuk University, Seoul, Gwangjin-gu Neungdong-ro 05029, Republic of Korea

* Corresponding author. Email: kimsj@konkuk.ac.kr

Abstract (10 pt, Times New Roman, Bold)

The main goal of this study is to estimate spring season fish assessment index (FAI) in South Korea using observed watershed environmental data and PyCaret-based AutoML (Automated Machine Learning). To develop input data for AutoML, observed hydrological data (e.g., streamflow, average depth, and velocity), water quality data (e.g., SS, T-N, T-P, DO, BOD, and COD), biological data (e.g., fish species, FAI score, trophic diatom index (TDI) score, and benthic macroinvertebrate index (BMI) score), and GIS spatial data (e.g., elevation, land use, stream order, and slope) were collected. Pearson correlation analysis was performed to understand the relationship between FAI and environmental factors. The positive correlation factors were forest area ratio, BMI, and DEM indicating R of 0.46~0.56, and negative factors were average COD, average BOD, average TOC showing R of -0.54~-0.47. The input variables of AutoML were selected as 58 variables based on the correlation results. The machine learning models of AutoML were compared to select optimal model using objective functions (R^2, coefficient of determination, NSE; Nash-Sutcliffe Efficiency, MAPE; Mean Absolute Percentage Error). The optimal model was random forest algorithm showing R^2, NSE, and MAPE of train set 0.79, 0.76, and 21.4, respectively. As a result of estimating FAI, the model performances of random forest were evaluated R^2, NSE, and MAPE of 0.68, 0.64, and 30.1, respectively.

Keywords: Fish Assessment Index (FAI), PyCaret, AutoML, Pearson Correlation, Random Forest

1. Introduction

River ecosystems in South Korea are increasingly threatened by climate change, watershed development, hydraulic structures, and pollutant inflows (Leprieur et al., 2008). To assess their ecological health, the Fish Assessment Index (FAI) is widely used as a key indicator based on fish communities and plays an important role in environmental policy and restoration planning (Cheimonopoulou et al., 2011).

However, its current field survey–based method is limited by seasonal and spatial constraints, hindering continuous monitoring. To overcome these challenges, this study explored the potential of machine-learning-based predictive models for FAI estimation. Using hydrological, water quality, biological, meteorological, and GIS-based watershed data from 164 monitoring sites (2008–2023), we applied the Python-based AutoML framework PyCaret to develop models for spring-season FAI prediction.

2. Materials and Methods

2.1. National observation station in South Korea

South Korea has established national monitoring networks for streamflow, water quality, and aquatic ecosystems. The observed monitoring data was provided by national websites. The streamflow station provides daily observed data (m^3/s), while the water quality station provides for 55 components including SS, T-N, and T-P at minimum 8-day interval. The biological station conducts surveys twice a year (Spring and Autumn) to assess aquatic ecosystem health using the TDI, BMI, and FAI.

2.2. AutoML - PyCaret

PyCaret is a python-based open-source machine learning library that simplifies code structure and automates model optimization by integrating various frameworks such as scikit-learn, XGBoost, LightGBM, CatBoost, Optuna, etc. In this study, total 18 machine learning models were tested, and the top four models from the decision tree and ensemble categories − AdaBoost, Gradient Boosting, LightGBM, and Random Forest − were selected for performance comparison. Model performance was quantitatively evaluated using R^2 (coefficient of determination), NSE (Nash-Sutcliffe efficiency), RMSE (root mean square error), and MAPE (mean absolute percentage error).

2.3. Fish Assessment Index (FAI)

Fish is top-level organisms in aquatic food web, making them highly representative of aquatic ecosystem health. FAI quantifies aquatic ecosystem health based on fish community characteristics.

$$FAI = M1 + M2 + M3 + M4 + M5 + M6 + M7 + M8 \quad (1)$$

where *M1* is number of native species; *M2* is number of riffle benthic species; *M3* is number of sensitive species; *M4* is proportion of tolerant individuals; *M5* is proportion of omnivores individuals; *M6* is proportion of insectivorous native individuals; *M7* is total number of native individuals; and *M8* is proportion of individuals with abnormalities.

2.4. Study Area

Study area is South Korea (109,411.8 km^2). South Korea operated 653 hydrological, 1,254 water quality, and 3044 biological stations. However, locations of these stations are different. Therefore, in this study, the hydrological and water quality stations were spatiotemporally linked based on the biological stations using ArcGIS. Finally, integration station is 164 stations (Figure 1).

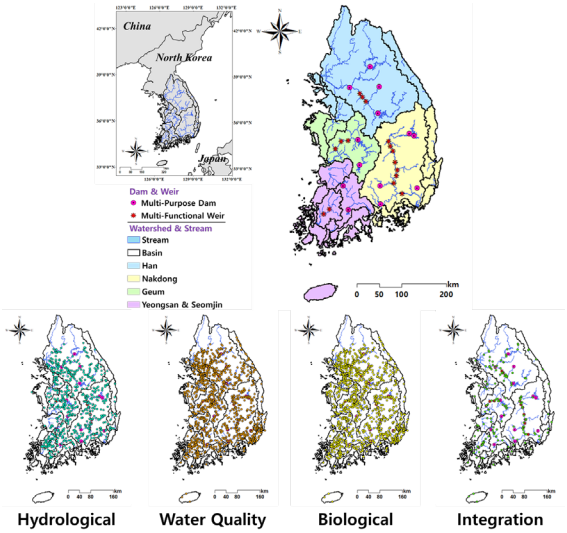

Figure 1. Study area and national observation stations.

3. Results and Discussion

3.1. Correlation analysis between FAI and variables

Pearson correlation analysis was performed to understand the relationship between FAI and environmental variables. The positive values are proportion of forest area (R: 0.56), fish species (R: 0.52), spring BMI (R: 0.46), and DEM (R: 0.46). The negative values are average COD (R: -0.54), spring COD (R: -0.52), average BOD (R: -0.50), and average TOC (R: -0.47). The negligible values are stream order (R: -0.14), spring SS standard deviation (R: -0.13), average depth (R: -0.12), and slope (R: 0.10).

3.2. Comparison of model performance

Top 4 ML models trained and tested with 8:2 data split and then iterated 100 times. AdaBoost showed overall low performance, weak generalization and High MAPE. Gradient boosting showed high train R^2 resulting in overfitting. Light GBM was evaluated strong overfitting tendency, unstable performance even in best case. Random Forest was evaluated most balanced train/test performance, highest test R^2 (0.68) and stable estimation (Table 1).

Table 1. Comparisons of model performance in best case.

Model	Train R^2	Test R^2	Train NSE	Test NSE	Train MAPE	Test MAPE
AdaBoost	0.60	0.65	0.57	0.62	29.3	27.5
Gradient Boosting	0.97	0.66	0.96	0.64	8.1	29.8
LightGBM	0.80	0.63	0.71	0.54	24.6	30.0
Random Forest	0.79	0.68	0.76	0.64	21.4	30.1

3.3. Estimation of FAI

FAI was estimated to use the best case of Random Forest algorithm. The results showed stable and consistent performance without overfitting. Compared to observed and estimated FAI, estimated points are evenly distributed along the 1:1 line. However, it showed slightly underestimation at high FAI. These results suggest that the spring FAI does not estimate high grades well, with scores ranging from 30 to 60 overall (Figure 2).

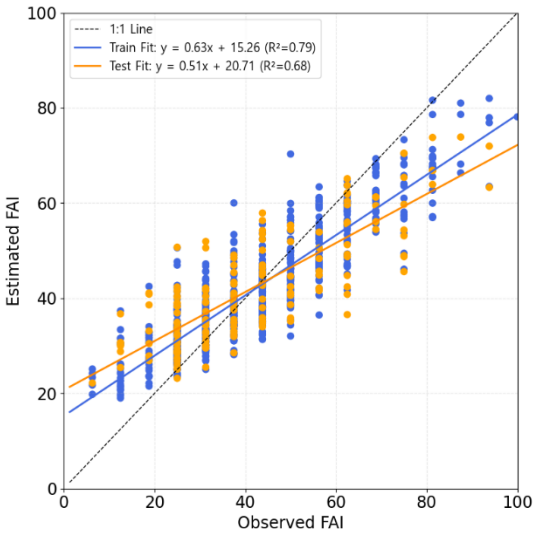

Figure 2. Results of FAI estimation

4. Conclusions

This study identified the relationship between environmental variables including GIS-based data and FAI and estimated FAI using AutoML-based machine learning model. The tree-based machine learning models were effective in interpreting nonlinear environmental variables and estimating ecological indicators. The machine learning-based FAI estimation approach can supplement conventional qualitative methods and is expected to be applicable for modeling other biological indicators.

Acknowledgements

This work was supported by Korea Environment Industry & Technology Institute (KEITI) through Aquatic Ecosystem Conservation Research Program, funded by Korea Ministry of Environment (MOE) (RS-2025-02304832). This work was supported by Korea Environment Industry & Technology Institute (KEITI) through Water Management Program for Drought Project, funded by Korea Ministry of Environment (MOE). (2022003610002)

References

Leprieur, F., Beauchard, O., Blanchet, S., Oberdorff, T., Brosse, S., and Simberloff, D., 2008. Fish invasions in the world's river system: when natural processes are blurred by human activities. PLoS Biol., 6(2), 0404-0410

Cheimonopoulou, M.T., Bobori, D.C., Theocharopoulos, I., and Lazaridou, M., 2011, Assessing ecological water quality with macroinvertebrates and fish: a case study from a small Mediterranean river. J. Environ. Manage., 47(2), 279-290

Integrating Modified Sheet-Pipe Technology in Rice Field Subsurface Water Management

Satyanto Krido Saptomo [1*], Heriansyah Putra [1], Ahmad Junaedi [2],

Raihan Muhammad Iqbal [1], Muhammad Faiq Alghifari [1], Ayda Hadyanti Hamzah [1]

[1] Department of Civil and Environmental Engineering, IPB University, Bogor, Jawa Barat 16680, Indonesia

[2] Department of Agronomy and Horticulture, IPB University, Bogor, Jawa Barat 16680, Indonesia

* Corresponding author. Email: saptomo@apps.ipb.ac.id

Abstract

The development of subsurface irrigation and drainage technology offers a sustainable solution to agricultural water management, enhancing efficiency and environmental resilience. This research focuses on the implementation of the sheet-pipe for subsurface water management system, designed to optimize water usage while mitigating excess runoff and soil saturation. The system features perforated pipes enveloped by calcite-reinforced sand, making it particularly suitable for narrow or hard-to-access farmland. Comparative flow capacity tests revealed that sheet-pipe (SP-C) and perforated PVC pipe (PP-C) systems with calcite-reinforced sand achieved discharge accumulation of 12,000 grams within 90 seconds and 100 seconds, which were faster water flow rates than geotextile-covered alternatives. Further experiments integrated the sheet-pipe system with the cultivation of eight rice varieties developed by breeders at IPB University. Results demonstrated that the average water productivity based on evapotranspiration at 1.4 $kg.m^{-3}$ and total water input at 0.1 $kg.m^{-3}$. The findings underscore the sheet-pipe system's potential to enhance irrigation practices, offering scalable and efficient water management solutions for various agricultural contexts.

1. Introduction

Efficient water management is a critical component of modern agriculture, especially in regions where water resources are scarce or unevenly distributed. Traditional surface irrigation methods often result in significant water losses and can contribute to issues such as soil erosion and nutrient leaching. The development of subsurface irrigation and drainage systems presents a promising alternative, offering improved water use efficiency and greater environmental sustainability. In this context, the current research explores the application of a modified sheet-pipe technology, designed to optimize water delivery and drainage in rice fields. By focusing on the integration of calcite-reinforced sand and innovative pipe configurations, this study aims to address the specific challenges associated with narrow or difficult-to-access farmland, thereby supporting more resilient and productive agricultural systems.

2. Materials and Methods

The study implemented a subsurface water management system utilizing sheet-pipe (Saptomo *et al.* 2025) and perforated PVC pipe technologies. Both systems featured perforated pipes encased in calcite-reinforced sand, a material chosen for its ability to enhance filtration and promote uniform water distribution. The making of calcite-reinforced sand was based on the method for soil stabilization with calcite precipitation (Lofianda *et al.* 2021).

Comparative flow capacity tests were conducted to evaluate the performance of the sheet-pipe system (SP-C) (Fig. 1) and the perforated PVC pipe system (PP-C) covered with calcite-reinforced sand against geotextile-covered alternatives. The PP-C is the same as SP-C but using perforated PVC pipes with similar orifice density as SP-C. The test was conducted by immersing the pipes under the water and let the water seep through the pore and flow out to one end of the pipes. Water discharge were measured and recorded, with particular attention to the time required to reach a specified discharge accumulation.

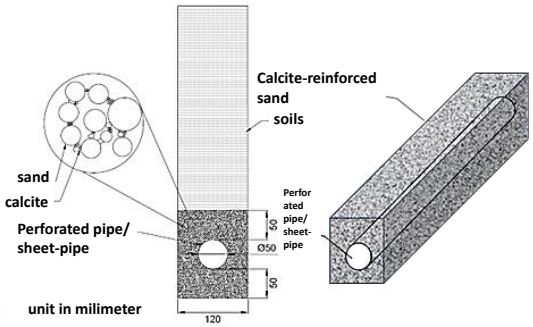

Figure 1. Calcite-reinforced sand covered sheet-pipe.

Additionally, the sheet-pipe system with calcite-reinforced sand was integrated into rice cultivation trials, where eight new rice varieties developed by breeders at IPB University were grown. The experiment was carried out on a land measuring 25 m x 12 m, with a sheet-pipe system at a depth of 40 cm underground (Fig. 2). Sheet-pipes were installed lengthwise with a distance of 4 m. This installation is a modification of the standard installation to adjust to conditions in narrow land. Measurements had been conducted by automatic weather station, water level sensors and flow meters. Water productivity was assessed by calculating yield based on both evapotranspiration (WP_{ETc}) and total water input (WP_{IR}) following (Molden dan Sakthivadivel 1999).

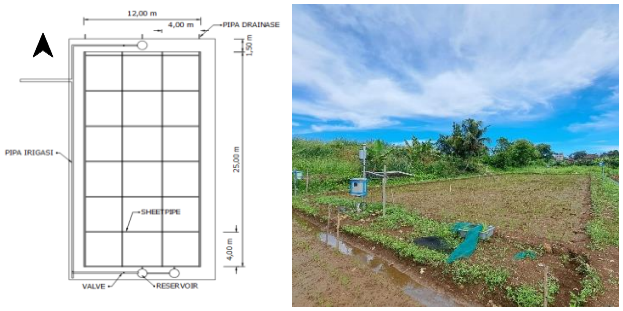

Figure 2. Sheet-pipe experimental field

3. Results and Discussion

The flow capacity tests (Fig. 3) revealed that both the SP-C and PP-C systems with calcite-reinforced sand significantly outperformed geotextile-covered alternatives in terms of water flow rates. Specifically, the SP-C system achieved a discharge accumulation of 12,000 grams within 90 seconds, while the PP-C system reached the same threshold in 100 seconds. These results indicate a faster and more efficient water movement through the subsurface system, which is essential for maintaining optimal soil moisture levels and preventing waterlogging.

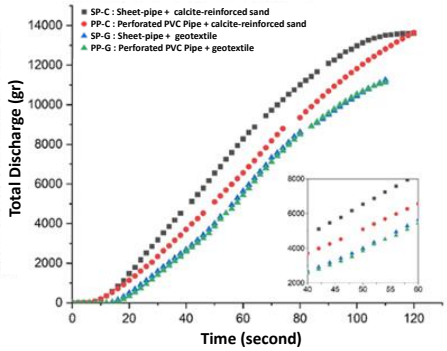

Figure 3. Flow capacity experiment results.

Crop evapotranspiration (Etc) was calculated based on reference evapotranspiration and paddy crop coefficient. Fig. 4 shows the fluctuation of Etc as well as water level during observation. In the rice cultivation trials, the sheet-pipe system contributed water productivity, with values the average water productivity based on evapotranspiration at 1.4 kg.m^{-3} and total water input at 0.1 kg.m^{-3}, where each of variety's yield and water productivity are enlisted in table 1.

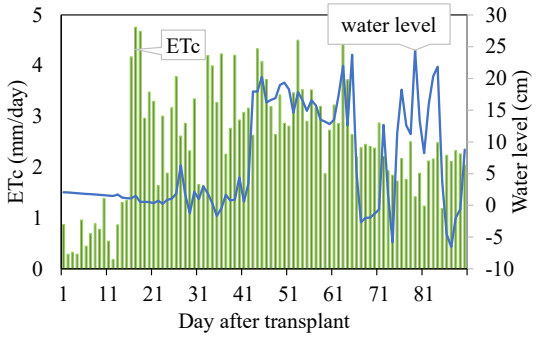

Figure 4. Evapotranspiration and water level fluctuation

Table 1. yield, water productivity

Variety	Yield (kg)	WP_{ETc} (kg.m^{-3})	WP_{IR} (kg.m^{-3})
IPB V01	4.5	1.0	0.1
IPB V02	5.3	1.1	0.1
IPB V03	5.9	1.3	0.1
IPB V04	5.0	1.1	0.1
IPB V05	9.1	2.0	0.2
IPB V06	6.9	1.5	0.1
Nat V01	6.0	1.3	0.1
Nat V02	8.7	1.9	0.2

These findings underscore the potential of the sheet-pipe technology to enhance irrigation practices, reduce water wastage, and support the cultivation of high-yield rice varieties. The success of the system also suggests its scalability and adaptability to various agricultural settings, particularly where land accessibility poses a challenge.

4. Conclusions

This research demonstrates that integrating modified sheet-pipe technology with calcite-reinforced sand presents a viable and effective approach to subsurface water management in rice cultivation. The system's superior flow rates and positive impact on water productivity highlight its potential to optimize irrigation efficiency and support sustainable agricultural practices. Given its adaptability to different field conditions and crop varieties, the sheet-pipe system offers a scalable solution for improving water management in diverse farming contexts. Future studies may further explore its long-term benefits, economic feasibility, and potential integration with other sustainable agricultural technologies.

References

Lofianda L, Putra H, Erizal E, Sutoyo S, Yasuhara H. 2021. Potentially of Soybean as Bio-Catalyst in Calcite Precipitation Methods for Improving the Strength of Sandy Soil. *Civil Engineering and Architecture*. 9(7):2317–2325.doi:10.13189/cea.2021.090719.

Molden D, Sakthivadivel R. 1999. Water Accounting to Assess Use and Productivity of Water. *Int J Water Resour Dev*. 15(1–2):55–71.doi:10.1080/07900629948934.

Saptomo SK, Purwanto MYJ, Arif C, Setiawan BI, Tamura K, Matsuda H. 2025. Implementation of sheet-pipe subsurface drainage system in Indonesia: Enhancing soil aeration and water management. *BIO Web Conf*. 171:04009.doi:10.1051/bioconf/202517104009.

The Impact of Alternate Wetting and Drying (AWD) on Methane Emissions and Groundwater Recharge in Organic Paddy Fields

Ying-Chi Liao[1], Yi-Zhih Tsai[1], Zhi-Wei Yang[2], Shao-Yiu Hsu[1]

[1]Department of Bioenvironmental Systems Engineering, National Taiwan University, Taipei, Taiwan

[2]Taoyuan District Agricultural Research and Extension Station, Taoyuan, Taiwan

Abstract

This study investigates the effects of Alternate Wetting and Drying (AWD) irrigation on methane emissions and groundwater recharge in organic paddy fields. The experiment was conducted at the Taoyuan District Agricultural Research and Extension Station in two organic fields: a continuous cropping field managed under traditional continuous flooding and a rotational cropping field managed using AWD. The results show that AWD significantly reduced methane emissions, with annual emissions in the rotational field markedly lower than those in the continuous cropping field. However, during the first crop season, AWD did not reduce irrigation water use; a simplified water balance analysis revealed that the rotational field exhibited higher percolation, which may have increased irrigation demand. Nevertheless, because the rotational field was planted with upland crops and not irrigated during the second crop season, its total annual irrigation volume remained lower than that of the continuous cropping field. Although percolation was higher in the AWD field during the first crop season, the annual total percolation volume was greater in the continuous cropping field, indicating that the rotational field contributed less to overall groundwater recharge. On the other hand, groundwater level monitoring showed a significant rise after irrigation began in the first crop season, and this elevated level was maintained until the end of the second crop season, demonstrating that irrigation activities had an immediate and substantial effect on groundwater dynamics. While this study cannot directly confirm the effectiveness of AWD in enhancing groundwater recharge, the field observations suggest that paddy field irrigation plays a critical role in influencing groundwater fluctuations.

Keywords: Alternate Wetting and Drying (AWD), methane emissions, paddy field, groundwater recharge

1. Introduction

Paddy fields are one of the major sources of methane emissions among greenhouse gases. Conventional irrigation practices often keep fields continuously flooded, creating anaerobic soil conditions that promote substantial methane production. As climate change intensifies, the world is increasingly facing challenges related to water scarcity. Alternate Wetting and Drying (AWD) has gained attention in recent years as an irrigation strategy that balances crop productivity with environmental sustainability, as it can reduce both irrigation water use and methane emissions. However, such water-saving practices may also alter infiltration dynamics in the field, thereby affecting groundwater recharge processes.

2. Materials and Methods

The study was conducted at the Taoyuan District Agricultural Research and Extension Station (WGS84: 24.95°N, 121.03°E), where two organic experimental fields were selected for on-site monitoring. These included a continuously flooded paddy field under conventional irrigation (continuous cropping) and a field managed with alternate wetting and drying (AWD) as part of a rotational cropping system. Monitoring activities included methane emission measurements using a gas analyzer, groundwater level observations using water level loggers installed in monitoring wells, and, in the AWD-managed field, the installation of soil moisture sensors, tensiometers, and the application of electrical resistivity tomography (ERT) to evaluate the effects of irrigation and rainfall on soil water dynamics and groundwater response.

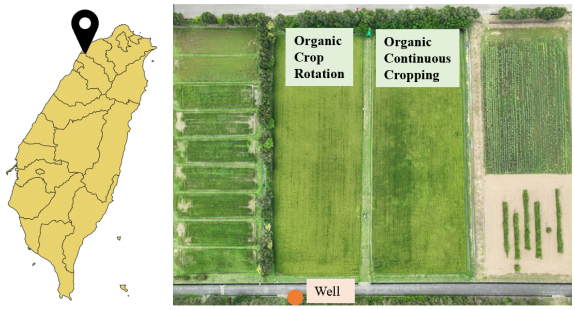

Figure 1 Taoyuan District Agricultural Research and Extension Station

3. Results and Discussion

3.1. Methane Emissions

The results showed that the rotational field managed with alternate wetting and drying (AWD) effectively reduced methane emissions. In 2024, the AWD field emitted 422.5 kg CH_4 ha^{-1}, which was significantly lower than the 4,545.4 kg CH_4 ha^{-1} observed in the continuously flooded field; a similar trend was observed in the first half of 2025.

Table 1 Methane Emissions

	Total CH_4 emissions (kg ha-1 season-1)	
	Organic Continuous Cropping	Organic Rotational Cropping
2024	4545.4	422.5
2025 (as of June 5)	1285.8	246.3

Table 2 Nitrous Oxide Emissions

	Total N_2O emissions (kg ha-1 season-1)	
	Organic Continuous Cropping	Organic Rotational Cropping
2024	0.2	0.86

2025 (as of June 5)	0.11	0.19

3.2. Irrigation Water Volume

On the other hand, in terms of irrigation water use, the AWD field received more irrigation than the continuously flooded field during the first crop season in both 2024 and 2025. Even in 2025, when rainfall was more abundant, the AWD field still required greater irrigation input to meet crop water demands during the growing period.

Table 3 Irrigation Water Volume and Rainfall

	Irrigation Water Volume (mm)		Rainfall (mm)
	Organic Continuous Cropping	Organic Rotational Cropping	
First Crop Season, 2024 (Jan 31 – Jul 3)	1107.34	1518.15	616.5
Full Year, 2024	2643.83	2106.36	1372.63
First Crop Season, 2025 (Feb 4 – Jul 16)	810.8	1020.64	1165.5

3.3. Groundwater Level

Groundwater level data indicated a clear rise following the onset of irrigation in the first crop season. This elevated water table was sustained throughout the first and second crop seasons and only began to decline after the second season ended, suggesting a strong influence of irrigation on groundwater dynamics.

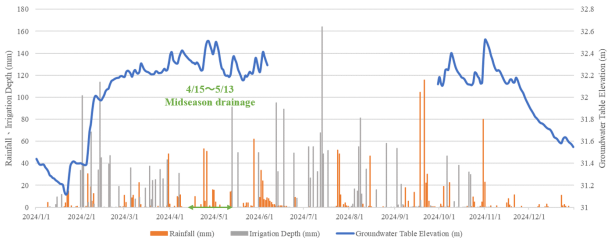

Figure 2 Groundwater Level, Rainfall, and Irrigation Water Volume in 2024

3.4. Percolation

Further analysis based on a simplified water balance indicated that the percolation volume in the rotational cropping field was higher than that in the continuous cropping field during the first crop season. This indicates that, although the rotational field required more irrigation water, it also had a higher percolation volume. However, since the rotational field was planted with upland crops and not irrigated during the second crop season, the total annual percolation remained higher in the continuous cropping field.

Table 4 Percolation Volume

	Organic Continuous Cropping(mm)	Organic Rotational Cropping(mm)
First Crop Season, 2024 (Jan 31 – Jul 3)	730.99	964.29
Full Year, 2024	3429.3	2229.82
First Crop Season, 2025 (Feb 4 – Jul 16)	1203.24	1264.96

3.5. Electrical Resistivity Tomography (ERT)

According to the measurements obtained from Electrical Resistivity Tomography (ERT), soil resistivity is influenced by field management practices such as rainfall, irrigation, and midseason drainage, showing either increasing or decreasing trends. During the midseason drainage period from mid-April to mid-May, soil resistivity exhibited an increasing trend due to the suspension of irrigation. However, rainfall events during the drainage period and subsequent irrigation after drainage completion resulted in a noticeable decrease in soil resistivity. After irrigation ceased in late June, soil resistivity increased again, reflecting a reduction in soil moisture content and a gradual drying of the soil.

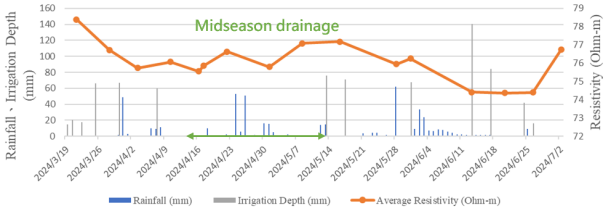

Figure 3 Rainfall, Irrigation Depth, and Average Resistivity during the First Crop Season of 2024

4. Conclusions

This study demonstrates that alternate wetting and drying (AWD) irrigation can effectively reduce methane emissions in organic paddy fields, with the rotational cropping field showing significantly lower methane emissions compared to the continuous cropping field. Although the AWD field required a greater amount of irrigation water during the first crop season, it was also associated with increased water percolation, which enhanced groundwater recharge. Groundwater levels rose rapidly after irrigation and remained at higher elevations, indicating a clear influence of irrigation on groundwater dynamics. However, due to the absence of irrigation during the second crop season with dryland cultivation, the total annual percolation was still higher in the continuously flooded field. Overall, AWD simultaneously provides the dual benefits of mitigating methane emissions and enhancing groundwater recharge during the first crop season. Although the results of this study cannot directly confirm the long-term effects of AWD on regional groundwater recharge at the current experimental scale, AWD may potentially influence water resource utilization and groundwater recharge under different cropping systems, such as dryland cultivation in the second crop season.

Acknowledgements

This work was supported by the Ministry of Agriculture, Project No. 114-AgriSci-4.4.1-hydraulic-02.

References

1. Qian, H., Zhu, X., Huang, S., Linquist, B., Kuzyakov, Y., Wassmann, R., ... & Jiang, Y. (2023). Greenhouse gas emissions and mitigation in rice

agriculture. Nature Reviews Earth & Environment, 4(10), 716-732.

2. Zhuang, Y., L. Zhang, S. Li, H. Liu, L. Zhai, F. Zhou, Y. Ye, S. Ruan, W. Wen(2019), Effects and potential of water-saving irrigation for rice production in China, Agricultural Water Management, 217, 374-382.
3. 殷祥玲(2023)，利用田間試驗與模式模擬探討水稻田灌溉策略，國立台灣大學生物資源暨農學院生物環境系統工程學系碩士論文

Assessment of Salinity and Soil Loss in Reclaimed Land Under Climate Change Using the APEX Model

Ye-Jun Lee [1], Won-Ho Nam [2*]

[1] Graduate Student, School of Social Safety and Systems Engineering, Hankyong National University, Anseong, Republic of Korea

[2] Professor, School of Social Safety and Systems Engineering, National Agricultural Water Research Center, Hankyong National University, Anseong, Republic of Korea

* Corresponding author. Email: wonho.nam@hknu.ac.kr

Abstract

Reclaimed farmlands are vital for securing arable land and ensuring food security, especially in countries with limited agricultural land. However, they are highly vulnerable to climate change-related stresses such as sea level rise, intensified rainfall, and groundwater fluctuations. These factors increase the risks of salinization and waterlogging, threatening crop productivity and the long-term sustainability of farmland. Poor soil aggregation from elevated salt concentrations restricts water movement in the topsoil and subsoil. Moreover, shallow groundwater tables require careful water input and drainage strategies from early land development stages. Given these physical and hydrological vulnerabilities, a quantitative risk assessment addressing both crop viability and land usability is essential. Integrated evaluation approaches that consider the combined effects of salinity and waterlogging—accounting for local soil and hydrological conditions—are critical for effective, long-term agricultural management and policy. This study employs the Agricultural Policy/Environmental eXtender (APEX) model to assess the impacts of climate change-induced salinity and soil loss in a representative reclaimed coastal area in South Korea under various Shared Socioeconomic Pathways (SSPs). The objective is to identify spatial and seasonal hotspots of salinity and excess moisture risk, and to analyze future risk trends under projected climate scenarios. The findings aim to support the development of farmland infrastructure standards and provide scientific evidence for policy measures that mitigate salinity and soil loss risks in vulnerable coastal regions.

Keywords: Reclaimed farmland, Coastal agriculture, Salinity stress, Waterlogging, SSP scenarios.

1. Introduction

Reclaimed land refers to areas created by filling public waters or tidal flats to secure arable or residential land. In South Korea, large-scale reclamation projects have been actively implemented since the 1960s to enhance food self-sufficiency and expand cultivable land. As national-level initiatives, these reclaimed farmlands have facilitated land consolidation and infrastructure development, thereby contributing significantly to increased agricultural productivity. They are now regarded as strategic resources for ensuring stable food supply in response to future challenges such as climate change and population growth.

However, reclaimed farmlands inherently exhibit structural limitations such as high groundwater levels and poor vertical drainage, which restrict soil aeration and permeability. These characteristics lead to soil oversaturation during heavy rainfall events, increasing the risks of severe soil erosion and saltwater/waterlogging damage. Soil erosion not only results in the loss of fertile topsoil but also causes sediment deposition in reservoirs and irrigation channels, thereby degrading the functionality of hydraulic structures and worsening downstream water quality (Lee et al., 2006). Additionally, continuous salt accumulation weakens soil aggregation, inhibits crop growth, and further deteriorates drainage capacity (Sohn et al., 2010). In particular, climate change-induced variability in rainfall patterns and the increasing frequency of extreme precipitation events exacerbate drainage issues in reclaimed lands, heightening the risk of salinity, waterlogging, and soil erosion (Park et al., 2014).

In this study, the APEX model, a field-scale simulation tool capable of evaluating various land management strategies, was employed to assess soil erosion and salinity/waterlogging risks in reclaimed lands under future climate change scenarios.

2. Materials and Methods

2.1. Study area

The study areas selected for this research are the Saemangeum reclaimed areas. The Saemangeum district is located in the vicinity of Gunsan, Gimje, and Buan in Jeollabuk-do.

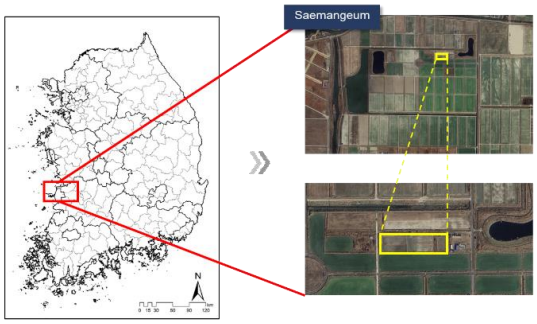

Figure 1. Locations of study area

2.2. Model input and calibration

In this study, the APEX model was employed to evaluate salinity, waterlogging, and soil erosion in reclaimed farmlands. The APEX model was originally developed to assess the impacts of agricultural practices on soil and water resources at farm and small watershed scales. The input data for the model are categorized into three main groups: climate data, soil and texture data, and crop management data.

To analyze soil erosion, the reliability of the APEX model in simulating soil moisture was verified. Observed soil moisture data collected from sensors installed in the pilot sites were compared with the model outputs, and the applicability of the model was evaluated using the

coefficient of determination (R^2).

2.3. Climate and Management scenarios

In this study, climate change scenarios were derived from General Circulation Model (GCM) data based on the SSPs provided by the Coupled Model Intercomparison Project Phase 6 (CMIP6). The Sixth Assessment Report of the Intergovernmental Panel on Climate Change (IPCC) presents SSP1-2.6, SSP2-4.5, SSP3-7.0, and SSP5-8.5 as standard future scenarios. Among these, this study adopted SSP1-2.6 (a low greenhouse gas emission scenario) and SSP5-8.5 (a high emission scenario) for analysis. Climate data were collected for the future period spanning 2040 to 2100, and six key meteorological variables—precipitation, maximum and minimum temperature, wind speed, relative humidity, and solar radiation—were utilized to evaluate future soil erosion as well as salinity and waterlogging risk.

3. Results and Discussion

3.1. Results of APEX Model Applicability Verification

The comparison between observed soil moisture values and those simulated by the APEX model revealed acceptable levels of agreement. The coefficients of determination (R^2) were found to be 0.53 for the flat and 3° slope plots, and 0.67 for the 5° slope plot. According to Francesconi et al. (2014), the APEX simulation can be considered reliable when the R^2 value exceeds 0.5. Based on these criteria, the model demonstrated sufficient applicability to the study area.

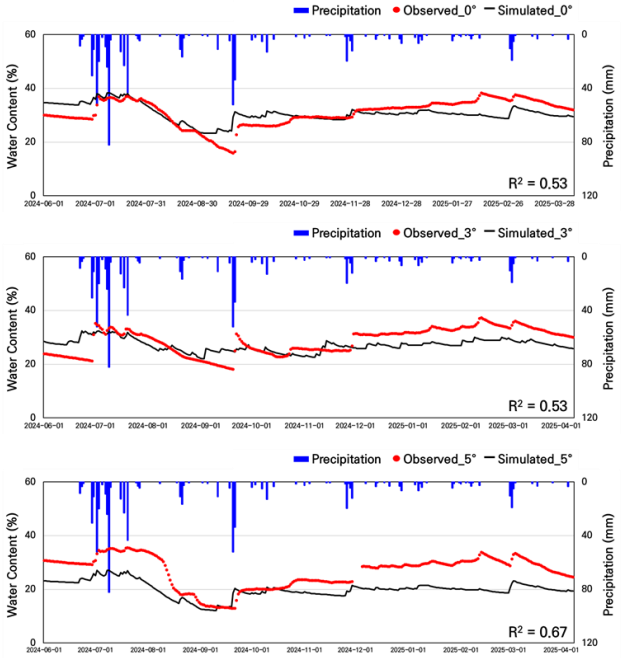

Figure 2. Soil Moisture Analysis Results for the Saemangeum District

3.2. Soil Erosion Analysis Results under Different Scenarios

For the scenario-based soil erosion analysis, simulations were conducted for two future periods: the near future (NF, 2041–2070) and the far future (FF, 2071–2100). The results indicated that soil erosion is projected to increase in the FF compared to the NF under both SSP1-2.6 and SSP5-8.5 scenarios. Moreover, overall soil erosion was higher under SSP5-8.5 than under SSP1-2.6, and the increase in soil erosion from the NF to the FF was also greater under SSP5-8.5.

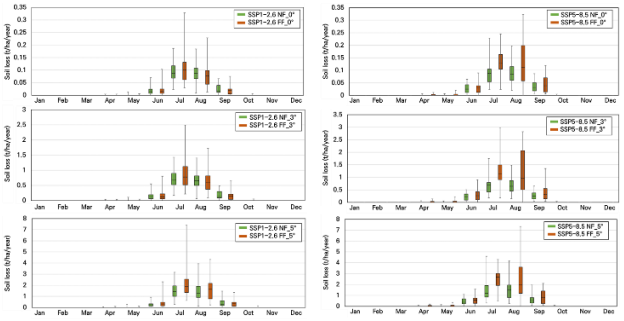

Figure 3. Scenario-Based Soil Erosion Analysis Results by Slope Gradient

4. Conclusions

In this study, the APEX watershed management model was applied to analyze soil erosion in reclaimed farmlands under climate change scenarios. The applicability of the model was validated by comparing observed and simulated soil moisture values, and based on this validation, soil erosion was comparatively analyzed according to slope gradients and climate scenarios. The findings of this study are expected to provide a foundation for ensuring stable crop cultivation in future reclaimed farmlands and to enable the prediction and characterization of soil movement processes in these areas.

Acknowledgements

This work was carried out with the support of "Cooperative Research Program for Agriculture Science and Technology Development (Project No. RS-2023-00224283)" Rural Development Administration, Republic of Korea.

References

Francesconi, W., Smith, D.R., Heathman, G.C., Wang, X., and Williams, C.O., 2014. Monitoring and APEX modeling of no-till and reduced-till in tile-drained agricultural landscapes for water quality. *Transactions of the ASABE*, 57(3), 777-789.

Lee, E.J., Cho, Y.K., Park, S.W., and Kim, H.K., 2006. Estimating soil losses from Saemangeum watershed based on cropping systems. *Journal of the Korean Society of Agricultural Engineers*, 48(6), 101–112 (in Korean).

Park, J.H., Kim, D.J., Kim, M.K., Jang, C.H., Kang, H.W., Kwm, D.H., and Lim, K.J., 2014. The evaluation of soil loss considering the R-factor value following the climate change. *Korean National Committee on Irrigation and Drainage*, 21(1), 64–77 (in Korean).

Sohn, Y.M., Jeon, G.Y., Song, J.D., Lee, J.H., Kim, D.H., and Park, M.E., 2010. Effect of soil salinity and soil-wetting by summer-rising of water table on the growth of fruit trees transplanted at the Saemangeum reclaimed tidal land in Korea. *Korean Journal of Soil Science and Fertilizer*, 43(1), 8–15 (in Korean).

Time-Dependent Groundwater Flows with Similarity Properties

Shuntaro Togo[1*], Koichi Unami[1], Masayuki Fujihara[1]

[1]Graduate School of Agriculture, Kyoto University, Kyoto, 606-8502, Japan

* Corresponding author. Email: togo.shuntaro.66s@st.kyoto-u.ac.jp

Abstract

In recent years, considerable attention has been directed towards groundwater due to its noteworthy characteristics. These include its interaction with diverse ecosystems, its status as the world's largest freshwater source, and its critical impact in regions experiencing water scarcity. The Boussinesq equation, a special case of the porous media equation (PME), is widely employed to simulate groundwater flows in unconfined aquifers having free surfaces. However, the nonlinearity of the governing equation makes it challenging to identify the well-posedness of problems. This study aims to deepen understanding of time-dependent groundwater flows when the water level of an adjacent water body fluctuates. Applying the Boltzmann transformation reduces the Boussinesq equation to a system of ordinary differential equations (ODEs) under three admissible boundary conditions. The resulting initial value problems are then solved numerically. The analysis develops and organizes similarity solutions within the framework of groundwater hydrology. The first type of boundary condition represents scenarios in which the water level of an adjacent water source decreases or increases. Explicit solutions under these conditions represent groundwater's instantaneous depletion, groundwater redistribution by gravity, and self-similar groundwater flows. The second type of boundary condition is regarded as the limiting case of the first. The third type of boundary condition models a sudden rise in the water level beyond the abovementioned situations. This limiting case corresponds to a fixed waterfront. This analysis offers a unified perspective on the similarity properties of groundwater flows.

Keywords: Boussinesq equation, Similarity solutions, Shampine's method

1. Introduction

Groundwater has an important role in the global water cycle and is recently known as a keystone ecosystem (Saccò et al. 2024). Wise use of groundwater is crucial, especially in arid and semi-arid regions (Stevanovic and Iurkiewicz 2009). As far as paddy fields are concerned, rice farming and groundwater are mutually influential: groundwater is extracted to meet the increasing water demand for irrigation (Zhang et al. 2024), and, on the other hand, rice fields largely contribute to the groundwater recharge (Hama et al. 2020). Therefore, it is desirable to simulate groundwater flows to establish an efficient water management strategy aiming for the sustainable development of paddy agriculture.

The Boussinesq groundwater equation is usually used to model unconfined groundwater flow. However, the intrinsic nonlinearity of the governing equation makes it difficult to obtain the general solution. Gilding (1982) classifies all the known explicit solutions of PME into three admissible similarity solutions: forward self-similarity, exponential self-similarity, and backward self-similarity. This approach is also applicable to the Boussinesq equation and illuminates the similarity properties of groundwater flows. For forward self-similarity, see Barenblatt et al. (1990), Lockington et al. (2000); for exponential self-similarity, see Telyakovskiy and Allen (2006); for backward self-similarity, see Togo and Unami (2025). In the current work, these similarity properties of groundwater flows are overviewed.

2. Materials and Methods

2.1. Problem statement

For simplicity, we employ the one-dimensional Boussinesq groundwater equation

$$S\frac{\partial h}{\partial t} = \frac{K}{2}\frac{\partial^2 h^2}{\partial x^2}, \tag{1}$$

where the constant S is the specific storage, the constant K is the saturated hydraulic conductivity, and $h(t,x)$ denotes the height of the water table above the horizontal impermeable base, defined on the set $\mathbb{R}_+ \times (0,T)$. The finite speed of propagation derived from the nonlinearity of the equation (1) yields a boundary condition

$$h(x_0, t) = 0, \tag{2}$$

where x_0 represents the position of the wetting front. Then, we consider the following inlet conditions using constants $U > 0, T > 0$, which admit similarity transformations.

(I) Forward power-law head condition at the inlet

$$h(0,t) = U(T+t)^{\alpha}, \ \ where -1/2 < \alpha. \tag{3}$$

(II) Exponential power-law head condition at the inlet

$$h(0,t) = Ue^{\beta(T+t)}, \ \ where\ 0 < \beta. \tag{4}$$

(III) Backward power-law head condition at the inlet

$$h(0,t) = U(T-t)^{\gamma}, \ \ where\ \gamma \le -1. \tag{5}$$

2.2. Similarity transformations

For the boundary value problem (1), (2), (3), we can conduct Boltzmann's transformation with the dimensionless variables

$$H(\xi) = U(T+t)^{-\alpha}h, \tag{6}$$

$$\xi = x\sqrt{2S(1+\alpha)/KU}\,(T+t)^{-\frac{1+\alpha}{2}}. \tag{7}$$

For (1), (2), (4),

$$H(\xi) = Ue^{-\beta(T+t)}h, \tag{8}$$

$$\xi = x\sqrt{2S\beta/KU}\,e^{-\frac{\beta}{2}t}. \tag{9}$$

For (1), (2), (5),

$$H(\xi) = (T-t)^{-\gamma}h, \tag{10}$$

$$\xi = x\sqrt{2S/KU}\,(T-t)^{-\frac{1+\gamma}{2}}. \tag{11}$$

Then, the original partial differential equation (PDE) is reduced to ODEs

$$\frac{d^2H^2}{d\xi^2} + \frac{a}{2}\frac{dH}{d\xi} + bH = 0, \tag{12}$$

where $a = \xi$, $b = -\alpha/(1+\alpha)$ for the condition (I), $a = \xi$, $b = -1$ for the condition (II), and $a = -(1+\gamma)\xi$, $b = \alpha$ for the condition (III). The boundary conditions are transformed into

$$\boldsymbol{H(0) = 1}, \qquad \boldsymbol{H(\xi_0) = 0}, \tag{13}$$

where ξ_0 denotes the front in relation to x_0. Then, the derived ODEs (12) can be numerically solved using Shampine's method (Lockington et al. 2000) under the transformed boundary conditions (13).

3. Results and Discussion

Figure 1 illustrates existing numerical solutions of the problem (12), (13) under specific conditions after converting to real scale, including all the known explicit solutions of the problem (1): the waiting time solution (a), the traveling wave solution (c), the point source solution (e), and the dipole solution (f). These similarity solutions are classified in relation to the rate of water-level rise at the inlet.

First, when the water level at the inlet drops to zero instantaneously because of abrupt high-rate pumping, the dipole solution appears ($\alpha = -1/2$). As the value of α increases, the pumping rate decreases, and when $\alpha = -1/3$, the free spreading of a point source water at the inlet is achieved. Then, the water level at the inlet starts to rise after reaching the stationary boundary condition ($\alpha = 0$). When $\alpha = 1$, constant-shape fronts are formed, moving with constant speed. With an increase in the value of α, the speed of the front propagation continues to grow.

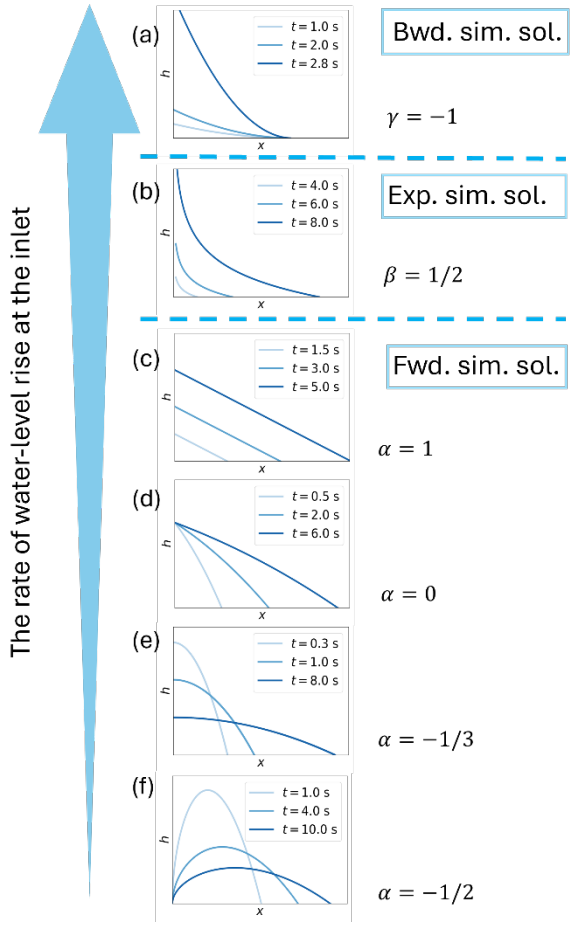

Figure 1. Classification of three types of similarity solutions in relation to the rate of water-level rise at the inlet.

In this context, exponential similarity solutions are considered to be the limiting case of forward similarity solutions. Finally, backward similarity solutions come into consideration, which represent a sudden rise in the water level at the inlet. Unlike previous situations, the water level diverges in finite time at the inlet. This type begins with the solution which has a fixed waterfront ($\gamma = -1$). As the value of γ decreases, the propagation speed of the waterfront increases.

4. Conclusions

Similarity solutions of the Boussinesq groundwater equation are classified in relation to the rate of water-level rise at the inlet, which enables us to establish conceptual continuity among three types of similarity solutions. Forward similarity solutions describe the behavior of groundwater infiltration ranging from a decrease to an increase, exponential ones are the limiting cases, and backward type represents the rapid rising of the water level.

Consequently, similarity properties of groundwater flows appear when the water level at the inlet is either monotonically increasing, decreasing, or constant based on a simple condition, though a monotonic change in water level doesn't always mean these properties will appear.

References

Barenblatt, G.I., Entov, V.M., and Ryzhik, V.M., 1990. *Theory of Fluid Flows through Natural Rocks*. Theory and Applications of Transport in Porous Media, v. 3. Kluwer Academic Publishers.

Gilding, B.H., 1982. "SIMILARITY SOLUTIONS OF THE POROUS MEDIA EQUATION." *Journal of Hydrology* 56: 251–63.

Hama, T., Fujimi, T., Shima T, Ishida, K., Kawagoshi, Y., and Ito, H., 2020. "Evaluation of Groundwater Recharge by Rice and Crop Rotation Fields in Kumamoto, Japan." *Journal of Water and Climate Change* 11 (4): 1042–49. https://doi.org/10.2166/wcc.2019.045.

Lockington, D.A., Parlange, J.-Y., Parlange, M.B., and Selker, J., 2000. "Similarity Solution of the Boussinesq Equation." *Advances in Water Resources* 23 (7). www.elsevier.com/locate/advwatres.

Saccò, M., Mammola, S., Altermatt, F., et al., 2024. "Groundwater Is a Hidden Global Keystone Ecosystem." *Global Change Biology* 30 (1). https://doi.org/10.1111/gcb.17066.

Stevanovic, Z., and Iurkiewicz, A., 2009. "Groundwater Management in Northern Iraq." *Hydrogeology Journal* 17 (2): 367–78. https://doi.org/10.1007/s10040-008-0331-0.

Telyakovskiy, A.S., and Allen, M.B., 2006. "Polynomial Approximate Solutions to the Boussinesq Equation." *Advances in Water Resources* 29 (12): 1767–79. https://doi.org/10.1016/j.advwatres.2005.12.006.

Togo, S., and Unami, K., 2025. "Backward Similarity Solution of the Boussinesq Groundwater Equation." Preprint, arXiv. https://doi.org/arXiv:2509.07478.

Qingsong, Z., Jiahao S., Changlei D., Guangxin Z., and Yanfeng W., 2024. "Sustainable Development of Groundwater Resources under the Large-Scale Conversion of Dry Land into Rice Fields." *Agricultural Water Management* 298: 108851. https://doi.org/10.1016/j.agwat.2024.108851.

Spatio-Temporal Variability Assessment of Groundwater Level in the Drought-Prone Region in India

Yuvraj Nanasaheb Dhivar [1*], Madan Kumar Jha[1], and Masayuki Fujihara[2]

[1] Department of Agricultural and Food Engineering, Indian Institute of Technology Kharagpur, West Bengal, 721302, India

[2] Graduate School of Agriculture, Kyoto University, 606-8501, Japan

* Corresponding author. Email: yuvrajdhivar97@gmail.com

Abstract

To map vulnerable areas with declining groundwater levels and to sustainably manage aquifers, groundwater level trends must be accurately analyzed, especially in drought-prone arid and semi-arid regions. The spatio-temporal variation of groundwater level helps to understand the aquifer's response under varied groundwater recharge rates and abstraction conditions. Therefore, this study examined the pre- and post-monsoon groundwater level (GWL) and their fluctuation trends in 154 observation wells (OBWs) located in the Buldhana district of Maharashtra state, India, from the year 2008 to 2023. The non-parametric statistical tests used to detect the trend in the study includes: Modified Man-Kendall Test (MMK), Innovative Trend Analysis Test (ITA), and Spearman Rank Correlation Test (SROC). The results revealed that the post-monsoon GWL trend was increasing at 111 OBWs. Whereas, no significant trend was found in 93 OBWs for pre-monsoon GWL. Moreover, the GWL fluctuation trend was found to be increasing at 72 and decreasing 19 OBWs.

Keywords: Modified Man-Kendall Test, Innovative Trend Analysis Test, Spearman Rank Correlation Test, Groundwater level, spatio-temporal variability

1. Introduction

Proper water resources management is extremely important to achieve the majority of sustainable development goals, especially in arid and semi-arid regions. Groundwater is dynamic, less susceptible to contamination, and a free source of freshwater available for the entire world (Barman et al., 2025). It is a vital source as far as irrigation and domestic water supply are concerned. Due to rapid population growth, urbanization, especially in developing nations, is in a vulnerable situation, with India being no exception.

Maharashtra is one of the important states in India with rapid agricultural growth and industrialization. Around 82% of its area is underlain by Deccan basalts, which makes the geology trickier, and because of the poor transmissivity of the aquifer due to hard rock, the movement of groundwater is restricted. Therefore, quantification of groundwater resources becomes critical (CGWB, 2021). Buldhana is one of the districts facing the groundwater salinity problem due to such a geological setup. Therefore, for effective management of groundwater, the study was conducted with the objective of assessing the pre- and post-monsoon groundwater levels and their fluctuation trend.

2. Materials and Methods

2.1. Study area and data collection

Pre-monsoon and post-monsoon groundwater levels of 154 observation wells (OBWs) were collected for 16 years (2008 to 2023), from the Groundwater Survey and Development Agency of Buldhana District. The total area of the district is 9661 km^2, and is divided into 13 blocks. The map of the study area is shown in Figure 1.

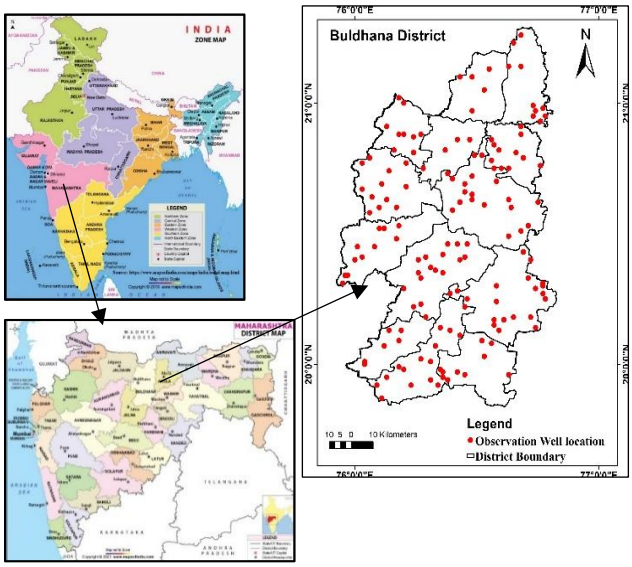

Figure 1. Location map of the study area.

2.2. Statistical tests for trend analysis

Three statistical methods were used, viz., MMK, ITA, and SROC, to identify the significant trend, and it was determined whether two or more tests provide the same results. Figure 2, shows the flowchart of the methodology.

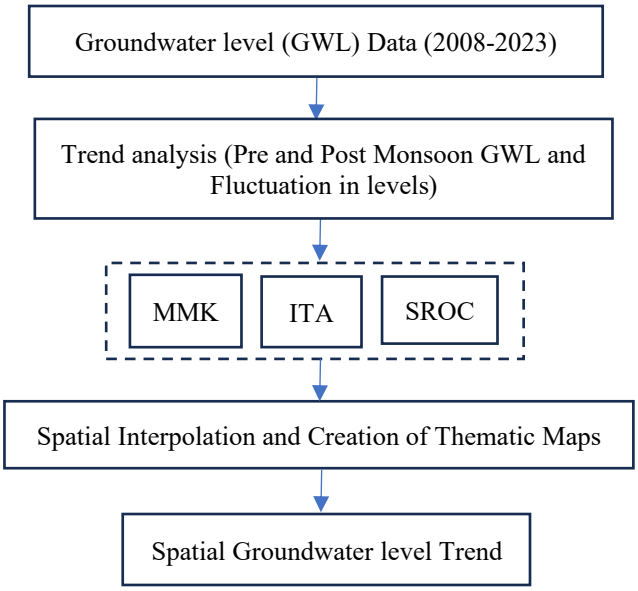

Figure 2. Flow chart of methodology.

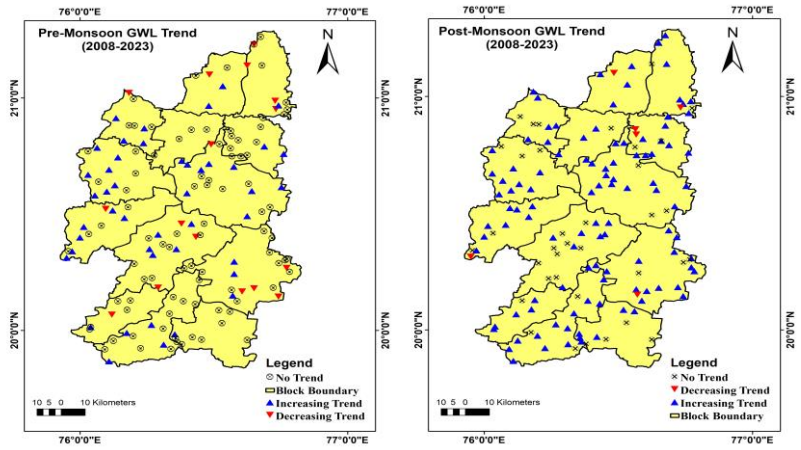

Figure 3. Pre-monsoon and post-monsoon groundwater level trend of Buldhana district during the year 2008-2023.

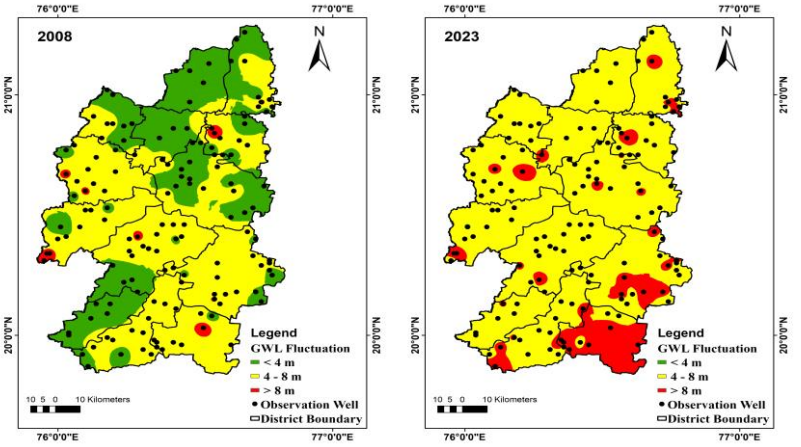

Figure 4. Groundwater level fluctuation of the year 2008 and 2023.

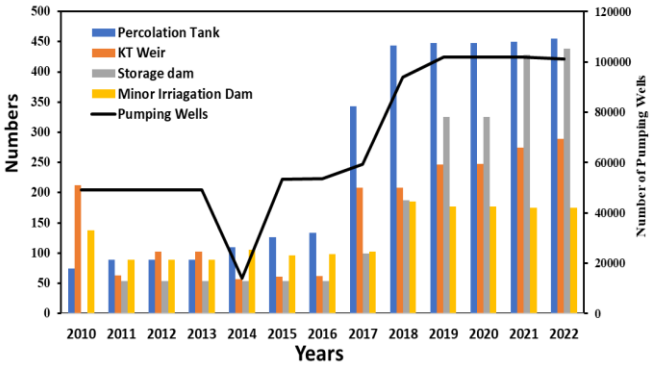

Figure 5. Annual variations in the number of artificial recharge structures and pumping well from the year 2010 to 2022.

3. Results and Discussion

3.1 Trend analysis of pre- and post-monsoon GWL

Figure 3 demonstrates that there is an increasing pre-monsoon GWL trend in 45, decreasing in 16 and no significant trend in 93 OBWs during 2008 and 2023 year and, there is an increasing post-monsoon GWL trend in 111, decreasing trend in 6 and no significant trend in 37 OBWs.

3.2 Trend analysis of GWL fluctuation

Figure 4 shows the GWL fluctuation for the year 2008 and 2023, which is classified into three classes, < 4 m, 4 – 8 m and > 8 m. The area of GWL fluctuation below 4 m decreased to 37%, increased to 26% and 11% for 4-8 m and > 8 m respectively.

Previous research revealed, overall declining rainfall trend in Buldhana district (Singh et al., 2021) and there is a reduction in normal precipitation (Kumar et al., 2025). Based on the statistical report of Buldhana district, number artificial recharge/water conservation structures and number of pumping well has been increased from year 2010 to 2022 (Figure 5).

The current study discovered an increasing trend in GWL fluctuations, despite the presence of more groundwater recharge structures and a rising post-monsoon GWL trend. This suggests increased in groundwater pumping during the non-monsoon season, as evidenced by growing number pumping wells.

4. Conclusions

Based on the findings of the study following conclusions are made:

a. The post-monsoon GWL trend was found to be increasing in 111 OBWs, due to increase in number of recharge structures.

b. No significant pre-monsoon GWL trend was detected at 93 OBWs, likely due to intensive groundwater pumping for irrigation in non-monsoon season, which offsets recharge and averting pre-monsoon GWL rise.

c. GWL fluctuation trend shows increasing trend in 72 OBWs.

d. The fluctuations in groundwater level utilized to forecast aquifer storage, influenced by recharge structures and groundwater draft.

The research will help in long-term management of groundwater in Buldhana district.

References

Barman, J., Biswas, B., & Soren, D. D. L. (2025). Groundwater trend analysis and regional groundwater drought assessment of a semi-arid region of Rajasthan, India. Environment, Development and Sustainability, 27(2), 3415-3439.

CGWB, (2021). Ground Water Year Book Of Maharashtra and Union Territory of Dadra and Nagar Haveli, Department of Water Resources, Rd & Gr Central Ground Water Board. Government of India, Ministry of Jal shakti.

Kumar, P. K., Madhnure, P., and Lamsoge, B. R. (2025). Long-term monsoon rainfall variability (1998–2023) and its impact on groundwater level dynamics in Maharashtra state. Theoretical and Applied Climatology, 156(6), 335.

Singh, R. N., Sah, S., Das, B., Vishnoi, L., and Pathak, H. (2021). Spatio-temporal trends and variability of rainfall in Maharashtra, India: Analysis of 118 years. Theoretical and Applied Climatology, 143(3), 883-900.

Water reuse and groundwater augmentation
－Focus on New Valley, Egypt－

Abdelhafez A Ahmed・Yoshida Shuichiro

Abstract

This study examines the strategic significance of water reuse and groundwater augmentation as solutions to the escalating global water crisis. It assesses the historical development, contemporary technologies, and practical applications of these approaches, emphasizing their essential role in sustainable water resource management. Water reuse entails the reclamation of treated wastewater for constructive uses, thereby reducing dependence on traditional freshwater sources and conserving natural resources. Groundwater augmentation, especially through Managed Aquifer Recharge (MAR), contributes to the sustainability of aquifers by replenishing them with treated water. The urgency of these practices is particularly evident in Egypt's New Valley Governorate, where groundwater serves as the primary-albeit non-renewable-source of water. An excessive reliance on this limited resource, coupled with insufficient monitoring and management, poses significant risks to water security and agricultural sustainability. This study underscores the imperative of consistently monitoring groundwater quality and quantity in the New Valley and accentuates the necessity of artificial recharge initiatives to compensate for excessive extraction. The augmentation of groundwater through treated wastewater not only increases water availability but also enhances groundwater quality, providing a sustainable alternative to meet rising demands in the context of climate variability and restricted access to surface water. By implementing integrated strategies for water reuse and recharge, Egypt can advance toward a more resilient and self-reliant water management framework, ultimately preserving its essential aquifers for future generations.

Multi-Domain Joint Learning for Crack Detection in-Service Agricultural Infrastructure under Varying Illumination Conditions using UAV Imagery

Hiromu Tanaka [1*], Kazuma Shibano [1], Keika Tagami [2] and Tetsuya Suzuki [3]

[1] Graduate School of Science and Technology, Niigata University, Niigata, 950-2181, JAPAN

[2] Faculty of Agriculture, Niigata University, Niigata, 950-2181, JAPAN

[3] Institute of Agriculture, Niigata University, Niigata, 950-2181, JAPAN

* Corresponding author. Email: f25e015b@mail.cc.niigata-u.ac.jp

Abstract

Concrete materials are widely used in agriculture infrastructure. Cracks accumulate through long-term use under varying environmental conditions, potentially compromising hydraulic function and irrigation system reliability. Automatic crack detection using deep learning faces significant challenges when datasets contain images with varying appearances across different domains, particularly under diverse outdoor lighting conditions. This study implements a multi-domain joint learning approach that unifies dataset appearance across varying illumination conditions through scene classification and image processing. The method performs scene classification using U-net to classify pixels into noisy areas, sunlit pavement areas, and shaded pavement areas before crack detection. Image processing in L*a*b* color space normalizes appearance variations through piecewise linear interpolation and level shift operations. Measurements were conducted on pavements of three rural road bridges in Niigata, Japan acquiring UAV imagery. Results demonstrate that scene classification achieves high accuracy, and the highest crack detection performance is obtained when multi-domain joint learning with image processing is applied. The combination of scene classification training and domain-adaptive image processing proves highly effective for improving generalizability under varying lighting conditions, contributing to optimized maintenance strategies for sustainable agriculture activities.

Keywords: Image processing, Scene classification, Lighting condition, Piecewise linear interpolation, Level shift

1. Introduction

For maintenance and management of agricultural infrastructure such as bridges and canal structures, automation using digital technologies is being promoted as an alternative to visual inspection. Cracks accumulate through long-term use under varying environmental conditions, potentially compromising hydraulic function, irrigation system reliability and structural integrity. In pavement crack detection for maintenance, numerous studies have examined crack detection using deep learning (Kheradmandi and Mehranfar, 2022), where the quantity and quality of datasets significantly affect detection accuracy (Kizhevsky et al., 2017).

Deep learning-based automatic crack detection faces significant challenges when datasets contain images with varying appearances under diverse outdoor lighting conditions. In bridge images, sunlit and shaded pavement areas exhibit different brightness levels, resulting in decreased crack detection accuracy in shaded areas and necessitating dataset preprocessing.

Therefore, this study attempts to classify pavement areas into sunlit and shaded sections using scene classification models, and unify the lighting conditions to sunlit pavement areas through image processing. The study aims to create models capable of handling diverse datasets by enabling any pavement surface to be treated as sunlit pavement area and examines the impact of image processing on crack detection accuracy.

2. Measurement methods

Visual image acquisition was conducted targeting the pavement sections of Bridge A (27 years after construction), Bridge B (27 years after construction), and Bridge C (31 years after construction), which are rural road bridges in service in Niigata Prefecture, Japan. The degree of damage in the pavement sections varied among the bridges. Damage in the sunlit pavement areas was observed on all bridges, while damage in the shaded pavement areas was only observed on Bridge A. Images were captured vertically downward at regular intervals using a visible camera mounted on a UAV. To maintain consistent image conditions for the dataset input, the UAV was flown at a constant altitude of 5 m from the takeoff point. Overview of target bridges and UAV system specifications are shown in Table 1.

3. Analytical procedures

In this study, analysis is conducted using scene classification models and crack detection models constructed with U-net architecture. Raw images are classified into noisy areas, sunlit pavement areas, and shaded pavement areas by two scene classification models. Noisy areas are defined as images containing objects other than pavement surfaces, such as vegetation, railings, and white lines. Shaded pavement areas are converted to simulated sunlit pavement areas through image processing. The presence or absence of cracks is determined for each pixel in both sunlit pavement areas and converted shaded

Table 1 Overview of target bridges and UAV system specifications

	Slab material	Bridge length	UAV model	Camera model	Image size
Bridge A	RC slab	112.0 m	Matrice 210 (DJI)	Zenmuse XT2 (DJI)	4,000×3,000
Bridge B	RC slab	52.8 m	Matrice 210 (DJI)	Zenmuse XT2 (DJI)	4,000×3,000
Bridge C	RC slab	82.5 m	Matrice 350 RTK (DJI)	Zenmuse L1 (DJI)	5,472×3,648

pavement areas using crack detection models.

Image processing is performed in the L*a*b* color space. The image processing flow is shown in Figure 1. Piecewise linear interpolation is applied to L*, while level shifting is applied to a* and b*. In piecewise linear interpolation, the L* values of input and target images are obtained at specified interval widths. The L* values of the input image are replaced with those of the target image in the same interval, with linear interpolation between intervals. The interval width is set to 5 % intervals. In level shifting, the values of each pixel in the input image are uniformly adjusted so that the mode values of a* and b* in the input image become identical to those of the target sunlit pavement areas. Since crack areas are darker than pavement surfaces, L* is distributed in a smaller range, however, shaded pavement areas are inherently dark, resulting in a smaller difference in L* distribution range compared to sunlit pavement areas. Since level shifting applied to a* and b* cannot reproduce this difference in L* distribution range, piecewise linear interpolation is adopted.

For creating dataset for crack detection models, annotation is performed on images of sunlit and shaded pavement areas containing cracks. 1,312 images of sunlit pavement areas and 130 images of shaded pavement areas are prepared. To match the number of shaded pavement area datasets with that of sunlit pavement areas, data augmentation is applied only to shaded pavement areas, increasing them to 1,312 images. For crack detection models, four models with different lighting conditions are created: a sunlit pavement model, a shaded pavement model, an entire pavement model trained on both sunlit and shaded pavement areas (entire pavement model), and an entire pavement model where shaded pavement areas are processed and approximated to sunlit pavement areas (processed entire pavement model). Hyperparameter tuning is conducted for kernel size, number of epochs and batch size with 20 trials. Regarding the dataset ratio, 80 % of the images are used as validation and training data for hyperparameter tuning, while the remaining 20 % are used as test data. Image division is performed randomly.

4. Results and discussion

The crack detection accuracy of each crack detection model for each pavement section is shown in Table 2. The detection targets are test data of the entire pavement with and without image processing applied. The detection results of the sunlit pavement model and shaded pavement model are presented as the results of detection using the sunlit pavement model for sunlit pavement areas and the shaded pavement model for shaded pavement areas (sunlit & shaded pavement model). Regarding the detection results for the entire pavement, the F-measure is highest at 0.778 for the sunlit & shaded pavement model and lowest at 0.611 for the processed entire pavement model. The sunlit & shaded pavement model achieves the most accurate results because the datasets are unified for each lighting condition and the lighting conditions of the detection targets also match. In contrast, the processed entire pavement model shows difficulty in detecting shaded pavement areas since it is not trained on pure shaded pavement areas. Regarding the detection results for the entire pavement after image processing, the processed entire pavement model shows the highest F-measure of 0.784 among all cases. The processed entire pavement model has datasets unified to sunlit pavement areas, and the dataset volume is twice that of the sunlit pavement model and shaded pavement model. The results suggest that applying image processing to both training data and detection targets enables more accurate crack detection by ensuring dataset volume while unifying lighting conditions.

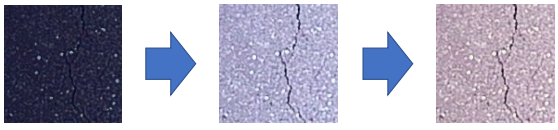

Piecewise linear interpolation (L*) Level shift (a* b*)

Figure 1. Schematic representation of image processing.

5. Conclusions

In this study, crack detection is conducted using deep learning that combines scene classification and image processing for visible images of bridges with different lighting conditions captured by UAV. The results show that the most accurate detection is achieved when the lighting conditions of both training data and detection targets are unified to sunlit pavement areas through image processing.

Acknowledgements

The authors are grateful to Niigata Prefecture for their assistance with the UAV measurements at each bridge.

References

Kheradmandi, N. and Mehranfar, V., 2022. A critical review and comparative study on image segmentation-based techniques for pavement crack detection. *Construction and Building Materials*, **321**, 126162, https://doi.org/10.1016/j.conbuildmat.2021.126162.

Kizhevsky, A., Sutskever, I. and Hinton, G.E., 2017. ImageNet Classification with Deep Convolutional Neural Networks, *Communications of the ACM*, **60**(6), pp. 84-90, https://doi.org/10.1145/3065386.

Table 2 Crack detection accuracy

Target: Entire pavement	Precision	Recall	F-measure
Sunlit & shaded pavement model	0.853	0.715	0.778
Entire pavement model	0.771	0.729	0.749
Processed entire pavement model	0.834	0.482	0.611
Target: Image-processed Entire pavement	**Precision**	**Recall**	**F-measure**
Sunlit & shaded pavement model	0.765	0.712	0.738
Entire pavement model	0.736	0.751	0.744
Processed entire pavement model	0.813	0.756	0.784

Quantitative Internal Damage Assessment of Irrigation and Drainage Concrete Structures by X-ray CT image based on DCNN

Koki Ikeda [1*], Kazuma Shibano [2], Moeka Mukai [2] and Tetsuya Suzuki [3]

[1] Faculty of Agriculture, Niigata University, Niigata 950-2181, JAPAN

[2] Graduate School of Science and Technology, Niigata University, Niigata 950-2181, JAPAN

[3] Institute of Agriculture, Niigata University, Niigata 950-2181, JAPAN

* Corresponding author. Email: a22n088k@mail.cc.niigata-u.ac.jp

Abstract

Deep Convolutional Neural Network (DCNN) has been applied to automated crack detection in X-ray Computed Tomography (CT) images of concrete cores. However, a major challenge is the extreme data imbalance arising from the complex geometry of cracks and their scarcity in datasets. This study develops a novel Class-Frequency-Aware Focal Loss (CFL) to address imbalanced data by focusing on minority classes during training. The method incorporates class imbalance into the γ parameter of Focal Loss (FL), enhancing the loss for minority classes that are difficult to detect. U-net architecture is employed for semantic segmentation using 591 CT images from 135 concrete cores extracted from irrigation and drainage structures and fabricated in the laboratory. Quantitative evaluation using confusion matrices demonstrates significant performance improvements. CFL achieves a crack true positive value of 0.48 compared to 0.11 for cross-entropy loss (CE) and 0.16 for FL, yielding F1-score improvements of up to 21 points. The results indicate that CFL facilitates efficient training by focusing on minority and detection-challenging classes.

Keywords: X-ray Computed Tomography, Deep Convolutional Neural Network, Loss function

1. Introduction

X-ray Computed Tomography (CT) is widely utilized for visualizing the internal structure of concrete cores, enabling high-resolution three-dimensional observation without destructive testing. Deep Convolutional Neural Network (DCNN) has achieved remarkable advances and is now being applied to automated crack detection in CT images of concrete cores (Cheniour et al., 2024). Such deep learning approaches enable the recognition and classification of complex patterns that are challenging for conventional image processing methods. A technical challenge in DCNN-based crack detection is the extreme data imbalance in datasets arising from the geometrical complexity of cracks and the scarcity of crack data. When datasets are imbalanced, training of deep learning models does not proceed efficiently (Johnson and Khoshgoftaar, 2019). This study proposes a loss function to address imbalanced data by focusing more intensively on minority classes during deep learning model training and validates its effectiveness.

2. Materials and Methods

2.1. Concrete Cores and CT images

135 concrete cores were served for dataset: 78 samples extracted from seven existing irrigation and drainage structures with varying service conditions, and 57 samples were casted in a laboratory to ensure dataset diversity. X-ray CT scanning was performed under identical scanning conditions to acquire 591 CT images for analysis.

2.2. DCNN model architecture

A CNN-based U-net architecture is employed for crack detection, which has been widely applied to semantic segmentation tasks in various applications (Ronneberger et al., 2015). U-net architecture is illustrated in Figure 1. For dataset preparation, a total of 591 CT images cropped to 512×512 pixels are utilized. Among these, 581 images are allocated for training and 10 for testing, with 10 % of the training data serving as validation data based on the hold-out method. The Adam optimizer is employed to ensure training stability and convergence.

2.3. Loss function

The design of loss functions is crucial for efficiently training minority classes such as cracks and voids. Cross-entropy loss (CE) is primarily employed in semantic segmentation tasks. Focal Loss (FL), which was proposed by Lin et al. (2017) to address class imbalance problems, is presented below. Adding a modulating factor to the CE significantly reduces the loss contribution from easy-to-detect classes and focuses learning on difficult-to-detect classes. Hyperparameter tuning is performed for γ values of (0.5, 1.0, 2.0, 3.0 and 5.0).

This study proposes a Class-Frequency-Aware Focal Loss (CFL) based on Focal Loss. The equation is presented below:

$$CFL(p_t) = -(1-p_t)^{\gamma_c}\log(p_t) \quad (1)$$

$$\gamma_c = \max\left(\lambda\frac{1-p_c}{p_c+\varepsilon}, \gamma_{max}\right) \quad (2)$$

where p_t represents the softmax output value from the model's output layer (the predicted probability for each class) and p_c denotes the class frequency. The proposed method incorporates class imbalance into the γ parameter

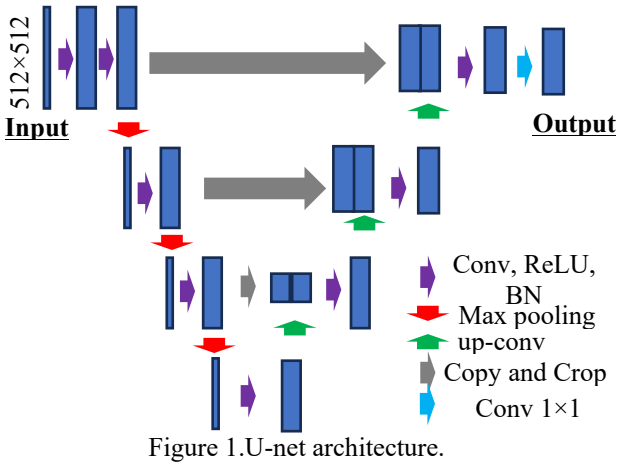

Figure 1.U-net architecture.

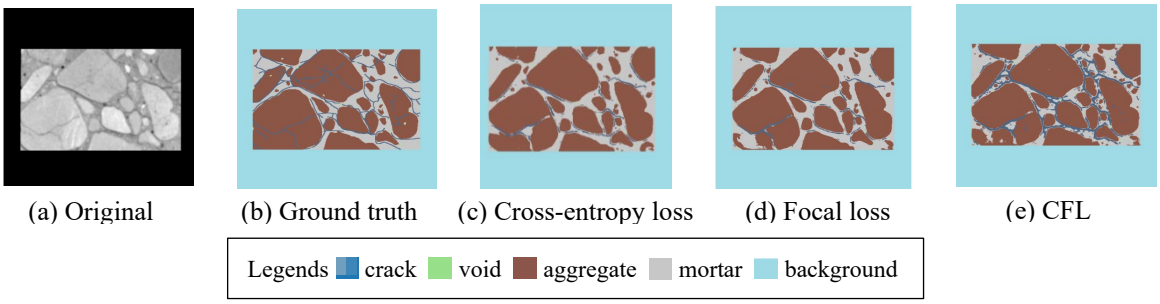

Figure 2. Prediction results.

of FL, establishing a mechanism that amplifies the loss for minority classes that are difficult to detect. Hyperparameter tuning includes the scaling factor λ (5, 10 and 15), maximum γ_c , γ_{max} (3, 5 and 7) and $\varepsilon(10^{-5}, 10^{-4}$ and $10^{-3})$.

2.4. Validation

Quantitative evaluation is conducted using confusion matrices. The obtained confusion matrices are employed to assess model performance based on precision, recall and F1-score metrics.

3. Results and Discussion

The prediction results by CE, FL and CFL are presented in Figure 2. CFL exhibits superior crack detection performance compared to both CE and FL. Especially, enhanced detection capability is observed at the interface between aggregates and mortar regions. However, the CFL approach exhibits numerous false positive detections that do not resemble crack-like geometry.

Quantitative evaluation results using confusion matrices are presented in Tables 1 to 4. For crack true positive values, CE achieves 0.11, FL achieves 0.16, while CFL achieves 0.48, yielding F1-score improvements of up to 21 points. These results suggest that efficient training is realized by effectively focusing on minority and difficult-to-detect classes such as cracks and voids. CFL detection shows lower precision calculated from confusion matrices compared to CE and FL, indicating the occurrence of false positives. Particularly, frequent false positive detections are observed in the mortar class, which can be attributed to the detection of crack-unrelated noise within mortar regions.

Table 1. Confusion matrix of CL

		Prediction label				
		1	2	3	4	5
True label	1	0.11	0.00	0.12	0.77	0.00
	2	0.11	0.56	0.06	0.37	0.01
	3	0.00	0.00	0.90	0.10	0.00
	4	0.01	0.00	0.14	0.85	0.00
	5	0.00	0.00	0.00	0.00	1.00

Table 2. Confusion matrix of FL

		Prediction label				
		1	2	3	4	5
True label	1	0.16	0.00	0.09	0.74	0.00
	2	0.01	0.52	0.10	0.36	0.01
	3	0.00	0.00	0.86	0.13	0.00
	4	0.01	0.00	0.11	0.88	0.00
	5	0.00	0.00	0.00	0.00	1.00

Table 3. Confusion matrix of CFL

		Prediction label				
		1	2	3	4	5
True label	1	0.48	0.01	0.12	0.39	0.00
	2	0.03	0.71	0.08	0.18	0.00
	3	0.01	0.00	0.92	0.07	0.00
	4	0.12	0.01	0.19	0.69	0.00
	5	0.00	0.00	0.00	0.00	1.00

* Class1: crack, 2: void, 3: aggregate, 4: mortar, 5: background

Table 4. Precision, Recall, and F1-score of crack detection by loss function

Loss function	Precision	Recall	F1-Score
CE	0.59	0.11	0.18
FL	0.58	0.16	0.25
CFL	0.33	0.48	0.39

4. Conclusions

This study designed CFL to address imbalanced data challenges in crack detection within concrete cores, and demonstrated its effectiveness. The proposed method significantly improves crack detection performance, though challenges with noise-induced false positives remain. Future work will focus on model optimization and dataset expansion to improve detection precision.

References

Cheniour, A., Asahina, D., Ramos, J. and Bolander, J.E., 2024. A mesoscale 3D model of irradiated concrete informed via a 2.5 U-Net semantic segmentation. *Construction and Building Materials*, **412**, 134392. DOI: https://doi.org/10.1016/j.conbuildmat.2023.134392

Johnson, J.M. and Khoshgoftaar, T.M., 2019. Survey on deep learning with class imbalance. *Journal of Big Data*, **6**, 27. DOI: https://doi.org/10.1186/s40537-019-0192-5

Lin, T.Y., Goyal, P., Girshick, R., He, K. and Dollár, P., 2017. Focal loss for dense object detection. Proceedings of the IEEE International Conference on Computer Vision, 2017, pp. 2980-2988. DOI: 10.1109/ICCV.2017.324

Ronneberger, O., Fischer, P. and Brox, T., 2015. U-Net: Convolutional Networks for Biomedical Image Segmentation. Medical Image Computing and Computer-Assisted Intervention – MICCAI 2015. Lecture Notes in Computer Science, Vol. 9351. Springer, Cham, pp. 234-241. DOI: 10.1007/978-3-319-24574-4_28

Influence of Input Frequency on Ultrasonic Velocity in Concrete Cores with Large Aggregate

Moeka Mukai [1*], Kazuma Shibano [1], Tetsuya Suzuki [2]

[1] Graduate School of Science and Technology, Niigata University, Niigata 950-2181, JAPAN

[2] Institute of Agriculture, Niigata University, Niigata 950-2181, JAPAN

* Corresponding author. Email: f24e021b@mail.cc.niigata-u.ac.jp

Abstract

Nondestructive testing techniques for concrete structures have essential role in the maintenance and management of facilities. Ultrasonic testing, one of the useful nondestructive testing method for concrete materials, is widely used in the maintenance and quality assessment of reinforced concrete structures. In this study, the relationship between ultrasonic velocity and the geometric properties of coarse aggregate at three input frequencies: 54 kHz, 150 kHz and 250 kHz, using concrete cores collected from the Uchinokura dam embankment is investigated. As a result, ultrasonic velocity for samples with a large coarse aggregate area rate and diameter exhibits higher than for one with a small coarse aggregate area rate and diameter. Increase trend of ultrasonic velocity is confirmed at 150 kHz and 250 kHz compared to 54 kHz. These results indicate that it is necessary to consider differences in coarse aggregate size, area rate and input frequency when using ultrasonic velocity testing to evaluate the damage degree of concrete.

Keywords: X-ray Computed Tomography (CT), Concrete, Aggregate, Ultrasonic test

1. Introduction

Ultrasonic testing, one of the nondestructive testing techniques for concrete materials, is widely used in the maintenance and quality assessment of concrete structures. Ultrasonic velocity is closely related to the mechanical properties of the material. It is important to clarify the relationship between the geometric features inside the material and the wave propagation characteristics to accurately interpret the results of ultrasonic testing. It has been expected that the use of particularly high-frequency ultrasonic waves improves the accuracy of detecting even smaller internal defects (Morozova et al., 2022 ; Philippidis and Aggelis, 2005). Evaluating the relationship between the internal structure of concrete and input frequency is essential for establishing nondestructive testing techniques. In this study, an influence of input frequency on ultrasonic velocity for concrete core with different coarse aggregate size and area rate is investigated.

2. Materials and Methods

2.1. Concrete cores

Concrete cores with a diameter of 70 mm were taken from the body of a hollow gravity concrete dam. A characteristic of dam concrete is that the maximum aggregate diameter generally exceeds 40 mm and diameter of some aggregates exceeds 150 mm. Therefore, the heterogeneity of the concrete due to the aggregate has a significant effect on ultrasonic velocity. This factor cannot be ignored when the degree of damage is assessed.

2.2. X-ray CT measurement

Internal structure of concrete core was visualized and quantified by X-ray CT measurements. CT images were acquired using an Aquilion One (Toshiba Corporation). Using coronal sections of the acquired CT data, couarse aggregates are visually classified (Figure 1). Using hierarchical cluster analysis, aggregates are classified into three clusters based on their number, area rate and feret diameter. A scatter plot of the three variables is shown in Figure 2 and the values of their respective centroids are listed in Table 1. Cluster 1 has a large average feret diameter and area rate, Cluster 2 has small feret diameter, and Cluster 3 has low values for all .

2.3. Ultrasonic velocity test

The ultrasonic velocity test was carried out using the transmission method, with input in the axial direction of the concrete core (ASTM, 2002). Three transducers with input frequencies of 54, 150 and 250 kHz were used.

3. Result and discussion

Figure 3 shows the ultrasonic velocity for each cluster

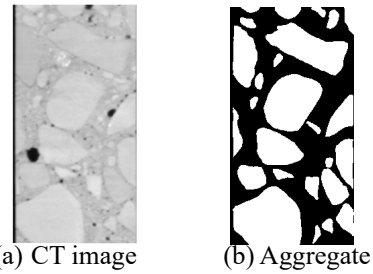

(a) CT image (b) Aggregate

Figure 1. Segmentation of internal structure for X-ray CT images.

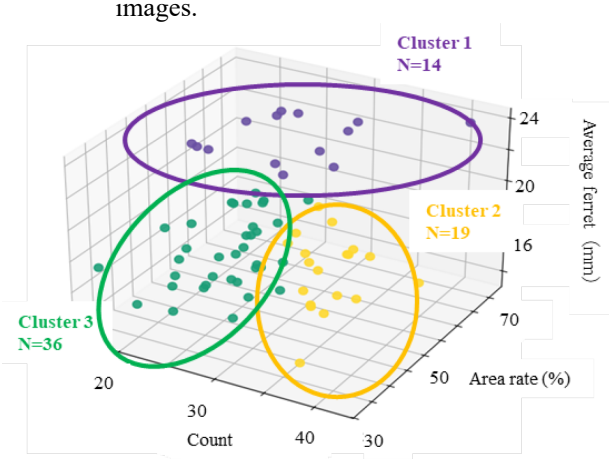

Figure 2. Cluster analysis results based on coarse aggregate geometric properties.

Table 1. Geometric properties centroid value for each cluster

Cluster number	Count	Area rate (%)	Average feret diameter (mm)
1	26	62.3	22.0
2	35	47.3	17.5
3	25	46.4	17.2

using a boxplot. A two-way analysis of variance (ANOVA) with input frequency and cluster as factors confirmed significant differences at the 5 % level between cluster and input frequency (Table 2). No significant differences were found for the interaction between the two factors. Multiple comparisons confirmed significant differences at the 5 % level between Clusters 1 and 2, and between Clusters 1 and 3 (Table 3). The high ultrasonic velocity values observed in Cluster 1 are influenced by the large coarse aggregate area rate, large feret diameter and high elastic modulus of the aggregates (Otsuki et al., 2000). Significant differences were also confirmed at the 5 % level between the frequencies of 150 kHz and 54 kHz and between 250 kHz and 54 kHz. The difference in mean ultrasonic velocity was 168 m/s between 150 kHz and 54 kHz, and 141 m/s between 250 kHz and 54 kHz. The

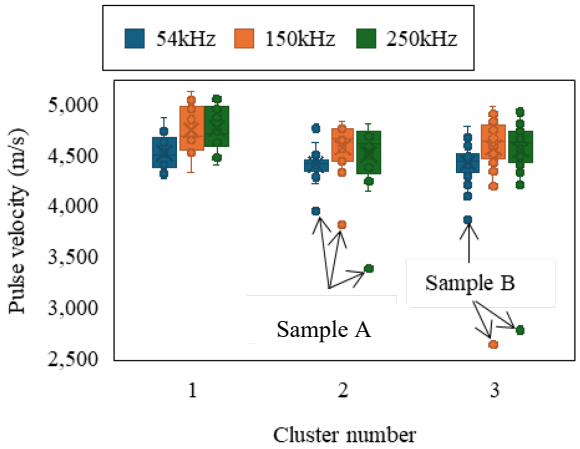

Figure 3. Relationship between ultrasonic velocities for each cluster.

Table 2. Two-way analysis of variance results

Factor	F-value	p-value
Cluster	6.76	<0.05
Frequency	5.67	<0.05
Interaction	0.31	>0.10

Table 3. Multiple comparison results

(a) Multiple comparisons between clusters

Cluster	Mean difference	p-value
Cluster 2-1	-180	<0.05
Cluster 3-1	-160	<0.05
Cluster 2-3	20	>0.10

(b) Multiple comparisons between input frequency

Frequency	Mean difference	p-value
250 kHz – 150 kHz	-27	>0.10
54 kHz – 150 kHz	-168	<0.05
54 kHz – 250 kHz	-141	<0.05

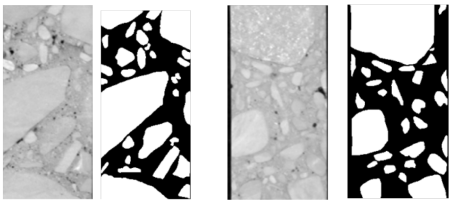

(a) Sample A (b) Sample B

Figure 4. Concrete cores that acquired lowest ultrasonic velocities.

results show that as ultrasonic frequency increases, the directivity becomes higher, with ultrasound propagating preferentially along the radiation axis (transducer axis), resulting in higher acquired ultrasonic velocities. These findings support previous studies (Fukushima and Uomoto, 1999). However, the ultrasonic velocities at 150 kHz and 250 kHz were significantly lower than the velocity at 54 kHz for two concrete cores (Figure 3, Figure 4). Low ultrasonic velocities in Clusters 2 and 3 indicate that small-diameter coarse aggregates contribute to the scattering of short-wavelength, high-frequency ultrasonic waves. These results conclude that a large coarse aggregate area rate reflects the high elastic modulus of concrete core, while a large diameter of aggregate minimize ultrasonic scattering (Yu et al., 2019).

4. Conclusions

In this study, concrete cores were extracted from the Uchinokura dam embankment, and the relationship between ultrasonic velocity and the geometric properties of coarse aggregate at three types of input frequencies: 54 kHz, 150 kHz and 250 kHz, was investigated. According to results, ultrasonic velocity for concrete cores with a large coarse aggregate area rate and coarse aggregate diameter was higher than one for concrete core with small coarse aggregate area rate and diameter. An increase in ultrasonic velocity was confirmed at 150 kHz and 250 kHz compared to 54 kHz. These results indicate that a large coarse aggregate area rate reflects the high elastic modulus of concrete core, while large diameter of aggregate such as those found in dam concrete minimize ultrasonic scattering.

References

ASTM, 2002. Standard test method for pulse velocity through concrete. West Conshohocken, *PA: ASTM International*, 10.1520/C0597-16.

Otsuki, N., Iwanami, M., Miyazato, S.I. and Hara, N., 2000. Influence of aggregates on ultrasonic elastic wave propagation in concrete. Non-Destructive Testing in Civil Engineering, *Elsevier, Amsterdam*, 313-322, 10.1016/B978-008043717-0/50033-7.

Fukushima, T. and Uomoto, K., 1999. Evaluation of defects in concrete structures using elastic waves (Non-destructive testing). *Proceedings of the Japan Concrete Institute Annual Convention*., **21**(2), 1255-1260.

Morozova, N., Shibano, K., Shimamoto, Y., Tayfur, S., Alver, N. and Suzuki, T., 2022. Visualization and evaluation of concrete damage in-service headworks by X-ray CT and non-destructive inspection methods. *Frontiers in Built Environment*, **8**, 947759, https://doi.org/10.3389/fbuil.2022.947759.

Philippidis, T.P. and Aggelis, D.G., 2005. Experimental study of wave dispersion and attenuation in concrete. *Ultrasonics*, **43**(7), 584-595, https://doi.org/10.1016/j.ultras.2004.12.001.

Yu, T., Chaix, J.F., Audibert, L., Komatitsch, D., Garnier, V. and Hénault, J.M., 2019. Simulations of ultrasonic wave propagation in concrete based on a two-dimensional numerical model validated analytically and experimentally. *Ultrasonics*, **92**, 21-34, https://doi.org/10.1016/j.ultras.2018.09.005.

A Study on Simplified Monitoring Methods for Water Leakage Evaluation in Aging Irrigation Reservoirs

Yixuan Li [1*], Moe Matsui [2], Naoki Nakamura [2], Mari Sato [3]

[1]Graduate School of Natural Science and Technology, Shimane University, Japan;

[2]Sanin Development Co.,Ltd. , Japan;

[3]Academic Assembly, Shimane University, Japan

* Corresponding author. Email: n25m513@matsu.shimane-u.ac.jp

Abstract

Aging irrigation reservoirs are vulnerable to damage from heavy rainfall and earthquakes, and establishing long-term management methods is essential to maintain their safety and functionality. In particular, increase in levee leakage volume is a sign of the embankment weakening and becomes a critical factor of dam failure during disasters.

In this study, we examined whether the condition of irrigation reservoirs can be easily assessed using water level, rainfall, and water quality indicators. The investigation was conducted on an irrigation reservoir in Matsue City, Shimane Prefecture, Japan. In addition to long-term monitoring of water level and precipitation, leakage volume at specific locations was recorded once a month. Furthermore, simple water quality parameters such as turbidity and total dissolved solids (TDS) were measured to evaluate their potential as indirect indicators of leakage.

As a result, surveys conducted one week after a significant rainfall event showed a marked increase in leakage volume, turbidity and other parameters, useful for detection of erosion risks. A correlation was observed between 48-hour cumulative precipitation and leakage volume.

Keywords: Levee seepage, Rainfall correlation, Infiltration

1. Introduction

In recent years, there have been reports of aging reservoirs being damaged by heavy rainfall, highlighting the need not only for regular comprehensive inspections but also for the development of simple monitoring methods for leakage in aging reservoirs. Matsui et al. (2022) conducted long-term observations by installing several kinds of sensors on embankments, clarifying the long-term and seasonal variation trends of reservoirs. However, since there are numerous reservoirs nationwide, it is difficult to install sensors on all of them. To establish a monitoring method for reservoirs without sensors is required.

This study focused on routine leakage and examined whether the condition of reservoirs can be monitored through simple, periodically conducted surveys centered on leakage. Additionally, we evaluated whether precipitation data observed by the Japan Meteorological Agency (JMA) could serve as a substitute for on-site rain gauges, and analyzed the correlations between precipitation, leakage volume, and reservoir water level to assess whether leakage trends can be understood using precipitation and water level data.

2. Materials and Methods

The survey target was an aging reservoir located within Matsue City, with a storage capacity of 10,000 m³. The most recent comprehensive reservoir inspection (Shimane Prefecture, 2021) was conducted in 2020, and the evaluation indicated that there were no items requiring immediate repair. For further details, please refer to Matsui et al. (2024). Since damage was confirmed in the bottom culvert, repair work began in October 2024. Prior to the repair work, regular surveys were conducted approximately every month from May to October 2024, resulting in a total of six surveys.

2.1. Water Quality Survey

Visual observations of the embankment were conducted, along with measurements of leakage volume from the bottom culvert to the inspection chamber where the regular leakage had been observed. Measurements were taken three times over a one-minute period, with the average recorded. Water samples were collected from both the reservoir and the leaked water in the inspection chambers; water temperature is also measured. The following day, turbidity, TDS, salinity, pH, and electrical conductivity were measured using portable water quality testing instruments, and the average value for each sampling bottle was calculated separately for the reservoir and leakage water.

2.2. Correlation Between Leakage Volume and Other Indicators

To analyze the correlation between leakage volume and precipitation or water level, existing long-term observation and JMA data were utilized. The results from Matsui et al. (2024), who installed precipitation and water level gauges and conducted long-term measurements at 10-minute intervals, were employed. Additionally, precipitation data from the Matsue Local Meteorological Observatory (hereinafter called JMA), located approximately 7 km in a straight line from the surveyed reservoir, were used. For precipitation, cumulative rainfall was calculated for 3, 24, 48, 72, and 240 hours preceding the approximate sampling time of 13:00 on each survey day. For water level, measurements at the sampling time and 6, 24, 48, and 72 hours prior were recorded.

3. Results and Discussion

3.1. Results of Water Quality Survey

From the survey results, it was confirmed, as shown in Figure 1, that leakage volume tended to increase with rising water levels. However, the correlation was low within the range of 9.2–10 m. This is likely due to the multiple piping holes, induced leakage from other locations. The temperature of the leakage water was lower

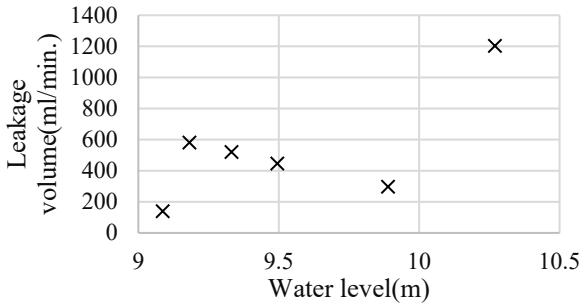

Figure 1. Water Level and Leakage Volume

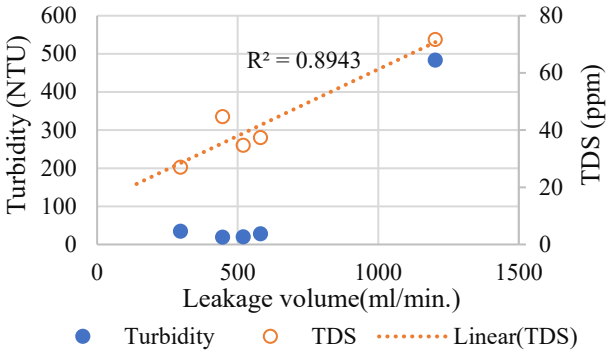

Figure 2. Turbidity and TDS in Leakage Water

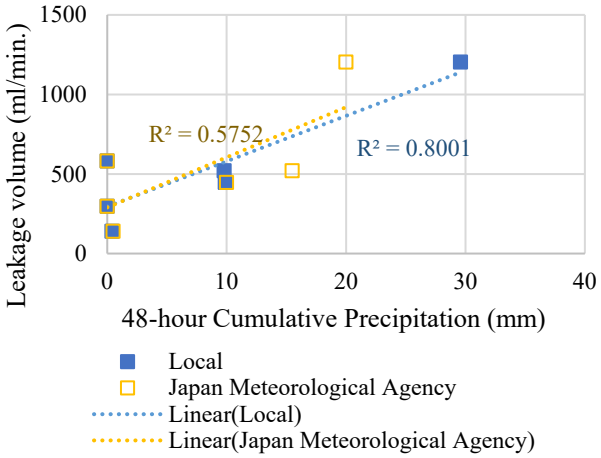

Figure 3. Relationship between 48-hour Cumulative Precipitation and Leakage Volume

than that of the reservoir water and showed smaller fluctuations.

Additionally, as shown in Figure 2, on July 16, turbidity and TDS of the leakage water temporarily increased, suggesting that rainfall may affect water quality. This is likely attributable to the heavy rainfall of 210 mm/day on July 9. Salinity and electrical conductivity showed similar trends to TDS, although slightly higher salinity was observed in the reservoir during measurements in August when the water level had decreased. For further details, refer to Li et al. (2025).

3.2. Results of Correlation Between Leakage Volume and Other Indicators

The relationship between cumulative precipitation measured by the on-site rain gauge and JMA, and leakage volume, was analyzed. The results indicated that the longer the cumulative period, the higher the correlation was verified; 24 hours: coefficient of determination (R^2) is 0.51 and 240 hours: R^2 is 0.98. As shown in Figure 3, the 48-hour cumulative precipitation measured by the on-site rain gauge exhibited particularly high correlation with leakage volume. Even at 72 hours, R^2 remained high at 0.79. The JMA data showed weaker correlation compared to on-site precipitation measurements. On the other hand, the correlation between reservoir water level and leakage volume was not as high as that for cumulative precipitation, with the highest correlation around 0.6.

4. Conclusions

Continuous surveys of the reservoir have been conducted even after the repair work, and in the future, further investigations and validations including other reservoirs, along with data accumulation, will be necessary. The insights obtained are summarized below.

- An increase in leakage volume was accompanied by rises in turbidity, TDS, and other measured parameters. This suggests that internal erosion may have occurred due to increased seepage velocity and water pressure within the embankment, causing fine soil particles to be eroded in the leakage. Repetition of erosion could lead to a reduction in embankment strength and the expansion of piping holes and cracks, being a potential risk for disaster.
- The on-site rain gauge and the JMA precipitation data showed low correlation for short-term cumulative periods, but high correlation over longer periods. To capture short-term rainfall trends, installation of on-site rain gauges is recommended. In addition, since leakage volume showed a high correlation with 48-hour cumulative precipitation, it is possible that, in addition to direct leakage from the reservoir, rainfall infiltration may cause leakage with a delay of several days.

Acknowledgements

This study was conducted as a collaborative research project between Sanin Development Co.,Ltd and Shimane University, and was supported by the 2024 Shimane University Support Program for Female Researcher-led Joint Research Projects.

References

Shimane Prefecture (2021): Report on the Seismic Inspection Survey of Agricultural Reservoirs under the Rural Area Disaster Prevention and Mitigation Project, FY2019 (Matsue, 20 Areas), Vol. 4, Icchoda, pp.1–36.

Matsui, M., Nakamura, N., and Sato, M.: Changes in Water Leakages and Long-term Monitoring at the Old Agricultural Reservoir, Ground Engineering, 40(1), pp.113–121 (2022).

Matsui, M., Sato, M., and Nakamura, N. (2024): Long-term Measurement of Soil Moisture on the Downstream Slope of a Reservoir Embankment in Relation to Storage Level and Rainfall, Proceedings of the 79th Conference of the Chugoku-Shikoku Branch, JSIDRE, pp.111–113.

Li, Y., Matsui, M., Nakamura, N., and Sato, M.(2025): Simplified Periodic Surveys of Aging Reservoirs, Proceedings of the 77th Annual Meeting of the Chugoku Branch, JSCE, III-38.

Japan Meteorological Agency: Past Weather Data, https://www.data.jma.go.jp/stats/etrn/index.php. Accessed September 3, 2025.

Strain behavior and mechanical properties of admixture-added mortars during air and water curing

Graduate School of General Science, Iwate University, Morioka, Japan

Hirotsugu Suzuki [*1], Kiyohito Yamamoto [*2]

1. Introduction

Aging agricultural irrigation facilities can lead to sudden accidents, so it is necessary to take measures to preserve their functionality. However, rebuilding the facility is not realistic from a cost perspective, and effective repair and reinforcement measures are considered necessary. Cement mortar with admixtures is often used to repair concrete structures, but its mechanical properties are largely unknown. In this study, we will discuss the strain behavior during hardening of mortar with different admixtures and hardening methods, and the dynamic elastic coefficient of hardened mortar determined from the elastic wave velocity.

2. Materials and Methods

The materials used were Portland cement, fine aggregate, water, AE water reducing agent, and admixtures (expansion agent and shrinkage reducing agent). Mortar specimens were prepared using a cylindrical mold with a diameter of 5 cm and a height of 20 cm, and a long column mold with a width of 10 cm, a height of 10 cm, and a length of 40 cm. There are four types of compounding patterns: no admixture added (N), standard amount of expansion material and standard amount of shrinkage reducer added (EXSR), double amount of expansion agent and standard amount of shrinkage reducer added (EX2SR), and triple amount of expansion agent and standard amount of shrinkage reducer added (EX3SR).

A strain gauge was attached to the prepared specimen to measure the strain. In the case of underwater curing, the strain gauge was waterproofed. Strain was recorded using a data logger. The elastic wave velocity Vp was measured by installing two AE sensors at the top and bottom of a cylindrical specimen, applying an impact by breaking the lead of a mechanical pencil at the end face, and dividing the propagation time of the elastic wave recorded by an oscilloscope by the specimen height by the propagation time. The dynamic elastic coefficient was calculated using Poisson's ratio, which was previously measured using a specimen created by the same synthesis as the elastic wave velocity Vp.

3. Results and Conclusion

Figures 1 and 2 show the results of strain behavior during curing. The W at the beginning of the legend letter indicates underwater curing, A indicates air curing, the middle letter surrounded by hyphens is the blending pattern, and the number at the end is the specimen identification number. Regarding Fig. 1, with air-cured N without any admixtures added, large shrinkage behavior was confirmed from the first day of age in all three specimens, whereas with underwater N, gradual expansion behavior was observed. In addition, in both cases of EXSR, expansion behavior was observed between the 1st and 2nd day of material age, and while the air-cured specimens showed a behavior that gradually turned to shrinkage, the underwater-cured specimens maintained this value after the expansion behavior subsided. After 40 days, the strain amounts for underwater-cured N and underwater-cured EXSR remained almost the same, suggesting that the difference in curing method has a greater effect on strain behavior than the addition of admixtures.

Regarding Figure 2, it was confirmed that there was an overall tendency for expansion to increase by increasing the addition of the expanding agent, but this effect was more likely to be seen with the material cured in air than with the material cured in water. In addition, in most of the specimens except for the EX3SR air-cured specimen, the strain value was within the range of 0 to 2000.

Figure 3 shows the results of the dynamic elastic modulus. During in-air curing, an increase in the dynamic elastic modulus was observed with the addition of standard amounts of admixtures. In-water curing resulted in a larger value than in-air curing for all compounding patterns, suggesting that the dynamic elastic modulus depends on the curing method.

Table 1 Mix proportion

Pattern	Cement	Fine aggregate	Water	Expansion agent	Shrinkage reducer	AE Water reducing agent
N	499	1544～1556	191～203	-	-	1248
EXSR	499	1544～1556	191～203	20	20	1248
EX2SR	499	1544～1556	191～203	40	20	1248
EX3SR	499	1544～1556	191～203	60	20	1248

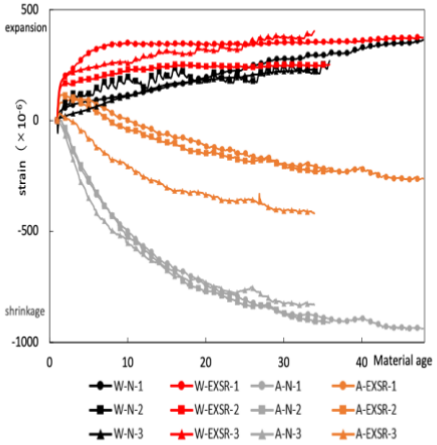

Figure 1 (N, EXSR)
Strain behavior during hardening

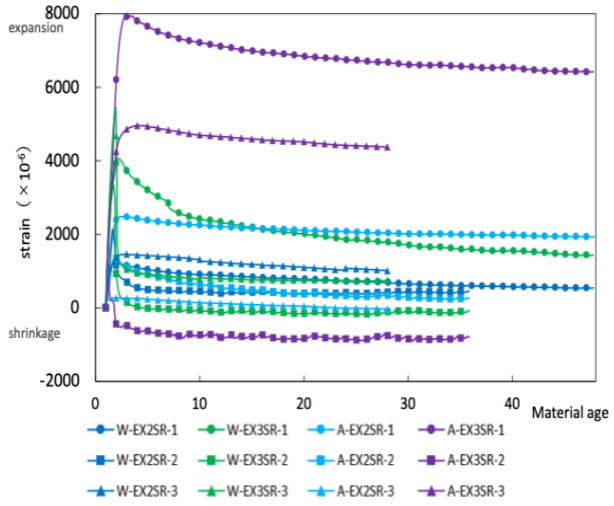

Figure 2 (EX2SR, EX3SR)
Strain behavior during hardening

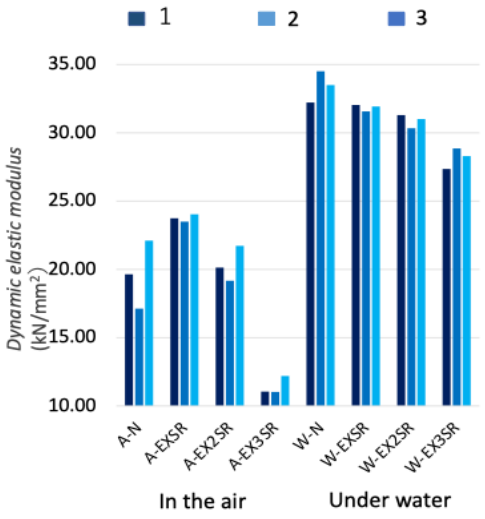

Figure 3
Dynamic modulus of elasticity calculated from V_p

Three-dimensional evaluation of in-service corroded steel sheet piles using laser scanning

Taiki Hagiwara [1*], Yuto Takahashi [2], Kazuma Shibano [2], Hiromu Tanaka [2], Koki Ikeda [3], Atsushi Chiyoda [4], Kakutaro Suematsu [4], Yuta Fujitani [4], Tetsuya Suzuki [3]

[1] Graduate School of Sciences and Technology for Innovation, Yamaguchi University, Yamaguchi, Japan

[2] Graduate School of Science and Technology, Niigata University, Niigata, Japan

[3] Institute of Agriculture, Niigata University, Niigata University, Niigata, Japan

[4] Nihon Suiko Consultant Co., Ltd, Omiya, Japan

* Corresponding author. Email: t-hagiwara@yamaguchi-u.ac.jp

Abstract

Numerous drainage canals in Japan's paddy field regions are constructed using steel sheet piles, which are thin-walled steel structural members. These sheet piles are commonly employed in soft, low-lying ground areas to enhance drainage efficiency. In recent years, corrosion has become a major issue, causing significant material deterioration. As corrosion progresses, the shape of the steel sheet piles changes, resulting in a decline in their mechanical performance. By precisely capturing the surface shape, corrosion-induced perforations, and deformations as 3D point cloud data, it becomes possible to account for the actual geometry of the structures. This study introduces a three-dimensional evaluation method for in-service corroded steel sheet piles using laser scanning technology. In field measurements, 3D point cloud data of the targeted agricultural steel sheet piles in Niigata, Japan, were acquired using a laser scanner. Based on this data, detailed 3D models are created, capturing the surface geometry and deformations of the sheet piles. The results demonstrate the potential of laser scanning to detect and evaluate the geometric deterioration of aging steel structures. Further work includes the mathematical modeling of corrosion textures and geometries to support more advanced structural assessments.

Keywords: Steel sheet pile, Corrosion, Laser scanning

1. Introduction

Steel sheet pile walls suffer localized corrosion in areas with water level fluctuations in drainage channels (Fig. 1). Severe corrosion can cause wall collapse. Corrosion measures focus on repair work to extend facility lifespan. However, coating material re-deterioration now occurs frequently in repaired steel sheet pile walls. These conditions of in-service facilities are reported in a review paper (Suzuki et al. 2025). Both localized corrosion and post-repair re-deterioration are essential information for facility maintenance.

Recent informatization trends in construction require BIM/CIM (Building/Construction Information Model) utilization for facility status assessment through 3D data acquisition and unified temporal-spatial management. While BIM/CIM benefits entire construction projects (Wang and Chen 2023), maintenance applications include incorporating localized damage into models (Artus et al. 2022), and AI integration (Pan and Zhang 2023). BIM/CIM application for steel sheet pile revetments enables easier information sharing in community meetings and stakeholder discussions through 3D visualization, promoting repair and renewal projects.

This paper presents 3D detection methods for BIM/CIM applications, addressing corrosion conditions in steel sheet pile walls of agricultural drainage channels and coating material re-deterioration in repair work.

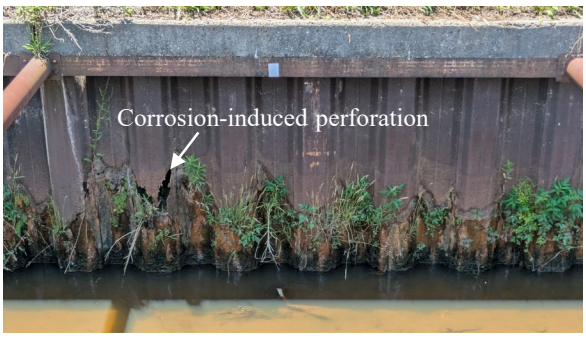

Figure 1. Steel sheet pile corrosion.

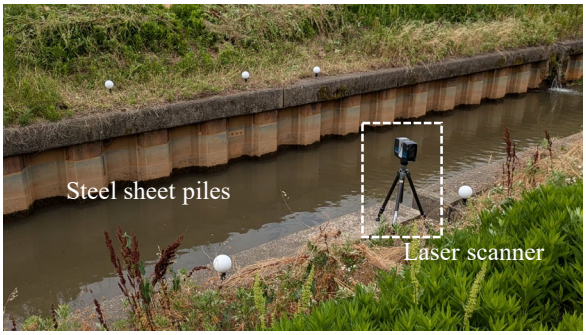

Figure 2. Setup for laser scanning.

2. Three-Dimensional Detection of Steel Sheet Piles

When focusing on perforation and buckling phenomena as corrosion conditions, capturing information about geometry is crucial. Steel sheet pile walls resist lateral loads such as earth pressure and water pressure through the flexural rigidity EI of members (E: elastic modulus, I: second moment of area). The thickness of steel sheet piles decreases due to corrosion. Thickness is an indicator of cross-sectional geometry and affects the second moment of area. In corroded steel sheet piles, both the elastic modulus E, which is a material property of steel, and the second moment of area I, which represents geometry, decrease. Therefore, capturing the actual three-dimensional geometry of perforations from existing facilities leads to detailed evaluation of the second moment of area. Additionally, capturing deformation associated with revetment tilting is expected to lead to inverse analysis of the stress field that causes it.

The technical challenge in coating material re-deterioration is considered to be understanding the

progression of corrosion in coated steel sheet piles. When coating blistering, swelling, or rust stain emergence occurs, corrosion in the coated steel sheet piles may be relatively advanced. When detecting such re-deterioration, easily visible swelling can be detected through image analysis, but for delamination conditions or relatively small blistering in early stages, point cloud measurement to capture three-dimensional surface geometry is useful. Recording such re-deterioration through sketches presents difficulties when later re-examining the site or when different investigators conduct inspections. Obtaining spatial geometry and distribution information aligns with BIM/CIM concepts.

Three-dimensional measurement of existing facilities is described below. Point cloud data acquisition was attempted for steel sheet pile revetments in agricultural drainage channels in Niigata Prefecture. Measurements were conducted using Faro® Focus S150 laser scanner (Fig. 2).

3. Results and discussion

In steel sheet pile walls where severe corrosion has progressed, repair work is implemented to extend the service life of in-service facilities, primarily applying methods using coating materials. In recent years, re-deterioration of coating materials has been reported to become apparent. The following are examples of re-deterioration conditions. In CV spray methods, blistering and rust stain re-deterioration can be confirmed (Fig. 3). Similarly, their detection can also be confirmed in laser scanning results (Fig. 4). Regarding blister detection, the technical challenge is whether small blisters that are difficult to detect visually can be detected by laser. In panel coating methods using precast concrete panels on the front face of corroded steel sheet piles, cracks in the panels can be confirmed (Fig. 5). Crack detection can also be confirmed in laser scanning results (Fig. 6). In the future, improvement of detection accuracy through combination with other sensing data, such as integration with thermal image data from infrared thermography, will also be considered.

4. Conclusions

This paper presents three-dimensional detection and informatization of corrosion conditions in steel sheet pile walls and re-deterioration conditions of coating materials for BIM/CIM applications. It is considered that detailed three-dimensional point cloud acquisition and localized deterioration detection will become possible. Three-dimensional detection is essential for capturing geometry, and evaluation of mechanical characteristics of steel sheet pile revetments and re-deterioration based on detailed geometry can be expected.

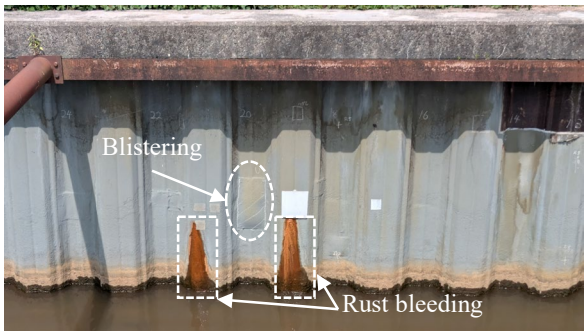

Figure 3. Re-deterioration of steel sheet piles with CV method.

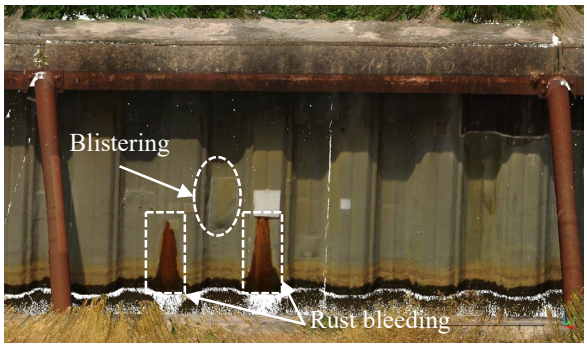

Figure 4. Laser scanning for steel sheet piles with CV method.

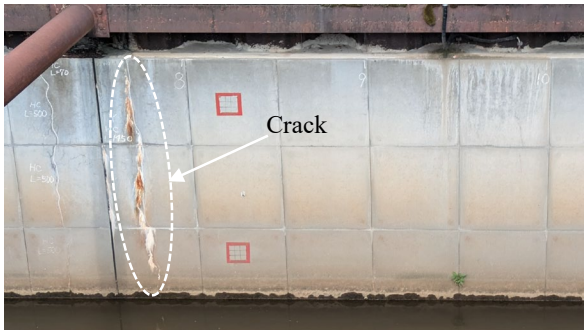

Figure 5. Crack of a concrete panel.

Figure 6. Laser scanning for a concrete panel crack.

References

Artus, M., Alabassy, M.S.H. and Koch, C., 2022. A BIM based frame-work for damage segmentation, modeling, and visualization using IFC. Applied Sciences 12(6), 2772.

Pan, Y. and Zhang, L., 2023. Integrating BIM and AI for smart construction management: Current status and future directions. Archives of Computational Methods in Engineering, 30(2), pp.1081-1110.

Suzuki, T., Hagiwara, T., Otaka, N., and Fujimoto, Y., 2025. A review of technical transition of steel sheet pile revetments development in agricultural drainage canal and corroded characteristics in service structures, Transactions of The Japanese Society of Irrigation, Drainage and Rural Engineering, 93(1), pp. III_1-III_13.

Wang, T., and Chen, H. M., 2023. Integration of building information modeling and project management in construction project life cycle. Automation in Construction, 150, 104832.

Non-Contact Detection of Water Pressure Transient Damping in Leakage Pipeline using DIC and TTBTs techniques

Yuto Takahashi [1*], Taiki Hagiwara [2], Toma Tsubota [3], Tetsuya Suzuki [4]

[1] Graduate School of Science and Technology, Niigata University, Niigata, Japan

[2] Graduate School of Science and Technology for Innovation, Yamaguchi University, Yamaguchi, Japan

[3] Obayashi Road Corporation, Tokyo, Japan

[4] Institute of Agriculture, Niigata University, Niigata, Japan

* Corresponding author. Email: f25e014d@mail.cc.niigata-u.ac.jp

Abstract

Transient Test-Based Techniques (TTBTs) have gained attention for their ability to detect pipeline leakage using pressure wave propagation phenomena. Expanding upon this foundation, we propose a novel leak detection technique that is non-contact and non-destructive, which is achieved by integrating Digital Image Correlation (DIC) into TTBTs. Laboratory tests were conducted using 65-meter-long polyvinyl chloride model pipeline. In the experiment, water hammer events were created by quickly closing a valve. A stereo DIC system measured external hoop strain on the pipeline surface. The experimental cases were set to one case without leakage and the other case with leakages at 22.6 meters upstream of the maneuver valve. Strain data were processed using continuous wavelet transform with the Gabor wavelet to calculate damping ratios. As a result, leakage conditions have higher damping ratios compared to the non-leakage case. This indicates that external strain measurements can serve as a reliable signal for detecting leaks.

1. Introduction

Agricultural pipeline systems are operating beyond their designed service lifespans, making them increasingly susceptible to water leakage problems. Traditional leakage detection methods such as acoustic techniques or hydrostatic testing require significant time and labor resources. Therefore, developing efficient leakage detection methods is urgently needed. To address these limitations, TTBTs have gained attention as promising alternatives for pipeline condition assessment (Brunone et al. 2022). TTBTs utilize pressure waves generated by transient events, such as sudden valve closure, to investigate internal pipeline conditions. These pressure waves propagate through the fluid and are altered by structural anomalies such as leakage. Previous studies by the authors demonstrated non-contact detection of pipe deformation associated with water hammer pressure using DIC method, evaluating water hammer damping due to leakage in existing pipeline (Hagiwara et al. 2025). This study aims to detect energy losses within pipes by measuring water hammer damping caused by leakage through non-contact measurement in a model pipeline system.

2. Materials and Methods

Laboratory experiments were conducted using a single pipeline at a laboratory of Niigata University. The pipeline consisted of PVC pipe with a nominal diameter of 100 mm, an outer diameter of 114 mm, and individual segments length of 2.0 meters, resulting in a total system length of 65.0 meters. The pipeline was connected to an upstream water reservoir and a downstream maneuver valve that discharges into the atmosphere. The downstream maneuver valve was used to control the flow conditions and generate transient events. A water pressure sensor was installed 0.5 meters upstream from the maneuver valve, with pressure data recorded at a sampling rate of 500 Hz. Pipeline deformation was measured using DIC at a location 1.6 meters upstream from the maneuver valve, with image data acquired at 50 Hz. Two test cases were conducted. Case A was a non-leakage condition, while Case B simulated leakage conditions. Leakage was introduced by removing a plug at 22.6 meters upstream of the maneuver valve.

Assuming free-free conditions and non-viscoelastic behavior, pipe hoop strain ε_θ can be calculated as:

$$\varepsilon_\theta = \frac{1}{E_p}\frac{pR}{d_w}, \tag{1}$$

where E_p; modulus of elasticity of pipe (N/m^2), p; internal pressure (N/m^2), R; internal radius (m), d_w; pipe wall thickness (m). The Continuous Wavelet Transform (CWT) is used for time-frequency domain analysis of both theoretical hoop strain calculated from Eq. (1) and measured hoop strain using DIC method. The wavelet coefficient of the ridge obtained from CWT is substituted into Eq. (2) to calculate the water hammer pressure damping ratio ζ (Slavič et al. 2003).

$$\ln\left(\frac{2\left|Wf\left(u,s(u)\right)\right|}{\left(4\pi\sigma^2 s^2(u)\right)^{\frac{1}{4}}}\right) \approx -\zeta\omega_d u + \ln A\,, \tag{2}$$

where parameter σ controls the width of the Gaussian window, ω_d; damped natural angular frequency.

3. Results and Discussion

The time-series results of theoretical and measured value of hoop strain are shown in Figure 1. The theoretical values of hoop strain are calculated using Eq. (1) based on water pressure data, while the measured values are obtained through DIC method. The measured hoop strain closely follows the trend of theoretical values, confirming the validity of the pressure-strain relationship under transient conditions. Slight fluctuations in measured strain are attributed to environmental noise such as light variation. The wavelet transform results of the theoretical hoop strain values are presented in Figure 2. High wavelet coefficients are confirmed near the frequency calculated from the water hammer propagation velocity (1.80 Hz) and near the natural frequency of the 2.0-meter beam (0.72 Hz). Comparing Case A and Case B shows that leakage reduces the duration of high wavelet coefficient regions near the water hammer frequency. The wavelet transform results of

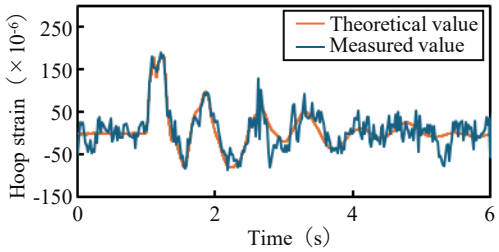

(a) Case A

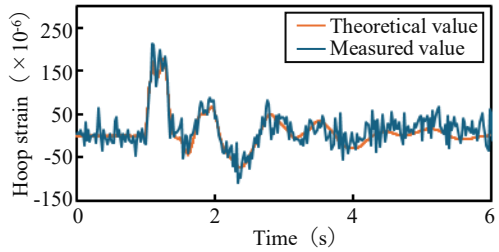

(b) Case B

Figure 1. Time-series of theoretical and measured hoop strain.

the measured hoop strain values are shown in Figure 3. Similar to the theoretical wavelet transform results, high wavelet coefficients are confirmed near the frequency calculated from water hammer propagation velocity and near the natural frequency of the 2.0-meter beam. The leakage case shows a reducing the duration of the high wavelet coefficient regions near the water hammer frequency. The damping ratio of hoop strain calculated from Eq. (2) are presented in Table 1. Both theoretical and measured hoop strain, leakage condition resulted in increased damping ratio. It is suggested that the damping of water hammer pressure can be evaluated through non-contact measurement of hoop strain from pipe outer surface.

4. Conclusions

In this study, hoop strain of pipeline was measured using DIC method in a model pipeline. The time-series results of hoop strain confirm that hoop strain fluctuations accompanying water hammer pressure can be detected through non-contact measurement. CWT results reveal that water hammer pressure damping due to leakage is observed in both theoretical and measured hoop strain values. The damping ratio calculated from CWT results reveals that leakage increases the damping of hoop strain fluctuations. These findings suggest that the damping of water hammer pressure can potentially be evaluated through non-contact measurement of hoop strain occurring in pipe materials.

References

Hagiwara, T., Asada, Y., Tsubota, T., Kurusawa, K. and Suzuki, T., 2025. Non-contact detection of leak-derived energy loss for an in-service pipeline system using digital image correlation. *Nondestructive Testing and Evaluation*, pp. 1-22. DOI; https://doi.org/10.1080/10589759.2024.2446647

Slavič, J., Simonovski, I. and Boltežar, M., 2003. Damping identification using a continuous wavelet transform application to real data. *Journal of Sound and Vibration*, **262**(2), pp 291-307. DOI: https://doi.org/10.1016/S0022-460X(02)01032-5

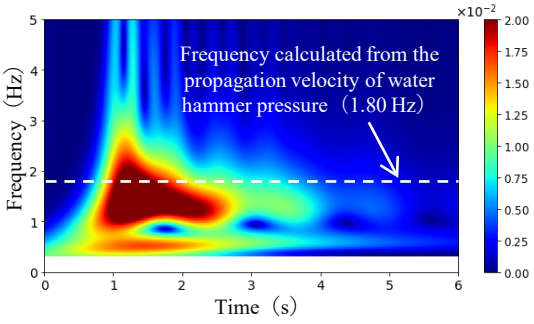

(a) Case A

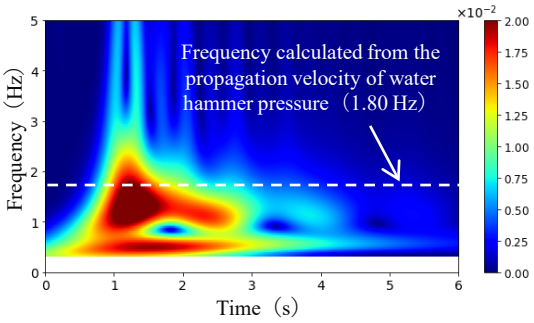

(b) Case B

Figure 2. Continuous wavelet transform results of theoretical hoop strain.

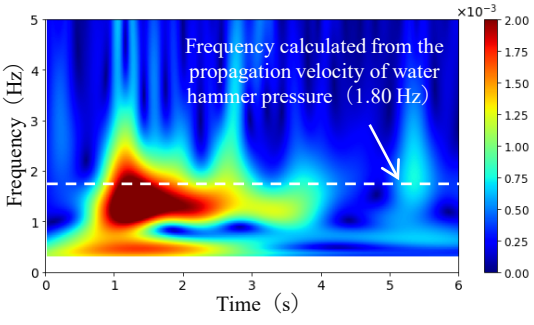

(a) Case A

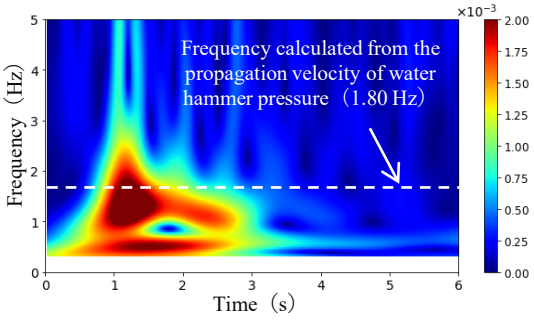

(b) Case B

Figure 3. Continuous wavelet transform results of measured hoop strain.

Table 1 Damping ratio of theoretical and measured hoop strain

	Theoretical hoop strain	Measured hoop strain
Case 1	0.063	0.049
Case 2	0.075	0.059

Comparison of Future Drought Vulnerability Based on Water Resource Systems in North and South Korea

Hyeon-Wook Shin [1], Won-Ho Nam [2*]

[1] Graduate Student, School of Social Safety and Systems Engineering, Hankyong National University, Anseong, Republic of Korea

[2] Professor, School of Social Safety and Systems Engineering, National Agricultural Water Research Center, Hankyong National University, Anseong, Republic of Korea

* Corresponding author. Email: wonho.nam@hknu.ac.kr

Abstract

Global warming is increasing abnormal climate events worldwide**,** and the Korean Peninsula is directly experiencing its impacts. Among climate hazards**,** drought is particularly complex—slow in onset, variable in space and time, with long-term impacts on agriculture, water, and energy sectors**.** Despite similar natural environments**,** South and North Korea show clear disparities in drought response and vulnerability due to differing socio-economic systems**.** This study sets South and North Korea as comparative subjects and aims to evaluate drought vulnerability based on their water resource systems. Global Climate Models (GCMs) data from the Coupled Model Intercomparison Project Phase 6 (CMIP6), based on the Shared Socioeconomic Pathways (SSP) outlined in the Intergovernmental Panel on Climate Change (IPCC) Sixth Assessment Report, were utilized. In particular, four drought indices reflecting key components of water resource systems such as precipitation, temperature, and evaporative demand were selected. Under the SSP5-8.5 scenario, the Standardized Precipitation Index (SPI), the self-calibrating Effective Drought Index (scEDI), the Standardized Precipitation Evapotranspiration Index (SPEI), and the Evaporative Demand Drought Index (EDDI) were applied. Through this approach, the study compares and analyzes the probability and spatial variability of future drought occurrence in South and North Korea, and evaluates drought vulnerability considering the impacts of differences in water resource infrastructure and management systems.

Keywords: Korea peninsula, climate changes, SSP5-8.5 scenario, drought index, drought vulnerability,

1. Introduction

Due to the recent increase in the average global temperature, the frequency of extreme weather phenomena such as heat waves, tropical nights, and droughts is increasing. The amount of annual precipitation between North Korea and South Korea averaged 900 mm and 1300 mm, respectively, showing a difference of about 30% (Lee et al., 2024). Drought is difficult to accurately determine the time and end point of occurrence, and due to the wide area of damage, it can have a serious impact on social and economic aspects, including water resources and agricultural systems as a whole (Savelli et al., 2022). Various drought indices are calculated using future climate data calculated by a SSP scenario based on the CMIP6. Vulnerable areas were analyzed using the drought index calculated based on this.

2. Materials and Methods

2.1. Data collection

The SSP scenario adopted in the IPCC 6th evaluation report is future forecast data for climate variables such as precipitation, temperature, wind speed, and humidity calculated by applying changes in radiation compulsion caused by artificial factors such as greenhouse gases and land-use changes to the GCMs. This study aims to forecast the future drought in Korean Peninsula using data from the SSP5-8.5 scenario, which is expected to emit the most greenhouse gases and increase temperature and precipitation the most. 18 GCM data are collected using the Simple Quantile Mapping (SQM) technique. The Multi-Model Ensemble (MME) method is applied to correct the deviation between the data of the 18 GCMs. It is selected as the Near Future (NF) from 2041 to 2070 and the Far Future (FF) from 2071 to 2100 (Choi et al., 2016). The SSP model-specific data includes precipitation, maximum temperature, minimum temperature, wind speed, relative humidity, and solar radiation in 87 observatory sites located on the Korean Peninsula from January 1, 2041, to December 31, 2100.

2.2. Drought index

SPI analyzes drought by selecting SPI6, a 6-month time scale recommended by the World Meteorological Organization (WMO), as an index that evaluates meteorological drought using only precipitation data. SPEI considers precipitation and evapotranspiration at the same time and evaluates drought using SPEI6. scEDI is an index that evaluates the severity of drought based on precipitation. EDDI is an index that evaluate drought based on atmospheric evaporation demand, and EDDI6 is selected to analyze drought.

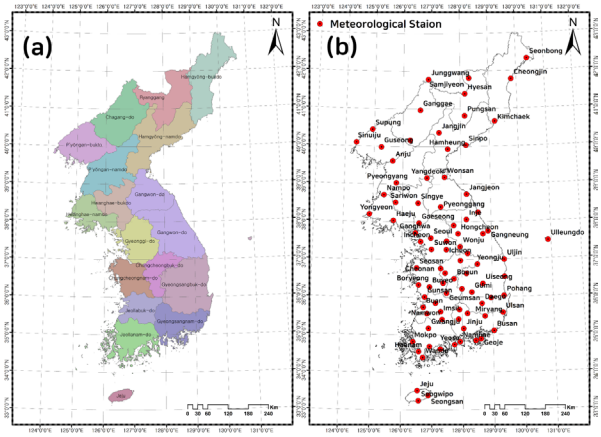

Figure 1. (a) Administrative divisions of the Korean Peninsula and (b) Location of 87 meteorological stations

Table 1. GCMs Representative Model (Kim et al., 2024)

Model Name	Institute
ACCESS-CM2	Commonwealth Scientific and Industrial Research Organisation, Australian Research council Centre of Excellence for Climate System Science (Australia)
ACCESS-ESM1-5	Commonwealth Scientific and Industria l Research Organisation (Australia)
CANESM 5	Canadian Centre for Climate Modelling and Analysis (Canada)
CNRM-CM6-1	Centre National de Recherches Meteorologiques (France)

3. Results and Discussion

The SPI6 index under the SSP5-8.5 scenario indicated distinct drought characteristics across the Korean Peninsula. In the near future, negative values were dominant, suggesting widespread drought risk. Strong negative anomalies were observed in Gangwon-do of North Korea and in Gyeongsangbuk-do and Gyeongsangnam-do of South Korea, highlighting their sensitivity to precipitation deficits. Although inland regions showed weaker signals, the overall pattern confirmed drought-dominant conditions in this period. In the far future, most regions shifted to positive values, reflecting wetter conditions due to increased precipitation. However, the wetting signal was not uniform. Gangwon-do and Gyeongsangnam-do consistently displayed relatively lower values compared with surrounding regions, indicating that localized drought vulnerability will persist despite the overall wetting tendency.

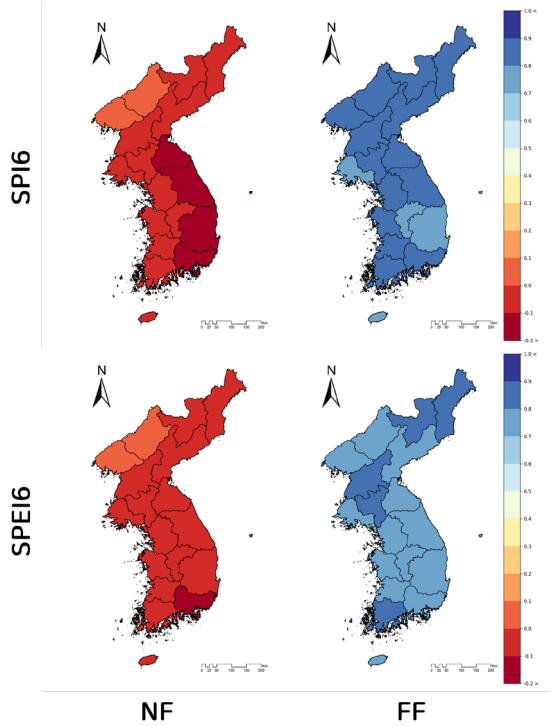

Figure 2. Spatial distribution of SPI6 and SPEI6 over the Korean Peninsula in the NF and FF

The SPEI6 index, which considers both precipitation and evapotranspiration, showed similar temporal tendencies to SPI6 but with stronger drought intensity. In the near future, negative values were widespread, and Gyeongsangnam-do in particular exhibited pronounced drought signals. This result reflects the combined effects of reduced precipitation and enhanced evapotranspiration due to warming. In the far future, most regions turned to positive values, suggesting wetter conditions. However, drought-prone signals remained in Gyeongsangnam-do and parts of Gangwon-do, implying that high evapotranspiration may offset precipitation increases in these areas. Thus, while both indices indicate a general wetting trend in the far future, regional disparities in vulnerability persist.

4. Conclusions

This study evaluated the future drought vulnerability of the Korean Peninsula using the SPI6 and SPEI6 indices under the SSP5-8.5 scenario of CMIP6 GCMs, focusing on the near future and the far future. The results showed that in the near future, negative anomalies dominated across the peninsula, with severe drought risks particularly evident in Gangwon-do of North Korea and Gyeongsangnam-do of South Korea. In the far future, most regions shifted to positive values, reflecting wetter conditions due to increased precipitation. However, these same regions consistently remained vulnerable, suggesting persistent drought risk despite the overall wetting trend.

Acknowledgements

This work was supported by Korea Environment Industry & Technology Institute (KEITI) through Water Management Program for Drought Project, funded by Korea Ministry of Environment (MOE) (RS-2023-00230286).

References

Choi, Y.W., Ahn, J.B., Suh, M.S., Cha, D.H., Lee, D.K., Hong, S.Y., Min, S.K., Park, S.C., and Kang, H.S., 2016. Future changes in drought characteristics over South Korea using multi regional climate models with the standardized precipitation index. *Asia-Pacific Journal of Atmospheric Sciences*, 52(2), 209–222.

Kim, S.H., Nam, W.H., Jeon, M.G., Hong, E.M., and Oh, C., 2024. Projected future extreme droughts based on CMIP6 GCMs under SSP scenarios. *Journal of the Korean Society of Agricultural Engineers*, 66(4), 1–15.

Lee, H.J., Nam, W.H., Otkin, J.A., Zhong, Y., Zhang, X., and Svoboda, M.D., 2024. Evaluation of flash drought characteristics using satellite-based soil moisture product between North and South Korea. *Journal of Korea Water Resources Association*, 57(8), 509–518.

Savelli, E., Rusca, M., Cloke, H., and Di Baldassarre, G., 2022. Drought and society: Scientific progress, blind spots, and future prospects. *Wiley Interdisciplinary Reviews: Climate Change,* 13(5), e791.

Quantitative Assessment of Agricultural Reservoir Response to Extreme Events with Consideration of Storage Capacity Variations

Mi-Hye Yang [1], Won-Ho Nam [2*]

[1] Ph.D Student, Department Integrated System Engineering, Hankyong National University, Anseong, Republic of Korea

[2] Professor, School of Social Safety and Systems Engineering, National Agricultural Water Research Center, Hankyong National University, Anseong, Republic of Korea

* Corresponding author. Email: wonho.nam@hknu.ac.kr

Abstract

According to the Food and Agriculture Organization of the United Nations (FAO, 2023), the agricultural sector has suffered nearly USD 380 billion in crop and livestock losses over the past 30 years due to disasters. From 2015 to 2020, droughts accounted for 49% of all agricultural losses, with floods also a major hazard. Agricultural reservoirs serve as critical infrastructure for irrigation, yet their performance is influenced by changes in storage capacity caused by sedimentation, erosion, or structural interventions. This study quantitatively evaluated the impact of such volumetric changes on drought and flood response. Design-based storage data were compared with recent survey measurements for Giheung, Sonhang 1, and Yongdang Reservoirs to assess variations in effective storage. Drought resilience was analyzed using the water utilization safety rate (based on the ratio of shortage volume to demand) and the water supply reliability rate (based on shortage days relative to total days). Flood mitigation was assessed through Probable Maximum Flood (PMF) flood routing analysis. Results showed effective storage losses of 10–21%, with Yongdang experiencing the largest decline and falling to Class IV in water utilization safety. PMF analysis indicated reduced flood retention volumes and a 0.17 m rise in peak flood level. These findings demonstrate that storage losses substantially weaken both drought and flood response, underscoring the need to integrate updated survey data into reservoir management.

Keywords: Irrigation Safety, Water Supply Reliability, Sedimentation, Water Balance Analysis, Probable Maximum Flood, Climate Change

1. Introduction

Agricultural reservoirs are essential for maintaining irrigation water supply, but their performance is strongly affected by changes in storage capacity. Sedimentation and structural modifications alter effective volume, which in turn influences both drought resilience and flood control. Despite this importance, limited studies have quantitatively evaluated how such volumetric changes impact reservoir response to extreme hydrological events. The aim of this study is to assess the effects of storage capacity variations on irrigation safety, water supply reliability, and flood mitigation capacity.

2. Materials and Methods

2.1. Study reservoirs

Three agricultural reservoirs—Giheung, Sonhang 1, and Yongdang—were selected considering their storage size, history of structural modification, and availability of recent survey data

2.2. Drought response evaluation

Drought response capacity was assessed using two indices:

- Water utilization safety rate (U_s):

$$U_s = 1 - \frac{D}{R}$$

where D is the total shortage volume (m^3) and R is the total required demand (m^3). Shortage was estimated by assuming that when storage fell below 20% of capacity, withdrawal efficiency decreased linearly, and the unmet portion was counted as deficit volume.

- Water supply reliability rate (S_r):

$$S_r = 1 - \frac{N_d}{N}$$

N_d is the number of shortage days and N is the total evaluation days.

2.3. Flood response evaluation

Flood mitigation capacity was evaluated through flood routing analysis under the Probable Maximum Flood (PMF). Results were compared between design and survey-based conditions in terms of flood storage change, retention volume, and peak flood level.

3. Results and Discussion

3.1. Analysis of volumetric changes in reservoir storage

By comparing the original design storage with the updated storage capacity derived from recent surveys, reductions in effective volume were identified. Even at full supply level, the actual storage volume was smaller than the design value, indicating a loss of usable capacity. These changes directly affect both irrigation safety and water supply reliability, while also limiting flood mitigation capacity.

Table 1. The changes in total storage capacity and effective volume for the selected reservoirs

Reservoir	Design effective capacity (10^3m^3)	Surveyed effective capacity (10^3m^3)	Change (%)
Giheung	11,630	9,993	-14.1
Sonhang 1	531	478	-10.0
Yongdang	6,832	5,382	-21.2

3.2. Evaluation of drought response capacity

3.2.1. Water utilization safety rate

Table 1 shows that effective storage capacities decreased by 10–21% compared with the design values. This reduction directly influenced irrigation safety (Table 2), where Giheung and especially Yongdang recorded lower safety rates under the updated conditions. In contrast,

Sonhang maintained a stable capacity and consistently high safety performance.

Table 2. Water utilization safety rates: (a) design storage condition and (b) survey-based storage condition

	Reservoir	Giheung	Sonhang 1	Yongdang
(a)	Shortage	197	1	216
	Demand	13,396	1,282	10,912
	U_s (%)	98.5	99.9	98.0
	Class	II	I	II
(b)	Shortage	216	1	1,143
	Demand	16,777	979	8,030
	U_s (%)	98.7	99.9	85.8
	Class	II	I	IV

3.2.2.Water supply reliability rate

Table 3 summarizes the water supply reliability rates of the selected reservoirs. Giheung and Yongdang maintained high reliability above 95%, remaining in Class I despite volumetric reductions. In contrast, Sonhang 1 showed a decline to Class II under the updated condition. Although Sonhang 1 maintained Class I in the irrigation safety rate (Table 2), its water supply reliability declined to Class II (Table 3). This discrepancy reflects the limitation of small reservoirs: shortage days are rare, but long-term stability against demand is less secure compared to larger reservoirs.

Table 3. Water supply reliability rates: (a) design storage condition and (b) survey-based storage condition

	Reservoir	Giheung	Sonhang 1	Yongdang
(a)	Shortage period	184	273	207
	Anaysis period	12,419	10,227	12,419
	S_r (%)	98.5	97.3	98.3
	Class	I	I	I
(b)	Shortage	168	527	590
	Demand	12,419	10,227	12,419
	S_r (%)	98.6	94.8	95.2
	Class	I	II	I

3.3. Evaluation of flood response capacity

3.3.1.Probable maximum flood

Tables 4–6 summarize the PMF-based flood routing results of Giheung, Sonhang 1, and Yongdang Reservoirs. In all reservoirs, the survey-based condition resulted in reduced flood storage change and retention volume compared with the design condition. For Giheung and Yongdang, this reduction led to an increase of 0.17 m in flood level. Sonhang 1 showed only minor differences between the two conditions, reflecting its smaller storage size. Overall, these results indicate that volumetric losses decrease flood mitigation capacity and elevate flood levels, particularly in larger reservoirs.

Table 4. Flood routing results of Giheung Reservoir under the PMF condition: (a) design storage condition, (b) survey-based storage condition, and (b–a) difference

Reservoir	Flood storage change (10^3m^3)	Flood retention volume (10^3m^3)	Flood level (EL.m)
(a)	37.90	13,344.78	46.71
(b)	32.62	11.475.95	46.88
(b)-(a)	-5.28	-1,868.83	+0.17

Table 5. Flood routing results of Sonhang 1 Reservoir under the PMF condition: (a) design storage condition, (b) survey-based storage condition, and (b–a) difference

Reservoir	Flood storage change (10^3m^3)	Flood retention volume (10^3m^3)	Flood level (EL.m)
(a)	1.85	739.86	226.61
(b)	1.50	642.33	226.21
(b)-(a)	+0.01	-0.35	0.00

Table 6. Flood routing results of Yongdang Reservoir under the PMF condition: (a) design storage condition, (b) survey-based storage condition, and (b–a) difference

Reservoir	Flood storage change (10^3m^3)	Flood retention volume (10^3m^3)	Flood level (EL.m)
(a)	26.78	8,085.52	129.19
(b)	23.88	6,239.62	129.36
(b)-(a)	-2.90	-1,845.90	+0.17

4. Conclusions

This study demonstrated that volumetric losses in agricultural reservoirs, caused by structural changes and sedimentation, reduce both drought and flood response capacities. While smaller reservoirs such as Sonhang showed limited sensitivity in safety rate, larger reservoirs like Giheung and Yongdang exhibited clear declines in reliability and flood mitigation performance. These findings highlight the need to incorporate updated storage conditions into reservoir operation and management strategies to ensure stable irrigation water supply under climate change

Acknowledgements

This work was supported by Korea Institute of Planning and Evaluation for Technology in Food, Agriculture, and Forestry (IPET) through Intelligent Agricultural Infra Management for Climate Change Development Program, funded by Ministry of Agriculture, Food and Rural Affairs (MAFRA) (RS-2025-02219764)

References

FAO. 2023. The impact of disasters on agriculture and food security: Avoiding and reducing losses through investment in resilience. FAO Flagship Report. Rome, FAO, p.10.

Yang, M.H., Nam, W.H., Shin, J.H., Yoon, D.H., and Yang, H.C., 2024. Evaluation of water supply reliability in agricultural reservoirs using water balance analysis. *J. Korean Soc. Agric. Eng.*, 66(5), 29-40.

Predicting water distribution amount using deep learning in the Aichi Irrigation Project

Taisei Hamaguchi [1*], Keigo Noda[2], Masashi Kiguchi[1], Taichi Sano[1], Taikan Oki[1]

1) Graduate School of Engineering, The University of Tokyo
(7-3-1 Hongo, Bunkyo-ku, Tokyo, 113-8656, Japan)
2) Graduate School of Agricultural and Life Sciences, The University of Tokyo
(1-1-1 Yayoi, Bunkyo-ku, Tokyo, 113-8657, Japan)
* Corresponding author. Email: hamaguchi-taisei257@g.ecc.u-tokyo.ac.jp

Abstract

This study explores the predictability of agricultural water demand for the Aichi Water Irrigation Project using machine learning, aiming to replace the current experience-based water allocation methods. We utilized the TimesNet model with five years of meteorological and water distribution data to forecast demand one day ahead. By comparing models trained with 3-month and 6-month data sequences, we found that a shorter sequence length yielded higher accuracy. This suggests that increasing the number of training iterations is more critical for prediction accuracy than learning long-term periodicity. The results also highlighted the significance of short-term agricultural cycles, such as weekly and monthly usage patterns, which are not fully captured by the current model. Future work will focus on refining the model to better quantify these agricultural cycles to further enhance prediction accuracy.

Keywords: *agricultural water demand, machine learning*

1. Introduction

The daily water allocation for the Aichi Water Irrigation Project is determined based on requests from farmers. Subsequently, Water Resources Agency staff compile the requested volumes and determine the final allocation. Consequently, the determination of water allocation currently relies heavily on the intuition and experience of the water supplier.

Research on predicting agricultural water demand has been conducted to achieve water supply that does not rely on experience or intuition. Classified by spatial scale, numerous studies have been conducted at the single-field unit level, beneficial for farmers (Suzuki & Wakabayashi, 2023; Nishida, 2022), and at the watershed unit level, beneficial for policy makers (Ide et al., 2020; Matsumura et al., 2021). However, the current state of prior research is that there are few studies on beneficiary area-level prediction, which is beneficial for water suppliers. Focusing on methodology, hydraulic models based solely on physical equations and water resource models with low spatial resolution are unsuitable for beneficiary area-level studies. Machine learning models can be considered the optimal approach, as they compensate for the shortcomings of both.

So why has research on predicting agricultural water demand using machine learning not progressed? Perea et al. (2021) have pointed out that it is necessary to consider not only crop-related variables such as evapotranspiration but also the behavioral characteristics of farmers. In other words, the factors determining agricultural water demand are complexly intertwined, making prediction difficult. Therefore, this study aims to explore the predictability of agricultural water demand using machine learning.

2. Materials and Methods

This study examined data and methodologies using the beneficiary areas of the Aichi Irrigation Project as the target region shown in Figure 1. The data covered a five-year period from April 2019 to March 2024. Data obtained from the Japan Meteorological Agency and Today's Earth was used, along with daily water distribution volume data for each branch canal. The machine learning model employed was the TimesNet model (Wu et al., 2023). This model can effectively extract periodic features from continuous data. Since much of the data handled in this study exhibits continuous periodicity, this model was considered optimal.

Figure 1. Aichi Irrigation Project overview diagram.

We trained the model on historical data to predict water distribution volumes one day ahead. During this process, we adjusted the number of days of past data used for each prediction, known as the sequence length. When the sequence length is set to 6 months, long-term periodicity can be learned, but the number of training cycles decreases. Conversely, when the sequence length is set to 3 months, the number of training cycles increases, but long-term periodicity cannot be learned. We compared which was more important for prediction: increasing training iterations or learning long-term periodicity.

3. Results and Discussion

The prediction results for water distribution volume are shown in Figure 2 and 3. Figure 2 shows results for a sequence length of 6 months, while Figure 3 shows results for a sequence length of 3 months. The loss function, representing the discrepancy between prediction and actual measurements, was smaller for the 3-month

sequence length. Prediction accuracy improved significantly, particularly during the non-irrigation period, peak distribution, and zero distribution periods. This suggests that increasing the number of learning iterations is more important than learning periodicity for predicting water distribution volume. Furthermore, it was suggested that learning the periodicity over the past three months is sufficient for prediction. So, what specific periodicity should be considered in the prediction?

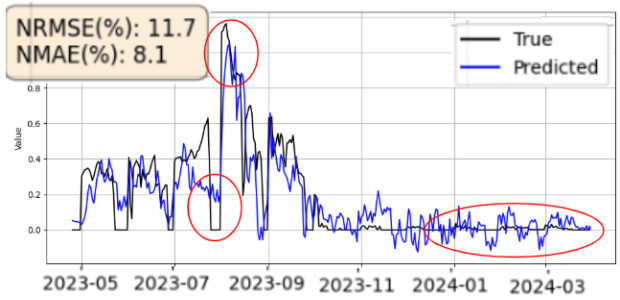

Figure 2. Predicted water distribution volume (sequence length: 6 months).

Figure 3. Predicted water distribution volume (sequence length: 3 months).

Next, we analyzed the differences in periodicity between the actual measured water distribution volume and the predicted values. Figure 4 visualizes the dominant cycles for both measured and predicted water distribution volumes over a three-month sequence length. The results show that the amplitude of the measured values was larger for several cycles, such as two weeks and one month. This suggests the need to consider short-term, agricultural cycles in the prediction, such as increased agricultural water use on weekends and decreased water use at month-end.

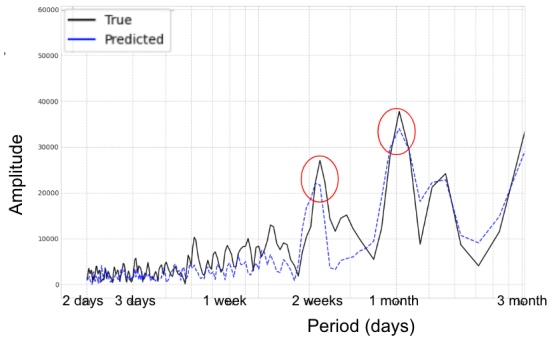

Figure 4. The cycle of water distribution volume and its amplitude.

4. Conclusions

This study conducted experiments to explore the predictability of agricultural water demand using machine learning. The results suggested that increasing the number of training iterations is more important than learning long-term periodicity, and that it is necessary to consider short-term and agricultural cycles. Looking ahead, we plan to further examine the experimental setup for machine learning, such as training models to quantify agricultural cycles.

References

鈴木翔・若杉晃介 2023. 圃場水管理システムを用いた普通期における減水深と用水量の算出手法. 農業農村工学会論文集 317: 53-60.

西田和弘 2022. 水田群の水需要の短時間変動が水田用水量に与える影響. 農業農村工学会論文集 315: 267-277.

Perea RG, Ballesteros R, Ortega JF, Moreno MA. 2021. Water and energy demand forecasting in large-scale water distribution networks for irrigation using open data and machine learning algorithms. *Computers and Electronics in Agriculture* 188.

井手 淨・井戸田 優希・吉岡 伸隆・田上 雅浩・松村 明子・小川田 大吉・花崎 直太・平林由希子 2020. 統合水資源モデル H08 で推計した灌漑水不足ポテンシャルと地盤沈下・地下水位の関係. 水工学論文集 76: 289-294.

松村明子・光橋 尚司・須賀 可人・寺島 明央・金山 拓広・小川田 大吉・矢野 伸二郎・花崎 直太・沖 大幹 2021. 全球水循環モデル H08 による都市の取排水システムを考慮した流域の水需給の評価. 水工学論文集 77: 205-210.

Wu H, Hu T, Liu Y, Zhou H, Wang J, Long M. 2023. TIMESNET: TEMPORAL 2D-VARIATION MODELING FOR GENERAL TIME SERIES ANALYSIS. *ICLR*

気象庁 2019-2024. https://www.data.jma.go.jp/stats/etrn/index.php Accessed September 15, 2025.

Today's Earth 2019-2024. https://www.eorc.jaxa.jp/water/index_j.html Accessed September 15, 2025.

Evaluation of Open-Source Digital Elevation Models for Watershed Hydrology Simulation

MISHRA KUMAR SURENDRA・PRASHANT PRASHANT・LOHANI KUMAR ANIL

Abstract

Digital Elevation Models (DEMs) are fundamental and crucial to a wide range of hydrological applications requiring spatial information. However, the fact that DEMs are accessible from various sources and at differing spatial resolutions presents challenges in watershed modeling, as they impact simulating hydrological features and the performance of the hydrological model. This study aimed to comparatively assess the impact of SRTM DEM and FABDEM (Forest and Buildings removed Copernicus DEM) selection on the delineation of streams and catchments, as well as the simulation of streamflow by setting up a hydrological model using the Soil and Water Assessment Tool (SWAT). The evaluation was carried out using the data of Ong River watershed, a forest-cropland dominated watershed of the Mahanadi River basin of India (area = 4650 sq. km). Various performance evaluation metrics were used to assess the performance of both the DEMs, including Willmott's index of agreement, Nash-Sutcliffe Efficiency (NSE), Coefficient of Determination (R2), Percent bias (PBIAS), and RMSE-observations standard deviation ratio (RSR). The findings offer valuable insights into the selection of DEMs for watershed modeling, emphasizing the importance of considering catchment-specific characteristics and desired accuracy levels.

Estimating rice NDVI-peaks with use of variety-specific time-series curves

Kyohei Onishi [1*], Takanori Nagano [1], Natsuki Yoshikawa [2], Yoshitaka Motonaga[2]

[1] Graduate School of Agricultural Science, Kobe University, 1-1 Rokkodai-cho, Kobe-shi, Japan

[2] Institute of Science and Technology, Niigata University, 8050 Igarashi2no-cho, Niigata-shi, Japan

* Corresponding author. Email: 248a004a@stu.kobe-u.ac.jp

Abstract

Rice cultivation in Asia is increasingly affected by climatic fluctuations and social changes, making continuous monitoring of growth dynamics essential. Remote sensing via satellites offers an effective way to capture vegetation changes over large areas. This study focused on estimating the maximum Normalized Difference Vegetation Index (NDVI) during the ear emergence stage, which strongly correlates with rice yield. The analysis targeted irrigation districts in Japan using Sentinel-2 imagery. Estimating peak NDVI from optical satellite data involves several challenges: cloud-related noise, discrete time-series observations, and the need for standard reference functions for individual paddies. To address these, we used Google Earth Engine per-pixel cloud evaluation data, reconstructed variety-specific standard NDVI curves from multi-year datasets and applied a parametric fitting approach. The fitting accounted for transplanting dates, temporal shifts, time scaling, amplitude variations, and baseline offsets, enabling robust estimation of phenological dynamics across diverse rice fields. This framework supports accurate monitoring of rice growth and provides insights into yield prediction and crop management.

Keywords: Remote Sensing, Sentinel-2, GEE, DTW

1. Introduction

NDVI is a key indicator for monitoring crop growth, and (Wakiyama et al.,2003) says its maximum value around the heading stage is particularly important for yield estimation. Satellite-based observation of NDVI is an effective approach for monitoring crop growth. However, it is often affected by noise due to clouds and atmospheric conditions, and the resulting data are temporally discrete. Moreover, direct comparison of NDVI time series across fields is complicated by differences in planting dates, growth rates, and varieties, which cause temporal shifts and variability in peak timing.

In this study, we focused on extracting the maximum NDVI value with high reliability by constructing standardized NDVI growth curves for rice cultivation. Dynamic Time Warping (DTW) (Sakoe and Chiba, 1978) was applied to align multiple time series, enabling the identification of a representative growth pattern while reducing the influence of temporal misalignment. This approach places greater emphasis on the heading stage, where accurate NDVI estimation is critical.

2. Materials and Methods

2.1. Study Area and Data

This study focused on rice cultivation areas within the command area of Yoshikawa Land Improvement District, Niigata. NDVI data were obtained from Sentinel-2 imagery for the 2023 and 2024 growing seasons (Apr. 1 to Sep. 30) and for 2025 until Aug. 30 through Google Earth Engine (GEE). Modified Normalized Difference Water Index (MNDWI) (Xu, 2006) data for the same periods were also used to aid transplanting date estimation. Transplanting dates and cultivar information were collected from farmers through questionnaires.

2.2. NDVI Preprocessing

To obtain high-frequency and reliable NDVI time series, cloud-affected pixels were removed using auxiliary cloud datasets (Cloud Score+ S2_Harmonized V1) instead of discarding entire images, and mixed pixels at field boundaries were excluded. The median NDVI within each field was calculated, and the resulting time series were smoothed using PCHIP interpolation to create continuous curves suitable for DTW alignment.

2.3. Time-Series Alignment for Standardized Curves

DTW was applied to the 2023 and 2024's PCHIP-interpolated NDVI time series to account for temporal shifts among fields. This alignment allowed multiple field-specific curves to be mapped onto a common reference, facilitating the construction of a representative standardized growth curve. The DTW-barycenter-averaged NDVI curves were further represented using a parametric model defined as Eq (1):

$$model(params, tau, t, tp) = a \cdot S\left(\frac{t - (\tau + tp)}{\kappa}\right) + b \quad (1)$$

where the parameters are defined as follows: κ: time scaling, a: amplitude scaling, b: offset adjustment, τ: temporal shift correction due to transplanting date estimation errors, and tp: estimated transplanting date defined as the first day when MNDWI (Sentinel-2) shifts from below to above zero followed by the minimum NDVI. These parameters (κ, a, b, τ) were optimized by least-squares fitting to the averaged curve, providing a smooth parametric representation of crop growth across fields.

3. Results

3.1. Transplanting date estimation

Transplanting dates were estimated based on the first minimum NDVI observed after MNDWI shifted from negative to values equal to or greater than zero.

The estimation accuracy was evaluated in several fields in 2023-2024, and the results are shown in Table 1.

Table1. Estimation error of Transplanting date estimation

Category	2023	2024
Number of Data	185	175
Mean Error (days)	-1.68	-1.58
Mean abs Error (days)	4.33	4.20
Max abs Error (days)	18	26
Standard Deviation (days)	5.03	5.11

3.2. Maximum NDVI estimation

To assess the predictive performance of the standardized NDVI curves, model curves derived from 2023–2024 data via DTW were applied to 2025 fields. For each field, NDVI data up to the end of May, June, and July were used for fitting, and the predicted maxim were compared with observed values. An example fit is shown in Figure 1, and the estimation result for selected varieties are summarized in Table 2.

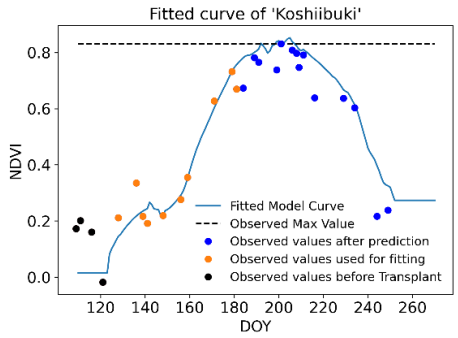

Fig. 1. Fitted result ex. of 'Koshi-Ibuki' in the end of Jun.

Table 2. Result of maximum NDVI estimation

Variety	N	Obs.Max Mean	Month	Est.Err. Mean	Est.Err .Std
Gohyaku mangoku	22	0.908	May	-0.023	0.058
			June	-0.022	0.026
			July	-0.030	0.015
Tsuki akari	78	0.874	May	0.019	0.053
			June	0.022	0.043
			July	-0.016	0.019
Koshi Ibuki	12	0.838	May	0.017	0.054
			June	-0.002	0.038
			July	0.001	0.017
Koshi Hikari	34	0.891	May	0.063	0.028
			June	0.070	0.020
			July	0.027	0.011

4. Discussion

4.1. Accuracy of Transplanting Date Estimation

Transplanting dates estimated from the first minimum NDVI after MNDWI $\geqslant$0 showed sufficiently small errors, demonstrating the method's effectiveness. Considering the 2-3 day revisit interval of Sentinel-2 and occasional limitations, the achieved accuracy is notable. Analysis of the largest errors indicated that they were not caused by missed observations, but rather by NDVI remaining low after transplanting, possibly reflecting poor early growth or unreported dates. Accuracy may fluctuate during rainy periods when satellite observations are restricted.

4.2. Accuracy of Maximum NDVI Estimation

The accuracy of maximum NDVI estimation was evaluated using standardized curves derived from 2023–2024 data and applied to 2025 fields not included in the training set. Fitting was performed on data from the sum of the estimated transplanting date and the error adjustment term τ through the end of May, June, and July. Parameter constraints were applied to prevent abnormal deformations with limited data: τ was restricted to integer values between -20 and 10, κ and a to 0.98–1.02, and b to -0.05–0.05, with τ set considering $\pm 2\sigma$ of the estimation error and the maximum observed error of +26 days.

Overall accuracy is good, at the end of July, the largest absolute mean error is 0.030. Although transplanting and harvesting dates varied among cultivars, mean errors and standard deviations tended to decrease as data accumulated, indicating effective parameter optimization. At the end of July, mean errors shifted from negative to positive in the order of Gohyakumangoku, Tsukiakari, Koshi-Hikari, and Koshi-Ibuki, matching the typical transplanting sequence reported by farmers. (noting that Koshi-Hikari and Koshi- Ibuki may switch order depending on production corporations and year) While later-transplanted cultivars inherently had fewer data by the end of July, the total precipitation observed at the nearby Takada Weather Station was only 0.5 mm in July, suggesting that late-transplanted cultivars were more prone to growth deficiencies due to drought, leading to overestimation. Conversely, for early-transplanted Gohyakumangoku, growth may have proceeded faster than the fitted curves could capture within the allowed parameter range, resulting in slight underestimation.

5. Conclusions

This study demonstrated that standardized DTW-based curves derived from multi-year Sentinel-2 NDVI data can effectively estimate maximum NDVI across rice fields in Niigata. Predictions were generally accurate, with minor biases likely due to drought or rapid early growth. The method proved robust across cultivars and could be further improved by adjusting parameter constraints and tailoring curves to growth stages.

Acknowledgements

The authors would like to express their sincere gratitude to Yoshikawa Land Improvement District for their valuable guidance and support, and to the farmers who cooperated in this study for their generous assistance.

This work was supported by JSPS KAKENHI Grant Number 24K01870.

References

・Journal articles:

Wakiyama, Y., Inoue, K., Nakazono, K., 2003. A Simple Model for Yield Prediction of Rice Based on Vegetation Index Derived from Satellite and AMeDAS Data during Ripenning Period, J.Agric.Meteorol., 59(4):277-286

Sakoe,H., Chiba, S., 1978, "Dynamic programming algorithm optimization for spoken word recognition," IEEE Transactions on Acoustics, Speech and Signal Processing, vol. 26(1), pp. 43–49.

Xu, H., 2006, Modification of normalized difference water index (NDWI) to enhance open water features in remotely sensed imagery. International Journal of Remote Sensing, Vol. 27, pp. 3025-3033.

・Internet resources:

Precipitation data were obtained from the Japan Meteorological Agency (Takada Weather Station), https://www.data.jma.go.jp/stats/etrn/view/monthly_s1.php?prec_no=54&block_no=47612&year=2025&month=7&day=&view= (accessed on Sep. 13, 2025).

Farmland polygon data were obtained from Field parcel polygon data (MAFF, 2025)

Impact of Climate Change-induced Warming on Adult Morphology in *Sympetrum frequens*

Shogo Sato *, Hiroshi Jinguji

Fukushima University Graduate School Faculty of Food and Agricultural Sciences, Fukushima-city, Japan

Email: shogo3103@hotmail.co.jp

Abstract

The population decline of *Sympetrum frequens,* a beneficial predator in rice-paddy ecosystems, has become increasingly severe in recent years. While insecticide use is a primary driver of this decline, climate change has also been implicated. However, the specific impact of climate change on *S. frequens* remains largely unexplored. The objective of this study was therefore to clarify the impact of climate change-induced warming on adult morphology in *S. frequens*. Adults undergoing reproductive diapause at high altitudes were collected, and morphometric measurements were recorded, including body weight, body length, forewing length, hindwing length, and wing area. Based on these measurements, the relative forewing length and relative hindwing length were calculated. Relationships between summer temperature and morphometric traits were then analyzed. In years with higher summer temperatures, body weight and relative forewing and hindwing lengths were significantly lower than in cooler years. These findings suggest that climate change induced by global warming may affect morphological traits in *S. frequens*. Previous studies on other dragonfly species have shown that reduced male body size is associated with decreased territorial behavior, reduced mating success, and potentially population decline. Consequently, clarifying the impact of climate warming on the adult morphology of *S. frequens* is important for the conservation of rice-paddy ecosystems.

Keywords body weight, global warming, relative forewing length, relative hindwing length

1. Introduction

Sympetrum frequens is a beneficial predator in paddy fields and is commonly referred to as the red dragonfly. Historically, large numbers of *S. frequens* were observed in paddy fields during autumn, and the species has played an important role in shaping the cultural landscape of rural areas. However, populations of red dragonflies have decreased markedly in recent years. The unique life history of *S. frequens* makes it particularly vulnerable to the effects of climate change. For instance, during the summer months (July–September), immature dragonflies migrate to cooler mountainous regions, away from the warmer lowland rice fields. Although insecticides and pesticides are considered the primary drivers of this decline (Jinguji et al. 2013), climate change has also been implicated (Nakanishi et al. 2020). Nonetheless, the specific effects of climate change on *S. frequens* populations remain largely unexplored. The objective of this study was to clarify how climate change-induced warming affects adult morphology in *S. frequens*.

2. Materials and Methods

2.1. Collection of adult *S. frequens*

Adult *S. frequens* individuals (50 males and 50 females/year) were collected over a five-year period from 2020 to 2024 at Mount Zao, Yamagata Prefecture. Sampling was conducted annually in late August. Feces samples were collected by keeping adults in folded triangular paper envelopes at room temperature.

2.2. Measurements

Body weight measurements were conducted using an electronic balance (CP2245, Sartorius, Japan). For morphometric measurements, adult specimens were photographed with a digital camera (PENTAX, RICOH, Japan), and the images were analyzed using ImageJ software (version 1.54g, Java 1.8.0_345). Traits for morphometric analysis included body length, forewing length, hindwing length, and hindwing area. Relative forewing length (forewing length/body length) and relative hindwing length (hindwing length/body length) were also calculated.

2.3. Statistics

Statistical analyses were performed separately for males and females using R (version 4.4.2). One-way analysis of variance followed by multiple comparison tests (Tukey's HSD test) was conducted to compare morphological traits among collection years.

3. Results and Discussion

3.1. Yamagata City temperature

The mean temperature in Yamagata city from May to August reached its highest values in 2023 and 2024 during the five-year study period. Compared with the 30-year climatological normal (1991–2020), temperatures were 1.8°C higher in 2023 and 1.9°C higher in 2024 (Table 1).

Table 1. Mean temperature in Yamagata city and the deviation from the climatological normal

	2020	2021	2022	2023	2024
Temperature (°C)	22.3	22.2	22.3	23.3	23.3
deviation	0.9	0.9	0.9	1.8	1.9

3.2. Body weight

In the years with higher temperatures (2023 and 2024), both males and females exhibited lower body weights than in the other years (Fig. 1). Significant inter-annual differences were observed in 2023 and 2024 (Fig. 2). In

Fig. 2, the *P*-values obtained from Tukey's test are presented as a heatmap.

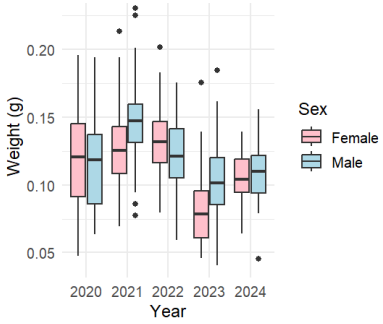

Fig. 1 Body weight by year.

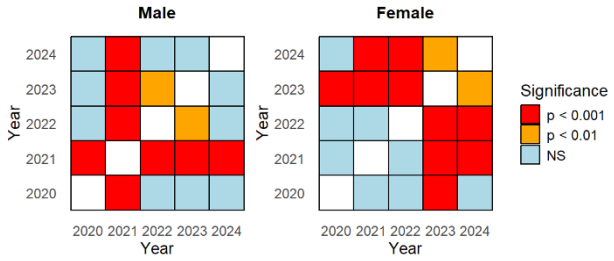

Fig. 2 Heatmap of body weight with Tukey test *P*-values.

3.3. Relative forewing and hindwing length

In the years with higher temperatures (2023 and 2024), both relative forewing length and relative hindwing length were smaller than in other years (Figs. 3 and Fig. 4). Significant inter-annual differences were observed in 2023 and 2024 (Fig. 5 and Fig. 6).

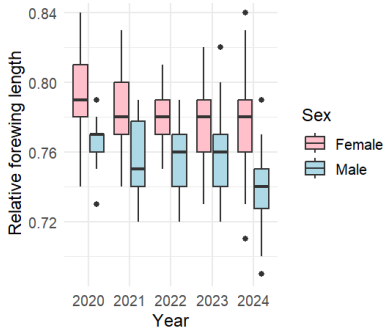

Fig. 3 Relative forewing length by year.

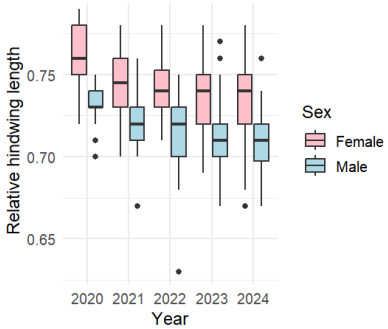

Fig. 4 Relative hindwing length by year.

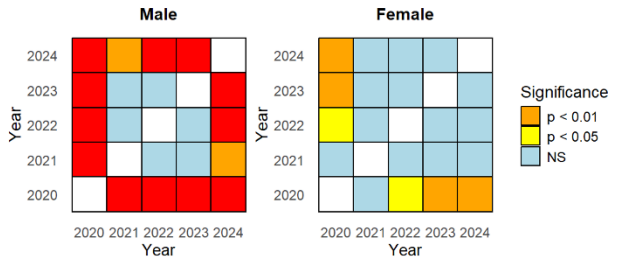

Fig. 5 Heatmap of relative forewing length with Tukey test *P*-values.

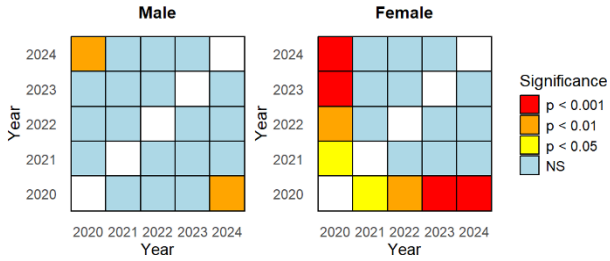

Fig. 6 Heatmap of relative hindwing length with Tukey test *P*-values.

4. Conclusions

This study confirmed a decrease in body weight and relative wing size of *S. frequens* associated with warming. In other dragonfly species, reductions in body size have been associated with deleterious effects. For example, elevated rearing water temperatures reduce egg hatching rates and increase larval mortality (Starr and Mclntyre 2019), and reductions in larval head width have also been reported. Furthermore, a decrease in male body size reduces territorial behavior (Ancco et al. 2020), potentially decreasing reproductive success. Taken together, these findings suggest that warming may lead to reduced body size in *S. frequens*, thereby contributing to population decline.

References

Ancco Valdivia, F.G., Alves-Silva, E., Del-Claro, K., 2020. Differences in size and energy content affect the territorial status and mating success of a neotropical dragonfly. *Austral Ecology*, 45: 748-758.

Jinguji, H., Thuyet, D.Q., Uéda, T., Watanabe, H., 2013. Effect of imidacloprid and fipronil pesticide application on *Sympetrum infuscatum* (Libellulidae: Odonata) larvae and adults. *Paddy Water Environ* 11, 277–284.

Nakanishi, K., Koide, D., Yokomizo, H., Kadoya, T., & Hayashi, T. I.,2020. Investigating effect of climate warming on the population declines of S*ympetrum frequens* during the 1990s in three regions in Japan. *ScientificReports*,10,12719.

Scott, M.S., and Nancy, M., 2020. Effects of Water Temperature Under Projected Climate Change on the Development and Survival of *Enallagma civile* (Odonata: Coenagrionidae), *Environmental Entomology*, 49(1), 230–237.

Comparative Analysis of Fish Habitat Suitability Characteristics in Han River Basin, South Korea

Lee Hyeokjin・Song Inhong

Abstract

This study investigates spatial variations in fish habitat suitability across 29 sub-basins in the Han River Basin, South Korea. Habitat Suitability Index (HSI) curves were developed for four representative fish species: Zacco platypus, Rhynchocypris oxycephalus, Zacco koreanus, and Squalidus japonicus coreanus using fish monitoring data collected twice annually from 2011 to 2023 under the national fish survey network. The HSI evaluation was conducted using the Instream Flow Aquatic System Group (IFASG) method based on key habitat variables including water depth, velocity, and temperature. Weibull distribution was applied to model the HSI response curves for each species. The spatial analysis reveals characteristic differences in HSI patterns between mainstream and tributary sub-basins, underscoring the importance of regional habitat conditions. These findings provide scientific insights for ecological stream flow assessments and the development of targeted habitat conservation strategies in the Han River Basin.

Modeling the Ecosystem Conservation Function of Agricultural Ponds in Urbanizing Regions

Jo Hamaguchi[1], Masayasu Maki[2], Koshi Yoshida[3], Tasuku Kato[4], Keigo Noda[1*]

[1] Graduate School of Agricultural and Life Sciences, UTokyo, Bunkyo-ku, Tokyo 1135841, Japan

[2] Faculty of Food and Agricultural Sciences, Fukushima Univ., Fukushima city, Fukushima 9601296, Japan

[3] Graduate School of Frontier Sciences, UTokyo, Kashiwa city, Chiba 2778563m Japan

4 United Graduate School of Agricultural Science, TUAT, Fuchu city, Tokyo 1838509, Japan

* Corresponding author. Email: nodakeigo@g.ecc.u-tokyo.ac.jp

Abstract

Farming ponds, managed for irrigation, are increasingly recognized for their ecosystem conservation functions, especially in regions undergoing rapid urbanization. These small water bodies support habitat connectivity, biodiversity retention, and microclimate regulation, yet their ecological value remains underrepresented in spatial planning models. This study aims to model the ecosystem conservation function of farming ponds in Vientiane, Lao PDR, where urban expansion is placing growing pressure on rural landscapes. We employed the InVEST Habitat Quality model to evaluate habitat conditions across the urban–rural gradient, with a methodological extension: a protection coefficient (β) was applied to reflect the positive ecological influence of farming ponds. Land use data and threat layers were incorporated into the model to reflect the local context. Our findings indicate that incorporating farming ponds as protective landscape elements significantly enhances habitat quality scores, particularly in suburban areas. By quantifying their ecological functions, this study provides a practical approach to integrating pond networks into urban spatial planning and ecosystem management.

Keywords: InVEST, Ecosystem services, Urbanization, Lao PDR, Vientiane

1. Introduction

In the evaluation of ecosystem services, the Integrated Valuation of Ecosystem Services and Tradeoffs (InVEST) model has become the de facto standard. Since InVEST was originally developed to explicitly assess the negative impacts of human activities on habitat quality, it treats not only urban areas but also secondary nature such as farmland as threats to ecosystems. However, in Monsoon Asia, including Japan, secondary natural environments such as paddy fields and satoyama landscapes serve as important habitats for various species.

In this study, we applied the Habitat Quality Model of InVEST to assess the ecosystem conservation functions of farming ponds from the perspective of habitat provision. The aim was to evaluate the changes in the ecological value of farming ponds associated with urbanization by adapting this model.

2. Materials and Methods

Five farming ponds located within Vientiane City, Laos, were selected to quantitatively evaluate changes in ecosystem conservation functions along with the progress of urbanization. The ponds were classified into five types according to their degree of urbanization and formation process, and analyses were conducted based on land-use data from four years: 1989, 2000, 2013, and 2021.

The ecosystem conservation function was assessed using the GIS-based InVEST Habitat Quality Model. This model estimates habitat quality based on the spatial relationship between land-use types defined as habitats and those defined as threats. Amphibians were assumed as the target species, and parameters such as the influence of each threat and the sensitivity of habitat types were set with reference to previous studies.

To express the conservation effects provided by farming ponds, a spatial buffering effect was incorporated to mitigate the influence of threats. The threat intensity was gradually reduced with distance from each pond, representing the pond's role in mitigating environmental pressures. For each pond, the total habitat quality within a 300 m radius was calculated as the habitat quality of the assessment area. Habitat quality was computed both with and without the buffering effect, and the difference between the two was defined as the "ecosystem conservation value of the pond." By comparing these values among the five ponds and across the four years, we quantitatively evaluated the temporal changes in ecosystem conservation functions under urbanization.

3. Results and Discussion

The habitat quality of each assessment area and the ecosystem value of each pond are shown in Tables 1 and 2.

At Nong Wat Panya, where surrounding farmland and vegetated areas have been developed into urban land, the overall habitat quality declined, while the relative conservation effect of the pond increased. Consequently, the calculated "pond value," expressed as the difference between cases with and without conservation effects, consistently increased over time. This indicates that as urbanization intensifies and acts as a threat, the ecological value provided by the pond as habitat becomes more significant.

In contrast, at the KM6 Regulation Pond, newly constructed during the same period of rapid urbanization, the overall habitat quality of the area improved despite the expansion of urban land use. Similarly, at That Luang Lake, although the surrounding habitat quality declined sharply due to urbanization, the presence of the pond helped to mitigate the rate of degradation. These results suggest that newly constructed ponds in urban environments can play two potential roles: improving habitat quality or suppressing its deterioration, both of which can be quantitatively evaluated through the proposed method.

On the other hand, for Beung Khayong Lake—located in the urban core—and Nong Tha Lake—where the pond area has significantly decreased—the proposed method could not adequately capture value changes associated with urbanization.

Acknowledgements

This work was supported by JSPS KAKENHI Grant Number JP23K27017.

Table 1. Habitat quality of each agricultural pond with/without conservation function

Habitat Quality								
	1989		2000		2013		2021	
β	with	without	with	without	with	without	with	without
①Nong Wat Panya	187.5	146.0	129.5	65.6	99.2	37.1	88.4	31.3
②KM6 Regulation Pond	-	284.9	343.8	243.7	280.4	167.4	202.0	87.9
③That Luang Lake	-	1304.6	-	1240.2	498.3	215.8	511.5	236.7
④Beung Khayong Lake	54.6	19.2	45.5	14.6	51.6	16.5	51.7	18.5
⑤Nong Tha Lake	1067.5	464.7	771.7	282.6	749.5	324.6	744.8	325.5

Table 2. Ecosystem value of each agricultural pond

The value of farming ponds				
	1989	2000	2013	2021
①Nong Wat Panya	41.5	64.0	62.1	57.1
②KM6 Regulation Pond	-	100.1	113.1	114.1
③That Luang Lake	-	-	282.5	274.8
④Beung Khayong Lake	35.4	30.9	35.1	33.2
⑤Nong Tha Lake	602.8	488.5	424.9	419.3

Estimation of Habitat Suitability Index Based on Water Quality Using Parametric Distributions in Korea

Seongju Jang [1], Hyeokjin Lee [1] , Inhong Song [1*]

[1] Department of Rural Systems Engineering, Seoul National University, Seoul 08826, Korea

* Corresponding author. Email: inhongs@gmail.com

Abstract

The objective of this study was to estimate habitat suitability index for fish in relation to water quality factors using parametric distributions. Water quality data were matched with fish monitoring data based on spatial and temporal proximity, considering station locations and observation periods. The dataset was organized by Korea's four major river basins: the Han, Nakdong, Geum, and Yeongsan Rivers. Four representative fish species in Korea—Zacco platypus, Zacco koreanus, Pungtungia herzi, and Carassius auratus—were selected. Nine water quality parameters, derived from Korea's national stream environment standards, were analyzed: water temperature, pH, biochemical oxygen demand, chemical oxygen demand, total organic carbon, suspended solids, dissolved oxygen, total phosphorus, and fecal coliforms. HSIs were calculated using gamma, Weibull, and logistic distributions for each species and parameter across the different river basins. The results were compared with those obtained using conventional nonparametric methods. The result of this study will be helpful to estimate ecological flow considering water quality in Korea.

Keywords: Habitat Suitability Index, Water quality, Ecological flow, Parametric distribution.

1. Introduction

The incorporation of aquatic ecosystems into environmental flow assessments has become increasingly important, and the use of habitat suitability index (HSI) for fish is essential in ecological flow estimation. In Korea, HSIs have been primarily developed based on physical factors such as water depth and flow velocity, with non-parametric methods frequently applied (Kang, 2012). More recently, studies have attempted to estimate HSI using probability density functions (Jang et al., 2018). In parallel, the Ministry of Environment has established and operates a national water environment monitoring network that provides data on water quality, fish populations, and other ecological variables. The objective of this study is to develop habitat suitability indices for water quality factors using a parametric distribution approach.

2. Materials and Methods

2.1. Water environment monitoring data

In this study, habitat suitability indices were estimated using water quality data from the Water Quality Monitoring Network and fish abundance data from the Biological Monitoring Network, both of which are part of the national Water Environment Monitoring System. Figure 1 illustrates the locations of the water quality and biological monitoring stations. Data collected between 2011 and 2013 were utilized. Since the monitoring datasets vary in terms of sampling locations and sampling periods, only data collected on the same day from adjacent sites were selected for analysis (Hong et al., 2021).

The water quality factors considered for the estimation of habitat suitability indices were selected based on Korea's riverine environmental standards and included pH, biochemical oxygen demand (BOD), chemical oxygen demand (COD), total organic carbon (TOC), suspended solids (SS), dissolved oxygen (DO), total phosphorus (TP), and fecal coliform counts. The target fish species were chosen as representative species in Korea, namely *Zacco platypus*, *Zacco koreanus*, *Pungtungia herzi*, and *Carassius auratus*.

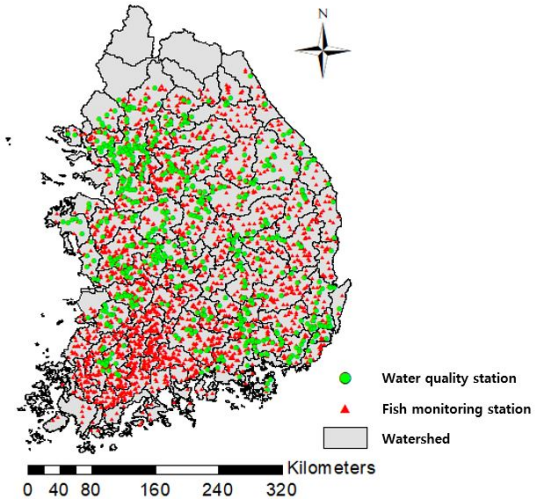

Figure 1. Location of water quality stations and fish monitoring stations.

2.2. Parametric distributions

The distribution functions used to estimate habitat suitability indices were selected with reference to the curves commonly applied for HSI estimation as suggested by IFASG (1986). In this study, the generalized Poisson, gamma, and Weibull distributions were employed (Figure 2).

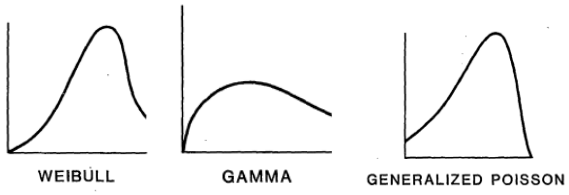

Figure 2. Distribute functions

3. Results and Discussion

Figure 3 and 4 show HSI curve of *Zacco platypus* and *Pungtungia herzi* for DO and BOD using Weibull distribution. For *Zacco platypus*, the species showed the highest preference at DO concentration of 10 mg/L and BOD concentration of 5 mg/L. For *Pungtungia herzi*, the species showed the highest preference at DO concentration of 17 mg/L and BOD concentration of 1 mg/L

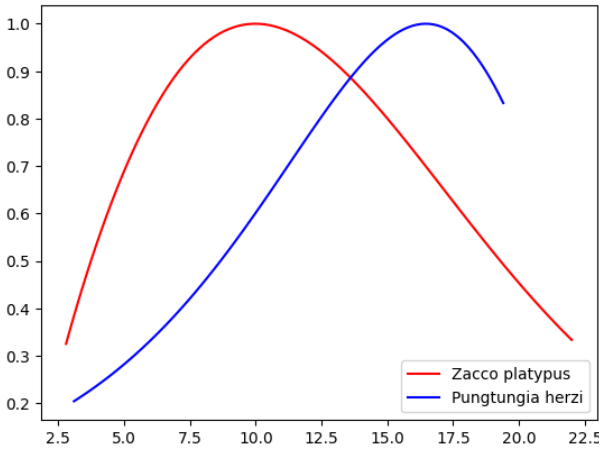

Figure 3. HSI curve of *Zacco platypus* and *Pungtungia herzi* for DO (Weibull distribution)

.

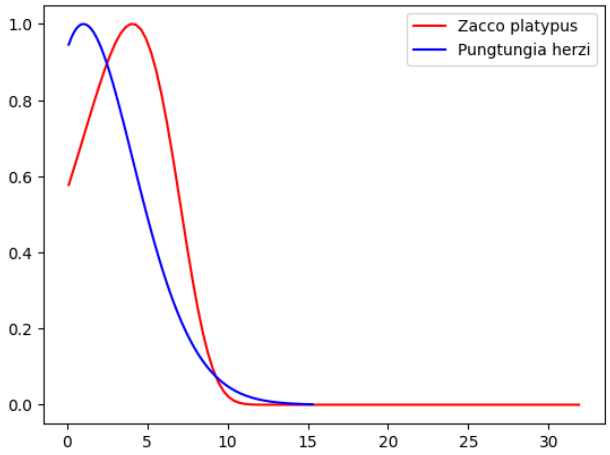

Figure 4. HSI curve of *Zacco platypus* and *Pungtungia herzi* for BOD (Weibull distribution)

4. Conclusions

In this study, habitat suitability indices for water quality factors were developed using parametric distribution approaches. A comparison of habitat suitability indices for dissolved oxygen (DO) and biochemical oxygen demand (BOD) between Zacco platypus and Pungtungia herzi indicated that Zacco platypus prefers lower DO and higher BOD levels than Pungtungia herzi. These findings are expected to provide useful insights for the estimation of ecological flow that incorporates water quality considerations.

Acknowledgements

This work was supported by the Korea Environment Industry & Technology Institute (KEITI) through the Aquatic Ecosystem Conservation Research Program, funded by the Korea Ministry of Environment (MOE) (Grant number 2020003050001).

References

Hong, R., Park, J., Jang, S., Song, I., 2021 Estimation of Fish Habitat Suitability Index for Stream Water Quality - Case Species of Zacco platypus -. Journal of the Korean Society of Agricultural Engineers., 63(6), 89-100.

IFASG (Instream Flow and Aquatic Systems Group), 1986. Development and evaluation of habitat suitability criteria for use in the instream flow incremental methodology. Instream flow information paper No. 21. Washington D. C.: National Ecology Center

Jang, K. H., Park, Y. K., Kang, J. I., Kim, M. H. 2018. Estimation of ecological flow rate for Zacco platypus based on habitat suitability index considering probability density function. Journal of Korea Water Resources Association. 51(3) 207-219

Kang, H., 2012. Comparision of Physical Habitat Suitability Index for Fishes in the Rivers of Han and Geum River Watersheds. Journal of the Korean Society of Civil Engineers B 32(1), 71-78

Spatiotemporal Analysis of Hydrological Connectivity in a Floodplain Wetland Using Geostatistical Methods: A Case Study of Bakhira Wildlife Sanctuary, India

Ashish Pandey[1]* Manish Rawat[1], Basant Yadav[1] and Praveen Kumar Gupta[2]

[1*] Department of Water Resource Development and Management, Indian Institute of Technology Roorkee, India,

[1] Department of Water Resource Development and Management, Indian Institute of Technology Roorkee, India,

[2]Space Applications Centre, Indian Space Research Organisation, Ahmedabad, India,

Corresponding author E-mail: ashish.pandey@wr.iitr.ac.in

Abstract

Hydrological connectivity plays a vital role in maintaining the stability and functioning of wetland ecosystems. Understanding the effects of changes in hydrological connectivity on wetland habitats is essential for wetland restoration and the preservation of species diversity. While most studies have focused on changes in land use and land cover (LULC) and their influence on ecosystems, few have quantitatively assessed the impact of different LULCs on hydrological connectivity. Bakhira, the largest natural floodplain wetland in eastern Uttar Pradesh, India, and a potential Ramsar site, is presently in a degraded state due to drying and fragmentation over the past two decades. In this study, multi-temporal NDVI derived from Landsat imagery (2000–2024) was used to monitor vegetation dynamics during both pre- and post-monsoon seasons. Hydrological connectivity was quantified through a time-series Index of Connectivity (IC) combined with the Connectivity Response Unit (CRU) framework, sustained by geostatistical analyses. The IC combined topography, vegetation cover, and upstream contributing area, while quartile-based CRUs classified the landscape into four connectivity categories ranging from very low to high. Results revealed marked seasonal variability, with post-monsoon conditions enhancing connectivity through rainfall recharge and vegetation recovery, whereas pre-monsoon periods exhibited weaker hydrological linkages. Sub-catchment analysis further emphasized spatial heterogeneity: SC-4 represented as the primary hydrological corridor, while SC-7 and SC-3 remained weakly connected due to vegetation and land-use impedances. Overall, this study provides a long-term, spatially clear assessment of wetland connectivity in the Ganga plains, demonstrating the CRU–IC framework as a robust and scalable tool for wetland restoration, adaptive management, and conservation planning under increasing anthropogenic and seasonal pressures.

Keywords: Connectivity index, Connectivity Response Unit (CRU), NDVI, Geostatistical, Wetland restoration**.**

1. Introduction

Wetlands are vital ecosystems that regulate hydrology, support biodiversity, and provide key ecological services. Their functioning depends on hydrological connectivity, which governs the transfer of water, sediment, and nutrients between wetlands and their catchments. However, across India, increasing pressures from land-use change, agriculture, and urban expansion have disrupted these linkages, causing many wetlands to dry, fragment, and lose resilience. This study applies the Connectivity Index (IC) in combination with the Connectivity Response Unit (CRU) framework to assess wetland–catchment linkages. The key objectives of this study are: (i) to assess seasonal variations in hydrological connectivity using the Connectivity Index (IC), and (ii) to analyse long-term spatio-temporal trends and sub-catchment contributions through the IC–CRU framework. Figure 1 illustrates the location of Bakhira Wetland in Uttar Pradesh, India, along with its sub-catchments (SC-1 to SC-8) and elevation distribution.

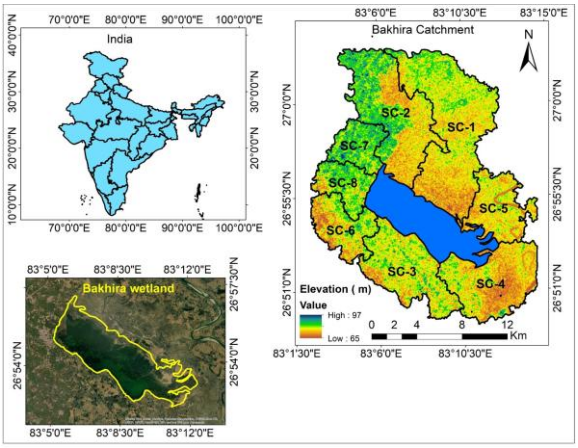

Figure 1. Study area map showing the Bakhira Wetland and sub-catchments

2. Materials and Methods

The hydrological connectivity of the Bhakira wetland and its sub-catchments was evaluated using a wetland-targeted Index of Connectivity (IC) framework integrated with Connectivity Response Unit (CRU) classification. Following Borselli et al. (2008) and Cavalli et al. (2013), the IC combines upslope contributing factors with downslope resistances to represent spatial hydrological connectivity. The analysis covered 2000–2024, focusing on pre- (March–May) and post-monsoon (October–December) seasons, which are hydrologically contrasting seasons. Input datasets included the 30 m SRTM DEM for terrain, the MERIT Hydro upstream drainage area for contributing catchment size, and Landsat imagery (Landsat 5 for 2000–2012; Landsat 8 for 2013–2024). Wetland boundaries and sub-catchment delineations were also incorporated. Connectivity components were derived in two steps. First, the upslope index (D_{up}) was estimated by integrating vegetation, slope, and contributing area. NDVI was calculated and converted into a normalized C-factor (0–1), which was combined with slope (tanΦ) to obtain a weighting factor. This was multiplied by the square root of the upstream contributing area to derive D_{up}. Second, the downslope component (D_{dn}) was calculated using a cumulative cost-distance algorithm, where the cost per pixel was defined as the inverse of the weighting factor. This represented resistance to flow, with steep vegetated areas offering low resistance and flat, bare areas offering high resistance. The cumulative distance was

measured from wetland polygons, representing the ease of flow transfer toward the wetland.

The Connectivity Index was computed for each pixel in Eq (1):

$$IC = \log_{10} \frac{D_{up}}{D_{dn}} \dots\dots\dots\dots\dots 1$$

Where higher values indicate stronger connectivity. Annual IC rasters were then classified into quartiles to generate CRUs with four categories: very low, low, medium, and high connectivity. These CRUs provided a standardized basis for spatial and temporal comparison of connectivity patterns. The CRU outputs were analyzed to examine seasonal and interannual variability and to evaluate the influence of vegetation dynamics, slope, and land-use changes on hydrological linkages

3. Results

The spatial classification of Connectivity Response Units (CRUs) for 2024, shown in Figure 2, reveals marked seasonal contrasts in hydrological connectivity across the Bhakira wetland catchment. During the post-monsoon season, northern and upland sub-catchments were characterized by very low to low connectivity, whereas southern areas and zones adjacent to the wetland exhibited medium to high connectivity, reflecting the influence of rainfall, soil moisture, and vegetation recovery. In contrast, the pre-monsoon season exhibited a reduction in high-connectivity zones, with more areas shifting to low and very low classes, indicating weakened linkages under drier conditions. Figure 2, Pixel-wise Connectivity Index (IC) maps support this pattern. IC values in 2024 ranged from −9.01 to 5.69 post-monsoon and −8.67 to 4.81 pre-monsoon. Higher IC values, concentrated near wetland margins and steeper slopes, indicate strong connectivity, whereas negative values in distant or flat sub-catchments denote disconnection. Post-monsoon IC values were consistently higher, highlighting the role of rainfall and vegetation in strengthening linkages.

Long-term IC Heatmaps shown in Figure 3 (2003–2024) reveal strong sub-catchment variability. Post-monsoon maximum IC values ranged 3.5–5.7, with SC-4 consistently highest (5.6–5.7) and SC-7 lowest (2.9–3.5). Minimum IC values varied from −7.0 to −11.5, with extreme lows in SC-2, SC-3, and SC-7, including −22.4 in SC-3 (2013). Pre-monsoon heatmaps showed slightly lower maxima (3.2–5.5), again with SC-4 most connected and SC-7 least. Minimum IC values ranged from −7.0 to −10.7, reflecting stronger disconnection during dry conditions.

The CRU and IC analyses exhibit that connectivity is governed by both seasonal and inter-annual variability. Post-monsoon periods consistently enhance connectivity, while pre-monsoon seasons show reduced linkages. Sub-catchment analysis confirms SC-4 as the primary hydrological corridor feeding the wetland, whereas SC-7 and SC-3 remain weakly connected, underscoring spatial heterogeneity and the need for targeted management to sustain the wetland's ecological integrity.

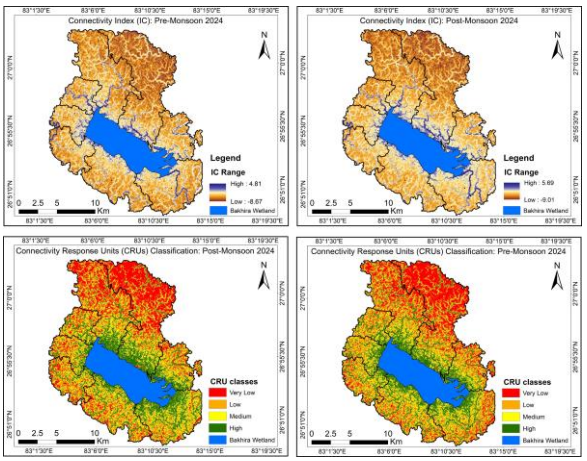

Figure 2. Seasonal Variations in Connectivity Index and Connectivity Response Units for the Bhakira Wetland Catchment

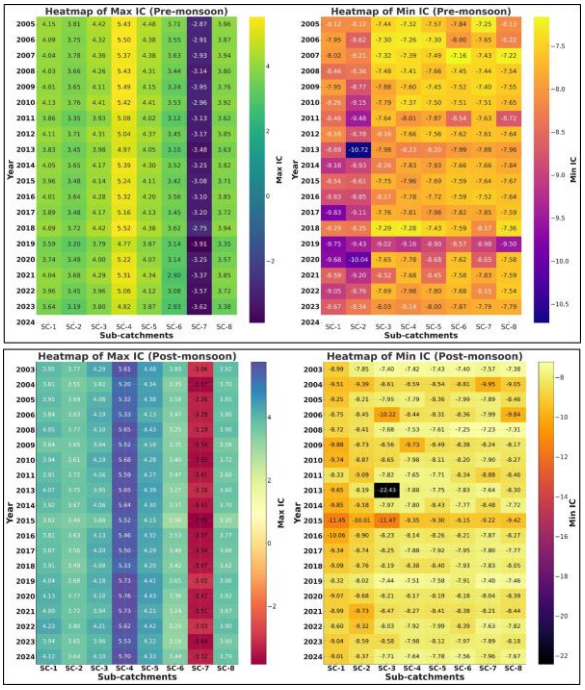

Figure 3 Temporal Variation of Max–Min Connectivity Index in Bhakira Wetland Sub-Catchments.

4. Discussion

This study shows that hydrological connectivity in the Bhakira wetland varies strongly with season and sub-catchment characteristics. Post-monsoon periods consistently exhibited higher connectivity due to rainfall and vegetation regrowth, while pre-monsoon conditions reflected weaker linkages under dry landscapes. Such seasonal contrasts align with earlier findings from Indian floodplain wetlands (Singh & Sinha, 2022) and highlight the need for long-term monitoring under a changing climate and land use. Sub-catchment analysis revealed SC-4 as the dominant hydrological corridor, while SC-7 and SC-3 remained weakly connected. This spatial heterogeneity parallels patterns in other Ganga plain wetlands (Singh et al., 2017). The CRU framework proved effective by simplifying IC values into actionable connectivity classes, consistent with its applications in Kaabar Tal and Haiderpur wetlands. The study advances

the IC framework proposed by Borselli et al. (2008) through its integration of DEM-derived slope, MERIT Hydro upstream area, and NDVI-based vegetation indices in Google Earth Engine. This workflow is replicable and scalable, adding to recent global applications of IC in China and Central Asia that address connectivity under climate change and land-use pressures (Liu et al., 2024).

5. Conclusions

This study reveals the effectiveness of the Connectivity Index (IC) and Connectivity Response Unit (CRU) framework for evaluating hydrological connectivity in the Bhakira wetland catchment. Using multi-temporal remote sensing and geospatial analysis, the approach captured both spatial heterogeneity and seasonal variability. Post-monsoon periods consistently showed stronger connectivity due to rainfall and vegetation recovery, while pre-monsoon seasons exhibited weaker linkages. Sub-catchment analysis identified SC-4 as the dominant hydrological corridor, whereas SC-7 and SC-3 remained weakly connected, highlighting uneven contributions to wetland inflows. Quartile-based CRU classification effectively translated continuous IC values into actionable categories, enabling the identification of connectivity hotspots and disconnection zones. The framework simplifies complex processes and provides a practical tool for wetland conservation and watershed management. Maintaining and restoring connectivity is critical for sustaining the ecological integrity of Bhakira, and future research should extend this approach to other wetlands, integrate climate change scenarios, and evaluate targeted management strategies.

Acknowledgements

The authors gratefully acknowledge the Department of Water Resources Development and Management (WRD&M), IIT Roorkee, for providing essential facilities and continuous encouragement throughout this research. This work was also supported by the Space Applications Centre, ISRO.

References

Borselli, L., Cassi, P., & Torri, D. (2008). Prolegomena to sediment and flow connectivity in the landscape: A GIS and field numerical assessment. Catena, 75(3), 268-277.

Cavalli, M., Trevisani, S., Comiti, F., & Marchi, L. (2013). Geomorphometric assessment of spatial sediment connectivity in small Alpine catchments. Geomorphology, 188, 31-41.

Singh, M., Tandon, S. K., & Sinha, R. (2017). Assessment of connectivity in a water‐stressed wetland (Kaabar Tal) of Kosi‐Gandak interfan, north Bihar Plains, India. Earth Surface Processes and Landforms, 42(13), 1982-1996.

Singh, M., & Sinha, R. (2022). Integrating Hydrological Connectivity in a Process–Response Framework for Restoration and Monitoring Prioritisation of Floodplain Wetlands in the Ramganga Basin, India. Water, 14(21), 3520.

Liu, C., Chen, Y., Huang, W., Fang, G., Li, Z., Zhu, C., & Liu, Y. (2024). Climate warming positively affects hydrological connectivity of typical Inland River in arid Central Asia. NPJ Climate and Atmospheric Science, 7(1), 250.

Life cycle impact assessment of radioactive isotope release on irrigated rice paddy environments

Chin Fong [1*], Chihhao Fan [2], Cheng-I Hsieh [3], Wen-sheng Lin [4]

[1] Department of Bioenvironmental Systems Engineering, National Taiwan University, Taipei 106319, Taiwan

* Corresponding author. Email: ntu.fongchin@gmail.com

Abstract

This study adopts a life cycle assessment (LCA) perspective to evaluate potential environmental and health implications of radionuclide releases during nuclear power plant decommissioning in Taiwan's rice-growing regions. To align with energy-transition and carbon-neutrality goals, the present study synthesizes literature on radionuclides of concern, transport pathways, and dose-conversion factors and compiles a preliminary life cycle inventory (LCI). In the initial test case, the exposure pathway—freshwater → irrigation supply → agricultural cultivated soil → rice root uptake—is delineated, and the water-transport segment is operationalized to generate irrigation-relevant concentration – time curves and indicators by pairing USEtox (steady-state screening) with GoldSim (time-resolved water transport). Analyses emphasize behavior in receiving waters and irrigation-side indicators that are directly interpretable for agricultural operations. As supporting data mature, the workflow will be extended stepwise along the pathway toward soil and root uptake, providing comparative, time-varying insights across radionuclides and priorities for refinement and monitoring within LCA/LCIA.

Keywords: Radioactive isotopes, Radionuclide exposure pathway, Interaction matrix, Rice paddy environment, Nuclear power decommissioning in Taiwan, LCA/LCIA

1. Introduction

In recent years, to achieve energy transition and carbon-neutrality goals, nuclear power has regained attention for its low operational carbon emissions and stable electricity supply; at the same time, its use has raised safety concerns about potential releases of radionuclides and their possible impacts on surrounding agricultural environments. In Taiwan's irrigated rice regions, waterborne transport is the principal pathway by which nuclides may reach farmland, because receiving waters (rivers and reservoirs) directly supply irrigation intakes. A paddy-centered perspective helps focus key questions: when and by what mechanisms source-water dynamics translate into concentrations at irrigation intakes, and how these conditions shape exposure in cultivated soils and crops.

Within an LCA/LCIA framework, this study combines screening-level characterization (for comparing nuclides or scenarios) with time-resolved interpretation to identify the temporal behavior of environmental exposure (e.g., peaks, lags, and persistence). In the initial test case, the analysis delineates a single exposure pathway—freshwater → irrigation supply → agricultural cultivated soil → rice root uptake—and, at this stage, implements only the water-transport segment to produce indicators relevant to irrigation management. This arrangement prioritizes verification of the model's feasibility and traceability; once initial testing is completed and both data and scope are more mature, simulations will be expanded to a broader domain and additional exposure pathways. This framing supports risk assessment and pragmatic management during decommissioning, while keeping the present work focused and defensible.

2. Materials and Methods

2.1 Environmental inventory and assessment lens (LCI)

This study first compiles an inventory of environmental components, parameters, and interactions relevant to paddy-field irrigation contexts. Components include the receiving freshwater body, irrigation intake, agricultural cultivated soil, and rice/crop compartments. Interactions/processes (e.g., advection, diffusion, sedimentation, precipitation/adsorption–desorption, resuspension, evaporation/spray, interception, root uptake) are gathered from existing reports and datasets with traceable sources and assumptions, and harmonized units/time bases. This LCI-style compilation keeps inputs consistent for both the screening model (USEtox) and the dynamic model (GoldSim) while remaining straightforward to interpret under an LCIA perspective.

2.2 Interaction-matrix construction

Based on Section 2.1, the compiled components and interactions are organized into an interaction matrix. The matrix provides a transparent map of how nuclides can move between modules (e.g., freshwater ↔ soil ↔ crop), and it serves as a boundary/scope control tool: current analysis focuses on water-transport–dominated links relevant to irrigation, while potential extensions are outlined for later stages when data permit.

2.3 Pathway and scope

Guided by the interaction matrix (Section 2.2), the present study adopts the pathway freshwater → irrigation supply → agricultural cultivated soil → rice root uptake. In the initial test case, only the water-transport segment is implemented to establish an irrigation-relevant baseline; site-specific soil or crop uptake is not modeled at this stage.

2.4 Model roles

USEtox (steady state) yields relative/normalized steady-state contributions—suited for screening and

comparison under simplified conditions. GoldSim (dynamic) specifies actual release/exposure amounts and simulates time-evolving concentrations/exposures in receiving waters, revealing early-time behavior, peak timing/magnitude, and decay.

2.5 Integration strategy

USEtox and GoldSim are executed in parallel using the same scenario and parameter set (with units and time bases harmonized). Outputs are then cross-checked—comparing USEtox's normalized steady-state contributions with GoldSim's time-series concentrations/exposures at irrigation-relevant locations—to verify consistency in nuclide ranking, plausible peak timing/magnitude, and overall trends. Any discrepancies trigger a targeted review of assumptions and parameter ranges. Results are finally integrated side-by-side: USEtox supplies the steady-state contribution signal for screening/interpretation, while GoldSim supplies the time dimension for timing and magnitude. Tight numerical coupling is not enforced at this stage to keep assumptions and uncertainties transparent. Current outputs include concentration–time curves at irrigation-relevant locations together with documented assumptions and parameter ranges.

3. Results and Discussion

3.1 From matrix to GoldSim exposure pathway setup

After constructing the interaction matrix, this study used its modules and links to configure a GoldSim model for the freshwater → irrigation segment and generated concentration – time curves at irrigation-relevant locations. The results show clear peak windows, early transients, and nuclide-specific persistence, and they reveal key sensitivities (e.g., advection versus dispersion).

	1	2	3	4
1	Surface Water Body	-Irrigation	-Interception	-Inhalation -Ingestion -External Irradiation
2	-Surface Runoff	Agricultural **Cultivated Soil**	-Root Uptake	-Inhalation -Ingestion -External Irradiation
3		-Weathering -Decomposition	Agricultural **Rice/Crops**	-Ingestion -External Irradiation
4	-Pumping	-Ploughing		**Humans**

Figure 1. Interaction matrix along the "Surface water → Irrigation intake → Agricultural cultivated soil → Rice/crops → Humans" continuum.

Major modules are arranged along the diagonal from top-left to bottom-right, and each cell at the intersection of two modules denotes their interaction—a potential pathway for radionuclide transfer (Figure 1). Based on the interaction matrix, the exposure pathway is configured in GoldSim for subsequent simulation of radionuclide transport (Figure 2).

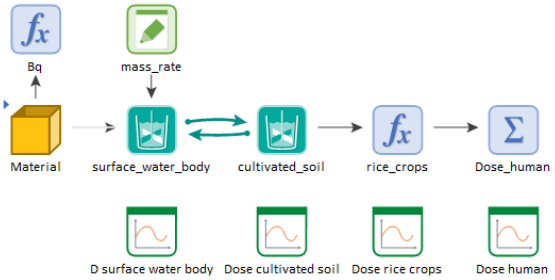

Figure 2. GoldSim exposure pathway for the "freshwater → irrigation" segment.

3.2 Implications for irrigated paddy management

Findings provide (i) a concise blueprint linking source-water dynamics to irrigation decisions and cultivated-soil conditions; (ii) actionable timing cues from peak windows; and (iii) time-varying differences that distinguish sharp-peaking from persistent nuclides. These insights support near-term operations and lay the groundwork for subsequent soil and root-uptake assessment.

3.3 Limitations, next steps, and screening cross-check (USEtox)

The current scope covers only water transport toward paddy fields; next steps will gradually expand parameters and reduce uncertainty in peak timing and magnitude. In parallel, steady-state screening with USEtox will serve as a cross-check: agreement in nuclide rankings builds confidence in assumptions and settings, whereas divergences indicate steady-state or time-scale effects and help prioritize nuclides and pathway segments for refinement and monitoring.

4. Conclusions

Within an LCA/LCIA framework, this study used the interaction matrix to set up the freshwater → irrigation exposure pathway in GoldSim, with USEtox serving as a steady-state cross-check. The model provides irrigation-relevant concentration – time curves and simple indicators, offering clear timing cues, linking source-water dynamics to paddy management, and highlighting which nuclides peak sharply versus persist. Next steps expand parameters, pathways, and interactions to strengthen the radionuclide exposure simulation and life cycle impact assessment (LCIA).

References

Paulillo, A. (2018). Operationalising the use of Life Cycle Assessment to nuclear waste management.

Kim, D., Kim, J., Lee, W., & Park, J. (2023). A systematic approach in the development of generic biosphere conceptual models for groundwater release into the Korean biosphere system from a spent nuclear fuel deep geological repository. Available at SSRN 4421426.

International Atomic Energy Agency. Division of Radiation, Waste Safety. Waste Safety Section, Biosphere Modelling, & Assessment (Program). (2003). " Reference Biospheres" for Solid Radioactive Waste Disposal: Report (Vol. 6). International Atomic Energy Agency.

Spatio-temporal characterization of compound heat and drought extremes in South Korea

Qudus Adeyi[1], Deepak Chaulagain[2], Kyung Sook Choi [1,2,3*]

[1] Department of Agricultural Civil Engineering, Kyungpook National University, Daegu 41566, Korea.

[2] Institute of Agricultural Science & Technology, Kyungpook National University, Daegu 41566, Korea.

*Corresponding author: Kyung Sook Choi

E-mail address: ks.choi@knu.ac.kr

Abstract

Compound drought and heatwave (CDH) events represent one of the most impactful forms of climate extremes, as their concurrent occurrence amplifies environmental and societal risks. This study investigates the spatiotemporal characteristics of CDH events across South Korea from 1973 to 2024 using a 3D connected components (CC3D) algorithm to identify contiguous events in space and time. CDH events were defined based on the overlap of drought and heatwave binary masks, and four key metrics—duration, frequency, projected area, and compound magnitude index (CDHMI)—were quantified. A total of 371 CDH events were detected, with most occurring in the central and southern regions. The majority were short-lived (mean duration: 3.8 days) and localized (median area: 927 km²), although occasional large-scale, long-duration events extended beyond 60,000 km². Seasonal analysis revealed a strong warm-season concentration, peaking in July and August, coinciding with monsoon withdrawal and intensified soil moisture–temperature feedbacks. Interannual variability showed substantial fluctuations, with a weak increasing trend of 0.195 events per decade. These findings highlight the episodic yet regionally concentrated nature of CDH events in South Korea and provide a framework for enhancing compound hazard monitoring, agricultural planning, and climate resilience under changing environmental conditions.

Keywords: Concurrent extremes, heatwave, drought,

1. Introduction

Compound climate extremes—particularly concurrent drought and heatwave (CDH) events—pose growing risks to ecosystems, agriculture, and water security under global warming (Zscheischler et al. 2018)(IPCC, 2021). When drought and heatwave conditions occur simultaneously, they interact through land–atmosphere feedback: soil moisture deficits enhance sensible heat flux, amplifying surface temperatures and reinforcing both extremes (Perkins and Alexander 2013). Such events often produce impacts greater than the sum of their individual effects, leading to crop losses, heat stress, and hydrological imbalance (Mukherjee et al. 2018).

East Asia, including the Korean Peninsula, is particularly vulnerable to CDH events due to strong monsoonal variability and teleconnections such as the El Niño–Southern Oscillation (ENSO) and Pacific Decadal Oscillation (PDO) (Mukherjee et al. 2020). South Korea's distinct wet–dry seasonal cycle, dominated by the East Asian summer monsoon, creates favorable conditions for CDH development during the warm, post-monsoon period (Krishnan et al. 2025). However, most regional studies have examined droughts and heatwaves separately, and few have explored their concurrent dynamics over multi-decadal scales.

This study addresses this gap by identifying and characterizing CDH events across South Korea from 1973–2024 using a 3D connected components (CC3D) algorithm. The objectives are to (1) detect concurrent drought–heatwave events through spatial–temporal clustering, (2) quantify their duration, frequency, spatial extent, and magnitude, and (3) examine long-term trends and seasonal patterns. By integrating drought and heatwave indices within a 3D analytical framework, this study provides new insights into the spatial heterogeneity and temporal evolution of compound extremes, supporting improved early-warning systems and climate adaptation strategies for the Korean Peninsula.

2. Materials and Methods

2.1. Compound extreme events identification

Concurrent drought and heatwave (CDH) events were defined as the simultaneous occurrence of both drought and heatwave on the same day and location. These were detected through the overlap of binary masks representing drought and heatwave states. The combined mask can be expressed mathematically as

$$CDH_{i,t} = \begin{cases} 1 & if\left(HW_i = 1 \cap D_{i,t} = 1\right) \\ 0 & otherwise \end{cases} \quad (3)$$

To identify distinct spatiotemporal CDH events, a 3D connected components (CC3D) labeling algorithm was applied. This algorithm groups contiguous grid cells across both spatial and temporal dimensions, allowing for the identification of independent CDH events following (Luo et al. 2022)

2.2. CDH event characterization

CDH events were characterized using four metrics: duration, frequency, projected area, and magnitude index. Duration is the number of days during which CDH persists, frequency is the count of distinct CDH events per year, projected area is the spatial extent of each CDH event on the Earth's surface, and magnitude index is the numerical measure of intensity or severity of an event. The magnitude index was calculated following the methodology outlined in (references)

3. Results and Discussion

3.1. Characteristics of CDH events

Using the CC3D algorithm, 371 CDH events were detected across South Korea from 1973 to 2024 (Figure 1a). Events were spatially concentrated in the central and southern regions, while fewer events occurred in the

mountainous northern regions. The CDH magnitude index (CDHMI) shows a strongly right-skewed distribution (Figure 1b), with most events exhibiting low-to-moderate magnitudes (CDHMI < 0.4). About 70% of all events fall below this threshold, suggesting that moderate concurrent extremes dominate South Korea's compound hazard landscape. The exponential decay pattern of CDHMI frequency mirrors findings in other East Asian regions, where weaker but frequent compound events outweigh extreme yet infrequent events (Kong et al. 2020; Fang et al. 2025).

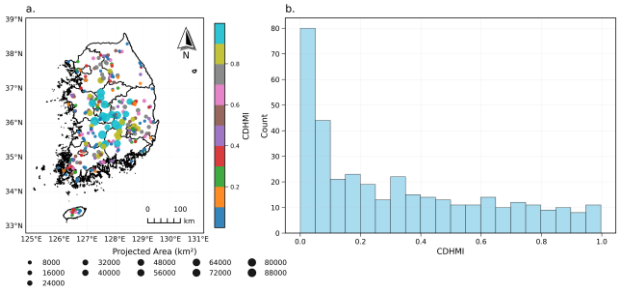

Figure 1. (a) Spatial distribution of the centroid of CDH events during 1973 – 2024, where the size and color of the dots represent the projected area and magnitude index of each event (b) Frequency distribution of CDH magnitude index

Most of the CDH events have short durations, with a median of 2.0 days and a mean of 3.8 days. About 60% of events lasted ≤ 3 days, consistent with transient atmospheric blocking and localized soil moisture deficits (Mukherjee et al. 2020). However, occasional long-duration events (up to 35 days) highlight episodes of persistent anticyclonic circulation and prolonged heat anomalies.

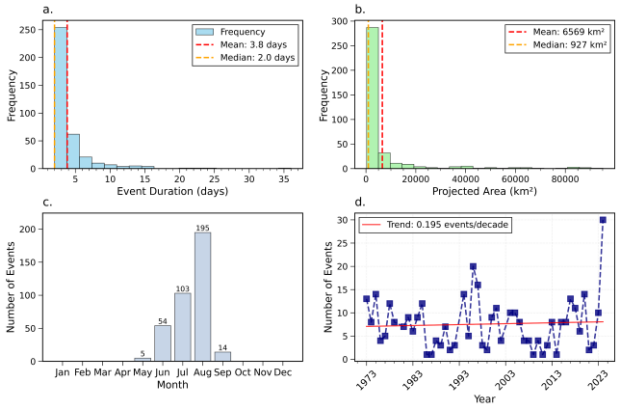

Figure 2. Characteristics of CDH events in South Korea during 1973-2024: Frequency distribution of (a) event duration, (b) projected area, (c) Monthly distribution of CDH events, and (d) Annual variation of CDH events

The projected area (Figure 2b) shows a mean of 6,569 km² and a median of 927 km², suggesting that while most events are localized, sporadic large-scale CDH events can impact extensive regions (> 60,000 km²). The events are pronounced during the summer season, peaking in August (155 events) and July (103 events). This pattern aligns with East Asia's post-monsoon period, characterized by strong solar radiation, limited rainfall, and soil desiccation (Pan et al. 2024). Interannual variability (Figure 2d) reveals pronounced year-to-year fluctuations, with annual event counts ranging from 5 to 30. A slight increasing trend (0.195 events per decade) is observed, though statistically weak.

4. Conclusions

This study provides a spatiotemporal assessment of concurrent drought and heatwave (CDH) events in South Korea (1973–2024) using an integrated CC3D approach. CDH events predominantly affect central and southern Korea, particularly agricultural regions. The majority of events last fewer than 4 days and cover less than 1,000 km². The highest frequencies occur during July–September, highlighting the role of monsoon withdrawal and soil moisture feedback. Despite global warming, the overall CDH frequency shows a marginal decrease, potentially due to enhanced atmospheric humidity and evolving monsoon dynamics. These findings emphasize the importance of compound event monitoring in regional climate adaptation strategies, particularly for agriculture and water resource management. The spatially heterogeneous but seasonally synchronized nature of CDH events suggests that integrated early warning systems combining hydrological and thermal stress indicators are critical for resilience planning in monsoon climates.

Acknowledgements

This work was supported by the National Research Foundation of Korea (NRF) grant funded by the Korea Government Ministry of Science and Information and Communication Technology (MSIT) (RS-2025-00562379).

References

Fang P, Wang T, Yang D, et al (2025) Substantial increases in compound climate extremes and associated socio-economic exposure across China under future climate change. NPJ Clim Atmos Sci 8:17. https://doi.org/10.1038/s41612-025-00910-7

Kong Q, Guerreiro SB, Blenkinsop S, et al (2020) Increases in summertime concurrent drought and heatwave in Eastern China. Weather Clim Extrem 28:100242. https://doi.org/10.1016/J.WACE.2019.100242

Krishnan R, Dhara C, Horinouchi T, et al (2025) Compound weather and climate extremes in the Asian region: science-informed recommendations for policy. Frontiers in Climate 6:1504475. https://doi.org/10.3389/fclim.2024.1504475

Luo M, Lau N, Liu Z, et al (2022) An Observational Investigation of Spatiotemporally Contiguous Heatwaves in China From a 3D Perspective. Geophys Res Lett 49:e2022GL097714. https://doi.org/10.1029/2022GL097714

Mukherjee S, Ashfaq M, Mishra AK (2020) Compound Drought and Heatwaves at a Global Scale: The Role of Natural Climate Variability-Associated Synoptic Patterns and Land-Surface Energy Budget Anomalies. Journal of Geophysical Research: Atmospheres 125:. https://doi.org/10.1029/2019JD031943

Mukherjee S, Mishra A, Trenberth KE (2018) Climate Change and Drought: a Perspective on Drought Indices. Curr Clim Change Rep 4:145–163. https://doi.org/10.1007/s40641-018-0098-x

Pan X, Wang W, Shao Q, et al (2024) Compound drought and heat waves variation and association with SST modes across China. Science of The Total Environment 907:167934. https://doi.org/10.1016/j.scitotenv.2023.167934

Perkins SE, Alexander L V. (2013) On the Measurement of Heat Waves. J Clim 26:4500–4517. https://doi.org/10.1175/JCLI-D-12-00383.1

Zscheischler J, Westra S, van den Hurk BJJM, et al (2018) Future climate risk from compound events. Nat Clim Chang 8:469–477. https://doi.org/10.1038/s41558-018-0156-3

This extended abstract template was updated on October 13, 2025

Water Scarcity Risk for Paddy Field Development Project in Pre-Modern Japan: Case Study of the Kinu-Kokai River Basin.

Adonis Russell Ekpelikpeze [1*], Atsushi Ishii [2], Yohei Asada [3]

[1] Graduate School of Life and Environmental sciences, University of Tsukuba, Ibaraki, Japan

[2] Faculty of Life and Environmental sciences, University of Tsukuba, Ibaraki, Japan

[3] Tokyo University of Agriculture and Technology, Tokyo, Japan

* Corresponding author. Email: aekpelikpeze@gmail.com

Abstract

Japanese water management for irrigation is a successful example of paddy field water governance. However, whether its successes are a product of the natural profusion of water or adequate management for water allocation is a matter of debate. This study investigates water scarcity risks for six irrigation schemes (Katsuriguchi, Sakagi, Ichinohori, Ooiguchi, Ezure, Kusakawa), chronologically developed in the pre-modern Kinu–Kokai River Basin (1603–1868), a period lacking large reservoirs, a canal system, and modern regulation technologies. Natural river flows were reconstructed using present-day discharge at the Sanuki headwork, adjusting the upstream dam impacts, canal efficiency, paddy field areas differences, and the return flow from drainage. The Japanese irrigation standard of 5 mm/day for minimum water requirements and 20 mm/day for easy management was applied as the water demand. Rainfall inputs, conveyance losses, and seasonal planting calendars were incorporated into approximate pre-modern conditions, while allocation followed priority rules based on the age of the scheme.

Results show that under high demand (20 mm/day), shortages occurred between 2/17 and 7/17 respectively for the fourth and the last irrigation schemes but were mitigated through intensive field-level management activities. For 5 mm/day, minimum evapotranspiration, shortages never followed, even during poor flow seasons, providing stable rice output without reliance on modern infrastructure. The findings suggest that pre-modern managers limited paddy growth to basins' hydrological capacity and applied coordinated allocation through Water User Associations (WUAs). It shows that adaptive governance and intense management, rather than hydrological abundance, facilitated Japanese irrigation's sustainability.

Keywords: Paddy field management, Pre-modern Japan, River flow reconstruction, Water scarcity risk.

1. Introduction

Japan's irrigation management is widely recognized as a successful case study in management systems. A key factor in this achievement has been Equitable Water Distribution (EWD) by Water User Associations (WUAs) that ensured fair allocation and collective maintenance. After World War II, irrigation infrastructures were improved through the development of multipurpose reservoirs and canal systems, reinforcing the perception that Japan's success derived from its abundant water resources. However, there are no records of damage during production during the pre-modern era (1603–1868), when large reservoirs, a modern canal system, and regulation were absent. Despite recurring droughts, rice productivity had not decreased severely, even during droughts, and several irrigation systems established at that time continue to sustain themselves till today.

This research aims to assess water scarcity risk in pre-modern Japan based on a case study of six irrigation systems in the Kinu–Kokai basin. Reconstruction of hydrologic conditions and water-demand/supply balance permits an examination of whether the irrigation achievements in Japan were founded upon natural water richness or upon flexible government administration, and how such a case can inform water-short areas in the contemporary world.

2. Materials and Methods

2.1. Materials

The materials used were hydrological data from the Ministry of Land, Infrastructure, Transport and Tourism (MLIT), for 17 years between 1952 and 1969. Dam inflow and outflow records were used to correct for modern storage impacts. Rainfall data were obtained from the Nikko AMeDAS station. Ministry of Agriculture, Forestry, and Fisheries (MAFF) and Land Improvement Districts (LIDs) have provided information about command areas, intake locations, and infrastructure characteristics. Field surveys were conducted in 2024, complemented by interviews to confirm land use patterns along with pre-modern water management practices.

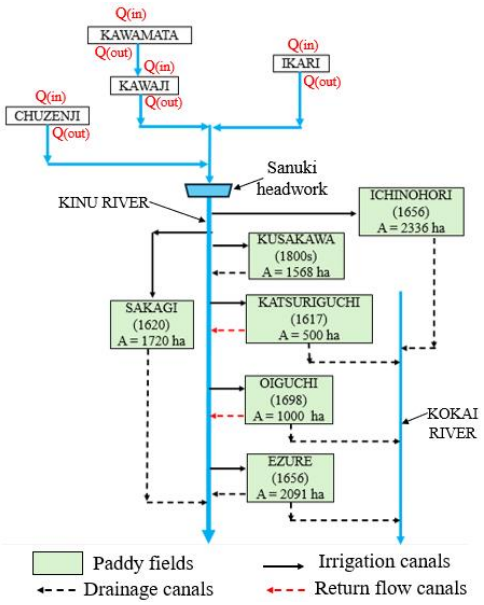

Figure 1. Irrigation schemes developed from 1617 to 1868 and reservoirs developed after WWII in Kinu river basin

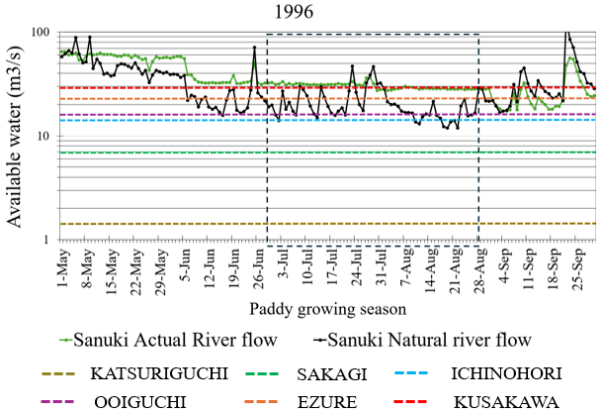

Figure 2. Water scarcity risk at 20 mm/d for 1996

2.2. Methods

Present-day discharge at the Sanuki headwork was used as the baseline for reconstructing natural flows. Adjustments removed the effects of four upstream dams, Ikari, Chu Zenji, Kawamata, and Kawaji, using the relation shown in Eq (1).

$$Q\ Natural\ flow = Q\ Sanuki - Q\ out(dams) + Qin(dams) \quad (1)$$

Canal efficiency was corrected by applying pre-modern conveyance loss rates of 30% compared with 15% in modern canals. Due to the absence of reservoirs in the pre-modern period, rice transplanting started in June, with scarcity risks in July and August, during the flowering and maturation phases. Water allocation followed the "First in Time, First in Right" principle, giving priority to older schemes, as well as the return flow from the Katsuriguchi and Ooiguchi schemes. Water demands for risk evaluation were based on the Japanese standard of irrigation at 5 mm/day, the minimum evapotranspiration for rice growth, and 20 mm/day, for easy water management activities. Rainfall was added directly to available river water, and ten consecutive days with less than 5mm/d considered to have damage on rice (Nougyou Suiri Kenkyukai, 1980).

3. Results and Discussion

Following the evaluation process described in the methodology, water scarcity risk was assessed over 17 years. Under a demand of 20 mm/day, scarcity occurred in 2/17 years from the third irrigation scheme (Ichinohori) and in 7/17 years for the last scheme (Kusakawa), indicating the need for intensive management activities (Fig. 2). In case of 10mm/d assuming the fact that in pre-modern water diversion infrastructure could take only half

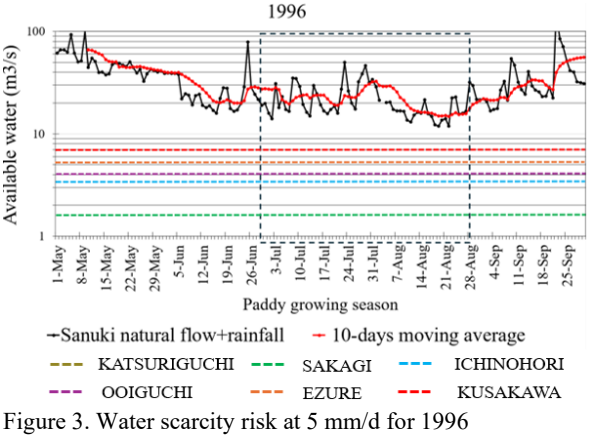

Figure 3. Water scarcity risk at 5 mm/d for 1996

Table 1. Water scarcity risk for paddy irrigation schemes

	KATUURI			SAKAGI			ICHINOHORI			OOIGUCHI			EZURE			KUSAKAWA		
	20 mm/d	10 mm/d	5 mm/d	20 mm/d	10 mm/d	5 mm/d	20 mm/d	10 mm/d	5 mm/d	20 mm/d	10 mm/d	5 mm/d	20 mm/d	10 mm/d	5 mm/d	20 mm/d	10 mm/d	5 mm/d
1956																		
1958							■			■			■			■	■	
1960							■			■			■			■	■	
1962																■		
1963													■			■		
1990							■			■	■		■	■		■	■	
1996													■			■		

■ Water scarcity risk

of the river water, the risk occurs 1/17 years from the fourth scheme (Ooiguchi) and 3/17 years for the last irrigation as shown in table1. With intensive management activity within the paddy field, the water scarcity risk has been reduced.

When demand was set at 5 mm/day, representing conditions under intensive management, no scarcity events were observed even during low-flow years, as shown in Figure 3.

Thus, there were no years with less than 5mm/d for ten consecutive days. It implies that there is no damage to rice production in the pre-modern Kinu River basin. The paddy fields area in the Kinu river basin has been developed within the extent of available water, suggesting a limited area expansion policy in pre-modern times.

In severe water conditions, intensive management activity through coordinated allocation mechanisms led by water user associations (WUAs) has been implemented to avoid the risk.

4. Conclusions

The evaluation of water scarcity in the pre-modern Kinu River Basin suggests that irrigation systems were operated within natural flow limits, with scarcity occurring in 7/17 years under high demand (20 mm/day) in downstream schemes but avoided through intensive field management.

At 5 mm/day, the minimum evapotranspiration, no shortages occurred even in low-flow years. This implies that rice cultivation was not damaged without the use of large reservoirs or an elaborate canal system. Past planners relied upon Water User Associations (WUAs) for water allocation. This shows that adaptive governance through intensive management activities has avoided water scarcity risk and has not depended upon abundant water supplies.

Acknowledgements

All the Land Improvement District (LID) officials, especially Ooiguchi and Ezure-hakkenbori LIDs for the facilitation of data collection, and the interviews.

References

Journal article:

Hamada, H., & Samad, M. (2011). Basic Principles for Sustainable Participatory Irrigation Management. Japan Agricultural Research Quarterly, 45(4), 371–376.

Satoh, M. and Ishii, A. 2021. Japanese irrigation management at the crossroads. Water Alternatives 14(2): 413-434.

Books.

Nougyou Suiri Kenkyukai. 1980. Nihon no Nougyou Yousui (in Japanese), Chikyusha, pp.29-39.

Shinzawa, K. 1978. Suiri no Kaihatsu to Chosei (in Japanese), Jichosha, pp.83-110, ,609-649.

Optimizing Irrigation Water Allocation in Sonosari Irrigation Area, Malang Regency Using Deterministic Dynamic Programming to Enhance Utilization Efficiency and Agricultural Profitability

Lufira Dara Rahmah・Limantara Montarcih Lily・Hamdany Ivan Muhammad

Abstract

Effective irrigation water management is essential to sustain agricultural productivity and food security in tropical regions. This study optimizes water allocation in the Sonosari Irrigation Area, Malang Regency, using deterministic dynamic programming. Covering about 800 hectares, the area faces seasonal water shortages and inefficient use. By analyzing secondary data on rainfall, discharge, climatology, and cropping patterns over ten years (2014-2023), an optimal multi-stage water distribution strategy was developed across key irrigation points. The model maximizes agricultural profit through efficient water use. Results show significant increases in irrigated land area and profitability compared to pre-optimization. This approach offers a practical decision tool for irrigation managers and policymakers promoting sustainable agricultural development. The findings contribute to improved water resource management and food security strategies in Indonesia.

A Preliminary Study on the Relationship between Tourism and Agriculture & Fishery

Takanori Nishino [1*], Takashi Wakabayashi [2]

[1] Institute of Current Business Studies, Showa Women's University, Setagaya, Tokyo, Japan

[2] Faculty of Agriculture, Shinshu University, Minamiminowa-Village, Kamiina-County, Nagano prefecture, Japan

* Corresponding author. Email: b10_t_nishino@swu.ac.jp

Abstract

The authors conducted a preliminary exploratory quantitative study of the relationship between tourism and agriculture and fisheries, reviewing previous studies to determine the extent to which quantitative empirical studies have been conducted. As a result, while sorting out issues such as insufficient data and the lack of a unified definition of "rural areas," which is one of the central concepts in this paper, the authors found that tourism have a particular impact on agriculture & fishery and that the relationship between tourism and agriculture & fishery has a certain degree of influence on the agricultural and fish areas. However, we were able to show that tourism has a particular impact on agriculture & fisheries by utilizing quantitative data obtained from the "Annual Report on Remote Islands Statistics" and other sources. The reason why we utilize "Annual Report on Remote Islands Statistics" is that we can make good use of data regarding tourism and agriculture & fisheries.

Keywords: tourism, agriculture, fishery, rural areas

1. Introduction

As inbound tourism to Japan continues to grow, regional policies are being promoted to ensure that tourism benefits not only tourist destinations but also brings economic gains to broader regions through the utilization of local resources, thereby further advancing regional development.

In Japan, the Tourism-based Country Promotion Basic Act was enacted in 2006, and the Japan Tourism Agency was established in 2008 to realize the vision of a tourism-based nation. The 2013 Japan Revitalization Strategy explicitly states the goal of increasing the number of foreign visitors to Japan and boosting employment through their consumption.

Furthermore, within the strategy's "Promotion of Sixth-Sector Industrialization through Agriculture-Commerce-Industry Collaboration," it promotes fostering exchanges between cities and rural areas through tourism collaboration.

In addition, this Japan Revitalization Strategy clearly states "ecotourism and green tourism" as part of "creating new tourism."

In 2014, the Ministry of Agriculture, Forestry and Fisheries and the Japan Tourism Agency signed a cooperation agreement to revitalize rural, mountainous, and fishing communities and realize Japan as a tourism-oriented nation.

Amidst this, tourism to rural areas is gaining greater attention than ever before from the perspective of promoting nationwide regional economic revitalization through tourism and exchange. Therefore, it is essential to accurately grasp the current state of tourism in agricultural and fishing villages and implement more reliable and effective measures. In government, promoting EBPM (Evidence-Based Policy-making) is crucial, and building future strategies by collecting data with the highest possible level of objectivity is of utmost importance.

Specifically, what are the effects of tourism on agriculture and fisheries—the core industries of rural and fishing communities—and how do tourism and these industries relate, or what mechanisms govern this relationship? How far has the foundational quantitative empirical research on these matters progressed? In fact, at present, these aspects are not fully understood, and their realization remains an ongoing challenge. One reason for this is that the definitions of "rural villages" and "fishing villages" are unclear. One reason for this is that the definitions of "farming villages" and "fishing villages" are unclear.

In addition, there are problems with the statistics. Specifically, it is impossible to determine from the statistics the number of tourists visiting small areas, which is a fundamental figure.

2. Materials and Methods

The effects of tourism on farming and fishing villages, particularly the impact of tourism on the agriculture & fisheries industries and the relationship between tourism and these industries, will be examined based on existing literature. First, we consider the effects of tourism on agriculture and fisheries within a relatively limited geographical area. While statistical data is often used to quantitatively assess these effects, such statistics are often underdeveloped, and figures illustrating the current state of tourism in farming and fishing villages are insufficient, resulting in few research findings based on numerical data. Japanese literature that has conducted quantitative analyses of tourism's effects on agriculture and fisheries includes Fujimoto (2000), Hirose (2001), and Fujimoto and Naito (2013). Provide sufficient details of the materials and methods to allow your work to be reproduced.

The use of input-output tables is a common analytical method that comprehensively measures the economic ripple effects within a specific region when a change occurs, and it also calculates the ripple effects on agriculture and fisheries. However, analysis using input-output tables also has several problems. While it is true that these estimates are based on certain assumptions and that separating agriculture and fisheries is difficult, fundamental issues exist. For example, input-output tables do not calculate figures by separating the sources of added value in the food service industry into those derived from tourism and those from other sources.

Next is the relationship between tourism and agriculture and fisheries. There are not many studies that discuss the relationship between tourism and agriculture and fisheries based on quantitative analysis.

Additionally, several studies exist concerning externalities, where measuring direct effects is difficult.

These research findings highlight several points regarding the relationship between tourism and agriculture/fisheries. First, when considering this relationship, it is necessary to account not only for positive effects but also for negative effects. Second, external economies must be taken into consideration. Third, it should be noted that no definitive consensus has been reached on the relationship between tourism and agriculture/fisheries, and there are points of contention with varying conclusions across different research outcomes.

Thus far, we have noted that while tourism to rural areas is gaining attention, rural and fishing villages remain undefined, fundamental statistical data on tourism within small-scale areas is unavailable, and literature quantitatively clarifying the relationship between rural areas and tourism—particularly agriculture and tourism—is limited. Given this current situation and a review of existing literature, the objective of this paper is to quantitatively confirm, based on fundamental data, the relationship between agriculture and tourism, and the connection between tourism/exchange and the agricultural/rural economy. More specifically, it aims to quantitatively clarify the extent to which the movement of people through tourism and exchange, along with the accompanying movement of goods and funds, and even the exchange of ideas, impacts the economy of so-called rural areas and the agriculture and fisheries industries—one of the main industries in these areas—and the economic effects this generates.

3. Results and Discussion

To conduct quantitative analysis from a nationwide perspective rather than through case studies of specific regions, a certain amount of comparable quantitative data for each region is required. The data set that overcomes this challenge is the "Statistical Yearbook of Remote Islands in Japan". The central hypothesis of this paper is that "the more active tourism and exchange are in a region (island), the more vibrant its rural economy becomes."

The analysis of variance indicates that the model is significant even at the 1% level, suggesting the regression equation can be used as a predictive model. Next, examining the significance probabilities of the coefficients, after adjusting using the variable reduction method, it was confirmed that Number of Primary Industry Workers in 2022, Number of Tourists in 2022, and Area of Natural Parks in 2022 were significant at the 1% level for Agricultural, Forestry, and Fisheries Production Value. Therefore, the slope of these regression coefficients is significantly non-zero. The regression equation is: and the 2022 natural park area as x_3, the regression equation can be expressed as "y = 3.833x_1 + 9.852x_2 - 12.417x_3 + 477.981". The goodness-of-fit of the regression equation is indicated by an adjusted R^2 value of 0.763, suggesting a reasonably high prediction accuracy. Furthermore, no particular issues regarding multicollinearity were observed.

Table 1

	Model 1		Model 2		Model 3	
Year 2022	Coefficient	Standard deviation	Coefficient	Standard deviation	Coefficient	Standard deviation
Number of Primary Industry Workers	3.778	0.363 ***	3.793	0.355 ***	3.823	0.354 ***
Number od tourists	9.233	5.883	10.568	2.997 ***	9.852	2.911 **
Area of natural parks	-12.858	3.274 ***	-12.624	3.124 ***	-12.417	3.117 ***
Working-Age Population Index	-29.620	29.003	-28.409	28.382		
Number of guests	1.707	6.452				
Constant	1,956.376	1,471.861	1,889.007	1,436.636	477.981	276.987 *
Adjusted R-squared	0.759		0.763		0.763	

*$p<0.1$, **$p<0.05$, ***$p<0.01$

Table 2

		Sum of squares	Degree of freedom	Mean square	F-number
Model 1	Regression	480,433,299	5	96,086,660	36.247 ***
	Residual	135,195,379	51	2,650,890	
	Total	615,628,678	56		
Model 2	Regression	480,247,814	4	120,061,953	46.116 ***
	Residual	135,380,864	52	2,603,478	
	Total	615,628,678	56		
Model 3	Regression	477,639,374	3	159,213,125	61.152 ***
	Residual	137,989,304	53	2,603,572	
	Total	615,628,678	56		

***$p<0.01$

4. Conclusions

We confirmed that the independent variables - "number of tourists," "number of primary industry workers," and "area of natural parks" - each exert positive or negative effects on the dependent variable "agricultural, forestry, and fisheries production value", with the latter exerting a greater impact on the dependent variable.

Acknowledgements

The authors thank the Institute of Current Business Studies, Showa Women's University, for financial support.

References

The Prime Minister's Office of Japan. https://www.kantei.go.jp/jp/singi/keizaisaisei/kettei.html, p83, Accessed on 25th May,2025

The Prime Minister's Office of Japan. https://www.kantei.go.jp/jp/singi/keizaisaisei/kettei.html p81, Accessed on 25th May,2025

Ministry of Agriculture, Forestry and Fisheries (2014): Agreement on Promoting Agricultural-Tourism Collaboration https://www.maff.go.jp/j/shokusan/sanki/pdf/kyoutei2.pdf Accessed on 15th November,2024

Cabinet Office (2018): Basic Policy on Economic and Fiscal Management and Reform https://www5.cao.go.jp/keizai-shimon/kaigi/cabinet/honebuto/2018/2018_basicpolicies_ja.pdf p68, Accessed on 25th May, 2025

Takashi FUJIMOTO,2000. Evaluation of Economic Impacts of Tourism in Mountainous Rural Experiment Station, Journal of Rural Problems Vol 140, p22-31

Makito HIROSE, 2001. Input-Output on Effect of Revenue from Tourism to Agriculture Sector, Journal of General Industrial Research,9, p157-172

Takashi FUJIMOTO & Shigeyuki NAITO, 2013. Distinctive Feature of Community Based Tourism and Its Territorial Economic Impact in Remote Islands: A Case Study in Ie Island, Okinawa, Japan, Journal of Osaka University of Economics, 64(1), pp.73-92

Factors Shaping Successful Participatory Irrigation Management in Vietnam: The Roles of Multi-Functional Cooperatives and the Public Sector

TRAN Hong Minh [1], ISHII Atsushi [2*], DOAN Doan Tuan [3], SHIN Moono [4], TRAN Viet Dung [3], ASADA Yohei [5], NGUYEN Duy Tien [3]

[1] Graduate School of Science and Technology, University of Tsukuba, Tsukuba, Ibaraki, Japan

[2] Faculty of Life and Environmental Sciences, University of Tsukuba, Tsukuba, Ibaraki, Japan

* Corresponding author. Email: ishii.atsushi.fu@u.tsukuba.ac.jp

[3] CPIM, Vietnam Academy for Water Resources, Hanoi, Vietnam

[4] Faculty of Food and Agricultural Sciences, Fukushima University, Fukushima, Japan

[5] Institute of Agriculture, Tokyo University of Agriculture and Technology, Tokyo, Japan

Abstract

This study examines motivations of upstream farmers to support equitable water distribution and identifies factors contributing to successful Participatory Irrigation Management (PIM) implementation through a case study in northern Vietnam. The research focuses on the Y2 Water Users Association (WUA), which manages the Y2 canal system serving 650 hectares of irrigated rice fields and supplies water to five Agricultural Cooperatives (AC or Coop). Prior to 2013, the public sector - Irrigation Management Company (IMC) centrally allocated water to each AC through 28 division points, restricting local negotiation. After the Y2 WUA was established, irrigation management shifted to PIM model. Field surveys conducted in September 2023 and April 2024, along with interviews with WUA representatives, IMC staff, and farmers, examined changes in water distribution and satisfaction before and after this transition.

Findings show that Y2 WUA introduced fixed seasonal schedules, flexible allocation negotiations, and a "downstream priority" mechanism, resulting in a 30% improvement in water access for downstream farmers. Multifunctional ACs—especially AC 3, which applies internal zoning—played a key role in encouraging upstream farmers to cooperate in equitable sharing. Furthermore, a formal agreement between IMC and Y2 WUA institutionalizes collaborative governance, outlining shared responsibilities in system operation and maintenance. These findings provide practical insights for scaling PIM in Vietnam and comparable settings.

Keywords: Participatory Irrigation Management, Agricultural Cooperatives, Equitable Water Distribution.

1. Introduction

PIM has been promoted worldwide to improve equity, efficiency, and sustainability in irrigation systems by enhancing farmers' involvement in decision-making and operation (Satoh, M. and Ishii, A., 2021). Yet, successful cases remain limited in developing countries. In Vietnam, PIM has been promoted by the government since the 1980s (MARD, 2020), but it differs from many international models in two key respects: (1) irrigation management is jointly conducted by public water management organizations and farmers' organizations, and (2) farmer irrigation organizations take the form of AC with multifaceted functions. Despite their importance, these functions have been insufficiently analyzed. This study examines a model PIM district in Vietnam to clarify how these two features shape irrigation management and their implications for system performance.

2. Materials and Methods

2.1. Study Site and Materials:

This study was conducted in the Y2 secondary canal of the Cau Son–Cam Son irrigation scheme, Bac Giang Province, northern Vietnam. Managed by the Bac Song Thuong IMC, the scheme irrigates about 12,000 ha of rice per season. The Y2 canal, 10 km long with 28 division points, serves 650 ha and 3,500 households. Since 2013, its management has been delegated to the Y2 WUA under a World Bank–supported project.

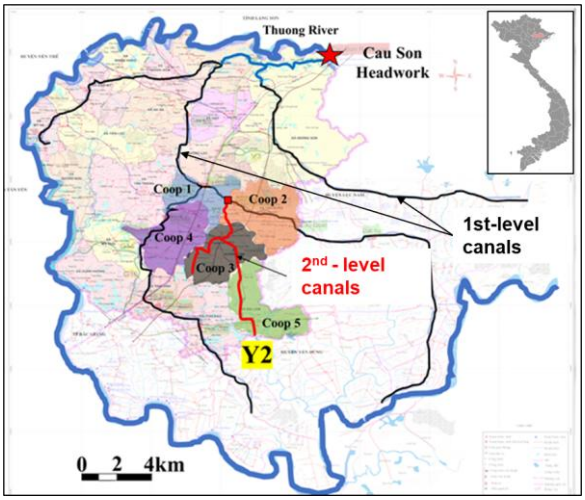

Figure 1. Y2 – canal system in Cau Son – Cam Son scheme.

The Y2 WUA functions as a meta-organization linking five ACs (Figure 1). While these ACs were originally collective production units, they have since expanded into multifunctional institutions. Each AC manages tertiary canals, coordinates cropping calendars, prepares seasonal irrigation plans, and collects on-farm irrigation fees to cover operation and maintenance. Beyond irrigation, ACs also distribute inputs, rent equipment, sell fertilizers, and provide community services. This multifunctional role enables ACs to mobilize resources, maintain leadership legitimacy, and embed irrigation governance within broader rural socio-economic development.

Data sources combined primary and secondary materials. Primary data included interviews with WUA leaders, AC representatives, and IMC staff, as well as field observations and financial records. Secondary data

comprised irrigation schedules, canal maps, and government regulations.

2.2. Methods:

Field surveys in September 2023 and March 2024 employed semi-structured interviews and document review. Analysis focused on (i) contributions of ACs and IMC to equitable water distribution (EWD) and (ii) upstream farmers' motivations to engage in collective water sharing. Triangulation across interviews, records, and field observations ensured validity.

3. Results

3.1. Equitable Water Distribution through ACs:

To enhance equity in water distribution, the Y2 system adopted rotational irrigation, alternating water access between upstream and downstream areas across day and night. A notable innovation within this arrangement is the practice of downstream priority, which grants cooperatives at the tail end of the canal extended nighttime access of up to 14.5 hours. This flexible scheduling ensures that all farms—regardless of location along the canal—have a fair opportunity to receive irrigation water. However, the effectiveness of rotational irrigation depends strongly on the role of ACs, which support the WUA in both technical water allocation and farmer mobilization. Among them, AC 3 is particularly significant, covering nearly 70% of the Y2 service area. Internally, AC 3 is subdivided into upstream and downstream groups, a structure that fosters cooperation by aligning farmers' interests under shared membership (Figure 2). As a result, upstream farmers accept rotational schedules that prioritize longer nighttime deliveries to downstream users. This arrangement illustrates how ACs leverage their multifunctional roles and embedded social capital to reinforce both equity and collective responsibility. Beyond irrigation management, ACs also coordinate agricultural production and provide community services, making them indispensable partners of the WUA.

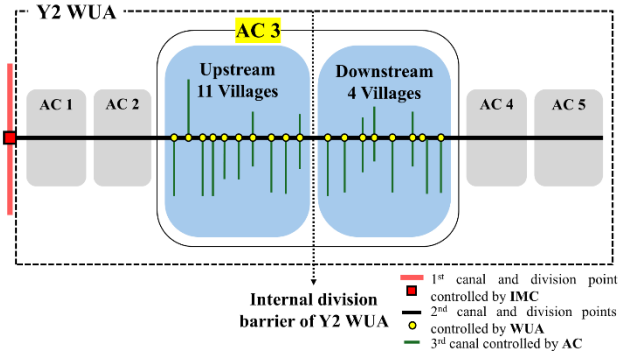

Figure 2. Conceptual map of Y2-canal system.

3.2. Continuous Support Role of IMC:

Despite strong local capacity, the Bac Song Thuong IMC remains central to system functioning. Responsible for the headworks, main canals, and first-level canals, the IMC provides the financial, technical, and institutional backbone for WUA operations. Seasonal contracts specify water delivery and O&M responsibilities. Following Decree 115 (2008), irrigation charges were waived nationwide and replaced with government subsidies for agricultural land and water use. After the transfer of irrigation management in the Y2 canal, only 12% of the subsidy was allocated to the Y2 WUA for secondary canal management, while 88% remained with the IMC. As noted by the WUA director, without this allocation the organization would be unable to cover canal cleaning, staff wages, or operational costs.

4. Discussion

In Vietnam, PIM facilitates the implementation of EWD in 2nd-level canals through flexible management practices and frequent farmer-to-farmer negotiation, while minimizing labor input requirements (Tran et al., 2025). The Y2 experience underscores the hybrid nature of irrigation governance in Vietnam. ACs provide legitimacy, organizational flexibility, and capacity to implement EWD, while the IMC ensures technical reliability, financial flow, and institutional authority. This dual arrangement creates strengths in responsiveness and participation but also weaknesses in long-term financial sustainability (Nguyen, T. D., and Le, M. H., 2018). The case suggests that the success of PIM in Vietnam depends not on full transfer of responsibility to farmers, but on strengthening partnerships between ACs and the IMC. Policy reforms should increase subsidy shares for WUAs, encourage more consistent ISF collection through AC structures, and clarify role delineations. Recognizing the multifunctional role of ACs while maintaining strong IMC support offers a pathway toward sustainable irrigation governance in large-scale paddy systems.

5. Conclusions

This study highlights that PIM in Vietnam functions most effectively as a co-management system in which multi-functional ACs and IMC assume complementary roles. ACs integrate irrigation with agricultural and community services, thereby mobilizing collective action and enhancing equity in water distribution. Meanwhile, the IMC provides essential public-sector support through subsidies, technical expertise, and institutional authority. Strengthening this dual structure—via more equitable subsidy allocation, improved irrigation service fee mechanisms, and clearer role delineation—offers a pathway toward sustainable and equitable irrigation governance in large-scale paddy systems.

Acknowledgements

This work was supported by JSPS KAKENHI Grant Numbers 25K09323.

References

Satoh, M., & Ishii, A. (2021). Japanese Irrigation Management at the Crossroads. Water Alternatives, 413-434.

Ministry of Agriculture and Rural Development (MARD). (2020). Irrigation and Agricultural Development in Vietnam.

Nguyen, T. D., & Le, M. H. (2018). Challenges and Opportunities in Vietnam's Irrigation Management. Asian Journal of Agriculture.

Tran, H. M., Ishii, A., Doan, D. T., & Moono, … (2024, October 23–25). Comparative study on joint irrigation management and farmer participatory irrigation management in Vietnam. Paper presented at the 2024 Conference of the International Society of Paddy and Water Environment Engineering (PAWEES), [Taiwan].

Functions and structures of Water User Associations (WUAs) in Egypt: A Focus on New Valley Governorate

El Gwely Samir・Iwasaki Erina・Sugiura Mikiko

Abstract

This presentation explores the role and impact of Water Users Associations (WUAs) in the New Valley Governorate, Egypt. Water scarcity and inefficient water management are critical challenges in the oasis society, affecting agricultural productivity and local livelihoods. The presentation will examine the structure, functions, and effectiveness of WUAs in the New Valley, with comparison with the WUAs in the Nile valley. Both WUAs are same in functions, but different in the water resource they depend upon, groundwater and Nile water. Additionally, it will discuss the potential for scaling up WUA initiatives to improve water management practices, support community empowerment, and achieve sustainable development goals in the region.

Development of a Drought Monitoring Method Using Multiple Vegetation Indices Derived from PlanetScope Imagery

Hyeok-Jae Choi[1], Won-Ho Nam[2*], Min-Gi Jeon[3], Min-Kyu Moon[4], Eun-Mi Hong[5], Jeong-Hwan Park[6]

[1] Graduate Student, School of Social Safety and Systems Engineering, Hankyong National University, Anseong, Republic of Korea

[2] Professor, School of Social Safety and Systems Engineering, National Agricultural Water Research Center, Hankyong National University, Anseong, Republic of Korea

[3] Associate Researcher, National Agricultural Water Research Center, Hankyong National University, Republic of Korea

[4] Assistant Professor, Department of Environmental Science, Kangwon National University, Republic of Korea

[5] Associate Professor, Department of Environmental Science, Kangwon National University, Republic of Korea

[6] Support Scientist, Hydrological Science Laboratory, NASA Goddard Space Flight Center, United States of America

* Corresponding author. Email: wonho.nam@hknu.ac.kr

Abstract

In recent years, the frequency and severity of droughts have increased due to climate change, causing significant agricultural losses. Effective monitoring is therefore required to assess drought impacts on farmland, particularly in regions dependent on rainfall. This study investigates the applicability of high-resolution PlanetScope imagery for agricultural drought monitoring in Korea. PlanetScope provides near-daily imagery at ~3 m spatial resolution, enabling the monitoring of small-scale fields. Four vegetation indices—Normalized Difference Vegetation Index (NDVI), Two-band Enhanced Vegetation Index (EVI2), Green Normalized Difference Vegetation Index (GNDVI), and Soil-Adjusted Vegetation Index (SAVI)—were derived from PlanetScope imagery for the year 2018. These indices were standardized using the Vegetation Condition Index (VCI) and Standardized Vegetation Index (SVI) to analyze drought response timing and lag periods. Validation was conducted by comparing PlanetScope-derived indices with Moderate Resolution Imaging Spectroradiometer (MODIS) data collected during the same period. The results showed that NDVI, EVI2, and SAVI exhibited high consistency with MODIS ($R^2 > 0.8$), while GNDVI displayed lower agreement. All indices responded with a lag of approximately 64–70 days after the drought period. These findings demonstrate that PlanetScope imagery provides strong potential for localized agricultural drought monitoring and can contribute to more accurate and timely drought management strategies.

Keywords: agricultural drought, Drought monitoring, Vegetation index, PlanetScope

1. Introduction

In Korea, the frequency of droughts has increased due to climate change, and rainfed farmland is particularly vulnerable because of insufficient irrigation infrastructure. Conventional meteorological indices rely on station data and spatial interpolation, which limit their ability to capture localized drought impacts. Therefore, this study aims to evaluate the applicability of PlanetScope-derived vegetation indices for agricultural drought monitoring.

2. Materials and Methods

The study area is Changnyeong County, Gyeongsangnam-do, where paddy and field boundaries were extracted using farm map data. PlanetScope imagery provides ~3 m spatial resolution with four bands (Red, Green, Blue, NIR) and was acquired from January to December 2018. Four vegetation indices—NDVI, EVI2, GNDVI, and SAVI—were calculated. These indices were standardized using VCI (Vegetation Condition Index) and SVI (Standardized Vegetation Index) to analyze drought response timing and lag days. Validation was performed by comparing PlanetScope-derived indices with MODIS indices collected during the same period. VCI and SVI are widely applied indices for evaluating drought intensity, duration, and spatial distribution (Singh et al., 2003; Quiring et al., 2010; Eyoh et al., 2019). SVI is derived from the conventional Z-score but removes seasonal components, thereby detecting abnormal vegetation responses independent of seasonality (Peters et al., 2002). The drought classification criteria applied in this study are presented in Table 1.

Table 1. Classification criteria of drought based on VCI and SVI.

Index	Range	Description
VCI	$\geq 50\%$	No drought
	$35\% \sim 50\%$	Low drought
	$< 35\%$	Severe drought
SVI	< -1	Agricultural drought

3. Results and Discussion

3.1. Validation with MODIS

Comparisons between PlanetScope and MODIS indices showed that NDVI, EVI2, and SAVI achieved high coefficients of determination ($R^2 > 0.8$), while GNDVI showed a lower value ($R^2 = 0.59$). This was attributed to differences in the green band reflectance.

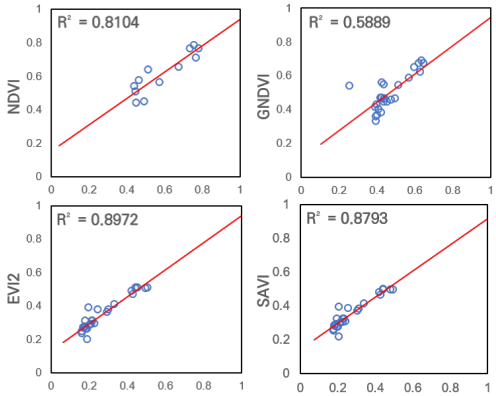

Figure 1. Regression results between PlanetScope and MODIS indices (NDVI, EVI2, GNDVI, SAVI).

3.2. Analysis of vegetation response to drought

The vegetation indices responded with a lag of approx

imately 64–70 days after the end of the 2018 drought. GNDVI showed the earliest response at 64 days, while NDVI, EVI2, and SAVI exhibited responses around 70 days. The relatively faster response of GNDVI can be attributed to its sensitivity associated with the green band reflectance.

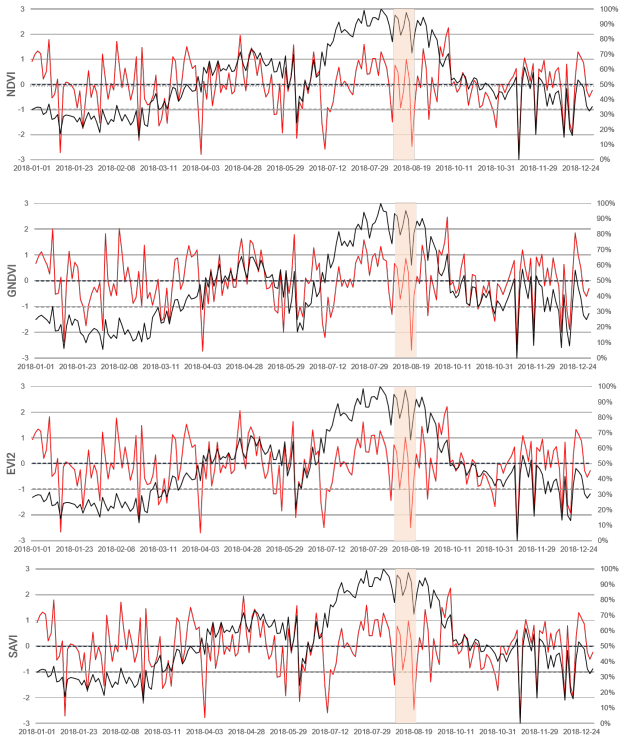

Figure 2. Drought response timing of individual vegetation indices (NDVI, GNDVI, EVI2, SAVI)

3.3. Applicability for Agricultural Drought Monitoring

The analysis confirmed consistent lagged response patterns across all indices, suggesting that PlanetScope imagery can be effectively applied for localized agricultural drought monitoring in Korea.

Table 2. Drought response timing of vegetation indices.

Indexs	First Response Date	Delay (days)
NDVI	2018-08-13	70
EVI2	2018-08-13	70
GNDVI	2018-08-13	64
SAVI	2018-08-13	70

3.4. Comparison with SPI and SPEI

To evaluate the applicability of vegetation indices for domestic drought monitoring, PlanetScope-derived indices were compared with climate-based indices, namely the Standardized Precipitation Index (SPI) and the Standardized Precipitation Evapotranspiration Index (SPEI). SPI is widely used to detect meteorological droughts based on precipitation, while SPEI incorporates both precipitation and potential evapotranspiration, thereby reflecting temperature effects. By comparing vegetation indices with SPI and SPEI, this study assessed their potential as reliable indicators for agricultural drought monitoring in Korea, highlighting their role as complementary tools to conventional climate-based indices.

4. Conclusions

This study validated the applicability of PlanetScope-derived vegetation indices for agricultural drought monitoring in Korea. The analysis demonstrated that NDVI, EVI2, SAVI, and GNDVI all exhibited consistent lagged responses of approximately 64–70 days following the 2018 drought period, with GNDVI showing a slightly earlier response due to its sensitivity to the green band reflectance. These results confirm that high-resolution PlanetScope imagery can effectively capture localized drought dynamics that are often overlooked by coarse-resolution satellite data. The validation against MODIS further highlighted the reliability of PlanetScope-based indices, with NDVI, EVI2, and SAVI showing strong correlations ($R^2 > 0.8$). The findings suggest that PlanetScope imagery has considerable potential for advancing localized drought monitoring frameworks in agricultural systems. However, the current analysis was limited to a single-year dataset. To strengthen the robustness of the approach, future research will incorporate multi-year datasets to capture interannual variability. Additionally, integrating meteorological indices such as SPI (Standardized Precipitation Index) and soil moisture datasets will allow for a more comprehensive assessment of drought conditions. Comparative analysis between vegetation indices (VCI, SVI) and climate-based indices (SPI, SPEI) will also provide deeper insights into drought onset, intensity, and recovery. Ultimately, these extensions will contribute to the development of a more reliable and practical drought monitoring framework, supporting timely decision-making and improved agricultural water management strategies in Korea.

Acknowledgements

This work is supported by the Korea Agency for Infrastructure Technology Advancement (KAIA) grant funded by the Ministry of Land, Infrastructure and Transport (Grant RS-2022-00155763).

References

Eyoh, A., Okeke, F., and Ekpa, A. 2019. Assessment of the effectiveness of the Vegetation Condition Index (VCI) as an indicator for monitoring drought condition across the Niger Delta region of Nigeria using AVHRR/MODIS NDVI. *European Journal of Earth and Environment*, 6(1), 12–17.

Ji, L., Peters, A.J., Walter-Shea, E.A., Vina, A., Hayes, M.J., and Sviatkovskii, V. 2002. Drought monitoring with NDVI-based standardized vegetation index. *Photogrammetric Engineering & Remote Sensing*, 68(1), 71–75.

Quiring, S.M., and Ganesh, S. 2010. Evaluating the utility of the Vegetation Condition Index (VCI) for monitoring meteorological drought in Texas. *Agricultural and Forest Meteorology*, 150(3), 330–339.

Singh, R.P., Roy, S., and Kogan, F. 2003. Vegetation and temperature condition indices from NOAA AVHRR data for drought monitoring over India. *International Journal of Remote Sensing*, 24(22), 4393–4402.

Comparative Assessment of CHIRPS v2.0 and v3.0 for Satellite-Based Agricultural Drought Monitoring in South Korea

Young-Sik Mun [1], Won-Ho Nam [2*]

[1] Ph.D Student, Department Integrated System Engineering, Hankyong National University, Anseong, Republic of Korea

[2] Professor, School of Social Safety and Systems Engineering, National Agricultural Water Research Center, Hankyong National University, Anseong, Republic of Korea

* Corresponding author. Email: wonho.nam@hknu.ac.kr

Abstract

Satellite-based precipitation datasets are vital alternatives to ground observations for drought monitoring. This study evaluated five widely used satellite precipitation products Climate Hazards Group InfraRed Precipitation with Station data version 2.0 (CHIRPS v2.0), CHIRPS v3.0, Precipitation Estimation from Remotely Sensed Information using Artificial Neural Networks Climate Data Record (PERSIANN-CDR), PERSIANN Cloud Classification System (PERSIANN-CCS), and Climate Prediction Center Morphing technique (CMORPH) against 56 Automated Synoptic Observation Stations in South Korea for the 2010–2023 period. Evaluation combined qualitative pattern analyses with quantitative metrics including Pearson correlation coefficient, Root Mean Squared Error (RMSE), Mean Absolute Error (MAE), Mean Bias Error (MBE), and Kling-Gupta Efficiency (KGE), supported by statistical significance tests. Results showed that CHIRPS v3.0 most reliably reproduced precipitation variability, while PERSIANN-CCS displayed severe underestimation. Based on the optimal dataset, drought indices were calculated the Standardized Precipitation Index (SPI), the Standardized Precipitation Evapotranspiration Index (SPEI), and the Soil Moisture Index (SMI) to analyze abnormal droughts across South Korea from 2014 to 2023. Short-term indices effectively captured rapid fluctuations and localized droughts, while long-term indices and SMI reflected cumulative water deficits. Integrating satellite precipitation with multi-index drought analysis provides a robust framework for understanding spatiotemporal drought variability in South Korea and offers practical insights for agricultural drought monitoring and early warning.

Keywords: drought monitoring, satellite-based precipitation data, drought indices, CHIRPS, South Korea

1. Introduction

Drought is one of the most critical hazards affecting agriculture and water resources in South Korea, where irregular rainfall and climate variability have intensified in recent decades (Bae et al., 2019). Accurate precipitation data are essential for monitoring drought, yet station networks remain limited in spatial coverage and fail to capture localized extremes. Satellite-based precipitation products (SPPs) provide consistent, long-term datasets and can complement ground observations, but their applicability under Korean conditions has been insufficiently evaluated (Ji et al., 2022). This study therefore aims to assess multiple SPPs through comparison with ASOS data, identify the most suitable dataset, and apply it to compute SPI, SPEI, and SMI for analyzing abnormal drought characteristics nationwide.

2. Materials and Methods

This study was conducted in three steps: (1) collecting long-term satellite and station precipitation data, (2) evaluating the reproducibility of satellite products against ground observations, and (3) applying the optimal dataset to derive drought indices and analyze abnormal drought characteristics.

2.1. Data collection

Five satellite precipitation products CHIRPS v2.0, CHIRPS v3.0, PERSIANN-CDR, PERSIANN-CCS, and CMORPH were compiled for 1995–2024. Ground-based precipitation from 56 ASOS was used as reference data. For intercomparison, monthly precipitation was analyzed during 2010–2023, while drought indices were derived for 2014–2023 using the optimal dataset (Funk et al., 2015).

2.2. Validation of satellite precipitation

Satellite precipitation estimates were compared with ASOS observations using both qualitative and quantitative approaches. Time series and spatial distribution patterns were visually examined to evaluate general agreement. Quantitative performance was assessed using correlation coefficient (r), RMSE, MAE, MBE, and KGE. In addition, statistical significance among datasets was tested with the Friedman test followed by the Nemenyi post-hoc analysis.

2.3. Drought index analysis

Grid-based drought indices were calculated using CHIRPS v3.0 precipitation combined with TerraClimate data. SPI and SPEI were derived using precipitation and PET, while SMI was calculated from soil moisture fields. All indices were computed at 5 km resolution. Abnormal droughts were defined when index values were below –1.5, and their frequency, duration, and intensity were analyzed nationwide for 2014–2023.

3. Results and Discussion

3.1. Satellite precipitation evaluation

Figure 1 and Table 1 compare observed and satellite-based precipitation. For the common evaluation period of 2010–2023, CHIRPS v3.0 showed the best agreement with ASOS data, while CHIRPS v2.0 had slightly lower correlations but the smallest bias. PERSIANN-CDR and CMORPH captured general variability but underestimated heavy rainfall, and PERSIANN-CCS performed worst. Overall, CHIRPS v3.0 was identified as the most reliable dataset for drought index analysis in South Korea.

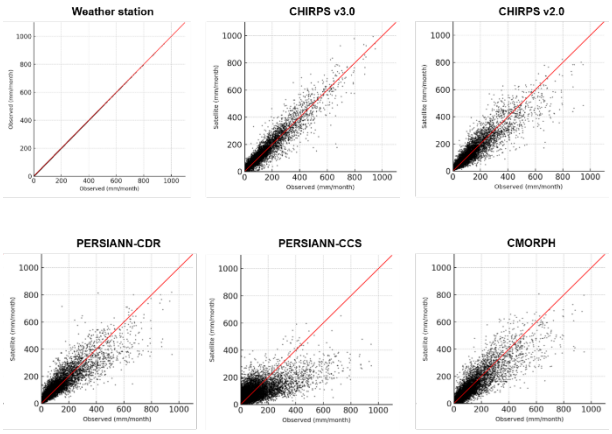

Figure 1. Scatterplot comparison of monthly precipitation

Table 1. Performance comparison of satellite precipitation datasets

Dataset	R	RMSE (mm)	MAE (mm)	MBE (mm)	KGE
v3.0	0.96	30	20	+4	0.93
v2.0	0.94	37	24	-2	0.88
CDR	0.90	47	31	+10	0.80
CCS	0.62	98	63	-20	0.35
CMORPH	0.88	50	32	-6	0.77

3.2. Grid-based drought indices

Figure 2 presents SPI3, SPI6, SPEI3, SPEI6, and SMI for August 2022, when contrasting hydrological conditions were observed. SPI largely detected the typhoon-driven wetness in central Korea and therefore indicated near-normal or wet conditions nationwide, failing to capture the persistent drought across the southern provinces. SPEI provided a more balanced picture: wet anomalies in the central region and severe drought signals in the south, where evapotranspiration demand remained high. SMI emphasized agricultural drought, showing concentrated soil moisture deficits in Jeolla and southern coastal areas, while not reflecting the temporary central wetness. These patterns show that SPI can misrepresent drought under localized rainfall, while SPEI and SMI better capture the contrast between central wetness and southern drought.

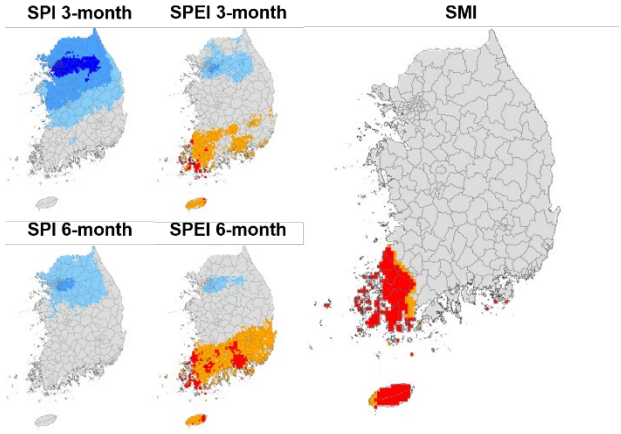

Figure 2. Spatial patterns of SPI, SPEI, and SMI in August 2022

3.3. Abnormal drought analysis

Table 2 summarizes the frequency, duration, and intensity of abnormal drought events during 2014–2023. Short-term indices such as SPI3 (3.8%, 1.36 months) and SPI6 (4.4%, 1.50 months) showed relatively low frequencies and short persistence, often missing prolonged stress. In contrast, SPEI3 (8.6%, 1.41 months) and SPEI6 (8.8%, 2.16 months) recorded nearly double the frequency of SPI, with SPEI6 indicating the longest duration, reflecting the impact of evapotranspiration. SMI (6.3%, 1.63 months) displayed intermediate frequency but highlighted persistent soil moisture deficits in southern regions. These results suggest that SPI alone underestimates abnormal drought, whereas SPEI and SMI provide more sensitive and realistic assessments for South Korea.

Table 2. Abnormal drought characteristics in South Korea (2014-2023, threshold -1.5)

Index	Frequency (%)	Duration (months)	Intensity (mean)
SPI3	3.8	1.36	0.42
SPI6	4.4	1.50	0.47
SPEI3	8.6	1.41	0.52
SPEI6	8.8	2.16	0.50
SMI	6.3	1.63	0.49

4. Conclusions

This study evaluated multiple satellite precipitation products against ASOS observations and identified CHIRPS v3.0 as the most reliable dataset for South Korea. Using this dataset, grid-based drought indices (SPI, SPEI, and SMI) were derived to examine abnormal drought characteristics from 2014 to 2023. Results showed that SPI often underestimated drought during localized heavy rainfall events, while SPEI and SMI more effectively captured both meteorological and agricultural drought conditions. These findings highlight the necessity of combining multiple indices for accurate drought monitoring and provide practical implications for strengthening agricultural drought early warning systems.

Acknowledgements

This work was supported by Korea Environment Industry & Technology Institute (KEITI) through Water Management Program for Drought Project, funded by Korea Ministry of Environment (MOE) (RS-2023-00230286).

References

Bae, H., Ji, H., Lim, Y.J., Ryu, Y., Kim, M.H., and Kim, B.J., 2019. Characteristics of drought propagation in South Korea: relationship between meteorological, agricultural, and hydrological droughts. *Natural Hazards,* 99, 1-16.

Ji, H., Peng, D., Gu, Y., Liang, Y., and Luo, X., 2022. Evaluation of multiple satellite precipitation products and their potential utilities in the Yarlung Zangbo River Basin. Scientific Reports, 12, 13334.

Funk, C., Peterson, P., Landsfeld, M., Pedreros, D., Verdin, J., Shukla, S., Husak, G., Rowland, J., Harrison, L., Hoell, A., and Michaelsen, J., 2015. The climate hazards infrared precipitation with stations—a new environmental record for monitoring extremes. Scientific Data, 2, 150066.

Parcel-Level Crop Classification from Structured SITS Features and Clustering Based Analysis

Jaejun Gou[1], Seongju Jang[1], Jinseok Park[1], Hyeokjin Lee[1], Inhong Song[1*]

1 Department of Rural Systems Engineering, Seoul National University, Seoul 08826, Korea
* Corresponding author. Email: inhongs@snu.ac.kr

Abstract

Low resolution of satellite data is one of the key challenges in satellite-based crop type mapping, especially in South Korea which has small field size. The objective of this study is developing a framework of accurate crop type classification using Sentinel-2 data for areas with small parcel sizes.

For this purpose, a satellite image time-series (SITS) was constructed for each parcel in the study area of Namhae-gun, South Korea. We systematically evaluated a diverse range of models, including tree-based ensembles (Random Forest and XGBoost), one-dimensional Convolutional Neural Network (1D-CNN) architectures, and more complex Transformer-based approaches. The 1D-CNN models were tested with and without a Convolutional Block Attention Module (CBAM) to assess the impact of attention. Model performance was rigorously assessed using Overall Accuracy (OA) and the Cohen's Kappa coefficient (κ) to account for class imbalance.

Our results demonstrated that the XGBoost model achieved the highest performance, with an OA of 0.7275 and a Kappa of 0.6749. Among the deep learning approaches, the simpler 1D-CNN models, particularly CBAM+MLP, consistently outperformed the more complex Transformer-based architectures. This suggests that for the structured, tabular SITS data used in this study, the complexity of Transformer models likely led to overfitting, whereas the tree-based ensembles and more constrained CNN architectures proved more robust.

The findings from this study highlight the potential of satellite-based approaches for accurate crop type mapping in small-field agricultural regions, offering a scalable and cost-effective alternative to high-resolution imagery

Keywords: Sentinel-2, Machine learning, Deep learning, Crop classification

1. Introduction

Crop type classification is essential for food security and agricultural policy, and Sentinel-2 Satellite Image Time Series (SITS) data is an effective tool as it captures the phenological stages of crop growth (Franch et al., 2015). However, in regions with small agricultural parcels, such as South Korea (KOSTAT., 2025), the 10m spatial resolution of Sentinel-2 presents a major challenge, as mixed pixels and edge effects degrade classification accuracy. A practical solution to mitigate this issue is a parcel-based approach that aggregates pixels to create structured data, thereby improving computational efficiency and classification stability.

This structured, parcel-based data allows for the application of not only traditional machine learning models like decision trees but also modern deep learning architectures like CNNs and Transformers, which treat the data as an image (Yıldız & Kalayci, 2025). However, there is a lack of research that systematically compares the performance of these diverse models for areas with small, irregularly shaped parcels like Korea. Furthermore, the use of post-hoc analysis techniques, such as k-means clustering for model interpretation, combined with agricultural and phenological analysis, remains largely unexplored in this context.

The objective of this study is to develop parcel-level crop classification framework, analyze the agricultural and phenotypic similarity using clustering algorithm, and reclassify with pseudo labels.

2. Materials and Methods

2.1. Study area

This study selected four research areas—Naju-si, Namhae-gun, Uiseong-gun, and Yeongcheon-gun—which exhibit diverse geographical and climatic characteristics, including plains, an island, and mountainous terrain.

2.2. Dataset

This research defined parcel boundaries using the farm map dataset from MAFRA, which is based on actual cultivation status, and used a drone imagery-based dataset from MSIT (2021-2022) for ground truth crop labels. To mitigate data imbalance, the initial set of crops was filtered to a final selection of 20 distinct classes.

The input data, consisting of mean spectral reflectance time-series for each parcel, was split into training, validation, and test sets at a 6:2:2 ratio. To prevent overfitting and balance the training data, all classes were adjusted to 2,000 samples by downsampling larger classes and augmenting smaller ones. The augmentation technique involved removing 5% of the temporal data points and reconstructing them with linear interpolation to simulate data loss from cloud cover.

2.3. Models

For our analysis, we compared a range of models, starting with two decision-tree based machine learning methods, Random Forest (RF) and XGBoost, known for their robustness on tabular data. We also investigated eight deep learning architectures by treating the SITS data as an image-like structure. These included foundational CNN models, some enhanced with a Convolutional Block Attention Module (CBAM), and hybrid models like CNN+MLP. To capture long-range dependencies, we tested CNN+Transformer hybrids and two pure Transformer architectures: a Vision Transformer (ViT) adapted for SITS data and a Spatio-Temporal Transformer (STTRE) designed to handle temporal and spectral

dimensions separately. Finally, we applied k-means clustering for post-hoc analysis to identify sub-patterns within each predicted class.

To ensure a fair comparison, all models were trained with a weighted cross-entropy loss function and incorporated dropout for regularization. We employed two distinct training strategies: for the Transformer-based models (ViT and STTRE), we used an Adam optimizer with a OneCycleLR scheduler to aid their training stability and convergence. For all other machine learning and deep learning models, we used an Adam optimizer with a step learning rate scheduler that periodically reduced the learning rate. Early stopping was applied across all experiments to prevent overfitting and select the best-performing model.

2.4. Model evaluation

To access the performance, Overall Accuracy (OA) and the Cohen's Kappa coefficient was used. Each metric is calculated by formular (1) and (2)

$$OA = \frac{N_c}{N_t} \quad (1)$$

$$\kappa = \frac{P_o - P_e}{1 - P_e} \quad (2)$$

3. Results and Discussion

Among all tested models, tree-based ensembles demonstrated superior performance, with XGBoost achieving the highest overall accuracy (OA) and Kappa score. Within the deep learning models, a clear performance hierarchy emerged: 1D-CNN based models (e.g., CBAM+MLP) outperformed 2D-CNNs, which in turn were superior to hybrid and pure Transformer architectures (ViT, SSTRE). This trend suggests that the complexity and weaker inductive biases of Transformers led to overfitting on the limited dataset, whereas the locality assumption of CNNs and the regularization from global average pooling in 1D-CNNs were more effective at capturing the dominant phenological patterns.

However, the top-performing models, XGBoost and CBAM+MLP, revealed a significant limitation tied to class imbalance. Both models demonstrated strong performance for majority classes with high support, such as Greenhouse and Sesame, achieving high F1-scores. Conversely, they failed significantly on minority classes with very low support, like Soybean and Maize, resulting in extremely poor F1-scores and demonstrating a failure to generalize effectively for the underrepresented classes.

Table 1 Overall error and Kappa score of each model for crop classification task.

Model	RF	XGBoost	CNN	CBAM CNN+MLP	
OA	0.6850	0.7275	0.6498	0.6709	0.6612
Kappa	0.6258	0.6749	0.6058	0.6268	0.6137
Model	CBAM+MLP	CNN+TF	CBAM+TF	ViT	SSTRE
OA	0.6817	0.6599	0.6227	0.5872	0.6049
Kappa	0.6391	0.6163	0.5780	0.5130	0.5321

4. Conclusion

XGBoost, are more effective than various deep learning architectures for structured SITS crop classification, although the performance on minority classes remains a critical challenge due to data imbalance. This study contributes a comprehensive benchmark that guides the selection of machine learning models for SITS-based crop classification in smallholder agricultural landscapes, highlighting the current superiority of tree-based ensembles and the persistent challenge of class imbalance.

Acknowledgements

This work was supported by Korea Institute of Planning and Evaluation for Technology in Food, Agriculture and Forestry(IPET) through Intelligent Agricultural Infra Management for Climate Change Development Program, funded by Ministry of Agriculture, Food and Rural Affairs(MAFRA)(500-20250172).

References

Franch, B., Vermote, E. F., Becker-Reshef, I., Claverie, M., Huang, J., Zhang, J., Justice, C., & Sobrino, J. A. (2015). Improving the timeliness of winter wheat production forecast in the United States of America, Ukraine and China using MODIS data and NCAR Growing Degree Day information. *Remote sensing of Environment*, *161*, 131-148. https://doi.org/https://doi.org/10.1016/j.rse.2015.02.014

KOSTAT. (2025). Agriculture, Forestry and Fishery Survey in 2024.

KMA. (2025). *Regional Climate Characteristics of Korea (in Korean)*. KMA. Retrieved 9/11 from https://www.weather.go.kr/w/climate/statistics/regional-char.do

Yıldız, A. Y., & Kalayci, A. (2025, 24-24 June 2025). Gradient Boosting Decision Trees on Medical Diagnosis Over Tabular Data. 2025 IEEE International Conference on AI and Data Analytics (ICAD),

Applying GeoAI to Paddy Area Estimation: A Case Study in Taibao, Taiwan

Zih-Ying Lee[1], Ting-Li Liu [2], Hsueh-Yen Shih[1], Candera Wijaya[1*]

[1] Agricultural Engineering Research Center, Taoyuan, Taiwan

[2] Department of Information Technology, Ministry of Agriculture, Taipei, Taiwan

* Corresponding author. Email: rbhung@aerc.org.tw

Abstract

Effective irrigation planning requires consideration of factors, including crop area, spatial distribution, soil texture, canal infrastructure, and historical irrigation data, etc. Among these, estimating the crop cultivation area is a labor-intensive task. Traditionally, surveyors had to visit fields in person to accurately assess cropping status. For efficiency, estimates were often based on surveyors' experience, making it difficult to balance accuracy and speed. To address this, we propose a GeoAI-based image classification solution for rapid and accurate estimation of paddy cultivation areas.

GeoAI offers a powerful tool for surveying paddy cultivation areas and supporting water resource management. With advances in AI and imaging sensors, high-resolution aerial imagery combined with deep learning enables efficient large-scale paddy mapping. A U-Net semantic segmentation model was trained using Leica DMCIII orthophoto (15 cm resolution, 4 bands) with labeled data. After fine-tuning the model with a limited dataset from regions beyond the training area, it was applied to Taibao, Taiwan. Integrating pixel-level classification with farmland parcel maps improved the practical accuracy of paddy area estimation.

This method mapped 14,000 hectares in Taibao within 2.5 hours, achieving accuracy exceeding 90%. Compared to traditional field surveys, it offers significant savings in both time and labor. In addition to supporting irrigation planning, classification results can be used to verify policy outcomes. For example, during droughts, subsidies are provided to fallow or non-irrigated fields. During cropping periods, image-based classification reliably verifies actual cultivation status, serving as a valuable reference for policy evaluation and future planning.

Keywords: GeoAI, paddy area, orthophoto

1. Introduction

Precision irrigation requires consideration of multiple environmental factors, including temperature, humidity, soil characteristics, and evapotranspiration. Among these, evapotranspiration is strongly influenced by the type and extent of cultivated crops. Paddy, as the staple food for much of Asia, occupies vast areas and demands substantial water resources. Therefore, accurate and timely interpretation of paddy cultivation areas is a critical first step toward implementing precision irrigation. However, conventional field surveys are often labor-intensive and time-consuming, limiting their scalability. To overcome these challenges, this study applies GeoAI techniques to rapidly and efficiently detect large-scale paddy cultivation, providing essential data support for precision irrigation planning.

2. Materials and Methods

The workflow included three steps: (1) data collection and preprocessing, (2) GeoAI model training, and (3) farmland parcelization, as detailed in the following subsections.

2.1. Data collection and preprocessing

This study utilized national-scale orthophoto and farmland parcel maps as the primary data sources for mapping paddy cultivation areas. The orthophoto, provided by the Ministry of Agriculture, has a spatial resolution of 15 cm. Paddy fields in Taitung County were annotated, and the orthophoto was subdivided into image patches according to the input size of the model. In total, the annotated paddy training data covered approximately 1,086 hectares. Each image patch was set to 224 × 224 pixels. Pixel-level masks representing paddy fields were generated from refined farmland parcel maps.

2.2. GeoAI model training

A semantic segmentation approach was adopted to interpretate paddy fields from orthophoto. The model architecture was based on U-Net, with Xception serving as the encoder for feature extraction. U-Net is well suited for pixel-level classification due to its symmetric encoder–decoder structure, which preserves spatial information while progressively reconstructing image details. Xception, through depthwise separable convolutions, enhances computational efficiency and feature representation with fewer parameters compared to conventional convolutional networks.

During training, image patches of 224 × 224 pixels from orthophoto were used as inputs, with the corresponding paddy masks as outputs. Cross-entropy loss was applied as the objective function, and data augmentation techniques were employed to improve robustness under varying image conditions. The trained model generated pixel-level paddy distribution maps, providing critical spatial information for precision irrigation planning.

2.3. Farmland Parcelization

In agricultural practice, the basic unit of field management is the land parcel, and the Ministry of Agriculture maintains farmland parcel maps on an annual basis. The model output is a pixel-level segmentation map; however, for practical applications, paddy cultivation must be quantified at the parcel level to facilitate governmental statistics and irrigation planning. The segmentation map and corresponding parcel map are shown as figure 1. This was achieved by calculating the proportion of paddy pixels within each parcel and applying a threshold, which was empirically determined and further optimized using validation data, to decide whether a parcel was classified as paddy-cultivated.

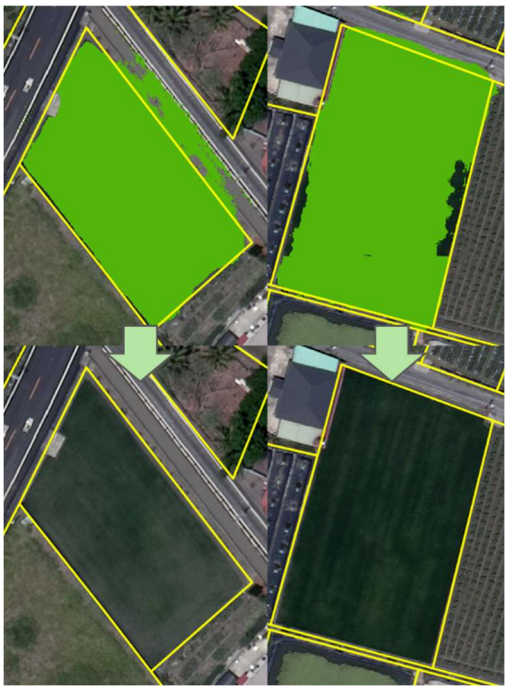

Figure 1. Segmentation results overlaid with corresponding parcel map.

3. Results and Discussion

The proposed paddy interpretating model was evaluated in Taibao. This section presents the results and accuracy assessment of the model, followed by discussions on its applicability for precision irrigation planning.

3.1. Study area

Taibao Township in Chiayi County, Taiwan, is an agricultural township with high paddy production. Figure 2 shows the boundary of Taibao along with the irrigation canals within the district. Since the crop types in this area are relatively homogeneous, once paddy cultivation is identified, the irrigation plan can be directly formulated based on the paddy-planted area. Therefore, this region serves as a relatively straightforward experimental site.

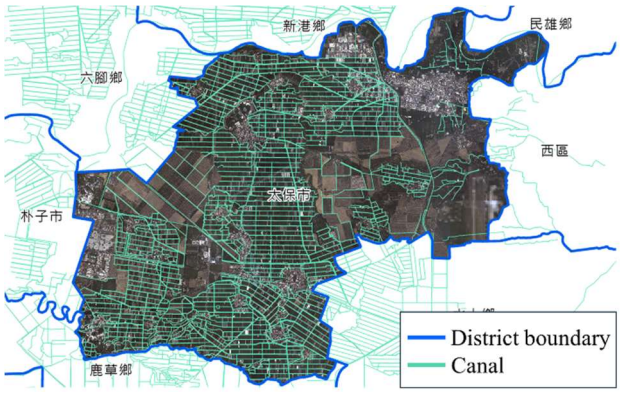

Figure 2. Study area: Taibao and surrounding irrigation canals.

3.2. Accuracy validation

After parcel-based quantification, expert visual interpretation of orthophoto was used as the ground truth. The confusion matrix of the proposed model's paddy interpretation results for Taibao is shown in Table 1. Based on the confusion matrix, the model achieved a precision of 0.97, a recall of 0.92, and an F1 score of 0.95 in this experiment. These results indicate that the proposed GeoAI-based approach provides highly reliable performance for paddy interpretation at the parcel level.

Table1. Confusion matrix of paddy mapping results in Taibao (unit: parcels).

		Prediction	
		Paddy	Non-paddy
Ground Truth	Paddy	7,208	606
	Non-paddy	230	7,271

4. Conclusion

By integrating GeoAI inference with the parcelization workflow, paddy cultivation areas within the entire 6,646-hectare region of Taibao were surveyed in just 3.5 hours. Expert visual interpretation of orthophoto indicated 2,144 hectares of paddy fields, while the GeoAI-based mapping estimated 2,064 hectares, resulting in a 3.7% area error rate. Compared with manual surveys, the proposed approach significantly reduces the time and labor required for large-scale agricultural mapping. For future irrigation planning, this error margin can be adopted as a safety coefficient to enhance both flexibility and reliability in water resource management.

Acknowledgements

We would like to thank the Department of Information Technology, Ministry of Agriculture, for providing the national farmland parcel maps and extensive ArcGIS Pro software licenses. Appreciation is also extended to the Aerial Survey and Remote Sensing Branch, Forestry and Nature Conservation Agency, Ministry of Agriculture, for supplying the orthophoto acquired with the Leica DMCIII aerial camera.

References

Journal articles:

Ronneberger, O., Fischer, P., & Brox, T. (2015). U-Net: Convolutional networks for biomedical image segmentation. In MICCAI.

Chollet, F. (2017). Xception: Deep learning with depthwise separable convolutions. In CVPR.

Yang, C. Y., Yang, M. D., et al. (2020). Assessment of rice developmental stage using time series UAV imagery for variable irrigation management. Sensors, 20(18), 5354.

Optimal IIS Deployment in Fragmented Paddy Fields via Geo-Clustering and Neighborhood Search

Runze Tian [1*], Keigo Noda [1], Kyoji Takaki

[1] Department of Biological and Environmental Engineering, The University of Tokyo, Bunkyo-ku, Tokyo 113-8657, Japan

* Corresponding author. Email: tianrunze@g.ecc.u-tokyo.ac.jp

Abstract

Paddy field fragmentation in Japan forces farmers to manage numerous spatially dispersed plots, leading to substantial labor costs in irrigation patrols. Intelligent Irrigation Systems (IIS) can alleviate this burden by reducing field visits, yet their benefits vary greatly depending on installation locations. The key challenge lies in selecting optimal fields for installation under limited capacity, where exhaustive search is infeasible and conventional cluster-first, route-second approaches suffer from solution space fragmentation. To address this, we propose a geo-clustering and Dual Neighborhood Search (DNS) framework that combines DBSCAN-based clustering with two complementary neighborhood operators: Incremental Addition (IA) for fine-grained local refinement and Large-scale Exchange (LE) for global diversification. Empirical validation using real farmer datasets demonstrates that the DNS framework consistently outperforms both DBSCAN-only and random baselines, achieving over 15% average improvement in labor reduction with statistically significant differences (Wilcoxon $p < 0.01$). These results confirm that the proposed approach provides an efficient and robust decision-support tool for maximizing IIS deployment benefits under practical constraints.

Keywords: Paddy Field; Intelligent Irrigation System; DBSCAN; Traveling Salesman Problem

1. Introduction

Japanese agriculture is significantly hindered by the structural fragmentation of paddy fields, forcing most farmers to manage numerous geographically dispersed plots. This spatial dispersion requires frequent inter-field travel for routine inspections, substantially increasing both time and labor input. The situation is further aggravated by an aging workforce and persistent labor shortages, making field patrols more costly and rendering paddy field fragmentation a critical bottleneck for improving irrigation efficiency and reducing labor burden.

Intelligent Irrigation Systems (IIS), which support remote monitoring and automatic water-level control, have been shown to reduce patrol frequency and enhance water-use efficiency—empirical studies report over 20% savings in irrigation management time in some regions[1,2]. However, high initial and maintenance costs have limited IIS adoption, especially among small and medium-sized farms[3,4]. Moreover, labor-saving benefits are highly dependent on installation locations: excluding an IIS-equipped field from patrol routes shortens travel distance, but the actual benefit varies with spatial configuration. Therefore, under constraints of limited budget and installation capacity, optimizing IIS placement to maximize overall benefit remains a major challenge.

To quantitatively evaluate the labor reduction effect of IIS deployment, the Traveling Salesman Problem (TSP) model is often employed, in which changes in optimal patrol routes before and after installation are compared to measure distance savings [5]. However, existing studies have mostly concentrated on route optimization itself and have not provided systematic solutions for "how to select optimal field combinations under limited device capacity." In practical optimization, the widely used "Cluster-first, Route-second" strategy reduces combinatorial complexity by applying spatial clustering prior to route optimization [6]. However, as show in Fig. 1, this approach suffers from the inherent limitation of solution space fragmentation, which weakens cross-cluster search integrity and restricts the ability to obtain globally optimal solutions.

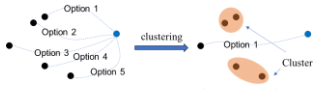

Fig. 1 Constraints on Search Space by Clustering

In summary, the objective of this study is to quantitatively identify field combinations that maximize labor reduction benefits from IIS deployment in fragmented paddy fields. This problem is challenging not only due to the combinatorial explosion of candidate subsets but also because clustering-based strategies induce solution space fragmentation, which hinders the achievement of global optimality. To address these challenges, this study proposes an optimization framework that reduces combinatorial complexity while retaining cross-cluster search capability, thereby enabling the maximization of IIS deployment benefits under limited installation capacity.

2. Methods

2.1. Problem Definition

This study formulates the IIS deployment optimization problem as follows: Given the set of all paddy fields P with known spatial coordinates, and a fixed number n of IIS units to be installed—where each field can host at most one unit—the objective is to select n fields for installation so as to maximize the reduction in total patrol-route length. The optimization model is given by:

$$\Delta L^*(n) = \max_{S \subset P, |S| = n} \Delta L(S) = D(P) - \min_{S \subset P, |S| = n} D(P \setminus S) \quad (1)$$

$$\text{s.t. } S = \{p_i \in P | x_i = 1\}, \sum_{i=1}^{M} x_i = n, x_i \in \{0,1\}, \ \forall i \in \{1,2,3,\dots,M\} \quad (2)$$

where $D(A)$ denotes the shortest patrol route length (i.e., TSP tour) for the set of fields A, and $\Delta L(S)$ represents the reduction in patrol distance achieved under installation plan S.

Since this problem is NP-hard, exhaustive search is infeasible for real-world scenarios. Therefore, it is essential to design an efficient heuristic framework that can reduce computational complexity while ensuring solution quality.

2.2. Method Overview

To address the challenges of combinatorial explosion and solution space fragmentation, this study proposes an optimization framework that integrates spatial clustering with Dual Neighborhood Search (DNS), as illustrated in Fig. 2. The method consists of two main stages:

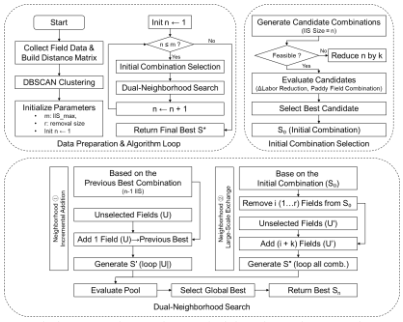

Fig. 2 Flow chart of the Dual-Scale Neighborhood Search

First, the DBSCAN algorithm is employed to cluster geographically proximate paddy fields, thereby compressing the solution space and generating an initial installation plan based on the clustering results.

Second, the Dual Neighborhood Search (DNS) strategy is introduced to iteratively improve the solution. This strategy utilizes two complementary neighborhood operations: Incremental Addition (IA), which performs fine-grained local adjustments independent of cluster boundaries; and Large-Scale Exchange (LE), which applies large-scale destroy-and-repair moves to introduce global perturbations and facilitate escape from local optima.

By alternating between these two neighborhood operators, the framework achieves a balance between intensification and diversification, effectively overcoming the limitations of cluster approaches. As a result, the proposed framework enables efficient exploration of the solution space and substantially enhances both the quality and global optimality of IIS deployment solutions under limited installation capacity.

2.3. Validation Method

This study evaluates the effectiveness of the proposed DNS framework using geospatial data from three real farmers with fragmented paddy fields (as shown in Fig. 3), with DBSCAN clustering parameters set based on the k-distance method.

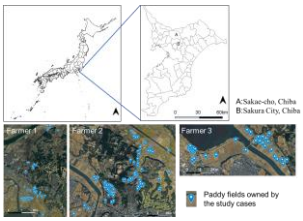

Fig. 3 Regional distribution of paddy fields

The validation consists of two parts:

First, ablation experiments are conducted to compare four schemes—DBSCAN only, and the full DNS—to quantitatively assess the incremental contribution of the dual-neighborhood mechanism.

Second, large-scale random sampling is used as a reference baseline to evaluate the practical improvement achieved by the DNS framework compared to random selection.

The evaluation metrics include:(a) Mean improvement rate (b)Wilcoxon test (c)Percentile. Through these multi-faceted comparisons, the proposed method is comprehensively validated for effectiveness and robustness under real-world conditions.

3. Results and Discussion

Fig. 4 illustrates the comparison of labor reduction across different numbers of IIS installations under the k-distance parameter setting. It can be observed that the proposed DNS framework consistently outperforms the DBSCAN-only baseline in most installation scales. When the number of installations increases, DNS continues to improve route reduction, whereas the baseline method tends to stagnate.

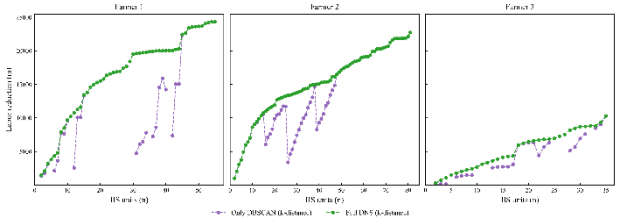

Fig. 4 Labor reduction (m) achieved with increasing numbers of IIS installations (n) for three farmers. Labor reduction (m) with increasing IIS installations (n) for three farmers. Purple denotes DBSCAN-only, green denotes DNS.

Quantitative results indicate that the DNS framework achieved a mean improvement rate of 13–17% over the random baseline for all farmer datasets, with statistical significance (Wilcoxon $p < 0.01$). DNS solutions consistently ranked above the 90th percentile in the random distribution, demonstrating robust and effective optimization performance.

Table 1 Key statistical indicators comparing DNS and random baseline

Farmer	Mean Δ (%)	Wilcoxon p	Percentile (%)
Farmer 1	17.3	<0.01	97
Farmer 2	14.6	<0.01	95
Farmer 3	13.1	<0.01	93

4. Conclusions

This study proposed a geo-clustering and DNS framework to optimize IIS deployment in fragmented paddy fields. The framework effectively mitigates solution space fragmentation and avoids local optima while maintaining computational efficiency. Validation with real farmer datasets demonstrated that DNS consistently outperforms the DBSCAN-only baseline and random selection, achieving statistically significant improvements in labor reduction. These results confirm that the proposed approach provides a practical and robust tool for maximizing the benefits of IIS under limited installation capacity.

References

[1] Wakasugi K, et al. 2017. J Jpn Soc Irrig Drain Rural Eng, 85:11–14. https://doi.org/10.11408/jjsidre.85.1_11.
[2] Umemoto M. 2010. Agric Econ Res, 82:102–11. https://doi.org/10.11472/nokei.82.102.
[3] Dibbern T, et al. 2024. Smart Agric Technol, 8:100459. https://doi.org/10.1016/j.atech.2024.100459.
[4] Kawamura M. 2019. Proc Annu Meet Jpn Soc Irrig Drain Rural Eng, pp.678–9.
[5] Nemoto T, et al. 2024. Smart Agric Technol, 8:100450. https://doi.org/10.1016/j.atech.2024.100450.
[6] Prins C, et al. 2014. Transp Res C, 40:179–200. https://doi.org/10.1016/j.trc.2014.01.011.

Evaluating Smart Gate Control Effects on Water Allocation in Terminal Canals of Thai Paddy Irrigation Schemes

Toru NAKADA [1*], Tadayoshi HITOMI [1], Tetsuo NAKAYA [1],

Attapan Diloksopon [2], Sarayut Ngootip [3], Katsuhiko YAMAUCHI [4]

[1] Institute for Rural Engineering, NARO, JAPAN

[2] Foreign Project Management Division, Bureau of Project Management, Royal Irrigation Department, Thailand

[3] Land Consolidation and On-farm Development Reginal Office 18, Royal Irrigation Department, Thailand

[4] Japanese Institute of Irrigation & Drainage (JIID), JAPAN

* Corresponding author. Email: nakada.toru364@naro.go.jp

Abstract

Advances in IoT and ICT enable water balance measurement in paddy fields, supporting demand-oriented irrigation and improved water allocation. While many studies focus on single-field efficiency using IoT data, evaluations at larger scales, such as irrigation schemes or watersheds, remain limited. This highlights the need to examine the impacts of smart irrigation devices on broader infrastructure, including irrigation blocks, secondary canals, and main canals. In northern Thailand's intensive land-consolidated irrigation scheme, we installed automatic water supply inlets to paddy plots irrigated from a terminal canal (FTO). Flow rates, along with the FTO, were measured before and after installation to assess the effects on water distribution. Under conventional irrigation with a 10-day rotation, upstream farmers often left gates open after securing water, delaying supply to downstream fields. Although overall water supply during the rotation period was sufficient, reliability under severe dry conditions could be improved. By installing smart devices in 10 upstream fields and enabling automatic gate closure when the target water depth is reached, unused irrigation water can be redirected downstream. This demonstrates the potential of smart irrigation to improve distribution efficiency and ensure more equitable water access across irrigation schemes.

Keywords: water use efficiency, automatic inlets, land consolidation, demand-oriented, upstream-priority

1. Introduction

Smart irrigation has great potential in the ASEAN countries. Smart water management systems play a vital role by optimizing water allocation, reducing waste, and improving overall irrigation efficiency, thereby enhancing the maximization of cultivated areas even under dry-season water shortages.

This study aims to evaluate the impact of implementing smart irrigation devices on water distribution within terminal irrigation canals (FTOs; Farm Turnouts) in northern Thailand's improved irrigation areas, where irrigation and drainage are separated. We introduced automatic water supply inlets to field blocks supplied by the FTO, measured flow rates at multiple points along the FTO to estimate the water provided to the fields, and conducted flow measurements before and after the installation of these inlets to assess changes in water distribution resulting from the smart irrigation devices.

2. Methods

2.1. Site description

The pilot site for this study is located in the irrigation scheme in Lampang Province, Northern Thailand, whose irrigation water resources are from two large dams: Kiw Lom Dam and Kiw Kho Mha Dam. The Right Bank Main Canal (RMC) area is divided into upstream and downstream sections, and each is supplied alternately every 10 days. There will be a 5-day supply shutdown period for maintenance after each 10 days of irrigation. Thus, each FTO has 25 25-day cycle, with 10 days of irrigation and 15 days of shutdown.

In this pilot site area, intensive land consolidation projects have successfully separated irrigation water from drainage systems. This terminal canal (FTO) is approximately 650 meters long. It distributes water along 40 inlet points to individual farm plots, supplying water to an irrigation area of roughly 15 hectares.

2.2. Field measurement

To verify water distribution in the FTO, flow was measured daily at four key points over a 10-day irrigation period. The flow rate was calculated using the measured velocity and water depth. The flow rate differences between these points divided the FTO into three field blocks, which enabled the calculation of the water intake volume for each block. Dividing this intake by the block's area yielded the water intake per unit area, expressed in millimeters (mm), which allows for direct comparison with crop water demand, such as evapotranspiration.

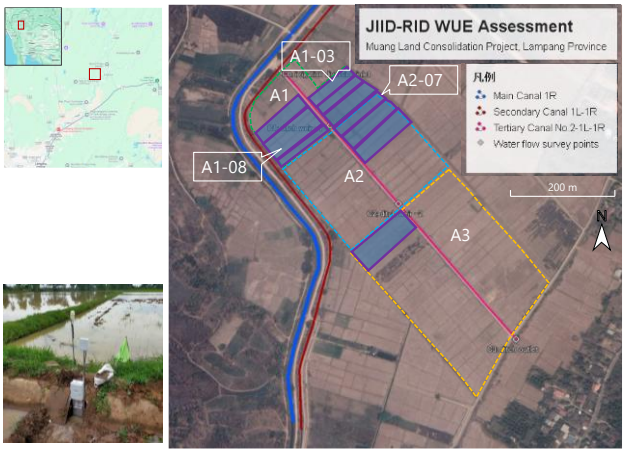

Fig. 1 Pilot site with smart irrigation devices installed plots

To facilitate collaborative analysis, the measurement results and measurement process photographs were shared among researchers in Japan and Thailand via Google Spreadsheets and the messaging application Line. This real-time data sharing enabled prompt feedback and discussion, enhancing the study's efficiency and effectiveness.

2.3. Smart irrigation device: Paditch

The Paditch system, developed by Enowa Co., Ltd., offers smart irrigation for paddy fields, enabling remote and automated control of water gates via smart devices. It includes timer scheduling and accumulates cloud-based data on water levels and gate openings for analysis.

To regulate excessive water usage in the upstream areas, 10 sets of Paditch were installed focusing on the upstream fields (Block A1).

3. Results and Discussion

3.1. Baseline survey before installation of smart irrigation devices

As a baseline survey before implementing smart irrigation devices, flow rate observations during dry (February-April 2023, January-April 2024) and wet (August-October 2023) seasons revealed significant temporal flow variations. This pattern shows upstream areas receive higher initial volumes, risking over-irrigation if field inlets remain open, while downstream fields receive sufficient but delayed flow.

Water withdrawal varied significantly by location: the upstream Block A1 (2.83 ha) recorded excessive withdrawal (>100 mm/day) from non-regulated inlets, causing water wastage. In contrast, Blocks A2(4.50 ha) and A3(7.75 ha) exhibited more balanced rates of approximately 50 mm/day, efficiently supporting crops. That said, the infiltration rate estimated from the September 2023 rainy season paddy field infiltration survey was approximately 20 mm/day, making the current value excessive by comparison. For reference, Thailand's standard irrigation design value for daily infiltration is 9 mm/day.

3.2. Follow-up survey after installation of smart irrigation devices

In rainy season of 2024, ten units of the smart irrigation device Paditch were installed at selected upstream plots along with the FTO. The implementation of smart devices faced several challenges, such as farmers unfamiliar with mobile app operations and technical failures. As a workaround, RID staff manually controlled the gates, which failed to replicate the benefits of autonomous operation. Consequently, water withdrawal did not significantly decrease, and improvements in water use efficiency and distribution fell short of expectations.

Despite these operational setbacks, the devices successfully collected useful water level data. In upstream Block A1, fields remained inundated throughout the 10-day distribution period, confirming previous observations of prolonged water usage. Midstream Block A2 showed a slight delay in water level rise compared to upstream, reflecting expected flow progression but also highlighting ongoing challenges in timely water delivery to downstream users.

Table 1 Water withdrawal per unit area in three blocks

			A1 (mm/day)	A2	A3	Rainfall
Conventional irrigation practice	Dry	2023-Feb.	29.3	22.5	57.5	
	Dry	2023-Mar	40.1	15.1	91.6	
	Dry	2023-Apr.	87.7	22.9	52.0	
	Dry	2023-Apr.	112.0	31.6	66.3	
	wet	2023-Aug	11.4	10.2	40.2	
	wet	2023-Aug	21.2	15.2	48.1	
	wet	2023-Sep	12.8	7.4	11.2	10.8
	wet	2023-Oct.	54.2	17.2	47.2	5.6
	wet	2023-Oct.	7.8	4.6	13.0	11.8
	Dry	2024-Jan	33.5	7.1	23.1	
	Dry	2024-Feb.	53.6	26.6	47.8	
	Dry	2024-Mar	78.1	69.5	28.3	
Smart irrigation	wet	2024-Jul	15.9	10.9	31.8	4.1
	wet	2024-Aug	23.6	21.5	65.2	1.3
	wet	2024-Aug	19.4	53.3	21.8	7.6
	wet	2024-Sep	31.6	108.2	48.3	20.9
	wet	2024-Oct	21.8	91.5	38.8	25.2
	Dry	2024-Dec	35.5	25.3	10.1	
	Dry	2025-Jan	51.1	36.4	39.0	
	Dry	2025-Feb	81.0	62.6	56.0	
	Dry	2025-Mar	56.5	44.7	67.7	

4. Conclusions

This study in Lampang, Thailand, used smart devices to address inequitable water distribution in a terminal irrigation canal (FTO). A baseline survey confirmed that upstream fields overused water, causing downstream shortages. Ten smart devices were installed upstream to automate intake and improve flow to downstream users.

While water use efficiency did not significantly improve due to some challenges, such as farmer unfamiliarity with the technology and technical failures, the project successfully collected data that revealed water usage patterns and key obstacles. These findings provide valuable insights for future smart irrigation projects in similar contexts.

References

Enowa Co., Ltd., paddich. URL: https://paditch.com/, (Accessed 2024-11-30)., [in Japanese]

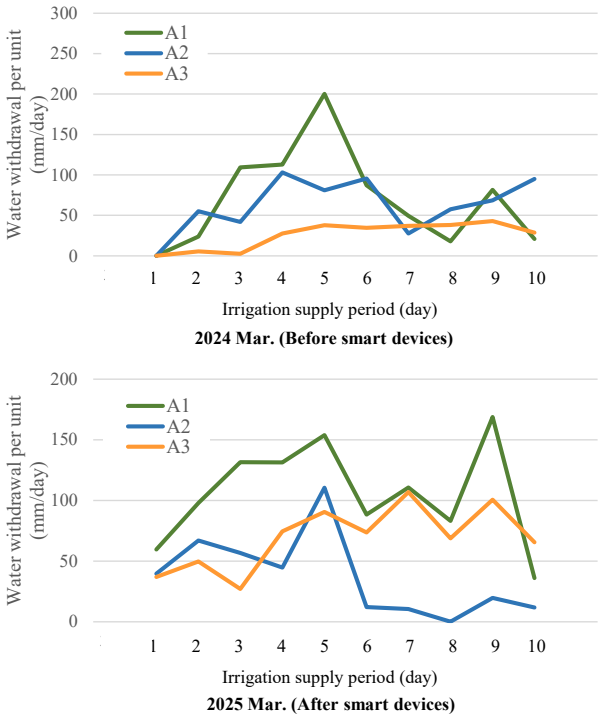

Fig. 2 Internal block-wise water withdrawal comparison between before and after smart devices

Uncovering Stakeholders in Agricultural Irrigation Governance: A Corpus-Based Text Mining Approach

Jou Jou Yu [1], Cheng Wei Yu [1*]

[1] Department of Bioenvironmental Systems Engineering, National Taiwan University, Taipei, (Province or State) 123456, Taiwan

* Cheng Wei Yu. Email: cwjyu@ntu.edu.tw

Abstract

Understanding stakeholder relationships in agricultural irrigation is essential for effective governance, as it highlights power dynamics, communication channels, and potential conflicts or cooperation. This study proposes a participatory framework to systematically identify and characterize stakeholders, integrating diverse perspectives into Taiwan's irrigation governance. Given the multi-sectoral nature of irrigation management—with overlapping jurisdictions and competing interests—robust strategies require a clear understanding of stakeholder interactions and institutional trade-offs across administrative levels.

Using the CORPRO corpus analysis tool with the Academia Sinica CKIPTagger and the CVAW4.0 Chinese sentiment lexicon, the study analyzed 51,427 texts from public and private sectors. Word frequency and semantic classification categorized the texts into five domains: actors, governance, economy, environment, and society. Results show that both sectors emphasized governance issues, followed by economy and environment. Co-occurrence and sentiment analyses further revealed annual variations in positive and negative attitudes across four thematic domains, providing deeper insights into stakeholder dynamics.

By integrating corpus and sentiment analyses, this study offers a robust framework for stakeholder identification in Taiwan's irrigation governance and contributes empirical evidence for participatory mechanisms and sustainable water management strategies.

Keywords: Agricultural water governance, Stakeholder analysis, Corpus analysis, Sentiment analysis , Sustainable water management

1. Introduction

The impacts of climate change have brought sustainability issues to the forefront of public concern. In pursuing sustainability goals, stakeholder perspectives must be considered not only in business and corporate contexts but also during the planning and execution of policy and project initiatives.

The essence of stakeholder analysis lies in identifying individuals or groups who may influence, or be influenced by, a specific action (e.g., a project, program, or event). Its purpose is to assess stakeholders' attitudes toward that action, providing information that helps determine which stakeholders should receive attention during particular phases of project or policy implementation.

The objective of this study is to define key stakeholders in Taiwan's agricultural irrigation governance and to establish effective participatory mechanisms. As agricultural irrigation encompasses diverse water-use demands, governance strategies must balance consensus among multiple stakeholders and trade-offs across administrative levels. Such considerations are critical to guiding irrigation governance toward sustainability. This research adopts corpus-based methods using the CORPRO corpus analysis tool (Chueh & Chen, 2016; Lischinsky, 2015; Chen, 2018; Kuo, 2020; Yang, 2023)) and sentiment analysis (Lin & Lee, 2023) to systematically identify and characterize stakeholders.

2. Materials and Methods

2.1. Text Collection

Using a Python-based web crawler, 18 keywords—including "agricultural irrigation," "agricultural water conservancy," "agricultural water resources," "farmland irrigation," "drought," "irrigation suspension," "irrigation district," "water rights," and "crop water demand"—were employed to retrieve news texts from both public and private sectors. A total of 51,427 texts were collected.

Table 1. Number of texts from public and private sectors

Category	Stakeholders	Number of Texts
Public	Ministry of Agriculture	799
	Water Resources Agency	299
Private	Agriharvest Media	3232
	Liberty Times	33863
	United Daily News	3158
	ETtoday	10146
Total		51427

2.2. Corpus Processing Methods

The CORPRO corpus analysis tool was applied for corpus construction. After word segmentation, stop-word removal, and synonym unification, word frequency analysis was used to extract high-frequency terms. These were semantically classified into five categories: actors, governance, economy, environment, and society. Co-occurrence analysis of key actors was then conducted to reveal interrelationships among stakeholders.

The co-occurrence results provided a basis for preliminary text organization, which was further classified into four domains—governance, economy, environment, and society—to facilitate sentiment analysis.

2.3. Sentiment Analysis Methods

Texts segmented by the Academia Sinica CKIP Tagger were analyzed using the CVAW4.0 Chinese multidimensional sentiment lexicon, producing positive and negative scores ranging from 0 to 9. Based on segmented tokens, words were matched with lexicon entries to determine sentiment polarity and intensity, which were then aggregated into sentence- and document-

level indices. This approach enabled the study to capture both the direction and strength of emotional expressions, providing a framework to evaluate stakeholder attitudes toward agricultural water issues over time.

3. Results and Discussion

3.1. Corpus Analysis

After removing meaningless words, the top 200 high-frequency terms were extracted and classified into five categories: stakeholder, governance, economy, environment, and society. Synonym functions were applied to consolidate terms with similar meanings. Co-occurrence analysis was then conducted to verify relationships among actors. The identified high-frequency words facilitated the identification of key topics within each category and enabled the analysis of trends in these topics over time.

Table 2. High-frequency term classification by sector

Category	Public	Private
Stakeholder	22	27
Governance	76	60
Economy	51	27
Environment	31	47
Society	38	35

3.2. Sentiment Analysis

As an example, in the private sector under the governance policy category, the stakeholders “citizens” and “government” (including their synonyms) were selected. High-frequency terms from the four thematic domains were used for text classification, after which paragraphs containing these actor terms were identified. The texts were then processed using the Academia Sinica CKIPTagger for segmentation and analyzed with the CVAW4.0 Chinese multidimensional sentiment lexicon, yielding the variations in positive sentiment scores of these stakeholders across the four domains in the private sector from 2005 to 2024.

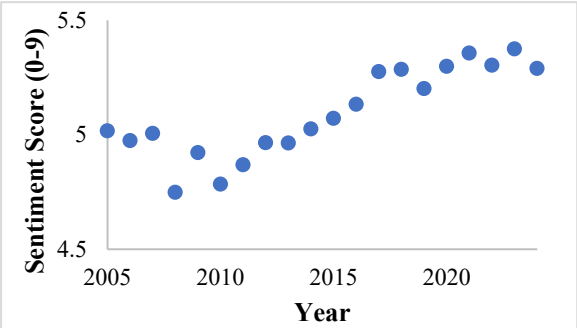

Figure 1. Variations in sentiment scores of stakeholders in governance-related texts of the private sector, 2005–2024.

4. Conclusions

This study collected 51,427 news texts from public and private sectors through Python-based web crawling. Using the CORPRO tool, frequency and classification analyses showed that public sector texts most frequently emphasized governance-related terms, with greater attention to economic issues compared to private sector texts, while the private sector emphasized environmental concerns. These findings indicate that stakeholders in both sectors are particularly attentive to governance-related issues.

Additionally, co-occurrence and sentiment analyses revealed shifts in positive and negative sentiments within the four thematic domains, providing deeper insights into the contexts of stakeholder interactions. The study demonstrates the value of integrating corpus and sentiment analyses to identify stakeholder dynamics in Taiwan’s irrigation governance, contributing to participatory mechanisms and evidence-based strategies for sustainable water management.

Acknowledgements

This research is supported by the Irrigation Agency of the Ministry of Agriculture (MOA) under the project titled “Net-Zero Strategies and Sustainable Circular Assessment for Agricultural Irrigation Systems.”. It has not been formally reviewed by the MOA. The views expressed in this document are solely those of the authors and do not necessarily reflect those of the Agency.

References

Chueh, H.-C., & Chen, K.-H. (2016). The development and application of the CORPRO Chinese Independent Corpus Analysis Tool. Digital Humanities: Between Past, Present and Future

Kuo, W.-P. (2020). Corpus-assisted media discourse analysis: An empirical study of Taiwan’s print media reports on the “Chinese Dream.” Journal of Information Society Studies.

Yang, C.-M. (2023). Exploring the characteristics of cultural and creative industry reporting through corpus analysis: A case study of United Daily News and China Times (2002–2021). Journal of Cultural Industries and Management Studies.

Chen, P.-F. (2018). From food safety to food sovereignty: A corpus-based discourse analysis of organic food news, 2011–2016 (Master’s thesis). Graduate Institute of Mass Communication, Tamkang University.

Lin, C.-M., & Lee, Y.-H. (2023). Topics of archival events and sentiment analysis in Taiwanese online forums. Journal of Library & Information Science Research, 17(2).

Liang-Chih Yu, Lung-Hao Lee, Shuai Hao, Jin Wang, Yunchao He, Jun Hu, K. Robert Lai, and Xuejie Zhang (2016). Building Chinese Affective Resources in Valence-Arousal Dimensions. In Proceedings of the 15th Annual Conference of the North American Chapter of the Association for Computational Linguistics: Human Language Technologies (NAACL-HLT'16), San Diego, California, USA, 12-17 June, 2016.

Lischinsky, A. (2015). What is the environment doing in my report? Analyzing the environment-as-stakeholder thesis through corpus linguistics. Environmental Communication.

Implementation plan development and monitoring status for agricultural water resources in Korea under the Comprehensive Basin Water Management Plan

Sungjin Cho [1], Kwangsik Yoon [1*]

[1] Department of Rural & Bio-Systems Engineering, Chonnam National University, Gwangju, 61160, Korea

* Corresponding author. Email: ksyoon@jnu.ac.kr

Abstract

The Korean government enacted the Framework Act on Water Management and established a new watershed plan. This new law and plan require an optimal water utilization strategy that considers not only water quantity and quality but also the current status of water resources and solutions to water-related challenges to achieve integrated water management. Following Korea's integrated water management guidelines, new strategies have been formulated for the efficient use of agricultural water. The primary strategies include: Measurement of agricultural water supply for scientific management, Establishment of intelligent agricultural water management information, Development of watershed water balance models for analyzing agricultural water supply and demand, Construction of pipeline-based irrigation canal networks for efficient agricultural water supply, Establishment of an integrated agricultural water supply management system encompassing rivers, surface water, and groundwater, Restructuring of agricultural water distribution systems and efficient water usage through reservoir operation, and Management of water-related conflicts. A five-year implementation plan has been developed, and annual performance evaluations are conducted. Quantitative and qualitative indicators for each task have been established, and performance results have been reported and evaluated. This paper introduces the process of developing and evaluating the implementation plan, analyzes the achievements of each task and the reasons for underperformance, and presents future implementation measures and directions for revision and supplementation during the re-establishment of the Basin plan.

Keywords: Integrated water management, basin plan evaluation, agricultural water, water safety, water environment, Korea

1. Introduction

Integrated water management in Korea seeks to overcome the fragmented and sectoral governance system that previously divided water policies across multiple ministries. By integrated water management, the framework now considers both water quantity and quality at the watershed scale, integrating flood control, water use, water quality, and aquatic ecosystems. This paradigm aims to propose nationally coordinated solutions to basin-level water challenges and conflicts, advancing cooperative and sustainable watershed management.

Recent shifts in national environmental policy reflect a transition from a focus on creating a prosperous human environment to ensuring sustainable water resources in response to climate change and emerging water-related challenges.

In June 2021, Korea announced its First National Water Management Plan (2021–2030). Furthermore, the Presidential National Water Management Committee and Regional Basin Water Management Committees were established to coordinate across ministries and foster public–private cooperation. However, integrated water management remains in progress, with limited tangible achievements so far.

In line with the National Water Management Plan and the Comprehensive Basin Water Management Plans, the Framework Act on Water Management and its Enforcement Decree mandate the inclusion of annual performance assessments for basin plans. These assessments serve to ensure plan implementation, with task-specific action plans evaluated to enhance accountability and effectiveness.

This study reviews the overall process of implementation evaluation within basin water management plans and focuses on agricultural water-related tasks included in the Yeongsan River, Seomjin River, and Jeju Basin Comprehensive Plans (2024).

2. Materials and Methods

The implementation evaluation assesses whether the basin plans are being carried out effectively, providing not only quantitative results such as scores but also qualitative insights such as strengths, areas for improvement, obstacles, and recommendations. These results are designed to feed back into future plan development and implementation.

Evaluation Indicators
Appropriateness of Implementation Tasks (10)
Feedback and Reflection of Evaluation Results (10)
Achievement of Implementation Tasks (40)
Efforts for Policy Communication (10)
Policy Effectiveness (25)
Performance Management Efforts (5)

For the Ministry of Agriculture, Food and Rural Affairs (MAFRA),15 projects were planned across five categories:

Water Use

- Mitigation of regional water use imbalances through efficient supply and utilization of agricultural water
- Establishment of a Rational Agricultural and Rural Water Use Plan to present efficiency targets by service areas
- Development of a watershed-scale water balance model and agricultural water supply management system
- Securing a stable irrigation supply system for upland fields and protected cultivation
- Exploration of groundwater utilization for agricultural water supply

Water Safety

- Expansion of Emergency Action Plans (EAPs) for agricultural reservoirs and stronger disaster prevention
- Enhancement of reservoir safety against earthquakes and floods
- Performance improvement of agricultural infrastructure and establishment of multi-purpose utilization systems
- Development of drought and flood forecasting models to support advanced early-warning systems

Water Environment

- Strengthened management of non-point source pollution from agriculture
- Establishment of preventive water quality management for agricultural water use
- Development of strategies for water quality improvement

Water Value

- Establishment of big data platforms for AI-based agricultural water management
- Evaluation of agricultural water use in the Yeongsan River Basin using the Wate – Energy – Food Nexus framework & development of integrated resource linkage indicators for policy application
- Creation of low-carbon, climate-resilient farming complexes to reduce greenhouse gas emissions

3. Results and Discussion

By the end of 2024, the evaluation of the Yeongsan–Seomjin–Jeju Basin Plan classified 74 implementation tasks into grades of Excellent, Good, and Average. Overall, 90.6% of tasks were rated Excellent or Good, suggesting that most projects are being implemented without major setbacks.

For the Ministry of Agriculture, Food and Rural Affairs (MAFRA), 16 projects were assessed across five categories:

Key Achievements and Implementation Efforts by MAFRA

- Installed water level gauges and flow meters (7 completed) to secure actual water-use data.
- Developed draft plans for rationalization of water use (total 130 sites).
- Introduced smart farming technologies for efficient water management
- Initiated development of big data-based flood prediction models using past precipitation data from KMA, real-time water level data, and rainfall records.
- Prepared EAPs for 23 reservoirs with capacity of 200,000 – 300,000 m^3 .
- Rehabilitation and reconstruction of aged reservoirs for 11 newly selected sites.
- Improved flood control capacity of small- and medium-sized reservoirs through gate construction projects
- Conducted seismic performance evaluations of 9 pumping stations.
- Carried out drainage improvement projects in flood-prone areas (85 districts: 52 under construction, 33 in design).
- Implemented tailored drought response measures, including education and promotion for water-saving practices for farmers.
- Conducted Agricultural Environment Conservation Programs in 15 cities/counties, 23 villages.
- Expanded agricultural water quality monitoring from 4 to 7 surveys per year at 234 sites.
- Promoted digitalization of irrigation and drainage system maps for irrigation districts.

Agriculture-related tasks received average scores in the 70-point range:

- Water use: 73.5
- Water safety: 70.6
- Water environment: 72.3
- Water value: 74.7

These results highlight particular weaknesses in water safety and water environment. The evaluation suggests the need for stronger agricultural reservoir emergency action plans (EAPs), improved drought and flood forecasting models, enhanced control of non-point source pollution from agriculture, and more preventive water quality management strategies.

4. Conclusions

Integrated water management in Korea represents a major institutional shift toward unified, basin-scale governance. While progress has been made, particularly in policy integration and plan implementation, challenges remain in the agricultural sector—especially in water safety and water environment.

The 2024 evaluation of the Yeongsan–Seomjin–Jeju Basin Plan underscores the necessity of reinforcing agricultural water strategies in light of increasing climate extremes. Moving forward, sustainable water security at the basin level must be pursued by:

1. Enhancing agricultural water infrastructure resilience to floods and droughts,
2. Expanding preventive water quality management and pollution control,
3. Establishing priority-based investment strategies, and
4. Strengthening inter-ministerial cooperation for strategic agricultural water management.

Ultimately, addressing climate-driven water challenges requires not only technical measures but also governance innovations to ensure sustainable and equitable water use across sectors.

References

Yeongsan River Basin Environmental Office. 2025 The 1st evaluation report on implementation of the Yeongsan–Seomjin–Jeju Basin plan.

Development of a Cascade Watershed Water Balance Model Integrating Agricultural Facilities

Dong-Hyun Yoon [1*], Won-Ho Nam [2]

[1] National Agricultural Water Research Center, Hankyong National University, Anseong-si, Gyeonggi-do, Republic of Korea

[2] School of Social Safety and Systems Engineering, National Agricultural Water Research Center, Hankyong National University, Anseong-si, Gyeonggi-do, Republic of Korea

* Corresponding author. Email: wonho.nam@hknu.ac.kr

Abstract

Quantitative assessment of agricultural water is essential yet remains difficult due to limited data and methodological shortcomings. Existing national-level analyses are constrained by the lack of separate demand nodes, the omission of river linkage, and the uniform application of return flow rates. To overcome these limitations, this study proposes a river-centric, network-based water balance model that defines topological relationships among facilities at the sub-watershed scale. By simplifying facility-level analyses and aggregating results to the rural water district and mid-watershed levels, the model provides a practical framework for evaluating agricultural water use in large-scale watersheds with limited observations, thereby supporting more realistic and integrated water resource management.

Keywords: Agricultural water, Water balance analysis, Watershed linkage model, Hydrological model, MODSIM

1. Introduction

Quantitative water balance analysis for agricultural water is essential from local-scale operational optimization to national-level water resources management (Nam et al., 2013). However, accurate evaluation remains challenging due to spatio-temporal uncertainties and the lack of fundamental data. Previous studies have mainly focused on small watersheds or individual reservoirs, where detailed modeling based on observed data has ensured high reliability. Nevertheless, such approaches are often highly site-specific and limited in their applicability to large-scale or data-scarce regions (Nam et al., 2014; Kang et al., 2022). To overcome these limitations, this study developed a generalized water balance model that can be applied even in ungauged or poorly monitored areas. The proposed model adopts sub-watersheds as the minimum analytical units and represents rivers and reservoirs as an interconnected network based on topological relationships. This structure enables the model to reflect hydrological interactions in a simplified yet realistic manner. In addition, improvements were introduced for estimating water demand and supply, as well as methods for river flow and return flow estimation, to enhance applicability under data-limited conditions. The developed model allows comprehensive assessment of agricultural water supply and demand characteristics at the watershed scale, even in regions with restricted data availability. It provides a generalized and versatile tool for supporting rational and realistic agricultural water management, thereby offering significant potential for application across diverse hydrological and geographical settings.

2. Materials and Methods

2.1. Study area and key factors of the water balance model

The study area was the mid-watershed of the Anseongcheon River, where the upstream irrigation districts are supplied mainly by large and medium-sized reservoirs, while the downstream districts rely on Asan Lake and pump stations. The watershed comprises 10 irrigation districts and 219 sub-watersheds, with a total of 513 water facilities including 165 reservoirs, 212 pump stations, and 136 weirs.

The basic data for the water balance analysis included meteorological records, river water data, facility information for reservoirs, pump stations, and weirs, as well as parameters such as percolation and canal loss rates. These datasets were used to estimate the major factors of water balance, including water demand, supply, inflow, and return flow.

2.2. Water balance analysis model algorithm

This study presents a model to improve nationwide agricultural water balance analysis by addressing limitations of existing plans. The model builds a sub-watershed-based network reflecting topological relationships among facilities, and separately analyzes reservoirs and rivers. Reservoirs consider primary and secondary sources with supplementary supply during shortages, while rivers use terminal outflows as available supply allocated from upstream to downstream. Results at the sub-watershed scale were aggregated to rural water districts and mid-watersheds.

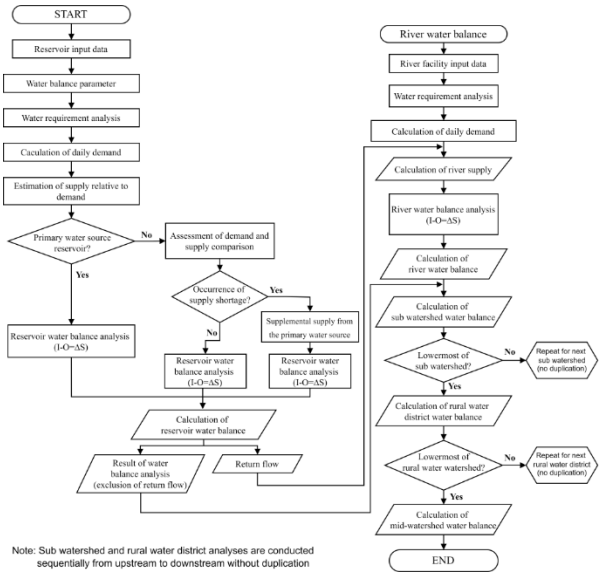

Figure 1. An example of a chart from Excel pasted here using Enhanced Metafile.

3. Results and Discussion

3.1. Results of model validation

Model validation was conducted at four observation sites within the Anseongcheon mid-watershed, using r, NSE, and RSR as evaluation indices. The Pearson correlation coefficient (r) assessed the correlation between variables, NSE evaluated the reproducibility of runoff patterns, and RSR quantified the level of error (Pearson, 1896; Nash and Sutcliffe, 1970; Moriasi et al., 2007). Model validation was conducted at four observation sites, and the simulated runoff showed a tendency to slightly underestimate the observed streamflow. However, since the r, NSE, and RSR indices satisfied the criteria suggested in previous studies, the model was considered suitable for watershed-scale agricultural water balance analysis.

Table 1. Analysis results based on evaluation metrics.

Observation station	r	NSE	RSR
Site 1	0.89	0.65	0.57
Site 2	0.92	0.73	0.52
Site 3	0.83	0.66	0.57
Site 4	0.87	0.69	0.55

3.2. Results of water balance analysis

This study classified rural water districts into reservoir-dominant, balanced supply, and river-facility-dominant types through a source-specific water balance analysis. The results showed greater shortages in primary sources, while some districts exhibited relatively stable river-facility supplies.

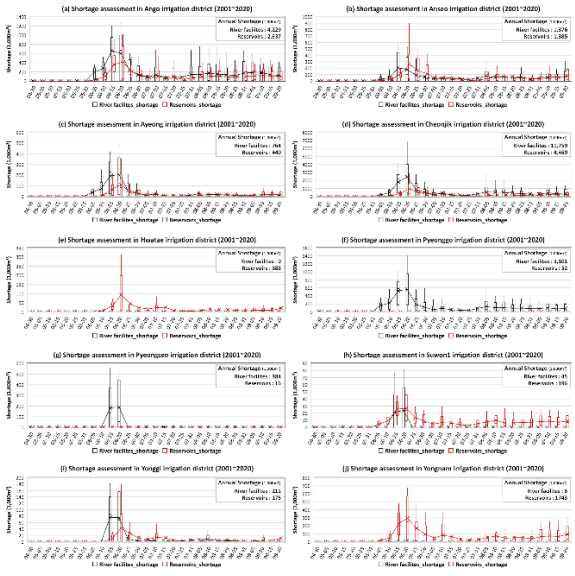

Figure 2. Analysis of shortage by water source in each rural water district.

The water balance analysis of the Anseongcheon mid-watershed revealed significant shortages during 2015–2018, with the Ango district showing the highest deficit rate (28%) and a low return flow ratio (36%), indicating its vulnerability. Overall, the watershed exhibited an average deficit rate of 12% and a return flow ratio of 42%. Compared to the uniform return flow assumption, the proposed model provided more realistic results by reflecting temporal, spatial, and source-specific characteristics.

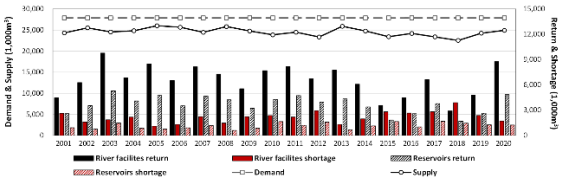

Figure 3. Water Balance Analysis Results in Anseongcheon mid-watershed.

4. Conclusions

This study proposed a watershed-based agricultural water balance model to overcome the limitations of existing national water management plans. The model improved realism by separating water sources, incorporating river water balance, and refining return flow estimation. Validation results showed that key performance indices (r, NSE, RSR) met established criteria, confirming its suitability. Application to the Anseongcheon mid-watershed revealed distinct supply characteristics and vulnerabilities across rural water districts and realistically reflected water shortages that could not be identified through the previous MODSIM analysis. The model is applicable at the national scale, and with further improvements such as incorporating municipal and industrial water use and refining fundamental input factors, it has the potential to contribute significantly to national water management planning and related research.

Acknowledgements

This work was supported by Korea Institute of Planning and Evaluation for Technology in Food, Agriculture, and Forestry (IPET) through Intelligent Agricultural Infra Management for Climate Change Development Program, funded by Ministry of Agriculture, Food and Rural Affairs (MAFRA) (RS-2025-02219764)

References

Nam, W. H., Choi, J. Y., Hong, E. M., and Kim, J. T., 2013. Assessment of irrigation efficiencies using smarter water management. J. Korean Soc. Agric. Eng., 55(4), 45-53.

Nam, W. H., Hong, E. M., Kim, T. G., and Choi, J. Y., 2014. Projection of future water supply sustainability in agricultural reservoirs under RCP climate change scenarios. J. Korean Soc. Agric. Eng., 56(4), 59-68.

Kang, S. K., Choi, S. J., Kim, G. H., and Choi, C. K., 2022. Application of water stress indicator and evaluation of water resource development indicator for stream flow management in dry season. *J. Korean Soc. Hazard Mitig.*, 22(6), 343-350.

Pearson, K., 1896. VII. Mathematical contributions to the theory of evolution.-III. Regression, heredity, and panmixia. Philos. Trans. R. Soc. A, 187, 253-318.

Nash, J. E., and Sutcliffe, J. V., 1970. River flow forecasting through conceptual models part I—A discussion of principles. J. Hydrol., 10(3), 282-290.

Moriasi, D. N., Arnold, J. G., Van Liew, M. W., Bingner, R. L., Harmel, R. D., and Veith, T. L., 2007. Model evaluation guidelines for systematic quantification of accuracy in watershed simulations. Trans. ASABE, 50(3), 885-900.

Assessing the awareness of information and communications technology in construction among enterprises engaged in agricultural and rural development

Yasushi Noguchi [1*], Teruhito Miyamoto [1], Atsushi Ishii [2]

[1] National Institute for Rural Engineering, National Agriculture and Food Research Organization,

2-1-6 Kannondai, Tsukuba, Ibaraki 305-8609, JAPAN

[2] Graduate School of Life and Environmental Sciences, University of Tsukuba,

1-1-1 Tennodai, Tsukuba, Ibaraki, 305-8572, JAPAN

* Corresponding author. Email: noguchi.yasushi956@naro.go.jp

Abstract

Motivated by Japan's i-Construction policy to enhance productivity and address labor shortages, this study examines disparities in the adoption and perceived effectiveness of ICT in construction across company sizes (Mega, Large, and SMEs). Using a web survey of executives, we analyzed ICT adoption rates and satisfaction levels. Results indicate a marked "digital divide": Mega firms show the highest adoption and perceived benefits, while SMEs lag significantly, especially regarding cost-effectiveness and productivity. These findings underscore the need for size-sensitive support, including simplified evaluation tools and knowledge sharing, to ensure equitable ICT diffusion and guide the industry's digital transformation.

Keywords: ICT-based construction, Information and communications technology (ICT), IT investment, Investment evaluation method, Mixed-mode survey

1. Introduction

1.1. Background

As a core sector of national infrastructure, Japan's construction industry faces persistent challenges—labor shortages, an aging workforce, and increasing demands for productivity and safety. To address these, the Ministry of Land, Infrastructure, Transport and Tourism (MLIT) launched the i-Construction initiative in 2016, promoting ICT use such as drone surveying, BIM/CIM, and automated machine control. Yet, despite proven potential, adoption remains uneven across the industry. Especially among enterprises engaged in agricultural land improvement projects, the diffusion of i-Construction remains limited.

A pressing issue is the "digital divide" within the sector. Large firms have the financial and technical capacity to invest in ICT, but SMEs—the majority of the industry—face greater barriers. This disparity risks widening productivity gaps and slowing overall modernization.

1.2. Objectives & Contributions

This study empirically investigates the state of ICT adoption in Japan's construction industry. Focusing on enterprises engaged in agricultural and rural development, the specific objectives are:

1) To assess ICT adoption status and willingness across company sizes (Mega, Large, and SMEs).
2) To compare the perceived effectiveness and satisfaction among adopting firms.
3) To provide data-driven evidence to inform targeted policies and support measures, especially for SMEs.

This study contributes to the literature by quantitatively analyzing the relationship between firm size, ICT adoption, and its perceived effects. Our methodology integrates traditional null hypothesis testing with effect size estimation (Cliff's delta) and clear data visualization, offering more nuanced, practical insights than significance testing alone. By focusing on SMEs, this research provides an evidence base for policymakers and industry practitioners aiming to bridge the digital divide and foster inclusive digital transformation.

2. Methodology

2.1. Survey Design & Target

An online survey was conducted to investigate the status of ICT adoption in the construction industry and the need for investment evaluation methods.

The questionnaire (19 items) captured firm profiles (capital, employees, sales, location), ICT engagement (adoption intention, adoption status, business sectors), and perceived effects (Q14-Q19).

The survey covered construction firms broadly, including those potentially engaged in agricultural land improvement projects as well as general construction enterprises.

1) Period: March 7–20, 2025 (14 days)
2) Respondents: Executives and board members
3) Response Rate: 300 / 630 (47.6%)

2.2. Firm Size Classification

Following Japanese industrial standards, respondents were grouped into three classes:

1) Mega-enterprises (Mega): >3,000 employees or annual sales > JPY 500 billion.
2) Large enterprises (Large): 1,000-3,000 employees or annual sales JPY 5-500 billion.
3) Small and Medium-sized Enterprises (SMEs): <1,000 employees or annual sales < JPY 5 billion.

2.3. Analytical Approach

Analyses combined descriptive and nonparametric statistics:

1) Cross-tabulations and chi-square tests for adoption status (Q12), intention (Q6), and sector (Q13).
2) Kruskal–Wallis tests for Likert-scale outcomes (Q14–Q19).
3) Post-hoc Mann–Whitney U with Holm correction when significant.
4) Effect sizes: Cliff's delta with 95% CI (bootstrap, 1,000).
5) Visualization: bar and radar charts with significance annotations..

3. Results

3.1. ICT Adoption Status and Intention

A statistically significant association was found between firm size and ICT adoption status ($\chi^2(2) = 28.5$, $p < .001$). As illustrated in Figure 1, 87% of Mega-enterprises reported using

ICT, compared to 50% of Large enterprises and less than 33% of Small and Medium-sized Enterprises (SMEs).

Similarly, the intention to adopt ICT differed significantly across classes ($\chi^2(10) = 45.1$, $p < .001$). Mega-enterprises had the highest proportion of firms reporting they were "fully committed" to adoption. In contrast, SMEs were more likely to be "planning to adopt" or have "no plans for adoption," suggesting a more cautious or resource-constrained approach .

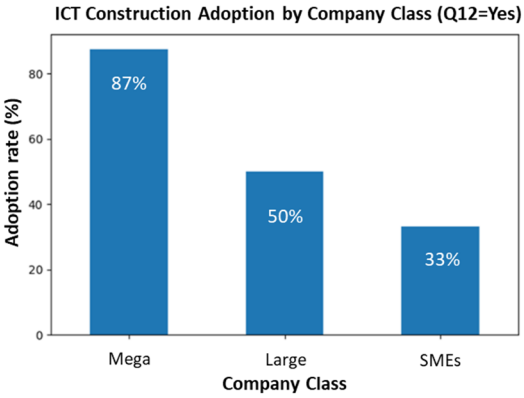

Figure 1. ICT Adoption Rate by Firm Class.

3.2. Primary Business Sectors

The primary business sectors also varied by firm size. Mega-enterprises predominantly engaged in large-scale public civil engineering and architectural projects. In contrast, SMEs were more concentrated in agricultural civil engineering and smaller-scale private construction. This suggests that the scope and type of applicable ICT may differ according to a firm's primary market.

3.3. Perceived Effects of ICT Adoption

For firms that have adopted ICT, a Kruskal-Wallis test revealed significant differences between the classes on three of the six perceived effects: cost-effectiveness (Q14, $H(2) = 8.9$, $p = .012$), productivity improvement (Q16, $H(2) = 11.2$, $p = .004$), and enhanced competitiveness (Q17, $H(2) = 7.5$, $p = .023$). No significant differences were found for error reduction (Q18) or the creation of new business opportunities (Q19).

Post-hoc analysis specified these differences. Mega-enterprises reported significantly greater satisfaction with cost-effectiveness compared to SMEs (Mann-Whitney U, p_{holm} = .01; Cliff's delta = 0.35, 95% CI [0.10, 0.55]). This gap was even more pronounced for productivity improvement (p_{holm} = .003; Cliff's delta = 0.40, 95% CI [0.15, 0.60]).

The radar chart in Figure 2 provides a comprehensive overview, showing that Mega-enterprises consistently reported more positive outcomes (scores closer to 4: indicating relatively positive evaluations) across all metrics compared to their smaller counterparts (scores around 3: reflecting more neutral perceptions).

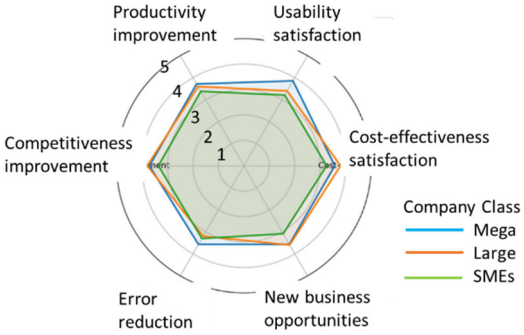

Figure 2. Radar Chart of Perceived Effects of ICT Adoption

4. Discussion

Key Findings & Implications are as follows.

4.1. Digital Divide

A clear digital divide exists as SMEs lag behind Mega-enterprises in ICT adoption and perceived benefits. Mega-enterprises show higher implementation rates and stronger satisfaction with productivity and competitiveness, while SMEs struggle with limited resources, fewer technical experts, and narrower markets. These disadvantages restrict effective ICT use and, without intervention, may widen productivity gaps and further marginalize SMEs, especially in agricultural and rural development where they play a key role.

4.2. Evaluation Gap

SMEs report low cost-effectiveness, largely due to the absence of robust ROI evaluation frameworks. Unlike Mega-enterprises with finance teams and structured models, SMEs often lack tools or expertise to measure benefits. This uncertainty discourages investment, creating a cycle where low adoption produces few success cases, which in turn reduces future uptake. Bridging this gap is vital for evidence-based decision-making.

4.3. Recommendations

Key measures include developing simplified ROI tools for smaller firms, promoting knowledge sharing so that successful cases can be adapted, and providing targeted subsidies or tax incentives. Sector-specific solutions are also essential; in agricultural civil engineering, ICT must fit smaller projects, seasonal conditions, and diverse sites. Lowering barriers in this way can make adoption more practical and beneficial.

4.4. Academic Contribution

This study demonstrates the value of combining effect sizes (Cliff's delta) with p-values to balance statistical and practical significance. Confidence intervals clarify reliability, while annotated visualizations—such as bar charts with markers and radar charts—strengthen clarity. Together, these practices enhance academic rigor and provide practical insights for digital transformation in construction.

5. Conclusions

ICT-based construction adoption is strongly influenced by company size. Mega firms lead in both adoption rates and positive evaluations, benefiting from their stronger financial and technical capacity. SMEs, by contrast, lag in both respects and often face barriers such as limited resources and uncertainty about investment returns. Bridging this divide requires targeted policies, accessible investment evaluation support, and systematic sharing of best practices across firm classes. The findings provide empirical evidence for designing support measures that are sensitive to company size and industry conditions, thereby contributing to the more equitable and effective diffusion of ICT in the Japanese construction sector.

Acknowledgements

This report was supported by JSPS Grant-in-Aid for Scientific Research 21K20608. We also express our gratitude to the Land Improvement Construction Association for their cooperation in this research.

References

Cliff, N. (1993). Dominance statistics: Ordinal analyses to answer ordinal questions. Psychological Bulletin, 114(3), 494–509

Gower, J. C. (1971). A general coefficient of similarity and some of its properties. Biometrics, 27(4), 857–874.

MLIT. (2016). i-Construction initiative policy report.

PHENOLOGY-BASED MAPPING OF DEEP-WATER FLOATING RICE IN MYANMAR USING GOOGLE EARTH ENGINE

Rudiyanto Rudiyanto・Ginting Irawan Frisa・Fatchurrachman Fatchurrachman

・Mohd Shah Ramisah・Che Soh Norhidayah

Abstract

Deep-water floating rice is a unique and climate-resilient cropping system cultivated in flood-prone regions of Myanmar, particularly within the Irrawaddy Delta. Accurate mapping of these rice areas is essential for agricultural planning, food security, and methane emission assessments. This study presents an integrated remote sensing approach to identify and map deep-water floating rice using Sentinel-1 synthetic aperture radar (SAR) and Sentinel-2 multispectral data within the Google Earth Engine (GEE) platform. Sentinel-1's cloud-penetrating capability and Sentinel-2's spectral sensitivity were leveraged to capture the phenological characteristics of floating rice throughout the monsoon season. A phenology-based k-means clustering method was applied to classify temporal patterns of vegetation dynamics. The results revealed extensive deep-water rice cultivation for 2022-2023 in three major regions: Ayeyarwady (142,162 ha), Bago (18,303 ha), and Yangon (7,667 ha). Based on satellite-derived phenological spectral profiles, these areas are typically flooded from July to October during the monsoon season, followed by the cultivation of deep-water floating rice from October to February of the following year. These findings underscore the significance of deep-water rice systems in Myanmar's agricultural landscape and demonstrate the utility of GEE-based analytics for large-scale, timely, and accurate crop mapping. The approach offers a scalable framework for sustainable agriculture monitoring and floodplain management across Southeast Asia.

Agricultural Street-View Survey System with Cabbage Field Object Detection

Hsueh-Yen Shih[1], Ting-Li Liu[2], Shin-Fu Ho[3], Zih-Ying Lee[4], and Candera Wijaya[5*]

[1]Assistant Researcher, Agricultural Engineering Research Center,

[2]Senior Systems Analyst, Ministry of Agriculture,

[3]Assistant Researcher, Associate Researcher, Agricultural Policy Research Center

[4]Assistant Researcher, Agricultural Engineering Research Center,

[5]Associate Researcher, Agricultural Engineering Research Center,

* Corresponding author. Email: rbhung@aerc.org.tw

Abstract

Cabbage is one of Taiwan's most important leafy vegetables, consistently ranking among the top three in national wholesale market volume. Therefore, the Ministry of Agriculture has assigned cabbage as a "price-conscious crop" that requires timely and precise monitoring of planting activities to avoid oversupply and associated price declines. In recent years, the total cultivation area of cabbage has remained around 9,000 hectares annually, with Changhua, Yunlin, and Nantou counties accounting for approximately 55% of the national total. The primary growing season occurs between October and December.

To enhance field mapping efficiency and data timeliness from traditional method, this study involves a roadside farmland street-view survey system. This system utilizes panoramic images captured by consumer-grade GoPro Max cameras mounted on motorcycles to collect crop conditions along rural roads. Thus, the YOLOv8 deep learning object detection model is employed for cabbage fields mapping.

Proposed method develops an object-based cabbage interpretation model by labeled street-view images, achieved the F1 score of 0.85 and the inference speed of 35 frames per second. And the roadside street-view survey system collects approximately 350 agricultural parcel images per hour, enabling rapid and scalable monitoring of cabbage cultivation patterns across major production regions.

Keywords: Cabbage field mapping, object detection, agricultural street-view survey s.

1. Introduction

Cabbage is one of the most important leafy vegetables in Taiwan, consistently ranking among the top three commodities in wholesale market trading volume. In 2020, it was the leading vegetable crop in terms of cultivation area and production, with an output of 409,000 metric tons—five times greater than that of cauliflower, which ranked second. Nevertheless, cabbage production is highly vulnerable to climatic disturbances, such as typhoons and torrential rainfall, which can severely reduce supply and drive up prices. Consequently, monitoring cabbage cultivation and ensuring a stable supply-demand balance has become a critical issue for agricultural authorities.

Historically, the government implemented the "Major Vegetable Seedling Supply Early Warning System" to track seedling distribution. However, due to incomplete registration and information asymmetry, the system has faced difficulties in capturing reliable data on actual cultivation areas and expected yields, thereby limiting its effectiveness in production-side regulation. To overcome these challenges, this study employs a consumer-grade panoramic action camera (GoPro MAX) to collect roadside farmland imagery and develops a deep learning–based object detection model for rapid interpretation of cabbage cultivation patterns. The proposed approach enables timely monitoring of overall cabbage production, thereby providing a more robust foundation for supply regulation and agricultural decision-making.

2. Materials and Methods

The overall workflow of this study is presented in Figure 1. Roadside farmland imagery acquired using the GoPro MAX was first subjected to positional correction for ensuring the precise spatial alignment with the corresponding farmland parcels. Following, the overlapping areas between farmland boundaries and the panoramic imagery were delineated, and the imagery was subsequently partitioned into fixed-size patches for analysis. These image patches were then processed using a cabbage object detection model to identify and map the spatial distribution of cabbage cultivation. The methodology is described in two major components: (1) positional correction of GoPro MAX imagery, and (2) development of the cabbage object detection model

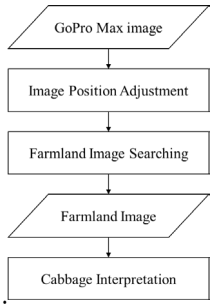

Figure 1. Flow chart

2.1. Positional Correction of GoPro MAX imagery

Since the GoPro MAX relies solely on GPS for positioning, the recorded locations typically contain errors from several meters to several tens of meters. To ensure that the imagery captured by the GoPro MAX can be accurately matched to the correct farmland parcels, positional correction of the GPS data was required.

The correction procedure was based on roadside boundaries as reference features. When the GPS trajectory indicated a movement speed exceeding 7 km/h and the point was located within 10 meters of a road boundary endpoint, that point was designated as the first reference point for correction. The distance and direction from this point to the road boundary endpoint were then calculated

and applied as adjustment values to correct next GPS points. This process was repeated iteratively. However, when the angle formed between consecutive trajectory segments and the road exceeded 135°, the location was considered a turning point. Such turning points were treated as new starting points for recalibration, using the second-nearest road boundary as the reference line. Consequently, a greater number of turning points provided more opportunities for refining the GPS correction.

After positional correction, farmland parcels intersecting with the corrected GPS trajectory within a 10-meter radius were identified, and their corresponding viewing angles were recorded. Image patches representing these farmland parcels were then extracted for subsequent interpretation using the cabbage object detection model, as illustrated in Figure 2.

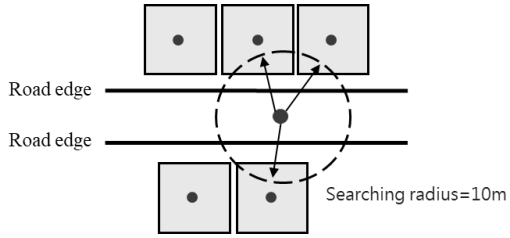

Figure 2. Farmland image searching

2.2. The Development of Cabbage Object Detection Model

This study developed a cabbage object detection model based on YOLOv8 (You Only Look Once) (G. Jocher, A. Chaurasia, and J. Qiu, 2023), YOLO is an end-to-end deep neural network that formulates object detection as a combined regression and classification problem (M. Lan, J. Wang, and L. Zhu, 2023). The overall workflow is presented in Figure 3.

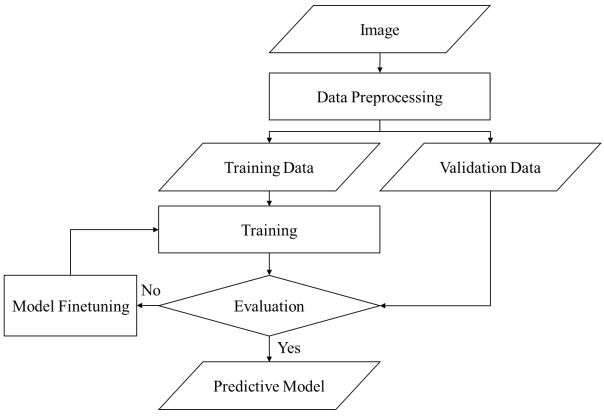

Figure 3. Flow chart for AI model development

To capture the growth dynamics of cabbage, image annotations were performed according to four phenological stages: seeding, vegetative, flowering, and harvest. The preprocessing and labeling scheme for these growth stages is shown in Figure 4, and the annotated dataset was subsequently used for model training.

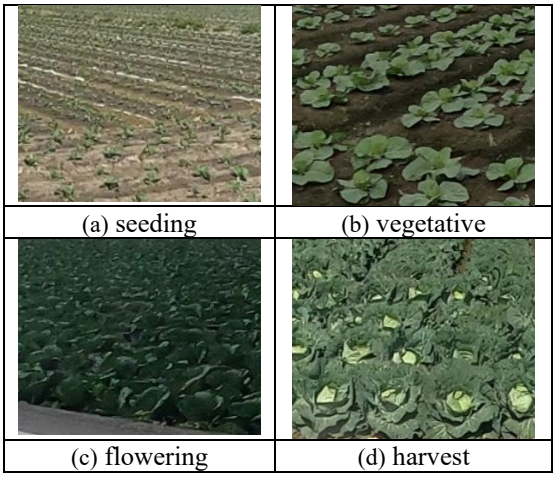

Figure 4. The four phenological stages of cabbage

3. Results

This study developed a cabbage object detection model based on YOLOv8, and the F1 for each growth stage: 0.87 for the seeding stage, 0.89 for the vegetative stage, 0.90 for the Flowering stage, and 0.89 for the harvest stage. To objectively evaluate the model's performance, a validation dataset was employed, and the resulting confusion matrix is presented in Table 1

Table 1. The confusion matrix of result

		Reference				F1
		Seeding	Vegetative	Flowering	Harvest	
Prediction	Seeding	**199**	5	1	0	0.87
	Vegetative	1	**307**	8	0	0.89
	Flowering	0	0	**341**	38	0.90
	Harvest	0	0	2	**107**	0.89

4. Conclusions

In this study, a consumer-grade action camera (GoPro MAX) was used to collect roadside farmland imagery, enabling the acquisition of at least 300 farmland parcels per hour. After positional correction, the images were accurately aligned with their corresponding farmland locations. Subsequently, the cabbage object detection model was applied to rapidly identify cabbage cultivation within the fields. The model achieved F1-scores greater than 0.87 across all growth stages, with an average inference time of less than 50 milliseconds per image.

References

J. Redmon, S. Divvala, R. Girshick, and A. Farhadi.,2016 You only look once: Unified, real-time object detection, *IEEE Conf. Comput. Vis. Pattern Recognit. (CVPR)*, Las Vegas, NV, USA , pp. 779–788.

G. Jocher, A. Chaurasia, and J. Qiu., 2023. *YOLO by Ultralytics (Version 8.0.0)*.: https://github.com/ultralytics/ultralytics

Yolov8 anchor-free bounding box prediction - issue 189.https://github.com/ultralytics/ultralytics/issues/189, 2023.

M. Lan, J. Wang, and L. Zhu., 2023 Perception and Range Measurement of Sweeping Machinery Based on Enhanced YOLOv8 and Binocular Vision, IEEE Access, vol. 11, pp. 126398–126408,

Experiments on Internet Environment Improvement in Mountainous Farmland Using Starlink and Mesh-net Wi-Fi Technology

Masaru Mizoguchi [1*], Yasuhiro Itakura [2]

[1] Graduate School of Agricultural and Life Science, The University of Tokyo, Bunkyo-ku, Tokyo1113-8657, Japan

[2] Misao Network Ltd., Kawaguchi, Saitama 334-0061, Japan

* Corresponding author. Email: mizo@g.ecc.u-tokyo.ac.jp

Abstract

Fourteen and a half years have passed since the 2011 Fukushima Daiichi nuclear disaster. In Iitate Village, Fukushima Prefecture, the evacuation order was lifted in 2017. Due to the limited number of farmers returning, farmland consolidation and centralization are progressing faster than in any other municipality in Japan. The Iitate Village Promotion Public Corporation (Agriculture Department) has led the management and cultivation of this land. However, many of the consolidated farmlands are in mountainous and forested areas, where cellular reception is poor and the latest smart agricultural machinery cannot be fully utilized.

In this study, we conducted an experiment to establish an internet environment in rice paddies lacking communication infrastructure, using Starlink satellite internet and mesh Wi-Fi technology. Our goal was to develop an independent communication infrastructure to support the implementation of smart agriculture. As a result, in the consolidated farmlands of District S, the status of water gates along an approximately 2-kilometer agricultural irrigation canal can now be monitored in real time via smartphone. The area has thus been transformed into an advanced model of farmland where smart agriculture is feasible. We believe that this technology has the potential to accelerate the adoption of smart agriculture in Japan significantly.

Keywords: Starlink, Mesh-net, Wi-Fi, Mountainous farmland

1. Introduction

Fourteen and a half years have passed since the 2011 Fukushima Daiichi nuclear disaster. In Iitate Village, Fukushima Prefecture, the evacuation order was lifted in 2017. Due to the limited number of farmers returning, farmland consolidation and centralization are progressing faster than in any other municipality in Japan. The Iitate Village Promotion Corporation (Agriculture Division) is currently operating this consolidated farmland. However, since the farmland lies between forested hills, mobile-phone reception is unavailable in many areas, preventing full utilization of smart-agriculture machinery. This study therefore constructed an internet environment using Starlink and mesh-net Wi-Fi technology to support smart agriculture applications such as remote monitoring of irrigation gates via Wi-Fi cameras.

2. Materials and Methods

At a consolidated rice-paddy area (approx. 12 ha) in the S district of Iitate Village, a Starlink internet base station was installed on a ridge, and Wi-Fi network coverage was extended across the field. (Fig.1, Fig.2)

2.1. Starlink Internet Base Station

Starlink, a broadband service by SpaceX using low-orbit satellites, provides stable communication even in remote mountainous or maritime areas. We installed the Starlink unit on a field ridge. Since there is no commercial power, power was provided by a box containing four 100 W solar panels. (Fig.2)

Figure 1. Layout of Wi-Fi communication network. A starlink internet base station (red), Wi-Fi repeaters (yellow), and Wi-Fi cameras (blue) were installed in a consolidated rice-paddy area.

2.2. Mesh-net Wi-Fi Repeater

An outdoor AP (EAP225Outdoor, TPLink) was connected via PoE Ethernet cable to the Starlink internet base station and mounted on a 3 m mast. From this base, two network routes were extended, each supporting five Wi-Fi repeaters powered by battery and 50 W solar panel, also mounted on 3 m poles. (Fig.2 right)

Figure 2. A Starlink internet base station (left) and a Wi-Fi repeater (right) installed on a ridge of paddy.

Rice fields in this district require water-management gates along approximately 2 km of waterways where mobile signals are absent. We installed Wi-Fi cameras (Reolink JP) at several gates to enable remote monitoring.

2.3. Weather Station Installation

As the fields lie in a mountain-surrounded wind corridor, we installed an ATMOS41 (METER Group, Inc) weather station and Wi-Fi data logger ZL6 (METER Group, Inc.) to monitor cultivation environment.

3. Results and Discussion

3.1. Starlink Internet Base Station

The power box was time-controlled and active from 6 AM to 6 PM. Real-time videos from the gates were transmitted during this period. Midday solar-voltage instability occasionally causes communication problems.

3.2. Mesh-net Wi-Fi Performance

Using the Omada cloud controller app (TP-Link Japan Inc.), we can monitor devices, clients, and the network topology map in the field. Table 1 shows distance between APs (m) and Signal Strength (dBm).

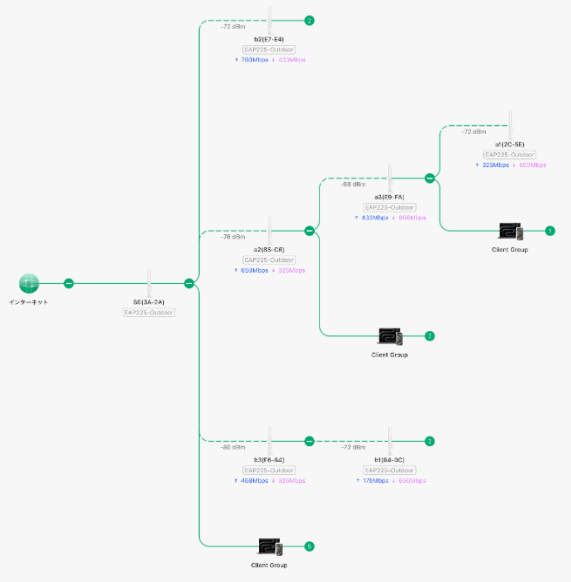

Figure 3. Mesh-net Wi-Fi Topology with the Omada cloud controller app (TP-Link Japan Inc.)

Table 1. Distance between APs (m) and Signal Strength (dBm). <number> indicates distance between APs (m). Signal strength (dBm) may vary by ±2 dB depending on weather conditions.

Path-a	S0	<421>	a2	<250>	a3	<211>	a1
Signal Strength		-76		-68		-72	
Path-b	S0	<396>	b2				
Signal Strength		-71					
Path-c	S0	<700>	b3	<325>	b1		
Signal Strength		-80		-75			

3.3. Water Gate Monitoring via Wi-Fi Cameras

When Starlink was active, smartphone or PC users could view gate conditions in real time. (Fig.4)

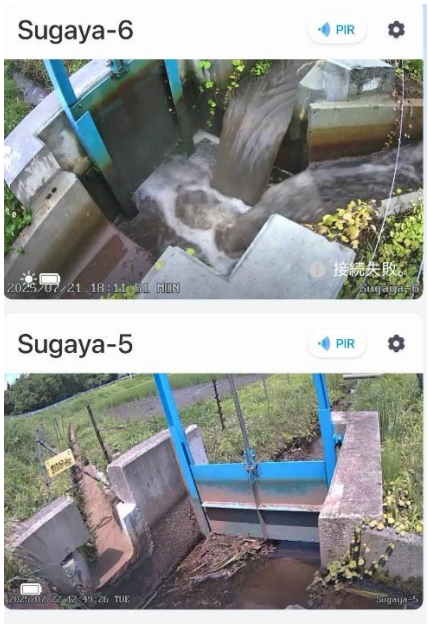

Figure 4. Monitoring water gates with Wi-Fi cameras.

3.4. Meteorological Data Acquisitions

Temperature, wind speed, precipitation, and solar radiation are recorded. Data can be collected even in areas without mobile signals. (Fig.5)

4. Conclusions

This experiment deployed Starlink in remote farmland with no mains power or mobile reception and expanded coverage via mesh-net Wi-Fi. As a result, the S district farmland gained digital infrastructure, enabling smart agriculture. If power and internet exist in nearby community buildings, leveraging those could reduce costs. Depending on the site conditions, this approach can enable remote farm management even in abandoned fields and contribute to resolving challenges in Japanese agriculture.

References

Mizoguchi, M., and Itakura, Y., 2024. Field WiFi expansion experiment in Iitate Village. J. Agricultural Reconstruction Science, 4(2), pp. 8-13

Mizoguchi, M., and Itakura, Y., 2025. Experiments on Internet environment improvement in mountainous farmland using Starlink and mesh net Wi-Fi technology. J. Agricultural Reconstruction Science, 5(2), pp. 23-28

Mizoguchi, M., and Itakura, Y., 2024. Proceedings of the Japanese Society of Irrigation, Drainage and Rural Engineering. pp. 135-136

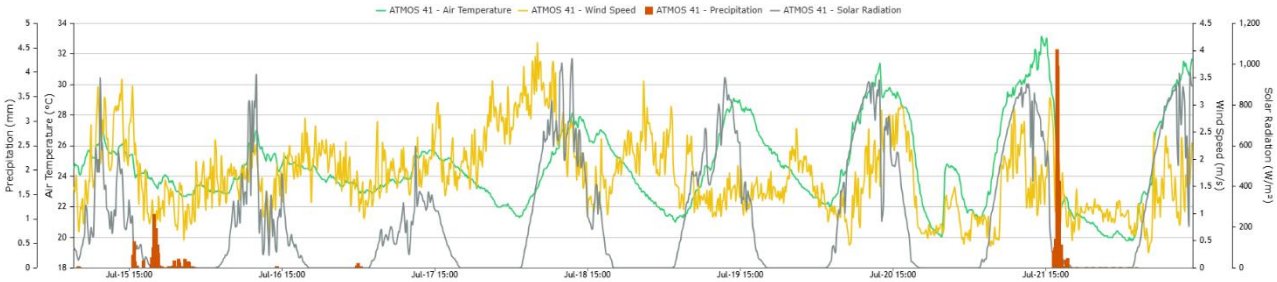

Figure 5. Meteorological data observed with Wi-Fi type ATMOS41 weather station.

Crop Cultivation Activity Impacts Evaluation using Water-Energy-Food-Carbon-Water Quality Nexus

Yoon PuReun・Kim Maga・Choi Jin-Yong・Hur Seung-Oh・Son Jeong-Woo

Abstract

To solve food security, concerns about the environmental load in the agricultural sector are increasing due to the high input farming method focused on productivity increase. Accordingly, in order to reduce environmental load and sustain the agricultural environment, activities such as AECP (Agricultural Environment Conservation Program). In addition, each resource affects other resources, and the relationship between resources is affected by external environmental conditions. Therefore, it is essential to analyze the inter-connections between nexus elements, including agricultural resources, carbon emissions and water quality, by applying the nexus concept. Crop cultivation activities such as irrigation, fertilization, tillage have a significant impact on nexus elements. For the impact evaluation of crop cultivation activities, it is necessary to establish a water-energy-food-carbon-water quality nexus, and a comprehensive analysis between nexus elements under the crop cultivation activity scenario is required. Therefore, this study conducted a linkage analysis according to the crop cultivation activity scenario. Crop cultivation activity scenarios included water, fertilizer, tillage management, conservation practices, performed in paddy and upland. The water-energy-food-carbon-water quality nexus was configured to derive standardized values for each nexus element, including agricultural resources, carbon and water quality elements. The APEX/ APEX-Paddy model was used to simulate the nexus elements. Besides, statistical data and national greenhouse gas emission factors were collected to simulate energy use and carbon emissions. This study is expected to be used as a policy decision-making tool for applying various crop cultivation activities to efficiently use limited resources and reduce environmental load and carbon emissions.

Improved Water Efficiency of Paddy Farming through Alternate Wetting and Drying Irrigation in Central Taiwan

Hsuan-Ju Tsai[1*], Pei-Jhen Wu[2], Dong-Hong Wu[3], Shin-Ruei Lee[2]

[1] Agricultural Technology Translation Center, Taiwan Agricultural Research Institute, Ministry of Agriculture, Taichung City, Taiwan

[2] Crop Science Division, Taiwan Agricultural Research Institute, Ministry of Agriculture, Taichung City, Taiwan

[3] Department of Agronomy, National Chung Hsing University, Taichung City, Taiwan

* Corresponding author. Email: hjtsai@tari.gov.tw

Abstract

Uneven precipitation distribution in Taiwan often leads to water shortages during the early stages of the first rice crop season. As rice (*Oryza sativa* L.) is a water-intensive crop, efficient irrigation strategies are essential. Alternate wetting and drying (AWD) is a practical, water-saving technique for rice cultivation. This study evaluated two AWD types—safe-AWD (field water level ⩽ 15 cm below the soil surface) and mild-AWD (15–20 cm)—in comparison with conventional flooding (CF) during the first and second crop seasons of 2024 in Taichung, Taiwan. The greatest difference in water consumption between AWD and CF occurred during the tillering stage in both crop seasons. In the first crop season, plant height and leaf area index under AWD were slightly lower during development stage, but grain yield differed by less than 5% compared to CF. AWD reduced irrigation water input over 58%, with water use efficiency (WUE) nearly double that of CF. In the second crop season, yields under AWD were approximately 20% lower than those under CF. Although AWD reduced irrigation water input at least 40%, abundant rainfall resulted in no differences in WUE between regimes. Overall, compared to CF, AWD reduced the number of flooded days up to 17 days, required only 40% of the irrigation hours and extended the re-irrigation interval by two days, thereby reducing labor demands for irrigation management. AWD demonstrated higher water use efficiency during the first crop season in central Taiwan, suggesting its potential as a water allocation strategy during periods of water shortage.

Keywords: rice, irrigation management, water shortage

1. Introduction

Agricultural irrigation in central Taiwan primarily depends on surface runoff, which is highly influenced by the amount and spatiotemporal distribution of rainfall. Precipitation is concentrated during the rainy season (June–August), whereas the dry season extends from November to April. The rainfall during the dry season typically accounts for only one-fifth to one-quarter of the annual total. There is also significant interannual variability in monthly rainfall, with spring often experiencing insufficient distribution. As a result, the early stage of 1st crop paddy rice frequently suffers from irrigation shortages. For 2nd crop, irrigation shortages are less frequent because rice enters the milk stage after October.

In 2024, the total rice cultivation area in Taiwan was approximately 240,000 hectares, with central Taiwan accounting for about 29% of national production. Water scarcity in this region can severely impact rice production — highlighting the necessity of developing effective irrigation strategies.

2. Materials and Methods

2.1. Experimental Site and Design

The study was conducted in Wufeng District, Taichung city, Taiwan (Fig.1.) for two crop seasons in 2024. Paddy rice (Tainung 71) was cultivated in plots of 0.5 hectares each. 1st crop was transplanted on 1 Mar. and harvested on 17 Jun. 2nd crop was transplanted on 23 Jul. and harvested on 29 Oct. The soil properties of the experiment field were analyzed (Table 1.). Fig. 2. shows the monthly rainfall and average temperature in 2024 versus average of past ten years of the experimental site.

Fig.1. Experimental plot layout in Taichung city, Taiwan.

Table 1. Soil properties of experiment field.

Soil property	Soil texture	Bulk density (g/cm³)	Saturated hydraulic conductivity (cm/sec)	Infiltration rate (mm/hr)
	Clay Loam	1.6	0.014	16.5

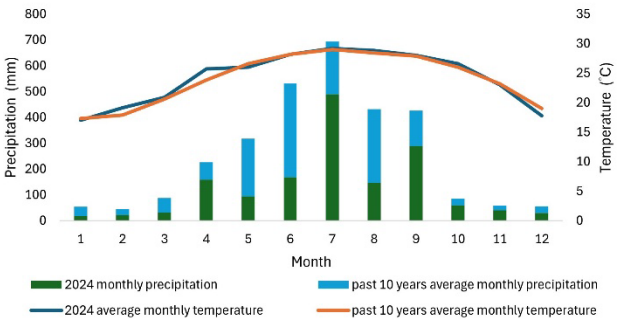

Fig.2. Monthly temperature and rainfall trends in 2024 vs. average of past ten years.

2.2. Irrigation regimes and data collection

Rice was grown under three irrigation regimes, conventional flooding, safe-AWD (field water level (FWL) ≤ 15 cm below the soil surface) and mild-AWD (15–20 cm below the soil surface). PVC tubes were used to monitor the FWL, and irrigation was applied when the FWL dropped to 15 cm or 20 cm below the soil surface. (Ishfaq et al., 2020). Plant height (PH), tiller number, and leaf area index (LAI) were measured, and grain yield was determined at harvest. Irrigation water input for each regime was recorded.

3. Results and Discussion

3.1. Effect of Different Irrigation Regimes on Growth Characters of Rice

3.1.1.First crop

The PH of CF was slightly higher than that of the other two AWD regimes during the panicle initiation to heading stages (Table 2); however, this difference was not significant at harvest. Similarly, no significant differences in tiller number or LAI were observed among the regimes.

Table 2. Growth characters of 1st crop rice under three irrigation regimes. Different letters represent significant differences ($p < 0.05$).

	Growth stage	Tillering		Panicle initiation	Booting stage	Heading stage	Dough stage	Maturity
Days after transplanting		19	40	51	61	69	79	97
PH	CF	29.09 a	76.59 a	85.75 a	98.75 a	102.00 a	103.42 a	103.09 a
	Safe-AWD	26.67 a	72.75 b	80.58 b	94.34 ab	98.92 ab	102.08 a	101.50 a
	Mild-AWD	26.00 a	69.25 c	77.92 b	89.75 b	95.50 b	98.75 a	99.00 a
Tiller	CF	14.34 a	29.92 a	32.09 a				
	Safe-AWD	13.83 a	29.84 a	31.75 a				
	Mild-AWD	12.34 a	28.25 a	31.00 a				
LAI	CF	0.14 a	2.49 a	3.41 a	4.15 a	4.26 a	4.19 a	3.64 a
	Safe-AWD	0.09 b	2.06 a	2.99 a	3.73 a	3.91 a	3.93 a	3.34 a
	Mild-AWD	0.01 c	1.98 a	2.98 a	3.59 a	3.73 a	3.72 a	3.15 a

3.1.2.Second crop

PH of CF was slightly higher than that of the other two AWD regimes during the heading stage (Table 3), while mild-AWD exhibited the lowest PH at maturity. No significant differences in tiller number or LAI were observed among the regimes.

Table 3. Growth characters of 2nd crop rice under three irrigation regimes. Different letters represent significant differences ($p < 0.05$).

	Growth stage	Tillering		Panicle initiation	Booting stage	Heading stage	Dough stage	Maturity
Days after transplanting		22	45	55	64	73	83	94
PH	CF	45.4 a	89.1 a	101.0 a	109.3 a	109.6 a	110.0 a	110.0 a
	Safe-AWD	46.7 a	85.1 b	97.3 ab	106.0 ab	109.4 a	109.8 a	109.8 a
	Mild-AWD	44.4 a	80.9 c	91.4 b	102.3 b	102.7 b	102.9 b	104.3 b
Tiller	CF	18.75 a	25.08 a					
	Safe-AWD	18.17 a	25.25 a					
	Mild-AWD	18.33 a	24.33 a					
LAI	CF	0.21 a	2.35 b	3.12 a	3.19 a	3.44 a	3.01 a	3.02 a
	Safe-AWD	0.26 a	2.73 a	3.50 a	3.57 a	3.61 a	3.39 a	2.56 a
	Mild-AWD	0.16 a	2.04 b	2.86 a	3.31 a	3.32 a	3.21 a	2.67 a

3.2. Effect of Different Irrigation Regimes on Yield and Water Use Efficiency of Rice

3.2.1.First crop

The greatest variation in irrigation water input occurred between late March and mid-May, corresponding to the tillering to heading stages of rice development (Fig. 3). Total irrigation water applied for CF, safe-AWD, and mild-AWD was 2,050.4 mm, 864.9 mm, and 603.6 mm, respectively. Grain yields of the AWD regimes differed by less than 5% compared to CF, while WUE was nearly double that of CF (Table 4).

3.2.2.Second crop

The greatest variation in irrigation water input occurred in August, corresponding to the tillering stage (Fig. 4). Total irrigation applied for CF, safe-AWD, and mild-AWD was 1,021.5 mm, 579.4 mm, and 549.7 mm, respectively. Grain yield of CF was 20% and 27% higher than that of safe-AWD and mild-AWD, respectively. Although AWD reduced irrigation input by more than 40%, abundant rainfall resulted in no significant differences in WUE among the regimes (Table 5).

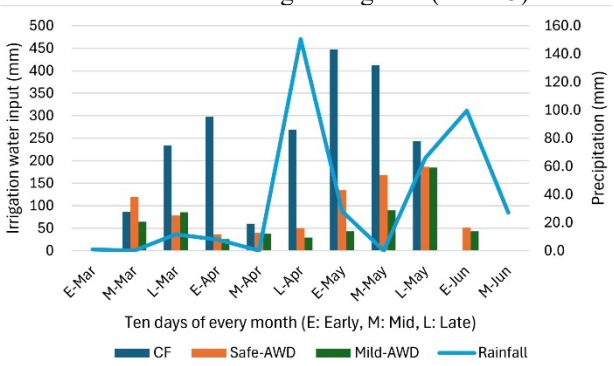

Fig. 3. Irrigation water input under three irrigation regimes of 1st crop. Total rainfall during growing season was 391.5 mm.

Table 4. Yield and WUE under three irrigation regimes of 1st crop. Total water input was the sum of irrigation and rainfall.

Treatment	Total water input (mm)	Yield (Kg/ha)	WUE (Kg/m³)	Flooding days	Irrigation hours	Re-irrigated frequency (days)
CF	2,441.9	6,092	0.25	60	233.3	2.2
Safe-AWD	1,256.4	6,230	0.5	55.3	88.7	3.9
Mild-AWD	995.1	5,832	0.59	43	87.7	3.9

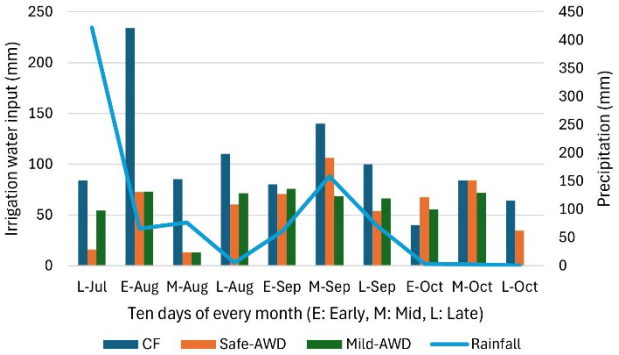

Fig. 4. Irrigation water input under three irrigation regimes of 2nd crop. Total rainfall during growing season was 865.0 mm.

Table 5. Yield and WUE under three irrigation regimes of 2nd crop. Total water input was the sum of irrigation and rainfall.

Treatment	Total water input (mm)	Yield (Kg/ha)	WUE (Kg/m³)	Flooding days	Irrigation hours	Re-irrigated frequency (days)
CF	1,886.5	7,062	0.37	43	271	2.2
Safe-AWD	1,444.4	5,930	0.41	26	68.7	4.8
Mild-AWD	1,414.7	5,572	0.39	26.8	72.7	4.4

Overall, compared to CF, AWD reduced the number of flooded days by up to 17 days, required only 40% of the irrigation time, and extended the re-irrigation interval by 2 days (Tables 4 and 5).

4. Conclusions

Considering the rainfall patterns in central Taiwan and the peak water demand period for rice, water shortages are most likely to occur from late March to May. AWD demonstrated higher water efficiency during the first crop season. Within an acceptable range of yield impact, AWD offers a practical basis for optimizing regional rotational irrigation scheduling and is worth repeated trials to improve effectiveness.

Acknowledgements This research was supported by the Ministry of Agriculture of Taiwan.

References

Ishfaq, M.; Farooq, M.; Zulfiqar, U.; Hussain, S.; Anjum, S.A. Alternate wetting and drying: A water-saving and ecofriendly rice production system. Agric. *Water Manag.* 2020, 241, 106363.

Establishing Corn Crop Coefficients for Precision Irrigation in Sustainable Paddy Rotation Systems

Shin-Ruei Lee [1*], Hung-Yu Dai [1] , Ping-Wei Sun [1]

[1] Taiwan Agricultural Research Institute, Ministry of Agriculture, Taichung City, Taiwan

Abstract

Paddy farming systems face significant water management challenges intensified by climate change. Integrating corn into paddy-corn rotation systems provides an effective strategy to improve water use efficiency. This study assessed daily crop coefficients (Kc) for corn, documenting values ranging from 0.11 to 1.75, with specific initial and mid-growth stage Kc values of 0.51 and 0.84 for spring, and 0.58 and 0.78 for autumn, respectively. Utilizing these Kc values in the CROPWAT model, daily crop evapotranspiration (ETc) was calculated, yielding seasonal ETc totals of 162, 127, 186, and 193 mm for four cropping periods in 2022 and 2023. Irrigation scheduling guided by these ETc estimations recommended more frequent irrigation than traditional practices but significantly reduced water wastage. These findings provide critical crop-specific water-use data, serving as an essential reference for enhancing precision irrigation practices and supporting sustainable water management in paddy-corn rotation systems.

Keywords: Sweet corn, Irrigation scheduling, CROPWAT

1. Introduction

Taiwan's climate shows pronounced wet and dry seasons that intensify irrigation pressure in paddy agriculture and complicate water allocation. Aligning irrigation with crop water requirements, expressed as crop evapotranspiration, ETc, is fundamental to climate resilient and water efficient management. The FAO 56 framework, based on reference evapotranspiration, ETo, and the crop coefficient, Kc, provides a robust basis for estimating ETc, and the CROPWAT model translates these parameters into operational irrigation schedules. However, stage specific Kc values for sweet corn are limited and highly dependent on local conditions, which underscores the need for locally derived coefficients and field validation. This study has two objectives. First, it establishes daily and growth stage Kc for sweet corn under contrasting spring and autumn climates. Second, it applies the resulting parameters in CROPWAT to generate irrigation schedules for comparison with conventional farmer practice. The broader aim is to position corn within paddy and corn rotation as a lower demand phase that reduces pressure on shared water resources.

2. Materials and Methods

2.1. Experimental Fields

Experimental fields for monitoring evapotranspiration were established in 2022 and 2023, with the aim of collecting fundamental data on sweet corn evapotranspiration and crop coefficients across three cropping seasons. The autumn 2022 crop was cultivated in Liujiao Township, Chiayi County (23.52°N, 120.27°E), with a field area of 3.5 hectares. In 2023, both spring and autumn crops were planted in Wufeng District, Taichung City (24.02°N, 120.68°E), each with an area of 1.1 hectares.

Figure 1. Experimental field, Liujiao Township, Chiayi County (left); Wufeng District, Taichung City (right).

2.2. Evapotranspiration and crop coefficients

To monitor ETc, eddy covariance systems were installed in the experimental fields. The system included an open-path CO_2/H_2O analyzer (7500DS, Licor Inc., USA), a three-dimensional ultrasonic anemometer (Gill WindMaster PRO, Gill Instruments Ltd., UK), and a net radiometer (NR-LITE2, Campbell Scientific, Inc., USA), all mounted at a height of 2.4 meters above the ground. Additional sensors included soil heat flux plates (HFP01, Campbell Scientific, Inc., USA) and soil moisture-temperature probes (CS616, Campbell Scientific, Inc., USA), installed at depths of 5 cm and 15 cm, respectively.

Figure 2. Eddy covariance system.

The Kc represents the ratio between ETc and ETo:

$$Kc = ETc/ETo \quad (1)$$

where Kc is crop coefficient; ETc is crop evapotranspiration, mm; ETo is reference evapotranspiration, mm.

ETc was calculated from the latent heat flux measured by the eddy covariance system, after appropriate unit conversion. ETo was calculated using the CROPWAT 8.0 software based on the Penman-Monteith equation (Allen et al. 1998; Smith 1992).

3. Results and Discussion

3.1. Crop coefficients

To establish local Kc for sweet corn in Taiwan, daily ETc was divided by ETo. The results indicated that Kc values were relatively low during the initial growth stage and gradually increased as the plants developed. A noticeable spike in Kc values was observed around 20 days after planting. The ranges of daily Kc values across the three cropping seasons were 0.11–1.75, 0.17–1.36, and 0.25–0.99, respectively. Growth stages were defined according to the FAO crop coefficient model and categorized into initial, development, and mid stages. The average Kc values with initial and mid-growth stage were 0.51 and 0.84 for spring, and 0.58 and 0.78 for autumn, respectively.

3.2. CROPWAT irrigation schedule

Using the locally established crop coefficients as inputs, CROPWAT was applied to estimate daily ETc and to generate irrigation schedules for four cropping seasons. Model outputs were then compared with field irrigation records (Table 1). In general, CROPWAT recommended a higher irrigation frequency than that adopted in practice. Except for autumn 2022, the model suggested lower total irrigation amounts than those applied in practice. In that season, excessive irrigation during the seedling stage led to waterlogging, which led to over-irrigation beyond the requirement and impaired crop growth. As a whole, the model's irrigation predictions during the high-yielding spring and autumn 2023 seasons closely matched observed applications, indicating that the CROPWAT-based schedule provides a useful reference for irrigation planning and water-saving management.

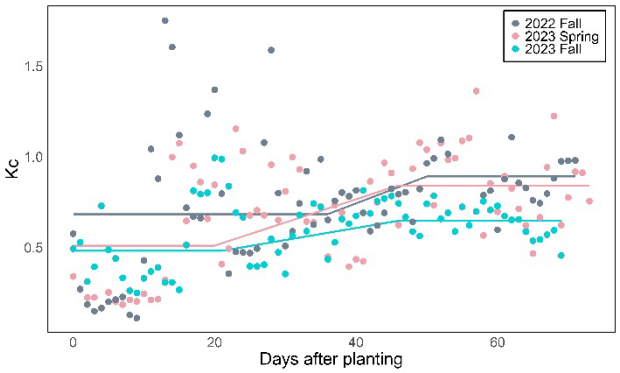

Figure 3. The daily crop coefficients of the three cropping periods and the average crop coefficient values in each growth stage.

Table 1. Comparison between CROPWAT irrigation schedule and actual irrigation practices.

Crop	Rain (mm)	ETc (mm)	Number of irrigations		Irrigation amount (mm)	
			Actual	Estimated	Actual	Estimated
2022 spring	406	162	1	4	14	76
2022 autumn	17	127	6	5	259	92
2023 spring	307	186	3	5	134	103
2023 autumn	45	193	3	8	181	190

4. Conclusions

This study developed locally validated crop coefficients for sweet corn by season and growth stage and applied them to simulate irrigation demand using the CROPWAT model. The resulting coefficients enabled accurate estimation of daily crop water use and informed stage-specific irrigation scheduling. Across four cropping periods, the seasonal evapotranspiration values were 162, 127, 186, and 193 millimeters, respectively. These findings confirm that corn rotation requires a comparatively moderate amount of water, making it a viable strategy to reduce irrigation pressure under limited water availability. Compared to actual field practices, CROPWAT generally recommended more frequent irrigation events, while the total irrigation amounts were comparable to observed values in the high-yielding seasons of 2023. Moreover, CROPWAT enables rapid calculation of daily crop water requirements, providing a practical reference for decision-makers in planning irrigation schedules. These findings offer a reliable technical basis for implementing precision irrigation and improving water use efficiency in paddy–corn rotational systems.

Acknowledgements

The authors gratefully acknowledge Pei-Jhen Wu for her assistance in the preparation of this poster.

References

Allen, R. G., L. S. Pereira, D. Raes and M. Smith. 1998. Crop evapotranspiration-Guidelines for computing crop water requirements-FAO Irrigation and drainage paper 56. Fao, Rome. 300:D05109.

Smith, M. 1992. CROPWAT: A computer program for irrigation planning and management. Food & Agriculture Org.

Evaluation of Return Flow and Reuse Efficiency Using Water Cycle Simulation in Irrigation Canal Networks

Hyeon-Ji Lee [1], Won-Ho Nam [2*], Ji-Hyeon Shin [3]

[1] Undergraduate Student, School of Social Safety and Systems Engineering, Hankyong National University, Anseong, Republic of Korea

[2] Professor, School of Social Safety and Systems Engineering, National Agricultural Water Research Center, Hankyong National University, Anseong, Republic of Korea

[3] Ph.D Student, Department Integrated System Engineering, Hankyong National University, Anseong, Republic of Korea

* Corresponding author. Email: wonho.nam@hknu.ac.kr

Abstract

Among various climate-related disasters, droughts are developing gradually and exhibiting significant temporal and spatial variability, with long-term implications for agriculture and water supply. Concurrently, the growing incidence of localized heavy rainfall has contributed to rising agricultural water variations, emphasizing the need to enhance the efficiency of rural irrigation systems. In reservoir-managed paddy field irrigation areas, part of the supplied water returns to canals via runoff or infiltration. This return flow, often overlooked in traditional analyses, can serve as a reusable resource for nearby irrigation areas. This study aims to quantitatively evaluate return flow and reuse efficiency through integrated water cycle analysis using the Environmental Protection Agency's Storm Water Management Model (EPA-SWMM), which enables simulation of irrigation canal networks. To this end, a detailed water supply network for agricultural reservoirs was constructed using SWMM, incorporating hydraulic control, canal characteristics, slope, and drainage structures. In this study, water balance analysis was employed to quantitatively assess the trends in return flow and the corresponding volume of water reuse according to the configuration of irrigation canals and networks, thereby elucidating the hydrological cycle associated with agricultural water supply. Ultimately, the findings of this study are expected to provide foundational data for efficient agricultural water management grounded in water cycle dynamics and to offer valuable insights for water allocation and operational strategies during periods of drought or water scarcity.

Keywords: Irrigation water, water balance analysis, return flow reuse, SWMM

1. Introduction

The frequency and intensity of droughts have been increasing worldwide due to abnormal climate conditions, posing significant challenges to agriculture and water resource management. Agricultural drought, caused by soil moisture depletion and reduced reservoir storage, directly affects crop growth and yield. In Korea, agricultural water use accounts for about 41% of total water resources, highlighting the need for systematic management. However, conventional experience-based water management practices often result in water loss and uneven distribution, emphasizing the necessity of quantitative research on rational water allocation and irrigation efficiency.

2. Materials and Methods

2.1. Study area

The study area was selected as the Sagok Reservoir, located in the Nakdong River basin. The reservoir is situated in Gyeongsangbuk-do, with an effective storage capacity of 5,175 × 10^3 m^3, a watershed area of 1,340 ha, and an irrigated area of 272 ha. The irrigation network consists of 20 main canals and 30 sub canals.

2.2. Definition and estimation method of return flow reuse

In this study, quick return flow and the quick return flow rate (RF_Q) were evaluated for each water supply, based on the drainage from the main canal (D_{mc}) and sub canal (D_{sc}). The calculation of (RF_Q) is defined in Equation (1).

$$RF_Q = (D_{mc} + D_{sc}) \times 100(\%) \quad (1)$$

2.3. EPA-SWMM

The EPA-SWMM model is a rainfall–runoff analysis model capable of simulating not only single rainfall events but also continuous rainfall events (Baffaut and Delleur, 1989). This model can be applied to analyze the hydraulic characteristics of agricultural water flow through canal networks that reflect the structural features of irrigation facilities such as open channels, pipelines, and intake weirs (Niazi et al., 2017). In addition, it enables simulation of irrigation water distribution by adjusting supply volumes and flow controls to account for regional water management strategies, and provides a detailed evaluation of irrigation return flow components—including supply, drainage, and infiltration—based on water sources, main and sub canals, and service areas (Rossman, 2010).

In this study, a canal network was developed for an irrigation district receiving actual agricultural water supply using the EPA-SWMM model. The analysis period was set from May 1 to September 30, 2024, and the required input data included source water supply, rainfall, evapotranspiration, and infiltration. The model simulated the distribution of water from a single source through main and sub-canals to individual paddy fields. Two water management scenarios were compared: Scenario A, without gate control, and Scenario B, in which gate operations were adjusted based on Scenario A results to mitigate water shortages and enhance irrigation efficiency.

3. Application and Discussion

3.1. Irrigation and drainage

For the estimation of irrigation return flow, monthly average irrigation and drainage volumes were analyzed. Irrigation was calculated based on field water supply,

while drainage was estimated from field drainage. Table 1 presents the 2024 results for Scenario A, and Table 2 for Scenario B. The analysis showed that irrigation volume was highest in August, reaching 539 × 10^3 m³ in Scenario A and 683 × 10^3 m³ in Scenario B. This suggests that the optimized water circulation applied in Scenario B contributed to a more stable water supply.

Table 1. Results of monthly irrigation and drainage analysis in Scenario A

Month	Irrigation (10^3 m³)	Drainage (10^3 m³)	Irrigation (%)	Drainage (%)
MAY	388	40	91	31
JUN	476	21	96	18
JUL	454	440	51	90
AUG	539	66	89	42
SEP	382	235	62	79

Table 2. Results of monthly irrigation and drainage analysis in Scenario B

Month	Irrigation (10^3 m³)	Drainage (10^3 m³)	Irrigation (%)	Drainage (%)
MAY	518	72	88	45
JUN	568	31	95	25
JUL	541	485	53	90
AUG	683	91	88	51
SEP	539	304	64	83

3.2. Water balance analysis

To understand the water flow in the irrigation district, a water balance analysis was conducted for the period from May to September 2024. Rainfall, water supply, evapotranspiration, infiltration, drainage, and storage were analyzed, and Table 3 presents the results of the 2024 water balance analysis. In Scenario A (SA), the storage was estimated at 962 × 10^3 m³, while in Scenario B (SB), it was 1,286 × 10^3 m³.

Table 3. Results of water balance analysis in paddy field

Category	Scenario A	Scenario B
Rainfall (R)	1,962	1,962
Water supply (D_1)	8,440	8,440
Evapotranspiration (ET)	1,773	1,991
Infiltration (I)	1,538	1,715
Drainage (D_2)	6,130	5,411
Storage (ΔS)	962	1,286

* Units: 10^3 m³

3.3. Estimation of return flow reuse

Figure 1 presents the comparison of reusable water volumes under the two scenarios. At a reuse rate of 10%, Scenario A yielded 613 × 10^3 m³ and Scenario B yielded 541 × 10^3 m³, representing the minimum values. At a 50% reuse rate, the volumes increased to 3,065 × 10^3 m³ for Scenario A and 2,705 × 10^3 m³ for Scenario B, showing the maximum values.

The return flow analysis revealed a clear difference between the scenarios. In Scenario A, July recorded the highest return flow, 2,546.48 × 10^3 m³, corresponding to 83.61% of the supplied water. In contrast, Scenario B recorded only 1,162.58 × 10^3 m³ in the same month, equivalent to 38% of the supply. This reduction in return flow ratio indicates that optimized gate control suppressed excessive drainage and improved overall irrigation efficiency compared with Scenario A.

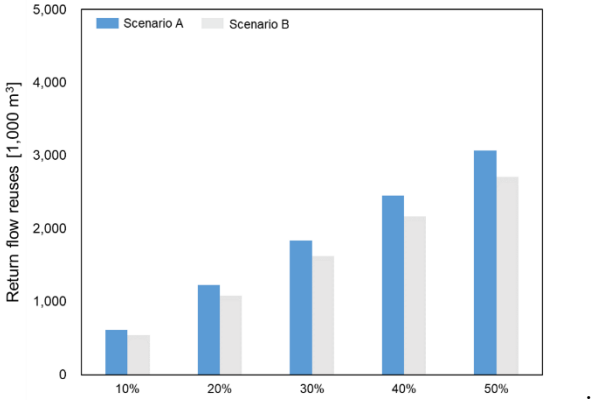

Figure 1. Results of return flow reuse estimation under assumed reuse rates

4. Conclusions

With the increasing frequency of droughts and floods under climate change, the concept of water circulation in irrigation reservoirs and districts has gained growing importance. It serves as a crucial mechanism for improving agricultural productivity, advancing sustainable water management, and protecting ecosystems. This study highlights the necessity of estimating irrigation water consumption through network-based modeling and of examining circulation processes—such as supply, drainage, return flow, irrigation water use, and demand—at both the source and district scales. The outcomes provide valuable insights for refining water policies, ensuring reliable and timely distribution, and promoting the sustainable use of rural water resources. In the future, establishing long-term monitoring of supply, drainage, and ponding depth will enable more precise estimates of irrigation water and deeper understanding of circulation dynamics.

Acknowledgements

This work was supported by Korea Institute of Planning and Evaluation for Technology in Food, Agriculture, and Forestry (IPET) through Intelligent Agricultural Infra Management for Climate Change Development Program, funded by Ministry of Agriculture, Food and Rural Affairs (MAFRA) (RS-2025-02219764)

References

Baffaut, C., and Delleur, J.W., 1989. Expert system for calibrating SWMM. *Journal of Water Resources Planning and Management*, 115(3), 278–298.

Niazi, M., Nietch, C., Maghrebi, M., Jackson, N., Bennett, B.R., Tryby, M., and Massoudieh, A., 2017. Storm water management model: Performance review and gap analysis. *Journal of Sustainable Water in the Built Environment*, 3(2), 04017002.

Rossman, L.A., 2010. Storm Water Management Model User's Manual Version 5.0. EPA/600/R-05/040, National Risk Management Research Laboratory, U.S. Environmental Protection Agency, Cincinnati, Ohio.

Estimation of Discharge Amount After Using Water Curtain Water in Greenhouse Complexes During Winter Season

Kim Sang Min

Abstract

Domestic facility cultivation complexes are distributed in areas adjacent to rivers where groundwater is easily available, and in particular, water curtain cultivation using groundwater is actively practiced during the winter. Water curtain cultivation sprays groundwater at night to maintain the temperature inside the greenhouse, and most of it flows into nearby rivers through irrigation channels or drainage ditches after use. Accordingly, the possibility of groundwater depletion and deterioration in water quality is raised. This study comprehensively analyzed the discharge amount and water quality characteristics after the use of water curtain water in a large-scale facility cultivation complex in Miryang, Gyeongsangnam-do. Based on the winter season (November 19, 2024, to January 16, 2025), when water curtain cultivation is performed, the drainage water level is monitored, and the return amount is calculated by applying the water level-flow relationship. Based on the individual buildings of House 4, the average daily discharge was 15.73 m3/day, the minimum was 9.33 m3/day, and the maximum was 20.97 m3/day. Repeated rises in water level were observed during the night, confirming regular diurnal variability.

Effect of Irrigation-Induced Distribution of Temperature and Nitrogen Concentration of Paddy Water on Rice Chalky Grain

Yuta AMAKAWA[1]*, Kazuhiro NISHIDA[1], Tadashi TSUKAGUCHI[2], Keita KOBUCHI[1], Kazuya SHIRAISHI[1], Shuichiro YOSHIDA[1]

[1] Graduate School of Agricultural and Life Sciences, The University of Tokyo,1-1-1 Yayoi, Bunkyo-ku, (Tokyo), Japan

[2] Faculty of Bioresources and Environmental Sciences, Ishikawa Prefectural University,1-308 Suematsu, Nonoichi-shi, (Ishikawa), Japan

* Corresponding author. Email: uts2-amakawa-yuta@g.ecc.u-tokyo.ac.jp

Abstract

Rice grain quality is influenced by irrigation, with its effects varying depending on the temperature and nitrogen concentration of the irrigation water; however, quantitative data on these effects remain limited.

The objective of this study was to assess the effects of irrigation water with low temperature and high nitrogen concentration on the thermal and nitrogen environments in a paddy field, and their effect on rice grain quality. Field measurements were conducted in a paddy field located in Tokyo, Japan, during the 2023 and 2024 growing seasons. The irrigation water was cold (17 °C) and contained a high nitrogen concentration (4 mgN/L), while average air temperatures in August including the grain-filling were high (29 °C). Paddy water temperature (Tw) and nitrogen concentration (Nw), grain nitrogen content (GNC), and the percentage of chalky grains (CG) were measured at multiple points along the flow path from the water inlet to the outlet. These data were analyzed using simple linear regression.

The following results were obtained, 1) Tw was lower and Nw was higher near the inlet, 2) GNC was higher and CG was lower near the inlet, 3) CG was positively correlated with Tw and negatively correlated with Nw and GNC. These results indicate that irrigation with water at low temperature and high nitrogen content improve rice quality (reduce CG). Future studies should focus on quantitative analyses to elucidate how thermal and nitrogen environments in paddy fields affect rice grain quality.

Keywords: Water Management, Heat Damage, Water Temperature, Grain Nitrogen Content, Appearance Quality, Cooling Effect

1. Introduction

Recently, heat damage during grain-filling has caused degradation of rice grain appearance quality (an increase in chalky grains). Water management techniques are among the well-known methods to improve quality. Generally, it is widely considered that lower water temperature (Tw) in paddy field improves rice quality.

However, irrigation also affects the nitrogen environment of the paddy field (including nitrogen concentration in surface or soil water), due to factors like nitrogen flux from irrigation.

Consequently, it has been suggested that changes in the nitrogen environment caused by irrigation can affect rice grain appearance quality (Nishida et al., 2019). In spite of this, few studies have investigated the effects of irrigation on rice appearance quality with considering both thermal environmental and nitrogen environmental changes.

Hence, the aim of this study was to elucidate the effects of irrigation on the thermal and nitrogen environments in a paddy field, and their effect on rice grain quality. A field research was conducted in a paddy field using low-temperature and high-nitrogen-concentration irrigation water. The distribution of temperature and nitrogen concentration in paddy surface water, as well as the chalky grains rate (CG) and grain nitrogen content (GNC) of rice were measured.

2. Materials and Methods

Field research was conducted in an experimental paddy field in Nishitokyo-shi, Tokyo, Japan in 2023 and 2024. Cultivar “Koshihikari” was cultivated in the paddy field. Irrigation water was cold (about 17 ℃ throughout the experiment) and high-nitrogen-concentration (about 3~4 mgN L^{-1}) underground water. Irrigation rate was very high because of a high percolation rate (7 cm d^{-1}). The temperature around the grain-filling stage (i.e., August) was 29.2 ℃ (2023), or 29.3 ℃ (2024), which was higher than the estimated threshold temperature for heat damage (27~28℃ during the 20 days after heading).

To analyze temperature and nitrogen concentration distributions in the paddy fields, measurements were taken at multiple points (7 in 2023 and 12 in 2024; Fig.1) Tw was measured every 10-30 min using thermometers. Total nitrogen concentrations (Nw) of water samples (collected multiple times: once in 2023 and fourth in 2024) were measured in the laboratory. 10-12 rice plants were sampled to assess their appearance quality and GNC. CG was measured as the sum of basal-white and back-white and milky-white grains. GNC was calculated on a dry weight basis.

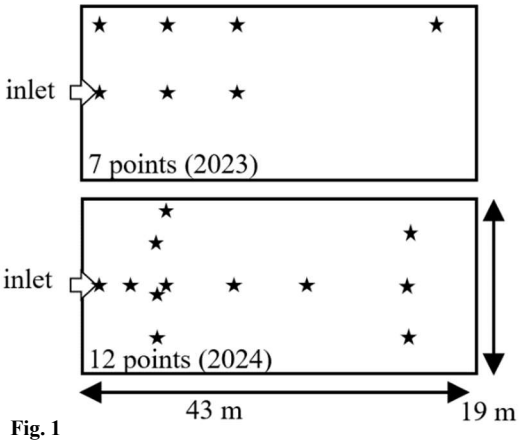

Fig. 1
Schematic representation of the experimental paddy field

3. Results and Discussion

Irrigation influenced the distributions of water temperature and nitrogen concentration in the paddy field. Fig.2 shows Tw was lower and Nw was higher near the inlet. Fig.3 shows the percentage of CG was lower (appearance was improved) and GNC was higher near the inlet. Irrigation influenced the distributions of water temperature and nitrogen concentration in the paddy field. These data were analyzed using simple linear regression. Fig.4 shows a significant positive correlation was observed between CG and Tw, and a negative correlation was observed between CG and GNC. These results suggest that irrigation with low-temperature and high-nitrogen concentration water caused an improvement in rice grain appearance and an increase in GNC.

On the other hand, previous research (Nishida et al., 2019) using irrigation water with low-temperature and low-nitrogen concentration reported distribution different from our results: the percentage of CG was higher (appearance was degraded) and GNC was lower near the inlet.Based on these contrasting results suggest that the rice appearance improvement (decrease of CG) in our research was the consequence of high nitrogen supply from irrigation water and high nitrogen uptake by rice.

Our research indicated that irrigation affects rice grain quality through the nitrogen environment, as well as the thermal environment. Therefore, to develop water management techniques to improve rice quality, it is essential to elucidate the effect of irrigation considering the nitrogen concentration of irrigation water and the impact of irrigation on the nitrogen environment of paddy fields.

4. Conclusion

With irrigating low-temperature and high-nitrogen water, Tw was lower and Nw was higher near the inlet. Consequently, rice grain appearance quality improved & N content lowered near the inlet. This result suggested that N supply from irrigation was the main cause of grain appearance improvement.To develop water management to improve grain appearance, it is necessary to consider the nitrogen environment as well as the thermal environment.

References

Nishida, K., Tsukaguchi, T., Shibata, S., Yoshida, S., & Shiozawa, S., 2019. Effect of continuous irrigation with running water using cool and low nitrogen concentration irrigation water during rice grain filling period on grain protein content and percentages of chalky grains of rice. Trans. Jpn. Soc. Irrig. Drain. Rural. Eng., 87(2), 219-226.

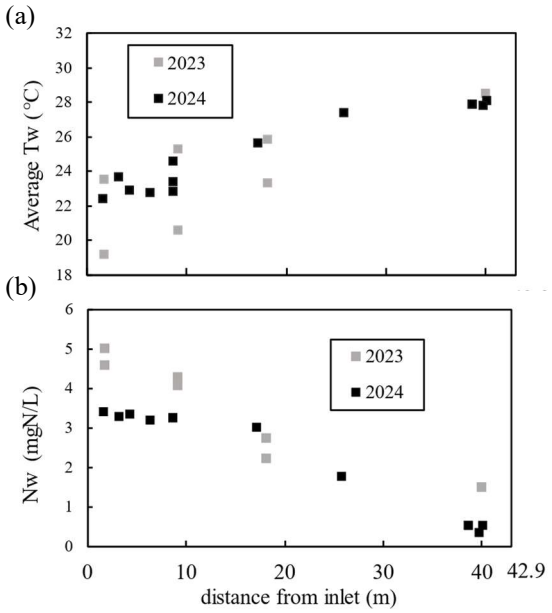

Fig. 2 Spatial distribution of (a) Average temperature during 20days after heading and (b) Nitrogen concentration of paddy water

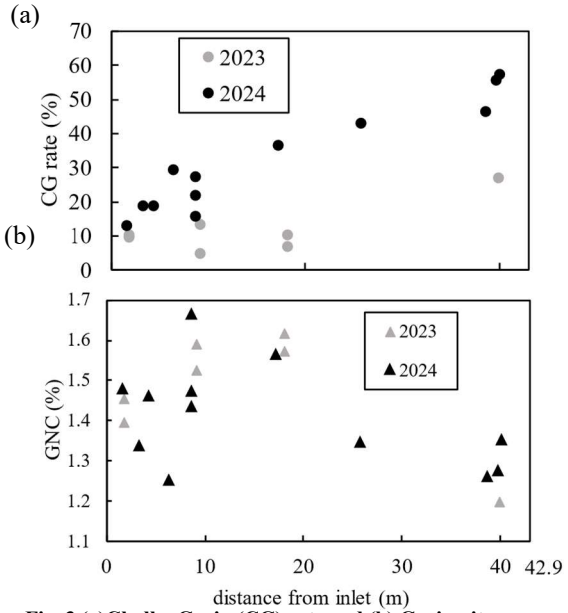

Fig. 3 (a)Chalky Grain (CG) rate and (b) Grain nitrogen content (GNC) percentage of rice

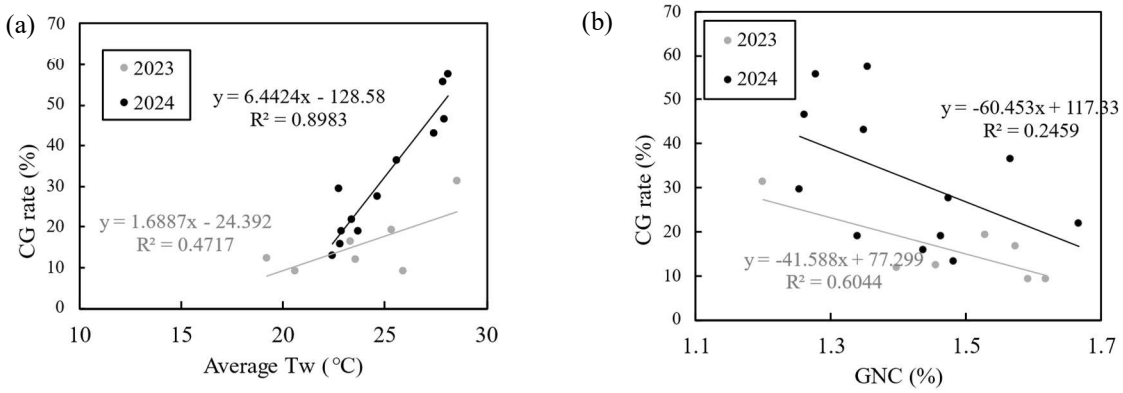

Fig. 4 BBWG vs (a)Average water temperatures during 20 days after heading and (b) GNC
*5% Significant，**1% Significant，***0.1% Significant

Methane gas emissions from meso-scale paddy soil columns affected by artificial macropore installation.

Nagatsuki Tanaka [1], Yasushi Mori [1*]

[1] Graduate School of Environmental, Life, Natural Science and Technology, Okayama University, Okayama, 700-8530, Japan

* Corresponding author. Email: yasushim@cc.okayama-u.ac.jp

Abstract

We are working to reduce GHG emissions from paddy soils as a climate change mitigation measure. To date, we have obtained results which alleviated anaerobic conditions and reduced methane emissions by combining artificial macropores (structures that mimic root-formed macropores) with drainage and applying them to the soil. However, this verification is limited to simple column experiments, and the effectiveness cannot be guaranteed in environments closer to actual field conditions.

In a previous experiment, we expanded the experimental scale by introducing rice into the columns and preparing six conditions combining 1) drainage (with or without) and 2) macropore structure (macropore only, macropore with soil layer, or none). However, our results from the drained columns indicated a possible underestimation of methane flux, likely due to bubbles escaping from the drainage.

In this experiment, the drainage section of the three drainage-applied columns was modified to trap all drainage and escaping bubbles and we attempted to evaluate the total GHG emissions from the columns.

Keywords: GHG, Methane gas, paddy soils, artificial macropore, drainage, redox potential

1. Introduction

Reducing CH_4 emissions from rice paddies is an important climate change mitigation measure in the agricultural sector.

Since CH_4 is produced in an anaerobic environment, our study group has attempted to improve soil drainage and downward infiltration by artificial macropores, which mimic natural macropore structure, to effectively deliver oxygen to the lower layers of paddy soil and reduce CH_4 emissions. Previous results from simple column experiments suggested that artificial macropore and drainage application were effective in reducing CH_4 emissions. However, these results did not fully take realistic conditions into account, such as emissions through the aerenchyma of rice plants, which is a well-known CH_4 emission mechanism in rice paddies.

The purpose of this study is to reduce CH_4 emissions from rice paddy soil using artificial macropore technology. Specifically, since we found possible CH_4 escape through column drainage, we redesigned the column to trap escaped bubbles from drainage and attempted to re-evaluate the total CH_4 emissions.

2. Materials and Methods

2.1. Soil column setup

2.1.1. Column Design

Air-dried alluvial clay soil (paddy soil), sieved to <2 mm, was saturated and used for the experiments. The column design was intended to bring the experimental scale closer to the field scale by introducing rice plants and applying gravity drainage by manual.

In this experiment, drainage design was minorly changed from our pre-conducted mesoscale experiment, to trap all gas bubble leakage and drainage water. Specifically, the drainage valve was directly connected to a 1 L Tedlar® bag, which formed closed system.

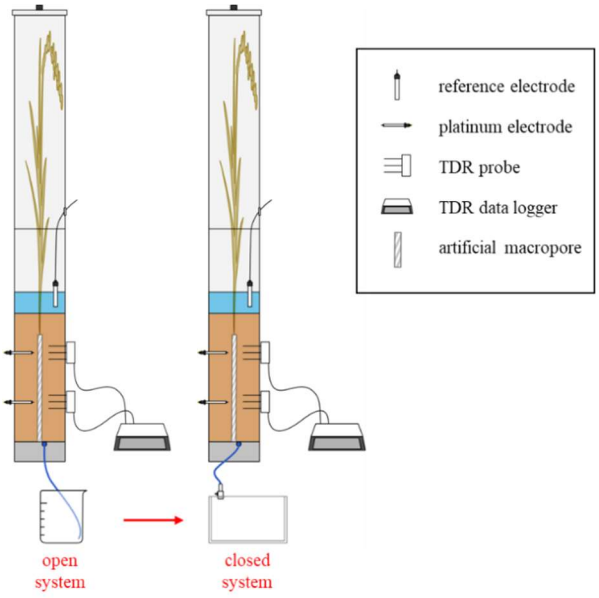

Figure 1. Column design.

2.1.2. Experimental Designs

A total of three column conditions were designed: macropore with soil layer (DML), macropore without soil layer (DM) without macropore (D).

These columns were kept in a growth chamber under constant temperature (30 °C), relative humidity (65%), and sunlight conditions (10 hours light and 14 hours dark) for 60 days.

Each column was drained every two days. The drainage was stopped when the water depth had decreased by 20 mm or after 3 hours, whichever occurred first.

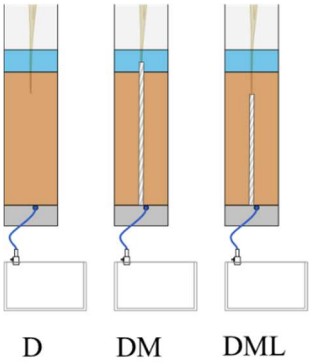

Figure 2. An experimental condition description.

2.2. Measurements and Analyses

During the 60-day experimental period, CH_4 and CO_2 gas concentrations, ORP, and other parameters were measured every two days.

CH_4 and CO_2 gas leakage through drainage were calculated as the product of the total volume of leaked bubbles collected in a Tedlar® bag, CH_4 and CO_2 concentrations in that bubble, and the gas densities of CH_4 (0.71607 kg m^{-3}) and CO_2 (1.9647 kg m^{-3}).

3. Results and Discussion

3.1. Soil water permeability

Firstly, soil water permeability for each column showed approximately one-tenth of those in a previous experiment with an open drainage system, suggesting that the column water could hardly have direct contact with the atmosphere, which led to smaller pressure gradient and weaker driving force for water movement. The difference in water permeability could have effects to other mass transfer processes and affected the results compared to the previous experiment. Therefore, it would be a limitation of the experiment design but may be interpreted with general ideas about mass transfer characteristics in soils.

3.2. Soil ORP

The upper soil ORP values were very high, approximately >400 mV, suggesting that high concentration of oxygen made by rice photosynthesis and transferred through aerenchyma to rhizosphere soils. However, such high ORPs should be only observed within column soils with very limited space of rhizosphere, which should be noted as an experimental limitation.

3.3. CH_4 emission

3.3.1. Upward emissions

CH_4 gas flux measured within upper side of the column during the experiment period is shown in Figure 3. There was little CH_4 emission from D and DML, while comparatively high emission from DM. These amount, however, were rather small compared to those in our previous experiment. CO_2 was not detected from the same gas samples in almost all days, which was same as the previous experiment, suggested that they were used up by rice photosynthesis.

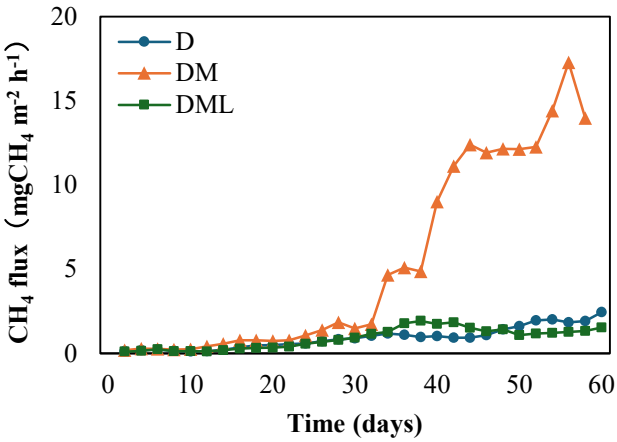

Figure 3. Upward CH_4 emission during the experimental period.

3.3.2. CH_4 leakage through drainage (Downward emissions)

CH_4 gas leakage through drainage during the experiment period is shown in Figure 4. Acertain amount of CH_4 leakage was observed in DML, while comparatively less leakage occurred in DM and almost none inD. Therefore, our overall interpretation are as follows; 1) for D, there was quite few methanogenesis, led to very low CH_4 emission, 2) for DM, the generated methane could be escaped through extruded artificial macropore, led to increasing CH_4 emission from upper side of the column, 3) for DML, surface soil layer effectively blocked the escape pass for methane bubbles, led to few emission from upper side but escape through drainage instead.

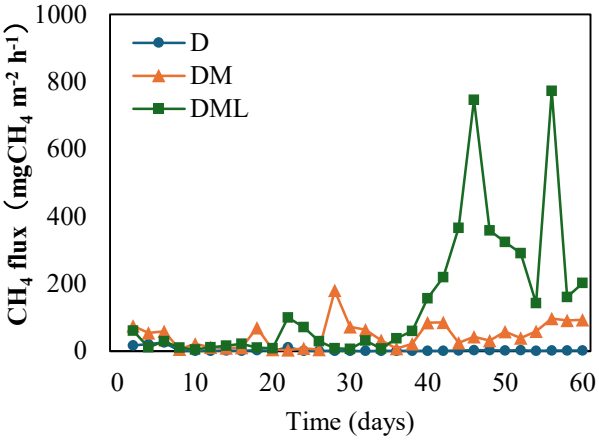

Figure 4. Downward CH_4 emission during the experimental period.

These results support our earlier finding that CH_4 emissions were effectively reduced by the combination of macropore and soil layer, compared to macropore without soil layer within simple column without rice and with continuous drainage. However, we found that there was also a risk of downward CH_4 emission with such soil structure.

4. Conclusions

In this study, we found that the soil structure with a macropore and soil layer may effectively block upward CH_4 emissions, compared to one with macropore without soil layer. However, the lowest CH_4 emissions were observed under the condition without a macropore in this experiment. Although dependent on drainage characteristics, some CH_4 leakage may occur.

We also found that there were limitations specific to this mesoscale column experiment, such as column-design-dependent water permeability and markedly high ORP in upper soils. Therefore, the results should be interpreted strictly within the context of our column system. It is necessary to interpret these results in light of general mass transfer principles, to clarify how macropore and drainage affect CH_4 emissions from paddy soils.

Acknowledgements

This study was partially supported by the Japan Society for the Promotion of Science NEXT Program (GS021, 2011–2014), KAKENHI (B) (26292127, 2014–2016), KAKENHI (A) (17H01496, 2017–2020), (21H04747, 2021–2024) and KAKENHI (S) (24H00057, 2024–2028). We are grateful to Professor Hirai for providing rice plants for this study.

Development of a Climate-Resilient Paddy–Upland Crop Rotation Model: A Case Study of Baby Corn and Heat-Tolerant Rice in Subtropical Taiwan

Ping-Wei Sun*, Charng-Pei Li, Li-Han Huang

Crop Science Division, Taiwan Agricultural Research Institute, Ministry of Agriculture, Taichung City, Taiwan

* Corresponding author. Email:pwsun @tari.gov.tw

Abstract

To address the challenges of climate change and water resource scarcity in paddy agriculture, this study proposes an innovative climate-resilient paddy–upland crop rotation model. The system integrates spring and autumn cultivation of baby corn, characterized by low water demand and short growth period, with summer cultivation of heat-tolerant rice varieties, thereby improving land use efficiency and contributing to sustainable agriculture. Field trials were conducted in 2024 in Wufeng, Taichung, Taiwan, using five baby corn varieties—including a newly developed line 110F-1-6—and three rice varieties (Tainung 77, Tainung 85, and the newly bred Tainung 88). Agronomic traits and yield performance were evaluated. Results indicated that in spring, 'Hongxu,' 'Xiaobao,' and 'Xiaoai' exhibited high ear density and yield per area, while 110F-1-6 had the highest husked ear ratio. In autumn, 110F-1-6, 'Xiaobao,' and 'Xiaoai' again showed favorable performance. For the intercropped rice, no significant differences were found among the three varieties in yield or seed-set ratio; however, TNG77 had the highest bulk density and thousand-grain weight, while TNG88 demonstrated outstanding heat tolerance and stable grain quality, making it suitable for summer cultivation. This model presents a viable strategy for enhancing food security and adapting to climatic extremes. Further research will focus on optimizing crop combinations and field management practices.

Keywords: paddy rotation, climate-resilient agriculture, baby corn, heat-tolerant rice, Taiwan, ecosystem services, sustainable water use

1. Introduction

To address the challenges of climate change and water resource scarcity in paddy agriculture, this study proposes an innovative climate-resilient paddy–upland crop rotation model. The system integrates spring and autumn cultivation of baby corn, characterized by low water demand and short growth period, with summer cultivation of heat-tolerant rice varieties, thereby improving land use efficiency and contributing to sustainable agriculture.

2. Materials and Methods

A novel paddy–upland crop rotation system was designed, in which baby corn is cultivated in spring and autumn, and rice is grown in the intermediate summer period (Figure 1). Appropriate baby corn and edible rice varieties were selected or bred to suit this cropping system. Standard cultivation protocols were followed for both crops, and agronomic traits, yield, and quality parameters were systematically evaluated.

a. The tested baby corn varieties included:
   - Hongxu
   - Xiaobao
   - Xiaoai
   - Fengchuan
   - the newly bred line 110F-1-6

b. The tested rice varieties included:
   - Tainung 77 (TNG77)
   - Tainung 85 (TNG85)
   - Tainung 88 (TNG88)

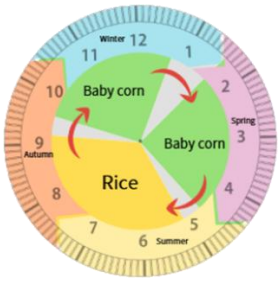

Figure 1. The novel paddy-upland crop rotation model developed in this study involves cultivating baby corn in spring and autumn, with rice grown as the intermediate crop.

3. Results and Discussion

During the spring baby corn cropping season, the varieties ‘Hongxu’, ‘Xiaobao’, and ‘Xiaoai’ demonstrated superior performance in terms of yield per unit area and number of ears per unit area. The line 110F-1-6 achieved the highest husked ear yield ratio. In the autumn season, the varieties 110F-1-6, ‘Xiaobao’, and ‘Xiaoai’ again showed promising yield performance. However, overall yields in late autumn were lower than in early spring, primarily due to Typhoon Usagi, which struck in mid-November 2024. Additionally, cooler winter temperatures likely suppressed plant growth and ear height, negatively affecting yield outcomes.

Table 1. Agronomic Traits of Spring 2024 Baby Corn Yield Comparison Trial.

variety	Traitz			
	Number of Ears per Unit Area (ear/m2)	Plant Height (cm)	Ear Height (cm)	Husked Ear Yield Ratio (%)
110F-1-6	14.67 b	162.67 c	87.27 b	26.59 a
Hongxu	20.47 a	189.6 a	111.4 a	22.5 b
Xiaobao	17.61 ab	179.8 ab	105.73 a	21.5 bc
Xiaoai	18.29 ab	188.2 a	109.27 a	22.31 b
Fengchuan	7.72 c	168.07 bc	70.27 c	19.72 c
Average	15.75	177.67	96.79	22.52
LSD	4.4	16.92	13.61	2.37

z Values are means of three replicates.

ζValues in the same column with the same letter are not significantly different according to the Least Significant Difference (LSD) test (α = 0.05).

Table 2. Agronomic Traits of Autumn 2024 Baby Corn Yield Comparison Trial.

variety	Traitz			
	Number of Ears per Unit Area (ear/m2)	Plant Height (cm)	Ear Height (cm)	Husked Ear Yield Ratio (%)
110F-1-6	10.40 ab	156.93 b	54.8 bc	19.92 a
Hongxu	6.93 bc	163.73 b	64.33 b	14.72 b
Xiaobao	11.02 ab	185.60 a	78.33 a	14.56 b
Xiaoai	13.01 a	188.53 a	82.33 a	17.41 ab
Fengchuan	5.15 c	159.27 b	44.93 c	17.53 ab
Average	9.30	170.81	64.95	16.83
LSD	4.38	10.36	10.69	3.00

z Values are means of three replicates.
ζValues in the same column with the same letter are not significantly different according to the Least Significant Difference (LSD) test (α = 0.05).

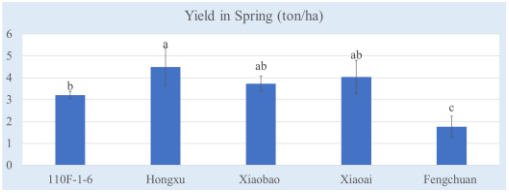

Figure 2. Yields of Baby Corn in Spring.

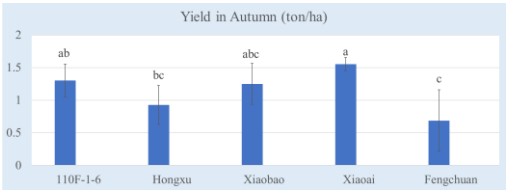

Figure 3. Yields of Baby Corn in Spring.

For the intermediate rice crop, the varieties Tainung 77, Tainung 85, and Tainung 88 showed no significant differences in yield or seed-setting rate. However, Tainung 77 exhibited the highest bulk density and thousand-grain weight. Notably, under the high temperatures encountered during the grain-filling stage, Tainung 88 maintained a low chalky grain rate and a high proportion of whole grains, suggesting strong heat tolerance.

Table 3. Agronomic Traits of Rice.

Variety	Yield (kg/ha)	Test weight (g/L)	Panicle length (cm)	Panicle weight (g)
TNG77	3991.2 ± 241.7 a	487.5 ± 4.6 a	19.1 ± 1.8 a	1.9 ± 0.2 a
TNG85	4995.3 ± 1213.1 a	473 ± 9.8 ab	17.2 ± 0.7 b	2.2 ± 0.6 a
TNG88	3954.6 ± 314 a	458.5 ± 5 b	18.6 ± 0.4 ab	2.2 ± 0.5 a

Table 4. Agronomic Traits of Rice.

Variety	Number of panicles per plant (NO.)	Number of filled grains per panicle (NO.)	Seed-setting rate (%)	1000-grain weight (g)
TNG77	19.6 ± 1.1 a	68.9 ± 6.4 a	81.8 ± 1.2 a	24.7 ± 0.6 a
TNG85	20.1 ± 2.2 a	85.7 ± 27 a	72.6 ± 12.2 a	22.9 ± 0.5 b
TNG88	18.5 ± 5.8 a	85.2 ± 19.5 a	78.1 ± 5.5 a	23.2 ± 0.9 ab

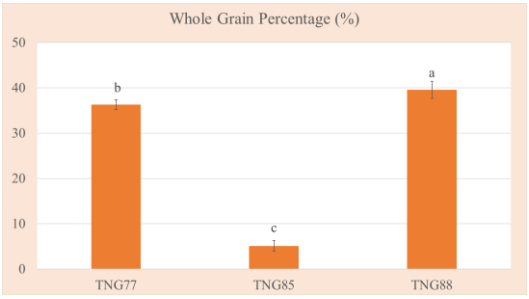

Figure 4. Whole Grain Percentage of Rice.

4. Conclusions

The paddy–upland crop rotation model developed in this study offers a promising strategy for enhancing food security in the context of climate change. Among the baby corn varieties tested, ‘Xiaobao’ and ‘Xiaoai’ consistently performed well across both seasons, while ‘Hongxu’ and the line 110F-1-6 also exhibited potential for rotational cultivation. For rice, Tainung 88 demonstrated notable resilience to heat stress, making it a strong candidate for the summer cropping period. Ongoing research will focus on breeding and optimizing varieties suitable for this rotational system, as well as conducting further field evaluations to validate long-term sustainability and productivity.

Effects of Lactobacillales Amendment and Soil Water Content on Carbon Dioxide and Methane Emissions in Paddy Soil

Liyuan Chen [1*], Kimihito Nakamura [1], Natsuki Nobe [1], Takanori Nagano [2]

[1] Graduate School of Agriculture, Kyoto University, Kyoto, Japan

[2] Graduate School of Agricultural Science, Kobe University, Hyogo, Japan

* Corresponding author. Email: chen.liyuan.32d@st.kyoto-u.ac.jp

Abstract

Microbial amendments have the potential to modulate carbon cycling in paddy soils by affecting carbon dioxide (CO_2) and methane (CH_4) emissions. This study investigated the effects of Lactobacillales amendment (LBA) in combination with different soil water contents on CO_2 and CH_4 emissions, as well as on partial global warming potential (pGWP). Laboratory experiments were conducted using soil columns subjected to three water content (WC) treatments: dry (0.3 WC; gravimetric water content of 0.3), moist (0.6 WC), and flooded conditions for one month, with LBA applied to each WC level alongside the respective control groups. Subsequently, all columns were flooded for an additional month. The results showed that LBA addition increased CO_2 emissions during the initial month, suggesting that LBA promoted the conversion of readily available carbon into CO_2 under 0.3 WC and 0.6 WC conditions, thereby reducing the substrate availability for CH_4 production under the subsequent flooded condition. However, the products generated by LBA under the flooded condition in the initial month could serve as substrates for methanogens, potentially enhancing CH_4 emissions in the subsequent flooded condition. These findings indicate that following LBA application in dry or moist soils, immediate flooding should be avoided to mitigate pGWP in paddy soils.

Keywords: paddy soil, Lactobacillales, methane, carbon dioxide, water content

1. Introduction

Methane (CH_4) is a potent greenhouse gas, with a 100-year global warming potential 27 times that of carbon dioxide (CO_2), making its mitigation critical for short-term climate warming, particularly in paddy fields (IPCC, 2021; Li and Zhou, 2020).

Lactobacillales are known to alter microbial community composition and are widely applied in food fermentation, yet their agricultural applications remain limited. In addition, water management such as intermittent irrigation has been shown to effectively suppress CH_4 emissions (Nunes et al., 2022; Oliver et al., 2019).

Thus, this study aimed to investigate the effects of Lactobacillales amendment (LBA) and soil water content (WC) on CO_2 and CH_4 emissions as well as the partial global warming potential (pGWP).

2. Materials and Methods

2.1. Soils and Lactobacillales amendment

Soil samples were taken from the 0–20 cm layer of a paddy field situated in Miyama Town, Nantan City, Kyoto Prefecture, Japan (35.33°N, 135.67°E). Following the removal of stones, roots, and debris, the samples were dried in air at 25 °C and sieved through a 2 mm mesh before being used. LBA was provided by Caltech Co., Ltd. (Japan), which included 63.73% Lactobacillales, 27.97% Enterobacteriales, and 5.94% Bacillales. The container used in the experiment had an inner diameter of 20 cm, with the soil layer approximately 6 cm high.

2.2. Experimental design

The experiment was conducted in two phases. Rice bran was added to all treatment soils. In the first phase, soils were adjusted to three soil water contents (dry: 0.3 WC; gravimetric water content of 0.3, moist: 0.6 WC, flooded: F) with or without LBA, and CH_4 and CO_2 fluxes were monitored daily for one month. Afterward, the soils were exposed to aerobic conditions for one week to simulate pre-flooding aeration. In the second phase, all treatments were flooded and incubated for another one month, with daily measurements of CH_4 and CO_2 fluxes.

2.3. Partial global warming potential equation

The partial global warming potential (pGWP, g CO_2-eq) was estimated over a 100-year time horizon by converting CH_4 emissions to CO_2 equivalents using a radiative forcing factor of 27 relative to CO_2.

3. Results and Discussion

3.1. Phase-specific changes in CH_4 emissions

In the first phase, CH_4 uptake was observed in the 0.3 WC and 0.6 WC treatments, whereas the F treatments exhibited CH_4 emissions (Fig. 1a). The CH_4 emissions in the F treatments increased progressively over time. Among the treatments with LBA addition, CH_4 emissions from F-LBA were higher than from F-C (Table 1), which may be attributed to metabolic products driven by LBA application that stimulated the growth of methanogens.

In the second phase, all treatments released CH_4 (Fig. 1b). However, CH_4 emissions in the 0.3 WC and 0.6 WC treatments were lower than those in the F treatments (Table 1). This reduction may be explained by the depletion of labile organic carbon during the aerobic period, thereby limiting the substrate available for methanogens under subsequent anaerobic conditions.

3.2. Phase-specific changes in CO_2 emissions

In the first phase, CO_2 was continuously and steadily released, while the D and M treatments showed a gradual decline in emissions after an initial peak during the first week (Fig. 2a). In the F treatments, LBA addition increased CO_2 emissions (Table 2), which may be attributed to the stimulation of methanotrophs by increased methanogens as well as the stimulation of microbial respiration. In the D and M treatments, the availability of labile organic carbon decreased after the

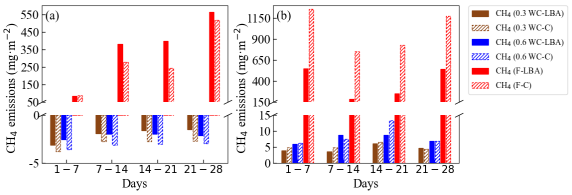

Figure 1. Weekly CH_4 emissions ($mg \cdot m^{-2}$) during the first phase (a), and the second phase (b).

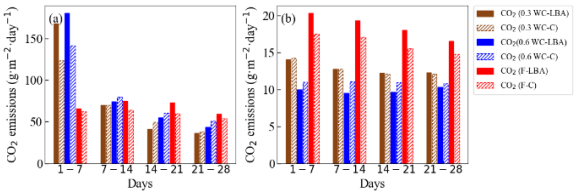

Figure 2. Weekly CO_2 emissions ($g \cdot m^{-2}$) during the first phase (a), and the second phase (b).

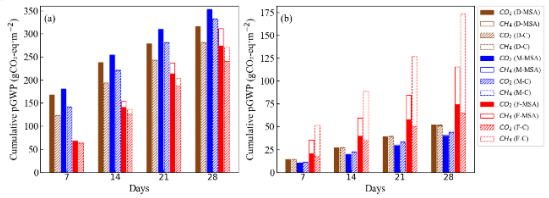

Figure 3. Temporal variations in cumulative pGWP during the first phase (a), and the second phase (b).

second week due to substantial consumption of labile organic carbon promoted by LBA during the first week, leading to a gradual reduction in CO_2 emissions (Fig. 2a).

In the second phase, the 0.6WC-LBA treatment exhibited the lowest CO_2 emissions (Fig. 2b), which may be attributed to the substantial consumption of labile organic carbon.

3.3. Phase-specific changes in pGWP

CO_2 was the main contributor to pGWP in the first phase, whereas both CO_2 and CH_4 contributed to pGWP in the second phase (Fig. 3).

D and M treatments substantially reduced pGWP during the second phase (Table 3).

4. Conclusions

WC had a greater impact on pGWP than LBA. During the first aerobic phase, LBA promoted the consumption of labile organic carbon by enhancing the decomposition of labile carbon sources, resulting in increased CO_2 emissions. In the subsequent second anaerobic phase, the reduced availability of labile organic carbon limited CH_4 emissions by restricting the substrates available to methanogens. In the D and M treatments, compared with the F treatment, prolonging the aerobic period could reduce the pGWP.

Acknowledgements

We are sincerely grateful for the financial support by JSPS KAKENHI (Grant Numbers: 23H00349), and Theme 4 of the Advanced Studies of Climate Change Projection (SENTAN Program, Grant Number JPMXD0722678534) supported by the Ministry of Education, Culture, Sports, Science and Technology (MEXT), Japan.

Table 1. Cumulative CH_4 emissions in all treatments ($mg \cdot m^{-2}$)

Treatments	The first phase	The second phase
0.3WC-LBA	-8.11	18.58
0.3WC-C	-12.01	20.95
0.6WC-LBA	-8.59	30.46
0.6WC-C	-12.67	34.13
F-LBA	1427.44	1523.92
F-C	1127.55	4014.93

Table 2. Cumulative CO_2 emissions in all treatments ($g \cdot m^{-2}$)

Treatments	The first phase	The second phase
0.3WC-LBA	315.52	51.28
0.3WC-C	281.09	51.28
0.6WC-LBA	353.42	39.54
0.6WC-C	332.29	43.84
F-LBA	273.17	77.25
F-C	240.30	63.64

Table 3. Cumulative pGWP in all treatments ($gCO_2\text{-}eq \cdot m^{-2}$)

Treatments	The first phase	The second phase
0.3WC-LBA	315.30	51.78
0.3WC-C	280.77	51.85
0.6WC-LBA	353.19	40.75
0.6WC-C	331.95	44.55
F-LBA	311.72	118.39
F-C	270.74	172.04

References

IPCC, 2021. 2021: the physical science basis: working Group I contribution to the sixth assessment report of the Intergovernmental Panel on Climate Change. Climate Change. Cambridge University Press, Cambridge, New York (No, A.R. WGI).

Li, T., Zhou, Q., 2020. The key role of Geobacter in regulating emissions and biogeochemical cycling of soil-derived greenhouse gases. Environ. Pollut. 266, 115135. https://doi.org/10.1016/j.envpol.2020.115135.

Nunes, J.A.S., Marchesan, E., Giacomini, S.J., Grohs, M., Taschetto, Â.M., Fortuna, C.R., Soares, C.F., Fleck, A.G., Donato, G., 2022. Emission of greenhouse gases and yield-scaled global warming potential of rice cultivars under permanent and intermittent irrigation. Bragantia 81, e2122. https://doi.org/10.1590/1678-4499.20210309.

Oliver, V., Cochrane, N., Magnusson, J., Brachi, E., Monaco, S., Volante, A., Courtois, B., Vale, G., Price, A., Teh, Y.A., 2019. Effects of water management and cultivar on carbon dynamics, plant productivity and biomass allocation in European rice systems. Sci. Total Environ. 685,1139–1151. https://doi.org/10.1016/j.scitotenv.2019.06.110.

The Effect of Soil Aggregation Forms to Water Content and Plant Biomass in Soil Columns

Kento Tajiri [1], Yasushi Mori [1*]

[1] Graduate School of Environmental, Life, Natural Science and Technology, Okayama University, Okayama City, Okayama, Japan

* Corresponding author. Email: yasushim@cc.okayama-u.ac.jp

Abstract

To improve the fertility of nutrient-poor soils in environments requiring crop cultivation, we investigated soil aggregation through the addition of natural polymer compounds and its effects on soil conditions and plant growth. A planting trial was conducted in soil columns to examine the impact of applying natural polymers to the topsoil layer. Results indicated that plots receiving natural polymer amendments tended maintain higher soil water content and showed positive effects on plant growth. Comparisons between amended and control plots revealed a correlation between surface soil water content and plant growth. These findings highlight the importance of soil aggregate formation and suggest potential applicability in actual crop cultivation. Further studies will focus on analyzing soil organic matter content and composition, in relation to plant growth, allowing for a deeper understanding of soil fertility improvement.

[Keywords] Soil organic matter, Soil aggregation, Natural polymer compounds, Cellulose Nanofiber (CNF), Natural rubber latex

1. Introduction

Soil supports diverse forms of life, including plants, soil fauna, and microorganisms, by storing water, facilitating root respiration and engaging microbial symbiosis. The development of soil aggregate structures has been essential for enhancing soil fertility since ancient times.

As the largest terrestrial carbon reservoir, it stores twice as much carbon as the atmosphere and three times as much as plant biomass. It mitigates the impacts of global warming and climate change, and as a plant growth medium, supports the ecological pyramid from its base.

For planting, the development of soil structure is considered crucial, and the formation of soil aggregates has long been essential for enhancing soil fertility.

Before the emergence of plants and animals on land, terrestrial soil contained no organic matter, and aggregates likely formed only in mineral gels. It is speculated that when plants colonized land, organic matter was supplied, enabling the formation of aggregate structures. However, how this influenced water retention, plant growth, and the accumulation of organic matter in the soil remains unclear. Two methods are considered for water retention in soil layers. One is aggregate formation by organic matter, and the other is the formation of root-created pores by vascular plants and the promotion of downward water movement.

In this study, we investigated the use of natural polymer compounds to promote soil aggregation in nutrient-poor soils and thereby improve their suitability for crop cultivation. We hypothesized that natural polymer compounds addition would enhance aggregation by binding clay particles and micro-aggregates. This experiment evaluated the effect of surface-applied polymers on plant cultivation in nutrient-poor soils under semi-arid environment. A planting trial was conducted using cowpea (Vigna unguiculate) grown in Masa soil columns, with measurements of soil water content, and plant height taken over time.

This experiment is still ongoing, and as an initial report, we present the results concerning soil moisture and early plant growth.

2. Materials and Methods

In the planting experiment, nutrient-poor Masa soil was packed to a depth of 30 cm in 40 cm deep acrylic columns fitted with base plates. Cowpea, a legume widely cultivated in Africa, was planted in each column. Soil moisture sensors (TEROS-12, METER) were installed at depths of 7.5 cm and 22.5 cm below the soil surface (Kobori, 2023). Two natural polymer compounds were tested: cellulose nanofibers (CNF) and natural rubber latex. Previous studies have shown that CNF improves water retention through soil aggregation, while natural rubber latex enhances aggregation. Leaf mold was added to the topsoil layer as fertilizer to support early plant growth.

The cross-sectional structure of the soil column can be described as follows: the 0-20 cm from the bottom consists solely of Masa soil, 20-25 cm from the bottom consists of Masa soil plus fertilizer, and 25-30 cm from the bottom consists of mixture of Masa soil, fertilizer and additional amendment (CNF, Latex, or control).

First, the lower layer of 20 cm of Masa soil (1494.4 g) is packed into the column. The middle layer of 5-cm soil is prepared by mixing 373.6 g of Masa soil and 1.04 g of fertilizer and place over the lower layer.

For preparing the top 5 cm of soil, we first prepared 373.6 g of Masa soil, 3.7 g of polymer compound (CNF or latex), and 74.7 g of deionized water per column. When using CNF, we placed Masa soil, CNF, and deionized water into a bag, sealed it, and mixed by shaking. When using natural rubber latex, a latex solution was first prepared by mixing it with deionized water, which was then mixed with the Masa soil. After thorough mixing, the bag was sealed and cured at room temperature for at least 48 hours. The sample was then removed from the bag, spread on a tray, and air-dried. Air-dried soil was then placed onto the intermediate layer. For the control area using only masa soil, it was simply filled directly onto the intermediate layer.

An experiment was conducted in a region with low organic matter and annual rainfall below 500 mm. Cowpea (Vigna unguiculate) was cultivated in this experiment (Omoigui, 2018).

For the experimental plots, we prepared a total of six conditions combining 1) rainfall intensity (light rain at 2 mm/h, heavy rain at 20 mm/h) and 2) CNF (Plot C), natural rubber latex (Plot L), and control (Plot X). Three columns

were set up in each condition, totaling 18 columns placed in a sunny location. Irrigation was performed daily at a fixed time using a pump. Based on the climatic conditions of the semi-arid region, daily rainfall equivalent to 3 mm was applied. This meant irrigating with 15.5 mL of water per day: 9 minutes at 2 mm/h and 90 minutes at 20 mm/h. During the experiment, volumetric water content and plant height were measured over time.

3. Results and Discussion

The results from the surface soil moisture sensor (Figure 1) showed that higher rainfall intensity tended to correlate with higher moisture content. This indicates that stronger rainfall promotes greater water retention in the surface layer. Plots C and L exhibited higher moisture content than Plot X, while Plot X's moisture levels were closer to those observed during light rainfall. This difference demonstrates the successful water retention achieved in Plots C and L due to aggregate formation. Furthermore, comparing plots C and L, the difference in moisture content was not significant, suggesting that the water retention characteristics of CNF and latex are similar.

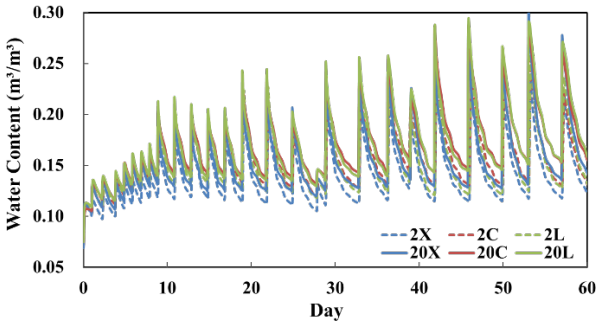

Figure 1. Top Water Content

Regarding the values from the soil moisture sensors installed below, at 20 mm/h, the increase values were observed in the order of plots L, C, and X. One possible reason is that the size of the formed aggregates was greatest in the order latex, CNF, and sandy loam, which may have resulted in better permeability in that order. On the other hand, differences in permeability due to root-formed pores based on plant growth suggested a pattern of latex, CNF, and sandy loam. Meanwhile, at 2 mm/h, the differences between experimental plots tended to be smaller compared to 20 mm/h. This is thought to occur because, during light rain, water movement via diffusion dominates, reducing the impact of permeability. Plot 2L tended to show lower values than other plots from the initial measurements, suggesting a possible issue with the sensor.

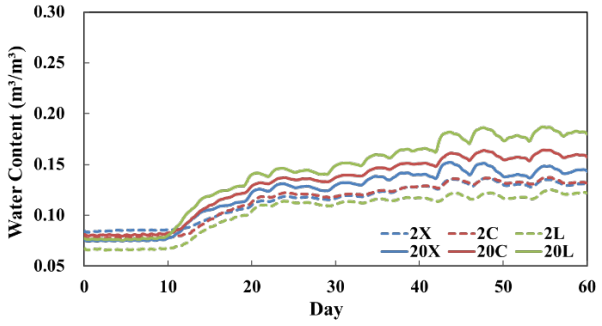

Figure 2. Bottom Water Content

Similar to moisture content, plants were larger in the 20 mm/h experimental plots, with greater growth observed in plots C and L compared to plot X. This trend aligns with moisture content, suggesting that aggregate formation progressed in the topsoil, first enhancing water retention there. Furthermore, aggregate formation likely increased topsoil permeability, promoting water movement downward even during heavy rainfall. This enabled greater water retention and effectively stimulated plant growth.

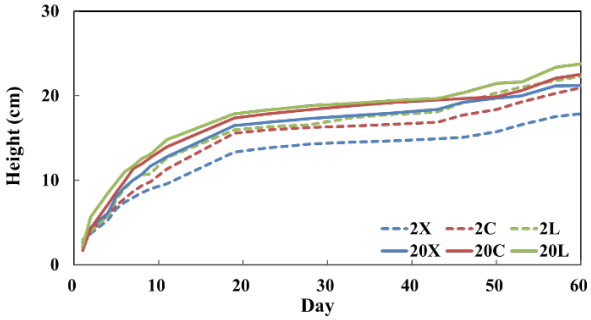

Figure 3. Plant Height

In this experiment, even with the same total irrigation volume, heavy rainfall resulted in greater water retention and higher plant growth. This suggests that developing soil aggregates may enable effective water retention in the surface layer or achieve high permeability to move water to deeper profiles, potentially allowing effective rainfall retention throughout the entire soil profile. Thus, the development of soil structure may have effectively achieved water retention within the soil profile.

4. Conclusions

The addition of natural polymer compounds tended to increase soil water content and positively influence plant growth. Furthermore, results for surface soil water content suggested that the formation of soil aggregate structure was important for plant growth. Moving forward, we intend to investigate in detail factors such as soil organic matter content and organic matter composition that influence soil water content and plant growth. We will examine their relationships and pursue a deeper understanding of the factors necessary for soil fertility enhancement and crop cultivation.

Acknowledgements

This study was partially supported by the Japan Society for the Promotion of Science NEXT Program (GS021, 2011-2014), KAKENHI (B) (26292127, 2014-2016), KAKENHI (A) (17H01496, 2017-2020), (21H04747, 2021-2024), and KAKENHI (S) (24H00057, 2024-2028).

References

Kobori, S. 2023. Enhanced Downward Permeation via Artificial Macropores and Increased Plant Biomass. Okayama University. Master's Thesis.

Omoigui, L.O., A.Y.Kamara, J. Batieno, T. Iorlamen, Z. Kouyate, J. Yirzagla, U. Garba, and S. Diallo. 2018. Guide to cowpea production in West Africa. IITA, Ibadan, Nigeria.

Molecular Characterization of Soil Organic Matter Using NMR and GC/MS in Relation to Total Carbon Content

Moeri Horiuchi [1*], Satoshi Hayakawa [2], Yasushi Mori [1]

[1] Graduate School of Environmental, Life, Natural Science and Technology, Okayama University, Okayama, 700-8530, Japan

[2] Graduate School of Interdisciplinary Science and Engineering in Health Systems, Okayama University, Okayama, 700-8530, Japan

* Corresponding author. Email: yasushim@cc.okayama-u.ac.jp

Abstract

This study aims to evaluate the quality of soil organic matter (SOM) by focusing on its structural characteristics rather than total carbon content (TC).

Samples included Japanese soils (paddy soil, andosols, masa soil, forest soil (cedar plantation)) and soils collected from Sweden, the Philippines, Vietnam, and Indonesia. These samples were analyzed using Gas Chromatography-Mass Spectrometry (GC/MS) and nuclear magnetic resonance (NMR) and compared with total carbon content.

NMR measurements showed peaks in the spectral regions attributed to aromatic and aliphatic carbons, methoxyl and carbohydrate carbons, and carboxyl group carbons in some soil samples. GC/MS analysis of Indonesian soils subjected to land restoration over time revealed that the compound peaks became more abundant as restoration progressed, suggesting GC/MS results may reflect soil organic matter to some extent. Furthermore, comparison of odd-chain fatty acids in Indonesian soils showed that levels comparable to forest soils were detected in the topsoil six years after mining.

Keywords: Soil organic matter, Gas chromatography–mass spectrometry (GC/MS), TMAH thermochemolysis, Total carbon, Van Krevelen diagram

1. Introduction

The ignition loss and the total carbon content are usually used to evaluate the organic matter contained in soils. These indicators evaluate soil organic matter as the amount of carbon, however, they do not provide information on molecular structure. If we can elucidate the properties of organic matter that extend beyond its total carbon content, we will gain insight into the history of organic matter accumulation on land and its resilience or vulnerability to global warming and climate change. This would be a major boon for global environmental research. In this study, soil organic matter is analyzed by GC/MS and NMR, and compared with the total carbon content (TC) to evaluate the age of organic matter, ease of decomposition, and nutritional status of the target soil.

2. Materials and Methods

The samples included paddy field soil, andosols, forest soil, and masa soil from Japan. In addition, soils from Sweden, the Philippines, Vietnam, and Indonesia were analyzed for GC/MS, NMR, and TC. 4μL of tetramethylammonium hydroxide (TMAH) was added to 1 mg of soil sample for better separation of compounds in the GC/MS analysis. The samples were heated inside the pyrolyzer, and 80 compounds were identified. The results were subjected to principal component analysis (PCA). Additionally, to visually represent these compounds, the pre-methylated state of the identified compounds was estimated and depicted using van-Krevelen diagrams. This diagrams were constructed by plotting the H/C ratio of each pyrolysis product on the y-axis and the O/C ratio on the x-axis (Sazawa, 2023). The size of each plot represented its area value.

3. Results and Discussion

Figure 1 shows the NMR spectrum. Some soil samples exhibited peaks in spectral regions attributable to aromatic carbons, aliphatic carbons, methoxyl groups/carbohydrate carbons, and carboxyl group carbons. Forest soil exhibited relatively large spectral peaks. Although paddy soil showed lower values for ignition loss compared to andosols and forest soil, they exhibited larger aromatic peaks. No prominent peaks were observed in the masa soil. Furthermore, PCA based on GC/MS results showed a clear separation between masa soils and other Japanese soils.

The Indonesian soil samples represented different restoration stages following tin mining. van Krevelen diagrams of the top 0 cm layer revealed that, after 6 years of restoration, the soil profile resembled that of nearby forest soils (Figure 2). Furthermore, comparison of odd-chain fatty acids (C15, C17) and even-chain fatty acids (C16, C18) by age and soil depth showed that odd-chain fatty acids were detected in the 0 cm soil layer after 6 years (Figures 3 and 4). Odd-chain fatty acids are generally regarded as biomarkers of microbial activity. Based on previous research (Putra et al.2022), this is considered to be due to microbial activity. Although differences in TC were observed among soils from the Philippines (Figure 5), Sweden, and Vietnam, their position on the van Krevelen diagram and in PCA were relatively similar.

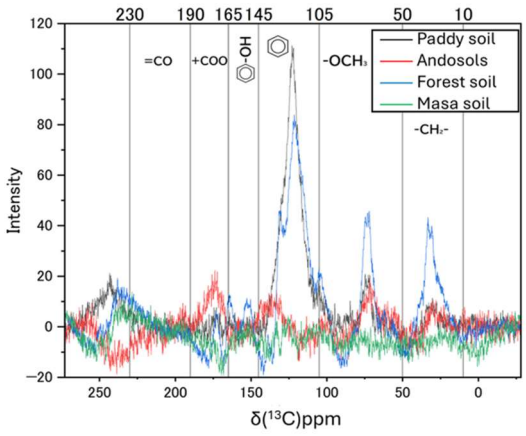

Figure 1. NMR spectra in Japanese soils (paddy soil, andosols, masa soil, forest soil)

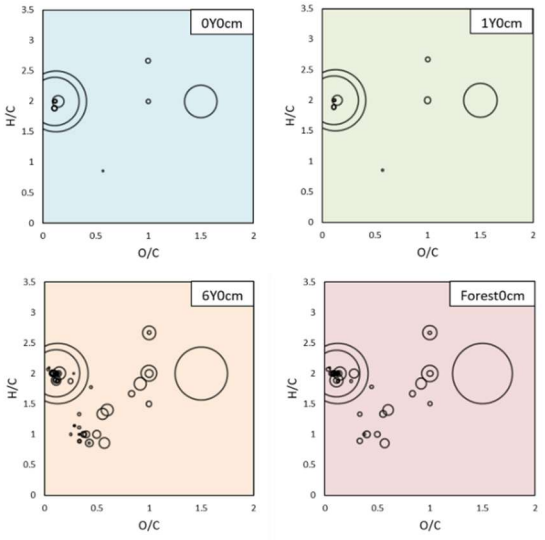

Figure 2. van Krevelen diagram for the top 0 cm layer at an abandoned tin mine site in Indonesia, by number of years since mining cessation (Plot created by estimating the unmethylated state of compounds identified by GC/MS)

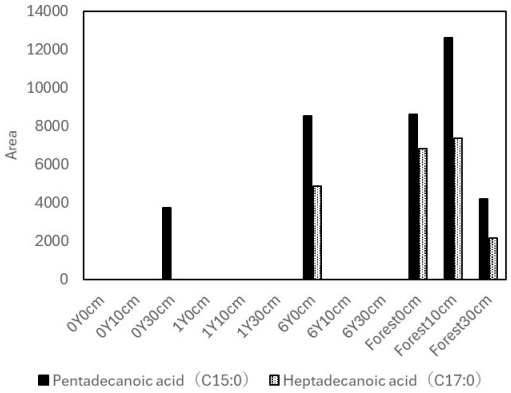

Figure 3. Area values of odd-chain fatty acids at Indonesian tin mine sites (by years since mining cessation and soil depth)

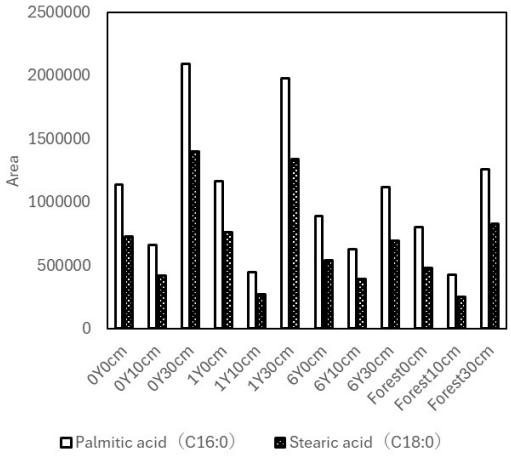

Figure 4. Area values of even-chain fatty acids at Indonesian tin mine sites (by years since mining cessation and soil depth)

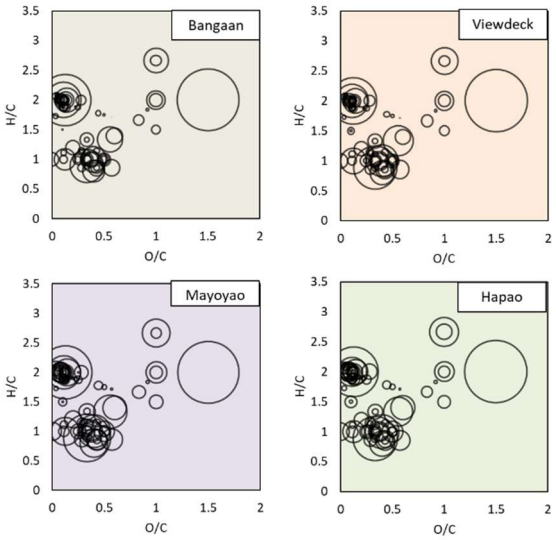

Figure 5.van Krevelen diagrams of soils from four locations in the Philippines (plot created by estimating the unmethylated state of compounds identified by GC/MS)

4. Conclusions

Japanese soils, particularly the nutrient-poor masa soil showed distinct separation from other soils (paddy soils, forest soils, andosols), in PCA based on GC/MS data. Aromatic peaks were prominent in both paddy soils and forest soils in NMR spectra.

Regarding overseas soils, particularly at former tin mining sites in Indonesia, six years after tin-mining, the molecular composition of SOM in the topsoil became relatively similar to that of nearby forest soils.

These findings highlight the usefulness of combining GC/MS, NMR, and TC for characterizing SOM quality. Further analysis focusing on other specific compounds by GC/MS is needed to deepen understanding of SOM dynamics.

Acknowledgements

This study was partially supported by the Japan Society for the Promotion of Science NEXT Program (GS021, 2011-2014), KAKENHI(B) (26292127, 2014-2016), KAKENHI(A) (17H01496, 2017-2020), (21H04747, 2021-2024) and KAKENHI(S) (24H00057, 2024-2028).

References

Sazawa, K.,2023. Molecular characterization of soil organic compounds by pyrolysis-GC/MS. Bunseki (Journal of the Japan Society for Analytical Chemistry), 499–500. [in Japanese]

Putra, H. F., Bui, L. T., & Mori, Y., 2024. Microbial community shifts indicate recovery of soil physical properties in a post‐tin‐mining area on Belitung Island, Indonesia. Land Degradation & Development, 35(7), 2395-2408.

Measurement of Guava Evapotranspiration in Southern Taiwan

Gao Bi-Shuang[1*], Hung-Yeh Hsieh [1], Chien-Hui Syu[2]

[1] Department of Tropical Fruit Trees, Fengshan Tropical Horticultural Experiment Branch, Taiwan Agricultural Research Institute, Ministry of Agriculture, Kaohsiung City, Taiwan

[2] Agricultural Chemistry Division, Taiwan Agricultural Research Institute, Ministry of Agriculture, Taichung City, Taiwan

* Corresponding author. Email: gao@tari.gov.tw

Abstract

Regional water resource management is a critical component of sustainable agriculture, and understanding water use is fundamental to effective management. This study, focusing on evapotranspiration, quantifies water requirements of guava to provide baseline data for regional water resource management in southern Taiwan. From August 2022 to May 2025, data were collected in Kaohsiung to examine guava evapotranspiration, soil texture, and infiltration rate, using a LICOR-7500DS system to monitor annual evapotranspiration, with the aim of establishing water demand characteristics for guava cultivation in southern Taiwan. Soil properties in the study area in the 0-150 cm layer include sandy loam or loam. The infiltration rate in the 0-40 cm soil layer ranges from 2-26 mm·hr^{-1}, with an available water capacity of 234 mm·m-1, indicating rapid drainage and high aeration. Guava crop evapotranspiration (crop evapotranspiration, ET_C) ranges from 1.51-3.84 mm·day^{-1}, potential evapotranspiration (potential evapotranspiration, ET_0) from 3.04-6.49 mm·day^{-1}, and crop coefficient (crop coefficient, K_C) from 0.42 to 0.6. Results indicate that guava evapotranspiration varies seasonally, suggesting that seasonal irrigation adjustments for guava are feasible. Furthermore, KC remains stable across years under dry or wet conditions, indicating that these data can be used by the government to precisely estimate guava water requirements for regional water resource management. This study continues to integrate these data into smart irrigation systems to optimize irrigation strategies, thereby enhancing water use efficiency and supporting sustainable agriculture and food security in southern Taiwan, while providing guidance for water resource management in tropical regions.

Keywords: crop evapotranspiration (ET_C), crop coefficient (K_C), tropical fruit

1. Introduction

Taiwan's average annual rainfall of 2,500 mm is unevenly distributed and poorly retained due to limited reservoir capacity, steep topography, and rapid river runoff. As a result, per capita freshwater availability is only one-third of the global average. With climate change intensifying the frequency of extreme weather events, rainfall patterns in Taiwan have become increasingly irregular, with lower frequency but higher intensity of precipitation events.

Water is a major limiting factor for crop growth, affecting both vegetative and reproductive development. Perennial fruit crops such as guava are particularly vulnerable because irregular drought and flooding influence not only current-year productivity but also long-term growth and fruit quality. Adaptive agricultural strategies are therefore crucial to mitigate the impacts of climate variability on water resources (Howden et al., 2007).

Irrigation is a fundamental management practice that enhances crop productivity, maintains landscapes, and rehabilitates degraded soils (Gavali et al., 2016). However, Improper irrigation may lead to reduced soil aeration, limited nutrient uptake, and decreased crop yields (Hillel et al, 2008). Crop-specific water requirements vary across growth stages, regions, and seasons, emphasizing the importance of crop coefficient (Kc)-based irrigation planning.

Guava (Psidium guajava L.) is a major evergreen fruit tree in Taiwan, with a cultivated area of 8,029 ha (2024 Agricultural Survey), and it ranks among the top ten fruit crops. Given its year-round production, water management is critical, and precision irrigation technology is increasingly recognized as a key component of sustainable guava production. Yet, local studies on guava evapotranspiration remain limited. This study aimed to quantify ET_0, ET_C, and K_C of guava under tropical field conditions in southern Taiwan and to evaluate the physical and hydrological properties of orchard soils.

2. Materials and Methods

2.1. Study Site

The study was conducted in a guava orchard located in Gangshan District, Kaohsiung City, Taiwan (22.80°N, 120.26°E). The cultivar was 'Jen-Ju Bar'. Trees were planted at 4 m × 4 m spacing with a canopy height of approximately 2.5 m. Orchard management followed conventional practices commonly adopted by local farmers.

2.2. Eddy Covariance Flux System

An eddy covariance flux system was installed at the orchard. Sensors included:(1)3D sonic anemometer: WindMasterPRO (Gill Instruments, UK), 1–32 Hz. (2)Open-path CO_2/H_2O analyzer: LI-7500DS (LI-COR, USA), max 20 Hz. (3)Soil moisture probe: CS616 (Campbell Scientific, USA). (4)Soil temperature sensor: Type-T thermocouple (Campbell Scientific, USA). (5)Net radiometer: NR-LITE2-L (Campbell Scientific, USA). (6)Heat flux plates: HFP01SC-L (Campbell Scientific, USA), buried at 5 cm depth. All sensors were connected to a Campbell CR1000 data logger.

2.3. Soil Analysis

Soil properties were assessed with the following methods:(1) Soil Texture: Soil texture was determined based on the relative proportions of sand, silt, and clay, according to the USDA soil texture classification system. (2) Available Water Content: The available water content

was measured using the pressure plate method at matric potentials ranging from 0.1 to 15 bar (Cassell and Klute, 1986). (3) Saturated Hydraulic Conductivity: Saturated hydraulic conductivity was determined using the constant-head method (Amoozegar, 1992). (4) Soil Water Infiltration Rate: The soil water infiltration rate was assessed in the field using a water infiltrometer.

2.4. Calculation of ET_0, ETc, and Kc

Reference evapotranspiration (ET_0) was calculated using FAO CROPWAT 8.0 software with meteorological parameters (minimum/maximum temperature, relative humidity, wind speed, and solar radiation). Actual crop evapotranspiration (ET_C) was obtained from flux measurements. The crop coefficient (K_C) was derived as $K_C = ET_C/ET_0$.

3. Results and Discussion

3.1. Evapotranspiration and Crop Coefficient

Between July 2022 and May 2025, ET_0 ranged from 3.04–6.49 mm/day, ET_C from 1.51–3.84 mm/day, and K_C from 0.35–0.60 (Table 1). Both ET_0 and ET_C followed seasonal temperature patterns, increasing during summer and decreasing during winter. K_C values showed minor seasonal fluctuations, reflecting guava's relatively stable evergreen canopy.

It is noteworthy that the orchard was managed according to conventional practices commonly adopted by local farmers. Therefore, the measured ET_C and derived K_C values reflect actual field conditions in commercial guava production, providing practical guidance for irrigation scheduling and water resource management under tropical conditions.

Table 1. The reference evapotranspiration (ET_0), crop evapotranspiration (ET_C) and crop coefficient (K_C) of 'Jen-Ju Bar' guava in Kaohsiung.

Year	2022		2023		2024		2025		K_C
Month	ET_0	ET_C	ET_0	ET_C	ET_0	ET_C	ET_0	ET_C	average
	mm/d	mm/d	mm/d	mm/d	mm/d	mm/d	mm/d	mm/d	
Jan			3.21	1.61	3.21	1.51	3.15	1.56	0.49
Feb			3.95	1.79	3.87	2.11	3.24	1.52	0.49
Mar			4.89	2.19	4.88	2.05	4.68	2.04	0.43
Apr			5.73	2.43	5.80	2.20	5.54	1.98	0.38
May			6.13	2.61	6.23	2.55	6.31	2.85	0.43
Jun			6.37	3.16	6.49	3.84			0.54
Jul	6.29	3.36	6.46	3.61	6.44	3.60			0.55
Aug	6.06	3.64	6.02	3.22	5.96	3.10			0.55
Sep	5.46	3.08	5.42	3.20	5.54	3.36			0.58
Oct	4.67	2.29	4.69	2.61	4.50	2.61			0.54
Nov	3.81	1.65	3.81	2.01	3.70	2.07			0.51
Dec	3.1	1.55	3.04	1.53	3.12	1.49			0.50

Average K_C values were comparable to those reported in India (0.55–0.86; Singh et al., 2007) and Egypt (0.55–0.86; Elnamas, 2020) but lower than values reported in Hawaii (0.8–1.0; Fares, 2008). These differences suggest that the K_C of guava is region-specific, influenced by cultivar, microclimate, and orchard management practices.

3.2. Soil Properties

Soil characterization revealed sandy loam in the 0–15 cm and 90–150 cm layers and loam in the 15–90 cm layer, with no plow pan observed. Soil pH ranged from 6.1 to 6.84, cation exchange capacity from 5.78 to 11.22 cmol/kg, and organic matter content from 1.31 to 5.25%, indicating moderate fertility. Infiltration rates in the 0–40 cm layer ranged from 2 to 26 mm/hr, and available water content was 234 mm/m, reflecting rapid drainage and high aeration. These results suggest that the soils in the study area have good air permeability and water movement, providing favorable conditions for root growth.

4. Conclusions

This study provides the first multi-year dataset of guava evapotranspiration and crop coefficients in southern Taiwan. These results can serve as a reference for developing precision irrigation strategies and improving water-use efficiency in guava orchards under tropical conditions.

Acknowledgements

This research was financially supported by the Ministry of Agriculture, Taiwan.

References

Amoozegar, A. 1989. A compact constant-head permeameter for measuring saturated hydraulic conductivity of the vadose zone. Soil Sci. Soc. Am. J. 53: 1356–1361.

Cassell, D.K.,and A. Klute. 1986. Water potential：Laboratory Methods. P. 635-662. In A. Klute(ed.)Methods of soil analysis. Part 1：Physical and mineralogical methods. 2nd ed.

Elnamas,A.E. 2020. Effect of irrigation systems and water regime on growth, yield components, water use efficiency and water productivity of guava (*Psidium guavaja* L.) grown in clay soil. Alexandria Science Exchange Journal, vol.41,259-273.

Gavali, M., Dhus, B., Vitekar, A., 2016. A smart irrigation system for agriculture based on wireless sensors. International Journal of Innovative Research in Science, Engineering and Technology, 6893-6899

Hillel, D., Braimoh, A.K., Vlek, P.L.G. 2008. Soil Degradation Under Irrigation. In: Braimoh, A.K., Vlek, P.L.G. (eds) Land Use and Soil Resources. Springer, Dordrecht. p101-119. https://doi.org/10.1007/978-1-4020-6778-5_6

Howden S.M., J. Soussana, F.N. Tubiello, N. Chhetri,, M. Dunlop, and H. Meinke, 2007. Adapting agriculture to climate change, Proc. Natl. Acad. Sci. U.S.A. 104 (50) 19691-19696, https://doi.org/10.1073/pnas.

Singh,B.K.,Tiwari,K.N.,Chourasia, S.K. and Mandal,S. 2007. Crop Water Requirement of Guava (*Psidium guajava* L.) cv. KG／KAJI under Drip Irrigation and Plastic Mulch. Acta Hortic. vol. 735, 399-405.

Determination of heat unit-based crop coefficient for rice in Taiwan

Ya-Ling Hou [1*], Dong-Hong Wu[2], Pei-Jhen Wu[1], Hsuan-Ju Tsai[3]

[1]Crop Science Division, Taiwan Agricultural Research Institute, Ministry of Agriculture, Taichung, Taiwan

[2]Department of Agronomy, National Chung Hsing University, Taichung City 402202, Taiwan

[3] Agricultural Technology Translation Center, Taiwan Agricultural Research Institute, Ministry of Agriculture, Taichung, Taiwan

* Corresponding author. Email: yalinghou@tari.gov.tw

Abstract

Optimizing agricultural water use efficiency is a pressing issue in Taiwan, due to increasing consecutive dry days from climate change. This situation leads to fierce inter-sectoral competition for water, resulting in mandated irrigation limitations and fallowed paddy fields, which impacts agricultural production stability and farmer livelihoods. Accurate estimation of agricultural water requirements is fundamental for establishing reliable irrigation schedules and supporting policy decisions. Crop water requirement (ETc) can be estimated by multiplying reference evapotranspiration (ETo) by a crop coefficient (Kc). This study aims to develop Kc equations based on crop thermal time, reflecting phenological development. An open-path eddy-covariance (EC) system was installed to measure ETc in an alternate wetting and drying (AWD) irrigated paddy field. ETc data from the first cropping seasons in 2023 and 2024 were computed with ETo to derive seasonal Kc values. Daily and 10-day averaged Kc equation models based on heat units were developed and validated in this study. The 10-day averaged Kc model yielded a higher coefficient of determination, likely due to smoother data and clearer seasonal trends. Meanwhile, the daily Kc model demonstrated better predictive performance on the 2024 validation dataset, with an RMSE of 0.178, slightly lower than the 10-day Kc model's RMSE of 0.183. These findings suggest that the daily Kc equation may maintain high prediction accuracy under high temporal resolution. The two heat unit-based Kc models demonstrate strong and versatile application prospects for estimating crop water requirements across diverse regional contexts, contributing to enhancing water use efficiency and sustainable agricultural production.

Keywords: Crop evapotranspiration, Growing degree days, Crop water requirement estimation

1. Introduction

Optimizing agricultural water use efficiency is a critical challenge in Taiwan under the impacts of climate change. The implementation of government-mandated irrigation restrictions has become more frequent and widespread, as evidenced by the increasing area of fallowed paddy fields. This trend underscores the critical need for accurate crop water requirement estimation. Reliable irrigation scheduling relies on precise quantification of crop evapotranspiration (ETc), which is typically determined as the product of reference evapotranspiration (ETo) and a crop coefficient (Kc). This study aims to establish Kc equations based on crop thermal time, aligning with phenological development stages and enabling broader transferability across locations and years.

2. Materials and Methods

2.1. Study site and field management

This study was conducted at the Taiwan Agricultural Research Institute (TARI), Taichung, Taiwan (24°01′55.5″ N, 120°41′30.4″ E). Rice (cv. TNG71) was transplanted with a 30 * 21 cm spacing and cultivated under the alternate wetting and drying (AWD) irrigation method.

2.2. Evapotranspiration and meteorological measurements

An EC measuring system was installed on the south side of the center of a 0.5 ha paddy field, considering the prevailing wind directions from the west-north and north. The system included a 3D ultrasonic anemometer (WindMaster Pro, Gill Instruments, UK) and an open-path infrared gas analyzer (LI-7500DS; LI-COR Biosciences, USA), were mounted at a height of 2.15 m above the ground. Flux data were collected at 10 Hz frequency and recorded as 30-minute averages within the SmartFlux® 3 system throughout the entire crop period.

2.3. Computing ETo and Kc

ETo was calculated from a nearby weather station (G2F820) located within 380 m from the experimental field. The FAO-56 Penman-Monteith equation (Allen et al., 1998) was used to compute daily timesteps ETo. Half-hourly ETc values derived from the EC method were cumulated over 24 h and divided by 2, then used to calculate daily Kc values, excluding data from days with rainfall and insufficient half-hourly ETc (hETc) data. Daily Kc values were obtained as the ratio of measured ETc to calculated ETo (Kc = ETc / ETo).

The time scale for the Kc curves was transformed from calendar days to cumulative growing degree days (CGDD), which provide a physiologically meaningful timescale. The growing degree days (GDD) were calculated using Equation (1):

$$\mathrm{GDD} = \frac{(T_{max}+T_{min})}{2} - T_{base} \qquad (1)$$

where T_{base} is the base temperature, and T_{max} and T_{min} are the daily maximum and minimum air temperatures respectively; where if $(T_{max}-T_{min})/2 < 10$, then GDD=0.

3. Results and Discussion

3.1. Weather and crop growth

Rice was transplanted on February 26, 2023, and March 9, 2024, and harvested after 102 and 100 days, respectively. During the first crop season, total precipitation was 358 mm with 23 rainy days in 2023, and 410 mm with 36 rainy days in 2024. In 2023, daily maximum air temperature (T_{max}) increased from 19.7 ℃ in February to a peak of 35.5℃ in May. In 2024, T_{max} increased from 16.7 ℃ in March to 34.9 ℃ in June, showing a similar trend across the two years (Fig. 1). The

CGDD from the day of transplant to harvest was 1439 in 2023 and 1603 in 2024, with an average of 1515 (Fig. 2).

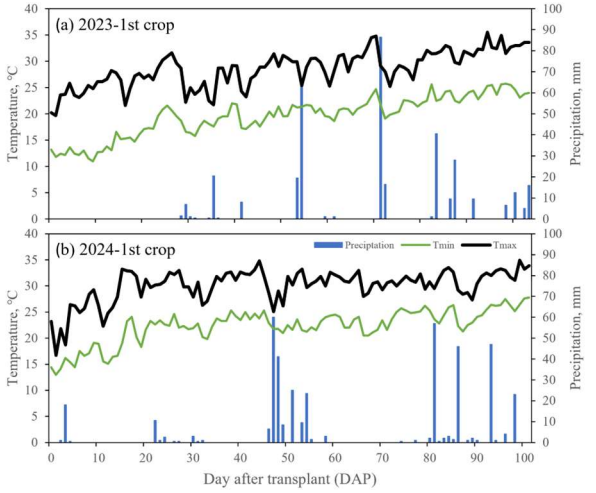

Figure 1. Daily maximum and minimum air temperatures and rainfall during the 2023 and 2024 1st crop season.

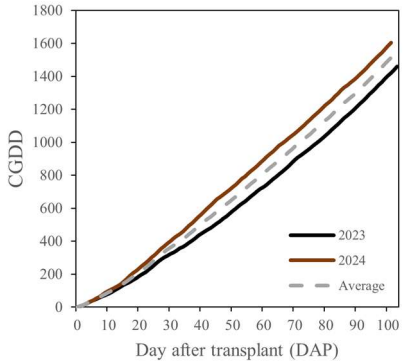

Figure 2. Cumulative growing degree days from rice transplanting to harvest in 2023 & 2024 1st crop season.

3.2. Measured crop ET and computed Kc

Pearson correlation analysis was conducted to examine the relationship between ETc and meteorological parameters. The results revealed that half-hourly ETc during the 2023-1st crop was strongly correlated with solar radiation (Rn, r = 0.94), vapor pressure deficit (VPD, r = 0.86), relative humidity (RH, r = –0.72), maximum wind speed (WS_{max}, r = 0.70), and mean air temperature (TA, r = 0.64) (Fig. 3). Consistent correlation patterns were also observed in the 2024 first growing season.

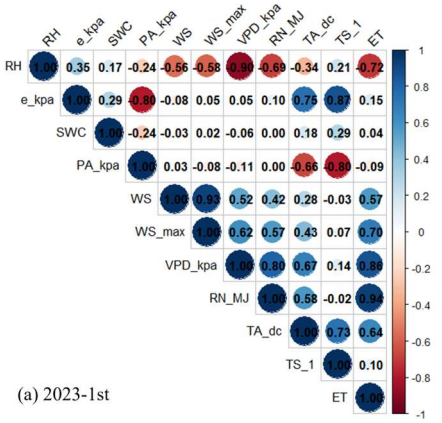

Figure 3. Pearson correlation coefficient among half-hourly ETc and meteorological parameters in 2023-1st crop season.

Half-hourly ETc values were aggregated to daily totals. Days with missing or insufficient ETc, or those affected by rainfall, were excluded. After data cleaning, 87 out of 103 days in 2023 and 79 out of 100 days in 2024 remained. Daily Kc values were then calculated as the ratio of ETc to ETo for subsequent analysis.

Daily and 10-day averaged Kc equation models based on heat unit were developed (Fig4 &Fig.5). The 10-day averaged Kc model yielded a higher coefficient of determination, likely due to smoother data and clearer seasonal trends. Meanwhile, the daily Kc model demonstrated better predictive performance on the 2024 validation dataset, with an RMSE of 0.178, slightly lower than the 10-day Kc model's RMSE of 0.183. Future research should incorporate multi-year Kc datasets to further enhance model development. Such an approach will allow for a systematic comparison of different Kc modeling strategies, thereby enabling a more rigorous evaluation of their accuracy and long-term stability under varying environmental and time scales.

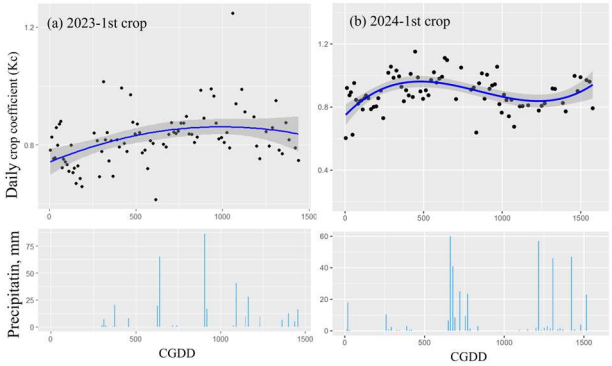

Figure 4. Daily Kc (black dots) and fitted cubic polynomial curves (blue lines) as a function of CGDD for the 1st crop seasons of 2023 (a) and 2024 (b).

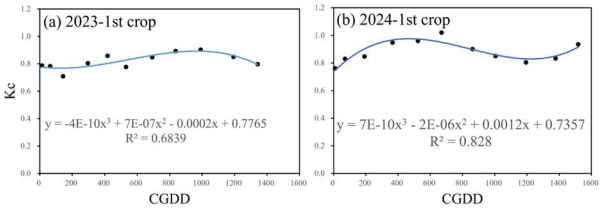

Figure 5. 10-day averaged Kc (black dots) and fitted cubic polynomial curves (blue lines) as a function of CGDD for the 1st crop seasons of 2023 (a) and 2024 (b).

4. Conclusions

Thermal-based daily Kc models established in this study provided better predictive performance compared to 10-day Kc model. It underscores the potential of thermal time-based Kc equations for improving irrigation requirement estimation across locations and years.

References

Allen, R. G., Pereira, L. S., Raes, D., & Smith, M. (1998). Crop evapotranspiration-Guidelines for computing crop water requirements-FAO Irrigation and drainage paper 56. Fao, Rome, 300(9), D05109.

Lin, S. H., Lu, C. T., Jwo, W. S., & Lu, H. Y. (2014). Establishment and validation of prediction model for rice growth stages. J. Taiwan Agric. Res, 63, 30-42.

Optimizing Banana Cultivation with CROPWAT 8.0 and Drip Irrigation to Mitigate Water Competition in Paddy-Dominated Watersheds and Promote Climate-Resilient Agriculture

Wei-Chen Wang[1], Yu-Yi Chen[1], Hsueh-I Chen[1], Chien-Hui Syu[2], Yao-Hsien Tsai[2], and Yung-Chou Lin[1*]

[1] Crop Science Division, Taiwan Agricultural Research Institute, Ministry of Agriculture, Taichung City, Taiwan

[2] Agricultural Chemistry Division, Taiwan Agricultural Research Institute, Ministry of Agriculture, Taichung City, Taiwan

* Corresponding author. Email: yongchou@tari.gov.tw

Abstract

Conventional banana farming using furrow or sprinkler irrigation is highly water-intensive and often competes with the limited water resources allocated to downstream paddy fields. To address this challenge, this study evaluates the potential of integrating drip irrigation systems with the CROPWAT 8.0 model to enhance irrigation water use index while maintaining yield and fruit quality in banana orchards. Field experiments were conducted in a subtropical region of central Taiwan, where bananas were cultivated on raised beds using a wide-narrow triangular row arrangement, with 4.8 m (wide row) and 2.4 m (narrow row) spacing, and 1.6 m between plants within rows. Crop evapotranspiration (ETc) and reference evapotranspiration (ET_0) were monitored to establish localized crop coefficients (Kc), crop phenology and soil moisture parameters were collected for input into the CROPWAT 8.0 model. Using historical meteorological data from the preceding week, irrigation water requirements were estimated, and the calculated irrigation depth was applied as the irrigation setting for the following week. Results showed that drip irrigation reduced total water input about 56% compared to conventional cultivation water requirement. Additionally, optimized irrigation scheduling helped to reduce peak water demand, allowing for more flexible and efficient water allocation within the watershed. This approach not only enhances the sustainability of upland banana cultivation but also alleviates irrigation pressure on downstream paddy fields. The findings highlight the importance of crop-specific, data-driven irrigation strategies for promoting climate-resilient and integrated water resource management in mixed-use agricultural landscapes.

Keywords: Banana cultivation, Evapotranspiration, Crop coefficients, Water requirements

1. Introduction

Banana (Musa spp.) cultivation is important for global food security and agricultural economies, with 2023 production reaching ~139 million tons on 5.9 million hectares, supporting millions of smallholder farmers and contributing to exports in tropical and subtropical regions (FAOSTAT, 2023).

Traditional banana cultivation is highly water-intensive, requiring 1,200–2,690 mm yr^{-1} (Panigrahi et al., 2021). Water stress reduces chlorophyll and photosynthesis, causes leaf senescence and weakened pseudo-stems, and lowers yield (Nansamba et al., 2020). A 100 mm yr^{-1} rainfall deficit can decrease bunch yield by 9%, mainly through reduced finger number (van Asten *et al.*, 2011).

Banana cultivation has traditionally relied on flood or furrow irrigation, which is inefficient and can cause both water excess and stress. Drip irrigation offers a precise alternative, aligning water application with crop demand to improve yield and quality while conserving water and reducing groundwater depletion (Ghosh et al., 2018). In Taiwan, although some farms have adopted sprinkler hose irrigation, overall irrigation efficiency remains suboptimal. Historically designed for rice cultivation, Taiwan's irrigation systems prioritize paddy fields, which consume substantial water and compete with upland crops, industry, and urban areas (Tsai and Hu, 2000). High water demands from both crops create direct competition, particularly during dry seasons or droughts intensified by climate variability, reducing agricultural system resilience.

This study evaluates CROPWAT 8.0-guided drip irrigation to improve water-use efficiency in banana cultivation and reduce competition in paddy-dominated watersheds, aiming to support climate-resilient production that maintains yield and quality while promoting sustainable water management.

2. Materials and Methods

2.1. Plant materials and treatments

Field experiments were conducted in a subtropical region of central Taiwan (24.034788°N, 120.686597°E) at 69 m above sea level, with a humid climate and distinct wet and dry seasons. Banana (Musa AAA, Cavendish, cv. 'Tai-Chiao No. 5') were grown on raised beds in a wide–narrow triangular row pattern (4.8 m and 2.4 m spacing; 1.6 m between plants in narrow rows), with standard fertilization, weeding, and pest management. Two irrigation treatments were compared in an RCBD: (1) conventional sprinkler hose irrigation (control) and (2) CROPWAT 8.0-guided drip irrigation, each with three replicated plots of six plants.

2.2. Irrigation management and CROPWAT 8.0 simulation

Irrigation was scheduled using CROPWAT 8.0, parameterized with local meteorological, soil, and crop data. Historical weather data from the preceding week—daily maximum and minimum temperature, relative humidity, wind speed, sunshine duration, and rainfall—were obtained from the nearest Central Weather Administration agricultural station. Reference evapotranspiration (ET_0) was calculated via the FAO Penman–Monteith method, and weekly irrigation requirements were estimated and applied to the plots the following week.

Crop evapotranspiration (ETc) was measured in the field using an LI-7500DS open-path gas analyzer (LI-COR Biosciences, Lincoln, NE, USA) before the irrigation experiment to determine localized crop coefficients (Kc) for each growth stage ($Kc = ETc/ET_0$), which were then used as input parameters in the CROPWAT 8.0 model for

irrigation scheduling.

2.3. Data collection and statistical analysis

Fruit yield was recorded at harvest, and total irrigation water applied was monitored with flow meters at each system's inlet. Irrigation water use index (IWUI) was calculated as banana yield per unit of irrigation water applied (Fairweather et al., 2011; Marković et al., 2012; Roth et al., 2013). Treatment effects were compared using a t-test, with significance at $p < 0.05$.

3. Results and Discussion

3.1. Reduction in Water Use with CROPWAT-Guided Drip Irrigation

Drip irrigation scheduled using the CROPWAT 8.0 model reduced total irrigation volume by 56% compared to conventional sprinkler irrigation (Figure 1), demonstrating the effectiveness of model-based planning in optimizing water application while meeting crop demand. This substantial reduction highlights the potential of CROPWAT-guided drip irrigation as a strategy to conserve scarce water resources and improve irrigation efficiency in banana cultivation.

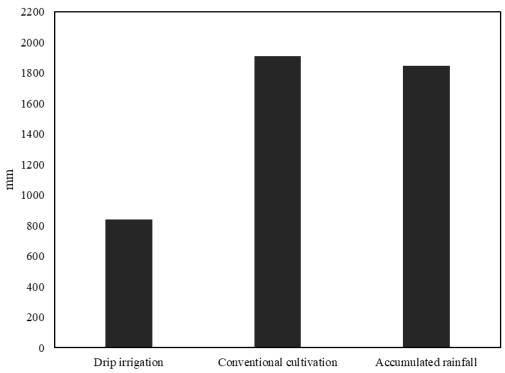

Figure 1. Total irrigation water applied under conventional sprinkler irrigation and CROPWAT 8.0-guided drip irrigation during this experiment. Drip irrigation reduced water use by 56% compared to the conventional method.

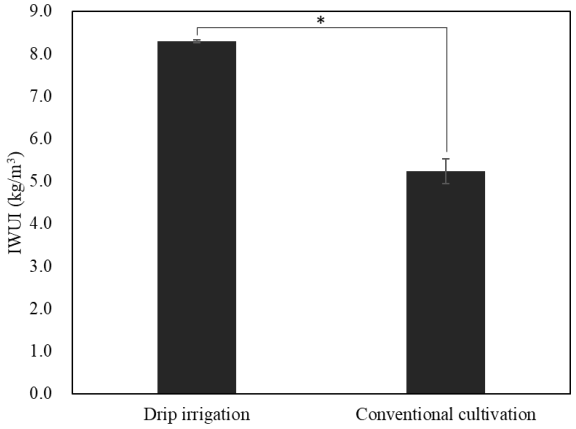

Figure 2. Comparison of mean of irrigation water use index for drip irrigation and conventional irrigation. Bars represent means ± standard error. A Student's t-test indicates a significant difference between treatments ($p < 0.05$).

3.2. Irrigation Water Use Index (IWUI)

According to Roth et al. (2013), IWUI is a suitable index for evaluating irrigation practices within a single growing season, as it accounts solely for the water applied. In this study, IWUI, calculated as banana yield per unit of irrigation water applied, was significantly higher under CROPWAT-guided drip irrigation than under conventional irrigation (Figure 2), indicating that precise, model-based scheduling improves crop water productivity and reduces competition for limited water resources. Furthermore, the results support the practical applicability of localized crop coefficients (Kc), derived from field ETc measurements using the LI-7500DS open-path gas analyzer, suggesting that the model reasonably approximated the actual water requirements of bananas throughout the growth cycle.

4. Conclusions

Integrating CROPWAT 8.0 with drip irrigation improved water use efficiency in bananas while maintaining yield. Model-guided drip irrigation reduced total water input versus conventional methods, easing competition in paddy-dominated watersheds and demonstrating a practical strategy for sustainable, climate-resilient production and watershed management.

Acknowledgements

This study was supported by the Ministry of Agriculture, Taiwan.

References

Fairweather, H., Austin, N., Hope, M., 2011. Irrigation Insights No. 5: Water use efficiency, an information package. Edited by Anne Currey. Designed and desktop published by Graphiti-design, Lismore.

FAO (Food and Agriculture Organization of the United Nations), 2023. FAOSTAT statistical database. Rome: FAO. https://www.fao.org/faostat/en/#home
Accessed September 12, 2025.

Ghosh, U., Sarkar, N., Biswas, R.K., Ranajit, 2018. A review on performance evaluation of drip irrigation system in banana cultivation. J. Pharmacogn. Phytochem., 7(1), 866–869.

Marković, M., Pepó, P., Sárvári, M., Kovačević, V., Šoštarić, J., Josipović, M., 2012. Irrigation water use efficiency in maize (Zea mays L.) produced with different irrigation intervals. Acta Agron. Hung., 60(1), 21–27.

Nansamba, M., Sibiya, J., Tumuhimbise, R., Karamura, D., Kubiriba, J., Karamura, E., 2020. Breeding banana (Musa spp.) for drought tolerance: A review. Plant Breed., 139(4), 685–696.

Panigrahi, N., Thompson, A.J., Zubelzu, S., Knox, J.W., 2021. Identifying opportunities to improve management of water stress in banana production. Sci. Hortic., 276, 109735.

Roth, G., Harris, G., Gillies, M., Montgomery, J., Wigginton, D., 2013. Water-use efficiency and productivity trends in Australian irrigated cotton: a review. Crop Pasture Sci., 64(12), 1033–1048.

Tsai, M.H., Hu, W.J., 2000. Irrigation performance and management in Taiwan. In: Proc. Challenges facing irrigation and drainage in the new millennium, Fort Collins, Colorado, USA, June 2000, pp. 523–534.

van Asten, P.J., Fermont, A.M., Taulya, G., 2011. Drought is a major yield loss factor for rainfed East African highland banana. Agric. Water Manage., 98(4), 541–552.

Detection of Initial Irrigation in Paddy Fields Using Remote Sensing Data for Monitoring Water Allocation in Traditional Irrigation System in Bali

Wily Goldramijaya [1*], Atiqotun Fitriyah [2], Fumi Okura [3], Tasuku Kato [1], Ni Nyoman Sulastri [5], I Wayan Tika [5], Sumiyati [5], Ida Ayu Gede Bintang Madrini [5], Mentari Kinasih [5]

[1] United Graduate School of Agriculture Science, Tokyo University of Agriculture and Technology, Fuchu, Tokyo, Japan

[2] The National Research and Innovation Agency of the Republic of Indonesia, Bogor, Jawa Barat, Indonesia

[3] Japan International Research Center for Agriculture Science, Tsukuba, Ibaraki, Japan

[4] Department of Agricultural and Bio-System Engineering, Udayana University, Jimbaran, Bali, Indonesia

* Corresponding author. Email: wilygoldramijaya.wg@gmail.com

Abstract

A comprehensive understanding of irrigation water management within an irrigation area is essential for developing effective adaptation strategies. This study investigates the water allocation scheme in a traditional irrigation system for rice cultivation during the dry season using Sentinel-1A imagery. The study area, located in the Tungkub Irrigation Area on Bali Island, Indonesia, consists of six groups of traditional water users known as Subak. To monitor water allocation during the dry season, we conducted the following steps: (1) generating dry-season paddy field maps using the Random Forest algorithm, and (2) detecting the initial irrigation in paddy fields through time-series analysis of backscatter values. The Random Forest classification successfully identified dry-season paddy fields, achieving an overall accuracy of 96.55% and a Kappa coefficient of 0.93. Furthermore, time-series analysis of Sentinel-1A backscatter effectively determined the first day of irrigation, with a root mean square error (RMSE) of 6.01 days compared with ground reference data. Our findings reveal that, under normal conditions, water users located upstream and downstream began irrigation almost simultaneously, whereas midstream users started later. Overall, this analysis provides insights into actual water allocation, shifts in irrigation schedules, disparities in allocation timing, and the influence of water availability on allocation practices.

Keywords: Sentinel-1, Random Forest, Time-series analysis, Subak system, Terraced paddy fields.

1. Introduction

A well-known traditional water user association in Bali, known as Subak, has played a key role in sustaining local rice production by managing irrigation water equitably under water-scarce conditions (Norken et al., 2015). However, with increasing demand for freshwater and declining availability due to climate change (Yamamoto et al., 2021; Kurniadi et al., 2024) evaluating the existing water management system is essential as an adaptive measure to strengthen local rice production. Furthermore, understanding the current state of actual water allocation is crucial for improving water management (Speed et al., 2013). Unfortunately, historical data related to water use are often scarce—for example, information on when farmers actually withdraw water from canals—and may not accurately reflect field conditions, particularly in developing countries. Yet such information is essential for understanding how water is allocated from the source.

Large-scale monitoring of water allocation requires significant time and extensive sampling to capture the dynamics of irrigation. As an alternative, remote sensing technology, particularly satellites equipped with active sensors, offers an efficient means of acquiring information on the Earth's surface. Active satellites such as Sentinel-1, which is equipped with synthetic aperture radar (SAR), have advantages over optical satellites. They can operate regardless of weather conditions, both day and night, and are capable of detecting water presence in paddy fields, making them highly suitable for monitoring irrigation systems in rice cultivation areas (Tsyganskaya et al., 2018). Therefore, this study was conducted to monitor water allocation during the dry season in a traditional irrigation system by identifying the initial irrigation in paddy fields through time-series analysis of Sentinel-1 imagery.

2. Materials and Methods

2.1. Study area

The study was conducted in the Tungkub Irrigation Area (TIA), located between Badung Regency and Tabanan Regency, Bali, Indonesia. TIA consists of six groups of traditional water users (*Subak*), covering a total area of approximately 1,092 hectares (Figure 1). Irrigation water is diverted from the Sungi river to supply the terraced paddy fields. The dry season in the region extends from April to September, and land preparation in each *Subak* typically takes about one month.

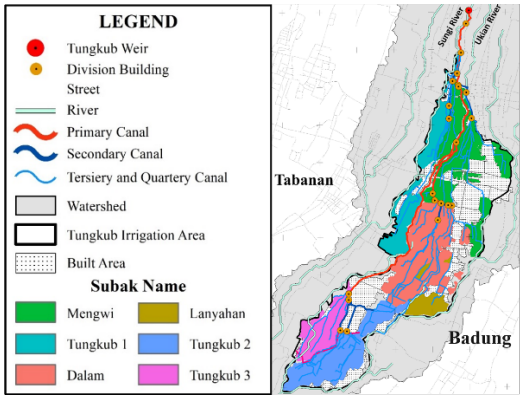

Figure 1. Map of Tungkub Irrigation Area

2.2. Data Preparation

A total of 601 Sentinel-1A images were used for the analysis from 2018 to 2024. Ground-truth data points of dry-season paddy fields and initial irrigation dates were collected through field surveys from June 14 to June 20, 2024, and supplemented with Planet Labs imagery. The Sentinel-1A imagery was preprocessed using SNAP software and R Studio to correct inherent distortions caused by topography, incidence angle, and atmospheric effects. The output of the preprocessing was a time-series

dataset of Sigma⁰ VH backscatter imagery.

2.3. Mapping dry season paddy fields

Since the main focus of this study is water allocation during the dry season, a dry-season paddy fields map was generated to mask non-paddy areas, leaving only pixels corresponding to dry-season paddy fields. The paddy map was produced using a Random Forest classifier trained with eight features derived from the time-series dataset of Sigma⁰ VH backscatter: standard deviation, maximum value, minimum value, backscatter difference, median, mean, R^2 of quadratic fitting, and the slope of linear fitting. The paddy maps were evaluated by a confusion matrix.

2.4. Detecting initial irrigation in paddy fields

The dry-season paddy field pixels were analyzed to determine when farmers initially withdrew water. We assumed that the point preceding the steepest slope in the time-series data of Sigma⁰ VH backscatter corresponds to the initial irrigation event. To identify this, the time-series backscatter data were converted into time-series slope data. The slope was calculated using a linear regression model with a sliding window technique, and the minimum slope value was considered indicative of the initial irrigation. This approach was then evaluated using the RMSE. The detected initial irrigation dates were aggregated from daily data to weekly data for easier visualization and analysis.

3. Results and Discussion

3.1. Dry season paddy maps

The Random Forest accurately identified dry-season paddy fields (Figure 2), as demonstrated by a confusion matrix showing a high overall accuracy of 96.5% and a Kappa coefficient of 0.93. Based on these maps, the areas of dry-season paddy fields in 2018 and 2019 were the smallest compared to other years, particularly in the downstream region. This reduction in 2018 was due to maintenance activities on the irrigation canal in the downstream area.

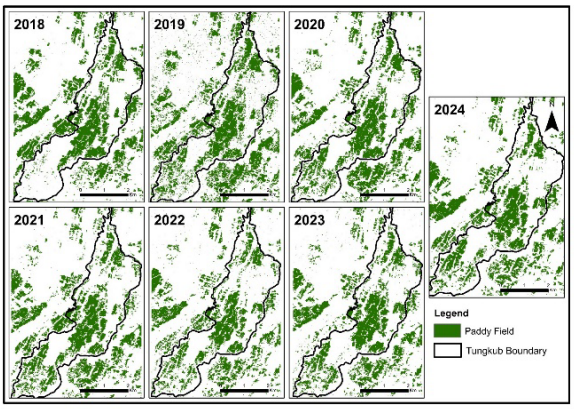

Figure 2. Dry season paddy maps

3.2. Weekly distribution of initial irrigation dates

The point preceding the significant drop in the time-series data likely represents the initial irrigation, with a root mean square error (RMSE) of 6.01 days. Water allocation can be visualized spatially and temporally through the distribution of initial intake dates. The results indicated that, during a normal year without El Niño, upstream Subaks typically began irrigation first, followed by downstream Subaks, and finally midstream Subaks (Figure 3). This pattern occurs because downstream areas receive a substantial amount of surplus water from upstream, resulting in higher water availability downstream compared to midstream. Between 2018 and 2024, each group exhibited changes in its allocation schedule, with Subak Dalam serving as a representative example (Figure 4). This phenomenon suggests that water allocation is determined by direct requests from farmers to the gatekeepers rather than by fixed schedules.

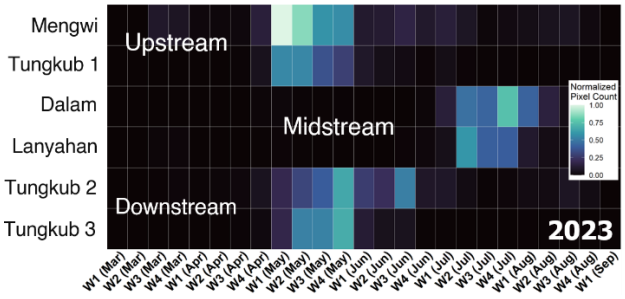

Figure 3. Weekly distribution of initial irrigation in 2023

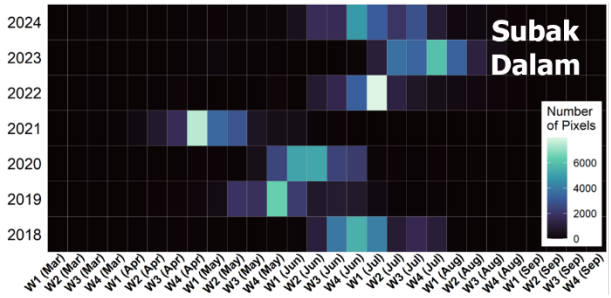

Figure 4. Weekly distribution of initial irrigation in Subak Dalam from 2018 to 2024

4. Conclusions

This study demonstrates the strong potential of Sentinel-1 for understanding traditional irrigation systems by analyzing the spatiotemporal distribution of initial water intake and delineating water user boundaries. The analysis provided valuable insights into actual water allocation, shifts in allocation schedules, disparities in planting, and the influence of water availability on irrigation management.

References

Kurniadi, A., Weller, E., Salmond, J., Aldrian, E., 2024. Future projections of extreme rainfall events in Indonesia. Int. J. Climatol. 44, 160–182. https://doi.org/10.1002/joc.8321

Norken, I.N., Suputra, I.K., Arsana, I.G.N.K., 2015. Water Resources Management of Subak Irrigation System in Bali. Appl. Mech. Mater. 776, 139–144. https://doi.org/10.4028/www.scientific.net/amm.776.139

Speed, R., Yuanyuan, L., Quesne, T. Le, Pegram, G., Zhiwei, Z., 2013. Basin water allocation planning: Principles, procedures and approaches for basin allocation planning. UNESCO, Paris.

Tsyganskaya, V., Martinis, S., Marzahn, P., Ludwig, R., 2018. Detection of temporary flooded vegetation using Sentinel-1 time series data. Remote Sens. 10, 1–23. https://doi.org/10.3390/rs10081286

Yamamoto, E.M.S., Sayama, T., Takara, K., 2021. Impact of Rapid Tourism Growth on Water Scarcity in Bali, Indonesia. Indones. J. Limnol. 2, 1–16. https://doi.org/10.51264/inajl.v2i1.14.

Improving SWAT performance in a snow-dominated basin via a two-season precipitation lapse rate: Case study of the Tedori River, Japan

Alexandru Tabacaru[1], Yoichi Fujihara[2]

[1] Graduate School of Bioresources and Environmental Sciences, Ishikawa Prefectural University, 1-308 Suematsu, Nonoichi, Ishikawa 921-8836, JAPAN tabacarualex@yahoo.com

[2] Faculty of Bioresources and Environmental Sciences, Ishikawa Prefectural University, 1-308 Suematsu, Nonoichi, Ishikawa 921-8836, JAPAN

* Corresponding author. Email: yfuji@ishikawa-pu.ac.jp

Abstract

Rainfall–runoff models are indispensable for understanding basin-scale water cycles in snow-dominated regions. This study applied the Soil and Water Assessment Tool (SWAT+) to the Tedori River basin (809 km²), a steep mountainous watershed in Japan, to evaluate the role of precipitation lapse rates (PLAPS) in improving discharge simulations. Twelve scenarios (Cases A–L) were developed, each representing distinct seasonal lapse rates, with a fixed temperature lapse rate (–0.0065 °C/m). Model performance was assessed against observed flow at the Tedorigawa Dam using Nash–Sutcliffe Efficiency (NSE) and Percent Bias (PBIAS). Results demonstrate that PLAPS calibration is critical: Case K achieved the best overall NSE (0.72) with reasonable PBIAS (10.75%), while Case J provided excellent bias control (PBIAS = 2.26%) and accurate flow representation (33.3 m³/s). The analysis revealed that modeled discharge is highly sensitive to precipitation input. Hydrographs confirm strong seasonal variability with spring snowmelt and summer typhoon peaks. These findings highlight the value of elevation-dependent precipitation adjustments and suggest that a two-season lapse-rate scheme balances simplicity and accuracy for snow-fed basins.

Keywords: Tedori River, SWAT+, precipitation lapse rate, snow hydrology, model calibration

1. Introduction

Hydrological models are widely used for watershed-scale water resource management and analysis. Among them, the Soil and Water Assessment Tool (SWAT) is one of the most representative and globally applied models. It allows for the simulation of runoff and water balance by incorporating spatial and temporal variations in land use, soil, and climate conditions.

In Japan as well, SWAT has been applied to many watersheds. Kibet et al. (2018) applied SWAT to the Yasu River basin and quantitatively evaluated the relationship between rainfall and agricultural runoff. In another study, Macalam et al. (2025) used SWAT to evaluate the water balance and seasonal variability of the Chikugo River basin. However, applications of SWAT in mountainous regions with heavy snowfall—where annual precipitation exceeds 4,000 mm, remain limited.

This study aims to evaluate whether incorporating elevation-dependent precipitation lapse rates (PLAPS) into SWAT+ can improve runoff simulations in a snow-fed basin. Focusing on the Tedori River basin in Ishikawa Prefecture (809 km²), we introduce multiple seasonal PLAPS scenarios and assess their impact on discharge simulations at the Tedorigawa Dam outlet.

2. Materials and Methods

2.1. Study area

Tedori River basin has a length of 72 km, originates at Mount Hakusan (2,702 m) in Ishikawa Prefecture, and features steep terrain with heavy winter snow and summer typhoon rain. Ishikawa has significant year-round rainfall, especially on the Sea of Japan coast.

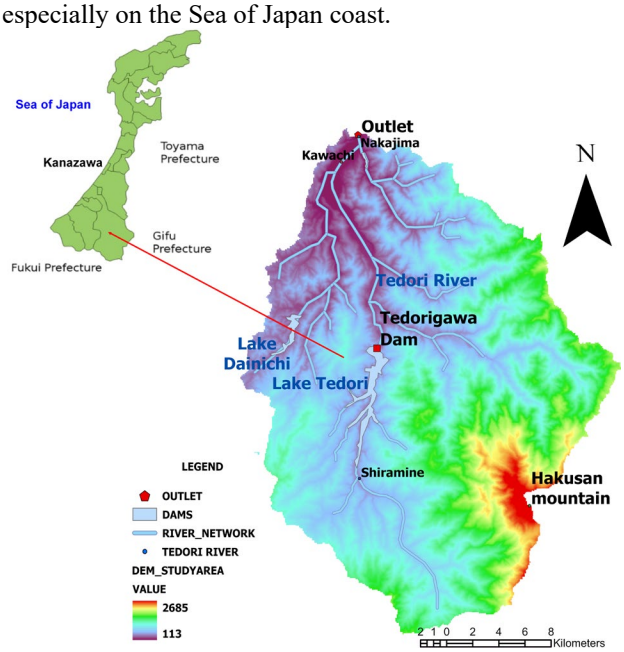

Figure 1. Location of the Tedori River basin, including stream network and elevation variations

2.2. Creating Virtual Weather Stations

The centroids (X, Y coordinates and elevation) of the 24 subbasins were used to define virtual weather station locations within the Tedori River basin. Observed flow data were obtained from Nakajima station.

2.3. Climate Data processing

Daily precipitation data from Shiramine, along with precipitation and temperature records from the Kawachi station (2014–2023), were used, with the years 2014–2015 serving as the model warm-up period. Wind speed, humidity and solar radiation came from Kanazawa station. The temperature used Kawachi data for all subbasins. Precipitation for virtual weather stations was taken from Kawachi or Shiramine, depending on which base station was closest.

PLAPS values were taken from Table 1. TLAPS was set to 0.65 °C per 100 m elevation gain, reflecting the typical decrease of temperature with height. Precipitation

for the new weather stations was estimated using Equation (1).

$$P_2 = P_1 \times [1 + PLAPS \times (Z_2 - Z_1)] \quad (1)$$

where P_2 = precipitation at target location (mm), P_1 = precipitation at source location (mm), PLAPS = precipitation lapse rate, Z_2 = target elevation (m), Z_1 = source elevation (m).

2.4. SWAT+ simulations

SWAT+ simulations used a 90 m DEM (USGS), 100 m land use map (4 classes), and 250 m soil map (4 classes) from the DSOLMap, along with flow and daily climate data. Twelve scenarios (Cases A–L) applied seasonal PLAPS for winter (Dec–Feb) and summer (Mar–Nov) (Table 1).

Table 1. Seasonal PLAPS Coefficients by Case Scenario

Case	Winter coefficient	Summer coefficient
A	0.0000	0.0000
B	0.0010	0.0010
C	0.0015	0.0015
D	0.0020	0.0020
E	0.0030	0.0030
F	0.0020	0.0010
G	0.0020	0.0005
H	0.0020	0.0001
I	0.0030	0.0020
J	0.0030	0.0015
K	0.0030	0.0010
L	0.0030	0.0005

Model performance was evaluated against observed discharge at Tedorigawa Dam using the equations for NSE (2) and PBIAS (3).

$$NSE = 1 - \frac{\sum_{t=1}^{T}(Q_m^t - Q_0^t)^2}{\sum_{t=1}^{T}(Q_0^t - Q_0^-)^2} \quad (2)$$

$$\text{PBIAS} = \frac{\sum_{t=1}^{T}(Q_m^t - Q_o^t) \times 100}{\sum_{t=1}^{T}(Q_0^t)} \quad (3)$$

Where Q_0^t is the observed flow at a given time, Q_m^t is the modeled flow at a given time, Q_0^- is the mean of observed flow.

3. Results and Discussion

Model results were highly sensitive to precipitation adjustments. Table 2 shows NSE and PBIAS at the Tedorigawa Dam outlet for all cases. Without lapse rates (Case A), flow was severely underestimated, confirming uniform inputs cannot represent snow hydrology. Uniform seasonal coefficients (Cases B–E) improved performance, while dual-season schemes (Cases F–L) further increased NSE but often raised bias. Case J was the best case because it best matched observed mean flow (33.3 m³/s) with low bias (2.3%) and solid NSE (0.69), whereas Case K achieved the highest NSE (0.72) with acceptable bias (10.8%). Overall, higher winter lapse rates with moderate summer values gave the most balanced results.

The simulations confirmed that precipitation lapse rates strongly influence runoff generation in the Tedori Basin. Higher winter coefficients improved snowmelt representation, while moderate summer values reduced bias. Peak flood events remained challenging to capture.

Table 2. NSE, PBIAS at Tedorigawa Dam outlet

Case	Observed Mean Flow (m³/s)	Modeled Mean Flow (m³/s)	NSE	PBIAS (%)
A	34.1	17.7	0.34	48.0
B	34.1	25.8	0.67	24.3
C	34.1	29.8	0.70	12.4
D	34.1	33.9	0.62	0.5
E	34.1	42.0	0.21	-23.2
F	34.1	28.1	0.71	17.5
G	34.1	25.2	0.65	26.0
H	34.1	22.9	0.56	32.8
I	34.1	36.2	0.59	-6.2
J	34.1	33.3	0.69	2.3
K	34.1	30.4	0.72	10.8
L	34.1	27.5	0.68	19.3

Hydrographs at Tedorigawa Dam (Fig. 2) captured key seasonal dynamics, including spring snowmelt and summer typhoon peaks. Wet years (2017–18, 2021–22) and dry years (2019–20) were represented, and baseflow during low-flow conditions reproduced reliably. Certain flood peaks (2017, 2018, 2022) were underestimated, while a few events were overpredicted, highlighting challenges in capturing extreme rainfall–runoff responses.

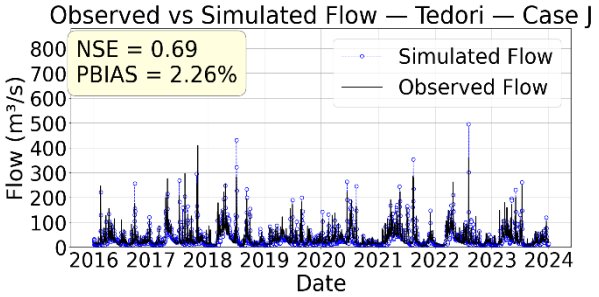

Figure 2. Observed and simulated flow hydrograph at Tedorigawa Dam station, Case J

Overall, results show calibrating PLAPS is a practical way to improve flow simulations in snow-fed basins. Seasonal PLAPS schemes enhance reliability for water resource and flood risk assessments, while their simplicity suits data-limited regions. Challenges in capturing rare extremes remain for future work.

4. Conclusions

The implementation of a dual season lapse rate scheme improved flow simulation accuracy, offered a practical calibration framework requiring minimal additional data, and enhanced model robustness without adding substantial complexity. These results provide guidance for hydrological modeling in snow-fed basins where dense meteorological networks are unavailable.

Acknowledgements

This research was supported by the Japanese International Cooperation Agency (JICA).

References

Kibet, K.B., Takeuchi,J., and Fujihara, M., 2018. Applicability of SWAT Model for Streamflow Simulation in a Highly Managed Agricultural Watershed: Yasu River basin, Japan. J. Rainwater Catchment Syst., 23(2), 19-27.

Macalam,F.J.,Wang,K.,Onodera,S.,Saito,M.,Nagano,Y., Yamazaki,M.,and War Nang,Y.,2025. Hydrological Modeling of the Chikugo River basin Using SWAT: Insights into Water Balance and Seasonal Variability.

High-resolution satellite monitoring of alpine snow patches for watershed water resource variability analysis

Ryoma Nonaka [1], Yoichi Fujihara [2*], Hiroshi Ogawa[2], Shunsuke Chono[2], Eiji Ichion[2]

[1] Graduate School of Bioresources and Environmental Sciences, Ishikawa Prefectural University, 1-308 Suematsu, Nonoichi, Ishikawa 921-8836, JAPAN

[2] Faculty of Bioresources and Environmental Sciences, Ishikawa Prefectural University, 1-308 Suematsu, Nonoichi, Ishikawa 921-8836, JAPAN

* Corresponding author. Email: yfuji@ishikawa-pu.ac.jp

Abstract

Alpine snow patch serves as a crucial summer water resource and a sensitive climate change indicator. However, frequent high-resolution observations in mountainous regions remain labor-intensive and logistically challenging. This study developed an automatic detection method using high-resolution Planet Labs satellite imagery, with a spatial resolution of 3.7m, daily acquisition frequency, and 4 bands (blue, green, red, and near-infrared). The method was validated against field surveys of the Senkagaike snow patch - the only perennial snow patch on MT. Hakusan. A multidimensional dataset (2016 - 2024) was constructed from 25 satellite scenes, integrating spectral and topographic features (DEM, slope angle, curvature). SVM classification using 2024 training data for three land cover classes (snow patch, wasteland, vegetation) showed that only 4 bands classification overestimated area (6,724m^2, 235%), while topographic integration improved accuracy: DEM (1,986 m^2, -0.8%), slope (2,181 m^2, 9%), and curvature (1,907 m^2, -5%). These results highlight the importance of terrain features in accurately detecting snow patch characteristics such as concave topography and shaded slopes.

Keywords: High-resolution satellite, Alpine snow patches, Water resource, Remote sensing, Climate change.

1. Introduction

The Senjagaike snow patch is the only perennial snow patch existing on Mount Hakusan in Ishikawa Prefecture (Ogawa et al, 2024). Snow patches are key water sources in alpine areas and shape nearby ecosystems (Goto et al, 2017). Therefore, continuously monitoring the snow patch's area is extremely important for assessing the impacts of climate change and establishing future water resource utilization plans and ecosystem conservation policies (Yamaguchi et al, 1998; Suzuki et al, 2018).

However, the Senjagaike snow patch is located near the high-altitude summit, requiring lengthy climbs and coping with environmental stress for on-site observation. Consequently, conducting frequent field surveys is practically difficult, and the low observation frequency may affect the continuity and accuracy of the data.

This study investigates methods to efficiently and continuously monitor changes in the area and shape of the Senjagaike snow patch by utilization high-resolution, high-frequency satellite data to overcome these challenges. This is expected to enable more frequent and wide-area snowfield monitoring in the future while reducing the burden on personnel.

2. Materials and Methods

2.1. Satellite and field surveying method

This study utilizes optical satellite imagery provided by Planet Labs as high-resolution, high-frequency satellite data. Planet Lab's satellites offer high spatial resolution of approximately 3.7 meters and capture images daily, making them well-suited for detailed monitoring of changes in snow patch shape and area. 4 bands are available: blue, green, red, and near-infrared.

Meanwhile, field surveys were also conducted to verify the detection accuracy of satellite data. These surveys were carried out in two phases, in August and October, to assess the condition of the snow patch during period. During the surveys, aerial photographs were acquired using a UAV, collecting approximately 50 to 100 high-resolution images per flight. These images were analyzed using the image processing software Metashape to create orthoimages. Furthermore, based on the created orthoimages, the snow patch contours were traced visually, and the precise area was measured.

2.2. Image analysis

A multidimensional dataset was constructed using the original 4 band images from 25satellite scenes (2016-2024). Additionally, three types of multidimensional datasets were constructed by combining the original images with three types of terrain information: DEM, slope angle, and curvature. Training data for images classification was extracted from the 2024 images, targeting three classes: snow patch, barren land and vegetation. Image classification was performed using the Support Vector Machine (SVM) method. For accuracy evaluation, actual measurements obtained from a field survey conducted on August 9, 2024, were used as the ground truth. The snow patch areas obtained through image classification were compared with these measurements for quantitative assessment.

2.3. Observation of snow patch area

Snow patches reach their smallest extent in October, then grow again with subsequent snowfall. Therefore, we focused on the snow patch area in October from 2016 to 2024 and extracted the snow patch area using the classification method with the highest accuracy. We also analyzed the relationship between the extracted snow patch area for each October and the annual average temperature in Kanazawa City.

3. Results and Discussion

Fig.1 shows the image classification results for snow patches on August 9 2024. The background is a drone

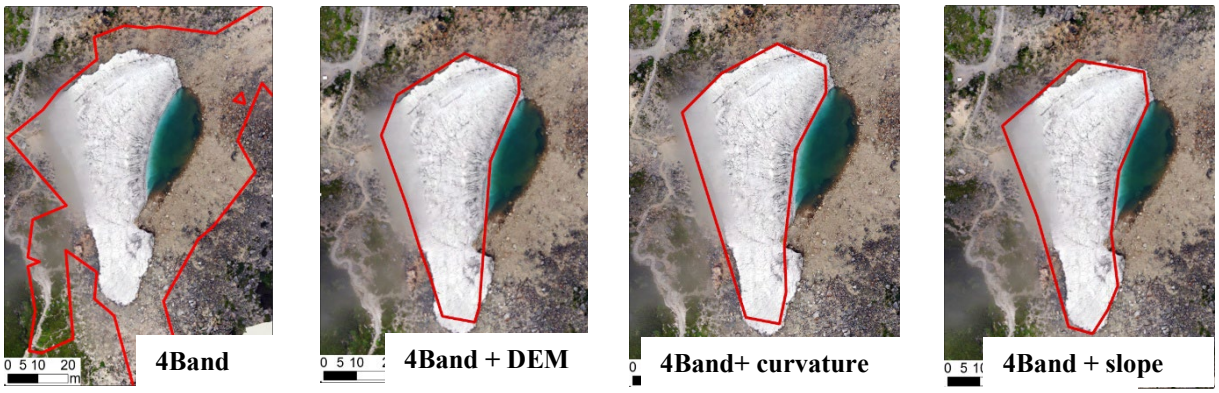

Fig.1 Comparison with drone imagery (August 9,2024)

image of the snow patch, with red lines indicating the shapes of snow patches extracted through image classification. Analysis using only 4 band data resulted in misclassification of barren land and vegetation as snow patch. However, analysis incorporating terrain data enable accurate extraction of the snow patch shapes.

Fig.2 shows the relative error between the calculated values and the true values for each image classification. Analysis using only the 4 bands data resulted in a very large relative error of 235% compared to the true values. However, incorporating terrain data into the image classification improved the relative error to less than 9%.

Fig.3 shows a graph comparing snow patch area calculated using conventional methods from collected October snow patch image data between 2016 and 2024 with Kanazawa City's average temperature. During this period, a trend was observed where snow patch area was large when average temperature was low and smaller when average temperature was high.

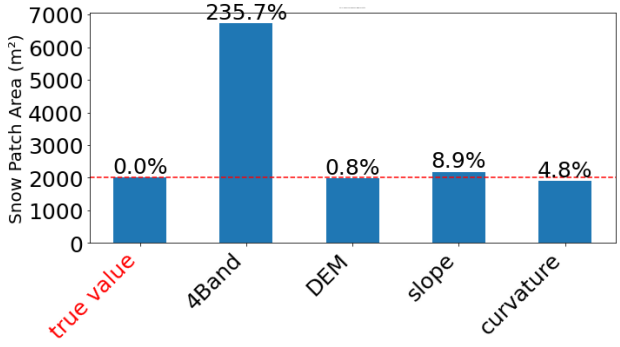

Fig.2 Snow patch area (August, 9, 2024)

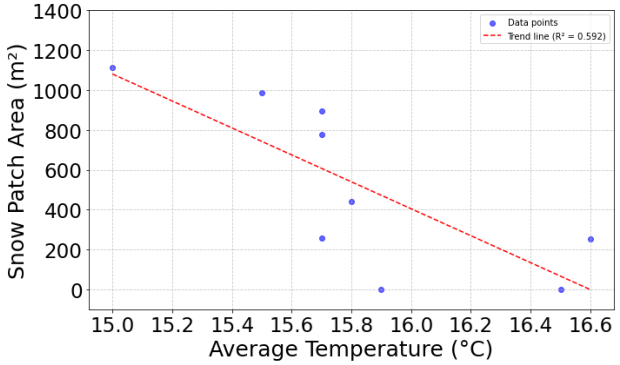

Fig.3 Relationship between temperature and snow patch area (2016-2024)

4. Conclusions

By utilizing Planet Scope's high-frequency, high-resolution satellite data, it has become possible to accurately determine the area of the Senjagaike snow patch. Integrating terrain data with the original images significantly improved image classification accuracy. Using this method to calculate snow patch area for October from 2016 to 2024 revealed a trend of gradual area reduction over this period. Thus, high-precision automated measurement enables detailed analysis of snow patch area fluctuations.

Going forward, we aim to utilize this methodology to conduct detailed and comprehensive analyses of long-term fluctuations in snow patches across alpine regions. By also investigating additional factors such as seasonal inflow volumes to dams located in downstream catchment areas, we seek to clarify and better understand the broader impact of environmental changes occurring in high-altitude zones on various aspects of human life and infrastructure.

Acknowledgements

This research was financially supported by the Japan Society for the Promotion of Science (JSPS) KAKENHI Grant Number 22H02461, the Japan Geographic Data Center, and the River Fund of the River Foundation, Japan.

References

Ogawa, H., Fujihara, Y., 2024. Long-term Variation Analysis of the Senjagaike Perennial Snow Patch on Mt. Hakusan. Journal of Japanese Society of Hydrology and Water Resources, Vol. 37, No. 2, pp. 125 – 141. https://doi.org/10.3178/jjshwr.37.1818

Goto, H., Kajikawa, M., Takahashi, Y., Takahashi, K., Yoshida, I., & Akita Yuki-no-Kai Sekkei Kansoku Group., 2017. Long-term Variations in Snowfield Size on the Northeastern Slope of Mount Chokai, Journal of the Japan Society of Snow and Ice, Vol. 79, No. 1, pp. 105 – 116. https://doi.org/10.5331/seppyo.79.1_105

Yamaguchi, S., Shiraiwa, T., Naruse, R., 1998. Recent variations in mass balance of the Hisago snow patch on the Daisetsu Mountains. Journal of the Japanese Society of Snow and Ice, Vol. 60, No. 4, pp. 279 – 287. https://doi.org/10.5331/seppyo.60.279

Suzuki, K., 2018. Recent Changes in Climate and Water Circulation in Kamikochi. Journal of the Japanese Society of Snow and Ice, Vol. 80, No.2, pp. 103 -113. https://doi.org/10.5331/seppyo.80.2_103

The Impact of Irrigation on Carbon Storage in Tea Plantations: Insights from the Static Chamber Method

Yan-Ning Huang [1*], Kuo-Wei Liao [2]

[1] Department of Bioenvironmental Systems Engineering, National Taiwan University, Taipei City, Taiwan

[2] Department of Bioenvironmental Systems Engineering, National Taiwan University, Taipei City, Taiwan

* Corresponding author. Email: r13622005@ntu.edu.tw

Abstract

Anthropogenic greenhouse gases (GHGs), particularly carbon dioxide (CO_2), are key drivers of global warming and climate change. In response, scientists have been exploring effective strategies for removing excess CO_2 from the atmosphere, with photosynthesis emerging as a natural and efficient solution. Through photosynthesis, plants absorb atmospheric CO_2, making them important carbon sinks in terrestrial ecosystems.

While extensive research has focused on forests as carbon reservoirs, less attention has been given to agricultural landscapes—particularly perennial crops like tea. Tea plants (*Camellia sinensis*), being woody shrubs with long lifespans and substantial biomass, may play a meaningful role in carbon sequestration.

This study employs the static chamber method, a widely adopted and cost-effective technique, to measure CO_2 fluxes at three sites in Yilan, Taiwan, including a well-irrigated tea garden, a rainfed tea garden, and adjacent barren land. The experiment was employed once per month under fair weather conditions from November 2024 to August 2025. Air samples were collected, stored at low temperatures, and analyzed using Gas Chromatography–Thermal Conductivity Detector (GC-TCD).

Preliminary results indicate that well-irrigated tea plantations exhibited greater CO_2 uptake than rainfed ones. Surprisingly, barren land, which was expected to show a net increase in CO_2 concentration, instead demonstrated a net decrease. This finding suggests that factors beyond the initial expectations may be influencing CO_2 dynamics in these areas. These results highlight the potential for the irrigation renovation project to enhance carbon sequestration alongside its original aim of stabilizing tea yields.

Keywords: *Camellia sinensis*, field chamber measurements, land management practices, greenhouse gas flux, agricultural carbon sequestration

1. Introduction

According to the IPCC Special Report on Climate Change and Land, terrestrial ecosystems are vital carbon sinks in both historically and current estimates of net CO_2 removal (IPCC, 2019). While forests are important carbon reservoirs, agricultural landscapes also contribute to carbon sequestration but remain less studied. Perennial crops such as tea (*Camellia sinensis*) can accumulate substantial carbon, in some cases exceeding secondary forests by up to 1.8 times (Chettri and Ghosh, 2023).

Management practices, particularly irrigation, may further influence carbon fluxes by altering plant growth, soil respiration, and ecosystem productivity. Soil moisture and water availability regulate photosynthesis and CO_2 exchange, with irrigation timing producing contrasting outcomes—spring irrigation may increase emissions, whereas summer irrigation can enhance net uptake (Zeng et al., 2017).

This study compares CO_2 fluxes in well-irrigated and rainfed tea gardens over a 10-month period, providing preliminary insights into irrigation's role in carbon sequestration within tea agroecosystems.

2. Materials and Methods

2.1. Site location

This field study was conducted in Dongshan Township, Yilan County in Taiwan. Two tea gardens, each covering approximately 0.5 ha were selected to represent contrasting management conditions: one well-irrigated and one rainfed. In addition, a patch of barren land adjacent to the rainfed garden was included as a baseline reference. For the tea gardens, three observation chambers were installed on different tea plants at each site, while two chambers were deployed in the barren land.

2.2. Experiment design

Transparent acrylic chambers were used to avoid interference with plant photosynthesis and ensure durability under field conditions. Each chamber consisted of a soil anchor and a detachable lid (approx. 0.5 × 0.5 × 1.2 m), with the anchor partially inserted into the soil and designed with a water-filled trench for airtight sealing (Collier et al., 2014). The lids were equipped with a fan powered by a portable charger for air circulation, a thermometer port, and a sampling port with a three-way valve for gas collection.

Air samples were collected monthly from November 2024 to August 2025 using pre-evacuated glass vials. Samples were stored at low temperature and analyzed within one week for CO_2 concentration using GC-TCD. Temperature and atmospheric pressure were recorded simultaneously to support data conversion.

2.3. Data analysis

CO_2 concentrations obtained from GC-TCD were first calibrated using a standard curve to convert signal areas into parts per million (ppm). These concentrations were then converted into $tCO_2 \cdot ha^{-1}$ using the Ideal Gas Law:

$$C_{tCO_2/ha} = \frac{n \times M}{A} = \frac{\left(\frac{PV}{RT} \times \frac{ppm}{10^6}\right) \times M}{A} \times 10^{-6}$$

where P is atmospheric pressure, Pa; V is the chamber volume, $0.3 m^3$; R is the ideal gas constant, 8.314 $Pa \cdot m^3 \cdot mol^{-1} \cdot K^{-1}$; T is chamber temperature, K; ppm is CO2 concentration; M is the molar mass of CO_2, 44.01 $g \cdot mol^{-1}$; A is the chamber area, $2.5 \cdot 10^{-5}$ ha; 10^{-6} converts grams to tons.

Outlier detection was conducted in two stages using the Modified Z-score method:

$$M_i = \frac{0.6745 \cdot (x_i - \tilde{x})}{MAD}$$

where M_i is the modified Z-score for data point i; 0.6745 is a scaling factor; x_i is the CO_2 concentration for data point i, $tCO_2 \cdot ha^{-1}$; $\tilde{x}$ is the group median, $tCO_2 \cdot ha^{-1}$; MAD is median absolute deviation.

Data points with M_i > 3.5 were excluded. The first stage was applied to replicate chambers at each site and time point within a month (e.g., A1, A2, A3 at t = 0). The second stage re-evaluated the remaining time-series data for each chamber across the month.

After outlier removal, replicate values at each site and time point were averaged to produce site-level concentrations (e.g., mean[A1(0), A2(0), A3(0)] = A(t=0)). These means were plotted against time, and linear regression was applied to estimate the rate of concentration change. Slopes were scaled to monthly values, yielding CO_2 fluxes in $tCO_2 \cdot ha^{-1} \cdot month^{-1}$.

3. Results and Discussion

By calculating the mean slopes from monthly linear regressions, Figure 1 illustrates the seasonal dynamics of CO_2 flux across the three study sites.

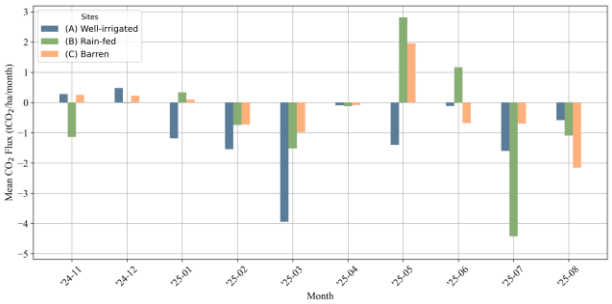

Figure 1. Mean CO_2 flux by month across sites

3.1. Seasonal Variability

Seasonal variability in CO_2 flux was evident across all sites. Net carbon uptake was generally higher in spring, coinciding with leaf flush, but a brief net release occurred in December, the coldest month. During summer, CO_2 fluxes became less predictable. The optimal temperature for tea photosynthesis is approximately 35 °C, yet average chamber temperatures from April onward consistently exceeded this threshold (Figure 2). Field observations confirmed signs of heat stress in tea leaves, which likely contributed to the irregular summer flux patterns.

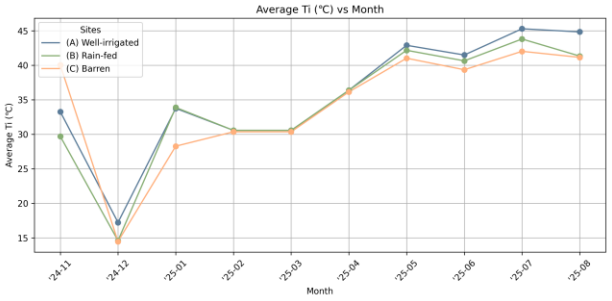

Figure 2. Mean chamber temperature by month

3.2. Site differences

The expected pattern was that the well-irrigated garden would exhibit greater carbon uptake than the rainfed garden. While this trend was generally observed, deviations occurred in certain months. Such variability may stem from site-specific microclimates, differences in plant phenology, or measurement constraints. The static chamber method is particularly sensitive to temporal variability, and perfect synchronization of lid deployment was not always feasible due to manpower limitations. Nevertheless, across the observation period, irrigation still emerged as the dominant driver of enhanced CO_2 uptake.

3.3. Averaged results

Despite monthly fluctuations, site averages revealed a clear pattern: the well-irrigated tea garden had the highest mean CO_2 uptake, followed by the rainfed garden, with barren land lowest (Table 1). Notably, the barren site showed a net negative flux, likely due to photosynthesis by mosses and weeds within the chambers, underscoring the sensitivity of static chamber measurements to small-scale vegetation dynamics.

Table 1. Mean CO_2 flux by month across sites

Date	(A) Well-irrigated Garden	(B) Rainfed Garden	(C) Barren Land
2024-11	0.277	-1.139	0.252
2024-12	0.477	-0.024	0.230
2025-01	-1.184	0.338	0.096
2025-02	-1.544	-0.743	-0.726
2025-03	-3.938	-1.521	-0.977
2025-04	-0.092	-0.121	-0.086
2025-05	-1.402	2.816	1.956
2025-06	-0.113	1.164	-0.683
2025-07	-1.601	-4.422	-0.700
2025-08	-0.582	-1.090	-2.155
Mean	-0.970	-0.474	-0.279

4. Conclusions

This study provides preliminary evidence that irrigation is associated with higher site-averaged CO_2 uptake in tea plantations. Despite pronounced month-to-month variability, 10-month means were greater in the irrigated garden than in the rainfed garden and barren land. These findings indicate that irrigation management can be an effective strategy for integrating climate mitigation into tea agroecosystems.

References

Chettri, V. and Ghosh, C. (2023) 'Tea Gardens, A Potential Carbon-sink for Climate Change Mitigation', *Current Agriculture Research Journal*, 11(3). DOI: 10.12944/CARJ.11.3.01

Collier, S.M., Ruark, M.D., Oates, L.G., Jokela, W.E., and Dell, C.J. (2014) 'Measurement of greenhouse gas flux from agricultural soils using static chambers', *Journal of Visualized Experiments (JoVE)*, 90, e52110. DOI: 10.3791/52110

Intergovernmental Panel on Climate Change (IPCC) (2019) *Climate Change and Land: Special Report of the Intergovernmental Panel on Climate Change*. Chapter 2. Available at: https://www.ipcc.ch/srccl/chapter/chapter-2/

Zeng, Y., Xie, Z., and Liu, S. (2017) 'Seasonal effects of irrigation on land–atmosphere latent heat, sensible heat, and carbon fluxes in semiarid basin', *Earth System Dynamics*, 8, pp. 113–127. DOI: 10.5194/esd-8-113-2017

XGBoost-Based Assessment of Groundwater Levels Influenced by Irrigation and Meteorological Factors

Chen Hui Chih・Ling You Ting・Zhuang Wei Ya・Wang Wei Sheng

Abstract

With increasing climate variability and the growing frequency of extreme weather events, paddy agriculture in Taiwan has become more reliant on groundwater, raising challenges for sustainable water resource management. Traditional numerical models often suffer from high uncertainty due to limited pumping data. To address this, electricity consumption from pumping wells is regarded as a critical feature for groundwater extraction in this study. Focusing on the Xiutan and Jiulong wells within an alluvial fan, this study applied the XGBoost algorithm to predict monthly groundwater levels from 2007 to 2023. Model features include the historical monthly groundwater levels, electricity consumption of pumping wells within a 2.5 km radius, and meteorological variables (temperature, wind speed, total rainfall, number of rainy days, and maximum daily rainfall). TimeSeriesSplit was used for time series cross-validation, and BayesSearchCV was applied for hyperparameter tuning. The model achieved R2 values of 0.78 and 0.51, and RMSE values of 1.28 and 0.43 m for Xiutan and Jiulong wells, respectively. SHAP analysis identified crop-season electricity use and lagged groundwater levels as key predictors. Irrigational pumping for rice cultivation had a strong negative impact on groundwater levels. Compared to traditional groundwater numerical models, which often exhibit high uncertainty in pumping rates calibration, this study demonstrates that electricity consumption provides a more reliable model input. This model enables rapid prediction of groundwater level responses under varying meteorological conditions and pumping scenarios. This study demonstrates the potential of machine learning approaches to support climate-resilient agriculture and to inform adaptation strategies for sustainable groundwater use.

Analysis of salinity dynamics in the estuary of the Hong River, Northern Vietnam

Keishi Inoue [1*], Masaomi Kimura [2], Yutaka Matsuno [2], Natsuki Yoshikawa [3]

[1] Graduate School of Agriculture, Kindai University, Nara, (Nara Prefecture) 6310052, Japan

[2] Faculty of Agriculture, Kindai University, Nara, (Nara Prefecture) 6310052, Japan

[3]Faculty of Agriculture, Niigata University, Niigata, (Niigata Prefecture) 9502102, Japan

* Keishi Inoue. Email: 2433680005j@nara.kindai.ac.jp

Abstract

The Red River Delta is one of Vietnam's two major rice-producing regions, with a cultivated area of about 570,000 ha. However, the coastal areas are highly vulnerable to natural disasters, and saltwater intrusion is particularly severe. During irrigation, sluice gates are operated to draw water from the river. However, because salinity must be measured each time, it is difficult to manage gate operations and establish irrigation plans in advance.

This study aims to investigate the salinity dynamics in the estuarine area of the Hong River, examine their temporal and spatial variations, and develop a hydrodynamic model. Field surveys revealed that electrical conductivity near the river mouth reached about 40,000 μS/cm. While conductivity decreased further upstream, salinity levels remained too high for agricultural use at most locations. In addition, strong and partially mixed saltwater intrusions were predominantly observed.

The numerical model was based on the governing equations of mass conservation, momentum conservation, and salinity transport. Water depth and discharge in each vertical layer were calculated using the Flux Difference Splitting (FDS) method. Salinity mixing was computed for each layer after solving the flow field using the FDS method.

Simulation results showed that strong mixing conditions could be reproduced with a freshwater discharge of 400-600 m³/s and an additional 25 cm in tidal level. However, other mixing patterns could not be replicated, indicating the need for further parameter adjustments to represent the full range of mixing conditions accurately.

Keywords: "irrigation", "saltwater", "intrusion", "simulation",

1. Introduction

The Red River, with a total length of about 1,200 km, is a major river flowing through northern Vietnam. At its mouth, the Red River Delta has developed as one of the country's two largest rice-producing regions, covering a cultivated area of about 570,000 ha. However, the coastal areas are particularly vulnerable to natural disasters, and saltwater intrusion is a serious issue. Salinity has been observed as far as 20 km upstream from the river mouth, with this tendency becoming more pronounced during the dry season when river discharge decreases. During irrigation, sluice gates are operated to draw water from the river, but because the salinity concentration must be measured each time to manage gate operations, it is difficult to establish irrigation plans in advance. Therefore, this study aims to investigate the salinity dynamics in the Red River estuary, clarify their variability characteristics, and develop a hydrodynamic model.

2. Target Area

The study area covers a stretch of about 30 km from the mouth of the Hong River in northern Vietnam (Figure 1). Within this section, the river width ranges from about 1,000 m near the estuary to around 250 m at its narrowest point. Along the main channel, several sluice gates have been installed for irrigation water intake. These gates are managed by closing them when the river salinity is high and opening them when the salinity is low.

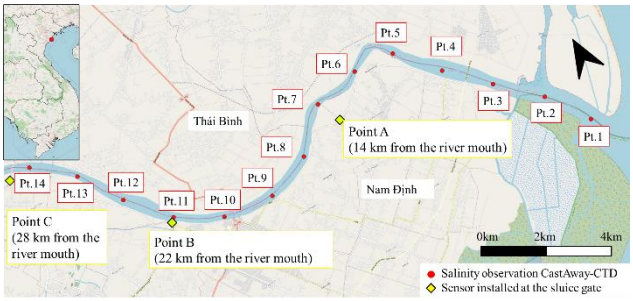

Figure 1.Target Area (Hong River mouth)

3. Materials and Methods

In December 2023 and February 2025, vertical salinity profiles and river cross-sectional surveys were conducted within the study area. For salinity measurements, a portable, deployable CTD sensor (measuring conductivity, temperature, and depth; CastAway-CTD) was used. The cross-sectional surveys were carried out by mounting a sonar device (GARMIN STRIKER VIVID 4CV) on a boat and traversing the river. In addition, CTD sensors (HYDROS 21) and data loggers (ZL6) were installed at three sluice gates (points A, B, and C in Fig. 1) to conduct continuous monitoring beginning in October 2024.

4. Survey Results

An example of the vertical distribution of electrical conductivity observed in December 2023 is shown in Figure 2. Electrical conductivity was as high as about 40,000 μS/cm near the river mouth and decreased with distance upstream; however, in most locations it remained too high to be suitable for agricultural use. Furthermore, strong and partially mixed salinity intrusions were predominantly observed, suggesting that the intrusion pattern varied depending on tidal strength and river discharge. A comparison between the electrical conductivity measured by sensors installed at sluice gates and that obtained from boat-based surveys in the Hong River showed no significant differences, indicating that

salinity did not decrease during the passage from the main river to the sluice gates. In addition, while saltwater intruded gradually upstream, it was observed to retreat rapidly when displaced by freshwater from upstream. These results indicate that salinity intrusion in the Hong River is not uniform but exhibits different patterns depending on tidal and discharge fluctuations. Based on this, we attempted to develop a hydrodynamic model capable of reproducing the vertical distributions under various intrusion conditions.

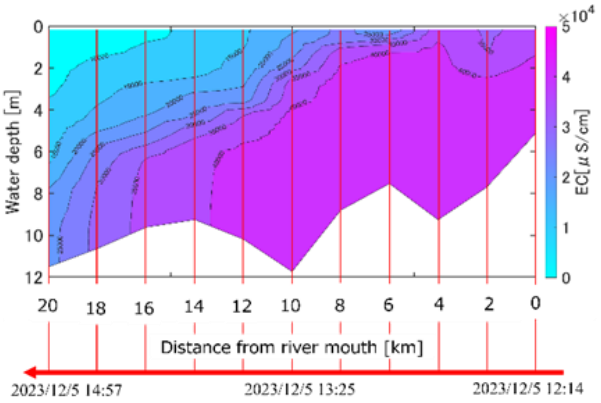

Figure 2. Estimated longitudinal distribution of electrical conductivity in the Hong River

5. Numerical Calculation

Governing equations for the numerical calculations consisted of the conservation of mass(Eq.1), momentum(Eq.2), and salinity(Eq.3).

(Governing equations)

Mass conservation

$$\frac{\partial A_i}{\partial t} + \frac{\partial Q_i}{\partial x} = \sum_{m=1}^{N}\{Wex(m,i) - Wex(i,m)\} \quad (1)$$

Momentum conservation

$$\frac{\partial Q_i}{\partial t} + \frac{\partial\left(Q_i^2/A_i\right)}{\partial x} + gA_i\frac{\partial}{\partial x}\left[\frac{1}{\rho_i}\{\sum_{l=1}^{i-1}(\rho_l h_l) + \sum_{m=i}^{N}(\rho_i h_m)\}\right] + gA_i S_{fi} = \sum_{m=1}^{N}\left\{\frac{\rho_m}{\rho_i}Wex(m,i)V_m - Wex(i,m)V_i\right\} \quad (2)$$

Salinity transport equation

$$\frac{\partial(A_i\rho_i)}{\partial t} + \frac{\partial(Q_i\rho_i)}{\partial x} = \sum_{m=1}^{N}\{\rho_m Wex(m,i) - \rho_i Wex(i,m)\} \quad (3)$$

The variables are defined as follows: i, computational layer; g, gravitational acceleration[m/s^2]; N, number of layers; A_i , cross-sectional area of the i-th layer[m^2]; Q_i, average discharge of the i-th layer [m^3/s]; h_i, thickness of the i-th layer[m]; V_i velocity of the i-th layer[m/s]; n, Manning's roughness coefficient; R_i, hydraulic radius of the i-th layer[m]; ρ_i, density of the i-th layer[kg/m^3]; S_{fi},friction slope of the i-th layer

Based on the conservation equations of volume and momentum, the water depth and discharge of each layer were calculated using the Flux Difference Splitting (FDS) method. Salinity mixing was then computed for each layer after solving the water flow with the FDS method. To maintain uniform density distribution, the Equivalent Density Method was applied to correct the density and water depth of each layer. As boundary conditions, freshwater discharge was prescribed at the upstream end, while tidal water level was imposed at the downstream end.

6. Simulation Results

The simulation was conducted for the one-week period from December 1 to December 8, 2023, and was validated by comparing the results with the general patterns of vertical salinity profiles observed in December 2023. Salinity intrusion is strongly influenced by freshwater discharge from upstream and tidal fluctuations at the estuary. However, due to limited availability of accurate data on freshwater discharge, tidal variation, and riverbed elevation, these three factors were treated as adjustable parameters in the simulation. The results showed that an increase in freshwater discharge flushed out surface-layer salinity, whereas bottom-layer salinity remained largely unchanged. Furthermore, the flow conditions that reproduced mixing states similar to the observed vertical profiles corresponded to discharges of about 400-600 m^3/s (Fig. 3), suggesting that the actual discharge of the Hong River during the study period likely fell within this range. Increasing tidal amplitude facilitated the flushing of bottom-layer salinity, and the model achieved higher reproducibility when the observed salinity structure approached a well-mixed state. This indicates that strong mixing conditions are more sensitive to tidal variations. In contrast, little effect was observed under other mixing regimes, implying that further refinement of parameters is necessary to better represent the diverse mixing states.

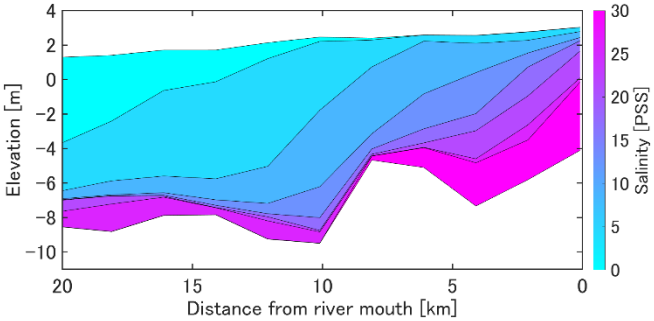

Figure 3. Simulation result for a discharge of 600 m^3/s

Acknowledgements

This study was supported by JST SICORP (JPMJSC20E1) and JSPS KAKENHI (24K01870). The authors would like to express their sincere gratitude to Ms. Lan Thanh Ha and Mr. Hung Dinh of the Institute of Water Resources Planning, Vietnam, for their considerable support in conducting the surveys.

References

Nguyen Yen Thi Bich, Kamoshita Akihiko, Dinh Van Thi Hai, Matsuda Hirotaka, Kurokura Hisashi. (2017) : Salinity intrusion and rice production in Red River Delta under changing climate conditions, Paddy and Water Environment, 15(1), 37-48.

KWON Sungill, KUBO Naritaka. (2005) : Study on Multilayer Model Development for Density Current Simulation in a Tidal River, Transactions of the Japanese Society of Irrigation, Drainage and Reclamation Engineering, 238, 69-77.

Effects of automated weed control robots on methane emissions from paddy fields in mountain areas of Northeast Japan

Chihiro Kato [1*], Tetsuya Nakamura[2], Taiichiro Ookawa [3]

[1] Faculty of Agriculture and Life Science, Hirosaki University, Hirosaki, (Aomori) 0368561, Japan

[2] NEWGREEN Inc., Koganei, (Tokyo) 1840012, Japan

3Institute of Agriculture, Tokyo University of Agriculture and Technology, Fuchu, (Tokyo) 1838509, Japan

* Corresponding author. Email: chihirok@hirosaki-u.ac.jp

Abstract

The automatic weed suppression robot (AigamoRobo) stirs the soil in flooded paddy fields using screw-driven water flow, suspending water to suppress weeds. Stirring the soil is expected to increase oxygen supply, potentially contributing to methane emission suppression. This study aimed to investigate the impact of AigamoRobo use on methane emissions in paddy fields located in the relatively cool mountainous area of Akita City. Within the experimental field, an Aigamo plot (operating the Aigamo -Robo for approximately one month starting immediately after rice planting) and a control plot (without Aigamo-Robo operation) were established. For two months after rice planting, soil samples were collected from the paddy soil surface and at depths of 3 mm and 50 mm once every two weeks. Microbial community analysis was performed using 16S rRNA v4 region amplicon sequencing. Methane flux emitted from the paddy fields was also measured on the same days as soil sampling. Soil methanogens increased from June to July regardless of plot or soil depth, but the increase rate was suppressed in the Aigamo plot. Conversely, methane flux tended to be low on all four measurement dates, regardless of robot use, with no significant differences observed between plots. This is presumed to be due to soil structure and climatic factors such as the soil characteristics and temperature conditions at this study site.

Keywords: Metahne, Paddy field, Automatic weed control robot, Mitigation.

1. Introduction

In Japan, methane (CH_4) emissions (FY2022) reached 29.9 million tons in CO_2 equivalent, with rice cultivation accounting for 44% of this total (Ministry of the Environment, 2023). Extending the mid-season drying period has been certified as a J-Credit method for reducing CH_4 emissions from paddy fields, but there is a need to establish CH_4 reduction technologies that can be applied across all areas, including those unsuitable for mid-season drying, and to achieve further reductions in CH_4 emissions. Therefore, this study focused on the use of the automatic weeding robot "AigamoRobo" (NEWGREEN Inc.). AigamoRobo suppresses weeds in paddy fields by stirring the soil with a screw-driven water flow, thereby suspending the water. It also suppresses weeds by burying seeds on the surface. It has been confirmed in several paddy fields in Japan that oxygen supply through soil stirring creates an oxidized state in the surface soil, leading to reduced CH_4 emissions. This study aimed to examine the impact of AigamoRobo use on CH_4 emissions in paddy fields, specifically targeting paddy fields in relatively cool regions. Differences in microbial communities involved in CH_4 production and CH_4 gas fluxes were investigated with and without AigamoRobo use.

2. Materials and Methods

2.1. Study site

This study targeted two adjacent organically cultivated paddy fields (hereafter referred to "Field A" and "Field B" respectively) in Uyashinai settlement, Akita City, Tohoku region, Japan. The study site is located approximately 25 km east of central Akita City, surrounded by mountains. The rice variety used was Kairyoshinko (sake rice), with transplanting conducted on May 30, 2024. On June 1, 2024, two sections measuring approximately 80 cm × 200 cm were established in each field using corrugated sheets. Subsequently, one AigamoRobo was deployed in each field and began operation. The AigamoRobo operated only outside the corrugated sheets (Aigamo plot) and did not enter the area inside the sheets (Control plot). In Field A, the first-generation AigamoRobo (IGAM1) was used, while the second-generation (IGAM2) was used in Field B. Both employ the same weed suppression mechanism but differ in their propulsion systems.

2.2. Soil Sampling and Soil Microbial Analysis

For approximately two months after rice planting, topsoil samples were collected from both the Aigamo and control plots using a 100-ml sampler (approximately 50 mm in height) at two-week intervals (June 15, June29, July 13, July 27). Using a microspatula, soil samples were collected from approximately 3 mm and 50 mm below the soil surface. These samples were brought back to the laboratory and stored frozen. Subsequently, amplicon sequencing analysis of the 16S rRNA v4 region was performed (Bioengineering Lab. Co., Ltd).

Separately, in September 2024, disturbed soil samples were collected at depth of 0-50 mm from the soil surface at the Aigamo plot in each field. Soil particle density (pycnometer method) and soil texture (pipette method) were measured. Furthermore, total carbon and total nitrogen ratios were measured using an NC analyzer (Vario EL Cube; Elementar).

2.3. Measurement of methane gas flux emitted from paddy fields

On the same day as soil sampling, CH_4 gas flux released from the paddy fields was measured using the closed chamber method for both the Aigamo and the control plots. Measurements were taken at two replicates per plot, meaning four points per field were measured for both Aigamo and control plots. For control plots, measurement points were selected several tens of centimeters away from each corrugated sheet. An acrylic

chamber with a base area of 0.1 m² (approximately 0.32 m square) and a height of 1 m was used. It was placed on the field surface to accommodate two moderately growing rice plants. The chamber was connected to a methane gas analyzer (LI-7800; LI-COR) to measure changes in CH_4 gas concentration within the chamber, thereby obtaining the CH_4 flux.

3. Results and Discussion

3.1. Soil physicochemical properties

Table 1 shows the soil particle density, soil texture, and total carbon and nitrogen for each field. The soils in both fields were classified as sandy clay loam (SCL). Furthermore, the C/N ratios for fields A and B were 12.1 and 13.3, respectively.

Table 1. Soil physicochemical properties

	Particle density (Mg m^{-3})	Soil texture	Total C (%)	Total N (%)
A	2.58±0.010	SCL	3.46±0.076	0.286±0.014
B	2.60±0.012	SCL	4.08±0.343	0.306±0.018

3.2. Microorganisms involved in methane production and oxidation

Analysis of 16S rRNA v4 region amplicon sequencing results from soil samples identified the following methanogen: *Methanobacterium*, *Methanocella, Candidatus, Methanoregula*, *Methanosaeta*, and *Methanosarcina*. For each sampling date, the total number of reads for all methanogen was calculated for soil samples taken at depths of 3 mm and 50 mm in each test plot. Using the values of June 15th (two weeks after the start of the AigamoRobo operation) as the baseline, the increase rate of methanogen was calculated for June 29 (two weeks later) and July 27 (six weeks later). Results for both fields are shown in Tables 2. At both fields and both depths, the Aigamo plots showed a tendency toward lower growth rates compared to the control plots. Significant differences at the 5% or 1% level were confirmed by chi-square tests except July 27 in field B. For methanotrophic bacteria, the low read counts did not reveal any clear trends (data not shown).

Table 2. Trend in methanogen read counts in amplicon sequence analysis (ratio relative to June 15th values) Chi-square test conducted for the Aigamo and control plot

Field A	Depth from the soil surface 3mm			50mm		
	Agm	Ctr		Agm	Ctr	
29th June	0.68	1.06	*	1.03	1.63	**
27th July	1.28	2.34	**	0.91	1.30	*

Field B	Depth from the soil surface 3mm			50mm		
	Agm	Ctr		Agm	Ctr-	
29th June	1.19	3.39	**	1.20	1.51	*
27th July	1.30	1.51		2.45	2.23	

3.3. Methane gas flux emitted from the paddy fields

Figure 1 shows a comparison of CH_4 gas flux trends between the Aigamo plots and control plots at each field. Reflecting the gradual progression of soil reduction in paddy fields, fluxes tended to increase from June to July. Although Tukey-Kramer tests were performed to assess significant differences, no significant differences were observed between the Aigamo plots and control plots at either field. The observed CH_4 fluxes tended to be smaller compared to other regions (e.g., Yagi and Minami, 1990). It is generally known that in paddy soils, when the infiltration rate is high, the redox potential is less likely to decrease, resulting in smaller CH_4 fluxes (Yagi and Minami, 1990). The study site has sandy soil, which may be less conducive to CH_4 generation. Furthermore, the area utilizes water drawn from mountain streams, resulting in lower water temperatures that may suppress the activity of methanogen. One possible reason for the lack of significant difference in methane flux despite the observed trend toward increased methanogen with the presence of the AigamoRobo is this low methane flux.

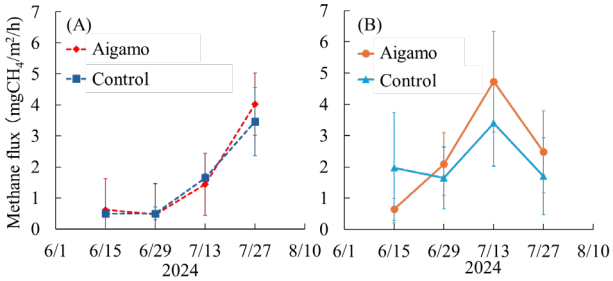

Figure 1. Trends in methane gas flux released from paddy fields in each field

4. Conclusions

The operation of the automatic weed suppression robot for approximately one month after rice planting prevented an increase in methanogen during the two months following planting. However, at this study site, the observed CH_4 fluxes tended to be smaller compared to other regions and no significant difference in CH_4 gas emissions was observed between plots with and without robot operation.

Acknowledgements

This research was conducted with funding from the Japan Science and Technology Agency (JST) (Grant Number JPMJPF2104). We gratefully acknowledge the cooperation of ARAMASA Co., Ltd. in conducting this research. We also express our deep gratitude to Professor Emeritus Shuichi Sugiyama of Hirosaki University for his valuable advice. Furthermore, we sincerely thank graduates of the Faculty of Agriculture and Life Science at Hirosaki University who assisted with the field observations.

References

Yagi, K. and K. Minami, 1990. Effect of organic matter application on methane emission from some Japanese paddy fields. Soil Sci. Plant. Nutr., 36 (4), 599-610

A Critical Review of Flood Risk Assessment Methodologies: Applicability and Framework for Agricultural Landscape Under Climate Change

Adisa Hammed Akinsoji*[1*], Kyung Sook Choi [2]

[1] Department of Agricultural Civil Engineering, Kyungpook National University, Daegu 41566, Korea.

* Corresponding author. Email: adisaakinsoji@gmail.com

Abstract

Agricultural systems are exposed to growing flood hazards, resulting in more than $123 billion of average annual losses globally, accounting for 5% of agricultural GDP. However, frameworks of flood risk assessment (FRA) remain largely geared to the urban environment, without addressing the agricultural-specific vulnerabilities of the landscape. This systematic review synthesizes the existing FRA frameworks to derive a comprehensive FRA framework applicable to agricultural landscapes. PRISMA approaches were utilized, and 47 peer-reviewed articles from 2020–2024 were acquired from the Scopus database and thoroughly reviewed to obtain FRA methodologies and applicable elements to be applied within agricultural contexts. The results indicate that Asia accounted for 70.2% of the studies, with China alone contributing 38.3%, while Africa's contribution was significantly lower at only 4.3%. In studies, hazard (89%), vulnerability (85%), and exposure (78%) were the most prevalent FRA components, respectively. Rainfall was the most common hazard indicator (31.2%), population density dominated for vulnerability (29.9%), and built infrastructure was the most common exposure component. Hybrid weighting approaches, which integrate expert opinion and data-driven techniques, were prevalent in 42% of the studies. According to these findings, the proposed agrarian-based FRA structure features crop-specific vulnerability matrices, precision agronomy technologies, and hydrodynamic models to accommodate data-scarce contexts. One of the key innovations includes agricultural resilience indicators, compound risk appraisal functionality, and policy integration output. The proposed structure fills relevant gaps in agrarian flood protection by virtue of standardized indicators for crops, greenhouse environments, and agrarian infrastructure while addressing uncertainty quantification as well as validation protocols. The results show practical, actionable pathways for strengthening agrarian resilience and climatic adaptation in the face of expanding flood hazards.

Keywords: Flood risk assessment, Agriculture, Urban, weight methods.

1. Introduction

Flooding is among the most frequent and destructive natural disasters worldwide, exacerbated by climate change, rapid urbanization, and land-use alterations (Darabi et al., 2020). The agricultural sector—responsible for feeding a growing global population—faces mounting exposure to extreme hydrological events that undermine food security and economic stability. Recent reports estimate annual agricultural flood losses exceeding USD 123 billion, representing 5% of global agricultural GDP (FAO, 2023).

Although urban FRA has evolved through advanced hydrodynamic modeling and geospatial decision-support systems, similar rigor is lacking for agricultural contexts. Agricultural landscapes differ markedly in spatial heterogeneity, crop sensitivity, drainage patterns, and resilience capacity. Most agricultural flood studies emphasize post-disaster damage estimation (Ahmad and Afzal, 2024) rather than proactive risk quantification and mitigation planning. Therefore, a tailored FRA framework is essential to evaluate hazard–exposure–vulnerability interactions specific to farmlands, greenhouses, and rural infrastructure.

The objective of this study is to critically review existing FRA methodologies, identify transferable frameworks for agricultural application, and propose a structured, data-driven FRA model that enhances resilience-based decision-making for agricultural systems..

2. Materials and Methods

A systematic review was conducted using the PRISMA framework to ensure transparency and reproducibility. The Scopus database was queried for publications between 2020 and 2024 using compound Boolean keywords related to “flood risk assessment,” “agriculture,” “vulnerability,” and “exposure.” After screening 248 initial records, 47 peer-reviewed articles met the inclusion criteria based on scope relevance, methodological clarity, and geographical representativeness.

Metadata analysis was performed to evaluate publication trends by year, continent, and thematic focus. Keyword clustering using VOSviewer identified emerging themes such as climate change adaptation and compound flood hazards. Indicators were categorized under hazard, vulnerability, and exposure components. Statistical aggregation quantified indicator frequencies, while methodological synthesis summarized data sources, weighting approaches, and modeling techniques.

3. Results and Discussion

3.1 Trends in FRA Studies

A sharp increase in FRA publications was observed between 2021 and 2024, with Asia contributing 70.2% of the studies—particularly China (38.3%)—while Africa accounted for only 4.3%, reflecting a research imbalance despite escalating flood occurrences.

3.2 FRA Components and Indicators

Across studies, hazard indicators were dominated by rainfall intensity and flood depth (Zheng et al., 2024), vulnerability by population density and GDP (Boultif et al., 2024), and exposure by built infrastructure and land use (Gu and Liu, 2024). The heterogeneity in indicator

selection reflects contextual data availability and research objectives.

3.3 Weighting Approaches

Subjective methods such as AHP and FAHP rely on expert judgment but are limited by inconsistency, while objective approaches like Entropy and PCA are data-driven but less adaptive to local contexts (Lu et al., 2024). Consequently, hybrid schemes—combining subjective and objective weighting (e.g., CRITIC-Entropy, GeoDetector-Dematel)—have emerged as the most robust, capturing both empirical evidence and expert insight.

3.4 Hydrodynamic Modeling and Validation

Integration of hydrological (HEC-HMS, SWMM) and hydraulic (MIKE 21, FLO-2D) models enhances hazard quantification by simulating runoff, inundation extent, and return periods under various climatic scenarios (M. Jibhakate et al., 2023). Model evaluations reported high reliability ($R^2 > 0.9$, NSE > 0.7). However, limited field data and high computational costs constrain application in developing regions.

3.5 Agricultural FRA Framework

Building on synthesized findings, a novel agriculture-oriented FRA framework is proposed. It incorporates crop-specific hazard thresholds, soil and drainage conditions, and farm-level exposure indicators such as greenhouse density and crop type. Vulnerability is conceptualized through sensitivity and adaptive capacity parameters aligned with IPCC AR6 definitions. The framework supports hybrid weighting, GIS-based integration, and scenario modeling for multi-hazard (flood–drought) interactions.

3.6 Data and Technological Integration

Emerging technologies—remote sensing, IoT sensors, and machine learning—offer pathways to overcome data scarcity and scale inconsistencies. Incorporating these into FRA enhances spatial precision and enables predictive analytics for early warning systems (Akinsoji et al., 2025).

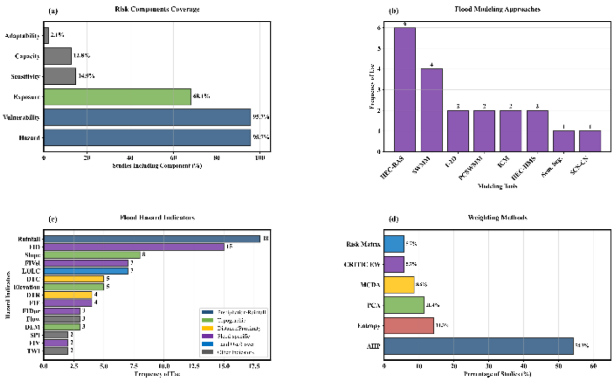

Fig 1: Flood Risk Component Analysis

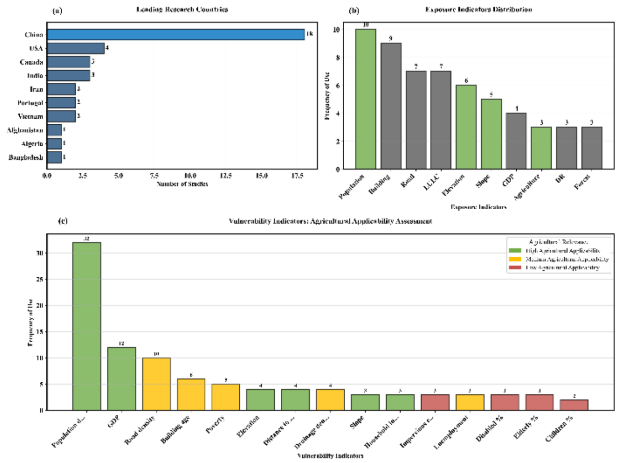

Fig. 2. Global Research Landscape of Flood Risk Assessment

4. Conclusions

This study underscores the urgent need for an agricultural-specific flood risk assessment framework that captures the unique vulnerabilities of agrarian systems. The review reveals significant regional and methodological disparities, with a predominant urban focus in existing FRA research. By introducing a structured, hybrid, and hydrodynamically informed FRA model, this work bridges the gap between conceptual understanding and practical application. The proposed framework provides a replicable blueprint for evaluating flood risks in agricultural settings, supporting evidence-based policy, precision agronomy, and resilient food systems. Future work should emphasize validation procedures, resilience quantification, and policy integration to enhance adaptive flood governance..

Acknowledgements

This work was supported by the Korea Institute of Planning and Evaluation for Technology in Food, Agriculture and Forestry (IPET) through the Intelligent Agricultural Infra Management for Climate Change Development Program, funded by the Ministry of Agriculture, Food and Rural Affairs (MAFRA) (RS-2025-02303335).

References

Ahmad, D. and Afzal, M. 2024. Climate change flood risks and post-flood agricultural and non-agricultural economic losses in flood-prone Bait households Muzaffargarh district of Punjab, Pakistan. Environment, Development and Sustainability. 27(8), pp.18275−18311.

Akinsoji, A.H., Adelodun, B., Adeyi, Q., Salau, R.A., Odey, G. and Choi, K.S. 2025. Prediction of spatial-temporal flood water level in agricultural fields using advanced machine learning and deep learning approaches. Natural Hazards., pp.1–26.

Darabi, H., Haghighi, A.T., Mohamadi, M.A., Rashidpour, M., Ziegler, A.D., Hekmatzadeh, A.A. and Kløve, B. 2020. Urban flood risk mapping using data-driven geospatial techniques for a flood-prone case area in Iran. Hydrology Research. 51(1), pp.127–142.

M. Jibhakate, S., V. Timbadiya, P. and L. Patel, P. 2023. Multiparameter flood hazard, socioeconomic vulnerability and flood risk assessment for densely populated coastal city. Journal of Environmental Management. 344.

Field Analysis of Infiltration Properties Before and After Restoration of Terraced Paddy Fields in Northern Taiwan

Qun-Zhan Huang [1*], Shao-Yiu Hsu [1]

[1] Department of Bioenvironmental Systems Engineering, National Taiwan University, Taipei, 106319, Taiwan

* Corresponding author. Email: d09622003@ntu.edu.tw

Abstract

Terracing is an important agricultural practice in regions with limited flat land. Beyond their practical function in cultivation, terraced paddy fields constitute a unique cultural landscape shaped by the historical development and human–environment interactions of local societies, and they carry substantial cultural and historical value. Moreover, irrigation in terraced fields provides additional ecosystem services such as water storage, maintenance of soil conditions, and year-round habitats for edible aquatic organisms. Consequently, the restoration of terraced fields—along with measures such as habitat creation and the revitalization of rural economies—has become a key policy focus for many government agencies in Taiwan. A critical indicator for evaluating restoration outcomes is the infiltration rate, which determines the field's capacity to store water. In this study, we measured the steady infiltration rate before and after the restoration of terraced paddy fields in Gongliao District, New Taipei City. The restoration engineering disturbed the original soil structure and resulted in the formation of a muddy surface layer. The surface soil texture at the study site was classified as clay loam, which typically exhibits a saturated hydraulic conductivity ranging from 0.1 to 380 mm/h. The measured vertical infiltration rate was 266.4 ± 28.5 mm/h before restoration, but this value significantly decreased to 0.293 ± 0.0012 mm/h after restoration, falling within the typical range suitable for paddy field conditions. Nevertheless, the underlying causes and long-term effects of these changes remain unclear, emphasizing the need for continued monitoring of infiltration performance.

Keywords: Terraced Paddy Fields, Infiltration.

1. Introduction

In regions lacking sufficient flat land, terraced fields serve as an important agricultural technique as well as a vital ecological habitat. Terraces perform key functions such as soil and water conservation (Chen, 2008) and water purification (Hakamata et al., 1992; Song et al., 2016). Beyond these ecological services, terraces embody distinctive landscapes shaped by historical trajectories of human–environment interactions, carrying significant cultural and historical value.

However, in Taiwan, with the progression of time, rural areas have experienced population outmigration, population aging, and declining agricultural labor, leading to the decline of hillside farming. Consequently, many rice terraces once established to meet food demand have been abandoned. Although rice terraces provide ecological and environmental benefits, their lack of proper management raises concerns such as soil erosion and water quality deterioration. To promote sustainable rural development and revitalize rural communities, the government of Taiwan has implemented policies aimed at improving basic production conditions while preserving rural ecology and culture. Within this context, the restoration of rice terraces—integrating tourism, cultural education, and ecological conservation—has become an important strategy for rural regeneration.

In Taiwan, rice paddies are typically maintained under 5–10 cm of standing water. Water use in paddy fields is consumed through crop evapotranspiration, surface evaporation, bund overflow, and seepage, with seepage accounting for 50–80% of the total water consumption (Sharma, 1989). Seepage is therefore a key factor in determining whether a field is suitable for rice cultivation. Rice farming favors conditions with low seepage rates, which can be classified as Excellent (1–2.5 mm/day), Good (2.5–5.0 mm/day), Marginal (5.0–10.0 mm/day), and Unsuitable (>10.0 mm/day) (Hasegawa et al., 1985).

To evaluate the effectiveness of terrace paddy field restoration, this study measured the steady infiltration rate before and after restoration in terraced paddies in Northern Taiwan.

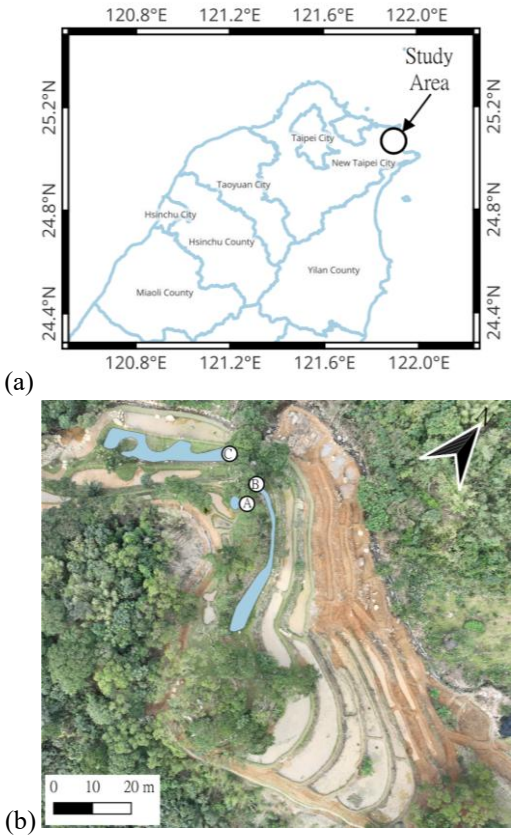

Figure 1. Study area.

2. Materials and Methods

The study area is located at Gongliao District, New

Taipei City (Figure 1a). We selected three plots for the experiment, designated as Fields A, B, and C from the upper to lower slope positions (Figure 1b). Prior to restoration, the steady infiltration capacity was evaluated using a double-ring infiltrometer. To reasonably estimate soil infiltration characteristics, soil samples from the 0–20 cm layer within the inner ring were collected and analyzed for texture in the laboratory.

After restoration, because the fields retained standing water, the steady infiltration capacity was assessed using a single-ring infiltrometer. The water depths inside and outside the ring were recorded using submersible pressure meters. Surface soil in the fields was also collected for soil texture analysis.

The stable infiltration rates were subsequently quantified from these measurements. Soil texture analysis was conducted using the sieve and hydrometer methods for both stages.

3. Results and Discussion

3.1. Before restoration

Before restoration, the surface soil texture was classified as clay loam (Figure 2). The infiltration curves of Fields A and C showed stable patterns, with steady infiltration rates of 41 ± 4 cm/h and 26 ± 2 cm/h, respectively. In contrast, the infiltration curve of Field B exhibited a shift in slope at approximately 50 minutes of cumulative infiltration time, where the rate decreased. Such a shift commonly occurs when the wetting front encounters a subsurface layer with hydraulic properties distinct from the overlying soil.

The data beyond 50 minutes this point were used to calculate the steady infiltration rate. The relationships between steady infiltration rate and ponding depth were expressed as follows:

$$I_{A,pre} = 0.69H + 37.59\ (\pm 4.02)\,, \quad (1)$$

$$I_{B,,pre} = -0.23H + 15.71\ (\pm 2.46), \quad (2)$$

$$I_{C,,pre} = 1.03H + 19.14\ (\pm 1.49), \quad (3)$$

where $I_{A,pre}$, $I_{B,pre}$, and $I_{C,pre}$ represent the steady infiltration rates (cm/h) of Fields A, B, and C, respectively, and H denotes the ponding depth (cm). Based on these equations, the estimated steady infiltration rates at $H = 5$ cm were 41.07 ± 4.02, 14.57 ± 2.46, and 24.30 ± 1.49 cm/h for Fields A, B, and C, respectively (Table 1).

Table 1. Steady infiltration at $H = 5$ (cm).

Field	Before restoration (mm/h)	After restoration	
		inside ring (mm/h)	outside ring (mm/h)
A	410.7 ± 40.2	0.263 ± 0.0005	1.101 ± 0.011
B	145.7 ± 24.6	0.132 ± 0.0019	1.049 ± 0.007
C	243.0 ± 14.9	0.484 ± 0.0005	2.181 ± 0.078

3.2. After restoration

Post-restoration infiltration tests were carried out from January 15 to 20, 2025, after maintaining ponding for more than one month. The soil samples were classified as silty clay (Figure 2), with a lower sand ratio than before restoration. During the tests, water supply was suspended. Because ponding depth and infiltration rate were not directly correlated, rainfall- and evaporation-corrected cumulative infiltration was analyzed by linear regression. The result is listed in Table 1.

As shown in Table 1, the infiltration rates measured inside were considerably larger than that outside the ring. The average infiltration rate inside the ring was 0.293 ± 0.0012 mm/h, significantly lower than the depletion rate (1.444 ± 0.045 mm/h), indicating substantial bund seepage. This discrepancy indicates substantial bund seepage, as the outer-ring infiltration rate accounts for both vertical infiltration and lateral seepage through the bunds, whereas the inner-ring rate reflects only vertical percolation.

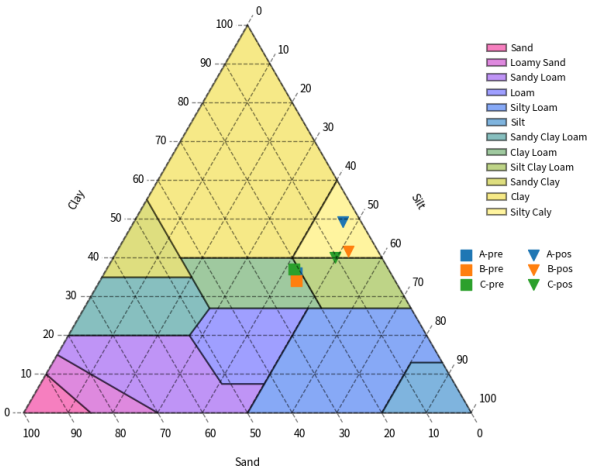

Figure 2. Soil texture.

4. Conclusions

Pre-restoration infiltration rates were much higher than expected for the soil texture, suggesting preferential flow paths such as macropores. After restoration, slurry deposition blocked these pathways and formed a compact layer, reducing infiltration capacity. Compared with the pre-restoration rate (266.4 ± 28.5 mm/h), the water retention capacity of the terraces was improved and had infiltration of 0.293 ± 0.0012 mm/h, falling within the typical range suitable for paddy field conditions. Nevertheless, the underlying causes and long-term effects of these changes remain unclear, emphasizing the need for continued monitoring of infiltration performance.

Acknowledgements

We gratefully acknowledge Yi-Zhih Tsai, Yung-Wei Lee, Yong-Ching Chang, Che-You Liu, and Ying-Chi Liao for their assistance with the infiltration tests and texture analysis.

References

Chen R-S (2008) Adaptability Study on USLE for Soil Erosion of Terraced Paddy Field. Retrieved from Council of Agriculture, Executive Yuan, R.O.C.

Hakamata, T., Hirata, T., Muraoka, K. 1992. Evaluation of land use and river water quality of the Tsukuba Mountains ecosystem, Japan. Catena 19(5):427-439.

Hasegawa, S., Thangaraj, M., & O'Toole, J. C. (1985). Root behavior: field and laboratory studies for rice and nonrice crops. Soil physics and rice, 383-395.

Sharma, P. K. (1989). Effect of periodic moisture stress on water-use efficiency in wetland rice. Oryza 26, 252-257.

Song, J.H., Ryu, J.H., Park, J., Jun, S.M., Song, I., Jang, J. et al (2016) Paddy field modelling system for water quality management. Irrigation Drainage 65:131-142.

This extended abstract template was updated on Sept 14, 2025

Impact on agricultural irrigation under the influence of climate change and adaptation strategies for stabilizing agricultural irrigation water supply

Ya-Zhen Huang[1], Chihhao Fan[12*]

[1]Department of Bioenvironmental Systems Engineering, National Taiwan University, No. 1, Section 4, Roosevelt Road, Taipei City, 10617 Taiwan (R.O.C.)

[2]Ecological Engineering Center, College of Bioresources and Agriculture, National Taiwan University, No. 1, Section 4, Roosevelt Road, Taipei City, 10617 Taiwan (R.O.C.)

* Corresponding author. Email: chfan@ntu.edu.tw

Abstract

Climate change has led to an increase in the frequency and severity of extreme weather events, posing significant challenges to the availability and reliability of water resources. Among the most affected sectors is agriculture, where irrigation supply is often disrupted due to policy-driven fallowing or suspension of irrigation in response to competing water demands from domestic and industrial sectors. These interruptions lead to reduced agricultural productivity, increased government expenditures on fallow land subsidies, and long-term degradation of farmland quality. This study aims to evaluate and propose strategies for enhancing the resilience and stability of agricultural water supply systems in the context of climate change. Drawing on existing research and survey reports, the study identifies key factors that influence the stability of irrigation supply and projects the potential short-term, medium-term, and long-term impacts of climate change on agricultural water management. Climate data is downscaled and spatially interpolated, then digitized into gridded formats to facilitate overlap analysis and identify high-risk regions. Nature-based adaptation solutions are proposed to support adaptive decision-making. The methodology is further tested and refined in a pilot area (Taoyuan City, Taiwan) to verify its practical applicability and scalability. Additionally, the study incorporates considerations such as alternative water resource utilization, ecosystem service benefits, economic impact assessments, and stakeholder engagement. By integrating these interdisciplinary perspectives, comprehensive, resilient strategies are formulated to strengthen the sustainability and adaptive capacity of agricultural irrigation systems in the face of a changing climate.

Keywords: Climate change, Agricultural irrigation, Water resource resilience, Adaptation strategies, Nature-based solutions

1. Introduction

Global population growth and industrial expansion have sharply increased competition for water, making agricultural and industrial use a central sustainability challenge. Over the past two decades, extreme climate events have intensified, driving more frequent droughts and floods. By 2030, global water demand is projected to reach 160% of available freshwater resources, with agriculture accounting for nearly 70%. Such imbalances pose severe risks to food security and socio-economic stability. Although international agreements such as the UNFCCC and the Paris Agreement promote mitigation and adaptation, climate change continues to intensify water allocation conflicts and threaten agricultural production.

Taiwan, a subtropical island nation, receives abundant rainfall, yet its steep terrain and short rivers cause most precipitation to flow rapidly into the sea. Coupled with uneven temporal and spatial distribution, central and southern regions frequently experience droughts. Agriculture—responsible for 70% of national water use and heavily dependent on direct river diversion—is highly vulnerable. Government responses, including crop rotation and financial compensation, have mitigated short-term crises but also created fiscal burdens and agricultural instability. Excessive groundwater extraction has led to land subsidence and a decline in water quality, underscoring the limitations of existing policies.

International experience suggests that precision agriculture, smart irrigation, and nature-based solutions (NbS) can enhance water resilience while sustaining crop yields and ecological services. This study therefore assesses climate change risks to Taiwan’s agricultural water resources and proposes adaptive strategies that strengthen resilience, ensure sustainable use, and safeguard long-term agricultural development.

2. Materials and Methods

2.1. Data and study area

This study collected and integrated domestic and international datasets to assess the impacts of climate change on agricultural water resources. Taoyuan, Taiwan, was selected as the case study, considering basic irrigation demand, economic development, alternative water sources, and climate change pressures. All data were digitized for spatial analysis using Geographic Information Systems (GIS).

2.2. Climate scenarios and indicators

Two scenarios were designed: (1) precipitation increase and (2) precipitation decrease. Extreme climate indices were adopted from the WMO Expert Team on Climate Change Detection and Indices (ETCCDI), supplemented by Taiwan’s 2019 climate index atlas. A total of 22 indicators (11 precipitation, 11 temperature) were applied. For precipitation increase, the key indices were annual total precipitation (prcpTOT) and simple daily intensity index (SDII); for precipitation decrease, the number of days with <10 mm rainfall and consecutive dry days (CDD) were selected..

2.3. Downscaling and assessment

Global climate data from CMIP6 were downscaled to 0.005° (~1 km) resolution through statistical bias correction using gridded observations. Variations in the selected indices were calculated under four SSPs (SSP1-2.6, SSP2-4.5, SSP3-7.0, SSP5-8.5) across short-term

(2021–2040), mid-term (2041–2060), and long-term (2081–2100) horizons relative to the 1995–2014 baseline. Normalized values (0–1) were classified into five levels, and high-priority areas were identified by overlapping grids with high index levels under each scenario.

3. Results and Discussion

3.1. Climate change scenarios and extreme weather indicators

Simulation results under CMIP6 projections revealed significant variations in precipitation and temperature indices across the four SSP scenarios. In the short term (2021–2040), moderate increases in prcpTOT appeared under SSP2-4.5 and SSP5-8.5, whereas mid- and long-term horizons showed greater variability. The SDII suggested rising rainfall intensity and higher flash-flood risk, while CDD increased markedly under SSP3-7.0, signaling greater drought potential. These findings indicate that both extremes—flooding and drought—are likely to intensify, increasing uncertainty for agricultural water management.

3.2. Spatial distribution of priority risk areas

Overlay analysis revealed contrasting high-risk regions under precipitation increase and decrease scenarios. Under precipitation surpluses, priority zones were concentrated in Fuxing District, where more frequent extreme rainfall may mobilize pollutants from agricultural lands. Approximately 325 hectares of dryland and 980 hectares of orchards were identified as potential non-point pollution sources, threatening irrigation water quality. Conversely, precipitation deficits placed Yangmei, Guishan, Longtan, Daxi, and Fuxing at high risk of drought. These regions encompass 7,670 hectares of farmland, 101 high-water-consuming industries, and a domestic water supply serving 78% of the population (Figure 1). Collectively, these results highlight that both water surpluses and shortages significantly threaten agricultural sustainability and socio-economic stability.

(a)

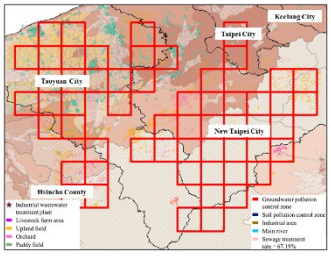

(b)

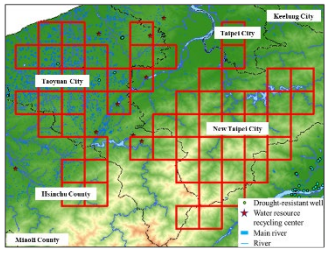

Figure 1. In the scenario of reduced precipitation, the overlap situation of surface water resources at the short-term and long-term in the concerned region: (a) Overlapping situation of surface water resources, and (b) Overlapping situation of various potential water use sectors.

3.3. Implications for agricultural water supply and management

The study area relies on river catchments and ~1,960 hectares of lakes and reservoirs, including Shimen Reservoir. However, these resources are insufficient during droughts. Supplementary reliance on groundwater and baseflow has become common, but over-extraction accelerates land subsidence and water quality deterioration, indicating the unsustainability of current strategies. Climate-driven variability, coupled with policy-driven fallowing and irrigation suspension, may further intensify competition among domestic, industrial, and agricultural sectors, underscoring the need for integrated management.

3.4. Adaptation perspectives

The dual risks of flood-induced pollution and drought-induced scarcity emphasize the importance of flexible adaptation. Strengthening pollution control in vulnerable zones, optimizing reservoir operations, and improving conjunctive use of surface and groundwater are essential. Precision agriculture, smart irrigation, and NbS—such as managed aquifer recharge and wetland restoration—can simultaneously enhance efficiency and provide ecological co-benefits. Prioritizing high-risk zones and engaging stakeholders in participatory governance will further strengthen equity, feasibility, and long-term sustainability.

4. Conclusions

This study comprehensively evaluated the impacts of climate change on Taiwan's agricultural water resources using high-resolution downscaled CMIP6 climate projections combined with spatial overlay analysis. The results revealed heightened risks from both flooding and drought, reflecting the dual challenges posed by climate extremes. Specifically, Fuxing District is projected to face more frequent extreme rainfall events, leading to pollution runoff and deterioration of irrigation water quality, while Yangmei, Guishan, Longtan, Daxi, and Fuxing are identified as drought-prone areas vulnerable to shortages. Current dependence on surface water and supplementary groundwater extraction is unsustainable, as it exacerbates land subsidence, reduces recharge, and compromises long-term water quality. To enhance resilience, integrated surface–subsurface water management, targeted non-point pollution control, and optimized reservoir operations must be prioritized. In parallel, adopting precision agriculture, smart irrigation, and NbS such as wetland restoration and managed aquifer recharge can improve water-use efficiency and provide ecosystem co-benefits. The proposed framework, validated in Taoyuan City, demonstrates strong applicability to other regions with similar climatic and hydrological challenges. Importantly, the findings highlight that successful adaptation requires not only technological innovation but also active stakeholder participation, institutional coordination, and cross-sector collaboration for sustainable agricultural water management under climate change.

Acknowledgements

Sincere appreciation goes to the National Science and Technology Council, Taiwan, for funding support under the grant number 113-2621-M-002-009. National Taiwan University also supported this research under the grant numbers NTU-CC-114L894803 and NTU-CC-114L8524.

Linking Reservoir Water Level with Lumped Models for Estimating Inflow to Agricultural Reservoirs

Seokhun Kang [1], Jung-Hun Song [2*]

[1] Department of Agricultural and Rural Engineering, Chungnam National University, Daejeon 34134, Republic of Korea

[2] Department of Agricultural and Rural Engineering, Chungnam National University, Daejeon 34134, Republic of Korea

* Corresponding author. Email: j.song@cnu.ac.kr

Abstract

Accurate estimation of reservoir inflow and outflow is essential for efficient operation and management of agricultural reservoirs. However, in most small- and medium-sized reservoirs managed by the Korea Rural Community Corporation (KRC), direct measurements of inflow and outflow are not conducted due to practical constraints. In contrast, real-time water level monitoring using level gauges is easier, and water levels can be converted to storage volumes using stage-storage curves. Nevertheless, inflow and outflow remain unknown variables, creating an ill-posed problem—solving two unknowns with one equation (the reservoir water balance). Recent studies proposed integrating reservoir water level data with expert operational knowledge to transform the ill-posed equation into a well-posed one during specific periods. Partial inflow data from these periods have been combined with hydrological models to reconstruct continuous inflow and outflow records. Lumped hydrological models typically require many parameters, reducing reliability in parameter estimation. Therefore, models with fewer parameters but high performance are preferred. Recently, the Five-Parameter Hyperbolic Model (FPHM), a simplified lumped model, was developed for Korean watersheds. However, its applicability to agricultural reservoir inflow estimation is yet to be fully evaluated. This study evaluates the applicability of FPHM by integrating it into a reservoir water level–based inflow/outflow estimation framework. The model's performance was compared with a modified 3-tank model at four reservoirs: Idong, Gopung, Gosam, and Cheongcheon. The findings aim to improve agricultural reservoir operation efficiency and hydrological modeling reliability.

Keywords: Reservoir water level, Reservoir inflow, Expert knowledge, FPHM, Ungauged watershed

1. Introduction

Agricultural reservoirs in Korea play a crucial role in supplying irrigation water, particularly to paddy fields. However, most small- and medium-sized reservoirs managed by the Korea Rural Community Corporation (KRC) lack continuous inflow measurements due to operational and financial constraints, with only water levels routinely recorded. This results in an ill-posed water balance where both inflow and outflow remain unknown. To address this, parsimonious models are preferred to reduce uncertainty in parameter estimation. The Five-Parameter Hyperbolic Model (FPHM), recently developed for Korean watersheds, offers a simplified alternative to traditional multi-parameter models. This study evaluates the applicability of FPHM for reservoir inflow estimation by integrating it into a water level–based framework and comparing its performance with the modified 3-Tank model.

2. Materials and Methods

2.1. Study Sites

This study targeted four agricultural reservoirs: Idong, Gopung, Gosam, and Cheongcheon. These reservoirs vary in catchment area, storage capacity, and hydrological response, providing diverse conditions for model evaluation. Reservoir water levels were obtained from KRC and converted into storage using stage–storage curves. Rainfall data were acquired from nearby meteorological stations.

2.2. Methodology

2.2.1. Water balance equation

Reservoir inflow (RI) and outflow (RO) were treated as unknowns in the reservoir water balance, with storage change (dS/dt) derived from observed water levels:

$$\frac{dS}{dt} = (RI + R) - (E + G + RO) \qquad (1)$$

2.2.2. Resolving the ill-posed problem with expert knowledge

Since both RI and RO are unknown, expert knowledge of reservoir operation was integrated to separate zero-outflow and nonzero-outflow periods

- Zero-outflow periods (RO = 0): inflow (RI) can be estimated as

$$RI = \left(\frac{dS}{dt}\right) + R - E \qquad (2)$$

- Nonzero-outflow periods (RO > 0): classified based on operation cases:

WS: irrigation water supply
PS: principal spillway release
ES: emergency spillway release

By combining these rules, periods with known RI or RO were identified and used as constraints for model calibration.

2.2.3. Hydrological modeling

The Five-Parameter Hyperbolic Model (FPHM) was applied to estimate continuous inflows, calibrated with the SCE-UA algorithm using the partial inflow data from 2.2.2.

2.2.4. Benchmark comparison

The modified 3-Tank model was also calibrated under the same conditions and used as a reference for performance evaluation.

2.2.5. Performance metrics

Model performance was assessed using NSE(Nash-Sutcliffe Efficiency) (Nash and Sutcliffe, 1970), NSE_{log}, NSE_{FDC}, and PBIAS.

3. Results and Discussion

3.1. Reservoir Inflow Estimation during Zero-Outflow Periods

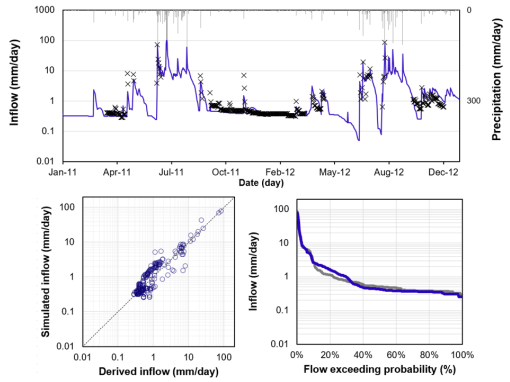

Figure 1. FPHM-Based Inflow Simulation for the Cheongcheon Reservoir Watershed

Figure 1 illustrates the FPHM-simulated inflows for the Cheongcheon Reservoir watershed, showing good agreement with derived inflows during zero-outflow periods. This confirms that the proposed framework can effectively utilize partial inflow information to reconstruct continuous inflow series.

3.2. Model Calibration Results

Calibration results (Table 1) demonstrate that both the modified 3-Tank model and the FPHM achieved high performance across the study reservoirs. In particular, FPHM consistently produced NSE values above 0.85 in all reservoirs, with Cheongcheon and Idong achieving NSE = 0.96. Moreover, PBIAS values remained within ±5% for most cases, indicating that FPHM effectively reduced systematic bias compared to the 3-Tank model. These results highlight the ability of FPHM, despite its parsimonious structure, to capture reservoir inflow dynamics reliably.

Table 1. Calibration Results

Reservoir	Model	NSE	NSE_{log}	NSE_{FDC}	PBIAS
Idong	3-Tank	0.93	0.53	0.76	-6.9
	FPHM	0.96	0.52	0.76	-2.2
Gopung	3-Tank	0.93	0.83	0.93	-7.0
	FPHM	0.90	0.78	0.90	-2.5
Gosam	3-Tank	0.90	0.75	0.95	-17.0
	FPHM	0.85	0.63	0.79	-3.1
CheongCheon	3-Tank	0.96	0.83	0.95	-2.6
	FPHM	0.96	0.52	0.92	-2.2

3.3. Model Validation Results

Validation outcomes (Table 2) further confirm the robustness of the FPHM framework. While the 3-Tank model showed strong performance during calibration, FPHM maintained stable accuracy during validation, particularly in Gopung and Cheongcheon Reservoirs where NSE_{log} and NSE_{FDC} values remained above 0.6. Even in Gosam Reservoir, which has relatively complex hydrological behavior, FPHM successfully reproduced overall inflow patterns, demonstrating its applicability under diverse watershed conditions.

Table 2. Validation Results

Reservoir	Model	NSE	NSE_{log}	NSE_{FDC}	PBIAS
Idong	3-Tank	0.87	0.67	0.87	-2.0
	FPHM	0.78	0.51	0.71	12.4
Gopung	3-Tank	0.78	0.62	0.80	-17.9
	FPHM	0.72	0.63	0.86	-12.8
Gosam	3-Tank	0.71	0.69	0.83	-32.4
	FPHM	0.68	0.21	0.40	-22.7
CheongCheon	3-Tank	0.86	0.59	0.78	-20.2
	FPHM	0.78	0.51	0.63	12.4

4. Conclusions

This study evaluated the applicability of the Five-Parameter Hyperbolic Model (FPHM) for estimating inflows to agricultural reservoirs by linking reservoir water levels with hydrological modeling. Results from four reservoirs demonstrated that FPHM achieved comparable performance to the modified 3-Tank model, with NSE values generally above 0.7 during both calibration and validation. PBIAS values were within ±5%, indicating stable performance without significant bias. Notably, the parsimonious structure of FPHM reduced parameter uncertainty while maintaining competitive accuracy. These findings highlight the potential of FPHM as a practical and reliable tool for inflow estimation in data-scarce agricultural reservoirs, contributing to improved reservoir operation and water resource management.

Acknowledgements

This work was supported by Korea Institute of Planning and Evaluation for Technology in Food, Agriculture and Forestry(IPET) through Intelligent Agricultural InfraManagement for ClimateChange Development Program, funded by Ministry of Agriculture, Food and Rural Affairs(MAFRA)(No. RS-2025-02215604)

References

Beven, K., 2002. Rainfall-Runoff Modelling: The Primer. Wiley-Blackwell.

Nash, J.E., Sutcliffe, J.V., 1970. River flow forecasting through conceptual models: Part I. Journal of Hydrology, 10(3), 282–290. https://doi.org/10.1016/0022-1694(70)90255-6

Song, J.H., Kang, M.S., Kim, S., 2019. Exploring parsimonious daily rainfall-runoff model structure using the hyperbolic tangent function and Tank model. Journal of Hydrology, 574, 574–587. https://doi.org/10.1016/j.jhydrol.2019.04.054

Song, J.H., Kang, M.S., Kim, S., 2022. Estimating reservoir inflow and outflow from water level observations using expert knowledge: Dealing with an ill-posed water balance equation in reservoir management. Water Resources Research, 58(4), e2020WR028183. https://doi.org/10.1029/2020WR028183

This extended abstract template was updated on September 15, 2025

Effect of irrigation with high nitrogen concentration water on the horizontal distribution and temporal changes in the nitrogen concentration in a paddy field

Keita Kobuchi*, Kazuhiro Nishida, Shuichiro Yoshida, Yuta Amakawa

Graduate school of agriculture and life science, Tokyo University, 1-1-1 Yayoi, Bunkyo-ku, Japan

* Corresponding author. Email: 12878978813@g.ecc.u-tokyo.ac.jp

Abstract

To understand the effect of high-nitrogen irrigation water on the nitrogen concentration in paddy water (Nw), a field investigation and a mechanism analysis using a model equation were conducted. The investigation was conducted in 2024 at an experimental paddy field in Tokyo, Japan. Both total Nitrogen concentration (TN) in irrigation water and the percolation rate were high (approximately 3.5 mgN/L and 7 cm/d, respectively). Irrigation was automatically managed based on water levels and each irrigation period lasted about 2 hours, and intervals between irrigations were roughly 10 hours. Over eight days during cultivation (late June to late August), paddy water was sampled multiple times a day (immediately after irrigation ceased and a few hours later) at six locations within the paddy field. TN was quantified in the laboratory and defined as Nw. The predictive model was derived considering horizontal advection due to irrigation and diffusion between the paddy water and the soil surface.

As a result, Nw was high near the water inlet and low near the water outlet throughout the entire survey period. Immediately after irrigation ceased, the difference between locations was substantial and Nw decreased over time, with decline more pronounced at higher concentration points near the water inlet. The model equation obtained by parameter fitting well represented the measured values. The study suggests that when investigating the impact of high-nitrogen irrigation water, it's necessary to account for the nitrogen concentration distribution and temporal changes, and that these phenomena are governed by horizontal advection and water-soil diffusion.

Keywords: model, paddy water, water management

1. Introduction

Irrigation influences rice growth by altering the water, thermal, and nitrogen environments in paddy fields. When irrigation water contains high concentrations of nitrogen, irrigation becomes a major source of nitrogen input to the field, and generates spatial and temporal changes in nitrogen concentration. These changes are expected to vary depending on the nitrogen concentration of irrigation water and water management methods, but this remains unclear.

This study investigated the effect of irrigation on the spatial distribution and temporal change of nitrogen concentration in paddy water in a field irrigated with high-nitrogen concentration water. Then, these distribution and change are analyzed using nitrogen concentration prediction model based on nitrogen transport and balance to understand the mechanisms underlying distribution formation and temporal changes.

2. Materials and Methods

The field measurements were conducted in 2024 in an experimental paddy field at the Institute for Sustainable Agro-ecosystem Services, The University of Tokyo (Andosol soil, cultivar: Koshihikari, transplanting from May 31 to June 1, topdressing on July 25). The irrigation water was sourced from groundwater with a high total nitrogen (TN) concentration of approximately 3–4 mg/L. Since infiltration was high (approximately 7 cm/d), large amounts of irrigation water were used. Irrigation was performed using an automatic water management system: irrigation started and stopped when the water depth was approximately 2 cm and 4 cm, respectively.

Paddy water samples were collected at six locations in the field (Fig. 1), and then their TN concentrations (Nw) were determined in laboratory. The sampling was conducted over eight days: three days before topdressing (June 27, July 5, July 18), the day of topdressing and the following day, and three additional days (July 29, August 19, August 27) when the effect of topdressing was considered minimal. On each sampling day, water was sampled 1–4 times (immediately after irrigation and 1–7 hours after irrigation). Water depth was measured to determine the flow velocity of paddy water.

3. Model Analysis

Considering horizontal advection in the paddy field and diffusion between paddy water and the soil surface, the nitrogen balance equation can be expressed as:

$$h\frac{\partial C}{\partial t} = -vh\frac{\partial C}{\partial x} - k(C - Cs) \qquad (1)$$

where C(x,t) is the TN concentration of paddy water (mgN/L), t is time (h), x is the distance from the inlet along the long side of the field (m), h is paddy water depth (cm), and v is the flow velocity of paddy water (m/h), k and Cs are parameters representing the diffusion coefficient (cm/h) and TN concentration at the soil surface (mgN/L), respectively.

TN concentration during irrigation where irrigation water reaches is expressed by Eq. (2), which is solution of Eq. (1) under the boundary condition ($C(0, t) = C_1$). TN concentration under no-irrigation is expressed by Eq. (3) , which is solution of Eq. (1) (with v=0) under the initial condition ($C(x, 0) = C_0$)

$$C(x,t) = Cs + (C_1 - Cs)exp\left(-\frac{k}{hv}x\right) \qquad (2)$$

$$C(x,t) = Cs + (C_0 - Cs)exp\left(-\frac{k}{h}t\right) \qquad (3)$$

The parameters k and Cs were determined by least squares method to minimize the difference between calculated and observed C(x,t) for six days excluding topdressing days using observed values of C_0, C_1, h, v. Model accuracy was evaluated using RMSE.

4. Results and Discussion

Nw was consistently higher near the inlet and lower near the outlet (Fig. 2). The concentration difference was the greatest when irrigation stopped, and became smaller with time after irrigation stopped. The spatial difference in Nw was particularly large at the point between 40% and 60% of the field immediately after irrigation stopped (Fig. 4). After irrigation stopped, Nw gradually decreased, with the most pronounced decline near the inlet where the Nw was initially high (Figs. 5).

The parameters of k and Cs were determined as 0.41 cm/h, 0.08 mgN/L, respectively. Eqs. (2) and (3) with these parameters reasonably reproduced both the spatial distribution and temporal changes of Nw (RMSE: 0.36 mgN/L, Figs. 4–6). This result indicates that considering horizontal advection and diffusion between paddy water and soil water is important to understand nitrogen concentration distribution and its temporal variation.

5. Conclusions

In paddy fields irrigated with high-nitrogen water, irrigation generated a distribution in which Nw was higher near the inlet. After irrigation ceased, Nw declined with time, and spatial differences decreased. Our research suggests these distribution formation and temporal change could be governed by horizontal advection and diffusion between paddy water and the soil surface.

Acknowledgements

This research was conducted at the Institute for Sustainable Agro-ecosystem Services, The University of Tokyo with the cooperation of technical staff.

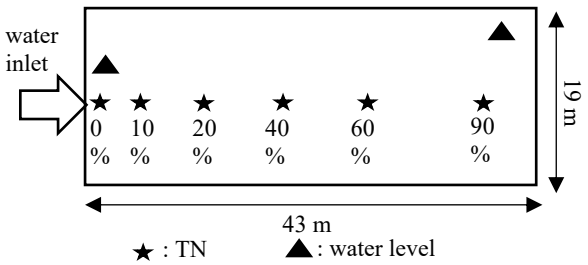

Fig.1 Schematic diagram of surveyed paddy field and measurement points (%: the distance ratio from the water inlet)

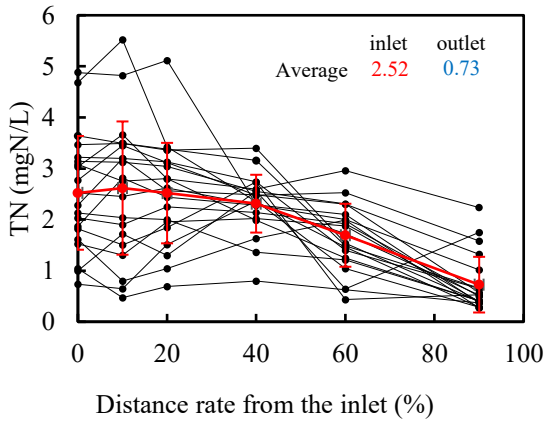

Fig.2 Nw distribution map for the entire survey period (red line: average value, red error bar: standard deviation)

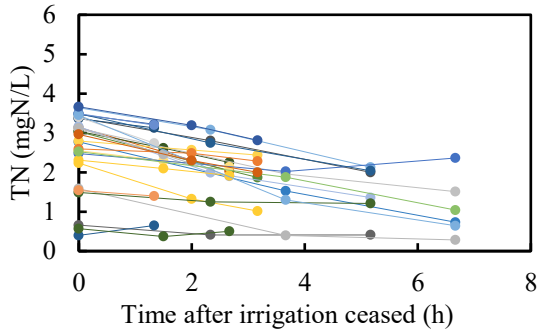

Fig.3 Time changes in Nw after irrigation stopped for the entire survey period

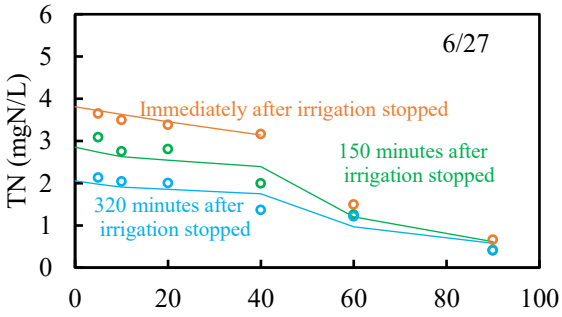

Fig.4 Nw immediately after irrigation (plot: actual measurements, line: calculated values)

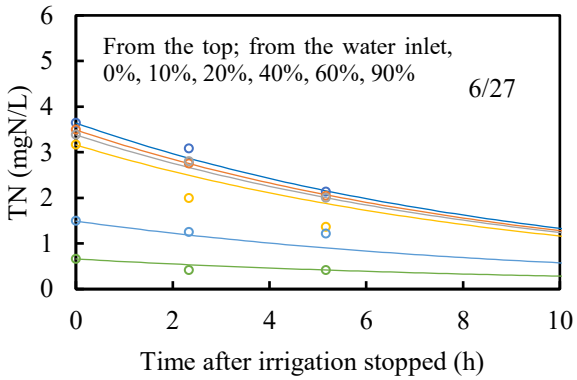

Fig.5 Time changes in Nw after irrigation stopped (plot: actual measurements, line: calculated values)

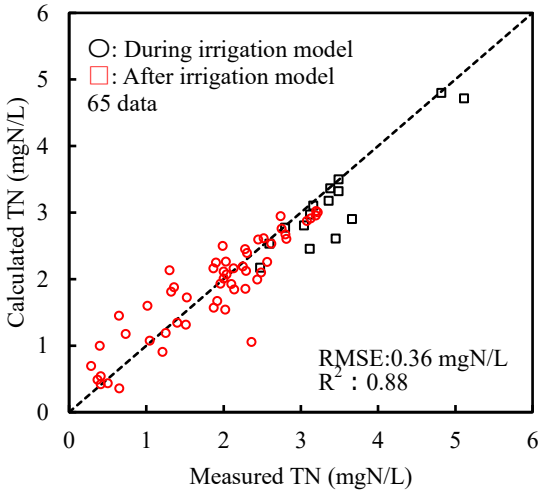

Fig.6 Comparison of model calculations and actual measurements (i: Immediately after irrigation, a: After irrigation)

Effects of Rice Straw Management on Greenhouse Gas Emissions and Soil Nitrogen Dynamics in Rice Paddy Soil

Wang Shan-Li・Kao Chuan-Fu

Abstract

While rice production is essential for the global food supply, it also contributes substantially to greenhouse gas (GHG) emissions. Among field practices, rice straw return is widely encouraged for its role in recycling nutrients and enhancing soil organic matter; however, its influence on nitrogen cycling in paddy systems remains insufficiently understood. To investigate this, a field experiment was conducted at the Experimental Farm of National Taiwan University, incorporating three straw management treatments, i.e., removal (-RS), incorporation (+RS), and surface cover (RS cover), under continuous flooding (CF) and alternate wetting and drying (AWD). Greenhouse gas fluxes were continuously recorded using a multichannel automated chamber system. Results indicated that CH_4 emissions were highest under straw incorporation (+RS), followed by RS cover, and lowest in -RS. AWD had limited effectiveness in reducing CH_4, likely due to weather-influenced water level fluctuations. Nitrous oxide (N_2O) emissions peaked 3-7 days after nitrogen topdressing and mid-season drainage, with the RS cover treatment exhibiting the greatest fluxes. Porewater analysis showed that total nitrogen and ammonium concentrations were higher in -RS, while RS cover had reduced levels, possibly due to enhanced denitrification. Straw application increased total carbon, nitrogen, and dissolved organic carbon in the soil, supporting long-term fertility improvements. However, the simultaneous rise in GHG emissions, particularly under RS cover, reveals a trade-off between enhancing soil quality and mitigating climate impacts. This study underscores the need for tailored management practices that optimize straw use and irrigation strategies to align both agronomic and environmental goals in rice cultivation.

Quantifying Absorbed Water via Matric Potential to Improve Dielectric Models

Makoto Hashimura[1*], Kumiko Tsujimoto[1]

[1] Graduate School of Environmental, Life, Science and Technology, Okayama University, Okayama, 700-8530, Japan

* Corresponding author. Email: pgxz9vtf@s.okayama-u.ac.jp

Abstract

What kind of dielectric permittivity model is effective in remote sensing? A dielectric permittivity model is an equation that relates soil water content to dielectric permittivity, but existing models have not been able to adequately cover wide regions. In this study, we attempted to theoretically construct a dielectric permittivity model by introducing the matric potential. If the relationships between matric potential and dielectric permittivity, as well as between matric potential and volumetric water content, can be clarified, it may be possible to estimate soil water content regardless of soil type. In this approach, the relationship between matric potential and dielectric permittivity is expressed using Debye's equation. However, how to represent the relationship between volumetric water content and matric potential still requires verification, and we are currently conducting comparative examinations using two different approaches. The key issue of discussion is how to define "bound water." One definition considers bound water as the state in which water exists only in the first molecular layer on the soil particle surface, while the other defines it as the boundary with free water in terms of relaxation time. Along with these validations, we also examined the appropriate matric potential values required for Debye's equation.
Keywords: Bound water, Matric potential, Dielectric permittivity model, Remote sensing, Volumetric water content

1. Introduction

When measuring soil water content, a "dielectric permittivity model" that relates volumetric water content (θ) to dielectric permittivity (ε) is typically employed. Such models have been applied to global-scale remote sensing using satellites, where accurate estimation across diverse soil types is required. Advances in this technology are expected to contribute to agriculture and disaster prevention in regions that are otherwise inaccessible.

However, existing models face limitations in measurement accuracy and often fail to achieve sufficient precision for soils different from those on which the models were originally constructed. Soil dielectric permittivity is commonly calculated based on Birchak's equation (1), which assumes a four-phase structure (soil particles *m*, free water *fw*, bound water *bw*, and air *a*):

$$\varepsilon_s^\alpha = V_\mathrm{m}\varepsilon_\mathrm{m}^\alpha + V_\mathrm{a}\varepsilon_\mathrm{a}^\alpha + V_\mathrm{fw}\varepsilon_\mathrm{fw}^\alpha + V_\mathrm{bw}\varepsilon_\mathrm{bw}^\alpha \cdots (1)$$

Here, Vi and εi denote the volume fraction and dielectric permittivity of component *i*, respectively, while α is a shape parameter, and $V_\mathrm{fw} + V_\mathrm{bw} = \theta$. The greatest challenge in improving the accuracy of dielectric permittivity models lies in accounting for bound water. Soil water can generally be divided into free water and bound water, but quantifying the amount and dielectric permittivity of bound water remains extremely difficult. To address this issue, Tsujimoto et al. (2022) attempted an approach that incorporates matric potential. Building on this concept, the objective of the present study is to experimentally link matric potential to volumetric water content and to determine the matric potential parameters necessary for deriving the dielectric permittivity of bound water, which has not been conclusively identified in previous research.

2. Materials and Methods

As target soils, Toyoura sand, bentonite, and seven types of volcanic ash soils were used. Two types of data were required for this verification:

- *Matric potential–volumetric water content* data for determining the volume of bound water
- *Dielectric permittivity–volumetric water content* data for determining the dielectric permittivity of bound water

2.1. Matric potential–volumetric water content

In previous studies, following Dirksen & Dasberg (1993), the water content at the air-dried state (= 100 MPa) was defined as the condition in which only bound water exists in the soil. In this study, we also employed the concept of Ito (1965), which defines the soil water content at the plastic limit (= 98 kPa) as the condition where only bound water is present.

For the experiment, soil samples with adjusted water contents were measured for matric potential using a WP4C (dewpoint potentiometer). From these measurements, the relationship between volumetric water content and matric potential was derived, and the volume of bound water was calculated.

2.2. Dielectric permittivity–volumetric water content

The dielectric permittivity–volumetric water content data were obtained by measuring the dielectric permittivity of water-adjusted samples using a Vector Network Analyzer (VNA). The measurement frequency was set to 200MHz.

2.3. Estimation of bound water permittivity

The dielectric permittivity of bound water is expressed by the Debye equation as follows:

$$\varepsilon_{bw} = \varepsilon_\infty + \frac{\varepsilon_0 - \varepsilon_\infty}{1 + \mathrm{j}\frac{f}{f_{r0}\exp\left(\frac{\Psi_{vw}}{RT}\right)}} \cdots (2)$$

In this equation, the value to be substituted for $\boldsymbol{\psi_{vw}}$ (the matric potential acting on bound water) has not yet been determined. One of the objectives of this study is to identify the appropriate value for $\boldsymbol{\psi_{vw}}$. Specifically, we substituted values of matric potential ranging from 0 to 800 MPa into the equation to estimate the dielectric permittivity of bound water. Subsequently, by substituting both the dielectric permittivity and volume of bound water into Birchak's equation and comparing the results with the

measured data obtained in section (2), we examined which value of $\boldsymbol{\psi_{vw}}$ is most appropriate for deriving the dielectric permittivity of bound water.

3. Results and Discussion

The volume of bound water was determined from the results of the psychrometer experiment (Fig. 1). Specifically, following the definition of Dirksen & Dasberg (1993), the intersection with a matric potential of 100 MPa was used as the reference point, while according to the definition of Ito (1965), the intersection with 98 kPa was taken as the reference for bound water volume.

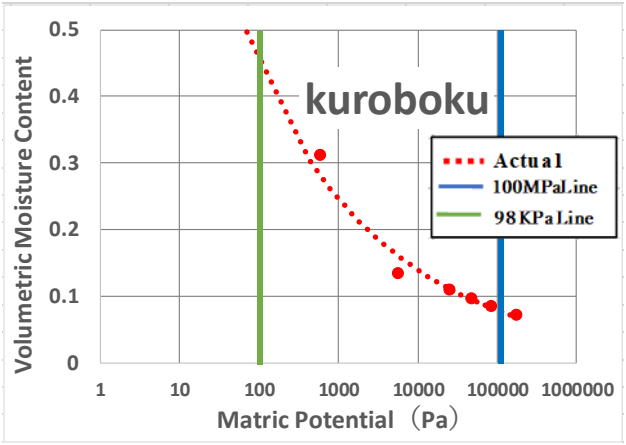

Fig. 1. Relationship between matric potential and volumetric water content obtained from the psychrometer experiment.

Next, Fig. 2 shows the comparison between the measured data obtained using the VNA and the estimated values derived from the dielectric permittivity model incorporating the calculated bound water volume (measurement frequency: 200 MHz).

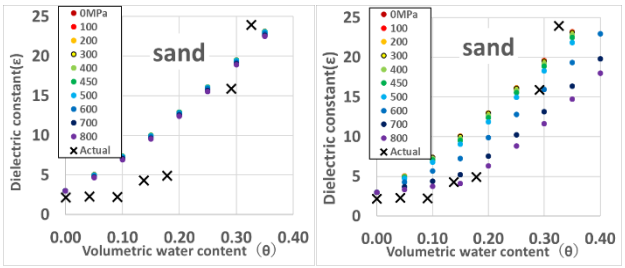

Fig. 2. Dielectric permittivity–volumetric water content: comparison of VNA measurements and dielectric model (left: $\boldsymbol{\psi_{vw}}$=100 MPa, right: $\boldsymbol{\psi_{vw}}$=98 kPa)

Although the trends varied depending on soil type, in many cases the model based on the definition of Dirksen & Dasberg tended to overestimate dielectric permittivity compared with the measured values. In contrast, the model based on Ito's definition more often reproduced the lower dielectric permittivity observed in the low water content region.

This difference is considered to arise from the method of deriving bound water volume. When Ito's definition was applied, the proportion of bound water relative to the total soil water increased. Since, at the same frequency range, the dielectric permittivity of bound water is generally lower than that of free water, a higher fraction of bound water results in a lower overall soil dielectric permittivity. Therefore, Ito's model can be interpreted as showing a closer agreement with the measured values.

Furthermore, in applying the Debye equation to estimate the dielectric permittivity of bound water, we aimed to determine the appropriate value of matric potential $\boldsymbol{\psi_{vw}}$ acting on bound water. However, in the present results, the measurement errors in the VNA data were larger than the variations caused by differences in $\boldsymbol{\psi_{vw}}$. Consequently, within the scope of this study, it was difficult to uniquely determine the value of $\boldsymbol{\psi_{vw}}$.

4. Conclusion

In this study, we attempted to implement a dielectric permittivity model incorporating matric potential, focusing on defining the volume of bound water and determining the matric potential to be substituted into Debye's equation. However, conclusive results were not obtained for either aspect. On the other hand, a significant outcome of this study was the demonstration that the definition of bound water volume has a substantial impact on model results. Future work should involve more rigorous theoretical and experimental investigations into the properties of bound water and the treatment of matric potential.

Acknowledgements

The authors gratefully acknowledge the financial support provided by the Japan Aerospace Exploration Agency (JAXA) through the Earth Observation Research Program (ER3AMF113, ER4AMF103-25RT000181), by JSPS KAKENHI (Grant Numbers 25H00760 and 23K26209), and by the "Initiative for Realizing Diversity in the Research Environment" from the Ministry of Education, Culture, Sports, Science and Technology (MEXT), Japan.

References

• **Journal articles:**

1. Dirksen, C., Dasberg, S., 1993. Improved calibration of time domain reflectometry soil water content measurements. Soil Sci. Soc. Am. J., 57(3), 660–667. https://doi.org/10.2136/sssaj1993.03615995005700030005x

2. Ito, H., 1965. On the properties of bound water in soils. J. Jpn. Soc. Soil Phys., 11, 11–18.

3. Tsuchiya, T., Maeda, T., 1987. Dielectric properties of wet soils at microwave frequencies from 1 to 36 GHz. Trans. IEICE B, J70-B(11), 1262–1269.

4. Tsujimoto, K., Ohta, T., Fujii, H., Komatsu, M., 2022. Dielectric behavior of wet soils in the 1–36 GHz microwave range: Modeling and validation. J. Jpn. Soc. Soil Phys., 151, 3–24. https://doi.org/10.34467/jssoilphysics.151.0_3

• **Books:**

1. Debye, P., 1929. Polar Molecules. Dover Publications, New York.

Estimation of short-term rainfall magnitude and intensity using forecast data based on artificial intelligence

Kwak Jihye・Kim Jihye・Kim Sinae・Park Seongjae・An Jaeyoung・Park Seonjae ・Park Suhwan・Kang Moon Seong

Abstract

Short-term heavy rainfall involves rapid temporal and spatial variations in inflow, making it essential to analyze relevant data and develop effective prediction algorithms. To this end, short-term forecast rainfall data from the Korea Meteorological Administration (KMA) were utilized. Artificial intelligence (AI) was used to analyze the occurrence of heavy rain based on KMA's forecast data. The AI model was trained to identify temporal and spatial patterns in the weather data, enabling it to predict the intensity and magnitude of imminent rainfall. These forecasts are updated every hour and provide predictions up to 6 hours in advance. Based on this, the AI model was designed to: (1) determine the likelihood of short-term heavy rainfall, (2) estimate its expected intensity and severity, and (3) update predictions every hour to improve responsiveness and accuracy. To implement the model, appropriate labels were defined by identifying the distribution of rainfall intensities. Probability distribution functions (PDFs) were derived from historical rainfall data to represent the statistical characteristics of precipitation. In addition, damage records-such as those found in disaster yearbooks-were reviewed and organized to link predicted rainfall events with actual downstream impacts. This approach enables the model to support not only rainfall forecasting but also impact-based prediction by associating rainfall intensity with observed damage.

Probabilistic estimation of future rainfall erosivity under climate change using sub-hourly disaggregation of daily rainfall in South Korea

Kim Sinae・Park Suhwan・Kwak Jihye・An Jaeyoung・Park Seongjae・Park Seonjae ・Kang Moon-Seong

Abstract

South Korea is highly susceptible to soil erosion due to its mountainous terrain and frequent heavy rainfall, characteristic of its topography and climate. Climate change is expected to increase the frequency of extreme precipitation events, thereby accelerating soil erosion through changes in rainfall erosivity. Among various influencing factors, the rainfall erosivity factor (R-factor) is directly affected by climate and shows high spatial and temporal variability. Thus, accurate estimation of future R-factors reflecting climate change is essential for reliable soil erosion assessment.

The Universal Soil Loss Equation (USLE) requires high-resolution rainfall data (≤15-minute intervals) to calculate the R-factor, while most climate change scenarios provide daily rainfall data, necessitating temporal downscaling and consideration of climate variability. Additionally, quantifying the uncertainty in future R-factor projections is critical.

This study aims to develop a sub-hourly rainfall time series generation method that incorporates climate change uncertainty and to estimate future R-factors and their associated uncertainties using the USLE framework. A stochastic weather generator and the Multiplicative Random Cascade model were applied to downscale daily rainfall data from Coupled Model Intercomparison Project Phase 6 (CMIP6) Shared Socioeconomic Pathways (SSPs) scenarios into minute-scale resolution. The resulting high-resolution rainfall data were used to probabilistically estimate future R-factors using the USLE method.

The significance of this study lies in quantifying both the magnitude and uncertainty of R-factor changes under future climate conditions. These findings can serve as fundamental data for developing reliable soil erosion vulnerability maps and effective erosion mitigation strategies in response to climate change.

High-resolution measurements of methane flux from paddy field

Natsuki Nobe [1*], Kimihito Nakamura [1], Liyuan Chen [1], Takanori Nagano [2]

[1] Graduate School of Agriculture, Kyoto University, Kyoto, Japan

[2] Graduate School of Agricultural Science, Kobe University, Hyogo, Japan

* Corresponding author. Email: nobe.natsuki.22e@st.kyoto-u.ac.jp

Abstract

Reducing methane (CH_4) emissions from paddy fields is essential for mitigating greenhouse gas impacts. Water management, including extended midseason drainage and alternate wetting and drying, is a promising strategy. However, detailed observations of daily CH_4 flux patterns and their relationships with water regimes, meteorological factors and soil physicochemical properties are needed to establish effective water management. This study monitored CH_4 fluxes in a paddy plot with Andosol soil in Kyoto Prefecture, Japan, using automated high-frequency monitoring. During the flooded period before mid-drying, a consistent diurnal pattern of CH_4 flux was observed, strongly influenced by soil temperature and redox potential (Eh). Throughout the entire flooded period, CH_4 flux gradually increased with rising air and soil temperatures and rice growth as Eh decreased, peaking just before mid-drying. During the non-flooded (intermittent irrigation) period after mid-drying, the daily variation pattern seen before mid-drying was not observed, suggesting greater influence from rainfall and water management. Fluxes were smaller compared to before mid-drying, turning negative in August during the late cultivation period.

Keywords: paddy soil, methane, water management, midseason drainage, high-resolution measurement

1. Introduction

In paddy fields, flooding creates a reduced soil environment that facilitates the activity of strictly anaerobic methanogens, leading to the release of decomposed organic matter as CH_4. CH_4 emissions from paddy fields account for 9% of global anthropogenic CH_4 emissions (Canadell et al., 2021) and CH_4 accounts for the second-largest share of global anthropogenic greenhouse gas emissions after CO_2 (IPCC, 2022). Given that the human influence to global warming is now considered unequivocal, suppressing CH_4 emissions from paddy fields is strongly demanded as one mitigation strategy.

The closed chamber method is the most common technique for measuring fluxes of various gases emitted from paddy fields. This method offers high sensitivity even for small fluxes, is inexpensive, and is easy to operate. However, the time required for each flux measurement and the labor involved in setting up the chamber and measuring concentrations imposed certain limitations on increasing the frequency of measurements. However, in recent years, gas analyzers utilizing spectroscopic techniques have become available, enabling much more frequent and convenient flux measurements. While most studies have focused on fluctuations throughout the entire rice growth period, few have examined flux variations at finer resolutions using automated closed-chamber methods with spectroscopic gas analyzers. To explore the relationship between detailed diurnal variations in CH_4 flux, changes throughout the cultivation period, and water management and meteorological conditions, this study conducted continuous CH_4 flux measurements using a spectroscopic gas analyzer in a paddy plot.

2. Materials and Methods

The measurement was conducted from May to August 2025 at a rice paddy field in Miyama Town, Nantan City, Kyoto Prefecture, Japan. An Opaque Long-Term Chamber (LI-COR, 8200-104) that automatically opens and closes was placed in the field, along with a Multiplexer (LI-COR, LI-8200) to control the opening and closing of the chamber and a Trace Gas Analyzer (LI-COR, LI-7810) on the ridges. These devices measured CH_4 fluxes at a frequency of once every 30 minutes or once per hour. Soil temperature and redox potential (Eh) at a depth of 15 cm, paddy water level, irrigation volume, air temperature, and precipitation were measured near the flux measurement points. Due to frequent malfunctions of the CH_4 measuring equipment, data was missing for some periods.

3. Results and Discussion

The observed plot was continuously flooded from May 8 to July 6, the period before mid-season drainage after rice planting in early May. From July 6 to August 27, the period after mid-season drying until harvesting, it was primarily non-flooded with intermittent irrigation. The following describes these flooded and non-flooded periods separately.

3.1. Flooding period

Methane flux exhibited a diurnal pattern with a minimum peak around 8:00–10:00 AM, an increasing trend during the day, and a maximum peak around 3:00–7:00 PM, matching the pattern of soil temperatures (Fig. 1a, 1b, 1c, 1d). The CH_4 flux gradually increased, reaching 0.004 μmol $m^{-2}s^{-1}$ by May 16 as Eh decreased during the early cultivation stage (Fig. 1a). From June 28 to July 1, the period immediately preceding mid-season drying, the diurnal variation range became very large, reaching a maximum of approximately 0.06 μmol $m^{-2}s^{-1}$, more than 15 times that observed during May (Fig. 1b).

Viewed over the entire flooding period, the CH_4 flux gradually increased, coinciding with rising soil temperatures from May to June. Factors contributing to this increase likely include increased organic matter (substrate for CH_4 production) secreted by roots as rice plants grow; and increased CH_4 emissions through the plants aeration tissues. A decrease in Eh associated with the prolonged flooded state was also observed (Fig. 1i, 1j).

3.2. Non-flooding period

The consistent diurnal pattern of CH_4 flux observed

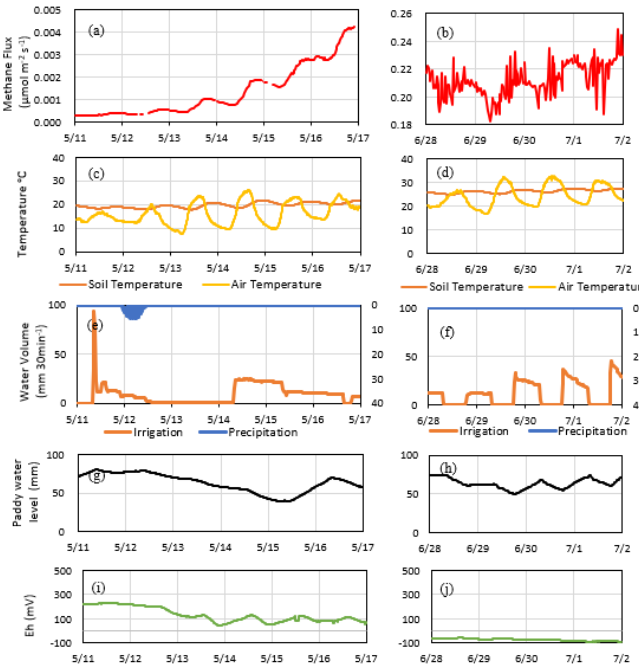

Figure 1. Methane flux (μmol m^{-2} s^{-1}) (a), (b), soil temperature and air temperature (°C) (c), (d), irrigation volume and precipitation (e), (f), paddy water level (mm) (g), (h), Eh (mV) (i), (j) during flooding period. The left column shows the early cultivation stage, while the right column shows the period immediately preceding mid-season drying. 0 mm in Figure 1g and 1h indicates the soil surface.

during the flooding period disappeared, and the flux exhibited different patterns from day to day. The magnitude of the flux decreased significantly compared to the flooding period before the mid-drying season (maximum approx. 0.25 μmol $m^{-2}s^{-1}$ on September 1). From July 12 to July 27, the maximum was 0.06 μmol $m^{-2}s^{-1}$ (Fig. 2a), and during August, it became slightly negative (approx. 0 to -0.01 μmol $m^{-2}s^{-1}$).

Although the effects of soil temperatures were not entirely eliminated, the impact of rising paddy water level and decreasing Eh associated with rainfall and irrigation appears to have been more significant. During July 12–27, increases in rainfall or irrigation water caused rises in water level and decreases in Eh. The timing of these water level rises coincided with the start of increased flux at five time points: July 15, 17, 20, 24, and 25 (Fig. 2a, 2d, 2e). However, even at its highest, the water level only reached the surface of the paddy plot and did not cause flooding. The decrease in Eh was also limited to around 200 mV, not reaching a reduced state in soil layer shallower than depth of 15 cm.

4. Conclusions

Methane flux emitted from a paddy plot exhibits a consistent diurnal pattern during the flooded period and is thought to be influenced by changes in soil temperatures and Eh. Over the entire flooded period, CH_4 flux gradually increased and Eh decreased with rising air and soil temperatures and rice growth. During the non-flooded period, no diurnal pattern was observed, and the flux was thought to be significantly affected by water management and rainfall.

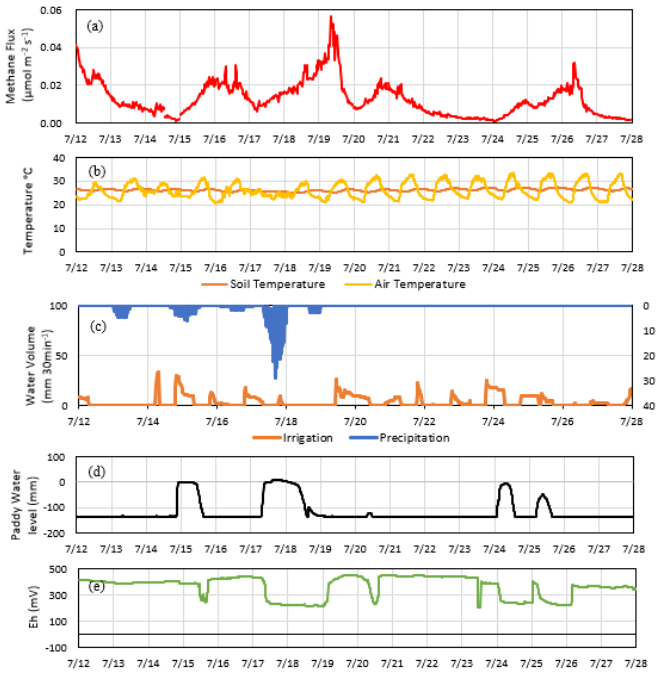

Figure 2. Methane flux (μmol m^{-2} s^{-1}) (a), (b), soil temperature and air temperature (°C) (c), (d), irrigation volume and precipitation (e), (f), paddy water level (mm) (g), (h), Eh (mV) (i), (j) during non-flooding period after mid-season drying. 0 mm in Figure 2d indicates the soil surface.

Acknowledgements

We are sincerely grateful for the financial support by JSPS KAKENHI (Grant Numbers: 23H00349), and Theme 4 of the Advanced Studies of Climate Change Projection (SENTAN Program, Grant Number JPMXD0722678534) supported by the Ministry of Education, Culture, Sports, Science and Technology (MEXT), Japan.

References

Canadell, J.G. et al., 2021: Global Carbon and other Biogeochemical Cycles and Feedbacks. In Climate Change 2021: The Physical Science Basis. Contribution of Working Group I to the Sixth Assessment Report of the Intergovernmental Panel on Climate Change [Masson-Delmotte, V. et al. (eds.)]. Cambridge University Press, Cambridge, United Kingdom and New York, NY, USA, pp. 673–816, doi:10.1017/9781009157896.007.

IPCC, 2022: Summary for Policymakers [P.R. Shukla et al. (eds.)]. In: Climate Change 2022: Mitigation of Climate Change. Contribution of Working Group III to the Sixth Assessment Report of the Intergovernmental Panel on Climate Change [P.R. Shukla et al. (eds.)]. Cambridge University Press, Cambridge, UK and New York, NY, USA. doi: 10.1017/9781009157926.001.

Comparison of Drought Response Capacities Based on Water Resources Under Extreme Drought Conditions in South and North Korea

Jun-Yeong Seo [1], Won-Ho Nam [2*]

[1] Undergraduate Student, School of Social Safety and Systems Engineering, Hankyong National University, Anseong, Republic of Korea

[2] Professor, School of Social Safety and Systems Engineering, National Agricultural Water Research Center, Hankyong National University, Anseong, Republic of Korea

* Corresponding author. Email: wonho.nam@hknu.ac.kr

Abstract

The frequency and intensity of extreme climate events such as droughts, heat waves, and floods have been increasing worldwide under climate change. Drought has emerged as a particularly critical environmental issue, threatening agricultural productivity and socio-economic stability on the Korean Peninsula. The situation is especially severe in North Korea, where weak infrastructure and limited water management systems heighten vulnerability to drought impacts. While most previous studies have relied on meteorological drought indices such as the Standardized Precipitation Index (SPI) and vegetation monitoring using MODIS data, the role of water-resource infrastructure in mitigating agricultural drought has often been overlooked. This study compared the drought response capacities of South and North Korea under extreme drought conditions by analyzing cropland NDVI distributions during a representative drought year (2015). MODIS MCD12Q1 data were used to delineate cropland areas, and NDVI imagery from October 16, 2015, was applied to capture vegetation conditions during severe drought. Results revealed distinct regional disparities: Jeollanam-do croplands in South Korea maintained relatively higher NDVI values, while Hwanghaenam-do croplands in North Korea exhibited lower NDVI values, reflecting stronger vegetation stress. These findings suggest that water-resource infrastructure plays a critical role in buffering agricultural drought impacts. Previous studies have reported that vegetation indices show a strong positive correlation with hydraulic structures such as dams and reservoirs (Polpanich et al., 2022). Accordingly, this study interprets the observed regional disparities as differences in drought response capacity attributable to water-resource infrastructure.

Keywords: Korea Peninsula, SPI, Extreme drought, MODIS, NDVI, Water-resource infrastructure

1. Introduction

Extreme drought is one of the most critical natural hazards, exerting severe impacts on agricultural productivity and food security. The Korean Peninsula is particularly vulnerable due to climatic variability and sharp disparities in water-resource infrastructure between South and North Korea. Recent events highlight these vulnerabilities. In South Korea, the 2012 extreme drought caused nationwide agricultural water shortages, with Jeollanam-do documented as one of the hardest-hit provinces by the National Drought Information Portal (drought.go.kr). Subsequent droughts in 2014 and 2015 further depleted reservoir storage and disrupted agricultural activities in southern regions. In North Korea, the 2012 drought damaged approximately 287,000 ha of cropland, while the 2015 and 2017 spring droughts were reported by the Food and Agriculture Organization (FAO) to have critically undermined crop production and food security. Although previous studies have widely applied indices such as the Standardized Precipitation Index (SPI) and the Normalized Difference Vegetation Index (NDVI) for drought monitoring, they often failed to account for the buffering role of water-resource infrastructure. This study aims to address this gap by comparing cropland NDVI distributions in Jeollanam-do and Hwanghaenam-do during the 2015 extreme drought, thereby providing insights into regional disparities in agricultural drought resilience.

2. Materials and Methods

2.1. Study area and period

The study focused on Jeollanam-do (South Korea) and Hwanghaenam-do (North Korea), two rice-producing provinces repeatedly affected by severe droughts. The analysis covered 2008–2017, encompassing major extreme drought events reported by the National Drought Information Portal (drought.go.kr) and the Food and Agriculture Organization (FAO).

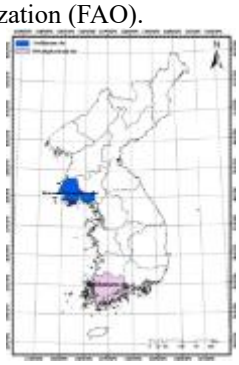

Figure 1. Study area: Jeollanam-do in South Korea and Hwanghaenam-do in North Korea

2.2. SPI calculation

Extreme drought events were identified using the Standardized Precipitation Index (SPI). CHIRPS precipitation data (5 km) were resampled to 500 m to match MODIS datasets. SPI-3 was selected as the most suitable timescale for agricultural drought monitoring in rice paddies(Park et al., 2009), and drought severity was categorized into five classes D0-D4 (Svoboda et al., 2002).

2.3. Cropland extraction

Cropland areas were delineated from the MODIS MCD12Q1 land cover dataset based on the International

Geosphere–Biosphere Programme (IGBP) classification. The 2024 dataset was applied as a reference mask to ensure spatial consistency across the Korean Peninsula.

2.4. NDVI analysis

MODIS NDVI data (500 m, 16-day intervals) were extracted for cropland areas using the MCD12Q1 mask. NDVI values corresponding to the 2015 extreme drought period were mapped to evaluate vegetation conditions in rice-growing regions.

2.5. Comparative assessment

Spatial patterns of NDVI and SPI were jointly analyzed within cropland areas to delineate drought-affected regions. Differences between Jeollanam-do and Hwanghaenam-do were interpreted as reflecting disparities in agricultural drought resilience, considering the buffering role of water-resource infrastructure such as reservoir storage and irrigation supply.

3. Results and Discussion

3.1. Cropland distribution

Figure 2(a) illustrates cropland areas delineated from the MODIS MCD12Q1 dataset. Jeollanam-do in South Korea and Hwanghaenam-do in North Korea were identified as major rice-producing regions highly vulnerable to extreme drought.

3.2. SPI-based drought conditons

Figure 2(b) presents SPI-3 distributions on October 16, 2015, applied to cropland areas. Results showed that Jeollanam-do experienced moderate drought conditions (SPI = –0.41), while Hwanghaenam-do was under severe drought stress (SPI = –1.70). These values highlight substantial differences in drought intensity between the two provinces during the same extreme drought period.

3.3. NDVI distribution under extreme drought

Figure 2(c) displays cropland NDVI values on October 16, 2015, derived from MODIS imagery. Jeollanam-do maintained relatively higher NDVI (0.554), indicating stronger vegetation vitality, whereas Hwanghaenam-do exhibited lower NDVI (0.424), reflecting reduced crop growth under severe drought. The contrast between SPI and NDVI responses suggests that water-resource infrastructure in South Korea contributed to buffering drought impacts.

3.4. Comparative interpretation

Table 1 summarizes the SPI-3 and NDVI values for the two provinces. The results demonstrate that, despite similar exposure to drought, Jeollanam-do sustained higher vegetation activity, likely due to irrigation systems and reservoir infrastructure, while Hwanghaenam-do exhibited severe vegetation stress in the absence of sufficient water-resource capacity. This combined interpretation of SPI and NDVI underscores the importance of infrastructural resilience in mitigating agricultural drought impacts.

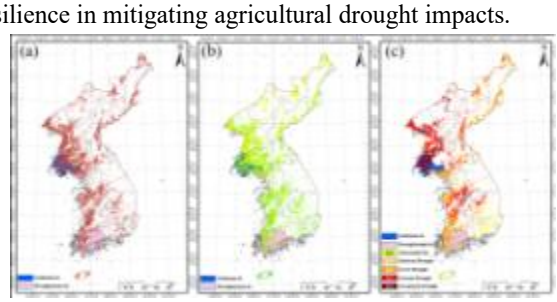

Figure 2. (a) Cropland distribution on the Korean Peninsula derived from MODIS MCD12Q1, (b) SPI-3 distribution on October 16, 2015, and (c) NDVI distribution on October 16, 2015, masked by cropland areas

Table 1. SPI-3 and NDVI values for Jeollanam-do and Hwanghaenam-do on October 16, 2015

Province	SPI-3	NDVI	Interpretation
Jeollanam-do	-0.41	0.55	Near-drought threshold / Relatively high vegetation vigor
Hwanghaenam-do	-1.70	0.42	Severe drought / Reduced vegetation vigor

4. Conclusions

This study compared the drought response capacities of South and North Korea under the representative extreme drought of 2015 by integrating cropland maps, SPI-3 indices, and NDVI imagery. The results demonstrated distinct regional disparities. As summarized in Table 1, Jeollanam-do recorded an SPI-3 of –0.41 and an NDVI of 0.554, suggesting relatively mild drought stress and resilient vegetation conditions. In contrast, Hwanghaenam-do exhibited an SPI-3 of –1.70 and an NDVI of 0.424, indicating severe drought and reduced vegetation vigor. These findings highlight that South Korea's water-resource infrastructure, including reservoirs and irrigation systems, played a critical role in buffering the impacts of meteorological drought, while North Korea's agricultural systems remained highly vulnerable. The combined use of SPI and NDVI proved effective in capturing these disparities, offering a practical framework for evaluating agricultural drought resilience on the Korean Peninsula. Future research will expand on this approach by incorporating NDVI change-rate analysis and lag-time correlations with SPI, enabling a more detailed understanding of temporal drought response mechanisms across different regions.

Acknowledgements

This work is supported by the Korea Agency for Infrastructure Technology Advancement (KAIA) grant funded by the Ministry of Land, Infrastructure and Transport (Grant RS-2022-00155763).

References

Park, J.S., and Kim, K.T., 2009. Evaluation of MODIS NDVI for drought monitoring: Focused on comparison of drought index. *The Journal of GIS Association of Korea,* 17(1), 117–129.

Polpanich, O., Bhatpuria, D., Santos, T.F.S., and Krittasudthacheewa, C., 2022. Leveraging multi-source data and digital technology to support the monitoring of localized water changes in the Mekong region. *Sustainability*, 14, 1739.

Svoboda, M., Lecomte, D., Hayes, M., Heim, R., Gleason, K., Angel, J., Rippey, B., Tinker, R., Palecki, M., Stooksbury, D., Miskus, D., and Stephens, S., 2002. The drought monitor. *Bulletin of the American Meteorological Society*, 83(8), 1181–1190.

Flood Damage Assessment in an Agricultural Irrigation Area with Motorized Gate Application

Daye Kim [1*], Ganghoon Lee [1], Seungwook Lee [2]

[1] Department of Agricultural & Rural Engineering, Chungbuk National University, 1 Chungdae-ro, Seowon-gu, Cheongju-si, 28644, Korea

[2] Chungbuk Research Institute, 102-1 Daesung-ro, Sangdang-gu, Cheongju-si, 28590, Korea

* Corresponding author. Email: kdy8462@naver.com

Abstract

On July 16, 2017, heavy rainfall caused flooding in an agricultural irrigation area in Goeun-ri, Cheongju, Korea, where a manual floodgate had previously failed due to corrosion and deterioration. This study evaluates flood damage before and after the installation of a motorized gate at the same location. Using water level data from the Cheongju gauging station and HEC-RAS modeling over a 15.9 km section of the river downstream from the gate, unsteady flow simulations were performed. The inundation area before installation was estimated at 141,309.3 m², while after the installation, no flooding was observed within the protected area. The findings suggest that motorized gate systems, especially when integrated with IoT-based disaster management platforms, can significantly mitigate flood risks in agricultural irrigation zones.

Keywords: Agricultural land inundation, Motorized floodgate, HEC-RAS, Flood simulation.

1. Introduction

On July 16, 2017, an extreme rainfall event resulted in significant inundation of agricultural areas in the upper reaches of the Musimcheon Stram. This event emphasized the need for resilient flood control infrastructure to mitigate damages from localized intense precipitation. Accordingly, this study applies HEC-RAS, a widely used one-dimensional hydrodynamic model, to estimate flood stages from the peak discharge. The spatial extent of inundation was then assessed for conditions before and after the installation of a motorized floodgate, enabling a comparative analysis of its effectiveness in mitigating floods.

2. Materials and Methods

2.1. Study area

The study area is located in Goeun-ri 655, Namil-myeon, Sangdang-gu, Cheongju-si, Chungcheongbuk-do, Korea, where agricultural land inundation occurred in the upper reaches of the Musimcheon Stream. The Musimcheon stream is a tributary of the Mihogang River, with a watershed area of 192.67 km², a channel length of 32.89 km, an average basin width of 5.86 km, a form factor of 0.18, a mean basin elevation of EL. 150.52 m, and an average basin slope of 24.29%. The basin exhibits a dendritic drainage pattern.

Along the right-bank levee of the study site, a manually operated floodgate had been installed. However, the structure had exceeded its design service life and was severely corroded, ultimately failing several years prior to this study.

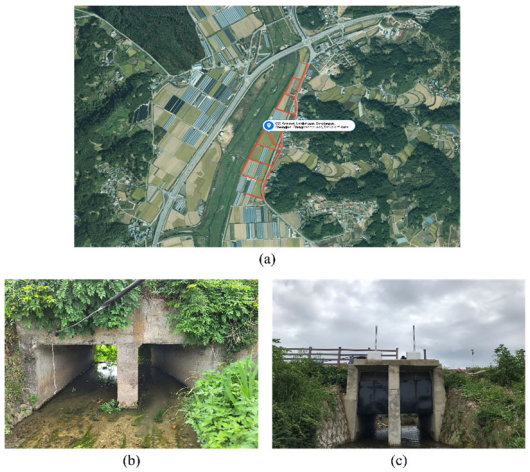

Figure 1. Location and installation status of the motorized floodgate: (a) Location of the motorized floodgate installation; (b) Before installation; (c) After installation.

2.2. Methods

The methodology of this study followed four steps.

First, data collection focused on topographic, hydrological, and land use characteristics of the Musimcheon Stram basin. These were used to set up input parameters for the HEC-RAS model. Second, the one-dimensional hydrodynamic model HEC-RAS was applied to estimate flood stages, with input data and boundary conditions set upto include channel geometry, discharge data, and hydraulic structures. Third, the model was run to generate unsteady flow simulations, producing spatial distributions of water surface elevations and inundation areas. Finally, the simulation results were analyzed to compare agricultural land inundation before and after installation of the motorized floodgate.This analysis provided an assessment of the flood mitigation effectiveness of the new system.

2.3. Collection of basic data for the study area

The Musimcheon Stram basin does not contain a meteorological station, so hydrological data were obtained from the nearby Cheongju Meteorological Observatory, which is operated by the Korea Meteorological Administration. To examine changes in river stage,

records from the Cheongju water level gauging station were analyzed. During the flood event of July 15–16, 2017, the maximum water level reached 5.52 m, accompanied by a peak discharge of 1,028.50 m³/s. A comparison between the design flood stage and the observed peak stage indicated that the design flood stage was EL.42.19 m, while the observed maximum was EL.41.95 m, resulting in a difference of 0.24 m.

2.4. Setup of HEC-RAS input data and boundary conditions

For the hydraulic simulation, the study reach extended approximately 15.87 km downstream from Goeun-ri 655 to the Heungdeokgyo water level station. Input data for the HEC-RAS model were classified into topographic and hydraulic datasets. Topographic information included longitudinal and cross-sectional profiles, structural details, and Manning's roughness coefficients, which were obtained from the Miho–Musimcheon Stram Master Plan (Ministry of Land, Infrastructure and Transport, 2019). Hydrological data comprised hourly stage and discharge records collected from the Heungdeokgyo gauging station, operated by the Ministry of Environment and accessible through the Geum River Flood Control Office.

The modeled reach was defined from station No.0 to No.15+871, consisting of 96 cross-sections. For unsteady flow simulations, boundary conditions were assigned as upstream inflow, lateral inflow, and downstream stage.

3. Results and Discussion

3.1. Results of HEC-RAS simulations

The HEC-RAS simulation for the flood analysis reach showed that, during the July 2017 flood event, maximum water surface elevations at individual cross-sections ranged from EL.41.92 m to EL.66.29 m, indicating spatial variation along the reach.

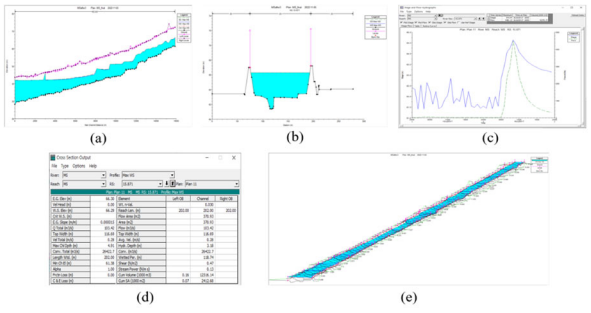

Figure 2. Results of HEC-RAS simulations: (a) Longitudinal water surface profile; (b) Cross-sectional water surface profile; (c) Hydrograph at the simulation point; (d) Maximum water surface elevation at the floodgate site; (e) Longitudinal distribution of maximum water surface elevation along the study reach.

3.2. Analysis of Agricultural Irrigation Area Inundation Before and After Motorized Floodgate Installation

At the Goeun-ri 655 cross-section, where the motorized floodgate was installed, the maximum water surface elevation during the simulated flood event reached EL.66.29 m. Using this elevation as the reference level, inundation extents were delineated for both pre- and post-installation conditions.

The flood simulation results indicated that, before the installation of the motorized floodgate, the inundated area within the protected zone covered 141,309.3 m². After installation, however, inundation in this zone was effectively eliminated, demonstrating the substantial flood mitigation effect of the motorized floodgate for the Goeun-ri agricultural irrigation area.

Figure 3. Comparative inundation analysis before and after motorized floodgate installation: (a) Inundation area before installation; (b) Inundation area after installation.

3.3. Discussion

The inundation analysis in this study was conducted only based on hydrological conditions, particularly observed water level and discharge records. Since hydraulic conditions such as channel roughness, structural characteristics, and local flow dynamics were not incorporated, the results could differwhen such factors are considered. Therefore, future studies should include hydraulic parameters to provide a more comprehensive assessment of inundation impacts.

Moreover, integrating the motorized floodgate system with emerging IoT-based monitoring technologies and linking it to municipal disaster management platforms could enhance flood resilience. Such integration would enable real-time monitoring and automated gate operations, thereby contributing to the reduction of similar inundation damages in agricultural irrigation areas.

4. Conclusions

Based on HEC-RAS simulations of the July 2017 flood, inundation extents were compared before and after the installation of a motorized floodgate at Goeun-ri 655. The analysis revealed that, before installation, the protected zone was inundated over an area of 141,309.3 m², whereas after installation inundation was effectively eliminated, demonstrating the flood mitigation benefit of the motorized floodgate. This result indicates that motorized floodgates, when integrated into local water management practices, can effectively support disaster risk reduction in agricultural irrigation areas.

Acknowledgements

This work was supported by Korea Institute of Planning and Evaluation for Technology in Food, Agriculture and Forestry(IPET) through Intelligent Agricultural Infra Management for Climate Change Development Program, funded by Ministry of Agriculture, Food and Rural Affairs(MAFRA)(RS-2025-02215604).

References

Investigation into effects of aging degradation of rice husk envelope of subsurface drainage for paddy fields on water conductivity at entrance of drainpipe

Yuji Kagei [1], Shuichiro Yoshida [1], Kazuhiro Nishida [1]

[1] Graduate School of Agricultural and Life Sciences, The University of Tokyo, Tokyo, Japan

* Corresponding author. yujikagei@g.ecc.u-tokyo.ac.jp

Abstract

The quantitative analyses of the water conductivity at the connecting areas of the ceramic drainpipe were conducted by using the real scale model of the connecting area of subsurface drainage system to simulate water conductivity reduction due to clogging at the area. The mixture of rice husk and bentonite were filled in the connecting area of ceramic drainpipes as densely as possible. Also, saturated hydraulic conductivity of the mixture under the predefined compression pressure were measured by falling head method.

As the mixture ratios of bentonite to rice husk (B-R Ratio) increased, the bulk densities of the mixture of bentonite and rice husk increased, lowering the conductivity under the equipment and the falling head method. The relationship formulae between the mixture ratios (B-R Ratio) and the bulk densities were derived based upon the experimental results. Furthermore, the approximation of water conductivity to dry density was derived under the equipment and the falling head method. It is implied that the conductivity of equipment and falling head method that can be estimated by the approximation formulae deviates by less than one order of magnitude.

Keywords: Subsurface Drainage, Conductivity, Density, Approximation

1. Introduction

The poor drainage is a major obstacle to enhance upland crop productivities in paddy fields. One of the solutions is to install a subsurface drainage system in the fields. Numerous reports have pointed out that deterioration of the subsurface drainage has been attributed to the subsidence and degradation of the filler and envelope materials and reappearance of plow pan above it. However, clogging at the interface between the rice husk envelope and ceramic drainpipes (near the drainpipe fittings) was recently found by the laboratory experiments as well as in-situ observations.

Fig.1 Clogging at the interface between the rice husk envelope and ceramic drainpipes

This research aims to clarify the quantitative effect of the clogging of the degraded rice husk envelope in the drainpipe fittings, i.e., entrance gaps for water, on drainage efficiency of the subsurface drainage system.

2. Materials and Methods

The mixtures of bentonite and rice husk were used as model of aging envelope and filler. The granulation through decomposition was reproduced by crushing rice husk. The cumulative weights of uncrushed rice husk and crushed one through a 1 mm sieve were 20% and 80%, respectively. Also, the soil contamination was reproduced by adding bentonite. The bentonite rice husk ratio (B-R Ratio) was defined as bentonite dry weight divided by rice husk dry weight. The B-R Ratio was set between 0.0 and 5.0. The experiment conditions were the combinations of uncrushed/crushed rice husk and the B-R Ratio (Table 1).

Table 1 Experiment Conditions

	Bentonite Rice Husk Ratio ω										
	0.0	0.1	0.2	0.5	0.6	0.7	0.8	1.0	2.0	3.0	5.0
Not Crushed Rice Husk	✓			✓	✓	✓	✓	✓	✓		✓
Crushed Rice Husk	✓	✓	✓	✓				✓	✓	✓	

The conductivity was measured by two methods. One was the equipment imitating the connecting area of ceramic drainpipe (Fig.1). The purpose of the equipment was to reproduce clogging at the connecting area. The mixture of bentonite and rice husk were filled in the space at the connecting area as densely as possible. The conductivity of the equipment was calculated in Eq (1) where *ke* is the apparent conductivity reflecting narrow channels at the connecting area and A denotes the area of the cylindrical gap at the fitting filled with the mixture.

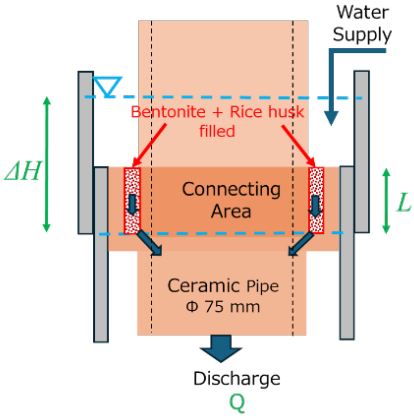

Fig.2 Equipment imitating the connecting area

$$k_e = \frac{Q}{A}\frac{L}{\Delta H} \qquad (1)$$

The other was falling head method for comparing the

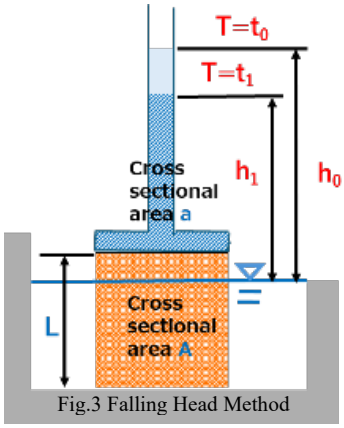

Fig.3 Falling Head Method

conductivity *ke* (Fig.2).

The conductivity by falling head method was calculated in Eq (2) where *kf* is the conductivity of falling water head method.

$$k_f = \frac{aL}{A}\frac{ln\left(\frac{h_0}{h_1}\right)}{t_1 - t_0} \qquad (2)$$

3. Results and Discussion

3.1. Discharge of Equipment (Fig.4)

As the B-R Ratio increased, the discharge of the equipment decreased. The decrease in the discharge by the bentonite addition was more remarkable for the crushed rice husk. It is presumed that water path is not completely clogged by the bentonite when the rice husk is not crushed and kept elastic macro-pore structure.

Taking account of the desired discharge of subsurface drain as per the engineering specifications in Japan, the desired discharge is 1.0×10^{-2} m^3 h^{-1}. The discharge under the crushed rice husk was below the desired level. On the other hand, the discharge under the uncrushed rice husk was below the desired level when the B-R Ratio was more than 0.5.

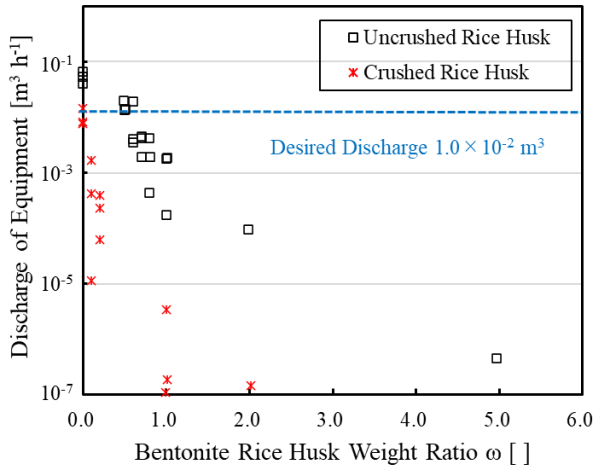

Fig.4 B-R Ratio and Equipment Discharge

3.2. B-R Ratio and Density at Equipment (Fig.5)

The dry bulk density of the bentonite and husk mixture filled in the equipment was increased with the ratio of bentonite.

Also, the crushed husk and bentonite mixture was more compressible than the uncrushed one. Furthermore, it was found that the relationship between dry bulk density and bentonite rice husk weight ratio ω followed exponential function.

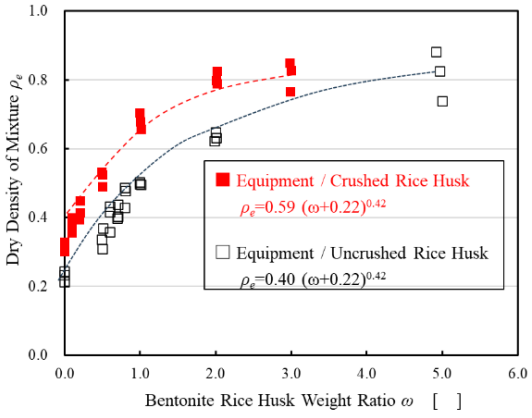

Fig.5 Bentonite Rice Husk Weight Ratio and Density

3.3. Conductivity and Density of Bentonite and Rice Husk (Fig.6)

The conductivities, k_e and k_f, were decreased when the densities of bentonite and rice husk were increased both for crushed and uncrushed conditions.

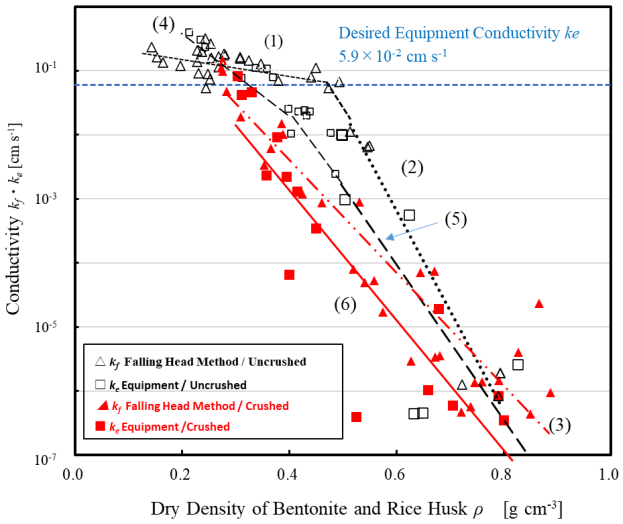

Fig.6 Dry Density and Conductivity

The approximation formulae were derived under the equipment and the falling head method (Table 2).

Table 2. Approximation for Conductivity

#	Rice Husk	Method	Approximation Line	R^2
(1)	Uncrushed	Falling Head	$\log_{10}kf=-1.1\rho-0.6$	0.27
(2)	Uncrushed	Falling Head	$\log_{10}kf=-15.6\rho+6.2$	0.96
(3)	Uncrushed	Equipment	$\log_{10}ke=-6.6\rho+1.1$	0.87
(4)	Uncrushed	Equipment	$\log_{10}ke=-12.1\rho+3.2$	0.54
(5)	Crushed	Falling Head	$\log_{10}kf=-8.6\rho+1.0$	0.87
(6)	Crashed	Equipment	$\log_{10}ke=-10.2\rho+1.2$	0.81

If the dry bulk density of the husk filled in the pipe fittings exceeds 0.3 g cm^{-3}, the apparent conductivity *ke* does not meet the desired level of 5.9×10^{-2} cm s^{-1}.

For the uncrushed husk, the difference between *ke* and *kf* is within one order of magnitude. On the other hand, for the crushed husk, the difference between *ke* and *kf* gets wider up to approximately one order of magnitude as the dry bulk density is increased.

4. Conclusions

As the mixture ratios of bentonite to rice husk (B-R Ratio) increased, the bulk densities increased, lowering the conductivity under the equipment and the falling head method. Furthermore, the approximation formulae of conductivity to dry density were derived under the equipment and the falling head method. It is implied that the conductivity of equipment and falling head method that can be estimated by the approximation formulae deviates by less than one order of magnitude.

Smart Agricultural Irrigation Enhances Management Efficiency

Tsai, Ming-Dou *

Engineer of Water Resources Agency (WRA), Ministry of Economic Affairs (MOEA), Taiwan

* Corresponding author. Email: A620160@wra.gov.tw

Abstract

Agricultural irrigation in Taiwan has traditionally relied on manual operations and empirical knowledge. In recent years, smart irrigation technologies have been gradually introduced to enhance management efficiency. By establishing a smart irrigation information management platform, real-time data such as channel water levels and flow rates are collected via sensors. The data is then analyzed using smart algorithms to automatically regulate gates and optimize water allocation. Managers can monitor irrigation conditions and perform remote operations through mobile phones or tablets, achieving the objectives of reducing labor requirements, minimizing response time, and enhancing the precision of water distribution.

Keywords: agricultural irrigation, smart irrigation

1. Introduction

Traditional enhanced irrigation management already has a well-developed water distribution plan and personnel experience, but it still relies on manual inspection, operation, and analysis. However, with challenges such as the gradual aging of management staff, smart agricultural irrigation plays an increasingly important role. By leveraging intelligent management platforms, the system can automatically collect and record irrigation data, issue warning notifications, and provide remote control or automatic regulation functions, thereby supporting and enhancing agricultural irrigation management.

2. Materials and Methods

2.1. Research scope

2.1.1 Test area

The Chianan Irrigation Area, located in the southwestern plains of Taiwan, covers 80,000ha, boasts 1,400km of channels, 7,000 water gates, and 1,200 waterworkers. The area's actual annual water use has averaged 680 million m^3. The test area from 2017 to 2020 was 114 ha at the Longtian Station.

2.1.2 Promotion Area

The Longtian Station in Chianan Irrigation Area covers 1,300ha, has 336 water gates, 347 channel outflow points. The average actual irrigation water consumption of first rice crop was 12.25 million m^3. The promotion method is to selectively build 35 water supply automatic gates and 80 channel outflow monitoring points.

The Fuxing Channel in Kaohsiung Irrigation Area covers 1,900ha and has a length of 9.6km. The average actual irrigation water consumption of first rice crop was 9.16 million m^3. The promotion method is to build 25 automated gates along the entire main line.

2.2. Research methods

From 2017 to 2020, the test area was built automated control gates and water level or flow meters at the end of channels. The smart irrigation management platform was developed, which features real-time data collection, historical records, remote control, alert notifications, and support for mobile device operation. The gate control strategy is shown in Figure 1.

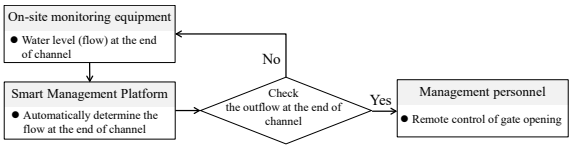

Figure 1. The monitoring and gate control strategy

Based on the test results, the system was extended to 1,300ha of the Longtian Station in Chianan Irrigation Area and 1,900ha of the Fuxing Channel in Kaohsiung Irrigation Area in 2024. A comparison of the gate control operations is shown in Figure 2.

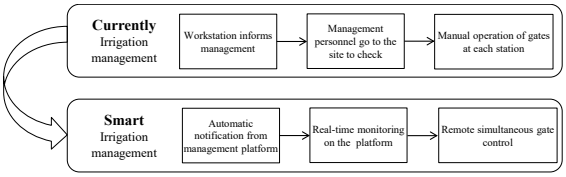

Figure 2. Comparison of gate control operations

2.3. Calculation formula

This study analyzes the expected water-saving benefits, which reflects the relationship between the outflow at the end of the channel and the actual irrigation water consumption. The formula is as follows:

$$E = C\frac{\Sigma I_{out}}{I_{in}} \quad (1)$$

E is the expected water-saving benefit, ΣI_{out} is the total outflow at the end of the channel, I_{in} is the actual irrigation water consumption, and C is the reduction coefficient of the difference in water delivery distance from the control gate to the end of the channel; C=0.9 in the test area.

This study analyzes the time-saving benefit to reflect the difference in operating time between remotely controlled gates and manually operated gates. The formula is as follow:

$$S = \Sigma M_t - \Sigma R_t \quad (2)$$

S is the time-saving benefit, ΣR_t is the total time of remote gate operation, and ΣM_t is the total time of manual gate operation. The time-saving by single gate operation at the Gangshan Station of Fuxing Channel is 1 hour as shown in Figure 3.

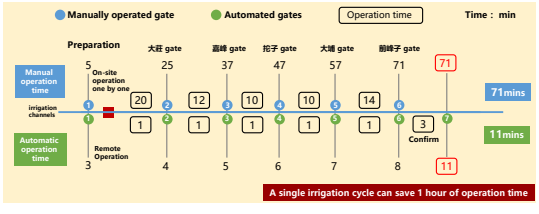

Figure 3. Remote gate operation benefit analysis

3. Results and Discussion

3.1. Test area

From 2017 to 2020, the expected water-saving benefits of the smart agricultural irrigation system were 3.6-6.3% in the first rice crop and 6.9-11.4% in the second rice crop, as shown in Table 1.

Table 1. the expected water-saving benefit

	2017	2018	2019	2020
I rice crop	-	4.9%	6.3%	3.6%
II rice crop	9.8%	10.7%	11.4%	6.9%

3.2. Promotion Area

3.2.1. Longtian Station in Chianan Irrigation Area

The ratio of automated gates and channel outflow monitoring at the Longtian workstation is shown in Table 2. During the first rice crop in 2025, gate openings and channel outflow information were automatically recorded every 5min, and gate operations were remotely 265 times, the time-saving was 35hr. The actual water consumption was 13.44 million m^3, and the monitored outflow was 73,000m^3, as shown in Figure 4. The outflow was relatively high in the early and late periods.

Table 1. The ratio of automated gates and channel outflow monitoring

	done	no-done	ratio
Auto. Gate	35	301	10.4%
Mon. Outflow	80	267	23.1%

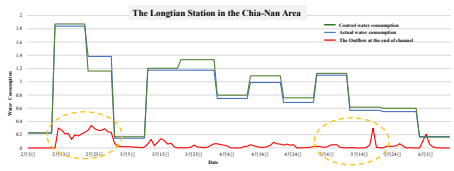

Figure 4. Monitoring results of the first phase of 2025

3.2.2 Fuxing Channel in Kaohsiung Irrigation Area

The Fuxing Channel main line was built 25 automated control gates in 2024. Its smart irrigation management platform has four operation modes as described below:

- General mode: remote control.
- Tracking mode: track branch line flow and adjust gate opening to meet, as shown in Figure 5.
- Linked mode: based on upstream flow, track and adjust gate opening.
- Special mode: if channel water level reaches warning value, automatically open gate.

During the first rice crop in 2025, gate openings and channel outflow information were automatically recorded every 10s, and gate operations were remotely 5,751 times, the time-saving was 758hr. The actual water consumption was 10.92 million m^3, achieving the control target of 11 million m^3.

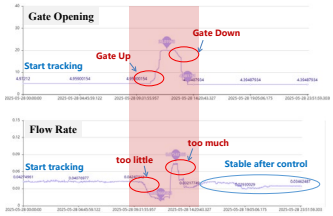

Figure 5. Tracking mode in Fuxing Area

3.3. Analyze

Due to the influence of effective rainfall in the Chianan Irrigation Araea, the expected water-saving benefits of the second rice crop are higher than the first rice crop. These benefits are positively correlated with the installation of automated gates and channel outflow monitoring. Therefore, new promotion sites should carefully evaluate gate water allocation, operation frequency, and manual operation time, and plan the construction sequence accordingly.

In the Kaohsiung Irrigation Area, the time-saving benefits are higher than in the Chianan Irrigation Area, as shown in Table 3. For new promotion sites, it could be first buildt automatic control gates on the main line and water level (flow) monitoring equipment, and then to be buildt automatic gates on waterways and water level (flow) monitoring equipment at the end of channels.

Table 3. Comparison of Chianan and Kaohsiung Area

	Auto. Gate	Remote control	Time-saving
Chianan	35	265	35hr
Kaohsiung	25	5,751	758hr

The smart irrigation management platform in the Kaohsiung Area provides four operation modes, gradually upgrading traditional manual operations to a smart control model. This approach can serve as a demonstration example for future promotion.

4. Conclusions

Smart agricultural irrigation can effectively improve efficiency and assist management, especially when gates are improved with automated control and remote monitoring. This can significantly save manpower, shorten operation time, and adapt the effects of aging managers. The promotion cases in Chianan and Kaohsiung irrigation Areas show that this technology has become more mature and feasible year by year. In the future, if it can be combined with more real-time monitoring information from irrigation areas, such as effective rainfall or field moisture content, and by analyzing historical irrigation water information, the irrigation water distribution operation model can be improved, it will help achieve the goals of energy saving and labor saving, real-time response and precise water supply in agricultural irrigation management.

Acknowledgements

Special thanks to Chianan and Kaohsiung Office of Irrigation Agency, Ministry of Agriculture for providing basic information on the irrigation area and related monitoring results.

References

Southern Region Water Resources Branch , Water Resources Agency (MOEA), 2017-2020, Improving Irrigation Water Saving Management Technique: A Case Study In Chianan Irrigation Area (Phase I-IV)

Nai-Fang Chou, et al., 2018, Journal of Water Resources Management Vol. 20, No. 1, Smart Water Management - Improving Field Irrigation Planning

Jih-Shun Liu, et al., Taiwan Water Conservancy Vo1. 70, No. 3, Investigations on the Application of Upgrading Irrigation Management with Internet of Things Technology

A Study on Establishing Appropriate Hydrological Design Frequency Criteria for Agricultural Reservoirs

So Euigeon・Yoo Seung-Hwan

Abstract

Recent climate change has intensified flood risks, altering design flood volumes and increasing heavy rainfall events by 225% in the last two decades. Downstream damage is escalating due to higher population density and land-use changes. While new flood volume estimation guidelines (2019) necessitate re-evaluating hydrological stability, current agricultural reservoir design lacks quantitative criteria for downstream conditions when applying the Probable Maximum Flood (PMF), despite having criteria for dam scale.

This study aims to establish PMF application criteria for small and medium-sized reservoirs by analyzing domestic and international approaches to downstream damage risk assessment (human and property). We propose quantitative criteria for human and property damage to be incorporated into domestic design standards, evaluating their economic feasibility and validity. This research will provide scientific, quantitative PMF criteria to support flood control capacity enhancement and revisions to agricultural embankment dam design standards.

Post-earthquake Deformation Detection in Drainage Wells by UAV-LiDAR for Prevention of Secondary Disasters in Paddy Field

Kazuma Shibano [1*], Hiromu Tanaka [1], Kazunari Inaba [2] and Tetsuya Suzuki [2]

[1] Graduate School of Science and Technology, Niigata University, Niigata 950-2181, JAPAN

[2] Institute of Agriculture, Niigata University, Niigata 950-2181, JAPAN

* Corresponding author. Email: kazuma3267@gmail.com

Abstract

Drainage wells serve as critical landslide prevention facilities in paddy agricultural regions, controlling groundwater levels during heavy rainfall. The 2024 Noto Peninsula earthquake (Mj7.6) caused significant damage to these structures, necessitating rapid assessment methods for secondary disasters such as landslides and paddy field erosions. This study develops a non-contact deformation detection methodology using UAV-LiDAR point clouds to identify structural damage in earthquake-affected drainage wells. Three drainage wells with depths ranging from 4.8m to 30.1m were investigated using DJI Matrice 350 RTK equipped with Zenmuse L1 LiDAR system. The multiple return capability enables point cloud acquisition through expanded metal lids and vegetation cover. Cylinder detection algorithms using RANSAC framework are applied to estimate well dimensions and establish reference geometries. Deformation detection is achieved by calculating distances between detected cylinder primitives and actual point clouds. Identification of vertical stiffener deformation and well curb damage were successful using distances between detected cylinder primitives and actual point clouds. Inward deformation of vertical stiffeners is detected using a -0.300m threshold, while outward deformation of well curbs is identified with a 0.200m threshold. The method effectively distinguished between damaged and undamaged structural elements, with detection accuracy comparable to conventional inspection methods, however, significantly reducing labor requirements and safety risks. This non-contact approach provides quantitative assessment capabilities essential for post-earthquake evaluation of landslide prevention infrastructure. The technology enables rapid damage assessment to prevent secondary disasters such as landslides and paddy field erosions.

Keywords: Point clouds processing, Primitive detection, RANSAC (Random Sample Consensus), Landslide

1. Introduction

This study addresses critical challenges in post-earthquake inspection of landslide prevention facilities. Drainage wells are essential for preventing landslides by lowering groundwater levels, however earthquakes can damage these facilities through shear destruction, potentially triggering secondary hazards. Traditional inspection methods face significant limitations: scarcity of expert engineers, difficulties accessing wells for measurements, time-consuming procedures, and unclear decision-making protocols. After disasters like the 2024 Noto Peninsula earthquake, conventional on-site inspections become impractical due to accessibility issues and the widespread distribution of facilities requiring urgent assessment. Therefore, this study develops a UAV-LiDAR-based non-contact deformation detection method to enable rapid, accurate evaluation of drainage well conditions without requiring expert personnel or dangerous site access, ensuring timely maintenance decisions for landslide prevention.

2. Materials and Methods

This study conducted UAV-LiDAR surveys on three drainage wells damaged by the 2024 Noto Peninsula earthquake in Ishikawa prefecture, Japan. The LiDAR's multiple return capability enables point cloud acquisition of well interiors even through overhead vegetation by capturing laser pulse reflections from different surfaces. Using RANSAC-based cylinder detection algorithms (Figure 1), the method quantitatively evaluates structural deformation by analyzing distance between point clouds and geometric primitives. The process begins by randomly selecting two points from the input point cloud and calculating normal vectors at each point. The cylinder's axis direction is determined through the cross product of these normal vectors, with nearly parallel pairs being discarded during sampling. Two parametric lines are created passing through the selected points along their normal directions. These lines are projected onto an axis-perpendicular plane to determine the cylinder's center,

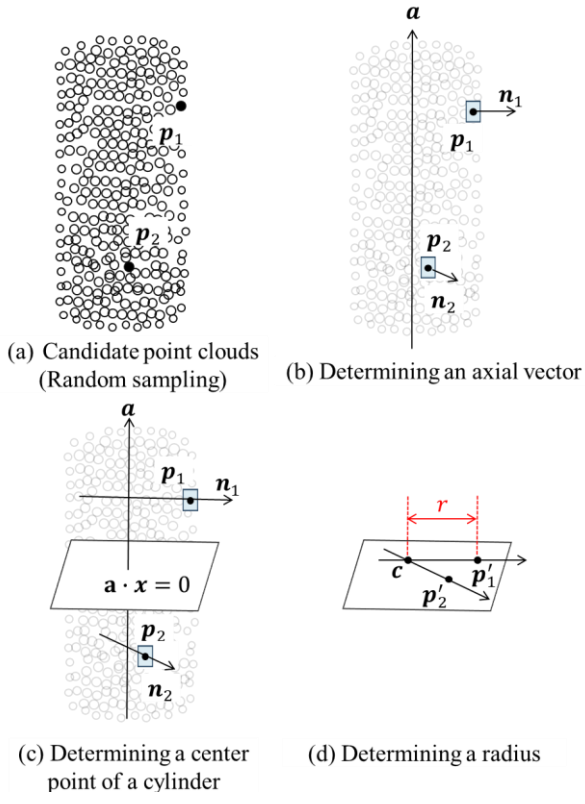

(a) Candidate point clouds (Random sampling)

(b) Determining an axial vector

(c) Determining a center point of a cylinder

(d) Determining a radius

Figure 1. Primitive detection.

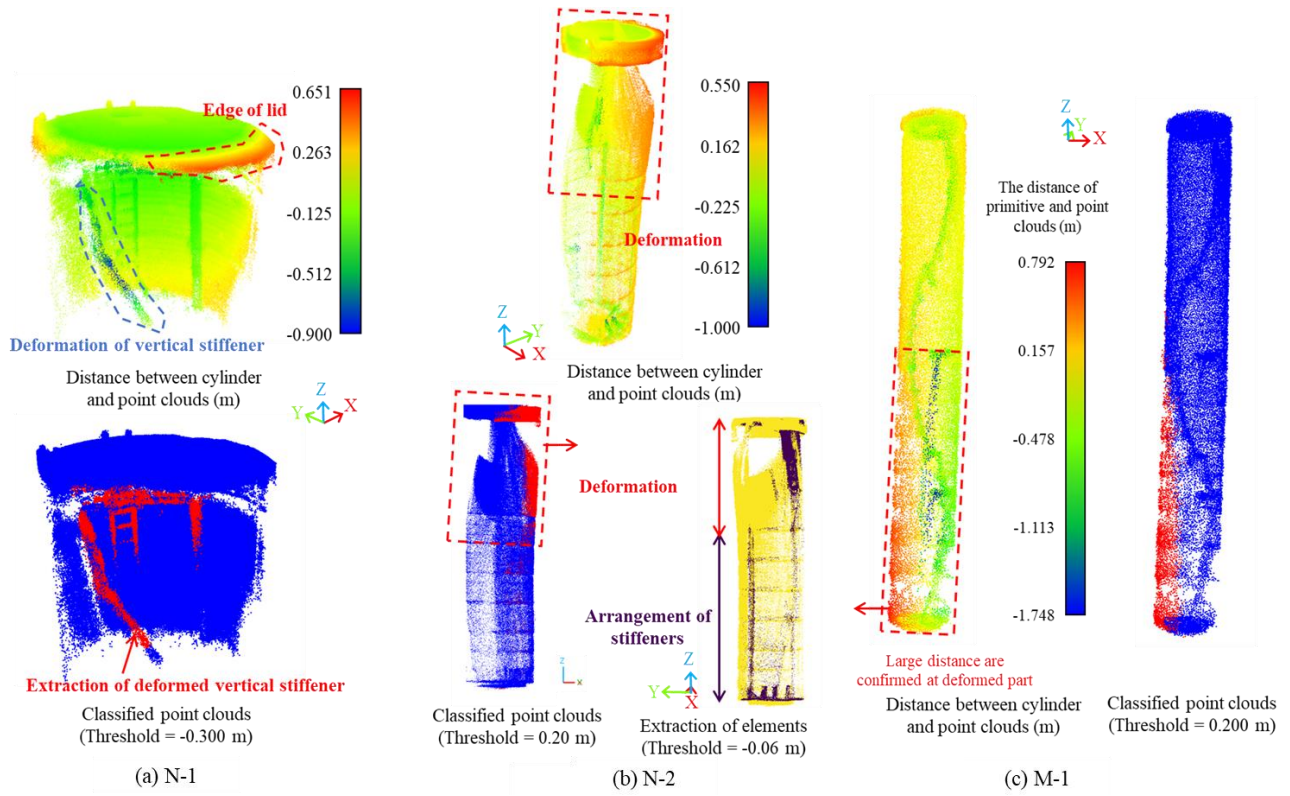

Figure 2. Deformation detection results for the three investigated drainage wells.

which satisfies both parametric equations and the plane equation. The cylinder's radius is computed as the distance from the center to the projected sampled point in the orthogonal plane, while height is estimated as the maximum distance between points along the axis direction. Model verification involves evaluating distance error (difference between point cloud points and the estimated model) and normal error (angular difference between point normals and cylinder surface normals). Points with errors below a threshold are classified as "inliers," while those with larger errors become "outliers." The model with maximum inliers after a predefined number of iterations is selected as the best fit. Three wells with different characteristics were investigated: N-1 showed severe shear fracture and missing components, while N-2 and M-1 appeared undamaged during visual inspection, demonstrating the method's applicability across various damage conditions.

3. Results and Discussion

For the severely damaged N-1 well, inward deformation of vertical stiffeners ranges from -0.125m to -0.900m, with distances decreasing farther from the well curb. Through threshold optimization comparing false positives in normal areas versus false negatives in deformed regions, a -0.300 m threshold successfully extracts deformed vertical stiffeners, though some false positives occur at upper ladders and normal stiffeners due to inaccurate cylinder detection caused by northeastern inclination. Considering cylinder detection accuracy and equipment dimensions, the 0.3 m threshold proves acceptable for extracting inward deformation in wells with missing sections (Shibano and Suzuki, 2025). For N-2, large distances in the upper well curb indicate outward deformation toward the northwest exceeding 0.162 m. Both N-2 and M-1 use a 0.20 m threshold for deformation extraction, with 0.1 m causing false positives and 0.3 m increasing false negatives. N-2's superior cylinder detection results from more complete point clouds. The deformation pattern suggests direct external forces without vertical stiffener involvement, as extracted stiffeners using -0.06 m threshold shows no overlap with deformation areas. M-1 exhibits deformation in the lower well curb toward the southwest, appearing as mid-level bending with undetermined causation. The study concludes that distance calculations between detected cylinders and point clouds effectively identify both vertical stiffener and well curb deformations. Optimal thresholds are -0.300 m for inward deformation detection and 0.200 m for outward deformation in typical drainage wells, providing a practical framework for automated damage assessment.

4. Conclusions

This study develops a UAV-LiDAR method for non-contact damage detection of earthquake-damaged drainage wells using RANSAC-based cylinder detection. Testing on three wells after the 2024 Noto Peninsula earthquake establishes optimal thresholds: -0.300 m for inward deformation and 0.200 m for outward deformation detection.

Acknowledgements

The authors are grateful to Tsuyoshi Okayama (Oku-Noto Agriculture and Forestry General Office, Ishikawa prefecture) for cooperating with the site investigation.

References

Shibano, K. and Suzuki, T., 2025. Non-contact damage detection of drainage wells during the Mj7.6 Noto Peninsula earthquake by UAV-LiDAR technique. Measurement, 117610.

Vulnerability Assessment of Agricultural Water Resources and Irrigation Reservoirs Using Multi-Model Ensembles Based on SSP Scenarios

Kim Hayoung・Na Ra・Joo Donghyuk・Yoo Seung-Hwan・So Euigeon

Abstract

As the climate crisis intensifies, extreme weather events-such as heatwaves, tropical nights, droughts, and floods-are becoming more frequent and severe, resulting in escalating agricultural damages. Climate change continues to shift crop-suitable zones, reduce agricultural water availability, increase pest and disease outbreaks, and intensify wildfires and landslides. However, the irregular and sporadic nature of these climate-induced agricultural disasters complicates forecasting and preparedness. Given the significant impact on agricultural productivity and food security, accurate projections of future climate scenarios and targeted adaptation strategies are essential. Global Climate Models (GCMs), widely used for climate scenario analysis, often yield divergent projections due to differences in climate system representation and parameterization. Relying on a single model risks embedding model-specific biases into policy. Therefore, multi-model analyses are necessary to strengthen the robustness of climate-informed decision-making. The Multi-Model Ensemble (MME) approach integrates outputs from various GCMs to offset individual biases and reduce uncertainty, offering more reliable estimates of mean climate conditions. However, this averaging process may underrepresent extremes such as droughts or floods. In this study, we analyzed 18 individual GCMs and their ensemble outputs under IPCC's Shared Socioeconomic Pathways (SSPs). We conducted vulnerability assessments for irrigation and flood control across all 167 administrative districts in the Republic of Korea, identifying spatially vulnerable regions. By addressing both model uncertainty and sensitivity to extreme events, this study provides a scientific basis for formulating adaptive agricultural policies and climate-resilient strategies to respond to future climate variability.

Estimation of Crack Width for Agricultural Infrastructure by Multimodal Approach with Point Cloud and Image Data Integration

Keika Tagami [1*], Hiromu Tanaka [2], Kazuma Shibano [2] and Tetsuya Suzuki [3]

[1] Faculty of Agriculture, Niigata University, Niigata, 950-2181, JAPAN

[2] Graduate School of Science and Technology, Niigata University, Niigata, 950-2181, JAPAN

[3] Institute of Agriculture, Niigata University, Niigata, 950-2181, JAPAN

* Corresponding author. Email: a22n096a@mail.cc.niigata-u.ac.jp

Abstract

This study presents an innovative multimodal approach for detecting and measuring crack dimensions in agricultural infrastructure. Integration of UAV-based point cloud and digital image analysis contributes to enhancement of meaningful information. Conventional crack detection methods have focused on extraction of crack features by image-based approaches. Adding point cloud with scale information enables estimation of crack dimensions. In this study, LiDAR and image capturing were conducted on a rural road in Niigata, Japan, using a DJI Matrice 350 RTK equipped with Zenmuse L1 sensor. Ground Sample Distance (GSD) is calculated by matching UAV image coordinates with point cloud data using kd-tree algorithms, enabling precise crack width estimation from digital images. The methodology involves coordinate transformation from WGS84 to UTM Zone 54N projection system, followed by nearest neighbor point matching to determine UAV altitude for each image. Crack widths were measured at 24 points using smartphone images, with three measurements per crack for validation. Thus, results demonstrate strong correlation between predicted and measured crack widths with R-squared of 0.948, with all predictions falling within ±1mm accuracy range. Smartphone images achieve higher precision with ground sampling distance of 0.023 cm/pixel and standard deviation of 0.154 mm compared to UAV images showing ground sampling distance of 0.195 cm/pixel and standard deviation of 0.618 mm. The multimodal approach combining point cloud and images indicates versatility for diverse applications including irrigation channels, drainage systems, concrete structures, and other agricultural facilities.

Keywords: UAV, GPS, GSD, EXIF information

1. Introduction

In recent years, a lot of attempts have been made toward automatic damage detection in agricultural infrastructure facility as an alternative to visual inspection. Our previous studies have investigated mechanisms for detecting crack width from images using deep learning (Tanaka et al, 2025). In bridge, crack width is used as performance indicators (AASHTO, 2024). Therefore, conversion from detected cracks in images to actual scale is necessary for practical applications. In this study, the Ground Sample Distance (GSD) is calculated by determining the capture altitude of each image from point cloud data acquired by UAV and EXIF (Exchangeable Image File Format) information of the images. By providing scale information to images using GSD, an attempt is made to estimate actual crack width from crack width in images.

2. Materials and Methods

2.1. Target structure and measurement methods

In this study, a survey was conducted on the Tochikura bridge which is located in Kashiwazaki city, Niigata prefecture. Tochikura bridge is a two-span continuous steel plate girder bridge that began service in 1996. Visible images and point cloud data were acquired using Zenmuse L1 (DJI) mounted on Matrice 350 RTK (DJI), which is the UAV used for measurement. The technical specifications of Zenmuse L1 are as follows: focal length of 8.8 mm, image resolution of 5,472×3,468 pixels, and sensor size of 13.2×8.8 mm. In UAV measurement, to maintain consistent conditions at an altitude where both ends of the bridge are visible, the flight was conducted at an altitude of approximately 5 m above the ground surface. For crack width measurement, 24 cracks were photographed at close range using a camera mounted on a smartphone iPhone SE (3rd generation). The crack width was measured at three locations for each crack. GSD is used when estimating crack width from images. The derivation formula for GSD is shown in Equation (1).

$$GSD = \frac{H \times \frac{SW}{ImW}}{F} \times 100, \quad (1)$$

where GSD is ground pixel dimension (cm/pixel), H is UAV altitude (m), SW is sensor size (mm), ImW is image size (pixel) and F is focal length (mm). GSD is an index representing the ratio between the length of one pixel and the actual length, and serves as a reference for identifying crack width from images.

2.2. Analysis procedure

GSD is calculated by matching the coordinates of images and point cloud data acquired by UAV and determining the altitude from the ground surface to the UAV for each image. The GSD of smartphone images is obtained from the pixel ratio between UAV images and smartphone images, and the actual crack width is calculated from the number of pixels of crack width and GSD, then compared with measured values. An overview of the GSD calculation method using UAV is shown in Figure 1. For coordinate matching, the coordinate system of images is converted from the geographic coordinate system WGS84 to the projected coordinate system UTM Zone 54N, which is the coordinate system of point cloud data. A kd-tree is used for matching coordinates between point clouds and images to find the nearest point from the coordinates of each image. The kd-tree search method is shown in Figure 2. A kd-tree is a method that divides multidimensional space and converts it into a binary tree structure, enabling efficient search for the nearest neighbor point of any point from point clouds. The altitude from the

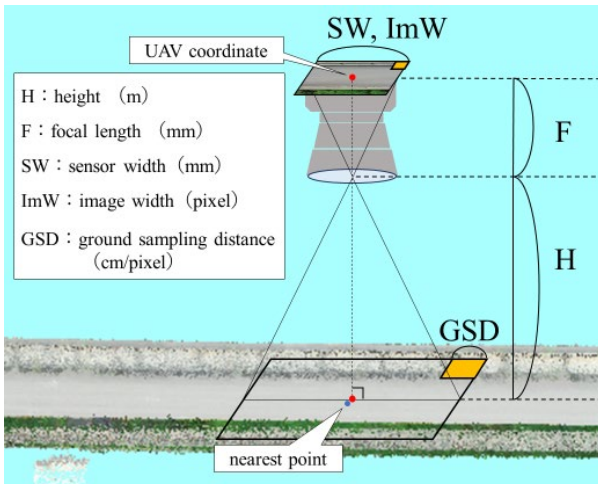

Figure 1. Diagrammatic illustration of calculation method for GSD using UAV image.

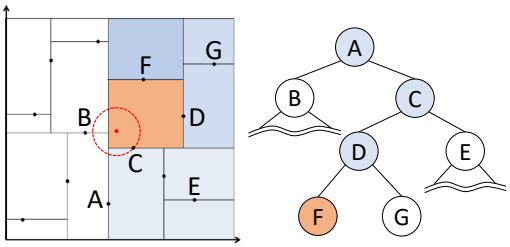

Figure 2. Diagrammatic illustration of kd-tree.

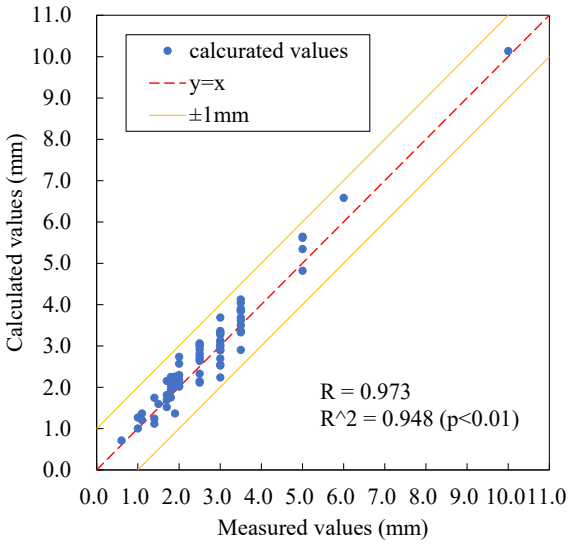

Figure 3. Relationship between calculated and measured values.

Table 1. Basic statistics of GSD and prediction error

Type of data	GSD (cm/pixel)		Prediction error (mm)	
Equipment	UAV	Smartphone	UAV	Smartphone
Mean	0.195	0.022	0.521	0.017
Median	0.194	0.022	0.425	0.129
Standard deviation	0.025	0.005	0.436	0.154
Max	0.241	0.027	2.174	0.596
Min	0.155	0.017	0.013	0.001

target point to the UAV is determined by the altitude difference between the matched image and the nearest neighbor point, and the GSD of UAV images is calculated from the obtained altitude and camera parameters. The GSD of smartphone images is calculated by using UAV images corresponding to each smartphone image and determining the pixel ratio for the same distance. For pixel measurement, distortion correction UAV images by calibration are used, and projective transformation is performed based on the UAV images. The locations measured in the field are identified from smartphone images, and the number of pixels of crack width is recorded using ImageJ. The predicted crack width is calculated from the obtained number of pixels and GSD, and compared with measured values.

3. Results and Discussion

The prediction results of crack width obtained by GSD estimation of smartphone images are shown in Figure 3. Figure 3 shows the relationship between predicted and measured values in a scatter plot, indicating the range where the error is 0 and within ±1 mm from that point. The correlation coefficient is 0.973 and the coefficient of determination is 0.948 ($p<0.01$), showing a strong positive correlation. Since the crack scale used to measure the crack width is in 0.5 mm increments in the range of 2~3 mm, detailed measurements in 0.1 mm increments are not possible. By measuring in 0.1 mm increments for all ranges, the variation in the range of actual values in the range of 2~3 mm is suppressed, and the coefficient of determination is thought to be larger than the current value. All predicted values fall within the error range of 1 mm. The statistical values of GSD and prediction error for UAV and smartphone images are shown in Table 1. GSD data consist of 15 UAV images and 24 smartphone images. The average GSD of UAV images is 0.195 cm/pixel, and the average GSD of smartphone images is 0.022 cm/pixel. The GSD of smartphone images is smaller than that of UAV images, enabling more accurate estimation of crack width. The standard deviation prediction error of UAV images is 0.436 mm, while that of smartphone images is 0.154 mm, suggesting that smaller GSD results in smaller error. In this prediction value calculation method, an objective method should be considered because it is prone to subjective human error when measuring the crack width on the image.

4. Conclusions

In this study, GSD estimation is performed using point cloud data and EXIF information of images to predict crack width. As a result, it is suggested that crack width can be predicted by GSD estimation from the altitude between the ground surface and UAV.

References

American Association of State Highway Officials (AASHTO). 2024. LRFD Bridge Design Specifications, Tenth Edition, p24.

Tanaka, H., Shibano, K. and Suzuki, T., 2025. Scene classification-assisted deep learning for crack detection in asphalt pavements. *Case Studies in Construction Materials,* **23**, e05064. DOI: https://doi.org/10.1016/j.cscm.2025.e05064.

Estimation of irrigation water quality and the effects of abrasion and leaching on water quality

Kanehira shusuke

Iwate Prefecture Land Improvement Association, 2-10-1 Motomiya, Morioka City, Japan

* Corresponding author. Email: kanehira_syusuke@yahoo.co.jp

Abstract

Half of the deterioration of concrete water channels is caused by abrasion. Previous research suggests that irrigation water is affected by physical effects of water flow as well as chemical effects such as leaching due to water quality. There is very little data on water quality items related to abrasion and leaching of concrete water channels. The main water sources for water utility services are rivers and lakes, and there are many commonalities in the water intake methods.Therefore,the author inferred the impact on concrete water channels in each region from the water quality items that contribute to leaching and abrasion, using the water source name and type of raw water for each water purification plant, and the average daily purification volume, which are published in the water supply water quality data. The average total hardness of irrigation water in Japan was 40 mg/L for 7,979 data points, water temperature was 17.4℃ for 28,531 data points, alkalinity was 31 mg/L for 8,585 data points, and Langelier index was -1.6 for 1,679 data points. Comparing by region, leaching of calcium components from concrete water channels is likely to occur in Hokkaido, Tohoku, and Chubu regions, where the total hardness is low and the water temperature is low. It is assumed that abrasion prediction can be improved by examining water quality in this way.

1. Introduction

The results of functional assessments of Japan operated concrete water channels have revealed that more than half of the changes in the inner surface of water channels are due to abrasion, drawing attention.Electron probe microanalysis (EPMA) has also revealed that leaching, which results in low concentrations of calcium components at the water contact surface, occurs in concrete canals and irrigation facilities that have been in service for a long time[1)]. It has also been reported that physical effects, such as flow velocity and the presence of sand and gravel mixed with the water flowing downstream, and chemical effects, such as water-mediated leaching, are involved[2)]. Here, we discuss the effects of abrasion and leaching on concrete irrigation facilities caused by irrigation water. Fig. 1 shows actual abrasion, which is a significant physical effect, observed in the field. However, in the cross-section of a concrete water channels using limestone aggregate, depressions in the coarse aggregate have also been observed, as shown in Fig. 2[3)]. Previous laboratory tests have confirmed that aggregate mass decreases over time when immersed in soft water in a still water environment. Furthermore, limestone coarse aggregate has slightly lower physical strength than aggregates of other rock types, and composition analysis has revealed that it has a higher proportion of calcium[4)]. This is thought to be why abrasion and leaching were so pronounced. In the water supply sector, facilities are already maintained and managed using the Langelier Index to measure the corrosivity (leaching) of facilities.

Fig. 1 coarse araggregate exposed by abrasion

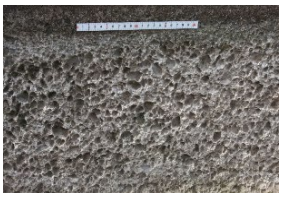

Fig. 2 Leaching of coarse aggregate (limestone)

The Japan Water Works Association publishes water quality data from water purification plants across Japan on the Web in its tap water quality database. It is believed that by using this data to clarify the risk of leaching from concrete irrigation facilities from a water quality perspective in each prefecture, it will be possible to contribute to improving predictions of the progress of wear and leaching in specific areas of irrigation water.

2. Reserchs and Methods

In a specific region, tap water and irrigation water are taken from lakes, dams, rivers, and headworks . Therefore, since the intake methods are similar, we assumed that the water quality would be similar. I estimated the quality of irrigation water based on raw water data for fiscal year 2018 obtained from the tap water quality database. However, the amount of irrigation water taken by irrigation facilities is difficult to grasp due to differences in the maintenance and management of large and small facilities. Furthermore, I could not find any documents summarizing the amount of water taken by each water intake facility. Therefore, I decided to proceed with the analysis assuming that the daily water intake volume of the irrigatin facilities and each water purification plant was the same. For the survey, I first obtained water quality data from the web using the initial screen shown in Figure 1. For the individual water quality tables, I selected raw water as the standard items for raw water for each regions.

The Langelier index is an index defined as the difference between the pH of water and the pH value when calcium carbonate in the water is in an equilibrium state, with neither dissolution nor precipitation. A value greater than 0 indicates a tendency for scale (white precipitates) to form, while a value less than 0 indicates a tendency for corrosion.

The management target setting is set to "above -1, with the goal of approaching 0 as close as possible." Water quality parameters related to corrosivity (leaching) were deemed appropriate. Hardness, pH, water temperature, alkalinity, and the Langelier index were extracted and organized from a water quality database(Fig. 3). The raw water before water treatment included surface water (natural flow), direct dam water, dam discharge water, underground water, and lake water.

Table 1 Compaison table of water quality by region

Region Name	Hardness (mg/L)		pH		Water Temperature(℃)		Alkalinity (mg/L)		Langelia Index	
	Value	Number	Value	Number	Value	Number	Value	Number	Value	Number
Hokkaido	33	583	7.2	3,399	11.0	6,018	20	3,372	-2.2	106
Tohoku	29	823	7.3	3,054	14.0	2,178	20	282	-2.0	246
Kanto	57	763	7.4	5,472	18.3	4,756	37	2,123	-1.3	294
Chubu	36	1,602	7.4	5,684	15.9	5,090	25	797	-1.5	239
Kinnki	38	2,117	7.4	5,927	18.7	5,112	33	444	-1.6	367
Chugoku	35	666	7.2	2,685	18.3	1,993	20	334	-1.7	157
Sikoku	37	412	7.4	1,574	18.4	1,358	31	753	-1.5	79
Kyusu	46	958	7.5	1,926	18.2	1,924	40	430	-1.5	190
Okinawa	46	50	7.4	102	23.7	102	39	50	-1.2	1
Average	40	7,979	7.4	29,824	17.4	28,531	31	8,585	-1.6	1,679

Fig . 3 Tap water quality database initial screen

The total hardness of irrigation water for each prefecture was calculated by multiplying the purified water volume (m3/day) of all individual water treatment facilities by the water quality item value, and dividing the aggregate value by the total purified water volume of all individual water treatment facilities. Similar calculations were performed for pH, water temperature, alkalinity, and the Langelier index.

3. Results and Discussion

Table 1 shows the average values of water quality items nationwide and each regions.The results of the estimated water quality of irrigation water are as follows. The average total hardness of irrigation water in Japan was 40 mg/L for 7,979 data points, water temperature was 17.4℃ for 28,531 data points, alkalinity was 31 mg/L for 8,585 data points, and Langelier index was -1.6 for 1,679 data points.

Next, we look at the water quality parameters by region. Based on the average corrosiveness (leaching) values for the water quality parameter, the region with the greatest concern for corrosiveness (leaching) is Hokkaido region (total hardness 33 mg/L, water temperature 11.0°C, alkalinity 20 mg/L, Langelier index -2.2). Next is Tohoku region (total hardness 30 mg/L, water temperature 14.0°C, alkalinity 19 mg/L, Langelier index -2.0). Next is Chubu region (total hardness 33 mg/L, water temperature 16.3°C, alkalinity 22 mg/L, Langelier index -1.7). Conversely, Kanto region is the region with the least concems (total hardness 57 mg/L, water temperature 18.3°C, alkalinity 37 mg/L, Langelier index -1.3). It is inferred that corrosiveness (leaching) is more suppressed in this region than in other regions due to the high total hardness, high water temperature, and high alkalinity.

As mentioned above, there are differences in water quality between regions. When the flow velocity is fast, physical action occurs and surface damage becomes significant, but the impact of leaching on water quality is also judged to be at a level that cannot be ignored, and we believe that close attention is needed.

4. Summary

The findings of this study are as follows

(1) Irrigation water in Japan varies by region. However, because it is soft water, it is prone to corrosion (leaching).

(2) When predicting deterioration due to wear of concrete irrigation facilities, the accuracy of the prediction formula can be improved by also considering water quality.

References

1) Masaru Tokashiki: Study on the abrasion mechanism and accelerated abrasion test in agricultural concrete waterways, Agricultural and Industrial Research Report 52, pp98-108 (2023)

2) Mitsuhiro Mori, Masaru Tokashiki, Daisuke Yamazaki, Tomotake Kato: Deterioration of the Concrete Surface of Long-Term Irrigation Channels, Proceedings of the Japan Concrete Institute 32(1), pp919-924 (2009)

3) Kanehira, Shusuke and Kitatsuji, Masafumi: Fundamental Study on Leaching of Limestone Coarse Aggregate in Concrete Water Supply and Utilities Facilities in the Tohoku Region, Journal of the Japanese Society of Irrigation, Drainage and Forestry Engineering 313, I_-387-I_396 (2021)

4) Shusuke Kanehira: Fundamental study on leaching of limestone coarse aggregate in concrete water facilities, Doctoral dissertation, pp86-88 (2022)

Development of Reservoir Operation Rules Using Machine Learning–Based Water Level Forecasting

Mi-Hye Yang [1], Won-Ho Nam [2*]

[1] Ph.D Student, Department Integrated System Engineering, Hankyong National University, Anseong, Republic of Korea

[2] Professor, School of Social Safety and Systems Engineering, National Agricultural Water Research Center, Hankyong National University, Anseong, Republic of Korea

* Corresponding author. Email: wonho.nam@hknu.ac.kr

Abstract

Agricultural reservoirs are critical infrastructure for ensuring a stable supply of irrigation water. Their efficient operation is essential for maximizing limited water resources and sustaining agricultural productivity. In Korea, however, existing operation guidelines are generally based on fixed flood and non-flood periods, which restrict flexibility in responding to short-term hydrological variations. This study proposes a method to quantitatively establish dynamic operation rules by predicting ten-day reservoir storage rates using an XGBoost regression model, which effectively captures nonlinear relationships among meteorological and hydrological variables. The model was trained on hydrological data from 1991 to 2024, with predictor variables including initial and terminal storage, cumulative rainfall, rainy days, prior-month storage, and seasonal indicators.

Operational rules were derived by linking predicted storage distributions to irrigation thresholds. Two approaches were applied: one based on statistical quantiles of predicted values and the other on prediction errors expressed as confidence intervals. These rules were evaluated through scenario analysis, including no-rainfall, high-rainfall, and low-rainfall conditions, as well as case studies for a drought year and a normal year. Results showed that the model achieved strong predictive performance, with higher accuracy in winter and larger errors concentrated in mid-August due to rainfall variability. Scenario testing highlighted clear differences in storage trajectories, confirming the framework's potential for adaptive rule-setting. The findings provide a quantitative analytical basis for reservoir operation and can support future irrigation water management under climate variability.

Keywords: XGBoost, Reservoir operation, Storage prediction, Operation rules, Drought response, Irrigation water management

1. Introduction

. Agricultural reservoirs are essential for irrigation, but climate change has increased the frequency and severity of droughts, adding uncertainty to their operation (FAO, 2023). In Korea, conventional guidelines rely on fixed seasonal rules, which limit flexibility in responding to short-term hydrological variability. To address this, data-driven approaches have been applied, and the XGBoost algorithm has proven effective in capturing nonlinear relationships among hydrological and meteorological variables (Chen and Guestrin, 2016). This study applies an XGBoost regression model to Najuho Reservoir to predict ten-day storage rates and establish a quantitative framework for dynamic operation rules.

2. Materials and Methods

2.1. Study area

Najuho Reservoir, located in Korea, was selected as the study site. The reservoir plays a key role in regional irrigation, and long-term hydrological records (1991–2024) are available for analysis.

2.2. Data collecion

The dataset included daily reservoir water levels, storage rates, precipitation, and meteorological records. Derived predictor variables were initial and terminal storage, 3-day and 5-day cumulative precipitation, number of rainy days, prior-month average storage, and seasonal dummy variables.

2.3. Modeling approach

An XGBoost regression model was applied to predict ten-day storage rates. The model was trained using data from 1991–2023 and validated with 2024 observations. Hyperparameters were optimized through cross-validation, and variables with zero importance were excluded based on sensitivity analysis. To construct the predictor set, both direct measurements and derived variables were considered, grouped into three categories:

- Rainfall-related variables: recent 3-day and 5-day cumulative rainfall, number of rainy days, standard deviation of rainfall, and changes and trends compared with the previous period.
- Storage-related variables: previous period start and end storage rates, monthly mean storage, and deviations from sequential averages.
- Seasonal indicators: dummy variables for spring, summer, autumn, and winter.

Feature importance analysis was then used to refine these predictors, resulting in an optimized input set for robust forecasting.

2.4. Derivation of operation rules

Operational rules were formulated from the predicted storage results using two complementary approaches:

- Statistical quantiles of storage distributions, setting irrigation thresholds based on the lower percentiles (e.g., 25%, 10%, 5%).
- Prediction error–based confidence intervals, adjusting operational decisions by incorporating uncertainty in forecast performance.

These rules were tested under no-rainfall, high-rainfall, low-rainfall, and normal scenarios, as well as through case studies of a drought year and a normal year, to evaluate applicability and sensitivity.

3. Results and Discussion

3.1. Model performance

The XGBoost model outperformed baseline regression in predicting ten-day storage rates. Errors were lowest during winter, with December showing the most reliable predictions, while mid-August exhibited larger errors due to high rainfall variability. Feature optimization eliminated redundant predictors and stabilized the model without sacrificing accuracy.

Table 1. Model performance summary

Ex.	n_ estimators	max_ depth	learning_ rate	RMSE
1	20	2	0.10	4.01
2	120	4	0.03	6.33
3	150	4	0.03	5.53

Table 2. Seasonal error distribution

Season/Period	Typical error (range)
Mid-August	−16 to −21
December (early)	−0.04 to 0.40

3.2. Scenario analysis

Scenario-based simulations were performed to examine reservoir responses under contrasting rainfall conditions. In the no-rainfall scenario, storage rates decreased continuously, indicating a high risk of depletion during dry spells. In contrast, under high-rainfall, low-rainfall, and normal scenarios, storage trajectories diverged significantly, demonstrating the model's sensitivity to precipitation variability.

Table 3 summarizes shortage probabilities under different rainfall scenarios and storage thresholds. Results highlight that shortage risks increase sharply when the storage level falls below 35–40%, suggesting this range as a practical boundary for operational planning.

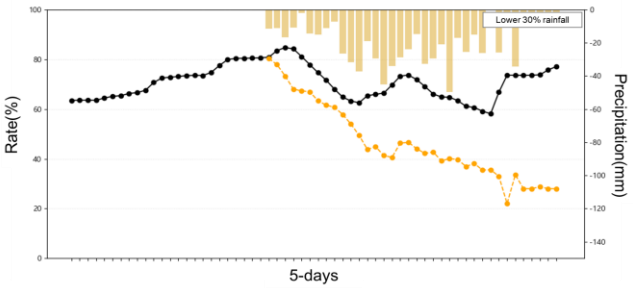

Figure 1. Reservoir storage trajectory under the lower 30% rainfall scenario

Table 3. Probability of water shortage under different storage thresholds and rainfall scenarios

Storage threshold (%).	Shortage prob. (Upper 30%)	Shortage prob. (Normal)	Shortage prob. (Lower 30%)
35.0	0.0	0.0	22.2
37.0	0.0	0.0	30.6
40.0	0.0	0.0	38.9
42.5	0.0	0.0	50.0
45.0	0.0	0.0	61.1

3.3. Operational thresholds

Operational thresholds were established to link predicted storage distributions with irrigation risk levels. A quantile-based method was applied, focusing on the lower 25%, 10%, and 5% storage distributions. These thresholds provided practical criteria for identifying water shortage risks under varying hydrological conditions.

As shown in Table 4, the threshold values for Najuho Reservoir were 45.5% (25%), 32.7% (10%), and 20.2% (5%). The shortage probability increased significantly once storage levels fell below the 10% quantile. Figure 2 illustrates the distribution of predicted storage values and the derived thresholds, demonstrating how quantile-based criteria can support dynamic operation rules.

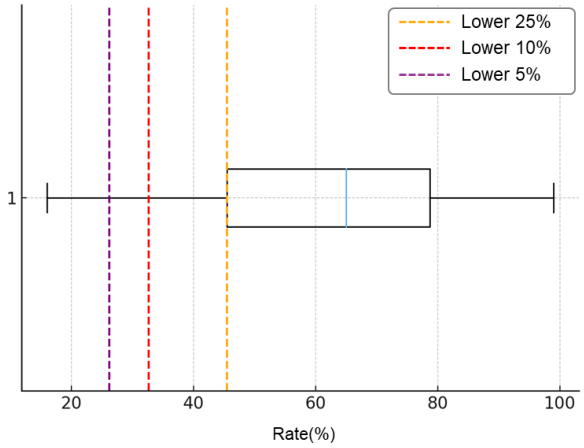

Figure 2. Boxplot of storage distribution for Najuho Reservoir with quantile-based thresholds

Table 4. Quantile-based thresholds for Najuho Reservoir

Quantile	Storage threshold (%)
Lower 25%	45.5
Lower 10%	32.7
Lower 5%	26.2

4. Conclusions

This study applied an XGBoost model to predict ten-day reservoir storage and derive adaptive operation rules. The model achieved stable accuracy (RMSE 4–6), with reliable performance in winter and larger errors in mid-August. Scenario analysis showed shortage risks increase sharply below 35–40% storage, while quantile thresholds for Najuho were identified at 45.5%, 32.7%, and 20.2%. These results highlight the potential of combining machine learning predictions with threshold analysis to support flexible and reliable reservoir operations under climate variability.

Acknowledgements

This work was supported by Korea Environment Industry & Technology Institute (KEITI) through Water Management Program for Drought Project, funded by Korea Ministry of Environment (MOE) (RS-2023-00230286).

References

Chen, T., Guestrin, C., 2016. XGBoost: A scalable tree boosting system. Proceedings of the 22nd ACM SIGKDD International Conference on Knowledge Discovery and Data Mining, 785-794.

Performance evaluation of agricultural pipeline system based on TTBTs with artificial leakage

Atsushi Chiyoda [1], Taiki Hagiwara [2*], Yuto Takahashi [3], Toma Tsubota [4], Kakutaro Suematsu [1], Hisaya Ito [1], Tetsuya Suzuki [5]

[1] Nihon Suiko Consultant Co., Ltd, Omiya, Japan

[2] Graduate School of Sciences and Technology for Innovation, Yamaguchi University, Yamaguchi, Japan

[3] Graduate School of Science and Technology, Niigata University, Niigata, Japan

[4] Obayashi Corporation Technology Research Institute, Kiyose, Japan

[5] Institute of Agriculture, Niigata University, Niigata University, Niigata, Japan

* Corresponding author. Email: t-hagiwara@yamaguchi-u.ac.jp

Abstract

In pipeline systems for the transportation of irrigation water to paddy fields, water leakage can cause significant energy losses, which lead to poor water delivery performance. In addition to water loss or service interruption, leakage may affect the surrounding ground and other social infrastructure. This study presents an experimental verification method to evaluate energy loss caused by artificial leakage in an in-service agricultural pipeline based on pipe deformation induced by pressure waves. By using pressure waves that contain information related to leakage, the proposed method enables leak detection over a long-distance pipeline on the kilometer scale. A field experiment was conducted on an in-service pump–tank pipeline system to assess the feasibility of the method. The results demonstrate that artificial leakage can be detected by identifying differences in the amplitude spectra of hoop strain caused by pressure waves following pump shutdown. Further work is expected to improve the accuracy of non-contact measurements and to enable detailed identification of leakage location and volume.

Keywords: Pipelines, Performance evaluation, Artificial leakage

1. Introduction

Agricultural pipelines require water transmission and distribution while maintaining specified flow rates and pressure. However, hydraulic performance degradation due to energy loss from leakage has not been sufficiently confirmed. This study targets an in-service pipeline in actual structures and utilizes simulated leakage and pressure waves, which the authors have been investigating, to develop performance verification methods. As a leak detection method considering the structural characteristics of pipelines, it is expected to be capable of detecting remotely located leaks and applicable even when direct access to facilities is difficult. The proposed method utilizes pressure waves generated by valve operations or pump operations in pipelines with leaks to capture information about remote leaks at measurement locations. Additionally, based on the concept of cylinders subjected to internal pressure in mechanics of materials, pipelines undergo increased pipe body deformation accompanying pressure waves. By capturing this, it becomes possible to detect flow conditions within pipes from pipe body deformation. Specifically, this paper presents experiment results using actual structures of relatively low-pressure pipelines in pump-reservoir systems.

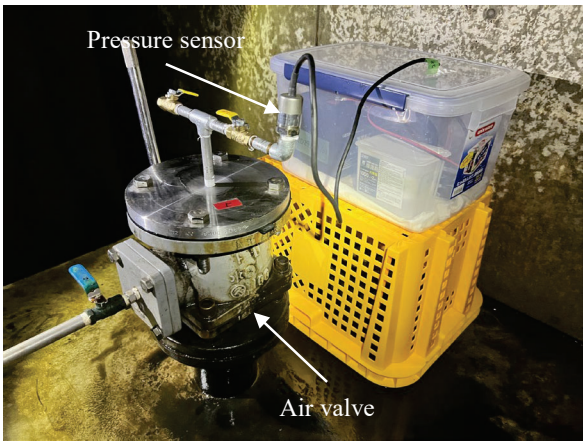

Figure 1. Setup for measurement.

Figure 2. Artificial water leakage.

2. Materials and Methods

An experiment was conducted to detect artificial leakage in existing pipelines. The pipeline extends approximately 5.5 km and consists of 600 mm diameter FRPM pipes, SP pipes, and VU pipes. A pumping station is located at the upstream end, and a diversion work with an overflow stand is at the downstream end, which is approximately 18.7 m higher than the upstream end. Various measurements in this experiment are described below. For water pressure measurement, flanges were installed on air valves to attach pressure sensors, and data was acquired at 500 Hz (Fig. 1). For strain measurement, strain gauges were attached in circumferential and axial

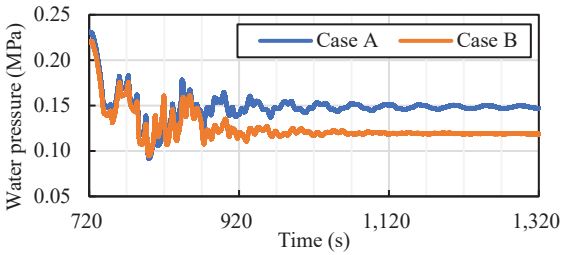

Figure 3. Water pressure after the pump shutting.

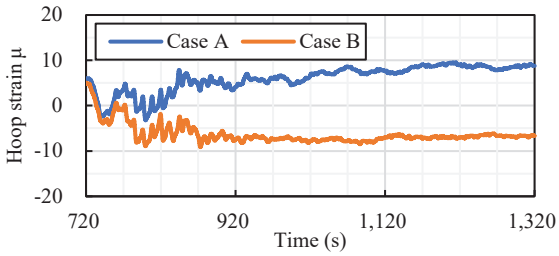

Figure 4. Hoop strain after the pump shutting.

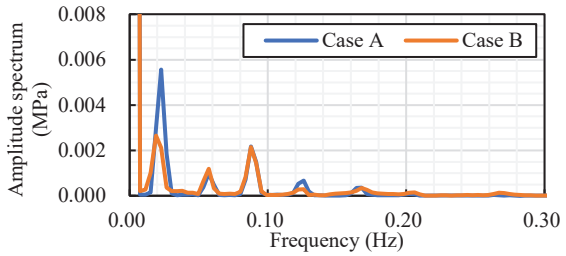

(a) Water pressure.

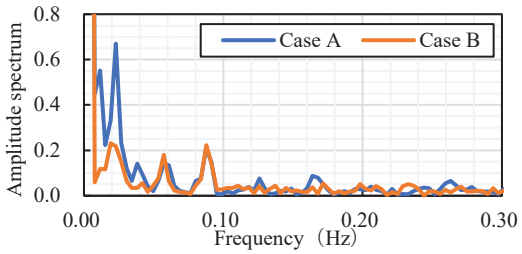

(b) Hoop strain.

Figure 5. Frequency distribution.

directions to exposed pipe sections in manholes, and data was acquired at 500 Hz.

The experimental cases presented in this study are Case A without leakage and Case B with leakage, with measurement results at 1,901.24 m from the upstream end. The experimental procedure involved starting various measurements, generating artificial leakage after 1 minute (for Case B, Fig. 2), starting pump operation after another minute, stopping operation after 10 minutes, and ending measurements after another 10 minutes (total 22 minutes). Artificial leakage was generated by opening the sediment discharge work located 1,703.96 m from the upstream end. This experiment was conducted to detect artificial leakage in the pipeline.

3. Results and Discussion

The examination results are described. Fig. 3 shows the time history waveform of water pressure, focusing on pressure waves following pump operation cessation after 720 seconds. In Case B, pressure wave attenuation and water pressure reduction due to leakage can be confirmed. Fig. 4 shows the results of measuring hoop strain of the pipe body caused by these pressure waves using strain gauges. Here, hoop strain could be extracted by applying a 0.3 Hz low-pass filter. Particularly in Case B, reduction in circumferential strain attributed to leakage was confirmed. To extract leakage characteristics, Fig. 5 shows frequency distribution obtained by FFT. In the frequency distribution up to 0.3 Hz for water pressure (Fig. 3) and circumferential strain by strain gauges (Fig. 4) in Fig. 4, peaks were confirmed at 0.023 Hz for Case A and 0.019 Hz for Case B. These values are close to the primary mode (0.018 Hz) of liquid column resonance in this pipeline. At these peaks, Case B with leakage shows smaller amplitude spectra than Case A without leakage. Considering the effects of energy loss due to leakage, it is inferred that leakage detection can be achieved from pipe body deformation as well as water pressure. The presentation will also address evaluation results using non-destructive and non-contact digital image correlation (DIC) methods.

4. Conclusions

This study examines a verification method focusing on energy loss in agricultural pipelines using artificial leakage. This method implements artificial leakage detection utilizing pipe body deformation caused by pressure waves. From the demonstration experiment on the in-service pump-reservoir system pipeline, it is confirmed that the presence or absence of leakage can be detected through differences in amplitude spectra of pipe body deformation caused by pressure waves generated during pump cessation.

References

Hagiwara, T., Asada, Y., Tsubota, T., Kurasawa, K. and Suzuki, T., 2025. Non-contact detection of leak-derived energy loss for an in-service pipeline system using digital image correlation. Nondestructive Testing and Evaluation.

Hagiwara, T., Tsubota, T., Takahashi, Y., Suzuki, T., Chiyoda, A., Suematsu, K., and Ito, H., 2025. New methodology for performance evaluation of an agricultural pipeline with artificial leakage. Water, Land and Environmental Engineering., 93(8), 17-20.

Tsubota, T., Hagiwara, T., Asada, Y., and Suzuki, T., 2024. Non-contact detection of water leakage in service pipeline by digital image correlation method with damping coefficients. Advanced Experimental Mechanics., 9, 24-0011.

Non-Contact Detection of Irregular Vibrations in Pump Rotors using Infrared-Stress Method

Suzuki Tetsuya・Oshima Keiichiro・Takahashi Yuto ・Hagiwara Taiki

Abstract

In agricultural water management systems, pump stations play a vital role in ensuring a stable and efficient water supply for irrigation. A reliable operation of these pumps is crucial, especially under conditions of aging infrastructure and increasing demands for sustainable water use. To maintain operational integrity, early detection of mechanical stress and potential failures in pump components is essential. In a rotating body, since stress fluctuations occur in each cycle, the temperature distribution also varies periodically. By capturing images of an operational pump shaft using an infrared camera, there emerges a possibility of non-contact measurement of the stress distribution based on the temperature variations caused by the thermoelastic effect. In this study, infrared stress measurements are performed on the pump shaft during operation to evaluate stress in a non-contact and non-destructive manner. The time-series data representing the temperature fluctuations of the pump shaft are analyzed using the Fast Fourier Transform technique. The analysis yielded results that suggest the detection of load frequencies corresponding to the rotational speed, which in turn implied the presence of irregular vibrations. By measuring stress distribution with a non-contact and easily installable infrared camera during pump operation, signs of failure can potentially be detected. This method may reduce maintenance costs by eliminating the need for periodic shutdowns.

Post-Earthquake Damage Assessment of Landslide Prevention Facilities by UAV-LiDAR

Norihiro Otaka [1*], Hiromu Tanaka [2], Kazuma Shibano [2], Yuji Fujimoto [1] and Tetsuya Suzuki [3]

[1] Nippon Steel Metal Products Co., Ltd., 4-14-1 Sotokanda, Chiyoda-ku, Tokyo 101-0021, JAPAN

[2] Graduate School of Science and Technology, Niigata University, Niigata 950-2181, JAPAN

[3] Institute of Agriculture, Niigata University, Niigata 950-2181, JAPAN

* Corresponding author. Email: nohtaka@ns-kenzai.co.jp

Abstract

Following the 2024 Noto Peninsula earthquake, rapid assessment of landslide prevention structures became critical for maintaining agricultural sustainability and protecting rural communities. This study presents a diagnosis procedure for rapid recovery and an innovative approach to post-earthquake damage evaluation of drainage wells, essential facilities for groundwater management in landslide-prone agricultural areas. Traditional post-disaster inspections face significant challenges, including limited accessibility to mountainous locations, safety concerns for inspection personnel, and time constraints for comprehensive damage assessment. Our research demonstrates the effectiveness of UAV-LiDAR technology for efficient off-site inspection of earthquake-damaged drainage wells in Ishikawa Prefecture, Japan. Key findings indicate that UAV-LiDAR can effectively capture three-dimensional structural conditions of drainage wells up to 30 m depth, providing critical data (shear deformation, inclination area and eccentricity) for emergency response and restoration planning. The methodology proved particularly valuable for accessing facilities in areas with compromised road networks and ongoing geological instability. This smart technology approach aligns with sustainable agricultural facility management by enabling prompt damage assessment, reducing inspection risks, and supporting rapid restoration of landslide prevention systems.

Keywords: Rapid inspection, Mj7.6 Noto Peninsula earthquake, Drainage well, Point clouds, non-contact detection, shear deformation

1. Introduction

The 2024 Noto Peninsula Earthquake caused damage to numerous structures. Heavy rainfall following the earthquake raised concerns about landslide occurrence. Against this background, comprehensive inspections of all drainage wells and landslide prevention facilities have been conducted. In the rapid inspection, 104 drainage wells were targeted in the district (Figure 1). These drainage wells are scattered throughout mountainous areas that are difficult to access. Moreover, earthquakes can serve as triggers for landslides, creating the possibility of secondary damage. Given these circumstances, it was difficult for engineers to visit the sites and conduct comprehensive inspections of all drainage wells. Therefore, this study proposes an offsite inspection method for drainage wells using UAV-LiDAR (Shibano and Suzuki, 2025). Additionally, from a practical standpoint, a rapid diagnostic procedure for drainage wells using realistically obtainable indicators (Figure 2) is also proposed, and the potential for UAV-LiDAR to serve as an alternative for indicator acquisition is discussed. In the

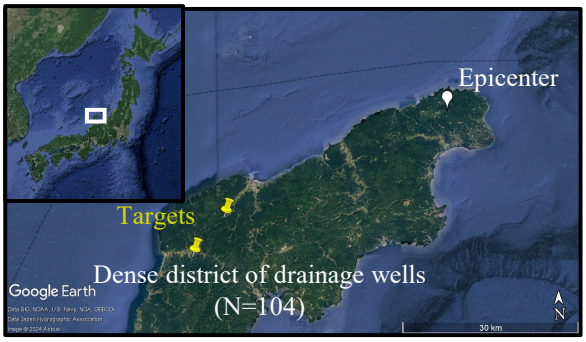

Figure 1. An example of a chart from Excel pasted here using Enhanced Metafile.

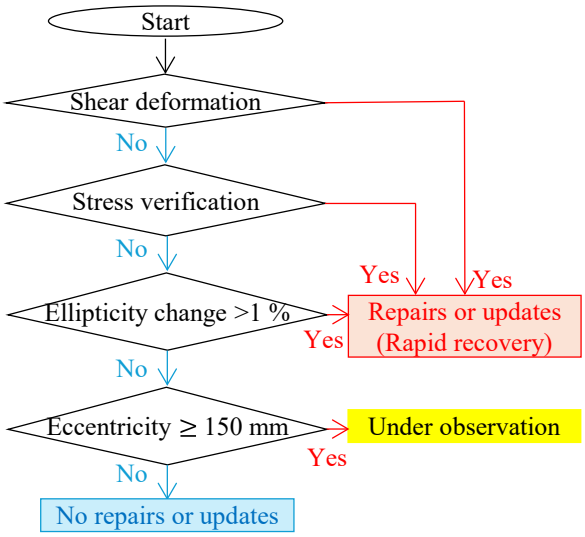

Figure 2. Diagnosis procedure.

design of liner plate drainage wells, it is common to perform stress verification for ring buckling and stress verification for bending compression. For this study, four items are used as evaluation indicators for drainage wells affected by earthquakes: presence or absence of shear deformation, stress verification under inclination, elliptical deformation amount and eccentricity (Figure 2). Among these, the presence or absence of shear deformation and stress verification under inclination (eccentricity) are examined.

2. Materials and Methods

LiDAR measures distance by calculating the time for laser pulses to return from target objects using the speed of light. UAV-LiDAR's unique multiple return capability allows it to capture several measurements from a single pulse, unlike SfM. For drainage wells beneath tree cover, the first return comes from canopy structure, while subsequent returns may reflect from the well lid or internal

surfaces like water or curbing. This multi-return feature enables point cloud acquisition of drainage wells even under vegetation cover, as laser pulses can reach targets through small gaps in the canopy structure.

Measurements were conducted on drainage wells damaged by the 2024 Noto Peninsula Earthquake (Mj 7.6) in Ishikawa prefecture. Three wells were surveyed: N-1 (constructed 1972, depth 4.805 m) showed severe shear fracture with deformed vertical stiffeners and missing water collection pipes, losing drainage function; N-2 (1977, depth 15.485 m) and M-1 (unknown construction year, depth 30.095 m) showed no visible deformation. All wells have 3.5 m diameter curbs.

3. Results and Discussion

Figure 3 shows the judgment of shear deformation in N-1 through point cloud processing. Figure 3 (a) is an image taken from inside the well through the lid. A slip surface occurred in the middle of the well body and shear deformation of the liner plates serving as earth retaining materials can be confirmed. The crescent-shaped area visible in the lower right direction of the figure is the slip surface that appeared due to the movement of the upper drainage well toward the valley side. Significant buckling deformation of the vertical stiffeners installed in the vertical direction can also be confirmed. When cylindrical detection is performed on the acquired point cloud and the difference between the cylinder and actual point cloud is calculated, the deformed section can be identified (Figure 3 (b)). Thus, it is considered possible to characterize shear deformation through well depth and member deformation that differ from design values.

Figure 4 shows the UAV-LiDAR point cloud of the drainage wells and the estimation results of their axial direction vectors. When soil mass above the drainage wells acts on the liner plate body, stress verification is performed for compressive forces generated by vertical loads. The calculation results plotted against depth and drainage well inclination are shown in Figure 5, where Region A represents the range where generated stress remains within allowable stress limits. N-1, which showed shear deformation, requires repair and renewal before stress verification, but also deviates from Region A from a stress verification perspective. For N-2 and M-1, the axial vector inclinations are 0.02 ° and 0.19 ° respectively, both within allowable stress limits. Focusing particularly on axial vector inclination allows estimation of stress verification indicators and eccentricity parameters when inclination occurs.

4. Conclusions

This research successfully demonstrates that UAV-LiDAR technology provides an effective solution for rapid, off-site inspection of earthquake-damaged drainage wells, enabling accurate detection of critical structural parameters including shear deformation and inclination angles without requiring dangerous site access.

Acknowledgements

The authors are grateful to Kazunari Inaba (Institute of Agriculture, Niigata University) and Tsuyoshi Okayama (Oku-Noto Agriculture and Forestry General Office, Ishikawa prefecture) for cooperating with the site investigation.

(a) Shear deformation

Extraction of deformed vertical stiffener

(b) Deformation detection by UAV-LiDAR

Figure 3. Shear deformation in N-1 by point cloud.

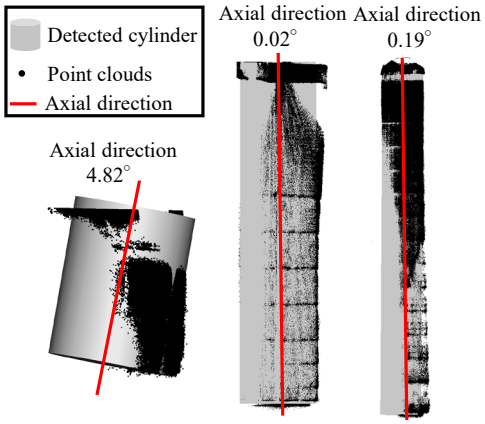

(a) N-1 (b) N-2 (c) M-1

Figure 4. Point cloud of the drainage wells and the estimation results of their axial direction vectors.

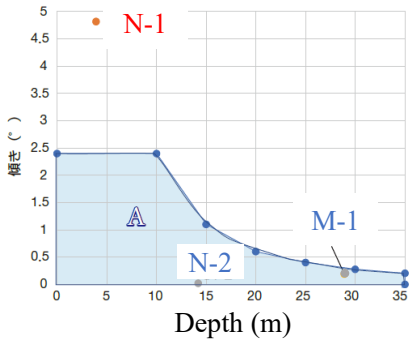

Figure 5. Stress verification results.

References

Shibano, K. and Suzuki, T., 2025. Non-Contact damage detection of drainage wells during the Mj7.6 Noto Peninsula earthquake by UAV-LiDAR technique. *Measurement*, 117610.

Estimation of Parameters in a Water Front Advance Model for Large-Scale Paddy Fields

Naoko Koshiyama*, Takeshi Otsu

Civil Engineering Research Institute for Cold Region, Sapporo, Hokkaido, Japan

* Corresponding author. Email: koshiyama-n@ceri.go.jp

Abstract

In Hokkaido, which is one of Japan's major agricultural regions, the number of farmers is decreasing and the management area per farmer is expanding rapidly. As one of the countermeasures, enlargement of plots has been pursued to improve farm work efficiency. Looking ahead to the further expansion of the management area, it is necessary to discuss how to design larger plots that can further reduce construction and maintenance costs in the future. The base for this discussion lies in analyzing the actual water management practices in large-sized plots that have already been developed. The authors focused on a water front advance model that quantitatively expresses the temporal changes in water front advance within a paddy field. This model incorporates parameters such as infiltration rates and so on, making it useful for evaluating the appropriate layout and scale of irrigation facilities within a field in response to specific conditions. However, in larger-sized paddy fields, estimating representative values for parameters becomes more difficult as the area of a single field increases. UAVs can easily capture images of water front advance during irrigation these days, making it is possible to estimate model parameters using this image data. In this study, the authors tried to estimate the parameters of the water front advance model using image data of temporal changes in the flooded area in some large-sized paddy fields captured by UAVs, and discussed the validity of these estimates.

Keywords: dry direct-seeding culture, flooded area, UAV.

1. Introduction

In the large-sized paddy field areas of Hokkaido, which is one of Japan's main agricultural regions, the aging and declining number of farmers has led to an increase in the size of areas managed by each farmer. As a measure to smoothly support such situations, large-block field consolidation projects are being implemented. Since the further expansion of farm management areas is anticipated, methods for designing extra-large paddy fields that can reduce both construction and maintenance costs are increasingly required. In response, the authors focused on a water front advance model that can quantitatively represent the temporal variation in water front advance distance within a field. Because this model incorporates parameters such as percolation rate, it allows the consideration of appropriate layouts for irrigation facilities under actual field conditions. Additionally, it becomes more difficult to estimate representative parameter values for large-scale paddy fields with increases in the field size. However, with the use of unmanned aerial vehicles (UAVs), the water front advance process can now be captured easily and accurately, raising the possibility of estimating model parameters directly from captured images.

In this study, the authors used UAVs to take photos of the temporal change in ponded area at first water intake at several large paddy fields in Hokkaido. From the image data, parameters of the water front advance model were estimated, and the validity of the results was examined.

2. Materials and Methods

Field surveys were conducted for four paddy fields in a paddy field area of Hokkaido in 2012, 2013 and 2024. The surveyed fields are outlined in Table 1. In all surveyed fields, the cultivation method was dry direct seeding. During the irrigation period, the ponding depth, groundwater level, water intake, and precipitation were monitored at 10-minute intervals. In addition, at the first intake stage, the water front advance from the start of water intake until irrigation water covered the entire field was recorded at 1-hour intervals by the following methods. In 2024, the water front advance was recorded by UAV imaging, and the images were orthorectified. In 2013–2014, poles were placed at fixed intervals along field ridges, and the water front advance was sketched by visual observation. From these images, the ponded area was determined by counting the number of wet pixels. Figure 1 shows an example of water front advanced in each field.

3. Model Overview

Haraguchi and Furuki (1995) conducted analysis of

Table 1 Outline of surveyed fields

Field name	Survey year	Area (ha)
IA23	2023	0.72
IA24	2024	0.72
NM13	2013	0.52
NM14	2014	0.62

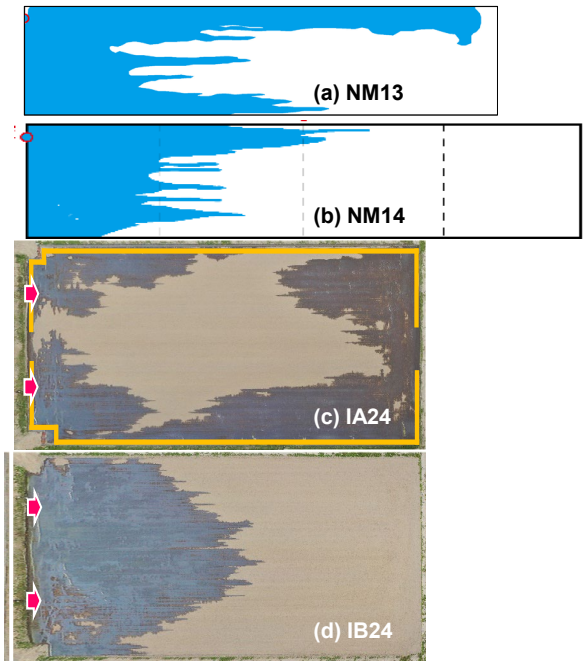

Figure 1. An example of water front advanced in each field.

flooding process in a paddy field using water front advance models based on water balance analysis (hereafter referred to as "the water front advance model"). In this study, the following water front advance model was applied to formalize the field survey results.

When irrigation water supplied from one side of the field advances uniformly, water front advance can be considered by a one-dimensional model along its longitudinal section. When the water front advances by the distance ΔX during duration Δt, the following water balance equation applies within the cell ($\Delta S \times \Delta X \times 1$).

$$\Delta S \cdot \Delta X = Q/b \cdot \Delta t - PX \cdot \Delta t \qquad (1)$$

where X is water front advance distance (m), Q is water intake rate (m^3/h), b is width of field supplied with water (m), P is percolation rate (m/h), and ΔS is increase in storage per unit area (m). The left-hand side of Equation (1) represents storage within the cell, while the first and second terms on the right-hand side represent inflow and percolation (the amount of water released from the farm block), respectively. From Equation (1), the water front advance model can be expressed as Equation (2).

$$\frac{dX}{dt} = \frac{Q/b - PX}{\Delta S} \qquad (2)$$

In Equation (2), percolation (PX) increases with ponded area. Consequently, the rate of increase in ponded area decreases over time. The increase in ponded area ceases when the intake rate equals percolation ($Q/b = PX$). Assuming that water supply begins at $t = 0$, ($X = 0$), solving Equation (2) yields Equation (3).

$$X = \frac{Q/b}{P}\left(1 - e^{-\frac{P}{\Delta S}t}\right) \qquad (3)$$

Multiplying both sides of Equation (3) by b gives Xb = ponded area A, expressed as Equation (4).

$$A = \frac{Q}{P}\left(1 - e^{-\frac{P}{\Delta S}t}\right) \qquad (4)$$

4. Results and Discussion

4.1. Water front advance in each field

Figure 3 and Figure 4 show the relationship between time elapsed from the start of the first intake and the flooded area during initial irrigation for each field. In all cases, as the ponded area approaches the total field area per unit time decreased. First intake rates were approximately 2-10 mm/h, and the time required for each field to become fully ponded ranged from about 8 to 12 hours.

4.2. Comparison of parameters

Here, we estimated the parameters (P, ΔS) for the water front advance model using two methods. The first method calculated and determined the parameters based on measured values such as the single-plot drawdown depth obtained from changes in water intake intensity and water depth (labeled "Calculated values" in the figure). The second method used UAV-captured flooded area and water intake intensity as measured values, estimating parameters that fit equation (4) via the least squares method ("Estimated values" in the figure). As a result, while some fields showed relatively well-fitted parameter values, differences were observed in other fields. Parameter values are influenced by conditions such as groundwater levels within the same area, but it is also thought that the relationship changes depending on the water intake intensity of the field.

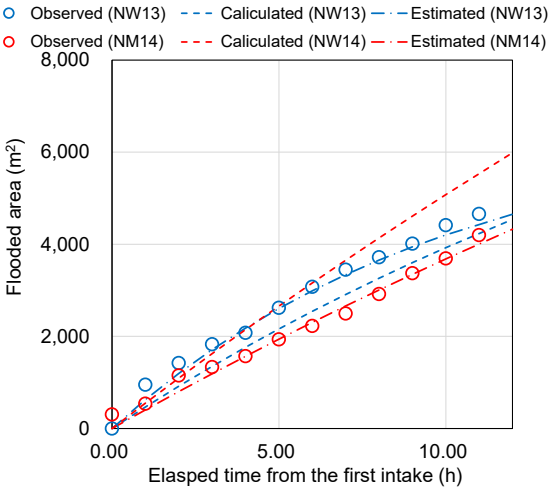

Figure 3. Relationship between time elapsed from the start of the first intake and the flooded area (NW13 and NW14).

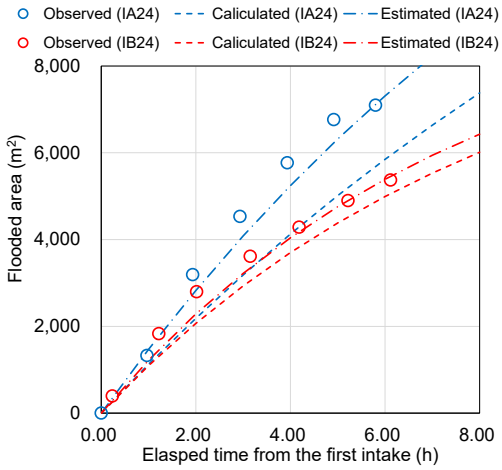

Figure 4. Relationship between time elapsed from the start of the first intake and the flooded area (IA24 and IB24).

Parameter estimation results showed relatively good agreement with estimated parameter values in some fields as shown in Figure 3 and Figure 4, while discrepancies were observed in others. It should be noted that parameter values may vary even within the same region due to differences in local conditions such as groundwater levels and abstraction intensity. Furthermore, since this model's parameters are determined based on abstraction volume, the use of high-accuracy data is considered essential to ensure reliable estimation.

5. Conclusions

It is expected that further data accumulation will enable parameters suited to field-specific characteristics to be more easily estimated in the future.

References

Haraguchi, N., Furuki, T., 1995. An investigation on suitable length of the long side and suitable intervals of inlet and outlet in a large paddy field lot based on water management time. Technical Report of National Research Institute of Agricultural Engineering, 190, 45-57 (in Japanese)

Effects of Land Use on Soil Microbial Community Composition and Predicted Nitrogen Metabolism in Paddy and Dry Fields

Yo-Jin Shiau[1]*, Ting-Kai Chen[1], Syu-Ruei Jhang[2], Yi-Ying Chen[3], Charles C.-K. Chou[3], Chia-Wei Lee[4], Wei-Nai Chen[3], Chih-Chung Chang[3], Chih-Feng Chiang[5], Pao-Kuan Wang[3,6]

[1]National Taiwan University, Taipei, Taiwan
[2] National United University, Miaoli, Taiwan
[3]Academia Sinica, Taipei, Taiwan
[4] National Kaohsiung University of Science and Technology, Kaohsiung, Taiwan
[5] Taiwan Agricultural Research Institute, Taichung, Taiwan
[6]University of Wisconsin-Madison, Wisconsin, United States
* **Corresponding author. Email: vshiau@ntu.edu.tw**

Abstract

Soils under different land uses harbor distinct microbial communities that regulate nitrogen cycling and ecosystem functioning. In subtropical Asia, flooded rice paddies and adjacent upland dry fields often receive similar fertilization regimes, yet differ greatly in redox conditions and nutrient dynamics. However, how these hydrological differences shape the soil microbiome and its nitrogen-related functional potential remains insufficiently understood. In this study, we collected surface soil samples (0–3 cm) from adjacent rice paddy and dry fields in central Taiwan during multiple fertilization stages in 2020. Genomic DNA was extracted and analyzed using 16S rRNA gene amplicon sequencing (515F/806R), followed by microbial diversity, taxonomic profiling, and functional prediction using PICRUSt2.

Results showed that Shannon and Chao1 diversity indices were significantly higher in paddy soils ($p < 0.05$). PCoA and RDA revealed distinct microbial communities shaped by hydrological conditions and nutrient availability. Taxonomic analysis indicated that potential complete denitrifiers such as *Denitratisoma* and *Zhizhongheella* were enriched in paddy soils, while dry fields were dominated by taxa such as *Sphingomonas* and *Luteimonas*, which lack key genes such as *nosZ* and may contribute to incomplete denitrification. Functional predictions supported this trend, suggesting enhanced dissimilatory nitrate reduction in paddy fields and partial denitrification in dry fields.

These findings demonstrate how land use and field hydrology influence microbial community structure and their predicted nitrogen transformation potential, providing insights for sustainable nutrient management in subtropical agroecosystems.

Keywords: soil microbiome; nitrogen cycling; 16S rRNA gene sequencing; paddy field; dry field

1. Introduction

Nitrogen is essential in ecosystems, but reactive forms such as N_2O, NO, and NO_2 strongly affect climate and air quality. Agricultural fertilization drives these emissions by stimulating soil nitrification and denitrification. While fertilizer use is known to enhance N_2O and NOx fluxes, less is understood about how soil microbial communities respond over time. This study investigated temporal changes in nitrifying and denitrifying communities in rice paddies after fertilization, and integrated microbial, chemical, and gas flux data from vegetable soils to assess links between microbial dynamics and nitrogen emissions.

2. Materials and Methods

2.1. Site description and sampling

The study was conducted in Wufun, Taichung, Taiwan. Rice paddies (Feb–Apr 2020) received urea top-dressing in April. Soils were collected daily for seven days from three plots, and composite topsoil (0–3 cm) samples were prepared.

2.2. Microbial and soil analyses

DNA was extracted for 16S rRNA sequencing. Soil C, NH_4^+, NO_3^-, pH, and EC were analyzed using standard protocols.

2.3. Flux measurement

An eddy covariance system and NOx analyzers were used to measure N_2O, HONO, and NO fluxes, calculated by covariance and flux-gradient methods.

2.4. Data analysis

Sequencing data were processed with Mothur and SILVA. Diversity and statistics were applied to link microbial communities with soil properties and gas fluxes.

3. Results and Discussion

Microbial abundance and diversity were higher in rice soils. Relative abundance analysis showed *Nitrospira* as the dominant nitrifier across sites, while denitrifier composition differed: *Thiobacillus* and *Geobacter* were enriched in rice, whereas *Massilia* and *Lysobacter* were more abundant in cabbage soils. These patterns may be linked to soil conditions, as higher NH_4^+ and NO_3^- in cabbage soils reflect more aerobic environments. Ammonium has been reported to affect proton balance and enzymatic activity in microbes (Gallert et al., 1998; Wang et al., 2015), while low water availability may further constrain diversity (Voroney, 2007). This may explain why microbial diversity indices were lower in cabbage soils (Figure 1).

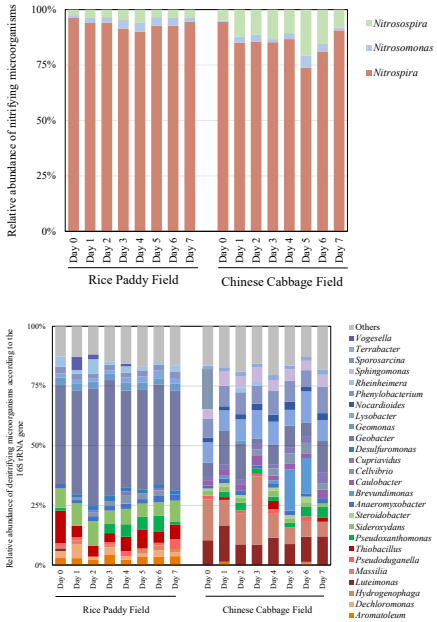

Figure 1. The community compositions of nitrifying microorganisms (a) and denitrifying microorganisms (b) in rice paddy field and Chinese cabbage soils.

Principal component analysis (PCA) revealed distinct microbial community compositions between rice and cabbage fields, although temporal variation after fertilization was limited. This suggests that cropping systems, rather than short-term fertilizer input, shaped community structures. The higher soil moisture in rice paddies may have facilitated microbial growth, while the more aerobic cabbage soils selected for narrower assemblages (Voroney, 2007). Thus, soil physicochemical differences likely drove the clustering patterns observed in PCA (Figure 2).

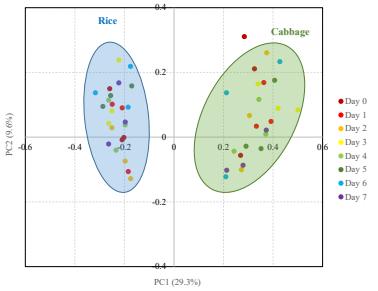

Figure 2. Plots of the first two principal components (PCs) showing differences in soil microbial community compositions between rice and Chinese cabbage fields after fertilizer application.

Redundancy analysis (RDA) showed incomplete denitrifiers in cabbage soils were strongly associated with N_2O and NO fluxes. Genera such as *Sphingomonas* and *Luteimonas*, which lack nitrous oxide reductase, tend to perform incomplete denitrification and produce N_2O as the end product (Lipski & Stackebrandt, 2015; Saddler & Bradbury, 2015). In contrast, rice soils harbored more complete denitrifiers such as *Denitratisoma* and *Luteitalea*, containing all functional genes required for denitrification (Fahrbach et al., 2006; Pessi et al., 2022). These site-specific community differences, together with soil moisture conditions, help explain why cabbage soils exhibited higher N_2O emissions than rice paddies (Figure 3).

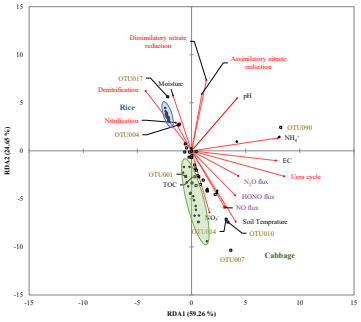

Figure 3. Redundancy analysis (RDA) linking soil properties, microbial activities, N species emissions (NO, HONO, N_2O), and dominant OTUs in rice and cabbage soils after fertilizer application.

4. Conclusions

This study examined temporal changes in soil microbial communities after fertilizer application in paddy and upland fields. Microbial population and diversity remained relatively stable, but community compositions differed. Paddy soils harbored more complete denitrifiers, while upland soils were dominated by incomplete denitrifiers, likely driving higher N species emissions. These results emphasize the role of microbial community structure in regulating agricultural N fluxes.

Acknowledgements

The funding was supported from Academia Sinica, Taiwan, under “2019 Sustainability Science Research Program (Project No. AS-SS-108-01)”.

References

Gallert C, Bauer S, Winter J (1998) Effect of ammonia on the anaerobic degradation of protein by a mesophilic and thermophilic biowaste population. Applied Microbiology and Biotechnology 50: 495-501.

Wang H, Fotidis IA, Angelidaki I (2015) Ammonia effect on hydrogenotrophic methanogens and syntrophic acetate-oxidizing bacteria. FEMS Microbiology Ecology 91: fiv130.

Voroney RP (2007) 2 - THE SOIL HABITAT. In: Paul EA, editor. Soil Microbiology, Ecology and Biochemistry (Third Edition). San Diego: Academic Press. pp. 25-49.

Lipski A, Stackebrandt ES (2015) Luteimonas. Bergey's Manual of Systematics of Archaea and Bacteria. pp. 1-3.

Saddler GS, Bradbury JF (2015) Xanthomonadaceae fam. nov. Bergey's Manual of Systematics of Archaea and Bacteria. pp. 1-3.

Fahrbach M, Kuever J, Meinke R, et al. (2006) Denitratisoma oestradiolicum gen. nov., sp. nov., a 17β-oestradiol-degrading, denitrifying betaproteobacterium. International Journal of Systematic and Evolutionary Microbiology 56: 1547-1552.

Pessi IS, Viitamäki S, Virkkala A-M, et al. (2022) In-depth characterization of denitrifier communities across different soil ecosystems in the tundra. Environmental Microbiome 17: 30.

This extended abstract template was updated on September 12, 2025

Farmers' Perceptions and Preferences of Land Management in Irrigated Area: A Case Study of the Rwamagana District Irrigation Scheme, Republic of Rwanda

KINOSHITA Kodai [1*], MATSUNO Yutaka [2]

[1] Japan Overseas Cooperation Volunteer, JICA Rwanda Office, Kigali City, Rwanda

[2] Faculty of Agriculture, Kindai University, Nara City, Japan

* Corresponding author. Email: kinoshita.kodai8@gmail.com

Abstract

In many developing countries, most farmlands are small and fragmented landholdings. Under such conditions, the land consolidation measure could be a solution for improving agricultural productivity. To assess the potential of the land consolidation, it is necessary to look at both the institutional aspect and perception of farmers' land use practices. However, such studies in developing countries have been limited.

This study investigates farmers' perceptions and land use practices in an irrigation scheme of Eastern Province of Rwanda. Interview surveys were conducted. and the results show that farmers face chronic labor shortages, particularly during labor demanding seasons such as transplanting and harvesting, and rely on temporary laborers to compensate. More than 95% of the farmers own less than 0.5 hectares, yet most want to expand their holdings. Landholding size was found to significantly influence farmers' annual income, while larger holdings also tended to increase travel time to the farthest plots. Furthermore, rice yields were significantly lower in areas where a higher proportion of farmers reported water shortages.

These results indicate the difficulty of sustainable production on small fragmented farms under labor constraints. Equitable water distribution could facilitate farmland consolidation and reduce farmers' travel burdens. Farther studies will be beneficial for development of effective farmland uses policies.

Keywords: Farmland Use, Farmers' Perceptions, Farm Management, Irrigation

1. Introduction

In rural areas of developing countries, most farmers are smallholders. In the East African region, land fragmentation is exacerbated by population growth, issues related to land tenure.

Under such condition, a renewal of land use policies can be an effective means to improve agricultural productivity. To examine specific approaches, it is important to account each country's social background and legal framework, as well as to understand the land use patterns and perceptions of farmers to identify key challenges.

This case study aims to clarify the land use patterns of farmers and their perceptions of farmland, to contribute to the examination of land use policies in Developing countries, particularly East African region

2. Materials and Methods

This study was conducted in an irrigation scheme located in Rwamagana District, Eastern Province, Rwanda. First, interviews were carried out with government officers and staff of the irrigation water user's organization to gather information on farmers' land use and the relevant legal framework. Subsequently, field interviews were conducted with a total of 110 farmers. To minimize sampling bias, survey sites were divided across four locations within the scheme. The data were compiled and analyzed to examine farmland use patterns and their relationship with farmers' basic attributes. Furthermore, the survey results were compared with rice yield data from the study area. Additional interviews with members of the irrigation water users' organization were conducted to clarify issues that emerged during the analysis.

3. Results

The survey revealed that more than 95% of farmers in the study area owned less than 0.5 hectares of farmland, while many farmers expressed a desire to expand their landholdings in the future. Multiple regression analysis of farmers' annual income indicated that landholding size was one of the major influencing factors on farmer's livelihood.

Table-1
Multiple Regression Analysis of Farmers' Income

	Estimate	Std. Error	PR(>|t|)
(Intercept)	-2.22	0.90	0.01 *
Paddy field size	0.08	0.01	<2e-16 ***
Academic background	0.51	0.23	0.03 *
Birthplace	-0.07	0.24	0.79
Yield	0.57	0.26	0.03 *
Farmland ownership	0.47	0.20	0.03 *

Adjusted R-squared: 0.64

In addition, a positive correlation was observed between the number of plots owned and the travel time to the farthest field.

Table-2
Correlation analysis between
travel time to fields and the number of fields owned

Travel time to fields	r	p-value	n
Nearest field	-0.03	0.72	108
Farthest field	0.22	0.02 *	108

Regardless of landholding size, approximately 80% of farmers reported experiencing a shortage of labor. Analysis of labor allocation across different stages of rice cultivation showed that during peak seasons, such as transplanting and harvesting, a substantial share of work was carried out by temporary laborers. They do not own any farmland.

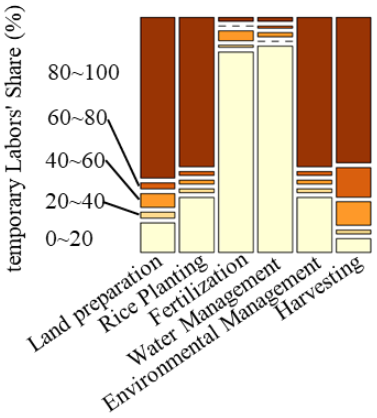

Figure-1
Proportion of temporary laborers' working hours at each stage of rice cultivation

With respect to water availability, significant regional inequalities were identified. When these results were compared with rice yield data across the study area, it was found that regions with a higher proportion of farmers reporting water shortages tended to have lower rice yields.

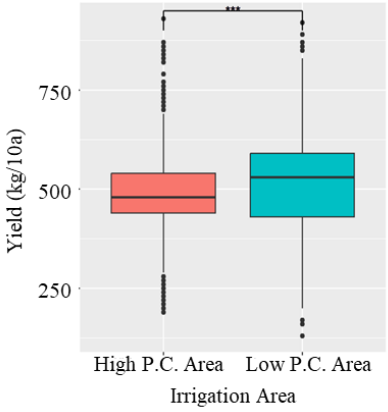

Figure-2
Boxplot of rice yields in areas with many farmers reporting water shortages and areas with few farmers reporting it

4. Discussion

Although many farmers face labor shortages, they still expressed a desire to expand their landholdings. The results of the multiple regression analysis on income suggest that most of their income depends on agriculture. In the study area, rice is purchased by cooperatives at a fixed price, meaning that yield directly determines income. This also implies that most farmers have limited alternative of income sources.

A positive correlation was observed between the number of plots owned and the travel time to the farthest field, indicating that as farmers' landholdings increase, their plots tend to be more dispersed. Consequently, expanding farmland may enhance income but could also increase the burden on farmers due to longer travel time to their fields and more complex field management.

Furthermore, the correspondence between farmers' perceptions of water shortages and rice yields demonstrates that farmers' perceptions accurately reflect the actual conditions. Equitable water distribution is considered to enable fair farming conditions for farmers, regardless of whether they are located upstream or downstream. This is considered to contribute to farmland consolidation.

5. Conclusions

This study identified several challenges related to farmland use in the study area. One major issue is the fragmentation of farmland. Rwanda is currently experiencing rapid population growth, and the demand for farmland is expected to increasing. Many farmers seek to expand their landholdings to improve their income. However, labor shortages persist, and a significant portion of farm work is delegated to temporary laborers. Given the high demand for farmland, since the immediate implementation of large-scale land readjustment is difficult, under the current conditions, promoting the consolidation of dispersed plots may contribute to improvements in agricultural productivity.

At the same time, farmland consolidation could potentially reduce farmers' burdens and increase agricultural productivity. Although limited, cases of land exchange among farmers to reduce travel time were observed. If the cooperatives or irrigation water user's organization could play a role in mediating farmland exchange, farmland consolidation could effectively progressed. Moreover, equitable water distribution, by eliminating differences in farming conditions between upstream and downstream areas, is considered to promote farmland consolidation. However, in the study area, field consolidation has not progressed, and a major challenge lies in how to facilitate exchanges between farmlands of different sizes.

Future research should continue to have more case studies, including those in rainfed agricultural areas, for better understanding of measures to improve the productivity and facilitate more efficient farmland use.

Acknowledgements

This study was conducted with the cooperation of Chariho Irrigation Water Users' Organization.

References

[1)]Arai S, Understanding Farmer Behavior and Agricultura l Policy Noukakoudou no rikai to nougyouseisaku (in Ja panese), Regional views, 2003, 16: 33-44.
[2)]The State of Food and Agriculture, FAO, https://www.fa o.org/publications/fao-flagship-publications/the-state-of -food-and-agriculture/en
Accessed August 2, 2025
[3)]Mayele, Joseph Mayindo, Jacob B. Kolle, and Joel Emm anuel Saburi. The impacts and causes of land fragmentat ion on farm productivity: Case review of East African co untries. Open Journal of Ecology 14.5 (2024): 455-482.
[4)]National Institute of Statistics of Rwanda, https://www.s tatistics.gov.rw/statistical-publications/population-size-a nd-population-characteristics
Accessed August 8, 2025

Enhancing Sustainable Agricultural Water Management through Participatory Local Governance: A Case Study from Korea

Daye Kim [1*], Seungjin Maeng [1], Eunryeong Lee [1], Bongkuk Lee [2]

[1] Department of Agricultural & Rural Engineering, Chungbuk National University, 1 Chungdae-ro, Seowon-gu, Cheongju-si, 28644, Korea

[2] Rural Research Institute, 870 Haean-ro, Sangnok-gu, Ansan-si, 15634, Korea

* Corresponding author. Email: kdy8462@naver.com

Abstract

As climate change, increasing water demand, and droughts intensify, sustainable and efficient agricultural water management is becoming more critical. This study introduces a participatory governance approach that engages local stakeholders in managing agricultural water resources. Two pilot sites in Korea—Wolseong District (Imsil County, upstream Seomjin River basin) and Boksim District (Buyeo County, downstream Geum River basin)—were examined. Governance activities included surveys, interviews, workshops, and education programs to promote collaborative decision-making. Results showed that in Wolseong district, perceived need for governance decreased (87.5% to 76.9%), while in Boksim-Chunghwa it increased (77.2% to 79.0%). Interest in water management improved in Boksim sites, though satisfaction with discussions slightly declined in Wolseong. These findings highlight regional differences in governance effectiveness. Policy recommendations include linking local governance with national programs such as the Public Direct Payment Program, basin-level funds, and renewable energy initiatives (e.g., floating solar power systems). The case demonstrates the importance of farmer-led governance in achieving sustainable agricultural water use, with implications extending to other rural contexts.

Keywords: Irrigation Water Supply, Water Governance, Water Management

1. Introduction

Integrated water management in agriculture requires a bottom-up approach, where farmers and local stakeholders lead in identifying problems and solutions. However, rural areas lack robust systems for managing agricultural water sources, resulting in inefficiencies and weak accountability. Existing governance frameworks in Korea primarily focus on river water quality and aquatic ecosystems, but little attention has been given to agricultural water circulation. This study aims to propose and test a socially acceptable, farmer-led governance model that strengthens rural water management through participatory activities, case studies, and stakeholder feedback.

2. Materials and Methods

Two pilot sites were selected: Wolseong Reservoir (Imsil, Jeollabuk-do, upstream Seomjin River basin) and Boksim Reservoir (Buyeo, Chungcheongnam-do, downstream Geum River basin).

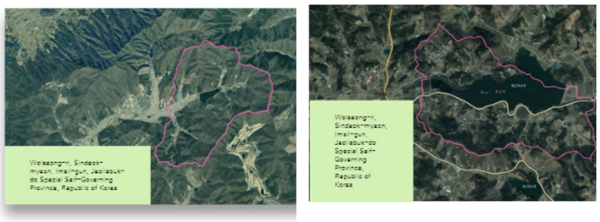

Figure 1. Locations of the pilot sites

At Wolseong, irrigation water is released into Oknyeodong Stream and coordinated through weirs, while Boksim supplies irrigation canals directly, with supplementary intake from Chilsan Stream when shortages occur.

Research methods combined qualitative and quantitative approaches. Pre- and post-surveys were conducted with more than 150 farmers and local managers, complemented by in-depth interviews with Korea Rural Community Corporation (KRC) staff. Participatory workshops and discussion forums were organized to address water-saving practices, governance awareness, and policy feedback. Monitoring plans were established to evaluate pilot district performance, with attention to governance gaps, water losses, and user practices.

3. Results and Discussion

A farmer-led governance system was developed with the involvement of national agricultural organizations, local water managers, and KRC branches. Activities included water-saving education, participatory forums, and environmental campaigns.

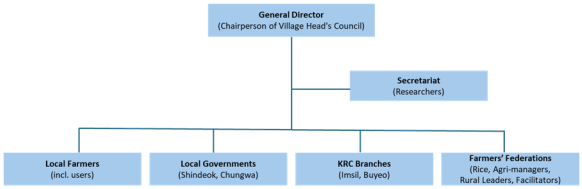

Figure 2. Organizational structure of farmer-led participatory governance for agricultural water management

Survey results revealed clear regional contrasts. In Wolseong, the perceived need for governance decreased (87.5%→76.9%) despite high baseline awareness, suggesting initial overestimation of governance benefits. In contrast, Boksim-Chunghwa increased significantly (77.2%→79.0%), while Boksim-Imcheon stabilized. Interest in water management improved in Boksim, indicating growing farmer engagement, while satisfaction with discussions declined slightly in Wolseong, reflecting

challenges in sustaining long-term interest.

Table 1. Summary of pre- and post- survey results for governance need, water management interest, and satisfaction with discussions

Item	Wolseong	Boksim-imcheon	Boksim-Chunghwa
Governance need (%)	87.5→76.9	57.1→51.9	77.2→79.0
Water management interest (%)	87.5→80.7	64.3→66.7	57.9→79.0
Satisfaction with discussions (%)	66.7→61.5	57.1→59.3	50.0→52.6

These findings show that participatory governance can enhance agricultural water management but that effectiveness varies depending on socio-economic context, prior awareness, and institutional support. The governance model not only facilitated dialogue among stakeholders but also highlighted the importance of continuous feedback and adaptive management.

Policy Recommendations: First, local governance initiatives should be systematically linked with national programs such as the Public Direct Payment Program to incentivize farmer participation. Second, basin-level funds could ensure stable financing for water infrastructure maintenance, while integration with renewable energy projects, such as floating solar power systems, can provide additional income streams for rural communities. Third, training programs, conflict resolution mechanisms, and transparent accountability systems are essential for strengthening governance capacity. Finally, regional councils should promote cross-district collaboration to reduce disparities in outcomes and build resilience against climate change.

4. Conclusions

This study demonstrates that farmer-led participatory governance can strengthen rural water management, though its impacts differ by region. Quantitative monitoring was constrained by physical limitations, but complementary evaluation approaches were employed. The results underscore the need to gradually expand governance systems, systematically integrate them with national programs, and reinforce them through continuous education and institutional support. Beyond Korea, this case provides valuable insights for other agricultural countries in Asia and globally that face similar challenges of water scarcity, fragmented governance, and climate change impacts.

References

Choi, Seul-Gi, and Choi, Kyung-Sook, 2021. *A Basic Study on Establishment and Operation of Agricultural Water Saving Governance*. Journal of Korean Society of Rural Planning, 27(3), 11-20.

Choi, Seul-Gi, and Choi, Kyung-Sook, 2022. *Development of a Bottom-up Agricultural Water Governance Model in Korea*. Journal of Korean Society of Rural Planning, 28(3), 49-59. DOI: 10.7851/ksrp.2022.28.3.049

Lee, Seung-Ho, and Kim, Seung, 2009. *Water Governance and the Act on the Management of Water Resources*. Proceedings of the Korean Water Resources Association Conference, pp. 385-389. (in Korean)

Korea Rural Community Corporation, 2024. *A Study on Governance for Integrated Water Management of Rural Irrigation Water*.

Climate Change and Adaptation in Coastal Agriculture: Impacts on Nutrient Cycling and Water Resources

Wen-Chi Chen [1], Yen-Yu Chen [1] , Sheng-Wei Wang [2*]

[1] Department of Water Resources and Environmental Engineering, Tamkang University, New Taipei City 25137, Taiwan (ROC)

[2] Department of Civil Engineering, National Central University, Chung-Li city, Tao-Yuan 320317, Taiwan(R.O.C.)

* Corresponding author. Email: wangsw@ncu.edu.tw

Abstract

Climate change has altered hydrological processes and nutrient dynamics, posing serious challenges to the sustainability of agricultural production and water resources. This study assesses the impacts of farming activities on ecosystem services in a coastal agrarian area of Taiwan. Key parameters were collected, including elevation, land use and cover, soil types, and meteorological data. By applying the Integrated Valuation of Ecosystem Services and Tradeoffs (InVEST) model, the research assesses the effects of climate change on annual water yield and nutrient retention. Future projections were analyzed under two Shared Socioeconomic Pathways (SSPs), SSP1-2.6 (sustainable development pathway) and SSP5-8.5 (high economic development pathway), utilizing downscaled IPCC climate projections. Under SSP1-2.6, mid-century projections show decreases in rainfall by 0.6%–8.87 %, water yield by 0.8%–11.58 %, and nutrient retention by approximately 2.2%. Under SSP5-8.5, reductions reach 22.71%, 29.78%, and 5.44%, respectively. Additionally, the frequency of extreme rainfall events is expected to rise by the end of the century, intensifying surface runoff and nutrient loss, and reducing nutrient retention by 3.46%–4.88%, which may threaten groundwater quality and ecosystem stability. Taiwan's agriculture faces structural issues, such as fragmented farmland, excessive fertilization, and poor soil water retention. Strengthening farmer education and policy support is critical to promote sustainable land management and climate resilience. The results of this study provide robust quantitative evidence to inform decision-making and enhance the long-term sustainability of agricultural ecosystem services under climate change.

Keywords: Ecosystem Services, Climate Change, Sustainable Agriculture

1. Introduction

The expansion of agriculture, urbanization, deforestation, and industrialization has progressively transformed ecosystems across the globe. These anthropogenic activities have diminished the capacity of ecosystems to deliver essential services. In natural landscapes, biodiversity and landuse systems are closely interrelated. Changes in land use not only alter surface characteristics but also affect regional climate, disrupt hydrological cycles, reduce biodiversity, and ultimately impair the functioning of ecosystem services. For instance, deforestation and the loss of wetlands weaken the ability of ecosystems to retain water and regulate flooding. Consequently, the risks of droughts and flood disasters increase significantly. According to the Millennium Ecosystem Assessment, ecosystem services can be categorized into four main types: provisioning, regulating, supporting, and cultural services. Water related ecosystems provide a variety of critical functions, including the supply of freshwater and food, mitigation of floods and droughts, carbon storage, regulation of nutrients and pollutants, stabilization of microclimates, and support for cultural and educational values. These services are closely tied to biodiversity and play an essential role in promoting human well-being and achieving sustainable development. This study is a coastal agricultural region in Taiwan using the Integrated Valuation of Ecosystem Services and Tradeoffs (InVEST) model to assess the spatial impacts of farming activities on ecosystem services. The analysis considers two Shared Socioeconomic Pathway (SSP) scenarios: SSP1 2.6, this pathway, policies focus on human well-being, clean energy technologies, and the preservation of the natural environment., and SSP5 8.5, which reflects a future with high emissions and continued reliance on fossil fuels. Simulation results reveal that climate change affects both annual water yield and nitrogen retention capacity, highlighting potential shifts in ecosystem service provision under different socio-environmental futures.

2. Materials and Methods

2.1. Study Area

The study area is located in Yunlin County, central Taiwan, which has the highest agricultural production value in the country. The county is bounded by the Taiwan Strait to the west and by the Zhuoshui River, the main river of the study area, to the north. The study area covers approximately 1,290 km^2. The region consists of about 90% plains and 10% mountainous terrain. The topography is relatively simple, but the hydrological characteristics exhibit considerable variability. The climate is classified as subtropical, with a mean annual temperature of 22.6°C and an average annual precipitation of about 1,028.9 mm, most of which falls between May to September.

In terms of topography (Fig1.), the eastern of the study area represents the upstream catchment zone, situated near the foothills of the Central Mountain Range. This area serves as the primary source of water inflow, characterized by pronounced terrain relief and dominated by forest land and mixed agricultural uses. The central region is a typical alluvial plain with intensive agricultural activity and diverse land-use patterns, where irrigation and drainage systems are extensively developed and interconnected. The western consists of the downstream coastal lowlands adjacent to the Taiwan Strait. This area is flat and highly flood-prone, with land use primarily consisting of aquaculture ponds and paddy fields, making it particularly sensitive to nutrient transport and water quality changes.

Figure 1. Steady Area

2.2. InVEST Model

This study collected key parameters, including elevation, land use and land cover, soil types, and meteorological data. The Integrated Valuation of Ecosystem Services and Trade-offs (InVEST) model, developed in the United States, was applied to analyze annual water yield and nutrient transport, and Shared Socioeconomic Pathway (SSP) climate scenarios were incorporated to enable comparative assessments of future conditions.

The nutrient delivery ratio (NDR) module was applied to identify the sources and pathways of nutrient transport within watersheds, thereby evaluating the capacity of vegetation and soils to retain nutrients. Key factors influencing nutrient transport include land use, nutrient loading, filtration efficiency, and watershed runoff. In this model, only the filtering capacity of vegetation was considered, while biogeochemical processes in soils were not included. The nutrient export is calculated as Eq(1).

$$x_{\exp i} = load_{surf,i} \cdot NDR_{surf,i} + load_{subs,i} \cdot NDR_{subs,i}$$

$$x_{exptot} = \sum_i x_{\exp i} \quad (1)$$

where $x_{\exp i}$ is the nutrient export from grid cell i; x_{exptot} is the total watershed export; $NDR_{subs,i}$ and $NDR_{surf,i}$ denote the nutrient delivery ratios for surface and subsurface water respectively; $load_{surf,i}$ and $load_{subs,i}$ represent surface and subsurface nutrient loads.

The annual water yield module sums grid water yield, enabling the evaluation of spatially explicit factors such as soil type, precipitation, and land cover on watershed hydrology. It further estimates the total and mean water yield within each sub-watershed. The computation is based on the Budyko curve and mean annual precipitation, with evapotranspiration and rainfall differentiated by landuse type. An equation is showed in Eq(2).

$$Y(x) = \left(1 - \frac{AET(x)}{P(x)}\right) \times P(x) \quad (2)$$

where $Y(x)$ is the mean annual water yield for landuse type; $AET(x)$ is the actual evapotranspiration; $P(x)$ is the annual precipitation.

2.3. Climate Change Scenario

This study employed the TaiESM1 model, which is adapted from the NCAR Earth System Model to reflect Taiwan's environmental conditions. Climate scenarios were based on the Shared Socioeconomic Pathways (SSPs) from the IPCC Sixth Assessment Report. The analysis considered two contrasting futures: SSP1-2.6, a low-emission sustainability pathway with radiative forcing reaching 2.6 W/m² and global warming limited to below 2°C by 2100; and SSP5-8.5, a high-emission fossil-fuel–intensive pathway with radiative forcing up to 8.5 W/m² and a projected temperature increase of about 4.4°C by 2100.

3. Results and Discussion

The results indicate that by the mid-century under the sustainability scenario (SSP1-2.6), rainfall decreases by approximately 0.6%–8.87%, while annual water yield decreases by 0.8%–11.58%. Under the high economic development scenario (SSP5-8.5), rainfall shows a greater reduction of 3.62%–22.71%, with annual water yield decreasing by 4.84%–29.78%. These findings suggest that reduced rainfall and more frequent droughts may increase the risk of soil erosion, lower soil moisture content, and limit plant evapotranspiration, thereby weakening regulating ecosystem services.

For nutrient retention (Table 1), the reduction is about 2.2% under SSP1-2.6 by mid-century, while under SSP5-8.5 the decrease ranges between 2.26% and 5.44%. Toward the end of the century, however, climate change is projected to intensify extreme rainfall events, with rainfall increasing by 0.91%–14.47% under SSP5-8.5. Higher rainfall intensity is expected to substantially increase surface runoff, leading to significant nutrient loss. Consequently, nutrient retention further declines by 3.46%–4.88%. These shifts may accelerate nutrient leaching, elevate the risk of groundwater contamination, and negatively affect water quality and ecosystem stability.

Table 1. Nutrient retention due to climate change .

scenarios	Near Future	Mid Future	Far Future
SSP1-2.6	-5.4~-0.5%	-4.9~-0.9%	-4.8~0.48%
SSP5-8.5	-5.4~-1.9%	-4.9~-1.3%	-3.5~-1.9%

4. Conclusions

Different climate change scenarios exert significant impacts on agricultural development. Under the low-emission scenario, reductions in water yield and nutrient retention remain relatively moderate. In contrast, under the high-emission scenario, greater rainfall variability and more frequent extreme events intensify the risks of water scarcity, nutrient loss, and ecosystem instability. Ensuring sustainable water resource management and resilient agricultural development therefore requires accurate assessment of climate change impacts on agricultural systems, as well as proactive preparation for the risks posed by extreme rainfall events..

Acknowledgements

The authors wish to express their appreciation to the National Science and Technology Council, Taiwan (R.O.C.) for their financial support under Grant Numbers NSTC 113-2621-M-150-001 -..

References

Natural Capital Project, 2025. InVEST 3.16.2. Stanford University, University of Minnesota, Chinese Academy of Sciences, The Nature Conservancy, World Wildlife Fund, Stockholm Resilience Centre and the Royal Swedish Academy of Sciences.

Hierarchical and Non-hierarchical Cluster Analysis of Standard Watersheds Considering Hydrology, Water Quality, and Aquatic Ecosystem in South Korea

Wonjun Jeon [1], Yonggwan Lee[2], Jeehun Chung[3], Yongwon Kim[3], Seongjoon Kim[4*]

[1] Division of Civil and Environmental Engineering, Graduate School, Konkuk University, Seoul, Gwangjin-gu Neungdong-ro 05029, Republic of Korea

[2] Asia Infrastructure Research Center, Konkuk University, Seoul, Gwangjin-gu Neungdong-ro 05029, Republic of Korea

[3] Department of Civil, Environmental and Plant Engineering, Graduate School, Konkuk University, Seoul, Gwangjin-gu Neungdong-ro 05029, Republic of Korea

[4] Division of Civil and Environmental Engineering, College of Engineering, College of Engineering, Konkuk University, Seoul, Gwangjin-gu Neungdong-ro 05029, Republic of Korea

* Corresponding author. Email: kimsj@konkuk.ac.kr

Abstract

This study applies hierarchical and non-hierarchical clustering to 850 standard watersheds in South Korea, classifying them by hydrology, water quality, and aquatic ecosystem characteristics. The datasets include Terra MODIS products (land surface temperature, NDVI, leaf area index), meteorological variables (precipitation; maximum, minimum, and mean temperature; relative humidity; wind speed; solar radiation), GIS-derived features (DEM, land use, slope, stream order), and hydrology–water quality–ecosystem health data (streamflow, suspended solids, total nitrogen, total phosphorus, ecosystem health indices). Clustering grouped watersheds by environmental characteristics, revealing spatial heterogeneity shaped by topography, temperature, precipitation, land cover, slope, and stream order. The results provide a framework for national ecological flow assessment and integrated watershed management.

1. Introduction

Watershed classification is essential for understanding spatial patterns of hydrology, water quality, and aquatic ecosystems, providing key information for ecological flow assessment and sustainable water management. While habitat-based models such as PHABSIM and River2D are effective locally, their limited scalability poses challenges for broader applications. Cluster-based classification can help overcome these limitations by reflecting regional biophysical variability, enabling scalable ecological flow estimations.

Previous studies support the value of integrative classification. Mayer et al. (2014) highlighted the value of combining hydrological, water quality, and ecological indicators, while Ahn et al. (2014) showed that topography, hydrology, meteorology, soil, and land cover are effective for watershed stratification. Hu et al. (2022) highlighted the influence of slope, stream order, and land cover on water quality and ecosystem health. Such frameworks capture spatial heterogeneity, supporting national ecological flow estimation and integrated management (Debnath, 2016). In this study, 850 standard watersheds in South Korea were classified using hierarchical and non-hierarchical clustering. By integrating satellite, meteorological, GIS, hydrological, and ecosystem health data, we identified coherent watershed types and established a practical stratification framework.

2. Materials and Methods

2.1. Study Area and dataset

The study covered 850 standard watersheds in South Korea (Figure 1) and utilized a comprehensive set of input data. Satellite-derived variables included MODIS Land Surface Temperature (LST), Normalized Difference Vegetation Index (NDVI), and Leaf Area Index (LAI). Meteorological data encompassed precipitation (mm), maximum, minimum, and mean temperature (°C), relative humidity (%), wind speed (m/s), and solar radiation(MJ/m^2). GIS-derived features incorporated Digital Elevation Model (DEM), land use, slope, and stream order, while hydrological and aquatic ecosystem health data comprised streamflow, suspended solids, total nitrogen, total phosphorus, and indicators of aquatic ecosystem health.

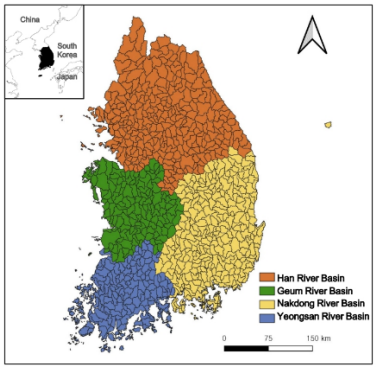

Figure 1. Description of 850 standard watersheds and the four major river of South Korea.

2.2. Statistical analysis

The dataset were summarized using descriptive statistics to examine temporal and seasonal patterns across the 850 standard watersheds. Normality tests were conducted to assess variable distributions, and Spearman correlation analyses was applied to identify key variables and reduce redundancy among predictors. Boxplots were used to visualize data dispersion and outliers, providing insights into variability and supporting robust inputs for cluster analysis.

2.3. Cluster Analysis

Hierarchical and non-hierarchical clustering were applied to explore watershed groupings based on selected variables. Spearman correlation identified correlated features, and cluster validity indices (Silhouette, Calinski–Harabasz) guided cluster numbers. This approach

characterizes watersheds by environmental and ecological features. Preliminary analyses suggest precipitation, temperature, land cover, slope, and stream order are influential, consistent with previous studies on landscape effects on water quality and ecology (Cupak and Kaczor, 2022).

3. Results and Discussion

Basic statistical analysis was conducted on the ecological flow-related factor dataset, and the Shapiro-Wilk test was applied to assess normality. Among the 59 variables, most exhibited *p*-values below 0.05, indicating deviation from normality, except for the DEM-derived aspect variable. Accordingly, non-parametric correlation analysis using Spearman coefficients was performed, followed by secondary factor selection to mitigate multicollinearity. Using the selected factors, cluster analysis was carried out for standard watersheds nationwide. While K-means is generally applied to datasets with more than 50 variables, hierarchical clustering can provide complementary insights when assumptions of normality and distance are uncertain. Therefore, both methods were employed. For K-means clustering, the analysis was repeated 100 times, and the optimal number of clusters was identified as 11. Evaluation using the Silhouette, Calinski-Harabasz, and Davies-Bouldin indices suggested this configuration as optimal (Silhouette = 0.152; Davies-Bouldin = 1.327). However, GIS mapping (Figure 2) indicated that clusters were not well separated, suggesting that further refinement of input variable selection may be necessary.

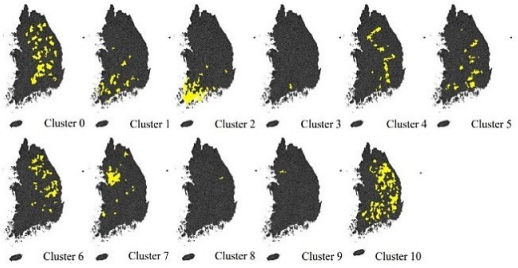

Figure 1. Results of K-means clustering

Hierarchical clustering, implemented with a bottom-up dendrogram approach (Figure 3), identified four clusters as optimal, highlighting differences in cluster granularity between the two methods.

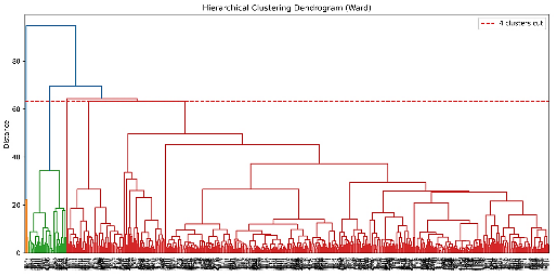

Figure 3. Results of hierarchical clustering

These results indicate that the choice of clustering method affects the number and composition of clusters. Non-hierarchical clustering yields a larger number of finer clusters, while hierarchical clustering emphasizes broader groupings, which can be useful for examining ecological patterns at different scales. Hierarchical clustering of the 850 standard watersheds (Table 1) showed that Cluster 1 and Cluster 4 contained 380 and 341 watersheds, respectively, forming similarly sized groups. In contrast, Cluster 2 and Cluster 3 comprised only 2 and 127 watersheds, with Cluster 2 showing a pronounced concentration. This imbalance suggests that hierarchical clustering may be unstable for representing characteristics across all standard watersheds.

Table 1. Clustering Results.

Cluster No.	Cluster 1	Cluster 2	Cluster 3	Cluster 4
Number of Standard Watersheds	380	2	127	341

4. Conclusions

This study applies hierarchical and non-hierarchical clustering to classify 850 standard watersheds in South Korea, considering hydrology, water quality, and aquatic ecosystem indicators. Emphasis is placed on evaluating the relative importance of input variables to ensure transparency in clustering outcomes and watershed characterization. The results are expected to provide a framework for nationwide ecological flow assessments, highlighting spatial variability among watersheds and supporting integrated management. Further research will incorporate additional datasets, temporal analyses, and modeling to enhance robustness and predictive reliability, contributing to sustainable river ecosystem management.

Acknowledgements

This work was supported by Korea Environment Industry & Technology Institute(KEITI) through Aquatic Ecosystem Conservation Research Program, funded by Korea Ministry of Environment(MOE) (RS-2025-02304832)

This work was supported by Korea Environment Industry & Technology Institute(KEITI) through Water Management Program for Drought Project, funded by Korea Ministry of Environment(MOE).(2022003610002)

References

Journal articles:

Mayer, A., Winkler, R., Fry, L., 2014. Classification of watersheds into integrated social and biophysical indicators with clustering analysis. Ecol. Indic., 45, 340–349

Ahn, S.-R., Kim, S.-H., Kim, S.-J., 2014. A study on hydrologic clustering for standard watersheds of Korea water resources unit map using multivariate statistical analysis. J. Korea Water Resour. Assoc., 47(2), 91–106

Debnath, R., 2016. A review of the sustainability of recent watershed management programmes in Bangladesh. Lakes Reserv. Res. Manag., 21(2), 152–161

Hu, Y., Yin, S., Xiao, W., Hou, B., Zhang, X., 2022. Spatial scale effects of landscape patterns on water quality changes in drinking water source protection areas: a case study in the Guishui River Basin, China. Arab. J. Geosci., 15(7), 685

Cupak, A., and Kaczor, G., 2022. Regionalization of low flow for chosen catchments of the upper Vistula river basin using non-hierarchical cluster analysis. Időjárás, 126(1), 27–45

Ecological Impact of Treated Effluent Irrigation in Rice Paddies: A Case Study on Aquatic Organisms

Chen Wuing Liu [1], Jin Jing Lee [1], Feng Wen Chen [2,3*], Yu Chien Cho [2], Guan Jia Chen [2], Mei Hwa Kuo [2], Yi Ji Tan [2]

[1] Department of Water Resources, Taoyuan Government, Taoyuan District, Taoyuan City, 330005, Taiwan

[2] Agricultural Engineering Research Center, Zhongli District, Taoyuan City, 320030, Taiwan

[3] Department of Water Resources and Environmental Engineering, Tamkang University, Tamsui, New Taipei City 251301, Taiwan

[4] Department of Entomology, National Chung Hsing University, South District, Taichung City 40227, Taiwan

* Corresponding author. Email: chenfw@aerc.org.tw

Abstract

In response to water scarcity, reusing treated effluent for irrigation offers potential to ease agricultural water stress. Yet its ecological impacts in paddy fields warrant careful assessment. This study monitored two rice fields in Yangmei, northern Taiwan, over two cropping seasons in 2024: one irrigated with treated effluent and the other with Shezi River water. Aquatic insects were used as ecological indicators, and biodiversity was evaluated using Margalef richness, Shannon–Wiener, Simpson, and Pielou's evenness indices. Statistical analysis with ANOVA (GLM procedure, SAS, significance at $P < 0.05$) tested differences between treatments. In the first season, biodiversity indices in effluent versus river irrigation were 2.038 vs. 1.333 (Margalef), 1.823 vs. 1.619 (Shannon–Wiener), 0.8344 vs. 0.7685 (Simpson), and 0.8768 vs. 0.8319 (Pielou). In the second season, values were 1.33 vs. 1.934, 1.666 vs. 2.058, 0.769 vs. 0.8482, and 0.8562 vs. 0.8282, respectively. Across both seasons, ANOVA revealed no significant differences ($P > 0.05$) in biodiversity between the two irrigation sources. These findings indicate that treated effluent irrigation did not adversely affect aquatic insect ecology in rice paddies, preliminarily supporting its environmental feasibility. Continued long-term monitoring, including terrestrial fauna and birds, is recommended to ensure comprehensive ecological evaluation of effluent reuse in agriculture.

Keywords: Aquatic Insects, Water Reuse, Ecology of Aquatic Environments.

1. Introduction

Water scarcity has emerged as a pressing global challenge, highlighting the urgency of enhancing water use efficiency and narrowing the supply–demand gap. Reusing treated domestic wastewater (effluent) for agricultural irrigation is considered a practical and sustainable option. While existing studies have primarily focused on water availability, quality, and crop safety, the ecological implications of effluent reuse remain underexplored. This concern resonates with international commitments such as the *Convention on Biological Diversity (CBD, 1992)* and the *United Nations Sustainable Development Goals (SDGs, 2015)*, which emphasize biodiversity conservation and sustainable water management. Paddy fields, with their distinct water-retention characteristics, provide an ideal setting to examine these issues. In this study, aquatic insects were selected as ecological indicators due to their sensitivity and ecological relevance. Over two cropping seasons in one year, insect communities were compared between effluent-irrigated and river-water-irrigated rice paddies to assess the potential ecological impacts of effluent irrigation.

2. Materials and Methods

2.1. Study Area

The study was conducted in Yangmei District, Taoyuan City, northern Taiwan. Two adjacent paddy fields were selected: the test field (1,479 m²) irrigated with treated effluent from the Yangmei Water Resource Recycling Center, and the control field (1,174 m²) irrigated with Shezi River water. Effluent was delivered by pumping through pipelines, while the control field received river water via an open-channel gravity system. Figure 1 illustrates the location and layout of the effluent- and river-water–irrigated paddy fields in Yangmei, Taoyuan, which served as the experimental sites for this study.

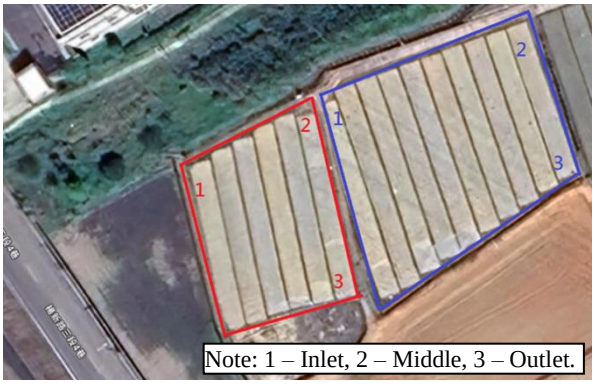

Figure 1. Location and layout of the effluent- and river-water–irrigated paddy fields in Yangmei, Taoyuan, Taiwan.

2.2. Sampling and Analysis Methods

Sampling was conducted in two cropping seasons of 2024 at three locations in each field (inlet, middle, outlet). Aquatic macroinvertebrates were collected using the core method with an acrylic frame (30 × 30 × 50 cm) inserted into the sediment. Disturbed water and organisms were scooped and filtered through a 250 μm mesh. The core sampling method is shown in Figures 2 and 3, demonstrating the use of an acrylic frame to collect aquatic macroinvertebrates in the paddy fields. Samples were preserved in 75% ethanol and identified in the laboratory. Aquatic insects were classified to the family level, while other macroinvertebrates were identified to the class level. Biodiversity was evaluated using four widely applied indices. First, the Margalef richness index (Eq. 1) was used to estimate species richness relative to total abundance (Margalef, 1958). Second, the Shannon–Wiener index (Eq. 2) was applied to quantify community

diversity based on both richness and proportional abundance (Shannon and Weaver, 1949). Third, the Simpson index (Eq. 3) was used to measure dominance, where higher values indicate greater diversity and lower dominance of single species (Simpson, 1949). Finally, the Pielou's evenness index (Eq. 4) was used to assess the distribution of individuals across species (Pielou, 1966).

$$d = S-1/\log(N) \quad (1)$$

$$H' = -\sum \quad p \quad (2)$$

$$1-\lambda = 1-\sum \quad (3)$$

$$J' = H'/\log(S) \quad (4)$$

These indices were calculated using PRIMER 6 software, and statistical comparisons were performed using ANOVA under the GLM procedure in SAS, with significance set at P<0.05P < 0.05P<0.05 (Krebs, 1999).

Figure 2. Core sampling method applied in paddy fields to collect aquatic macroinvertebrates.

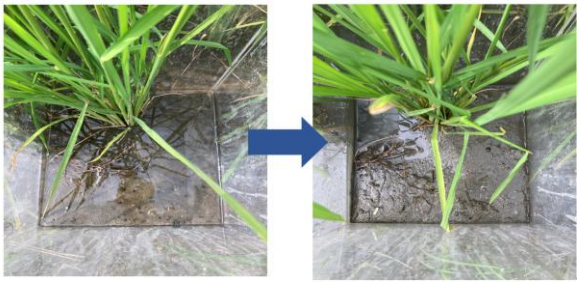

Figure 3. Field operation of the core sampling method using an acrylic frame

3. Results and Discussion

3.1. Survey Results

In the effluent-irrigated field, a total of 5 orders and 12 families of aquatic insects were recorded in the first season (45 individuals), increasing to 6 orders and 13 families in the second season (110 individuals). In contrast, the river-water field contained 7 orders and 14 families (107 individuals) in the first season and 6 orders and 14 families (297 individuals) in the second season. Non-insect macroinvertebrates such as Arachnida, Oligochaeta, Gastropoda, Branchiopoda, and Crustacea were also observed, with temporal variations across seasons. Detailed results are presented in Table 1.

3.2. Biodiversity Indices

Biodiversity indices, including Margalef richness, Shannon–Wiener, Simpson, and Pielou's evenness, showed temporal and spatial variations between the two irrigation sources. In the first season, most indices were higher in the effluent-irrigated field, whereas in the second season, the river-water field yielded higher values. Representative results are summarized in Table 1.

Table 1. Survey results of aquatic organisms observed in effluent- and river-water–irrigated paddy fields during two cropping seasons in 2024

Group	Effluent field		River-water field	
	1st period	2nd period	1st period)	2nd period
Arachnida	1	8	-	5
Oligochaeta	78	75	26	150
Gastropoda	81	117	134	19
Branchiopoda	-	32	-	113
Crustacea	-	-	1	-
Aquatic insects	5 orders, 12 families, 45	6 orders, 13 families, 110	7 orders, 14 families, 107	6 orders, 14 families, 297
Diptera pupae	1	-	-	2

3.3. Statistical Analysis

ANOVA results revealed no significant differences (P>0.05) in biodiversity indices between effluent- and river-water–irrigated fields across both cropping seasons. This indicates that the use of treated effluent for irrigation did not adversely affect aquatic insect communities in rice paddies. The findings suggest ecological stability under effluent irrigation, supporting its potential as a sustainable agricultural water resource.

4. Conclusions

This study evaluated the ecological impacts of irrigating rice paddies with treated effluent in northern Taiwan. Results from two cropping seasons in 2024 demonstrated that aquatic insect diversity in effluent-irrigated fields was comparable to that in river-water fields. Although biodiversity indices varied between seasons, ANOVA showed no significant differences (P>0.05P > 0.05P>0.05) between the two irrigation sources. These findings suggest that treated effluent irrigation does not adversely affect aquatic insect communities and may be considered environmentally feasible for paddy cultivation. To strengthen future assessments, long-term monitoring and expanded surveys including terrestrial organisms, amphibians, and birds are recommended to provide a more comprehensive evaluation of the ecological sustainability of effluent reuse in agriculture.

References

Krebs, C.J., 1999. *Ecological Methodology* (2nd ed.). Benjamin Cummings, Menlo Park, California.

Margalef, R., 1958. Information theory in ecology. *General Systems*, 3, 36–71.

Shannon, C.E., Weaver, W., 1949. *The Mathematical Theory of Communication*. University of Illinois Press, Urbana.

Simpson, E.H., 1949. Measurement of diversity. *Nature*, 163, 688.

Pielou, E.C., 1966. The measurement of diversity in different types of biological collections. *J. Theor. Biol.*, 13, 131–144.

Secretariat of the Convention on Biological Diversity, 1992. *Convention on Biological Diversity*. Montreal, Canada.

United Nations, 2015. *Transforming our world: The 2030 agenda for sustainable development*. United Nations, New York.

This extended abstract template was updated on Septempter 14, 2025

Development of a Practical Numerical Model for Predicting Paddy Field Dam Effect Based on the Actual Field Condition

Takaaki Abe [1*], Naoko Koshiyama [2], Nobuyuki Hotta [1]

[1] Cold-Region Hydraulic and Aquatic Environment Engineering Research Group, Civil Engineering Research Institute for Cold Region, Sapporo City, Hokkaido, 0628602, Japan

[2] Cold-Region Agricultural Development Research Group, Civil Engineering Research Institute for Cold Region, Sapporo City, Hokkaido, 0628602, Japan

* Corresponding author. Email: abe-t2ji@ceri.go.jp

Abstract

Recently, "Paddy Field Dam" is attracting a social attention for its flood mitigation effects. However, its local storage effect is unclear, since each paddy field has variabilities such as ground surface elevation, dike distribution and drainage installation situation. In this research, a new approach is introduced for modeling the flood mitigation effect of paddy field dams. The targeted field is in Iwamizawa city, Hokkaido. The surface elevation with refined resolution of the site is modeled using SfM (Structure from Motion) technique. Field observations of water level and discharge from the paddy field are conducted summer season in 2024. A 2D shallow water equation model is developed for the evaluation of flood mitigation effect of paddy field dam. The model is verified through the comparison between numerical prediction and the observed data, showing a good agreement of both observed and predicted data. Then, the model is applied to the same flood event with "paddy field dam" condition. As a result, installation of paddy field dam to the targeted field can decrease the water level in the drainage channel during the event. This model can be a reliable tool for facilitating consensus-building efforts among farmers and river-management offices.

Keywords: paddy field dam, numerical simulation, UAV-SfM technique, real scale

1. Introduction

The concept of "River Basin Disaster Resilience and Sustainability by All" has spread nationwide as a means of preparing for frequent flood disasters, and various efforts are being implemented by entities within river basins. This paper focuses primarily on "paddy field dam" (herein described as “PFD”) initiatives. The quantitative effects of PFDs for flood control remain unknown; such as which areas within a watershed should each farmer or district strategically promote such measures. Against such background, the research group of Civil Engineering Research Institute for Cold Region (CERI) pays attention to evaluation of flood control effect, taking into account field or water management conditions during farming. However, there is a few researches about the evaluation of this kind of perspective. In addition, the production of rice may also be affected depending on the growing stages and the duration of inundation of the farmland during a flood event. Since PFD installation is carried out by each local farmer, in order to ensure the flood control effects of PFDs, it is important to gain each farmer's approval for PFD activities while explaining the flood mitigation effects as well as the impact on farming itself.

This paper examines the flood control effects of PFDs as a flood control measure, especially focusing on local field conditions. Using a numerical analysis model considering the actual conditions of the paddy field, we aimed to understand the storage situation and runoff reduction effect. The accuracy of the model is verified through on-site observation results, and then numerical analysis with PFD conditions are performed and the effects of PFD of the targeted field are described.

2. Materials and Methods

To conduct observations with actual field conditions, observations were conducted during the summer season in 2024 at 15 rice paddy fields (7 ha) in Iwamizawa City, Hokkaido, Japan. The observation period was from July to November. Observations of paddy field water levels, water level of the drainage channel and drainage channel discharge were conducted. Aerial photography was taken and used for topographical survey. Based on the discharge observations, H-Q equations were created for the upstream and downstream ends of the drainage channels, and water level data was converted to discharge data. Topographic data was created using SfM techniques from UAV aerial images. Points such as the edges of typical structures within the field were used as GCPs, and elevations of them were obtained using GNSS surveying (Trimble Geo7). 3D point cloud data was created using Agisoft's Metashape Professional and used as topographic data for calculation. Figure 1 shows the topographic data used in this study. Although a culvert exists within the drainage channel, the channel bed topography was determined by a channel bed profile survey. The numerical model used here is an unsteady flow calculation model which takes rainfall into account and is based on the two-dimensional shallow water equations. For a full-scale farm field, runoff from the paddy field to the drainage channel via a drainage outlet was calculated using the orifice equation and

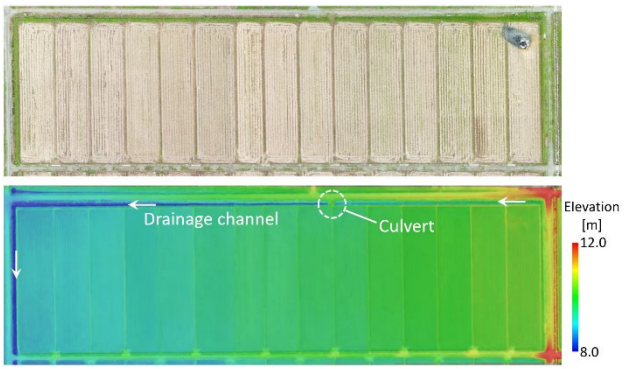

Figure 1. Created field elevation data using UAV-SfM technique

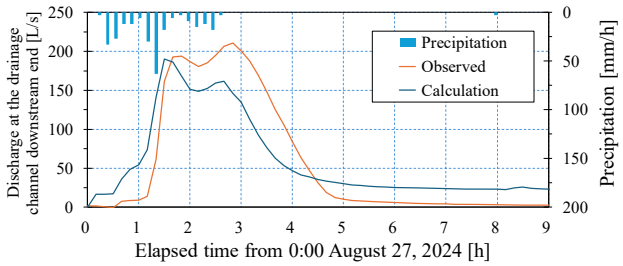

Figure 2. Comparison between calculation result and observed discharge in the rainfall event.

outflow volume equations for a square weir or a v-notch type weir plate, referring to the previous study (Minakawa & Miyazu, 2022). For the numerical analysis, iRIC software (iRIC Project) was used for generating computational mesh, initial and boundary condition settings, output and visualization of the calculation results. The numerical analysis focused on the rainfall event on August 27, 2024, which had the highest total rainfall in 2024. After verifying the validity of the numerical analysis model, the extent to which paddy field storage and drainage control would be possible with the PFD implementation condition.

3. Results and Discussion

First, the results of the simulation for the summer flood season in 2024 are described. Figure 2 shows a comparison of the temporal change in rainfall and the change in discharge at the end of the drainage channel, starting from midnight on August 27th. The total precipitation was 47 mm, the largest rainfall event of the season. During this event, the height of the weir plate was assumed to be the same as the elevation of the nearby field, since the field was in a drained state. The observed rainfall pattern had three peaks, but the observed hydrograph indicated by the orange line in the figure showed a two-peak runoff. The blue line representing the calculation result also shows the bimodal trend, showing good agreement between observed and predicted discharge hydrograph. However, the runoff during the initial stage of the rainfall began to increase earlier in the simulation. The reason is thought to be due to the analysis failing to take into account infiltration into the field. Considering infiltration volume in the continuity equation in the model may improve reproducibility.

Having confirmed that this model has reproducibility in predicting paddy field storage for rainfall, calculations are conducted to predict changes in storage conditions assuming the installation the PFDs. Rainfall conditions were the same as those for the August 27th event. Figure 3 compares the changes in storage conditions over time when (a) conventional water management plates are installed and (b) v-notch type plates are installed to simulate the effect of PFDs. The storage conditions after one hour (t = 1h) for each case and the storage conditions at the time the drainage channel peaked 1.5 hours later in (a) and 3 hours later in (b). In each case, differences in storage conditions became apparent after one hour, and a storage effect was clear when PFD weir plates were installed. At the point when the runoff volume reached its maximum, as shown in the bottom of each figure, a clear difference was shown, and it was found that the storage

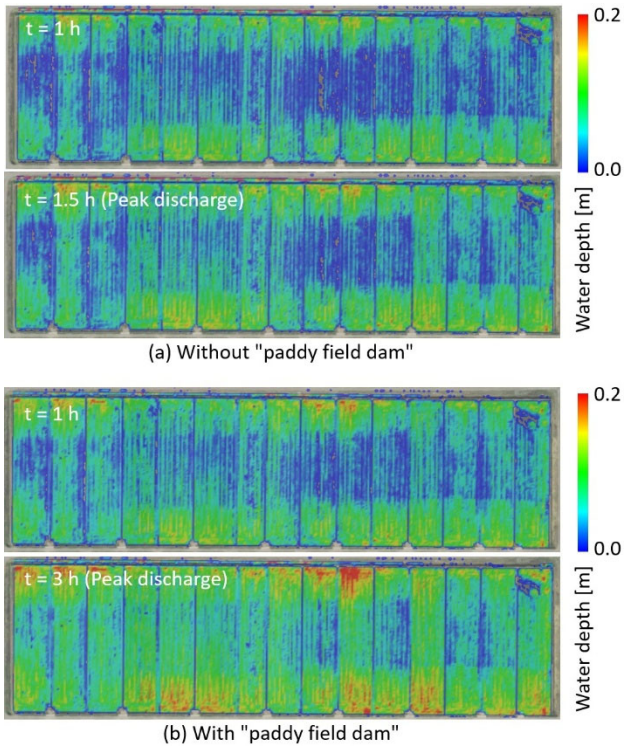

Figure 3. Comparison between calculation result (a) without and (b) with paddy field dam installation

volume increased when PFD weir plates were installed. It was also found that the time of peak flow was delayed by approximately 1.5 hours during event. At the same time, this model makes it possible to grasp the inundation depth distribution during flooding conditions in each field.

4. Conclusions

In this paper, we constructed a numerical analysis model to evaluate the effects of PFD initiatives. Using topographical data based on the actual conditions of the fields, we verified the validity of the model through a simulation of a rainfall event in August 2024. Then a comparative analysis was conducted to examine the extent of storage effect that could be achieved when a standard-type weir plate and v-notch type weir plate. Using the present model, it was confirmed that PFD initiatives were effective in storing water in rice paddies and delaying rainfall runoff.

Acknowledgements

The survey area in this paper is located in a Hokkaido government project site. The authors show their gratitude to members of Iwamizawa Regional Agreement for their assistance and insightful comments.

References

Minakawa, H. & Miyazu, S. 2022. Functional evaluation of paddy field dam devices with different characteristics using generated heavy rainfall data, Trans. Jap. Soc. Irrig. Drain. Rur. Eng. 90(1), I_157-I_165

Yoshikawa, N. & Koshiyama, N. 2024. Potential of Tambo Dam implementation as a flood control measure, Irrig. Drain. 73(5), 1854-1868.

iRIC Project. https://i-ric.org/ja/, Accessed September 15, 2025.

Quantitative PCR method to detect the invasive bitterling fish in agricultural channels using environmental DNA

Kaito MORIUCHI [1]*, Kanoko OTSUKI [2], Mayuko HAMADA [3], Rintaro TANIGUCHI [1], Takanari SUMIDA [4], Koki KATSUHARA [1] and Kazuyoshi NAKATA [1]

[1] Graduate School of Environmental, Life, Natural Science and Technology, Okayama University, 3-1-1 Tsushima-naka, Okayama, Okayama 700-8530, Japan

[2] Kaihatsu Co., Ltd., 6-20-24 Ima, Okayama, Okayama 700-0975, Japan

[3] Ushimado Marine Institute, Okayama University, Ushimado, Setouchi, Okayama 701-4303, Japan

[4] Okayama Prefectural Environmental Conservation Foundation, Inc., 665-1 Uchio, Okayama, Okayama 701-0212, Japan

* Corresponding author. Email: pjrl5usw@s.okayama-u.ac.jp

Abstract

We developed an eDNA-based monitoring method to detect the invasive fish species (*Rhodeus* sp.), which is a multi-species hybrid and has invaded rivers and agricultural channels in Okayama Prefecture, western Japan. We designed the species-specific primers and probes to the mitochondrial gene of each species for quantitative real-time PCR and conducted both aquarium and field experiments to evaluate whether their eDNA could be detected. Our results indicate that our method enables highly accurate and quantitative assessment of the distribution of *Rhodeus* sp. in agricultural channels and can thereby facilitate its efficient eradication.

Keywords: Bitterling fish, Environmental DNA, Invasive species, Real-time PCR

1. Introduction

Conservation of native species in agricultural ecosystems is important for maintaining the ecosystem services provided by rural environments (Zhang et al., 2007). However, the establishment of invasive species has had severe impacts on native organisms inhabiting rural ecosystems (Pyšek et al., 2020). The control of invasive species has thus become essential for conserving rural biodiversity.

Recently, environmental DNA (eDNA) analysis has emerged as a useful tool for assessing the distribution of aquatic species in freshwater environments (Lodge et al., 2012). Compared to capture survey methods using traps, eDNA analysis is less labor-intensive and enables more accurate estimation of species presence or absence. Therefore, it is essential for biodiversity conservation in rural areas to establish eDNA-based monitoring methods that can rapidly and accurately detect the distribution of invasive species.

An invasive bitterling fish species, *Rhodeus* sp. (Fig. 1), has begun to spread into rivers and agricultural channels in Okayama Prefecture, western Japan. *Rhodeus* sp. is a multi-species hybrid, comprising *R. atremius atremius*, *R. notatus*, and an undescribed species of *Rhodeus*. The invasion of *Rhodeus* sp. may negatively affect native bitterling fish species through interspecific competition and genetic disturbance, ultimately leading to a loss of biodiversity in agricultural channels and rivers and other freshwater habitats. In this study, we developed an eDNA-based monitoring method for detecting *Rhodeus* sp. that enables efficient monitoring of its distribution and supports the identification of appropriate areas for control measures in invaded waters.

Figure 1. *Rhodeus* sp. The black bar indicates 10 mm.

2. Materials and Methods

2.1. Design of primers and probes

Species-specific primers and probes targeting the *ND1* gene were designed for real-time PCR-based detection and quantification of *Rhodeus* sp. in eDNA samples, based on sequence alignments of *R. atremius atremius*, *R. notatus*, and undescribed species of *Rhodeus*.

2.2. Aquarium experiments

Aquarium experiments were conducted to evaluate the detection of *Rhodeus* sp. in eDNA samples using real-time PCR. In the experiments, six individuals—each of *R. a. atremius*, *R. notatus*, an undescribed species, and *R. a. suigensis*, which is closely related to these species—were placed in each plastic aquarium filled with water, and 1 L of water was collected from each aquarium. An aquarium without fish was also prepared as a negative control. After completing all experiments, water samples were filtered to collect eDNA.

2.3. Field experiments

Field experiments were conducted to detect *Rhodeus* sp. in natural water bodies using eDNA analysis and to verify that the eDNA analysis results accurately reflected the actual biomass of *Rhodeus* sp. In the experiments, we collected 20 water samples from a river where *Rhodeus* sp.

Figure 2. Water sampling conducted for eDNA analysis.

Figure 3. Individuals of *Rhodeus* sp. captured during the field survey.

has been confirmed (Fig. 2). After the water samplings, we captured *Rhodeus* sp. using a cage trap at the same 20 sites. The relationship between eDNA concentration and the number of *Rhodeus* sp. individuals captured was examined.

3. Results and Discussion

3.1. Aquarium experiments

In the aquarium experiments, the designed primers and probes specifically detected the target species. DNA amplification was successfully achieved using species-specific primers and probes targeting the three species comprising *Rhodeus* sp., and their specificity was verified.

3.2. Field experiments

Rhodeus sp. was detected in 19 out of 20 water samples by the eDNA analysis. During the field surveys, a total of 896 individuals of *Rhodeus* sp. were captured (Fig. 3). There was a significant positive correlation between the number of individuals of *Rhodeus* sp. and the eDNA concentration of *R. a. atremius* (Kendall rank correlation coefficient, $P < 0.01$) and *R. notatus* ($P < 0.01$), suggesting that our method was effective in estimating the population density of *Rhodeus* sp.

4. Conclusions

Our method enables highly accurate and quantitative assessment of the distribution of *Rhodeus* sp. in agricultural channels and can thereby facilitate its efficient eradication.

References

Lodge, D. M., Turner, C. R., Jerde, C. L., Barnes, M. A., Chadderton, L., Egan, S. P., Feder, J. L., Mahon, A. R., & Pfrender, M. E., 2012 Conservation in a cup of water: estimating biodiversity and population abundance from environmental DNA. *Molecular Ecology*, 21(11), 2555–2558.

Pyšek, P., Hulme, P. E., Simberloff, D., Bacher, S., Blackburn, T. M., Carlton, J. T., Dawson, W.,Essl, F., Foxcroft, L. C., Genovesi, P., Jeschke, J. M., Kühn, I., Liebhold, A. M., Mandrak, N. E., Meyerson, L. A., Pauchard, A., Pergl, J., Roy, H. E., Seebens, H., Kleunen, M. v., Vilà, M., Wingfield, M. J., Richardson, D. M., 2020. Scientists' warning on invasive alien species. *Biological Reviews*, 95(6), 1511–1534.

Zhang, W., Ricketts, T. H., Kremen, C., Carney, K., & Swinton, S. M., 2007. Ecosystem services and dis-services to agriculture. *Ecological Economics*, 64(2), 253–260.

Development of a Multi-Faceted Evaluation Framework for Agricultural Reservoir Clusters toward Sustainable Management

Masaomi Kimura [1*], Satoshi Watanabe [2], Keigo Noda [3], Yutaka Matsuno [1]

[1] Faculty of Agriculture, Kindai University, Nara 6318505, Japan

[2] Faculty of Social and Cultural Studies, Kyushu University, Fukuoka 8190395, Japan

[3] Graduate School of Agricultural and Life Sciences, The University of Tokyo, Tokyo 1138657, Japan

* Corresponding author. Email: mkimura@nara.kindai.ac.jp

Abstract

Agricultural reservoirs play a vital role in rural Japan not only as irrigation infrastructure but also as assets with multifunctional value, including flood mitigation, biodiversity conservation, and cultural significance. However, depopulation and aging in rural areas have made their maintenance increasingly difficult. To enable strategic and sustainable management of agricultural reservoir clusters, we propose a comprehensive evaluation framework based on four dimensions: (1) flood risk caused by potential dam breach, (2) future maintenance burden, (3) importance as irrigation water sources, and (4) ecological conservation potential.

Flood risk was assessed using a dam-breach inundation modeling software (SIPOND) to calculate inundation areas upon hypothetical dam failure. Maintenance burden was quantified as the projected number of labor hours per pond based on forecasted declines in agricultural labor force. The irrigation importance index combined future estimates of cultivated area with individual reservoir capacity. The ecological potential was evaluated through a GIS-based habitat index using InVEST, targeting amphibians as key indicator species.

The framework was applied to two contrasting case studies: a mountainous rural area in Saijo City, Ehime Prefecture, and an urban-fringe area in Osakasayama City. The application revealed distinct typologies and highlighted key considerations in planning site-specific maintenance strategies. This research demonstrates how a multifaceted and spatially explicit assessment can support prioritization and effective governance of aging reservoir networks under resource constraints.

Keywords: scenario-weighted prioritization, dam-breach inundation modeling, operation-and-maintenance burden, irrigation water security, habitat quality, InVEST

1. Introduction

Agricultural reservoirs in Japan function not only as irrigation infrastructure but also as multi-benefit assets that contribute to local flood mitigation, biodiversity, and cultural landscapes; however, depopulation and aging are eroding the capacity to maintain these pond networks, making strategic, evidence-based prioritization urgent. Policy responses since the 2018 heavy rain disaster and subsequent legislation in Japan have accelerated efforts to identify high-risk or high-priority ponds, but practical, reproducible tools for area-wide prioritization remain needed.

In this study, we adopt a cluster-level perspective and organize management needs into four dimensions—disaster risk upon potential dam breach, future maintenance burden, importance as irrigation water sources, and ecological conservation potential—so that heterogeneous ponds can be compared on a common, governance-ready basis. We apply this framework to two contrasting settings (Saijo and Osakasayama), compute standardized indicator scores for all ponds, visualize their spatial distributions, and derive pond typologies that clarify trade-offs among safety, operation/maintenance, water supply, and biodiversity. We further examine scenario-weighted prioritization schemes to translate these indicators into transparent, defensible priorities for local managers operating under tight resource constraints, and discuss implications for long-term, area-wide pond governance.

2. Materials and Methods

2.1. Study areas

We analyze two contrasting pond clusters in Japan. Saijo City (Ehime) represents a mountainous, agriculture-intensive setting with numerous irrigation ponds embedded in narrow valleys. Osakasayama City (Osaka) represents an urban-fringe environment with many small ponds—including the historic Sayama-ike—surrounded by residential land use. This pairing enables comparison of cluster-level priorities under different geomorphology and management contexts.

2.2. Data sources

We compiled four datasets: (i) municipal/prefectural pond ledgers (dam height, crest length, storage); (ii) 5-m DEM for breach-inundation hydraulics; (iii) national land-use polygons to extract “building land” for exposure overlays; and (iv) settlement-level agricultural statistics (farmer counts, cultivated area) for maintainer and cropping projections. Together, these sources enable a reproducible, municipality-scale evaluation.

2.3. Indicators

We evaluate each pond on four dimensions—Exposure, Maintenance, Resource, and Q (ecology)—and convert raw values to deviation scores (mean = 50, SD = 10) for within-cluster, relative comparison.

2.3.1.Exposure: breach damage potential

We simulate a hypothetical instantaneous dam-breach with SIPOND (Standard) using inputs of dam height, storage, 5-m DEM, and breach direction; the outflow hydrograph follows the Costa relation (peak at breach, exponential decay). From the 2-D routing we export depth/velocity at 1 h and intersect the inundation with “building-land” polygons; the overlapped area is the Exposure raw score.

2.3.2.Maintenance: future O&M burden

Maintenance represents the routine maintenance burden per available maintainer. We estimate future agricultural maintainers at the settlement level via a cohort-change method (age-class survival and net inflow/outflow), then normalize a geometry-based burden proxy by the projected maintainer count; higher scores indicate heavier future burden.

2.3.3.Resource: future irrigation importance

Resource reflects future irrigation demand/importance attributable to each pond. We apportion projected cultivated area within each settlement by the pond's storage share (or an equivalent capacity-based allocator) and use the apportioned area as the raw score; larger values indicate greater future importance as a water source.

2.3.4.Q (ecological value): habitat-quality–based index

We adapt InVEST Habitat Quality to agricultural reservoir landscapes: land-use serves as habitat suitability; built-up/roads are threats; pond presence acts as a positive, distance-decaying influence via multiple ring buffers. We set the half-saturation constant to half the maximum degradation from a preliminary run. From the resulting habitat-quality raster, we delineate a 500 m buffer per pond and sum the quality values within the buffer—this sum is the pond's Q value, standardized to a deviation score.

3. Results and Discussion

3.1. Saijo City

Across the mountainous cluster, Exposure hot spots appeared where breach paths funnel into narrow valley floors with mapped "building land," yielding elongated inundation footprints. Maintenance burdens were highest for ponds with tall embankments/long crests serving sparsely populated beneficiary settlements—our cohort-based projections indicate fewer future maintainers per pond, amplifying per-capita upkeep. Resource scores concentrated on larger-capacity irrigation ponds adjacent to fields with comparatively stable cultivated area, indicating that a small subset of ponds will carry a disproportionate share of future water-supply importance. Q (ecology) highlighted contiguous pond–wetland–woodlot linkages along valley sides and headwaters, suggesting opportunities to co-prioritize safety remediation and habitat stewardship within the same sub-catchments. Together, the indicator space separated ponds into clear typologies, enabling differentiated and defensible management pathways.

Using the four-indicator space (Exposure-Maintenance-Resource-Q), we classified ponds into clear typologies and linked each type to candidate, fit-for-purpose management options: e.g., High-Exposure/High-Resource → spillway/crest reinforcement and staged drawdown planning; High-Maintenance/Low-Resource → consolidation or decommissioning with downstream safeguards; High-Q with moderate Resource → vegetation management, buffer protection, and seasonal water-level rules to sustain habitat. This typology-to-action mapping provides a practical menu for area-wide O&M planning.

3.2. Osakasayama City

In the urban-fringe cluster, Exposure intersected more frequently with residential building land because many small ponds are embedded within or immediately downstream of residential areas; while individual inundation footprints were compact, cumulative downstream overlap increased area-wide risk. Maintenance tended to be driven less by embankment geometry (often modest) and more by limited agricultural labor availability, yielding high burden per maintainer even for small ponds. Resource scores were generally lower and more dispersed than in Saijo, reflecting the contraction and fragmentation of cultivated area; a few legacy ponds with relatively larger storage still emerged as locally important for irrigation security. These contrasts underscore how geomorphology and land-use context shift both the dominant constraints and the priority mixes across clusters.

Applying the same classification, urban-fringe ponds near housing that score High-Exposure are steered toward risk-first measures (alarm/monitoring, spillway upgrades, emergency drawdown protocols), while Low-Resource/High-Maintenance small ponds are candidates for management transfer, naturalization, or phased decommissioning. Legacy ponds with relatively higher Resource warrant selective capacity maintenance and irrigation reliability measures. The scheme thus translates heterogeneous scores into site-appropriate strategies under fiscal and labor constraints.

4. Conclusions

A cluster-level, four-dimensional evaluation (Exposure, Maintenance, Resource, Q) cleanly distinguishes management typologies in both mountainous and urban-fringe settings, clarifying trade-offs among safety, O&M capacity, irrigation security, and ecology. The results support scenario-weighted prioritization: e.g., risk-first remediation where residential exposure dominates; capacity-building or consolidation where maintenance burden outstrips labor; and targeted stewardship where ecological value co-locates with critical irrigation assets. This framework offers a reproducible, governance-ready basis for transparent decisions in aging reservoir networks.

Acknowledgements

This work was supported by the Japan Society for the Promotion of Science (JSPS) KAKENHI [grant number 21H05179]. The authors would like to express their sincere gratitude to the students from Gifu University, Kindai University, and Kyushu University, Japan who supported the fieldwork and laboratory analysis.

References

InVEST (Integrated Valuation of Ecosystem Services and Tradeoffs). https://naturalcapitalproject.stanford.edu/software/invest Accessed September 1, 2025.

SIPOND (dam-breach inundation modeling software). https://flood-soft.jp Accessed September 1, 2025.

Tsujioka, Y., Nakamura, S., Kimura, M., Noda, K., Nishihara, Y., Tanaka, T., Watanabe, S., 2022. Integrated evaluation indicator for irrigation ponds considering disaster prevention and maintenance: Case study of Saijo City, Ehime, Japan. J.JSHWR., 35(2), 122-133. DOI: 10.3178/jjshwr.35.122.

Effects of restoration methods on freshwater mussel distribution in the agricultural irrigation channels of Okayama City, western Japan

Rintaro TANIGUCHI [1*], Moyu SATO [2], Kaito MORIUCHI [1], Koki KATSUHARA [1], Tomohiro TAKEYAMA [3] and Kazuyoshi NAKATA [1]

[1] Graduate School of Environmental, Life, Natural Science and Technology, Okayama University, Okayama, Okayama 700-8530, Japan

[2] Graduate School of Science and Engineering, Okayama University of Science, Okayama, Okayama 700-0005, Japan

[3] Department of Biosphere-Geosphere Science, Okayama University of Science, Okayama, Okayama 700-0005, Japan

* Corresponding author. Email: pg2e9c1q@s.okayama-u.ac.jp

Abstract

In recent years in Japan, mussel habitats have drastically declined due to agricultural land improvements, leading to the decrease in bitterling fish populations as well because bitterling fishes have a unique reproductive ecology in which they spawn their eggs inside mussels. In this study, we conducted field surveys at 17 study sites, including 11 sites with restoration methods, to clarify the effects of restoration methods on freshwater mussel distribution in the agricultural channels of Okayama City, western Japan. We found 547 individuals belonging to six mussel species at 13 sites. The 11 sites where restoration methods had been introduced exhibited significantly higher numbers of species and individuals compared to the sites without any restoration measures. Sand deposition was observed on the channel beds at the sites where restoration methods had been introduced, suggesting a positive effect on the establishment of freshwater mussel populations.

Keywords: Agricultural channel, Bitterling fish, Freshwater mussel, Restoration method

1. Introduction

Agricultural channels have provided suitable habitats for aquatic species adapted to natural wetland ecosystems (Washitani, 2001). In Japan, however, agricultural land improvement projects, including the complete concreting of channels to enhance water management efficiency, have led to the loss of suitable habitats, threatening many aquatic species such as fish or mussels with extinction (Natsuhara, 2013; Katayama et al., 2015). Bitterling fishes are primarily distributed in East Asia and are predominantly found in agricultural channels in rural areas. Bitterlings have a unique reproductive ecology in which they spawn their eggs inside mussels (Smith et al., 2004). In recent years, due to agricultural land improvements, mussel habitats have drastically declined, leading to the decrease in bitterling populations as well (Negishi et al., 2008). In Japan, restoration methods have been introduced in some agricultural channels to create habitats with suitable environmental conditions for fish species, including bitterlings. However, no studies have evaluated the effectiveness of restoration methods in conserving mussel populations. In this study, we conducted field surveys to clarify the effects of restoration methods on freshwater mussel distribution in the agricultural channels of Okayama City, western Japan.

2. Materials and Methods

Mussels were collected at 17 sites, including 11 sites with restoration methods (Figure 1). At each site, six quadrats (100 cm×100 cm) were placed across the channel, and a single investigator collected mussels by hand or with a rake for 15 minutes within each quadrat. The number of mussel individuals and the shell length of each species were recorded. After the measurements, all mussels were returned at the original collection site.

In each quadrat, water velocity at three depths (surface, mid-layer, and near-bottom) and water depth were measured at five points: the four corners and the center, and the channel width was recorded at the locations where each quadrat was set. The bank structure at each site was categorized as either natural banks, banks with restoration methods, or banks without restoration methods; Figure 1). For the data obtained at 16 sites other than St. 15, where the natural banks were observed, a generalized linear mixed model (GLMM) was constructed. The model included three physical environmental variables and bank types at each site as explanatory variables, species richness or total mussel abundance as response variables, and the survey site as a random effect. The error distribution was set to Poisson.

3. Results and Discussion

We found 547 individuals belonging to six mussel species at 13 sites (Figure 2). The six mussel species collected all inhabit lotic environments. The 11 sites where restoration methods had been introduced showed significantly higher numbers of species and individuals compared to the sites without any restoration measures ($P < 0.05$; Figure 3). There was no significant correlation between water velocity, water depth, or channel width and the number of mussel species. A significant positive correlation was found between water velocity and mussel abundance ($P < 0.001$), whereas no significant correlations were observed with water depth or channel width.

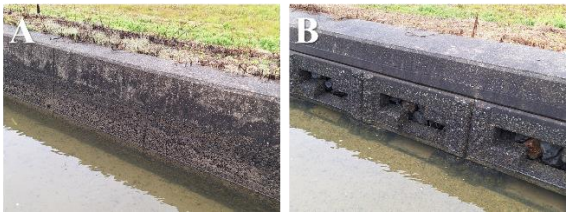

Figure 1. The channel wall of the study agricultural channel. A: the concrete channel wall without restoration methods, B: the channel wall incorporating fish nests as part of the restoration methods.

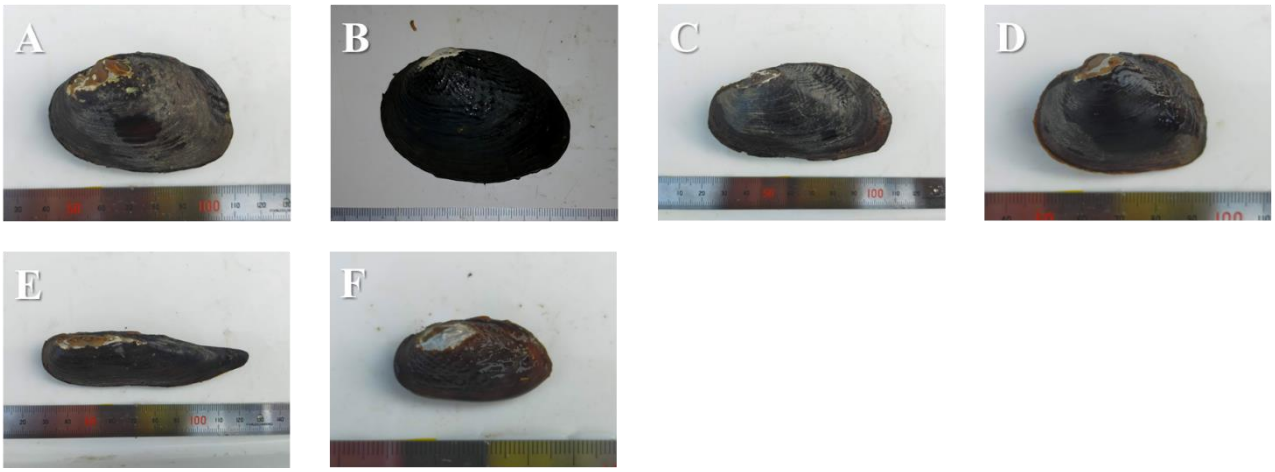

Figure 2. Mussel specimens collected in this study. A: *Inversiunio yanagawawensis*, B: *Pronodularia* cf. *japanensis*, C: *Obovalis omiensis*, D: *Inversidens brandtii*, E: *Lanceolaria oxyrhyncha*, F: *Nodularia douglasiae*.

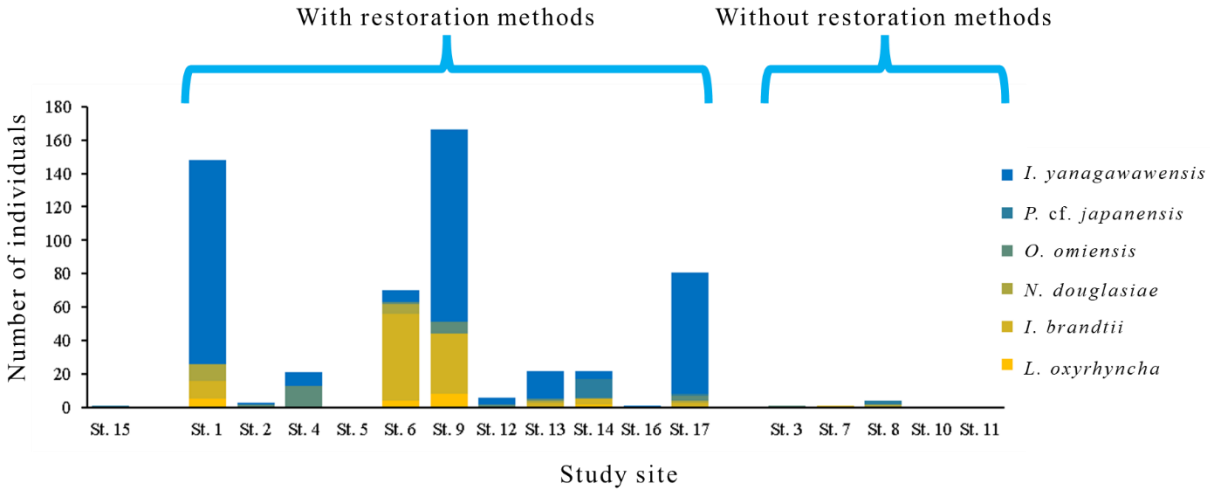

Figure 3. Number of mussel individuals collected by site and species.

4. Conclusions

We observed sand deposition on the channel beds at the sites where restoration methods had been introduced, suggesting that restoration efforts may facilitate habitat conditions favorable for the establishment of freshwater mussel populations.

References

Katayama, N., Baba, Y. G., Kusumoto, Y. & Tanaka, K., 2015. A review of post-war changes in rice farming and biodiversity in Japan. *Agricultural Systems*, 132: 73–84.

Natsuhara, Y., 2013. Ecosystem services by paddy fields as substitutes of natural wetlands in Japan. Ecological Engineering, 56: 97–106.

Negishi, J. N., Kayaba, Y., Tsukahara, K. & Miwa, Y., 2008. Ecological studies on Unionoida: current status and future challenges. *Japanese Journal of Ecology*, 58: 37–50 [in Japanese with English abstract].

Smith, C., Reichard, M., Jurajda, P. & Przybylski, M., 2004. The reproductive ecology of the European bitterling (*Rhodeus sericeus*). *Journal of Zoology*, 262: 107–124.

Washitani, I., 2001. Traditional sustainable ecosystem "SATOYAMA" and biodiversity crisis in Japan: conservation ecological perspectives. *Global Environmental Research*, 5: 119–133.

Improving Water Distribution and Reducing Labor in Hillside Irrigation Canals Using ICT Irrigation Devices

Shinichi Takeshita [1*], Maetawee Pingkanon [2]

[1] Faculty of Agriculture, University of Miyazaki, Miyazaki, (Miyazaki) 8892192, Japan

[2] Graduate School of Agriculture, University of Miyazaki, Miyazaki, (Miyazaki) 8892192, Japan

* Corresponding author. Email: rtakeshita@cc.miyazaki-u.ac.jp

Abstract

Hillside irrigation canals often suffer from inefficient water distribution, particularly in the downstream areas. This study investigated the effectiveness of introducing information and communication technology (ICT) irrigation devices to improve water distribution and reduce labor. A simulation model combining unsteady flow calculations (using the leapfrog method) and a paddy water balance model was developed to reproduce canal flow and the behavior of ICT devices. This study was conducted in the Shimono area of the Hamanose irrigation canal in Takachiho, Miyazaki, from May to September. Two experiments were conducted. The first compared two strategies for placing two ICT devices: paddy field size and along the canal from upstream to downstream. The second study examined the optimal number of devices, increasing from 2 to 16, using both spatial strategies. The results showed that when devices were installed based on paddy size, especially in downstream areas, water levels were more stable, leading to more efficient water use and a significant reduction in farmers' workloads. Additionally, installing 12–14 devices starting from upstream fields proved to be most effective during July, which is the peak irrigation period. These findings suggested that ICT irrigation devices enhance water stability and distribution reliability. Prioritizing the installation of smaller paddy fields is effective in cost-constrained scenarios. With fewer cost limitations, starting installations upstream maximizes water use efficiency and management benefits. While some modeling challenges remain, this study demonstrates that ICT-based irrigation can reduce water stress and labor demands compared to manual irrigation in hillside canal systems.

Keywords: Hillside irrigation canals, Water distribution efficiency, Labor reduction in irrigation, ICT irrigation devices, Unsteady flow simulation

1. Introduction

Information and communication technology (ICT) has improved agricultural efficiency worldwide, and automatic irrigation devices are increasingly applied to rice fields in Japan. However, their use has been limited to flatland paddies. In contrast, hillside irrigation canals, which are characterized by open channels on mountain slopes, still face serious water distribution problems, particularly in downstream areas (Takeshita *et al*., 2023). Previous studies demonstrated the benefits of ICT-based irrigation in flatlands; however, its effectiveness in hillside canals remains unclear.

The aim of this study was to quantitatively evaluate the effectiveness of ICT irrigation devices in hillside irrigation canals using a simulation model. Two numerical experiments were conducted to (1) determine the optimal placement strategy and (2) identify the effective number of devices required.

2. Materials and Methods

An integrated simulation framework was developed to evaluate the effectiveness of ICT irrigation devices in hillside canal systems quantitatively. The framework comprised three components: (i) a canal flow model based on unsteady flow equations solved by the leapfrog method; (ii) a paddy water balance model incorporating precipitation, intake, drainage, infiltration, and evapotranspiration; and (iii) an ICT device control algorithm. Field data from the Shimono area of the Hamanose irrigation canal in Takachiho, Miyazaki, were used for parameterization and validation.

The ICT device algorithm was designed to automatically regulate irrigation according to the water depth in paddy fields. Each device monitors the water level and initiates irrigation when the depth falls below a certain threshold (Hod). Irrigation continues until the depth reaches an upper threshold (Hcd), at which point the valve closes, as shown Figure 1. Devices record the water level, valve status, and temperature every 20 min and transmit the data to a cloud server via LPWA, enabling remote monitoring and control through smartphones. This dual capability of local automatic regulation and remote adjustment enables flexible water management to adapt to the field conditions.

Two numerical experiments were conducted using the integrated model. Experiment 1 focused on identifying the most effective placement of the two devices in the study area. Two strategies were compared: (a) sequential installation from upstream to downstream (U2 cases) and (b) allocation based on descending order of paddy size (A2 cases). Multiple combinations were simulated to assess the relative benefits of stabilizing upstream flows versus prioritizing smaller paddies, which typically face greater water stress.

Experiment 2 examined how the number of devices influences the system performance. The simulations tested incremental installations, increasing from 2 to 16 devices. Again, two strategies were considered: (a) sequential

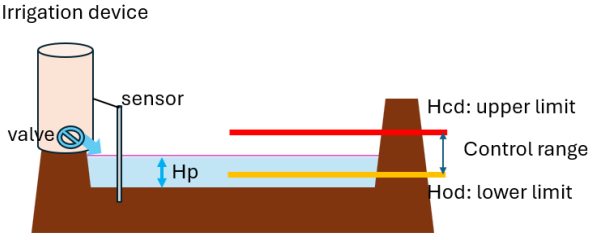

Figure 1. Operation of the irrigation device

upstream-to-downstream installation (U2 cases), and (b) allocation beginning with the largest paddies (A2 cases). This approach enables the evaluation of cost-constrained scenarios (limited devices) and more intensive implementations (several devices).

By integrating canal hydraulics, paddy water dynamics, and ICT control algorithms, this modeling framework provided a quantitative tool for assessing irrigation performance under varying deployment strategies. The methodology enabled the comparison of spatial placement and device density, clarifying how ICT irrigation can stabilize the downstream water supply and enhance the overall water use efficiency in hillside canal systems.

3. Results and Discussion

Numerical experiments revealed clear differences in water management outcomes depending on both the placement and number of ICT irrigation devices in hillside irrigation canals.

Experiment 1 compared two strategies for introducing the two devices: allocation by paddy field size (A2) and sequential upstream installation (U2). Figure 2 shows that the A2 cases generally produced more stable downstream water levels with lower coefficients of variation than current conditions. The larger paddies prioritized in Cases 1 and 2 showed high water-use efficiency and reduced fluctuations, indicating improved resource utilization. In contrast, the U2 cases demonstrated that upstream installation increased downstream water levels and enhanced distribution efficiency, whereas devices placed in downstream fields (Cases 7 and 8) contributed less to water saving, but significantly reduced farmers' operational workloads. Overall, the A2 strategy outperformed the U2 strategy in stabilizing canal water levels, although both strategies provided benefits depending on the management objectives.

Experiment 2 investigated the cumulative effects of increasing the number of devices used. In the A2 scenario, average water levels were generally lower than the baseline, except in September. Yet, variability was reduced in critical irrigation months, particularly in August, when more than eight devices were introduced. Table 1 shows the results of the U2 scenarios, where 12–14 devices were installed sequentially from the upstream section. This resulted in higher average water levels than under the current conditions and reduced fluctuations during June, July, and August. These findings demonstrated that sequential upstream installation of a sufficient number of devices stabilized canal water levels and ensured reliable downstream distribution.

A comprehensive comparison suggested that the most effective configuration is the installation of 12–14 devices beginning from upstream paddies, especially in July when irrigation demand peaks. This approach optimizes water-use efficiency and reduces stress on the canal system. However, prioritizing smaller paddies yielded meaningful improvements in water-level stability in cases where cost constraints limit large-scale deployment. Moreover, while downstream installations are less effective in saving water, they play an important role in reducing farmers' management burdens, underscoring the trade-off between hydrological efficiency and labor reduction.

In summary, the results demonstrated that ICT irrigation devices are effective in stabilizing canal water levels and alleviating farmers' workload. The optimal water-saving strategy is sequential upstream deployment of 12–14 devices. However, partial- or downstream-oriented installations provide practical advantages. These insights highlighted the potential of ICT to enhance the resource efficiency and sustainability of hillside agricultural systems.

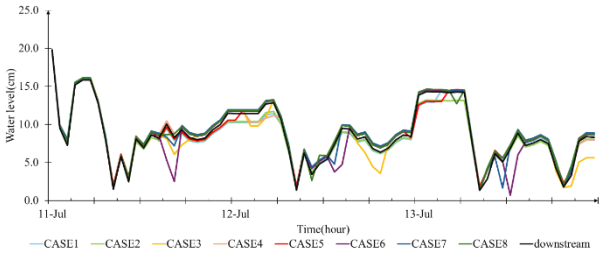

Figure 2. Comparison of water levels in experiment 1 – case A2 from July 11 to 13.

Table 1. Average water level at canal's bottom of experiment 2 – case U2. The blue cells indicate that the average water level was higher than the current condition.

		May	Jun	Jul	Aug	Sep
	Current	12.0	12.1	8.7	11.0	11.1
E2U2	CASE1	11.9	12.1	8.7	11.0	11.2
	CASE2	11.6	11.9	8.8	10.8	11.1
	CASE3	11.4	11.8	8.7	10.8	11.2
	CASE4	11.5	12.2	8.7	10.5	11.7
	CASE5	11.6	12.4	9.2	11.2	12.0
	CASE6	11.6	12.5	9.7	11.5	12.2
	CASE7	11.2	12.3	10.0	11.5	12.2
	CASE8	10.2	11.4	10.2	10.5	11.0

4. Conclusions

This study showed that ICT irrigation devices enhance water distribution efficiency and reduce the workload of farmers in hillside canals. The experiments revealed that the device placement and number strongly influenced the outcome. Installing two devices based on paddy size improved stability, whereas upstream placement secured downstream supply. The results indicated that installing 12–14 units sequentially upstream provided the most effective and stable distribution, particularly in July. Although large-scale deployment offers the best efficiency, prioritizing smaller paddies or downstream fields remains valuable under cost or labor constraints. Overall, ICT promotes sustainable water use and efficient water management.

Acknowledgements

This study was supported by the KAKENHI(grant number JP24K09131).

References

Takeshita, S., Hirai, N., Eto, S., and Sato, M., 2023, Irrigation feature of hillside irrigation canals based on the operation history of ICT irrigation devices, Water, Land and Environ. Eng. Jun., pp. 19-22.

Sentinel-2 Time-Series Analysis for Detection and Monitoring of *Alternanthera philoxeroides*

Kengo Shinohara[1*]

[1] Institute for Rural Engineering, NARO, 2-1-6 Kannondai, Tsukuba-shi, Ibaraki 305-8609, Japan

* Corresponding author. Email: shinohara.kengo338@naro.go.jp

Abstract

Spatiotemporal trends in colonies of the invasive alien species *Alternanthera philoxeroides* were evaluated using a time-series analysis of Sentinel-2 satellite data in the Hachiken River, Chiba Prefecture, Japan. First, the applicability of Sentinel-2 satellite data for monitoring of the river was evaluated by performing a correlation analysis between high-resolution WorldView-3 satellite data and Sentinel-2 satellite data, confirming a significant correlation (r= 0.96). Next, the positional deviation of the Sentinel-2 satellite data was evaluated and corrected (up to 17 m) using the georeferencing function of QGIS. Then the temporal changes in the Normalized Difference Vegetation Index (NDVI) values of the river area were examined. The results showed that the high-density colony zone in the target area tended to move downstream starting around the summer of 2022. Furthermore, it was suggested that the stable dominance of this species is caused by its ecological characteristics and the artificial eradication work. The proposed method are expected to be useful for river administrators in areas where *A. philoxeroides* dominated, helping them to implement efficient eradication plans and river management.

Keywords: Invasive alien species, Normalized Difference Vegetation Index (NDVI), Spatiotemporal trend.

1. Introduction

The invasive alien species *Alternanthera philoxeroides* forms mat-like colonies in rivers, causing damage such as ecosystem disruption, water flow obstruction, and pumping station blockage. Because the stems of this species are easily fragmented and root from the fragments, disturbance events (e.g., eradication work or flooding) can carry many fragments downstream, resulting in the expansion of the dominated area. To prevent the spread of this species, it is important to understand the distribution of this species' colonies and how they change over time (i.e., spatiotemporal trends) in order to implement efficient eradication plans and river management.

For vegetation monitoring, satellite remote sensing technology is widely used. However, it is important to combine high-resolution satellite data (such as WorldView-2 and -3) with freely available satellite imagery (e.g., Sentinel-2, Landsat), because of the trade-off between spatial resolution and data accessibility (Kristen L. Wilson et al., 2022).

In this study, the applicability of Sentinel-2 satellite data for monitoring *A. philoxeroides* in river area was first evaluated through a correlation analysis between Sentinel-2 satellite data and WorldView-3 satellite data. Next, spatiotemporal heatmap of NDVI value was created using Sentinel-2 satellite data from 2019 to 2024. Using the heat map, spatiotemporal trends of *A. philoxeroides* colonies in the target area were considered.

2. Materials and Methods

2.1. Study area

This study focused on the downstream basin of the Hachiken River in Katori City, Chiba Prefecture (Figure 1 (a)). This river is 7.3 km long with a very slow flow, and occasionally backflow depending on the operation of the pumping station. Colonies of *A. philoxeroides* has been observed downstream from its junction with the branch river, 3.5 km upstream. While river administrators conduct removal activities on an irregular basis, the complete eradication of this species has not yet been achieved.

2.2. Data and Analysis

From 2019 to 2024, under clear-sky conditions, Sentinel-2 satellite data covering the Hachiken River, were downloaded at a frequency of approximately one scene per month, and used for the following analysis with QGIS 3.34.8. First, image of NDVI was created using Band 4 (Red) and Band 8 (NIR) data from the Sentinel-2 satellite data (Fig. 1 (b)). Next, Analysis polygons were prepared by dividing the water's edge polygon (downloaded from the Geospatial Information Authority of Japan website) into 10 m pitches in the east-west direction (Fig. 1 (c)) and overlaid onto each NDVI image. The average of the pixel values located within the polygons (hereafter referred to as "plot-averaged NDVI values") was then calculated. Finally, using the plot-averaged NDVI values for the entire period, a heatmap was created with the vertical axis representing time (January 1, 2019, to December 31, 2024) and the horizontal axis representing the distance from the upstream end, using the spatiotemporal interpolation process (Kriging method) in Surfer 23.2.176 (Golden Software, LLC).

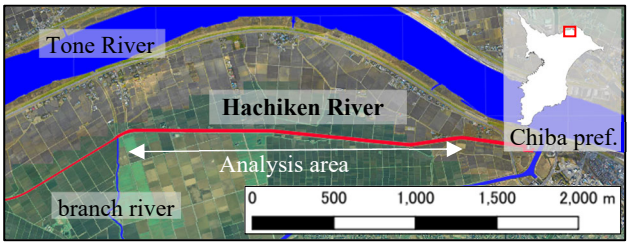

(a) Study area

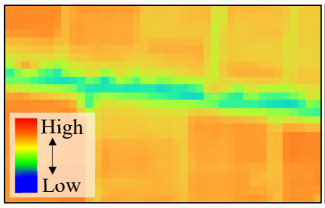

(b) NDVI image using Sentinel-2 satellite data

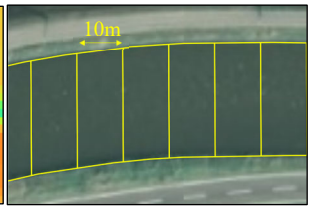

(c) Polygons of river's edge divided at 10 m intervals

Figure 1. Test area and examples of analysis data.

3. Results and Discussion

3.1. Examining the applicability of Sentinel-2 satellite data to monitoring *A. philoxeroides*

Sentinel-2 satellite data potentially contains positional errors depending on observation conditions. In this study, the shift between images was evaluated by visually inspecting each image and marking points on intersections of farm roads. As a result, it was found that maximum shift was approximately 17 m, for this reason, positional corrections were performed using the georeferencing function in QGIS.

Prior to main analysis, the applicability of Sentinel-2 satellite data for detecting *A. philoxeroides* was verified through correlation analysis using Sentinel-2 and high-resolution WorldView-3 satellite data collected at approximately the same time points (August 4, 2024, and August 3, 2024, respectively). As a result, a significant correlation (r= 0.96) between the plot-averaged NDVI values from both datasets was revealed (Fig. 2), suggesting that the plot-averaged NDVI values derived from Sentinel-2 satellite data can reasonably evaluate the distribution of *A. philoxeroides* colonies. Thereafter, a spatiotemporal heat map was created by calculating the plot-averaged NDVI values using multi-temporal Sentinel-2 satellite data for subsequent analyses.

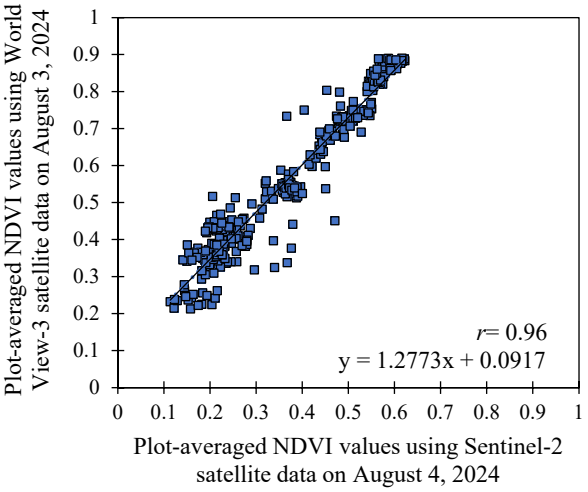

Figure 2. Comparison of plot-averaged NDVI values obtained from Sentinel-2 and WorldView-3 satellite data

3.2. Characteristics of *A. philoxeroides* distribution using an NDVI spatiotemporal heatmap

The NDVI spatiotemporal heatmap in the Hachiken River using Sentinel-2 satellite data revealed the following trends of *A. philoxeroides* distribution (Fig. 3). I: The colonies decreased once in 2021 but expanded in the following years. II: Vigorous proliferation was observed in the mid-stream area from the summer of 2022, and the proliferation area shifted downstream in 2023 and 2024. III: The increasing trend during the summer became more pronounced over time.

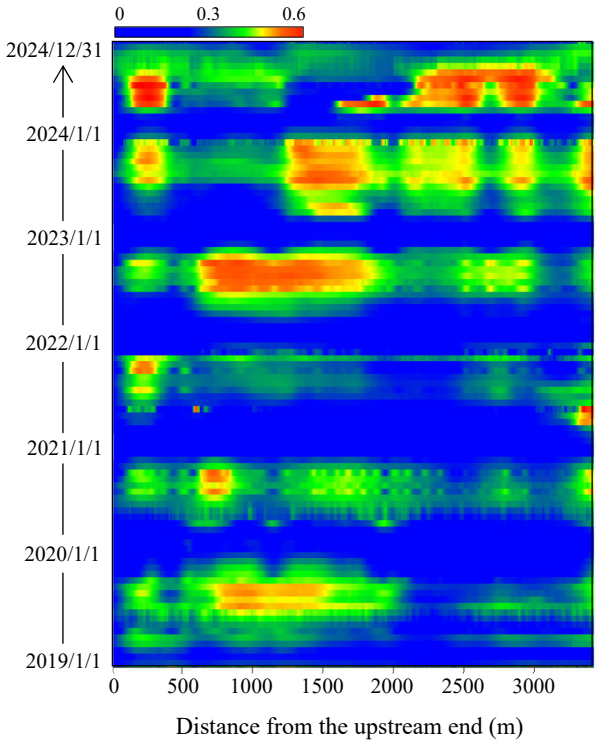

Figure 3. Spatiotemporal heatmap of NDVI values for the Hachiken River using Sentinel-2 satellite data. (The plot-averaged NDVI values at any given location and time are represented by the color intensity)

The ease of establishment and proliferation of this species may be related to the fragmentation of plant bodies. In the *A. philoxeroides* removal work, heavy machinery is often used to grab the colonies with a bucket, lift and collect them, and then incinerate them after drying (Mineta et al., 2018). Since the stems of this species are easily broken, they are often fragmented and flow downstream when the colonies are grabbed and lifted by the bucket. This may be contributing to spread of the colonies in the downstream areas. These results suggest that the stable dominance of this species is caused by its ecological characteristics and the artificial eradication work.

4. Conclusions

In this study, after examining the applicability of Sentinel-2 satellite monitoring, we visualized the spatiotemporal trends of *A. philoxeroides* communities in the Hachiken River through time-series analysis. In the future, we aim to integrate and complement high-resolution satellite data and drone data for more detailed monitoring of this species.

Acknowledgements

This study was supported by the Cabinet Office, Government of Japan, programs for Bridging the gap between R&D and the Ideal society (Society 5.0) and Generating Economic and social value (BRIDGE).

References

Wilson, K., L., Wong, M., C. and Devred, E., 2022. Comparing Sentinel-2 and WorldView-3 Imagery for Coastal Bottom Habitat Mapping in Atlantic Canada. Remote Sens. 2022, 14(5), 1254.

Mineta, T., Sasaki, T., Ichikawa, Y., Shibaike, H., Takahashi, O., Minakawa, H., Suzuki, H., Yamaoka, M., 2018. Invading and spreading of *Alternanthera philoxeroides* in the Inbanuma area. Water, Land Environ. Eng. 86, 687–690.

Geospatial Information Authority of Japan website. https://service.gsi.go.jp/kiban/app/map/
Accessed September 11, 2025.

Groundwater Level Forecasting Based on Time Series Clustering and Transformer

Chueh, Chia-Jung [1*]

[1] Department of Bioenvironmental Systems Engineering, National Taiwan University, Taipei, Taiwan

* Corresponding author. Email: venus159951@gmail.com

Abstract (10 pt, Times New Roman, Bold)

Groundwater plays a crucial role in sustaining agricultural production and securing regional water resources, especially in areas prone to seasonal droughts. In this study, we propose a groundwater level forecasting framework that integrates time series clustering (TSC) with Transformer deep learning models. The analysis focuses on the Zhuoshui River Basin, utilizing long-term groundwater level data from monitoring wells across the fan-top, fan-mid, and fan-tail regions.

Time series data from all stations were first standardized using Z-score normalization, followed by K-shape clustering to group wells based on similar temporal fluctuation patterns. After clustering, feature importance was assessed using XGBoost to identify key meteorological and human-related drivers for each cluster. Individual Transformer models were then trained per cluster to predict one-step-ahead (T+1) groundwater levels.

The results show that the combination of shape-based clustering and targeted Transformer models improves prediction accuracy and reveals meaningful spatiotemporal groundwater behavior. This framework provides a robust foundation for future drought warning systems and sustainable water management strategies.

Keywords: Groundwater forecasting; Time series clustering; K-shape; Transformer; XGBoost; Zhuoshui River Basin; Water resources management

1. Introduction

The Zhuoshui River Basin, the longest river system in Taiwan (~186 km, 3,156.9 km²), is one of the most intensively developed regions, spanning Changhua, Yunlin, Chiayi, and Nantou counties. It hosts industrial zones, irrigated farmland, and the Central Taiwan Science Park, leading to high and competing water demands. Excessive groundwater extraction has caused severe land subsidence and infrastructure risks, highlighting the urgent need for accurate groundwater prediction models (Chang et al., 2024).

2. Materials and Methods

2.1. Study area and data

This research specifically concentrates on the Zhuoshui River alluvial fan, which can be subdivided into proximal, mid-fan, and distal fan zones based on geomorphological characteristics (Fig. 1). The dataset includes records from 39 groundwater observation wells (GL1–GL39), 26 rainfall stations (R1–R26), 9 river flow stations (F1–F9), as well as irrigation water-use data from the Changhua–Yunlin agricultural districts. Through the integration and analysis of these multi-source datasets, this study establishes a systematic framework encompassing clustering, feature selection, and deep learning-based forecasting. The framework provides groundwater level predictions for all 39 monitoring wells across the basin, offering critical scientific insights for regional water resource management and sustainable utilization.

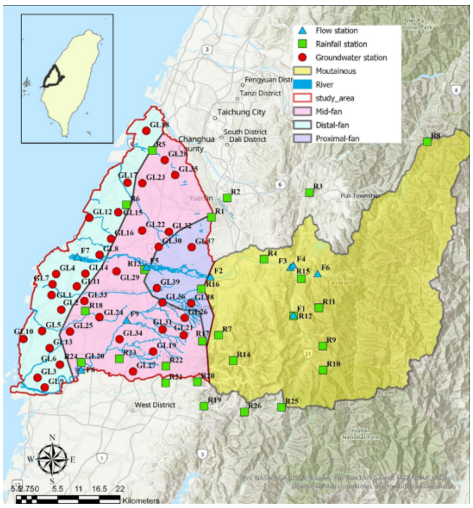

Fig.1 Study area and locations groundwater stations (GL1~GL39), flow stations (F1~F9), and rainfall stations (R1~R26)

2.2. Methods

This study integrates groundwater (39 wells), rainfall (26 stations), river flow (9 stations), and irrigation data to develop a forecasting framework for the Zhuoshui River alluvial fan. Using K-shape clustering (Lin et al., 2024), XGBoost feature selection, and cluster-specific Transformer models (Chang et al., 2024), the framework provides accurate and adaptive groundwater predictions to support sustainable management and mitigate subsidence.

2.2.1. Time series clustering

This study applied Time Series Clustering (TSC) to 39 groundwater wells in the Zhuoshui River Basin. Relative groundwater levels were derived by normalizing observations against site-specific minima, followed by Z-score standardization. Clustering was conducted using the K-shape algorithm with Shape-Based Distance (Eq. 1),

$$SBD(x,y) = 1 - \frac{\max(NCCc(x,y))}{\|x\|_2\|y\|_2} \qquad (1)$$

where $NCCc(x,y)$ denotes the normalized cross-correlation function that evaluates the similarity between two time series x and y under various temporal shifts (lags), and the maximum value is used to represent their optimal alignment.

Enabling classification by temporal patterns rather than absolute magnitudes. Results identified six clusters with distinct dynamics: C2 had the largest annual amplitude (10.094 m, distal fan), C3 showed the strongest decline (–0.1255 m/year, mid-fan), and C6 exhibited a clear rising trend (0.2439 m/year), likely linked to management or recharge. Other clusters displayed moderate or stable variations across upland and transitional zones.

Table 1. Summary Statistics of Each Groundwater Cluster

Cluster	Numbers of Stations	Annual Amplitude (m)	Dry Season Decline (m)	Trend Slope (m/year)
C1	8	3.604	0.284	-0.0327
C2	10	10.094	-0.106	0.0209
C3	8	3.896	0.370	-0.1255
C4	2	1.922	0.404	-0.0140
C5	3	1.423	0.384	0.0218
C6	8	4.364	0.221	0.2439

2.2.2. Transformer neural network

The Transformer model, driven by its self-attention mechanism and multi-head attention, excels at capturing complex dependencies in sequence-to-sequence tasks. In this study, we apply the Transformer to predict groundwater levels in the distal fan zone of the Zhuoshui River Basin, treating rainfall、streamflow and irrigation as input sequences and groundwater level as the output sequence. Preliminary results focus on the distal fan zone, with future work extending to mid-fan areas through separate models.

3. Results and Discussion

3.1. Results

Figure 2 shows the predictive performance of the Transformer model across groundwater clusters (C1–C6), evaluated using R^2, MAE, and RMSE. C1 achieved the most stable and consistent results, while C6 also performed well with relatively concentrated errors. In contrast, C2 and C3 were less stable; for example, GL10 and GL11 in C2 showed lower accuracy. C4, despite containing only two stations, achieved excellent performance with high R^2 and low errors. C5 showed moderate performance, with acceptable error levels but slightly lower accuracy than C1 and C6.

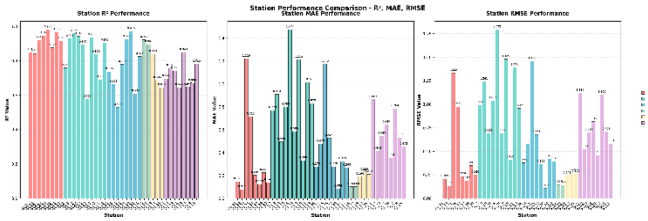

Fig. 2. Station-wise performance of the Transformer model across groundwater clusters (C1–C6), evaluated using coefficient of determination (R^2), mean absolute error (MAE), and root mean square error (RMSE)

3.2. Discussion

The results indicate that the Transformer model can effectively capture groundwater dynamics in clusters with stable hydrogeological conditions (C1, C6), while performance decreases in areas with higher variability or stress (C2, C3). The strong performance of C4, even with limited data, highlights the model's adaptability. Meanwhile, the moderate accuracy of C5 suggests that regional characteristics, such as transitional fan zones, may reduce model stability. Overall, the findings underscore that cluster-specific hydrogeological conditions strongly influence prediction accuracy.

4. Conclusions

This study developed a groundwater forecasting framework for the Zhuoshui River alluvial fan by integrating time series clustering, feature selection, and Transformer-based deep learning. The clustering results revealed distinct groundwater dynamics across fan zones, with C2 showing strong seasonal variability, C3 exhibiting a long-term decline, and C6 indicating recovery trends under management efforts. Cluster-specific Transformer models improved prediction accuracy compared to a uniform model, particularly in stable clusters (C1 and C6), though performance in highly stressed areas (C2 and C3) remained less consistent. These findings demonstrate that combining clustering with deep learning effectively captures spatiotemporal heterogeneity, providing a practical tool for sustainable groundwater management and subsidence mitigation in Taiwan.

Acknowledgements

This study is supported by National Taiwan University (NTU-CC-112L893501) and National Science and Technology Council, Taiwan (NSTC 113-2313-B-002-029-MY3). The datasets provided by Water Resources Agency, MOEA, Taiwan, were acknowledged.

References

Journal articles:

Chang, C.H., Wang, P.L., Hsu, K.C., 2024. Transformer-based groundwater level forecasting in the Zhuoshui River Basin, Taiwan. Journal of Hydrology, 631, 130584. https://doi.org/10.1016/j.jhydrol.2024.130584

Lin, Y.C., Kuo, C.M., Chen, C.F., 2024. Identifying groundwater dynamics using time series clustering in the Zhuoshui River Basin, Taiwan. *Journal of Hydrology*, 632, 130629. https://doi.org/10.1016/j.jhydrol.2024.130629

Water Stress Detection in Persimmon Cultivation Using A Pre-Trained Machine Leading Model

Naoki Onishi [1*], Atsushi Okayama [2], Yutaka Matsuno [1], Kuniomi Kimura [1]

[1] Faculty of Agriculture, Kindai University

[2] Graduate School of Agriculture, Kindai University

* Email: naokiagri0927@gmail.com

Abstract

Appropriate irrigation management is essential for sustaining crop quality and yield, and the recent decline in agricultural labor has intensified the need for efficient irrigation practices. In persimmon cultivation, irrigation timing has traditionally been determined by visual assessment of leaf condition, which is subjective and difficult to quantify. Deep learning, particularly convolutional neural networks (CNNs), offers an alternative by enabling automatic feature extraction from images. Previous studies achieved around 80% accuracy in estimating water stress from RGB images of persimmon leaves, but these models were limited to single-orchard datasets. To develop a more generalized model, this study investigated the use of a pre-trained ResNet-50 CNN with multi-orchard data. Field data were collected from two orchards in Gojo-Yoshino, Nara Prefecture, Japan, between 2022 and 2024, including hourly RGB leaf images and soil moisture sensor data, which were converted to pF values and categorized into five stress levels. Two training cases were evaluated: Case 1 used 8,993 images, and Case 2 used a randomly sampled subset of 4,496 images. Case 1 achieved 80% accuracy, while Case 2 reached 76.35%. The F1-score stabilized with around 3,000 training images, and further increases yielded only limited performance gains. These results demonstrate the feasibility of pre-trained CNNs for estimating water stress in persimmon leaves under practical conditions.

Keywords: Convolutional Neural Network (CNN), pre-trained model, ResNet-50, irrigation

1. Introduction

In agriculture, appropriate irrigation management is crucial for maintaining crop quality and yield, making it necessary to optimize both the timing and amount of irrigation. Additionally, the declining number of agricultural workers has increased the demand for labor-saving and efficient irrigation practices. In persimmon, the fruit tree targeted in this study, irrigation timing is traditionally determined based on leaf condition; however, this approach is subjective and difficult to quantify.

In recent years, deep learning based on artificial neural networks has gained attention as a complementary approach to empirical knowledge. Deep learning mimics the structure of biological neural circuits and enables automatic feature extraction. Previous studies have applied convolutional neural networks (CNNs), a type of deep learning, to estimate water stress from RGB images of persimmon leaves, achieving an accuracy of approximately 80% (Okayama et al., 2025). However, these models were developed using data from a single orchard, and constructing a generalized model applicable across multiple orchards requires a larger dataset, making data acquisition a critical challenge. In this context, pre-trained models are of particular interest. These models have already been trained on large datasets and have learned general features and patterns, making it possible to construct classification models with relatively limited data.

Accordingly, this study investigates the feasibility of using pre-trained models to develop a water stress estimation model from RGB images of persimmon leaves.

2. Materials and Methods

The study area is the Gojo-Yoshino region in central Nara Prefecture, Japan. This study targeted two persimmon orchards in the Gojo-Yoshino region. In each orchard, one soil moisture sensor and two fixed cameras were installed, and hourly measurements of soil moisture and RGB images of persimmon leaves were collected from 2022 to 2024. Soil moisture values were converted to pF values using the soil water retention curve. To account for the lag in plant water use, pF values measured five hours earlier were used as the reference. Water stress levels were classified into five categories based on the criteria of Kamoda (1987) (Table 1).

For model development, a pre-trained ResNet-50 CNN architecture was employed (Figure 1). Two cases were considered for model evaluation. Case 1 used all available data (8,993 images), whereas Case 2 used a randomly sampled subset of half the images from Case 1 (4,496 images). The number of images for each case is shown in Table 2. Comparing these cases allowed us to assess the effect of training data volume on model accuracy. The datasets were divided into training and test sets at a 9:1 ratio.

Table. 1 "Optimal Soil Moisture Range for Each Growth Stage" (Kamoda, 1987)

Class	pF range
Class1	0 – 2.0
Class2	2.0 – 2.3
Class3	2.3 – 2.7
Class4	2.7 – 3.0
Class5	3.0 -

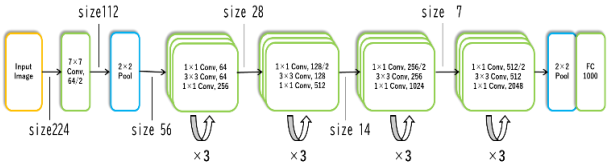

Fig.1 Model Architecture (ResNet50)

Table. 2 Training images per case

(images)	Case1	Case2
Class1	1078	556
Class2	301	157
Class3	720	353
Class4	1148	584
Class5	5746	2846

Model performance was evaluated using accuracy, recall, precision and F1-score. Recall evaluates the model's ability to avoid false negatives, precision evaluates its ability to avoid false positives, and the F1-score represents the harmonic mean of these two metrics. All indices range from 0 to 1, with values closer to 1 indicating higher performance. The formulas for calculating recall, precision, and F1-score are shown below.

$$Precision = \frac{True\ Positive}{True\ Positive + False\ Positive}$$

$$Recall = \frac{True\ Positive}{True\ Positive + False\ Negative}$$

$$F1 - score = \frac{2 \times Precision \times Recall}{Precision + Recall}$$

3. Results and Discussion

Figure 2 shows the overall accuracy for the two cases. Case 1, which used all available images, achieved an accuracy of 80%, while Case 2, with a randomly reduced dataset, achieved 76.35%, approximately 4% lower than Case 1.

Figure 3 presents the precision, recall, and F1-scores for each class in the two cases. In both cases, Class 5 exhibited the highest precision, recall, and F1-score. The variation in class-wise performance showed similar trends across both cases. However, in all classes, the F1-scores of Case 2 were lower than those of Case 1. Among them, Class 2 showed the greatest decline in F1-score (by about 0.1), while Class 5 showed the smallest decline (about 0.02). Classes 1, 3, and 4 decreased by approximately 0.06.

Based on these results and the number of training images per class shown in Table 2, it can be inferred that model performance stabilizes when approximately 3,000 training images are used, as observed in Class 5 of Case1. Furthermore, increasing the number of training images beyond 3,000 is unlikely to yield substantial performance improvement (Class5 of Case2), suggesting that the model may have reached its performance ceiling under the conditions of this study.

4. Conclusions

This study demonstrated that water stress in persimmon leaves can be estimated from RGB images collected across multiple orchards by using a pre-trained convolutional neural network (ResNet-50). Even when the number of training images was reduced by approximately half, model performance did not decline substantially. However, class-wise accuracy was affected by the imbalance in training sample sizes. Future work should therefore focus on balancing the number of training images across classes and exploring alternative pre-trained models.

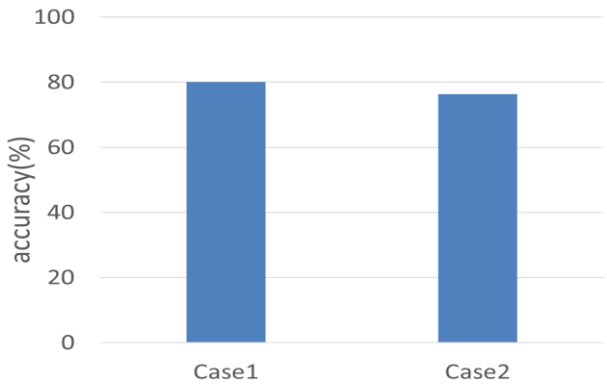

Fig. 1 Evaluation of model performance for each case

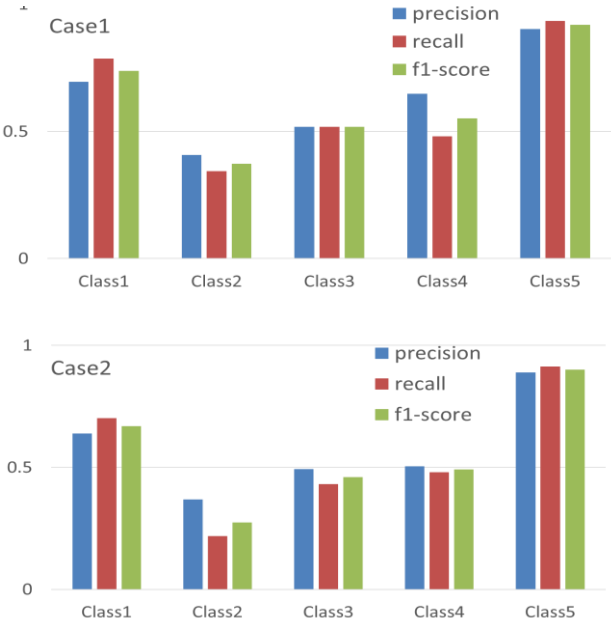

Fig. 2 Evaluation of the model for each class

Acknowledgements

The authors extend their sincere appreciation to the Food and Agricultural Promotion Depart-ment, Nara Prefecture, and the Gojo Yoshino Land Improvement District for their support and facilitation of the research activities, as well as to the anonymous referees for their comments and constructive suggestions, which have significantly enhanced the manuscript quality.This research received financial support from the development and improvement program of strategic smart agricultural technology grants provided by the Project of the Bio-oriented Technology Research Advancement Institution (BRAIN).

References

Kamoda, S. (1987). Environmental control in facility cultivationof fruit trees. Abstracts of Symposium of the Horticultural

Society, 1–8. (In Japanese)

This extended abstract template was updated on April 11, 2025

Deep Learning-Based Estimation of Water Stress in Persimmon Trees for Data-Driven Irrigation Management

Atsushi Okayama [1*], Naoki Onishi [2], Masaomi Kimura [2], Rena Sanada [1], and Yutaka Matsuno [2]

[1] Graduate School of Agriculture, Kindai University

[2] Faculty of Agriculture, Kindai University

* Corresponding author. Email: 2544680002w@nara.kindai.ac.jp

Abstract

Nara Prefecture is a major persimmon-producing region in Japan, where effective irrigation management is crucial for maintaining fruit quality and yield. Conventional irrigation practices often rely on farmers' empirical knowledge, which may be inadequate under increasingly variable climatic conditions. To address this issue, we developed a deep learning model to estimate water stress in persimmon trees using RGB leaf images. Morphological changes, such as wilting and curling, were used as visual indicators of water stress. Data were collected from multiple orchards in the Gojo-Yoshino region of Nara Prefecture during the 2022–2024 growing seasons. Leaf images were paired with soil moisture measurements and categorized into six water stress levels. A convolutional neural network (CNN) with six convolutional layers was trained to classify the leaf images. Balanced datasets and data augmentation were applied, and training sizes of 1,000, 2,000, and 3,000 images per class were evaluated. Model performance was assessed using accuracy and F1-score. Accuracy increased with larger training sizes, reaching approximately 68% with 3,000 images per class. Extreme moist and dry conditions were classified more reliably than intermediate states, as indicated by higher F1-scores. These findings demonstrate the potential of CNN-based leaf morphology analysis to support irrigation management in persimmon orchards. Future work will focus on improving generalizability and accuracy by incorporating data from additional orchard sites.

Keywords: Smart Agriculture, irrigation management, Deep learning, CNN

1. Introduction

Effective soil moisture management is essential for sustaining fruit quality and yield in orchard production (Tanaka et al., 1971; Matsuda et al., 2011). However, current irrigation practices largely depend on farmers' empirical knowledge, and increasing climatic instability due to global warming has reduced the reliability of conventional approaches. Consequently, there is a growing demand for quantitative irrigation decision-making methods that do not rely solely on experiential judgment.

In recent years, deep learning, a branch of artificial intelligence, has emerged as a promising tool. Deep learning models, inspired by the structure of human neural networks, can transform qualitative, experience-based assessments into objective, data-driven evaluations.

Previous studies have shown that leaves under severe water stress undergo morphological changes, such as wilting and curling, which farmers traditionally use as irrigation cues. Therefore, image-based analysis of leaf morphology offers a potential basis for determining irrigation timing. In this study, we developed a convolutional neural network (CNN) for estimating water stress levels from RGB images of persimmon leaves and compared classification accuracy across different training dataset sizes. The objective was to evaluate the effectiveness of this model as a decision-support tool for irrigation management.

2. Materials and Methods

This study was conducted in four persimmon orchards in the Gojo-Yoshino region of Nara Prefecture. Each orchard was equipped with two fixed-point cameras (eight in total) and one soil moisture sensor (four in total). Data were collected hourly from June to September during the irrigation periods of 2022–2024, resulting in 14,812 RGB images of persimmon leaves paired with soil moisture measurements.

Soil moisture values were converted into pF values using soil moisture retention curves. To account for the lag in plant water uptake, the pF value measured five hours earlier was used as the reference. Based on this reference, water stress levels were classified into six categories (Table 1).

A convolutional neural network (CNN) with six convolutional layers was constructed (Figure 1). The model used RGB images as input and classified them into six water stress levels as output. Since class imbalance can negatively affect performance (Altalhan et al., 2025), the number of training images was equalized across classes. Training dataset sizes of 1,000, 2,000, and 3,000 images per class were evaluated, while validation and test sets contained 300 images per class. For classes with insufficient images, data augmentation was applied by dividing each image into four segments, while excluding segments that did not contain leaf regions. Because deep learning results vary depending on random initialization of weights, each training condition was repeated ten times. Model performance was evaluated based on the average overall accuracy and F1-score. An F1 value closer to 1 indicates higher classification accuracy. Early stopping was employed during training to prevent overfitting.

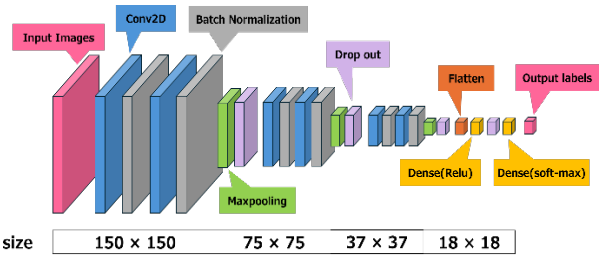

Fig. 1 Model Architecture (CNN)

Table. 1 Water Stress Classification by pF Value (X : pF value)

Classification	Range
Class1	X < 2.0
Class2	2.0 ≤ X < 2.5
Class3	2.5 ≤ X < 2.8
Class4	2.8 ≤ X < 3.0
Class5	3.0 ≤ X < 3.5
Class6	3.5 ≤ X

3. Results and Discussion

The overall classification accuracy according to training dataset size is shown in Figure 2. The model achieved an average accuracy of 51% with 1,000 training images, 58% with 2,000 images, and 68% with 3,000 images. Standard deviations were 1.6% for 1,000 images, 0.9% for 2,000 images, and 0.5% for 3,000 images. Accuracy improved by as much as 10% between 2,000 and 3,000 images, suggesting that fewer than 2,000 images per class are insufficient for the model to capture morphological features related to water stress. Balancing the dataset at 3,000 images per class yielded the highest accuracy and minimized performance variation caused by random initialization. However, the use of augmented data may have limited accuracy to approximately 70%.

Figure 3 presents the F1-scores of each class under different training sizes. The model trained with 1,000 images indicated the lowest F1-scores across all classes, whereas training with 3,000 images produced the highest scores. In particular, for Classes 1, 2, and 3, a difference of more than 0.1 was observed between 2,000 and 3,000 training images. Comparison of F1-scores revealed that Class 6 (dry condition) consistently achieved the highest value, followed by Class 1 (moist condition). Classes 2, 4, and 5 showed relatively small F1-scores, all below 0.2, compared with Classes 1 and 6.This indicates that extreme moist and dry conditions are more easily distinguished, whereas intermediate stress levels are more difficult to classify. These findings highlight the need for larger and more diverse datasets that capture more detailed information about leaf condition to improve performance in intermediate water stress states.

In a previous study by Okayama et al. (2025), a model trained with data from two orchards achieved accuracy exceeding 80%. By contrast, the present study incorporated data from a larger number of orchards, which reduced accuracy. This suggests that orchard-specific environmental factors may exert stronger effects than common morphological features of persimmon leaves.

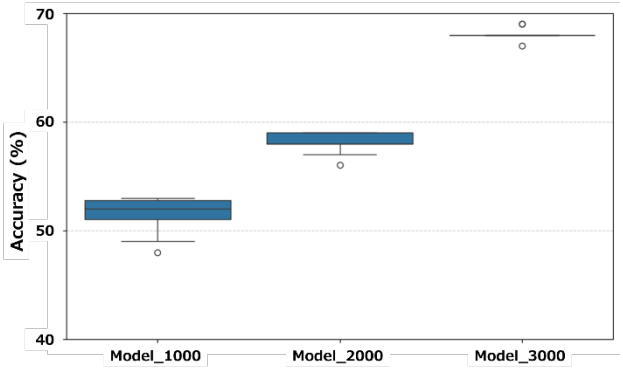

Fig. 2 Performance Comparison of Three Models
Model_1000: trained with 1,000 images; Model_2000: trained with 2,000 images; Model_3000: trained with 3,000 images.

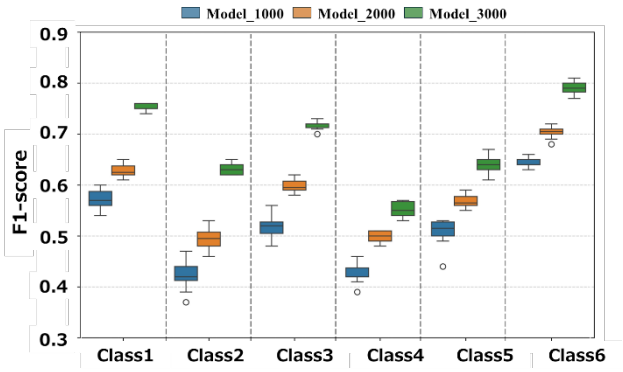

Fig. 3 Model Performance in Classifying Six Water Stress Levels (F1-Score)

4. Conclusions

When the number of training images was balanced across classes, model performance became stable with at least 3,000 images per class. The model effectively distinguished extreme moist and dry conditions but was less accurate for intermediate stress levels. These results indicate that the proposed model has sufficient potential to be applied as a decision-support tool for irrigation management.

The results of this study, which included a larger number of orchards, showed lower accuracy compared to the previous study by Okayama et al (2025), which was conducted with fewer orchards. To improve both accuracy and applicability, future work will focus on collecting and utilizing data from a broader range of orchard sites. Expanding the dataset across more diverse environments will be crucial for enhancing both generalizability and robustness of the model.

Acknowledgements

The authors extend their sincere appreciation to the Food and Agricultural Promotion Department, Nara Prefecture and the Gojo Yoshino Land Improvement District for their support and facilitation of the research activities.

This research received financial support from the development and improvement program of strategic smart agricultural technology grants provided by the Project of the Bio-oriented Technology Research Advancement Institution (BRAIN).

References

Altalhan, M., Algarni, A., & Turki-Hadj Alouane, M. (2025). Imbalanced data problem in machine learning: A review. IEEE Access, 13, 13686–13699.

Matsuda, M., Habu, T., Konishi, T., Nonaka, K., Kusumi, K., Kurosawa, T., & Kitajima, A. (2011). Effect of the drip irrigation system with plastic mulch on fruit quality in Japanese persimmon cv. 'Taisyu'. Bulletin of the Experimental Farm, Kyoto University, 20, 29-32. (In Japanese)

Okayama, A., Yamamoto, A., Kimura, M., & Matsuno, Y. (2025). Utilizing convolutional neural network (CNN) for orchard irrigation decision-making. Environmental Monitoring and Assessment, 197(2), 168.

Tanaka, K., & Aoki, M. (1971). Effect of Irrigation and Nitrogen Application in Summer on the Fruiting of 'Fuyu' Kaki. Research bulletin of the Aichi-ken Agricultural Research Center. Series B, 3, 9-18. (In Japanese).

Fundamental Evaluation of Convolutional Neural Networks for Automatic Identification of Spider Mite Damage in Edible Roses (*Rosa* spp.)

Rena Sanada [1], Honami Nakasuji [1], Atsushi Okayama [1],

Munetaka Hosokawa [2], Masaomi Kimura [2], Yutaka Matsuno [2]

[1] Graduate School of Agriculture, Kindai University, Nara Prefecture, Japan

[2] Faculty of Agriculture, Kindai University, Nara Prefecture, Japan

Abstract

Spider mites are major agricultural pests due to their extremely small body size, rapid reproductive capacity, and strong resistance to pesticides, making early control essential for crop protection. However, initial damage symptoms are often subtle and difficult to detect, leaving diagnosis dependent on the experience and skill of growers. In recent years, AI-based approaches for automated diagnosis have been explored, yet the reliable identification of early spider mite damage remains challenging and insufficiently addressed.

This study investigated the potential of convolutional neural networks (CNNs) to identify early spider mite symptoms using a small dataset. Leaf images were captured with an iPhone 16 and classified into two categories: “damaged” and “healthy.” A total of 496 training images and 40 validation images were employed. To emphasize subtle damage features, the RGB values of the training images were carefully adjusted. Model performance was evaluated using accuracy and F1-score, comparing results between adjusted and unadjusted datasets. Grad-CAM visualization was further applied to examine which regions the model focused on during classification.

The results demonstrated that models trained with RGB-adjusted images achieved approximately 0.1 higher accuracy and F1-scores compared with unadjusted data. Heatmap analysis also confirmed that adjusted models more effectively extracted relevant features from damaged areas. These findings suggest that RGB adjustment enhances the detection of early spider mite damage even with limited data. Future improvements will require larger datasets and more advanced preprocessing techniques to achieve higher accuracy and practical reliability.

Keywords: Deep Learning (DL), heatmaps, Cultivation Management, pest infestation in plants.

1. Introduction

Spider mite damage has been frequently reported in edible roses, but cultivation management is generally difficult because pesticide use must be minimized. Spider mites are parasitic organisms that feed on leaf nutrients and reproduce rapidly. Therefore, once detected, they must be removed promptly. However, roses are often cultivated densely in greenhouses, and spider mites are very small (approximately 0.5 mm in body length), making visual detection challenging. Consequently, the assessment of spider mite damage has relied heavily on the expertise of agricultural workers. With the aging of the agricultural workforce, concerns have been raised regarding the decline in observational ability (Inoue, 1990). The establishment of methods that enable simple and expertise-independent assessment of plant damage is highly desirable. In recent years, increasing attention has been directed toward the potential application of artificial intelligence (AI) technologies for the automatic diagnosis of plant diseases and pest damage. In this study, we conducted a fundamental evaluation of spider mite damage identification using an image recognition model.

2. Materials and Methods

A binary classification model was constructed to discriminate the presence or absence of spider mite on rose leaves by utilizing a convolutional neural network (CNN), one of the deep learning algorithms. The number of training epochs was set to a maximum of 100, and early stopping was introduced to prevent overfitting, with the patience parameter set to 15. The dataset was collected from edible roses cultivated in a greenhouse at the Faculty of Agriculture, Kindai University. During the survey in September, pesticide application for mite control had been carried out, and no spider mites were observed. Subsequently, on October 9, 100 images each of damaged and undamaged leaves were captured. To increase the number of images, cropping was applied to the original photographs, resulting in 266 images of damaged leaves and 290 images of undamaged leaves. These images were used for model validation..

In Experiment 1, 236 damaged leaf images and 260 undamaged leaf images were employed as training data for model evaluation. In Experiment 2, cropped images were further processed to emphasize the red component of the RGB channels (Fig. 1), and the same number of images as in Experiment 1 were used.

Figure 1 Normal cropped image (left) and color processed image (right)

Each experiment was repeated 10 times. In this study, the F-measure was used as an evaluation metric for classification performance. The F-measure is defined based on Precision and Recall, as expressed in Eq. (1).

$$F = \frac{2 \cdot Precision \cdot Recall}{Precision + Recall} \quad (1)$$

Furthermore, Grad-CAM was employed to verify whether the model appropriately extracted features from the damaged areas. The heatmaps generated by Grad-CAM visualized the image regions that the CNN focused on during classification, with red indicating high attention and blue indicating low attention (Toda et al., 2019).

3. Results and Discussion

A comparison of classification of the accuracy between Experiment 1 and Experiment 2 revealed that the mean accuracy in Experiment 1 was 0.647, whereas Experiment 2 achieved a higher mean accuracy of 0.747. (Table .1)

Table 1. Comparison of Accuracy

	Maximum	Minmum	Mean
Experiment 1	0.733	0.600	0.647
Experiment 2	0.833	0.650	0.747

Next, a comparison of the F-measures from the both experiments (Figure 2) revealed that, similar to the accuracy results, Experiment 2 (orange) was distributed at higher values than Experiment 1 (blue). In Experiment 1, the median F-measure (0.621) was lower than the mean (0.641), indicating a tendency toward lower values. In contrast, Experiment 2 showed a median (0.774) higher than the mean (0.764), suggesting a bias toward higher values. These results for both the accuracy and F-measure demonstrate that applying color adjustment to the data enhances the precision of spider mite damage classification.

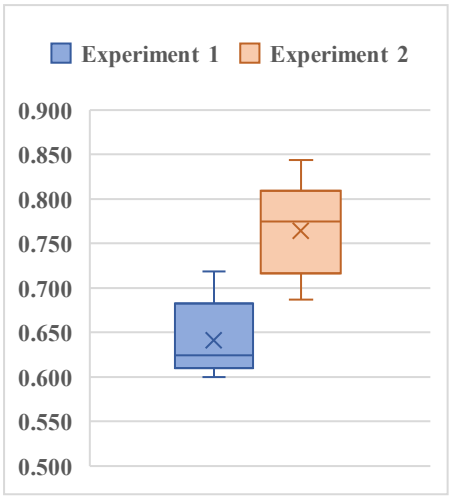

Figure 2. Comparison of F value results between Experiment 1 (blue) and Experiment 2 (orange).

Figure 3 shows the images used in Experiment 1 (upper left) and Experiment 2 (upper right), as well as the corresponding heatmaps of the Experiment 1 model (lower left) and the Experiment 2 model (lower right). In the Experiment 1 model, the entire leaf was covered in blue, and the brownish damaged areas could not be extracted. In contrast, the Experiment 2 model highlighted the damaged areas in red, indicating appropriate feature extraction. However, it was found that predicting small spots, which may represent early symptoms, remains difficult. Furthermore, in other test images, both models showed a tendency for blank regions in the heatmaps to appear in red and be recognized as features of damaged leaves.

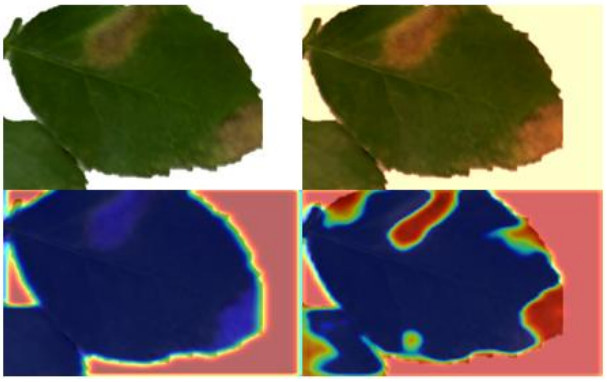

Figure 3. Comparison of heatmaps from Experiment 1 (bottom left) and Experiment 2 (bottom right)

Overall, RGB value adjustment facilitated the extraction of damage-related features and enhanced the classification accuracy of damaged leaves. Previous studies on plant image classification often employed approximately 1,000 images per class (Yatomi, 2019). In contrast, this study suggests that reliable classification is possible even with a limited dataset. Future work will not only increase the number of leaf images but also apply data augmentation techniques, such as image rotation, to further improve model performance.

4. Conclusions

The study demonstrated that even with a limited dataset, adjusting RGB values enabled the learning model to achieve high accuracy and F-measure, suggesting improved classification performance under small data conditions. Verification using Grad-CAM further confirmed that RGB adjustment facilitated feature extraction from damaged areas. However, the heatmaps indicated a tendency for the model to also learn blank regions as features, highlighting the need for improvement in this aspect. While severe damage symptoms were successfully identified, the complete automatic recognition of early symptoms remains challenging. These findings suggest that RGB adjustment has potential for the identification of early-stage spider mite damage, and further improvements in accuracy can be expected through dataset expansion and enhanced preprocessing strategies.

Fast,J.D.,Zong,S.,Whiteman,C.D.,1996. Boundary layer evolution with in a canyonland basin. J.Appl. Meteor.,35(12),2162-2178

References

Inoue, M., 1990. Influence of Ageing on Grower's Ability to Detect the Occurrence of Spider Mites. Jpn. J. Appl. Entomol. Zool., 34, p254–257.

Toda, Y., Okura, F., Ito, J., Okada, S., Kinoshita, T., & Tsuji, H. (2019). How convolutional neural networks diagnose plant disease. Plant Phenomics, 2019, 1–14.

Yatomi, H., 2020. Trends and Challenges of Automatic Diagnosis Techniques for Plant Diseases and Pests. Jpn. J. Nematol. Sci., 26, p123–130.

Effect of nighttime irrigation using automatic irrigation systems on preventing cold water damage of rice

Kazuhiro Nishida[1*], Kazuya Shiraishi[1], Tadashi Tsukaguchi[2], Shuichiro Yoshida[1], Kazuyoshi HIRAI[3], Yuji SUNAHASE[3]

[1] Graduate School of Agricultural and Life Sciences, The University of Tokyo, Tokyo, Japan

[2] Faculty of Bioresources and Environmental Sciences, Ishikawa Prefectural University,

[3] Hokutsu Co. Ltd., City, (Province or State) 54321, Country

* Corresponding author. Email: knishida@g.ecc.u-tokyo.ac.jp

Abstract

Nighttime irrigation is a promising measure to mitigate cold-water damage in rice cultivation; however, the additional labor required for water management remains a major challenge. Automatic irrigation systems offer a potential solution by enabling efficient nighttime irrigation without extra labor. This study evaluated the effects of nighttime irrigation using an automatic system on paddy water temperature (T_w), rice growth, yield, and grain quality. Field experiments were conducted in 2023 and 2024 in a paddy field in Hukushima, Japan, where irrigation water was consistently cold. In both years, T_w, rice plant height, grain quality (percentage in green immature grains), and grain yield were measured at multiple locations within the field. Water level fluctuations were also monitored to evaluate irrigation practices. A comparative analysis was conducted between 2023 (conventional water management) and 2024 (nighttime irrigation with the automatic system). The results showed that: (1) the automatic system successfully conducted nighttime irrigation when the temperature difference between irrigation water and T_w was minimal; (2) nighttime irrigation effectively increased Tw, particularly near the water inlet, where Tw is often lowered by cold irrigation water; and (3) these thermal improvements led to increased plant height, improved grain quality, and higher yields. These findings indicate that nighttime irrigation using an automatic system is an effective, labor-saving approach for mitigating cold-water damage in rice.

Keywords: Nighttime irrigation, Automatic irrigation systems, cold water damage of rice.

1. Introduction

Nighttime irrigation is known as a countermeasure against yield reduction in rice caused by the inflow of low-temperature irrigation water (cold-water damage). This method prevents a decline in paddy water temperature by applying irrigation at night, when the temperature difference between paddy and irrigation water is small. However, it requires considerable labor for water management, posing a practical challenge. Recent advancements in automated irrigation systems may provide an effective solution to this issue enabling nighttime irrigation without substantial labor input. To evaluate this effect, this study examines the impact of nighttime irrigation using an automatic system on paddy water temperature, rice growth, yield, and grain quality.

2. Materials and Methods

Field experiments were conducted in 2023 and 2024 in a paddy field located in Fukushima, Japan. The rice cultivar was *Akitakomachi*, transplanted on May 17. The field had high percolation rate (20 mm d^{-1}), and the average temperature of irrigation water during the early growth stage was low (14 °C). In 2024, an automatic irrigation system (“Mizumawari-Gate-kun”) was installed, and nighttime irrigation using this system was implemented starting on May 30.

The temperature of paddy water (T_w), water depth, rice plant height, grain quality, and yield were measured at multiple points in the field (Fig.1). T_w was measured every 10–20 min using a thermometer, and the time-averaged water temperature during the early growth stage (June 1-24) was calculated. Water depth change was measured using a water pressure sensor and used to evaluate irrigation practices. The average height of five to ten rice plants was measured at 50 days after transplanting. Ten rice plants were sampled at maturity and then assess their grain quality (percentages in green immature grain) and yield. A comparative analysis was conducted between 2023 (conventional water management) and 2024 (nighttime irrigation with the automatic system).

3. Results and Discussion

In 2023, water depth fluctuated irregularly, whereas in 2024 it exhibited a regular pattern, rising at night and declining during the daytime (Fig. 2(a)). This indicates that while low-intensity continuous irrigation was applied in 2023, the automatic irrigation system enabled ideal nighttime irrigation in 2024.

Consequently, the large temperature drops observed near the water inlet in 2023 were not observed in 2024 (Fig.2(b)(c), Fig.3). These results demonstrate that nighttime irrigation with automated irrigation system effectively increased paddy water temperature.

The large differences in rice plant height and the percentages in green immature grains observed within the paddy field in 2023 were reduced in 2024 (Fig.4). These results indicate that nighttime irrigation using an automatic irrigation system mitigated growth delay, yield loss, and quality deterioration of rice caused by cold-water damage.

4. Conclusion

Nighttime irrigation using an automatic irrigation system suppressed the decrease in paddy water temperature and alleviated growth delay, yield reduction, and quality deterioration of rice.

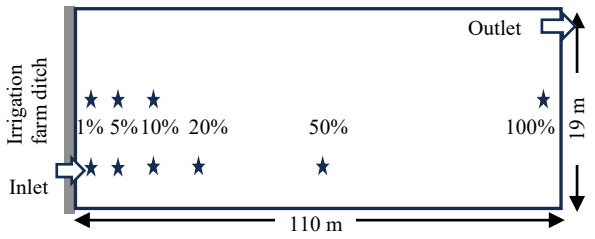

Fig.1 Schematic diagram of the field and measurement points

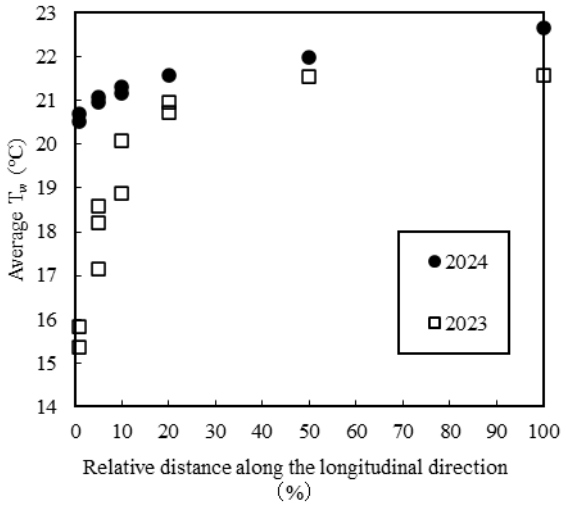

Fig.3 Comparison of time-averaged water temperature distribution during June 1-24.

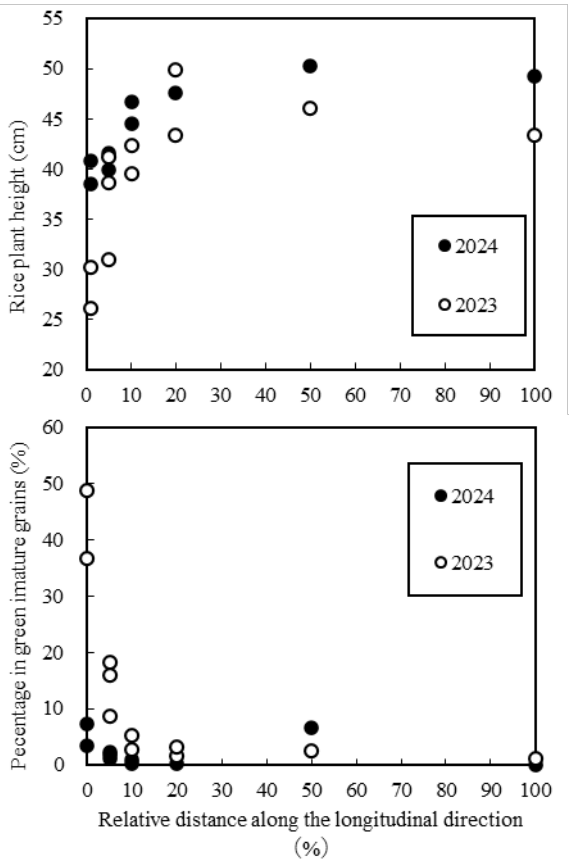

Fig.4 Rice plant height at 50 days after transplanting and percentage of immature grains

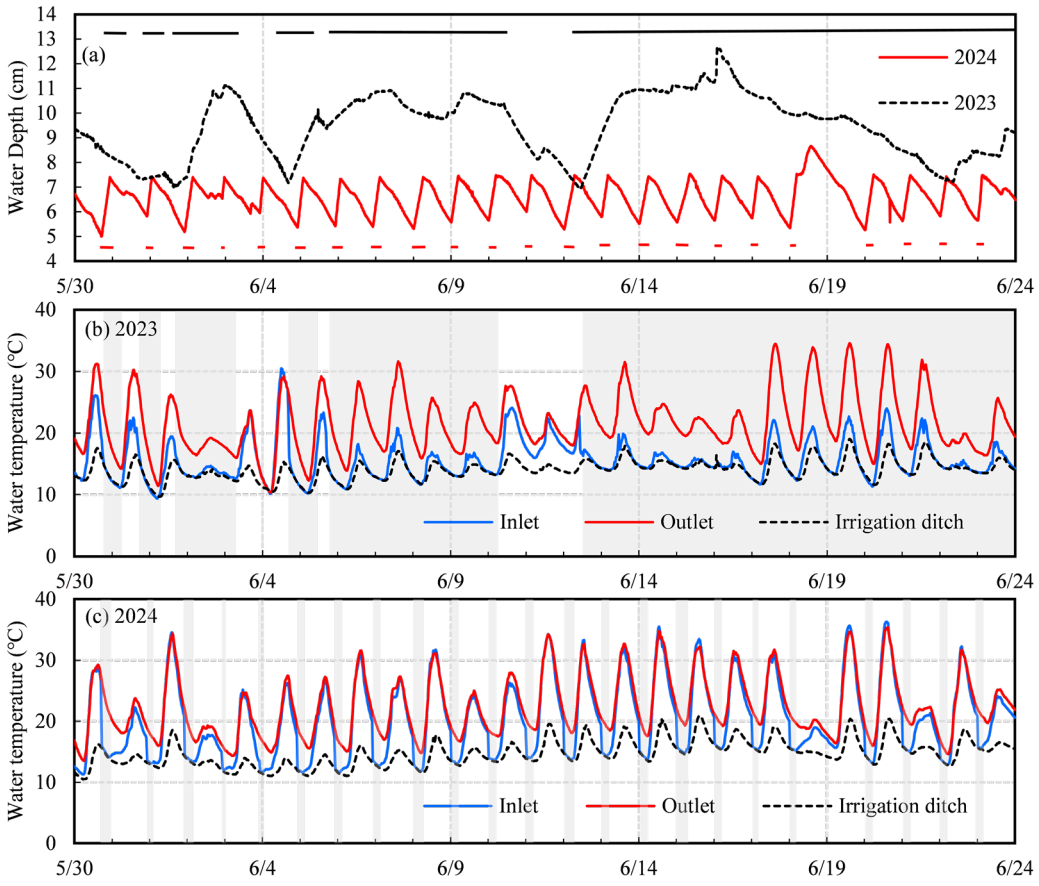

Fig.2 Changes in water depth and temperature at 2023 (conventional water management) and 2024 (nighttime irrigation with automatic irrigation system). (background color: irrigation)

Integrating Groundwater Forecasting and Climate Risk Mapping to Enhance Adaptive Water Management: A Case Study of Tainan, Taiwan

Tsai Wen-Ping・Wang I-Hsuan・Tsang Pei-Ju

Abstract

Taiwan faces recurring water shortages despite high annual rainfall, due to steep terrain, uneven precipitation patterns, and dense population. Climate change has increased drought frequency, intensifying pressure on groundwater-now a critical source for agriculture and urban use. However, groundwater levels are highly sensitive to climatic variability and human extraction, making accurate forecasting essential for adaptive and sustainable water management.

This study develops an integrated framework combining deep learning-based groundwater forecasting with climate risk assessment to support water adaptation strategies in Tainan, a region with mixed urban-agricultural land use and high vulnerability. A Long Short-Term Memory (LSTM) model was trained using historical meteorological and well data to predict groundwater trends at multiple sites. K-means clustering and within-group normalization were used to enhance prediction accuracy across hydrologically similar zones.

Risk was assessed using a three-pillar framework: Hazard, Exposure, and Vulnerability. Hazards were evaluated using the Standardized Precipitation Index (SPI) and extreme climate trends; exposure considered irrigation demand and population; vulnerability was based on groundwater fluctuation amplitudes and historical depletion patterns. The resulting risk maps identified groundwater-stressed zones under potential drought scenarios.

Findings demonstrate the LSTM model's strength in forecasting groundwater dynamics and provide spatial insights for managing aquifer sustainability. The approach supports smarter irrigation planning and water allocation, contributing to climate-resilient paddy agriculture and sustainable water governance across vulnerable rural landscapes.

Development of a Crop Yield Estimation Technique Based on Integrated Analysis of Hydrological and Growth Indicators in Paddy Fields Using SAR Imagery

Chung Jeehun・Lee Yonggwan・Kim Yongwon・Jun Wonjun・Kim Seongjoon

Abstract

This study aims to develop a machine learning-based rice yield prediction model by integrating crop growth and hydrological indicators derived from Sentinel-1 C-band Synthetic Aperture Radar (SAR) imagery. Time-series backscatter data from 2015 to 2024 were preprocessed using the SNAP(Sentinel Application Platform) to generate co and cross-polarized images, from which vegetation indices were extracted. These indices were used to monitor rice phenology at the field scale, using digital farm map paddy field boundaries. Agricultural reservoirs boundaries were extracted using Otsu threshold method to SAR imagery, and their surface water area dynamics were validated against optical water indices and land cover maps. Reservoir storage volumes were estimated using empirical surface area-volume curves, enabling the assessment of water availability across irrigation districts. Growth indicators and hydrological variables were combined to generate a multivariate feature set. Automated machine learning (AutoML) was used to select optimal algorithms and tune hyperparameters for yield prediction, based on national rice production statistics. The proposed framework enables early-season, spatially explicit yield forecasting by linking remote sensing-derived indicators of crop status and water supply, offering practical applications for agricultural planning and food security policy.

Integrated Application of Ultrafiltration and Fine Bubble Diffusion in a Hybrid Recirculating Aquaculture Paddy Farming System

Teuku Assiddiqi Devan・Setiawan Indra Budi

Abstract

The availability of fish from natural waters is decreasing due to overexploitation, environmental pollution, and the disruptive effects of climate change on aquatic ecosystems. As a result, these conditions are further depressing wild fish populations globally. To overcome this crisis, modern aquaculture technologies such as recirculating aquaculture systems (RAS) are essential, as they allow for more efficient, sustainable management and significantly enhance aquaculture productivity. This research integrates a hybrid RAS with paddy farming (rice-fish farming), aiming to optimize water reuse and nutrient cycling in an integrated agri-aquaculture system. The wastewater treatment process employs multimedia filters, activated carbon filters, SRUF-4040 ultrafiltration membranes, and fine bubble diffusers to ensure water quality suitable for both fish culture and irrigation of rice paddies. Preparation phase involves designing the system configuration that supports both aquaculture and paddy irrigation. Testing phase includes monitoring water quality parameters. In the data analysis phase, water quality, fish survival, fish growth, and potential benefits for rice irrigation are evaluated. The recirculation system operates continuously with an average distribution discharge of 2.486 L/min in row A tanks and 2.463 L/min in row B tanks. The integrated system demonstrates the ability to reduce toxic parameters such as ammonia and nitrite to average concentrations of 0.4 mg/L and 0.009 mg/L, respectively, and increase dissolved oxygen to an average of 5.7 mg/L. This performance supports healthy fish culture, indicated by a survival rate of 93.13% and a specific growth rate of 4.10%, while also producing treated water suitable for sustainable rice cultivation.

Paddy Irrigation Tools developed on Farmers Viewpoint

OZAWA Yoshihiro

Technical Adviser, Showa Concrete Industry, Khoran 1 Gifu City(Gifu pref.), Japan

Email: ozawa-y@showa-con.co.jp

Abstract

Recently, counter measures to climate change are becoming new challenges in paddy irrigation. AWD, Alternate Wetting and Drying, is effective method for reduction of methane, a type of GHG, emission from paddy field. Paddy Dam, which retains heavy rainfall on paddy surface, is effective method for mitigation of flood damage.

For smooth introduction of AWD and Paddy Dam, we developed low-cost and easy-to-use tools as follows.

ITAOTOSHI Gate: Half-automatic paddy irrigation gate for limiting water depth on paddy surface

GETAMIZU Block : Streamline shaped concrete block for raising canal water depth

HONEN Water Gage : Ground water check gage

T-DAM Pipe : Floating overflow regulating pipe

T-DAM Board : Notched orifice flow regulating board

Keywords: AWD, Paddy Dam, limiting water depth, raising canal water depth, ground water check

1. Introduction

GHG emissions from agriculture and forestry occupies 20% of world whole emission. Especially methane, which has strong greenhouse effect compared to CO2, attracts much attention. In Western world methane is from caw burps, but in Asia emission from paddy soil under reduction state is dominant, especially double or triple cropping areas. From the past Intermittent Irrigation has been regarded as a method for water saving, recently AWD, which lowers water surface below soil surface for a few days, has been noticed as effective way for reduction of methane emission.

Enhancing flood storage function of paddy field is effective and low-cost countermeasure to flood disaster. By ponding 20cm depth on one hector is equivalent to 2000 m3 of disaster prevention dam capacity. Recentry, measures for enhancing flood storage function named Paddy Dam are proactively introduced in Japan.

Implementation of AWD and Paddy Dam in large areas generates significant social benefit. For acceleration of farmers' participation in these challenges, tools should have features such as simple, low cost, easy O&M, etc.

2. Tools for AWD

ADW is a method which repeats following operations. Start intaking water from canal to paddy field and stop intake just after paddy water depth reaches a certain level. Leaving water level down until it becomes ground water to provide soil with oxygen.

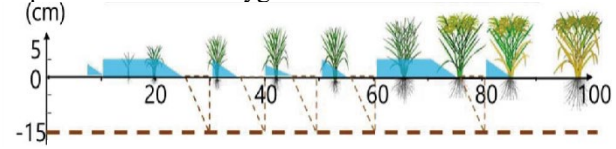

Figure 1. Conceptual diagram of AWD

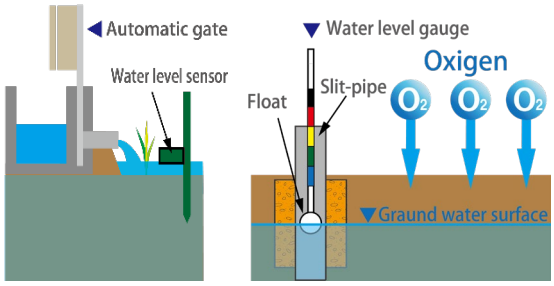

Figure 2. Tools for AWD

2.1. ITAOTOSHI Gate

2.1.1. Useful irrigation gate for AWD

For controlling water intake, automatic gate is helpful. Followings are requirements for gate familiar to farmers.

- Operation is simple and easy.
- Both initial and running cost are inexpensive.
- Farmers can easily install and remove it.
- Durable, easy to repair and parts-procuring.

2.1.2. Functions of ITATOSHI Gate

- ITAOTOSHI is half-automated irrigation gate, whose automated function is only stop water intake. Start of water intake can be done with minimum workload, if farmers open gate during daily field patrol for watching crops growing, pest etc. Farmer open gates by only lifting handle, which needs only a few seconds.
- Main functional parts of ITAOTOSHI are gate-panel, gate-handle, water revel sensor, solenoid, and AA type batteries etc. By raising gate-handle manually, gate-panel is held at high position. When sensor detects water surface reaches a certain level, solenoid loosens the hold of gate-handle then gate-panel falls by gravity.

2.1.3. Features of ITAOTOSHI Gate

- Initial & Running cost: It costs 300 US dollars. It is far lower than ICT type automatic gate, because motor, gear, solar panel, etc. are not used. Running cost is only expense for four AA batteries per one cropping.

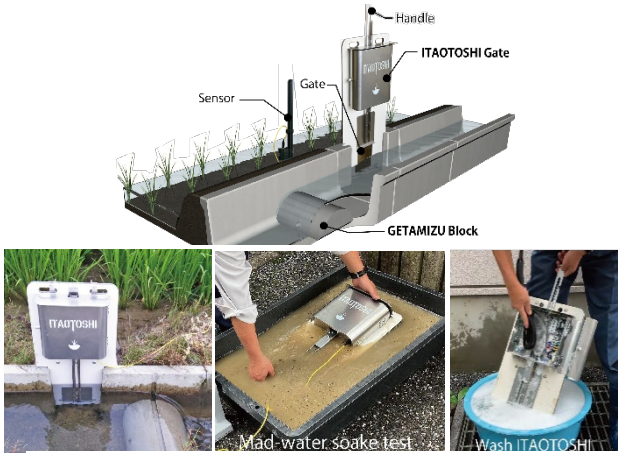

Figure 3. ITAOTOSHI Gate & GETAMIZU Block

- Installation and Removal: Installation is only fitting to stop-log groove at inlet. If there are no stop-log groove, use Stop-log Flame shown in Fig.-5.
- Durability and Maintenance: It will not be easily deteriorated by weathering, because the structure is made of stainless steel and plastic. Even if it is soaked in mad water during flood, function recovers by only washing and dry. Daily maintenance is oiling. Parts such as sensor, switches etc. are available at electric parts shop.

2.2. GETAMZU Block

GETAMIZU Block is concrete block for raising canal water surface for intaking during little flow. It can dam-up water surface of shallow flow. But it does not cause water spilling in case of deep flow, because flow velocity above the block increases smoothly due to streamlined shape.

2.3. HONEN Water Gage

It is water surface gage for checking ground water level for AWD. It consists of plastic pipe with many slits and colored plastic rod with float ball. Farmers can easily check ground water level in invisible paddy soil.

Figure 4.
HONEN Water Gage

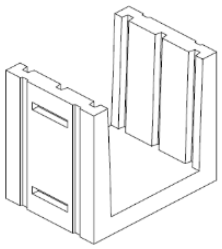

Figure 5.
Stop-log Frame

3. Tools for Paddy Dam

Function of Paddy Dam is to retain heavy rainfall on paddy surface by regulating discharge from outlet. For accelerating many farmers' participation, demerits accompanying Paddy Dam should be as little as possible, because it does not have direct merits to farmers. Anticipated demerits in farming are as follows.

- Excessive deep ponding causes levee overflow & failure.
- Clogging by trash such as rice straw causes ill drainage.

3.1. T-DAM Pipe

T-DAM Pipe is discharge regulator for vertical pipe type outlet. It is plastic pipe with floats and small spillways.

Light rain overflows through spillways with less than 4cm of flow depth. When flow depth reaches 4cm during heavy rain, T-DAM Pipe rises by buoyancy of float while keeping the same depth. When top of T-DAM Pipe approaches levee top, the rising stops. Then only water surface continues to rise, and spillway discharge increases. Finally, water surface rises above floats crest, and overflows on floats starts. Thus, it can prevent excessive ponding by increasing discharge.

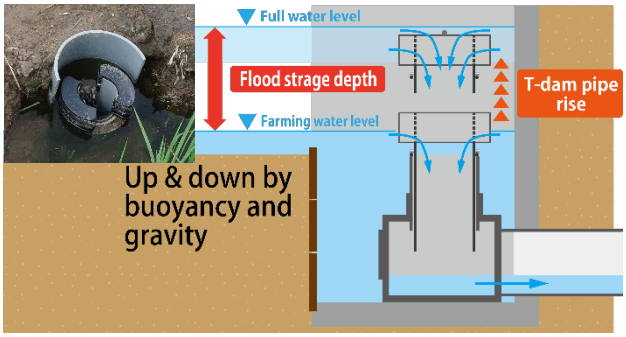

Figure 6. T-DAM Pipe

Even after rain, spillway discharge continues, and water surface descend gradually. Thus, T-DAM Pipe rises and descends automatically only by buoyancy and gravity. It costs 20 US dollars. It is far lower than ICT type Paddy Dam gate.

Floating trash flows away because surface water discharge continues throughout entire ponding process.

3.2. T-DAM Board

T-DAM Board is discharge regulator for stop-log type outlet. It is plastic board with half circle shaped notch at bottom. This notch forms orifice when the board bottom touches surface of concrete outlet structure. Board crest is lower than levee top.

Light rain discharges through the notch orifice. When rainfall on paddy surface exceeds discharge flow during heavy rain, water surface rises. When the surface elevation surpasses board crest, overflow at board crest start. Thus, it can prevent excessive ponding by increasing discharge.

Floating trashes accumulate in front of the board when no overflow and clogging to notch orifice when water surface lowered. It causes ill drainage. In this case, by only 5cm of lifting of the board, downward stream occurs, and clogged trash is removed and flows away. Maintenance of notch orifice type regulating board is far easier than hole orifice type regulating board.

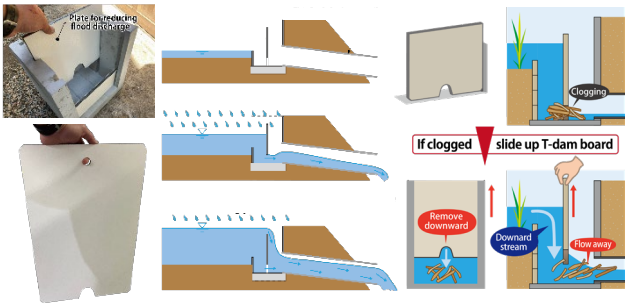

Figure 7. T-DAM Board

4. Others

Through introduction of tools for AWD, not only GHG reduction but also significant water saving will be realized . For farmers viewpoint, water saving is very important achievement because it can increase irrigation areas especially in dry season cropping in developing countries. By making use of water saving as an incentive for farmers, AWD will be introduced smoothly.

In areas such as developing countries where enough labor work is available, instead of expensive automatic gate, only installation of Stop-log Frame at inlet will improve paddy water control and contribute to AWD.

5. Finally

Simple tools developed on farmers viewpoint will effectively assist farmers challenges to important social themes, not only in Japan but also in rice cropping country in the world.

A Differentiable Two-Layer Energy Balance Model Coupled with a Residual Temporal Convolutional Network for Sparse-Observation Paddy Water Depth Inversion

Xie Wenpeng・Kimura Masaomi・Li Hongmei・Tian Runze

Abstract

Accurate knowledge of water depth in rice paddies is vital for regulating soil nutrient release, ensuring adequate root aeration, and optimizing crop transpiration, all of which underpin high and stable yields. However, traditional depth measurements-whether manual gauge readings or automated sensors-are laborious, prone to fouling by sediment and weeds, and often impractical for large-scale deployment. To overcome the scarcity of direct water depth observations, we reformulate the classic two-layer energy balance model as a differentiable, deep-learning-compatible module and introduce a two-stage hybrid learning framework: first, a lightweight residual network learns and corrects systematic biases of the physics module using discrepancies between simulated depth and sparse labels; second, a multi-layer temporal convolutional network (TCN) performs end-to-end depth sequence modeling on the corrected outputs by integrating physical priors with meteorological forcings. The unified network is trained end-to-end by jointly minimizing temperature and sparse-depth losses, requiring true depth labels at only 5 % of time steps. Field experiments demonstrate a water depth RMSE of approximately 2 cm, outperforming standalone physical or purely data-driven approaches. The proposed modular framework is adaptable to other agricultural and hydrological settings where direct depth observations are limited, offering a cost-effective, high-precision tool for precision irrigation and sustainable water resource management.

Analysis of Critical Input Features in LSTM-Based Inundation Forecasting Optimized by Multi-Objective Genetic Algorithms

Bing-Chen Jhong [1*], Hsiang-Kuan Chang [2], Jung-Lien Chu [3]

[1] Department of Marine Environment and Engineering, National Sun Yat-sen University, Kaohsiung, 80424, Taiwan (R.O.C.)

[2] Center for Weather and Climate Disaster Research, National Taiwan University, Taipei, 106319, Taiwan (R.O.C.)

[3] Meteorology Division, National Science and Technology Center for Disaster Reduction, New Taipei, 231007, Taiwan (R.O.C.)

* Corresponding author. Email: jhongbc@mail.nsysu.edu.tw

Abstract

Heavy rainfall induced by typhoons frequently causes severe urban inundation events, underscoring the need for accurate and timely forecasting systems. This study investigates the identification and optimization of critical input features in a Long-Short-Term-Memory (LSTM)-based inundation forecasting model enhanced by a Multi-Objective Genetic Algorithm (MOGA). The proposed framework systematically analyzes the contribution of various hydrometeorological and hydraulic factors to improve model accuracy and robustness across different lead times. Yilan County, Taiwan, was selected as the study area, encompassing nine reference inundation points. A cross-validation procedure was employed to rigorously evaluate model performance. Comparative experiments with conventional machine learning approaches highlight the superior ability of the LSTM-MOGA framework to identify key inputs and achieve consistent predictive accuracy. The results demonstrate that optimizing input features via MOGA not only enhances model performance but also mitigates overfitting, ensuring reliable forecasts during both training and testing phases. This research provides valuable insights into feature selection for deep learning-based hydrological forecasting and offers practical implications for urban flood risk management and disaster mitigation planning.

Keywords: Urban inundation forecasting, Long Short-Term Memory, Multi-Objective Genetic Algorithm, critical input feature analysis

1. Introduction

Climate change has intensified hydrometeorological hazards, with more frequent and severe rainfall events—especially typhoons—amplifying flood risks in urban areas. Global climate models consistently project rising extreme precipitation, posing challenges for densely populated cities with aging drainage systems. In Taiwan, typhoon-driven storms often cause flash floods and prolonged inundation, underscoring the urgent need for reliable short-term flood forecasting.

Artificial intelligence (AI), particularly deep learning, offers strong potential to surpass conventional hydrological models. Long Short-Term Memory (LSTM) and Gated Recurrent Units (GRU) capture nonlinear and temporal dynamics for near-real-time forecasting. Yet challenges remain in interpretability, feature selection, and generalization. Poorly chosen inputs or lag structures can degrade model performance, especially under rapidly changing typhoon conditions.

To address these issues, evolutionary algorithms such as Genetic Algorithms (GA), Particle Swarm Optimization (PSO), and Simulated Annealing have been applied, with Multi-Objective Genetic Algorithms (MOGA) showing particular promise in balancing accuracy and complexity. However, few studies have used MOGA for systematic input–lag optimization in flood forecasting. While GA-assisted LSTM tuning has been applied in energy and finance (Santra & Lin, 2019; Huang et al., 2021), most efforts remain single-objective. Reviews (e.g., Bansal et al., 2022) highlight potential in combining LSTM with evolutionary algorithms, but automated input selection remains underexplored.

This study proposes a hybrid framework integrating LSTM with MOGA-based feature optimization for short-term inundation forecasting. Objectives include: (i) building an LSTM model for grid-level inundation prediction; (ii) implementing a MOGA procedure for selecting predictors and lag structures; (iii) evaluating performance across multiple typhoon events; and (iv) benchmarking against baseline SVM and LSTM models.

2. Materials and Methods

2.1. Materials

This study targets Yilan County in northeastern Taiwan, a humid subtropical region with complex terrain and among the most rainfall-prone areas of the country, as shown in Figure 1. Frequent typhoons and seasonal monsoons bring prolonged precipitation, raising inundation risks across both urban and rural areas.

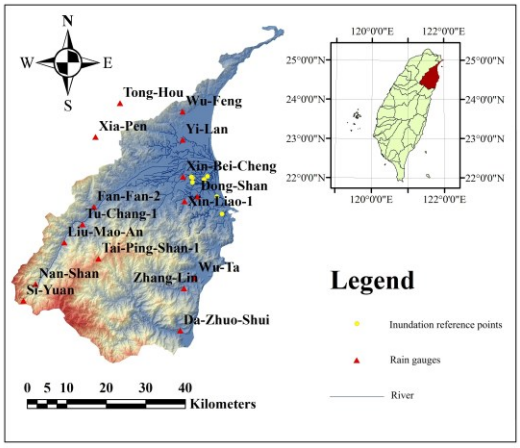

Figure 1. Study area with the distribution of rain gauges and inundation reference points.

To represent hydrological and drainage dynamics, nine reference sites and six sewer-level monitoring stations were selected, supplemented by rainfall data from 16 gauges. Several typhoon events (2005–2022) were used for training and validation to capture diverse flood conditions. Input features included (i) observed and KRID

rainfall data, (ii) SOBEK-simulated flood depths, and (iii) sewer water levels, providing a comprehensive view of surface and subsurface responses. The forecast target was inundation depth at 1–6 h lead times to support urban flood early warning. KRID, derived from radar–gauge integration through the QPESUMS system and processed by NCDR, offers high-resolution rainfall data suitable for flood modeling.

Baseline SVM and LSTM models with manually selected inputs were built for comparison. In contrast, the proposed framework integrates MOGA with LSTM to automatically optimize input features and lag lengths, reducing subjectivity and enhancing adaptability, robustness, and forecasting accuracy.

2.2. Methods

Support Vector Machine (SVM) is a supervised learning method effective for small datasets and nonlinear rainfall–inundation relationships, making it a robust baseline model in flood forecasting. Long Short-Term Memory (LSTM) networks, designed to capture sequential dependencies, are well suited for modeling lagged rainfall–inundation responses and enabling accurate multi-lead-time predictions in data-rich early warning systems. Multi-Objective Genetic Algorithm (MOGA) is an evolutionary technique that balances competing objectives to identify Pareto-optimal solutions. In flood forecasting, it is particularly effective for input feature and lag selection, enhancing both model accuracy and generalization.

Traditionally, feature selection has relied on expert judgment or correlation filtering, which often overlook nonlinear dependencies. To address this, this study integrates MOGA with LSTM to optimize input features and temporal lags, while using SVM and LSTM as baseline models for comparison. Through iterative genetic operations, MOGA systematically explores input configurations, guiding models toward more accurate, efficient, and reproducible forecasts.

3. Results and Discussion

3.1. Comparative assessment of forecasting performance

As shown in Figure 2, during testing, SVM and LSTM models using conventional feature selection performed worse than the proposed model at all nine inundation sites. LSTM showed the greatest instability, with inconsistent results across lead times, such as at reference point 1. At points 4 and 8, only the proposed model achieved positive CE values for all horizons. These results highlight that traditional feature selection risks overfitting, whereas the proposed framework improves robustness and forecasting accuracy.

3.2. Evaluation of effective input features in the optimized flood forecasting model

The proposed model demonstrates the ability to optimize input feature selection in an automated manner while also adapting feature importance to specific forecast lead times (1- to 6-h). In this study, Factors 1–2 represent KRID rainfall and its accumulated values, Factors 3–18 correspond to observed rainfall records, and Factors 19–25 denote sewer water levels. As illustrated in the figure, KRID rainfall, selected observed rainfall variables, and sewer water level information contribute significantly to longer lead-time forecasts, whereas not all features are equally effective. A key advantage of the proposed framework lies in its capacity to autonomously identify effective predictors without manual intervention, thereby enhancing both efficiency and robustness in inundation forecasting.

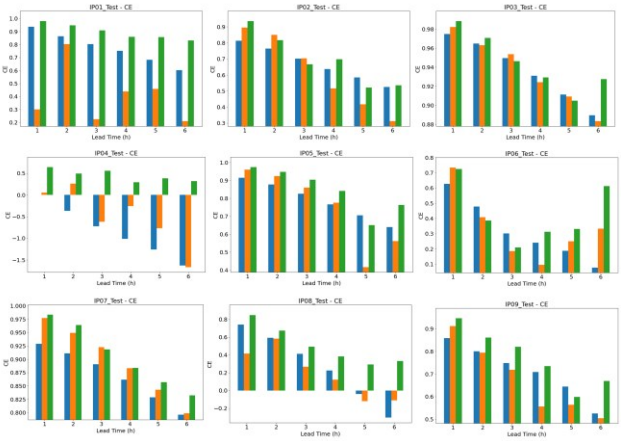

Figure 2. Comparison of coefficient of efficiency (CE) values for SVM (blue), LSTM (orange), and the proposed model (green) at nine inundation reference sites during the testing phase.

Figure 3. Proportion of inundation reference sites utilizing each input feature across forecast lead times (1–6 h).

4. Conclusions

This study integrates MOGA with LSTM to optimize input features and lag structures, achieving higher accuracy and robustness than baseline models. The fully automated feature selection reduces subjectivity and overfitting risks, making the framework well suited for operational flood forecasting. Future work may extend the approach by combining other optimization or AI algorithms to further enhance generalization and adaptability.

Acknowledgements

The authors acknowledge the support of the National Science and Technology Council of Taiwan (Grant No.: NSTC 114-2625-M-110-001).

References

Bansal, M., Goyal, A., & Choudhary, A. (2022). A comparative analysis of K-nearest neighbor, genetic, support vector machine, decision tree, and long short term memory algorithms in machine learning. Decision analytics journal, 3, 100071.

Huang, Y., Gao, Y., Gan, Y., & Ye, M. (2021). A new financial data forecasting model using genetic algorithm and long short-term memory network. Neurocomputing, 425, 207-218.

Santra, A. S., & Lin, J. L. (2019). Integrating long short-term memory and genetic algorithm for short-term load forecasting. Energies, 12(11), 2040.